Contents

INTRODUCTION TO PART II

In the following chapters we present the theory of bifurcations of dynamical systems with simple dynamics. It is difficult to over-emphasize the role of bifurcation theory in nonlinear dynamics the reason is quite simple: the methods of the theory of bifurcations comprise a working tool kit for the study of dynamical models. Besides, bifurcation theory provides a universal language to communicate and exchange ideas for researchers from different scientific fields, and to understand each other in interdisciplinary discussions.

Bifurcation theory studies the changes in the phase space as we vary the parameters of the system. In essence, this is the authentic notion of bifurcation theory proposed originally by Henry Poincaré when he studied Hamiltonian systems with one degree of freedom. We must, however, note that this intuitively evident definition is not always sufficient at the contemporary stage of the development of the theory. One needs, in fact, to have an appropriate mathematical foundation to define the notions of the structure of the phase space and the changes in the structure.

The first attempt at creating such formalization had been made by Andronov and Pontryagin in 1937: they introduced the notion of a *rough* system. For a system to be rough, it means that any sufficiently close system is to be topologically equivalent to the given one. Moreover, the conjugating homeomorphism must be close to identity. In other words, the two systems must have matching phase portraits and corresponding trajectories can differ only slightly.

In the same paper, Andronov and Pontryagin had presented the necessary and sufficient conditions of roughness for systems on the plane. Consequently,

many problems of nonlinear dynamics that can be modeled by two-dimensional dynamical systems has since attained a necessary mathematical foundation.

The main statements of the Andronov and Pontryagin theory are presented in the first section of Chap. 7, which opens Part II of this book. We also give the definition of structural stability (due to Peixoto) there. The difference between the notion of structural stability and that of roughness is that, the conjugating diffeomorphism defining the structural stability is not assumed to be close to identity in the former case. This is rather convenient from a purely mathematical point of view as it follows immediately from the definition that structurally stable systems form an open set. Even though numerous known proofs had only concentrated on structural stability, roughness itself follows from the same proofs as a by-product. Hence, the difference of these two notions does not seem to be that essential. Note, nonetheless, that the notion of structural stability has become much more widely known outside of Russia, especially in the West. In this book we will frequently utilize this term as well. In spite of that, we believe that the notion of roughness is, in principle, more reasonable as it gives the natural image of small changes of real processes caused by small variations of parameters.

The multi-dimensional extension of two-dimensional rough systems is the Morse–Smale systems discussed in Sec. 7.4. The list of limit sets of such a system includes equilibrium states and periodic orbits only; furthermore, such systems may only have a finite number of them. Morse–Smale systems do not admit homoclinic trajectories. Homoclinic loops to equilibrium states may not exist here because they are non-rough — the intersection of the stable and unstable invariant manifolds of an equilibrium state along a homoclinic loop cannot be transverse. Rough Poincaré homoclinic orbits (homoclinics to periodic orbits) may not exist either because they imply the existence of infinitely many periodic orbits. The Morse–Smale systems have properties similar to two-dimensional ones, and it was presumed (before and in the early sixties) that they are dense in the space of all smooth dynamical systems. The discovery of dynamical chaos destroyed this idealistic picture.

The fundamental question of "what distinguishes systems with simple dynamics from systems with chaotic dynamics?" can only be answered if we can correspond certain types of trajectories to physically observable processes. We began the classification with the study of quasiperiodic trajectories (Chap. 4 in the first part of this book). Even though these trajectories are non-rough, they were shown to model adequately such phenomena as beats and modulations.

Quasiperiodic trajectories are a special case of Poisson-stable trajectories. The latter plays one of the leading roles in the theory of dynamical systems as they form a large class of center motions in the sense of Birkhoff (Sec. 7.2). Birkhoff had partitioned the Poisson-stable trajectories into a number of subclasses. This classification is schematically presented in Sec. 7.3. Having chosen this scheme as his base, as early as in the thirties, Andronov had undertaken an attempt to collect and correlate all known types of dynamical motions with those observable from physical experiments. Since his arguments were based on the notion of stability in the sense of Lyapunov for an individual trajectory, Andronov had soon come to the conclusion that all possible Lyapunov-stable trajectories are exhausted by equilibrium states, periodic orbits and almost-periodic trajectories (these are quasiperiodic and limit-quasiperiodic motions in the finite-dimensional case).

Thus, it appeared naturally to assume that every interesting dynamical regime possesses a discrete frequency spectrum. In this connection, it is curious to note that Landau and Hopf had proposed quasiperiodic motions with a sufficiently large number of independent frequencies as the mathematical image of hydrodynamical turbulence (the number of the frequencies was supposed to increase to infinity as some structural parameter, such as the Reynolds number, increases).

All other Poisson-stable trajectories are unstable in the sense of Lyapunov. How can such trajectories be of any use in dynamics? The answer was found nearly 30 years later. For the first time, the significance of a stable limit set consisting of individually unstable trajectories for explaining the complex and chaotic behavior of nonlinear dynamical processes was recognized by Lorenz in 1963 [87].

In the rough case an analysis of the structure of such a limit set (called a quasiminimal set, which is defined as the closure of an unclosed Poisson-stable trajectory) may be performed using Pugh's closing lemma. The main conclusion that follows from this analysis (see Sec. 7.3) is that periodic orbits are dense in a rough quasiminimal set. In particular, we will see that the number of periodic orbits is infinite. Systems possessing such limit sets are called systems with *complex dynamics*.

A more vivid characteristics of systems with complex behaviors is the presence of a Poincaré homoclinic trajectory, i.e. a trajectory which is biasymptotic to a saddle periodic orbit as $t \to \pm\infty$. The existence of a homoclinic orbit which lies at the transverse intersection of the stable and unstable

invariant manifolds of the saddle periodic orbit implies the existence of infinitely many other saddle periodic orbits in the phase space (Sec. 7.5).

However, rough systems (both types — with simple and complex dynamics) with dimension (of the phase space) greater than two are not dense in the space of dynamical systems. In fact, it turns out that a key role must have been given to *non-rough* attracting limit sets with unstable behaviors in their trajectories.

An example of such a set is the Lorenz attractor which occurs in a variety of models. The wild spiral attractor [153] is another fascinating example.[1]

The similarity between both strange attractors is that none contains stable periodic orbits. The difference between them is that all Poincaré homoclinic orbits in the Lorenz attractor are rough, whereas the featuring property of the wild attractor is the coexistence of rough and non-rough Poincaré homoclinic orbits due to homoclinic tangencies. The similarity is that both attractors are "concentrated" on a rough equilibria state which is a saddle in the case of the Lorenz attractor, and a saddle-focus in the case of the wild attractor. Among other features of models with such strange attractors, we may single out the existence of regions in the parameter space where the parameter values corresponding to homoclinic loops to the equilibrium state are dense.

A complete understanding of such complex phenomena is impossible without a thorough knowledge of basic bifurcations, both local and global. General aspects of this theory are reviewed in Chap. 8. We begin the analysis with the simplest non-rough systems in the two-dimensional case, following the pioneering works by Andronov and Leontovich. They carried out a systematic classification of all principal bifurcations of limit cycles on the plane of which there are four sub-types: namely, the birth of a limit cycle from:

(1) a simple weak focus;
(2) a simple semistable limit cycle;
(3) a separatrix loop to a simple saddle-node; and
(4) a separatrix loop to a saddle at which the divergence of the vector field is non-zero.

The Andronov–Leontovich classification employs an additional notion of the so-called degree of non-roughness. A further development of the theory

[1]The spiral-like shape of this attractor follows from the shape of homoclinic loops to a saddle-focus (2, 1) which appear to form its skeleton. Its wildness is due to the simultaneous existence of saddle periodic orbits of different topological type and both rough and non-rough Poincaré homoclinic orbits.

had taken yet another direction, namely by selecting bifurcation sets of codimension one for primary bifurcations, and of arbitrary (though finite) codimension in the general case. Moreover, even though all two-dimensional flows on a connected component of a bifurcation surface of a given finite codimension are all topologically equivalent (Leontovich–Mayer theorem), this is no longer true in the multi-dimensional case.

This result is due to Palis, who had found that two-dimensional diffeomorphisms with a heteroclinic orbit at whose points an unstable manifold of one saddle fixed point has a quadratic tangency with a stable manifold of another saddle fixed point can be topologically conjugated locally only if the values of some continuous invariants coincide. These continuous invariants are called moduli. Some other non-rough examples where moduli of topological conjugacy arise are presented in Sec. 8.3.

Surprisingly, even non-rough systems of codimension one may have infinitely many moduli. Of course, since the models of nonlinear dynamics are explicitly defined dynamical systems with a *finite* set of parameters, this creates a new obstacle which the classical bifurcation theory has not run into. Although the case of homoclinic loops of codimension one does not introduce any principal problem, nevertheless codimensions two and higher are much less trivial as, for example, in the case of a homoclinic or heteroclinic cycle including a saddle-focus where the structure of the bifurcation diagrams is directly determined by the specific values of the corresponding moduli.

Therefore, Andronov's approach (Sec. 8.4) for studying dynamical models has to be corrected in cases where a complete bifurcation analysis may not be possible without moduli. We note, however, that if some fine delicate phenomena may be ignored, or if the problem is restricted to the analysis of non-wandering orbits like equilibrium states, periodic and quasiperiodic motions, a study of the main bifurcations in systems with simple dynamics still remains realistic within the framework of finite-parameter families under certain reasonable requirements (Sec. 8.4).

We note parenthetically that the situation becomes drastically different for the systems with complex dynamics. In the majority of cases (at least in those cases where homoclinic tangencies appear) the introduction of the moduli is inexorable because they serve as the essential parameters governing the bifurcations (see [63]).

Although the theory of the typical bifurcations of limit cycles in two-dimensional systems was created by Andronov and Leontovich in the

thirties,[2] a systematic development of the bifurcation theory of periodic orbits and equilibrium states in multi-dimensional systems was initiated only after their results became available to the scientific community (the work of Hopf in 1942 was, perhaps, the only exception).

A straightforward generalization of two-dimensional bifurcations was developed soon after. So were some natural modifications such as, for instance, the bifurcation of a two-dimensional invariant torus from a periodic orbit. Also it became evident that the bifurcation of a homoclinic loop in high-dimensional space does not always lead to the birth of only a periodic orbit. A question which remained open for a long time was: could there be other codimension-one bifurcations of periodic orbits? Only one new bifurcation has so far been discovered recently in connection with the so-called "blue-sky catastrophe" as found in [152]. All these high-dimensional bifurcations are presented in detail in Part II of this book.

In Chaps. 9 and 10 we consider structurally unstable equilibrium states and periodic orbits. The bifurcations of these limit sets are studied in Chap. 11. These three chapters belong to a theory of *local* bifurcations. The results with local bifurcations are well presented in the literature and this theory continues to develop rapidly. We therefore restrict ourselves here to a detailed study of the basic cases. First of all, for a bifurcating equilibrium state whose characteristic exponents do not lie on the imaginary axis, we assume that they lie strictly to the left of it. On the imaginary axis we assume that there is either a single zero exponent,[3] or a complex-conjugate pair of pure imaginary ones. Analogous assumptions are made in the case of periodic motions: the multipliers which do not lie on the unit circle must lie inside it, and those on the unit circle consist of a single multiplier equal to $+1$, or -1, or a complex-conjugate pair $e^{\pm i\varphi}$, $0 < \varphi < \pi$. The corresponding bifurcations in these cases are sufficiently simple, so wherever it is possible we do not impose restrictions on the nonlinear terms.

The reason for our assumption on the spectrum of characteristic exponents is quite obvious: we focus special attention on the problem of the loss of stability of equilibrium states and periodic motions and on the bifurcations accompanying the loss of stability. It is clear that these problems are a primary subject of nonlinear dynamics.

[2] This was reported in the preface of the first edition of the book "The Theory of Oscillations" by Andronov, Vitt and Khaikin (which was printed without the name of Vitt in 1937).

[3] The case of a double-zero characteristic exponent is partly considered in Sec. 13.2.

Of course, the cases of higher degeneracies in the linear part are also very interesting; for example, an equilibrium state with three characteristic exponents 0, $\pm i\omega$, or with two pairs of purely imaginary exponents $\pm i\omega_1$, $\pm i\omega_2$, etc. In such cases of codimension two it is typical that the associated (truncated) normal form reduces to a two-dimensional system with a finite number of parameters. A systematic study of these normal forms is presented in [21, 40, 64, 82].

One must bear in mind, however, that a truncated normal form does not always guarantee a complete reconstruction of the dynamics of the original system. For instance, when the truncated normal forms possess additional symmetries, these symmetries are, in principle, broken if the omitted higher-order terms are taken back into account, and this can even lead to an onset of chaos in some regions of the parameter space. These regions are extremely narrow near a bifurcation point of codimension two but their size may expand rapidly as we move away from the bifurcation point over a finite distance.

The significance of higher degeneracies (starting from codimension three) in the linear part is that the effective normal forms become three-dimensional, and may, as a result, exhibit complex dynamics, the so-called instant chaos, even in the normal form itself. Such examples include the normal forms for a bifurcation of an equilibrium state with a triplet of zero characteristic exponents, and a complete or incomplete Jordan block, in which there may be a spiral strange attractor [18], or a Lorenz attractor [129], respectively (the latter case requires an additional symmetry). Since we will focus our considerations only on simple dynamics, we do not include these topics in this book.

The key methods in our presentation of local bifurcations are based on the center manifold theorem and on the invariant foliation technique (see Sec. 5.1. of Part I). The assumption that there are no characteristic exponents to the right of the imaginary axis (or no multipliers outside the unit circle) allows us to conduct a smooth reduction of the system to a very convenient "standard form." We use this reduction throughout this book both in the study of local bifurcations on the stability boundaries themselves and in the study of global bifurcations on the route over the stability boundaries (Chap. 12).[4] These

[4]In the general case where there are both stable and unstable characteristic exponents, or stable and unstable multipliers in the spectrum, the local bifurcation problem does not cause any special difficulties, thanks to the reduction onto the center manifold. Consequently, the pictures from Chaps. 9–11 will need only some slight modifications where unstable directions replace stable ones, or be added to existing directions in the space. However, the reader must

global bifurcations are related to the fact that in contrast to an equilibrium state which always persists on any boundary of its stability region, a periodic orbit may not exist on the stability boundary. In particular, a periodic orbit may disappear via one of the following scenarios:

(1) it shrinks to an equilibrium state;
(2) a saddle-node equilibrium state appears suddenly on it;
(3) it adheres into a homoclinic loop to a saddle equilibrium state; and
(4) it undergoes a blue-sky catastrophe, when its period and length both become infinite when it approaches a stability boundary. In contrast to homoclinic bifurcations, no equilibrium state is involved in a blue-sky catastrophe.

In Chap. 12 we will study the global bifurcations of the disappearance of saddle-node equilibrium states and periodic orbits. First, we present a multi-dimensional analogue of a theorem by Andronov and Leontovich on the birth of a stable limit cycle from the separatrix loop of a saddle-node on the plane. Compared with the original proof in [130], our proof is drastically simplified due to the use of the invariant foliation technique. We also consider the case when a homoclinic loop to the saddle-node equilibrium enters the edge of the node region (non-transverse case).

The bifurcation of a separatrix loop of a saddle-node was discovered by Andronov and Vitt [14] in their study of the transition phenomena from synchronization to beating modulations in radio-engineering. Specifically, they had studied the periodically forced van der Pol equation

$$\ddot{x} - \mu(1 - x^2)\dot{x} + \omega_0^2 x = \mu A \sin \omega t \,,$$

where $\mu \ll 1$ and $\omega_0 - \omega \sim \mu$. In the associated averaged equation, they showed the existence of the saddle-node bifurcation which explained the simple transition from a stable equilibrium state to a periodic motion. However, the question of the correspondence between the limit sets of the averaged equation and those of the original one was not solved then. Andronov and Vitt returned to this problem in their succeeding paper [15] where, using the method of a small parameter by Poincaré, they proved the correspondence between the rough equilibrium state of an averaged system and a periodic orbit

be aware that since a reduction to the standard form is not always smooth in this general case, it cannot be applied in a straightforward way to the analysis of certain global bifurcations (such as the disappearance of saddle-saddle equilibria or saddle-saddle periodic orbits).

of the original system. Later on, Krylov and Bogolyubov [81] proved the correspondence between the rough periodic orbit in the averaged equations and the two-dimensional invariant torus in the original system. Thus, a rigorous explanation of the transition from synchronization to modulations in the original system requires a study of the bifurcation of the possible birth of an invariant torus at the disappearance of a saddle-node periodic orbit.

The general setting of the problem of global bifurcations on the disappearance of a saddle-node periodic orbit is as follows. Assume that there exists a saddle-node periodic orbit and that all trajectories which tend to this periodic orbit as $t \to -\infty$ also tend to it as $t \to +\infty$ along some center manifold. In other words, assume that the unstable manifold W^u of the saddle-node returns to the saddle-node orbit from the side of the node region. In this case, either:

(1) W^u is a two-dimensional invariant manifold such as a torus, or a Klein bottle, or
(2) W^u is not a manifold.

If the system has a global cross-section (which always exists when we treat a periodically forced autonomous system), the unstable manifold W^u will only be a torus. The intersection of W^u with the cross-section is a closed curve which is invariant under the Poincaré map. Consequently, the following two cases are possible:

(1) the curve is smooth, and
(2) the curve is non-smooth.

If the curve is smooth when the saddle-node disappears, a closed attracting invariant curve remains on the cross-section. This result is due to Afraimovich and Shilnikov [3]. If the invariant curve is non-smooth, the situation becomes essentially more complicated, because the disappearance of the saddle-node may now lead the original system out of the Morse–Smale class, i.e. the system may exhibit complex structures. Afraimovich and Shilnikov discovered if the so-called "big lobe" or "small lobe" conditions are satisfied, then there exists a sequence of parameter intervals corresponding to the occurrence of complex dynamics. This result was subsequently improved by Newhouse, Palis and Takens [97] who proved that there exists a sequence of parameter values corresponding to a transverse homoclinic orbit (and, hence, there always exists a sequence of intervals corresponding to complex dynamics),

without using the big lobe condition but restricted to one-parameter families of a special kind. An analogous result for this bifurcation for general one-parameter families is also obtained in [151] where it is shown that if the big lobe condition is satisfied, then chaos exists for all (small) parameter values just after a saddle-node's disappearance. On the contrary, if this condition is not satisfied, then intervals of complex dynamics and those exhibiting only simple dynamics (a continuous invariant curve exists) must alternate on the parameter axis.

Note that the effect of alternating zones of simple and complex behavior was discovered for the first time by van der Pol [154] in his experiments on the periodic forcing of a lamp generator (this effect occurs when one tunes a radio, and a characteristic noise is heard while moving from one station to another). The first theoretical explanation was given by Cartwright and Littlewood [36] for the van der Pol equation.

We will present in Sec. 12.2 a summary of results for the case where the unstable manifold W^u of the saddle-node is homeomorphic to a torus along with the proof of a theorem on the persistence of the invariant torus in the smooth case. There, we will also develop a general theory for an effective reduction of the problem to a study of some family of endomorphisms (smooth non-invertible maps) of a circle.

When a system does not have a global cross-section, the unstable manifold W^u of the saddle-node may also be a Klein bottle (if the system is defined in R^n with $n \geq 4$). If the Klein bottle is smooth at the bifurcation point, it will persist after the disappearance of the saddle-node. For topological reasons, a pair of periodic orbits will always exist on the Klein bottle such that the length of both orbits will increase to infinity while approaching the event of the sudden appearance of the original saddle-node. Generically, these periodic orbits will change stability infinitely many times via a forward and backward period-doubling bifurcations. If the Klein bottle is non-smooth at the bifurcation point, then the big lobe or the small lobe conditions should be applied. The former guarantees complex dynamics for all small values of the parameter beyond the demise of saddle-node. In contrast, the small lobe condition can only guarantee the existence of a sequence of intervals of parameter values where complex dynamics occurs. Note that unlike the case where W^u is homeomorphic to a torus, in the case of a non-smooth Klein bottle the dynamics may be simple for all small parameter values when the small lobe condition is not satisfied (the case of a "very small lobe"). These results are presented in Sec. 12.3.

A totally different situation becomes possible in the case where the system does not have a global cross-section, and when W^u is not a manifold. In this case (Sec. 12.4), the disappearance of the saddle-node periodic orbit may, under some additional conditions, give birth to another (unique and stable) periodic orbit. When this periodic orbit approaches the stability boundary, both its length and period increases to infinity. This phenomenon is called *a blue-sky catastrophe*. Since no physical model is presently known for which this bifurcation occurs, we illustrate it by a number of natural examples.

Note that in the n-dimensional case, where $n \geq 4$, other topological configurations of W^u may be realized. Such saddle-node bifurcations will definitely lead the system out of the class of systems with simple dynamics. For example, it is shown in [139, 152] that a hyperbolic attractor of the Smale–Williams type may appear just after the disappearance of a saddle-node periodic orbit.[5]

Another typical codimension-one bifurcation (left untouched in this book) within the class of Morse–Smale systems includes the so-called saddle-saddle bifurcations, where a non-rough saddle equilibrium state with one zero characteristic exponent (the others lie in both left and right half-planes) coalesces with another saddle having a different topological type. If, in addition, the stable and unstable manifolds of the saddle-saddle point intersect each other transversely along some homoclinic orbits, then as the bifurcating point disappears, saddle periodic orbits are born from the homoclinic loops. If there is only one homoclinic loop, then only one periodic orbit is born from it, and respectively, this bifurcation does not lead the system out of the Morse–Smale class. However, if there are more than one homoclinic loops, a hyperbolic limit set with infinitely many saddle periodic orbits will appear after the saddle-saddle vanishes [135].

A similar effect occurs when a saddle-saddle periodic orbit (with one multiplier equal to 1 and the rest of the multipliers both inside and outside of the unit circle) disappears. If the stable and unstable manifolds of the saddle-saddle periodic orbits intersect across two (at least) smooth tori, then the disappearance of such a periodic orbit is followed by the birth of a limit set in which an infinite set of smooth saddle invariant tori is dense [6].

[5] A more general case is also considered in [139] concerning the disappearance of a saddle-node torus and followed by the appearance of Anosov attractors and multi-dimensional solenoids.

In Chap. 13 we will consider the bifurcations of a homoclinic loop to a saddle equilibrium state. We start with the two-dimensional case. First of all, we investigate the question of the stability of the separatrix loop[6] in the generic case (non-zero saddle value), as well as in the case of a zero saddle value. Next, we elaborate on the cases of arbitrarily finite codimensions where the so-called Dulac sequence is constructed, which allows one to determine the stability of the loop via the sign of the first non-zero term in this sequence.

In the case of a non-zero saddle value, we present the classical result by Andronov and Leontovich on the birth of a unique limit cycle at the bifurcation of the separatrix loop. Our proof differs from the original proof in [9] where Andronov and Leontovich essentially used the topology of the plane. However, following Andronov and Leontovich we present our proof under a minimal smoothness requirement ($\mathbb{C}^1$).

The case of zero saddle value was considered by E. A. Leontovich in 1951. Her main result is presented in Sec. 13.3, rephrased in somewhat different terms: in the case of codimension n (i.e. when exactly the first $(n-1)$ terms in the Dulac sequence are zero) not more than n limit cycles can bifurcate from a separatrix loop on the plane; moreover, this estimate is sharp.

In the same section we give the bifurcation diagrams for the codimension two case with a first zero saddle value and a non-zero first separatrix value (the second term of the Dulac sequence) at the bifurcation point. Leontovich's method is based on the construction of a Poincaré map, which allows one to consider homoclinic loops on non-orientable two-dimensional surfaces as well, where a small-neighborhood of the separatrix loop may be a Möbius band. Here, we discuss the bifurcation diagrams for both cases.

The bifurcations of periodic orbits from a homoclinic loop of a multi-dimensional saddle equilibrium state are considered in Sec. 13.4. First, the conditions for the birth of a stable periodic orbit are found. These conditions stipulate that the unstable manifold of the equilibrium state must be one-dimensional and the saddle value must be negative. In fact, the precise theorem (Theorem 13.6) is a direct generalization of the Andronov–Leontovich theorem to the multi-dimensional case. We emphasize again that in comparison with the original proof due to Shilnikov [130], our proof here requires only the $\mathbb{C}^1$-smoothness of the vector field.

[6] Only one-sided stability is naturally considered.

We consider next the homoclinic bifurcation of the saddle whose unstable manifold is still one-dimensional, but the saddle value is now assumed to be positive. Unlike the case of the negative saddle value, here we need some additional non-degeneracy conditions to be imposed on the system. These conditions, in fact, imply the existence of a stable two-dimensional invariant $\mathbb{C}^1$-manifold in the system, which is either a cylinder or a Möbius band, depending on the sign of the so-called separatrix value. Hence, our problem is reduced, essentially, to the two-dimensional case considered in Sec. 13.2. Since this problem is a particular case of a more general problem (the case of the multi-dimensional unstable manifold) considered in Sec. 13.5, we focus more on the geometry underlying the result. Such an approach is relevant to the study of the Lorenz attractors, as well as some other homoclinic bifurcations of higher codimensions.

We end this section with a consideration of the homoclinic loop to a saddle-focus whose unstable manifold is one-dimensional. It is shown that when the saddle value is positive, infinitely many saddle periodic orbits coexist near such a homoclinic loop of the saddle-focus (Theorem 13.8).

The existence of complex dynamics near a homoclinic loop to a saddle-focus was discovered by L. Shilnikov for the three-dimensional case in [131]. Subsequently, the four-dimensional case[7] was considered in [132]; and the general case in [136].

In Sec. 13.5 we consider the bifurcation of the homoclinic loop of a saddle without any restrictions on the dimensions of its stable and unstable manifolds. We prove a theorem which gives the conditions for the birth of a single periodic orbit from the loop [134], and also formulate (without proof) a theorem on complex dynamics in a neighborhood of a homoclinic loop to a saddle-focus. Here, we show how the non-local center manifold theorem (Chap. 6 of Part I) can be used for simple saddles to reduce our analysis to known results (Theorem 13.6).

In the case of the saddle-focus, the result of [136] in its full generality cannot be obtained by a reduction to any invariant manifold. However, generically (i.e. under some simple non-degeneracy conditions) the problem can be reduced to a three- or four-dimensional invariant manifold [120, 150].

Section 13.6 discusses three main cases of codimension-two bifurcations of a homoclinic loop to a saddle. These cases were selected by Shilnikov in [138]

[7] Here, the saddle-focus has two pairs of complex-conjugate characteristic exponents and the divergence of the vector field is non-vanishing at the saddle-focus.

for explaining the immediate onset of the Lorenz attractor from a homoclinic butterfly. Later, these bifurcations attracted much interest (see references in Sec. 13.6). Here we consider a multi-dimensional case of a homoclinic loop to a saddle with zero saddle value and those cases of the so-called "orbit-flip" and "inclination-flip" bifurcations which do not lead to complex dynamics. Although the corresponding bifurcation diagrams are widely known (see [126, 77, 129] for the inclination-flip case, [119] for the orbit-flip case, and [99, 38, 77, 65] for the case of zero saddle-value), an explicit and complete proof is published here, probably for the first time.

In Sec. 13.7 we describe two other cases of codimension two, namely the bifurcations of a homoclinic-8 and a heteroclinic cycle with two saddles. Both cases are considered within the Morse–Smale class (we require the saddle-value to be negative in the case of the homoclinic-8; in the case of the heteroclinic cycle, either the saddle values must be negative or the conditions which guarantee the existence of a two-dimensional invariant manifold must be satisfied). The results surveyed in this section are extracted from [148, 151, 50, 149] for the homoclinic-8, and [121, 122, 123, 124, 125] for the heteroclinic cycles. Some other results on heteroclinic connections with a different topology [34, 35] are also presented. The structure of bifurcation diagrams in the case where two saddle-foci are involved is much more complicated in contrast to the case of the connection between two saddles (even though the dynamics remains simple in both cases). According to [158], the fine structure of the bifurcation diagrams for the saddle-focus case is sensitive to arbitrarily small changes of the continuous topological invariants (moduli) discussed in Sec. 8.3.

The last chapter focuses on the general problems of the transition over the stability boundaries of equilibrium states and periodic orbits. These questions have an immediate significance for the subject of nonlinear dynamics, specially in cases where changes in the parameters of a working device may push it out of its stability region, or when the control parameters are deliberately chosen as close to the stability boundary as possible in order to achieve maximal performance. For stationary regimes, the corresponding problems were addressed by Bautin in his monograph first published in 1949. He classified stability boundaries as either safe or dangerous. When a safe boundary is crossed, the representative phase point does not leave a small neighborhood of the bifurcating equilibrium state or periodic orbit, although the latter becomes unstable. In the case of a dangerous boundary, the phase point blows out from

a small neighborhood of the bifurcating trajectory. Evidently, a local analysis becomes inadequate in the case of dangerous boundaries: one must investigate here how the unstable sets behave at the critical moment. For instance, if a stable limit cycle adheres to a homoclinic loop of a saddle, it becomes crucial to know where the other separatrix goes to since its ω-limit set will be the new dynamical regime of the system. In other cases, it turns out, however, that there may be more than one stable limit set included in the boundary of the unstable set at the critical parameter value (if this bifurcation is within the Morse–Smale class, these limit sets are stable equilibria or periodic orbits). Another option embraces the so-called dynamically indefinite stability boundary where a random choice of the new regime occurs as a natural dynamical phenomenon — the dynamical uncertainty.

The number of papers and monographs on the theory of bifurcations is very large and increasing rapidly. Some of the questions considered in this book are, to a certain extent, reflected in other books as well (see especially the books marked by an asterisk in the list of references). We stress, however, that in many works, while studying global bifurcations, the assumption of smooth linearization of the equations near equilibrium states and periodic orbits is very often made only for the sake of maximal convenience. The linearization assumption requires the absence of resonances, which in turn imposes an infinite set of unnecessary additional conditions on the system (or, the number of such assumptions, first finite, may grow very fast as the dimension of the system grows). Therefore, any approach based on linearization will cast some doubts on the full applicability of the theoretical results to dynamical models.[8] The methods presented in this book are free from these problems. This is achieved by the use of techniques developed by our research group in Nizhny Novgorod. It is applied in Chaps. 12 and 13 to non-local bifurcations. We stress that we need only a very small degree of smoothness. This, perhaps, makes our analysis more complicated, but it guarantees and enhances the validity and the adequacy of our global bifurcation results. The methods presented in this book are applicable also for systems with complex dynamics, in particular, for systems with homoclinic tangencies [58, 59, 62], see also [100, 101].

[8] It happens rather often that some results which sound fine mathematically, being formulated for "typical" or "generic" families of dynamical systems, when applied to a specific problem require the verification of their stipulated conditions. It is unfair, however, to force a researcher to consume time and computational resources only to check on conditions which are, in fact, unnecessary.

We would like to acknowledge the help given to us while working on this book. In particular, we wish to thank S. Gonchenko, M. Shashkov, O. Stenkin, L. Lerman and J. Moiola. We would also like to acknowledge the generous supports from the USA Office of Naval Research and the Swiss Federal Institute of Technology (EPFL and ETH).

Chapter 7

STRUCTURALLY STABLE SYSTEMS

The qualitative theory of dynamical systems was initiated in the 19th century by problems from celestial mechanics. The equations from celestial mechanics, as we know, are Hamiltonian, a rather special form from a general point of view. In essence, there was no particular need for a qualitative theory of non-conservative systems at that time. Nevertheless, Poincaré had created a significant part of a general theory of dynamical systems on the plane along with its key result — the theory of limit cycles, and so had Lyapunov — a general theory of stability. These mathematical theories were both applied later, in 1920–1930 in connection with the invention of the radio and the further intensive development of radio-engineering.

The dynamical regime in radio-engineering is self-oscillations. Any real device, such as a neon bold or a vacuum tube, possesses a certain set of adjustable parameters. In practice, the parameter values corresponding to a self-oscillatory regime of the same device, or of a series of similar ones, cannot be exactly identical. Therefore, if a device exhibits repeatedly a similar oscillation, this means that small parameter deviations within some tolerance margins do not change the qualitative character of the process. Naturally, any realistic mathematical model of the system must also exhibit this property of real physical systems.

In the case where the physical system can be adequately modeled by a dynamical system on the plane, precise mathematical meaning can be given to this feature of physical "robustness", and this was done by Andronov. First of all, he applied the Poincaré theory of limit cycles and the Lyapunov theory of stability for studying modeling equations that allowed him and Vitt to explain many real phenomena in radio-engineering. Then, he linked the

notion of a stable Poincaré limit cycle with the observable periodic oscillations which he called "self-oscillations". Moreover, Andronov introduced the notion of a "rough" cycle as the mathematical image of robust self-oscillation, i.e. a cycle which persists under small smooth perturbations of the system.

However, over some parameter range, the governing parameters can cause fundamental changes in the oscillatory regimes. For a dynamical system this causes qualitative modifications of the phase portrait. In his perspective review on "Mathematical problems of the theory of self-oscillations" [8], Andronov had emphasized that the comprehensive study of bifurcations of the oscillatory regimes requires the expansion of the notion of roughness from a stand-alone trajectory (as a limit cycle, or an equilibrium state) onto the system as a whole. This problem was solved by Pontryagin and himself. Below, we sketch their theory of systèmes grossièrs, "rough" systems on a plane.

7.1. Rough systems on a plane. Andronov–Pontryagin theorem

Consider a set of two-dimensional systems on the plane defined by the equation

$$\dot{x} = X(x)\,, \tag{7.1.1}$$

where $X(x_1, x_2)$ is a $\mathbb{C}^r$-smooth ($r \geq 1$) function defined in a closed bounded region $G \subset \mathbb{R}^2$.

Let us introduce the following norm in this set

$$\|X\|_{\mathbb{C}^1} = \sup_{x \in G} \left(\|X\| + \left\| \frac{\partial X}{\partial x} \right\| \right) . \tag{7.1.2}$$

Endowed with this norm, the set of systems becomes *a Banach space* which we denote by $\mathcal{B}$ or $\mathcal{B}_G$, thereby stressing the choice of the domain G.

We can also introduce a δ-neighborhood of the system X as the set of all systems $\tilde{X}$ satisfying the condition

$$\|\tilde{X} - X\|_{\mathbb{C}^1} < \delta\,.$$

Definition 7.1. *A dynamical system X is said to be rough in the region G if given $\varepsilon > 0$ there exists $\delta > 0$ such that*:

(1) *all systems $\tilde{X}$ in a δ-neighborhood of X are topologically equivalent to X; and moreover*

(2) *the homeomorphism, which establishes this topological equivalence, is ε-close to the identity, i.e. the distance between two corresponding points is less than ε.*

Like it was done in the original definition of roughness, it is natural to impose some assumptions regarding the boundary ∂G of the region G: namely, that ∂G must be a smooth closed curve without contact with the vector field[1] (i.e. not tangent to it). Notice that in the case of dynamical systems on compact smooth surfaces, the domain G is just taken to coincide with the whole surface, so no conditions on the boundary appear.

Theorem 7.1. (Andronov–Pontryagin) *A system X is rough in the region G, if and only if,*

(1) *no equilibrium state has a characteristic exponent on the imaginary axis*;
(2) *no periodic orbit has a characteristic multiplier on the unit circle*; *and*
(3) *no separatrix starts from one saddle and ends at another* (*or at the same*) *saddle.*

The last condition may be reformulated as the absence of homoclinic and heteroclinic trajectories.

It follows from the above theorem that a rough system on the plane may possess only rough equilibrium states (nodes, foci and saddles) and rough limit cycles. As for separatrices of saddles, they either tend asymptotically to a node, a focus, or a limit cycle in forward or backward time, or leave the region G after a finite interval of time.

Obviously, this picture is preserved under small smooth perturbations. Therefore, *the rough systems form an open subset of $\mathcal{B}_G$.*

Moreover, it follows from simple arguments based on the rotation of a vector field to be presented below that, if X is a non-rough system, then given any $\delta > 0$ there exists a rough system $\tilde{X}$ which is δ-close to X. In other words, *the rough systems form a dense set in $\mathcal{B}_G$.*

[1]This condition may be weakened so that a finite number of points of a quadratic contact with the vector field can be allowed on ∂G. In such a case, the fourth condition that neither periodic orbits nor separatrices pass through these contact points should be added to the Andronov–Pontryagin Theorem.

It follows immediately from the Andronov–Pontryagin theorem that *a rough system may possess only a finite number of equilibrium states and periodic orbits in G.*

Equilibrium states, periodic orbits and separatrices of saddles are *special* trajectories. Together they determine *a scheme* — a complete topological invariant (see Chap. 1 for details). One may easily conclude that all systems δ-close to a given rough system have the same scheme.

The necessity of conditions (1) and (2) of the Andronov–Pontryagin theorem is obvious. Indeed, if a system is rough in G, it must remain rough in any sub-region of G. Hence, by choosing a small neighborhood that contains an equilibrium state, one concludes that the system corresponding to this equilibrium state must be rough too. An analogous observation also holds for rough limit cycles.

Let us now explain why there are no separatrices which connect saddles in rough systems.

Let us rewrite the system X in the form

$$\begin{aligned} \dot{x} &= P(x,y)\,, \\ \dot{y} &= Q(x,y)\,. \end{aligned} \tag{7.1.3}$$

Consider a special perturbed system $\tilde{X}_\mu$

$$\begin{aligned} \dot{x} &= P(x,y) + \mu Q(x,y)\,, \\ \dot{y} &= Q(x,y) - \mu P(x,y)\,, \end{aligned} \tag{7.1.4}$$

where μ is a parameter. Observe that the equilibrium states of the system (7.1.4) do not move when μ varies. At any other point, the angle ψ between the phase velocity vectors of $\tilde{X}_\mu$ and X is given by:

$$\tan\psi = \frac{\dfrac{Q-\mu P}{P+\mu Q} - \dfrac{Q}{P}}{1 + \dfrac{Q-\mu P}{P+\mu Q}\cdot\dfrac{Q}{P}} = -\mu\,, \tag{7.1.5}$$

i.e. the angle ψ is constant.

Due to this feature, the family X_μ is called *a rotation* of the vector field X through a constant angle. This angle is positive if $\mu > 0$ or negative if $\mu < 0$, respectively. Hence, if at $\mu = 0$, a separatrix of one saddle is connected to

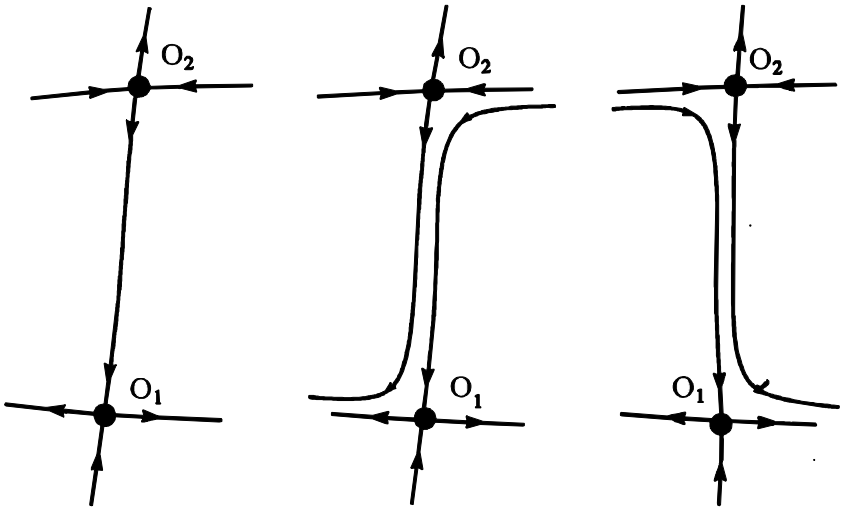

(a) (b) (c)

Fig 7.1.1. (a) A non-transverse heteroclinic connection between two saddles in $\mathbb{R}^2$ at $\mu = 0$ is split in two ways: (b) $\mu < 0$ and (c) $\mu > 0$.

another saddle [See Fig. 7.1.1(a)], then for an arbitrarily small non-zero μ, this connection will be split in either way shown in Figs. 7.1.1(b) and 7.1.1(c).

Similarly, if there were a separatrix loop to a saddle at $\mu = 0$, it would be split for some non-zero μ, as shown in Fig. 7.1.2. We see that an arbitrarily small smooth perturbation of the vector field will modify the phase portrait of a system with a homoclinic loop or a heteroclinic connection; this obviously means that such a system is non-rough.

The proof of sufficiency of the conditions of the Andronov–Pontryagin theorem relies heavily on the Poincaré–Bendixson theory which gives a classification of every possible type of trajectories in two-dimensional systems on the plane (see Sec. 1.3). We refer the reader to the books [11, 12] for further details.

The Poincaré–Bendixson theory is also applicable for systems on a cylinder, as well as on a two-dimensional sphere. As for other compact surfaces like tori, pretzels (spheres with a handle) etc., there may exist vector fields that possess, besides equilibria and limit cycles, unclosed Poisson-stable trajectories as well.

Of special interest in nonlinear dynamics are the flows on a two-dimensional torus. We consider the systems on a torus which have no equilibrium states

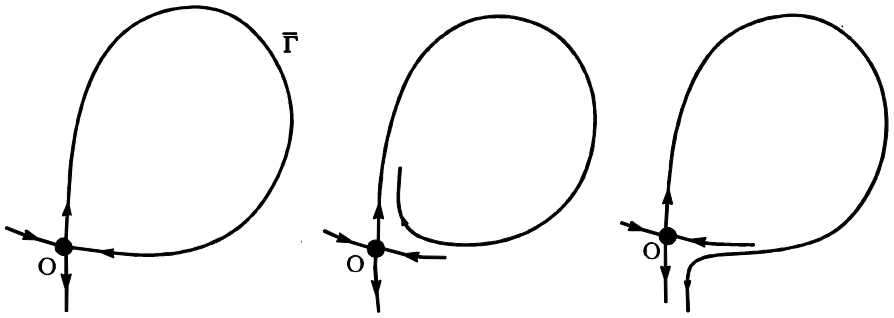

(a) (b) (c)

Fig 7.1.2. (a) A homoclinic loop to a saddle is structurally unstable. A separatrix behavior (b) prior and (c) after the loop.

and which can be reduced to an orientable diffeomorphisms of the circle in the form

$$\bar{\theta} = \theta + f_0(\theta) \equiv f(\theta) \mod 2\pi\,.$$

By introducing the metrics

$$\text{dist } (f_1, f_2)_{\mathbb{C}^1} = \max_{\theta}(\|f_1(\theta) - f_2(\theta)\| + \|f_1'(\theta) - f_2'(\theta)\|)$$

the set of these diffeomorphisms comprises a metric space where (in view of Mayer's theorem from Chap. 4) *rough diffeomorphisms are dense*.

Rough systems are also dense in the space of systems on two-dimensional orientable compact surfaces for which the necessary and sufficient conditions of roughness are analogous to those in the Andronov–Pontryagin theorem. The theory of such systems was developed by Peixoto [107]. The key element in this theory proves the absence of unclosed Poisson-stable trajectories in rough systems (they may be eliminated by a rotation of the vector field).

It must be noted here that Peixoto employs a different definition of roughness. In the case of systems on a plane, it is to be redefined in the following way:

Definition 7.2. *A system X is said to be structurally stable in region G if there exists $\delta > 0$ such that if $\|X - \tilde{X}\|_{\mathbb{C}^1} < \delta$, then X and $\tilde{X}$ are topologically equivalent.*

Compared to the definition of rough systems, the above definition has an advantage: it follows immediately that structurally stable systems form in

an open set. The analogous claim for rough systems follows only from the Andronov–Pontryagin theorem. In fact, Peixoto showed that the necessary and sufficient conditions of roughness in the sense of Definition 7.1 coincide with the necessary and sufficient conditions in the sense of Definition 7.2 for two-dimensional systems.

The notion of roughness/structural stability can be extended to the high-dimensional case without any problem. However, some other problems do arise here when we need to find out explicitly the necessary and sufficient conditions for roughness. We have remarked that Andronov and Pontryagin, as well as Peixoto, had used the classification of proper two-dimensional systems in an essential way. So, we must stop here to get acquainted with some basic notions and facts from the general theory of dynamical systems.

7.2. The set of center motions

Back to radio-engineering in the 1920' and the 1930's, we may presume that there still remained problems which would have required modeling in terms of dynamical systems of order higher than two. We may wonder what kind of oscillatory motions other than periodic ones might have been observed in complex physical systems and which mathematical image could be adequately associated to them. To settle this question, one must have a comprehensive classification of all possible trajectories. Its first stage begins with the selection of *wandering* and *non-wandering* points. The definition of points of both sorts was given in Chap. 1 for systems on compact sets. We will consider below the system

$$\dot{x} = X(x)\,,$$

where $X \in \mathbb{C}^1$ in a bounded and closed region $G \subset \mathbb{R}^n$ whose boundary consists of smooth $(n-1)$-dimensional surfaces without contact with the vector field, which is oriented inwards, i.e. entering G. Hence, for any point $x_0 \in G$ a positive semi-trajectory $x(t, x_0)$ is defined from any starting point x_0 at $t = 0$.

Definition 7.3. *A point x_0 is said to be wandering if it has a neighborhood U such that for some $T > 0$ and for all $t \geq T$*

$$U \cap x(t, U) = \emptyset\,.$$

Here, as before,

$$x(t, U) = \bigcup_{\xi \in U} x(t, \xi)\,.$$

It follows from the above definition that each point $\xi \in U$ is wandering too. Therefore, the set of all wandering points is open. Besides, it is easy to see that if x_0 is a wandering point, then the point $x(t, x_0)$ is also wandering for any t. Hence, one may call $x(t|_{t\geq 0};\, x_0)$, *a positive wandering semi-trajectory.* Moreover, if $x(t, x_0) \in G$ for all $t < 0$, i.e. if a negative semi-trajectory passing through the point x_0 lies entirely in G, then $x(t, x_0)_{t<0}$ will also consist of wandering points. Hence a whole trajectory $x(t, x_0)$ may be called wandering. For obvious reasons, a wandering (semi-) trajectory is unlikely to be associated with the type of motion we have been looking for.

Therefore we shall focus on non-wandering points. Even from the name, one may anticipate a certain "recurrence".

Definition 7.4. *A point x_0 is called non-wandering if for any neighborhood U of x and for any $T > 0$ there exists $\bar{t} \geq T$ such that*

$$U \cap x(\bar{t}, U) \neq \emptyset\,.$$

In this case, given an arbitrary sequence $T_n \to \infty$, one can find a sequence $\bar{t}_n \to \infty$, such that U returns to itself infinitely many times. One may easily see that if a point x_0 is non-wandering, then $x(t, x_0) \in G$ for all $t \in (-\infty, +\infty)$, and any point on the trajectory is non-wandering too.

Since the set of wandering points is open, its complement, which is the set of non-wandering points, is closed. We will denote it by $\mathcal{M}_1$. Let us show that it is not empty under our assumptions. First of all, notice that the set of ω-limit points of any semi-trajectory is non-empty. This follows from the compactness of G.

Statement 7.1. *Any ω-limit point of any trajectory $x(t, x_0)$ is non-wandering.*

Proof. Let $x(t, x_0)$ be a semi-trajectory and y be its limit point. Let U be an arbitrary neighborhood of y. Choose an arbitrarily large $\bar{t}$. Since y is an ω-limit point, one may find two arbitrarily large t_1 and t_2 such that $y_1 = x(t_1, x_0) \in U$ and $y_2 = x(t_2, x_0) \in U$. We may assume that $t_2 - t_1 > \bar{t}$. It follows then that $x(t_2 - t_1, U) \cap U \neq \emptyset$ (this intersection contains the point y_2). Therefore, y is a non-wandering point indeed.

The reverse statement is not true. In general, there may exist non-wandering points which are not ω-limit points or α-limit points of any trajectory.

Equilibrium states and periodic orbits are non-wandering trajectories. In the former case, any neighborhood of an equilibrium state will contain it forever; in the case of a periodic orbit, any of its points returns infinitely many times to an initial neighborhood simply because of periodicity.

The central sub-class of non-wandering points are points which are stable in the sense of Poisson. The main feature of a Poisson-stable point is not only the recurrence of its neighborhood but the recurrence of the trajectory itself. The definition of Poisson-stable points below is different in some ways but equivalent to the definition given in Chap. 1.

Definition 7.5. *A point x_0 is said to be positively stable in the sense of Poisson (P^+-stable) if there exists a sequence t_n, where $t_n \to +\infty$ as $n \to +\infty$, such that*

$$\lim_{n\to+\infty} x(t_n, x_0) = x_0 \,.$$

In other words, the point x_0 is an ω-limit point of its positive semi-trajectory.

The definition of a negative Poisson stable (P^--stable) point is analogous to the above except that $t_n \to -\infty$ here. In the case where the point x_0 is both P^+-stable and P^--stable, it is said to be stable in the sense of Poisson.

One can see that if x_0 is P^+ (P^-)-stable, its trajectory is P^+ (P^-)-stable too. Hence, we may generalize the notion of the Poisson stability over semi-trajectories and whole trajectories.

It is important to distinguish the P^+, P^- and P-stable trajectories from each other. Indeed, consider the example from Sec. 1.2 of a system on a two-dimensional torus which possesses an equilibrium state with a P^+-trajectory which is α-limiting to the equilibrium state and a P^--trajectory which is ω-limiting to it; all other trajectories on the torus are Poisson-stable, and cover it densely.

Let us return to the set $\mathcal{M}_1$ of non-wandering points. We have established that it is non-empty, closed and invariant (consists of whole trajectories). The set $\mathcal{M}_1$ may be regarded as the phase space of a dynamical system, and therefore one may repeat the procedure and construct the set $\mathcal{M}_2$ consisting of non-wandering points in $\mathcal{M}_1$. Clearly, $\mathcal{M}_2 \subseteq \mathcal{M}_1$. Just like $\mathcal{M}_1$, the set $\mathcal{M}_2$

is also a compact invariant set. If $\mathcal{M}_2 = \mathcal{M}_1$, then $\mathcal{M}_1$ is said to be *the center* or *the set of center motions*. This is exactly the situation we have when considering structurally stable two-dimensional systems.

In the general case, we have

$$\mathcal{M}_1 \supset \mathcal{M}_2 \supset \cdots \supset \mathcal{M}_k \supset \cdots .$$

If $\mathcal{M}_k = \mathcal{M}_{k+1}$ beginning with some k, then $\mathcal{M}_k$ is also called *a center*, and k is called *the ordinal number* of center motions.

If $\mathcal{M}_k \neq \mathcal{M}_{k+1}$ for any k, then we may introduce the set

$$\mathcal{M}_\omega = \bigcap_{k=1}^{\infty} \mathcal{M}_k .$$

which is the intersection of closed invariant sets. Therefore, the set $\mathcal{M}_\omega$ is closed and invariant as well. Indeed, if $x_0 \in \mathcal{M}_\omega$, then $x_0 \in \mathcal{M}_k$ for any k. All $\mathcal{M}_k$ are invariant, and therefore $x(t, x_0) \in \mathcal{M}_k$ for all t and any k, whence $x(t, x_0) \in \mathcal{M}_\omega$.

We can repeat the above procedure to obtain a *transfinite* sequence of closed sets

$$\mathcal{M}_1 \supset \cdots \supset \mathcal{M}_k \supset \cdots \supset \mathcal{M}_\omega \supset \cdots \supset \mathcal{M}_\alpha \supset \cdots .$$

It is known (from Cantor's theorem for finite-dimensional sets) that one can find a countable α such that $\mathcal{M}_\alpha = \mathcal{M}_{\alpha+1} = \cdots$, i.e. the process terminates. In such a case, $\mathcal{M}_\alpha$ is *a center* where α is *the ordinal number*. If α is finite, it is called *a transfinite ordinal number of the first class*; if $\alpha \geq \omega$ it is called *a transfinite ordinal number of the second class*.

It seems bizarre, but dynamical systems with a transfinite ordinal number α of the second class do exist. Mayer [93] had proved that for any given transfinite α of the second class, there exists a system whose ordinal number of center motions exceeds this transfinite number.

For rough systems on a plane, the Andronov–Pontryagin theorem gives $\alpha = 1$. The case where $\alpha = 2$ takes place in systems which has a loop of separatrix Γ to a saddle O, the loop is the limit trajectory for nearby orbits (see Fig. 7.2.1) and is non-wandering. Here, $\mathcal{M}_1 = \Gamma \cup O$. On the second step of the above procedure, one obtains $\mathcal{M}_2 = O$, i.e. the center of the region G is minimized to the equilibrium state.

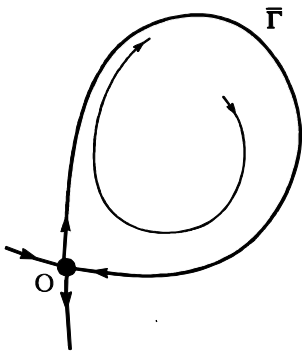

Fig. 7.2.1. The homoclinic loop to saddle is an ω-limit for a trajectory from the interior region.

Why is the center so remarkable? First, this is the set about which all trajectories of the system linger much longer than elsewhere, most of the time. Second, this center is characterized by Birkhoff's theorem.

Theorem 7.2. (Birkhoff) *The Poisson-stable trajectories are dense everywhere in the set of center motions.*

This theorem resembles the known theorem by Poincaré on recurrence of the regions for the case of conservative systems, i.e. for volume preserving flows and diffeomorphisms provided the volume of the phase space is finite. Strictly speaking, that was the goal which Birkhoff wished to achieve while creating the theory of center motions; namely, to single out the set of trajectories from a dissipative system, on which the system would behave like a conservative one. For example, on a periodic orbit, the equation of motion in the normal coordinates is given by $\dot{\theta} = 1$. This flow preserves the length of the arc. An analogous situation occurs on a stable invariant torus covered densely by a quasiperiodic trajectory. For example, this is the motion described by the equations:

$$\dot{\theta} = \omega_1 \,, \quad \dot{\varphi} = \omega_2 \,,$$

where ω_1 is not commensurable to ω_2.

Finally, we remark that the reader may find deeper insights to the above issues in the book "Dynamical Systems" by Birkhoff [31] and in the book "Qualitative Theory of Differential Equations" by Nemytskii and Stepanov [98].

7.3. General classification of center motions

We have already noticed that the theory of structurally stable systems of second order on a plane is based essentially on the theory of Poincaré–Bendixson, and on the classification of all possible kinds of motions. Below is the diagram suggested by Andronov which describes the general classification of motions due to Birkhoff.

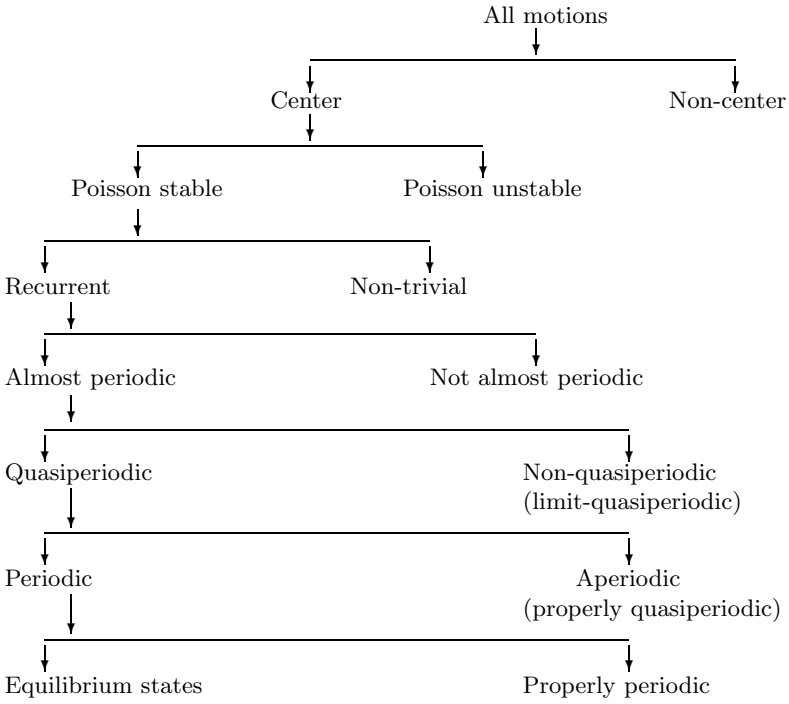

In the preceding sections, we have discussed the set of center motions. In essence, we have found that it is the closure of the set of Poisson-stable trajectories. It does not exclude the case where the latter ones may simply be periodic orbits. But if there is a single Poisson-stable unclosed trajectory, then by virtue of Birkhoff's theorem in Sec. 1.2, there is a continuum of Poisson-stable trajectories. As for the rest of the trajectories in the center, it is known that the set of points which are not Poisson-stable is the union of not more

than a countable number of sets that are closed and nowhere dense in the center. This means that the majority of trajectories in the set of center motions consists of the Poisson-stable trajectories.

The Poisson-stable trajectories may be sub-divided into two kinds depending on whether the sequence $\{\tau_k(\varepsilon)\}$ of Poincaré return times of a P-trajectory to its ε-neighborhood is bounded or not. Birkhoff named the trajectories of the first kind *recurrent trajectories*. Such a trajectory is remarkable because regardless of the choice of the initial point, given $\varepsilon > 0$ the whole trajectory lies in an ε-neighborhood of the segment of the trajectory corresponding to a time interval $L(\varepsilon)$. Obviously, equilibrium states and periodic orbits are the closed recurrent trajectories.

Let us recall next the notion of a minimal set.

Definition 7.6. *A set $\mathcal{M}$ is called minimal if it is non-empty, closed, invariant and contains no other subsets of the same properties.*

We remark that under the above assumptions on the system and on the region G, the minimal set always exists. It is curious that to prove their existence Birkhoff also applied the transfinite procedure.

The relationship between a minimal set and a recurrent trajectory is constituted by the following theorems.

Theorem 7.3. (Birkhoff) *Any trajectory of a minimal set is recurrent.*

Theorem 7.4. (Birkhoff) *The closure of a recurrent trajectory is a minimal set.*

It follows from these theorems that the trajectories of a minimal set (other than an equilibrium state or a periodic orbit) form a totality of "twins".

The closure of an unclosed Poisson-stable trajectory whose return times are unbounded for some $\varepsilon > 0$ is called *a quasiminimal set*. A quasiminimal set contains, besides Poisson-stable trajectories which are dense everywhere in it, some other invariant and closed subsets. These may be equilibrium states, periodic orbits, non-resonant invariant tori, other minimal sets, homoclinic and heteroclinic orbits, etc., among which a P-trajectory is *wandering*. This gives a clue to why the recurrent times of the non-trivial unclosed P-trajectory are unbounded. Furthermore, this also points out that Poisson-stable trajectories of a quasiminimal set, due to their unpredictable behavior in time, are of

major interest in non-transient oscillating processes having an empirical chaotic character.

In the case of recurrent trajectories, there are certain statistics in Poincaré return times which are "weaker" than that characterizing genuine Poisson-stable trajectories. Nevertheless, there is a particular sub-class of recurrent trajectories which is interesting in nonlinear dynamics. This is the class of the so-called *almost-periodic motions*. The remarkable feature which reveals the origin of these trajectories is that each component of an almost-periodic motion is an almost-periodic function (whose analytical properties are well studied, see for example [49, 66, 84]).

An almost periodic function is uniquely defined "in average" by a trigonometric Fourier series

$$f(t) \approx \sum_{n=-\infty}^{+\infty} a_n e^{i\lambda_n t}\,,$$

where λ_n are real numbers. If all λ_n are linear combinations (with integer coefficients) of a finite number of rationally independent elements from a basis of frequencies $\omega_1, \ldots, \omega_m$ (see Chap. 4), then we have a particular case of almost-periodic functions, namely quasiperiodic functions. It is correct to write a quasiperiodic function in the form

$$f(t) = \varphi(\omega_1 t, \ldots, \omega_m t)\,,$$

where φ is periodic in all its arguments, with the same period. If a k-dimensional system of differential equations

$$\dot{x} = X(x) \tag{7.3.1}$$

has a quasiperiodic solution

$$x(t) \equiv \varphi(\omega_1 t, \ldots, \omega_m t)\,,$$

then it admits also a solution

$$x = \varphi(\omega_1 t + C_1, \ldots, \omega_m t + C_m)\,,$$

where $C_1, \ldots, C_m$ are arbitrary constants. This means that the associated minimal set (the closure of $x(t)$) is an m-dimensional invariant torus. Andronov and Vitt [15] had established that its dimension must meet the following condition

$$m \leq k - 1\,.$$

If a finite-dimensional system has an almost-periodic solution, that is not quasi-periodic, then the coefficients λ_n are linear compositions of a finite number of basis frequencies $\omega_1, \ldots, \omega_m$ with *rational* factors. Such solutions are called *limit-quasiperiodic*. For this case Pontryagin [112] had proven that the dimension m of the minimal set must satisfy the following inequality

$$m \leq k - 2\,.$$

In particular, for a system of third order we have $m = 1$, i.e. its limit-quasiperiodic solutions have the form

$$f(t) = \sum_{n=-\infty}^{+\infty} a_n e^{ir_n \omega t}$$

with some rational r_n, so that a finite segment of the Fourier series

$$f(t) = \sum_{n=-N}^{N} a_n e^{ir_n \omega t}$$

of $f(t)$ is some periodic function with a period tending to infinity as $N \to \infty$.

The structure of the minimal set of a limit-quasiperiodic trajectory is a fractal. In other words, it is characterized locally as a direct product of an m-dimensional disk and a zero-dimensional Cantor set $\mathbb{K}$. Obviously, in the limit-periodic case, it has the form of a direct product of an interval and $\mathbb{K}$.

In order to visualize the structure of the minimal set of a limit-periodic trajectory in $\mathbb{R}^3$, it is instructive to construct an object called *the Wietorius-van Danzig solenoid*.

The first stage in this geometrical construction is as follows. Consider a solid-torus $\Pi_1 \in \mathbb{R}^3$, where $\Pi_1 = \mathbb{D}^2 \times \mathbb{S}^1$, $\mathbb{D}^2$ is a two-dimensional disk and $\mathbb{S}^1$ is a circle. Let us embed a similar solid-torus Π_2 into Π_1 so that it intersects every disk $\{\varphi = \text{constant}\}$ in Π_1, where $\varphi \in \mathbb{S}^1$ is an angular variable, in two disjoint disks so that Π_2 makes two revolutions along $\mathbb{S}_1$ without self-intersections as illustrated in Fig. 7.3.1. It is also assumed that Π_2 is about twice as long as that of Π_1, and four times thinner. At the second stage, we embed a torus Π_3 into Π_2 in the same way as above, so that there are now four intersections of Π_3 with each disk $\{\varphi = \text{constant}\}$, two inside each previous pair of intersections.

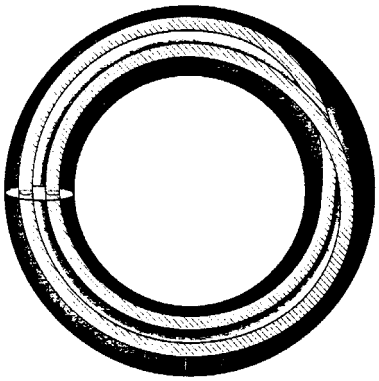

Fig. 7.3.1. The second stage in constructing the Wietorius–Van Danzig solenoid.

Repeating this procedure, we obtain a sequence of solid-tori Π_n such that $\Pi_{n+1} \subset \Pi_n$. The resulting solenoid is defined by the set

$$\Sigma = \bigcap_{n=1}^{\infty} \Pi_n \,.$$

This set is closed, and $\Sigma \cap \{\varphi = \text{constant}\}$ is a Cantor set. Wietorius and van Danzig showed that a flow may be defined on Σ so that Σ becomes a minimal set of almost-periodic motions. It is apparent that they have used the notion of almost-periodicity from a qualitative point of view.

Definition 7.7. *A motion $x(t)$ is said to be almost-periodic if for any $\varepsilon > 0$ there exists a value $L(\varepsilon)$ and a countable sequence of numbers $\{\tau_{k(\varepsilon)}\}$ satisfying $|\tau_{k+1} - \tau_k| < L(\varepsilon)$, such that*

$$\operatorname{dist}(x(t), x(t+\tau_k)) < \varepsilon \,, \quad -\infty < t < +\infty \,. \tag{7.3.2}$$

A periodic orbit, which is the special purest case of an almost-periodic motion, admits, besides its least period τ, also any multiple $k\tau$ of τ as periods, where k is an integer. The collection $\{\tau_k\}$ plays almost the same role for an almost-periodic trajectory as the periods for a periodic orbit; this is why the numbers $\tau_k(\varepsilon)$ are called *almost-periods*.

The closure of an almost-periodic trajectory contains only almost-periodic trajectories. Moreover, the value $L(\varepsilon)$ and the almost-periods remain the same.

The above observation poses a basic question: what feature distinguishes almost-periodic trajectories from recurrent ones? To answer this question, we must introduce one more definition.

Definition 7.8. *A trajectory possesses the S-property if, given* $\varepsilon > 0$, *there exists* $\delta > 0$ *such that, for any* t_1 *and* t_2,

$$\operatorname{dist}(x(t_1, x_0), x(t_2, x_0)) < \delta\,,$$

implies

$$\operatorname{dist}(x(t + t_1, x_0), x(t + t_2, x_0)) < \varepsilon\,,$$

for $0 \le t < +\infty$.

In essence, the above condition is a hidden property of uniform stability in the Lyapunov sense.

Theorem 7.5. (Franklin, Markov) *If a recurrent trajectory possesses the S-property, then it is almost-periodic.*

One of the conclusions from this theorem is that an authentic recurrent trajectory must be unstable. A few exotic examples of dynamical systems on some compact manifolds, called nil-manifolds, are known where all trajectories are recurrent. Moreover, these trajectories are unstable. However, their instability is not exponential but only polynomial. In contrast to an almost-periodic trajectory whose frequency spectrum is discrete, the spectrum of a recurrent trajectory has in addition a continuous component. For further details see [23].

7.4. Remarks on roughness of high-order dynamical systems

Many oscillatory regimes must be modeled by high-order dynamical systems. As in the low-dimensional case, the equilibrium states and periodic orbits of such systems correspond to stationary regimes and periodic oscillations, in particular, self-oscillations. In Chap. 4, we touched upon questions related to the description of self-modulation and multi-frequency regimes by means of quasiperiodic motions on invariant tori. But the large variety of possible kinds of oscillating phenomena in high-order dynamical systems is not exhausted by the above motions alone. What mathematical image corresponds to such more

complex oscillatory behavior? Can the latter be explained via the language of dynamical systems? In order to answer these questions, we need to reveal the role of unclosed Poisson-stable trajectories. Meanwhile, one must bear in mind that any mathematical idealization of an observable process must be stable in time and robust against small smooth perturbations of the dynamical system.

In this context, the following question raised by Andronov and Vitt is remarkable: Which P-trajectory is stable in the sense of Lyapunov? Its answer is settled by the following theorem.

Theorem 7.6. (Markov) *If a Poisson-stable trajectory is uniformly stable in the sense of Lyapunov, then it is almost-periodic.*

The proof of this theorem is presented in [98]. In essence, it is based on the S-property only and therefore requires the additional property of uniformity of stability.[2]

This result shows that an individual trajectory cannot give an adequate image of chaotic oscillations. Looking ahead we note that all unclosed Poisson-stable trajectories in structurally stable systems are, in fact, unstable, or more precisely, of the saddle type.

If a P-trajectory is unstable in the sense of Lyapunov, this should imply that each trajectory from its quasiminimal set is also unstable. Nevertheless, this set can be attractive as a whole, and in this case it may be a mathematical image of the complex oscillatory process that we have been seeking. However, a clear understanding of the necessity of having such attractors in nonlinear dynamics came years later, only in the seventies.

Let us explore the properties of the geometrical objects of our consideration from the point-of-view of their persistence under small smooth perturbations. Again, this is well understood in the case of equilibrium states and periodic orbits. But what about the case when a structurally stable system has an unclosed P-trajectory? What features does such a system possess?

We have already mentioned that a P-trajectory $\varphi(t, x_0)$ is a self-limit, i.e. it approaches its initial point x_0 arbitrarily close. It appears intuitively clear that by the appropriate choice of a sufficiently small perturbation the perturbed system will have a periodic orbit going exactly through the point x_0. As it

[2]In the case of a uniform stability in the sense of Lyapunov, the sizes of both small neighborhoods included in the definition do not depend on a choice of an initial point, i.e. they are the same for each point on a trajectory, see Malkin [91].

often happens in mathematics, a simply formulated statement may require a rather non-trivial proof. This hypothesis was proven by Pugh in 1968. This result follows from the following theorem called *the closing lemma* [113].

Theorem 7.7. (Closing lemma, Pugh) *Let x_0 be a non-wandering point of a smooth flow. Then, arbitrarily close in $\mathbb{C}^1$-topology, there exists a smooth flow which has a periodic orbit passing through the point x_0.*[3]

Since each point on a P-trajectory is non-wandering, this result is also valid for points stable in the sense of Poisson. The closing lemma implies the following meaningful corollary: *a rough system with a P-trajectory possesses infinitely many periodic orbits.*

Indeed, since the original system is rough, it is topologically equivalent to any sufficiently close system. By Theorem 7.7, this means that the original system has a periodic orbit that goes through a point x_1 near enough to x_0 (it should also be noted that the smaller the perturbation, the longer the period of the periodic orbit will be). By the same arguments, the system must have another periodic orbit which passes through an even closer point x_2, and so on.

So, one can see that the original system with a Poisson-stable unclosed trajectory will possess infinitely many periodic orbits $\varphi(t, x_k)$, where $\varphi(0, x_k) = x_k (k = 1, 2, \ldots)$ with periods τ_k, such that $x_k \to x_0$ and $\tau_k \to +\infty$ as $k \to +\infty$.

Note that in this proof, we use essentially the roughness (versus structural stability) of the system, i.e. we assume that the homeomorphism establishing the topological equivalence of sufficiently closed systems is close to identity. However, without this assumption the claim is still true, though the proof becomes more involved.

To characterize the structurally stable systems with P-trajectories, the following result is very useful.

Theorem 7.8. (Pugh) *Arbitrarily close (in $\mathbb{C}^1$-sense) to any smooth flow, there exists a flow for which the periodic orbits are dense everywhere in the non-wandering set.*[4]

Therefore, if a structurally stable system has an attractive quasiminimal set — *a strange attractor*, then periodic orbits will be dense in it.

[3] The validity of the $\mathbb{C}^r$-version of this theorem with $r \geq 2$ remains unknown up-to-date.
[4] Strictly speaking — in the non-wandering set minus the equilibrium states.

As for attractive minimal sets, it follows from Pugh's theorem that they are structurally unstable. Although the minimal sets composed of recurrent and limit-quasiperiodic orbits are by far not key players in the nonlinear dynamics, quasiperiodic motions have always been of major interest because they model many oscillating phenomena having a discrete spectrum.

Resuming our consideration, we may make a preliminary conclusion: typical dynamical systems are divided into two basic classes depending on whether the system has a finite number of periodic orbits in a bounded subregion of its phase space or the number of periodic orbits is infinite. In the first case such systems are usually called systems with simple dynamics. The second class is composed of systems with complex dynamics. The notion of roughness or structural stability is easily applied to the systems with simple dynamics. The situation for systems with complex dynamics is more uncertain.

The point is that structurally unstable (non-rough) systems with complex dynamics may form *open regions* in the space of dynamical systems. Moreover, it must be emphasized that structurally stable (rough) strange attractors *have never been observed* so far in any model in nonlinear dynamics, remaining purely geometrical or algebraic constructions. Therefore, it seems that typical systems with strange attractors fall exactly into the regions of structural instability. These *structurally unstable strange attractors* enjoyed a great success in our exploration of dynamical chaos. For such attractors, the strict requirement of roughness obviously makes no sense; only some typical features must persist under small perturbations.

Usually, a reasonable high-order model must exhibit both types of dynamics — simple and complex. Of course, the first step in the analysis of such models is the study of the structure of the partitioning of the phase space into trajectories in those parameter regions which correspond to simple dynamics. In the next section, we will be focusing on a rather broad class of structurally stable systems with simple dynamics which are called *the Morse–Smale systems*. Systems with complex dynamics require special care, and will be the subject of a further monograph.

7.5. Morse–Smale systems

Morse–Smale systems are introduced axiomatically. Consider a dynamical system

$$\dot{x} = X(x)\,, \tag{7.5.1}$$

where $X(x) \in \mathbb{C}^r$ $(r \geq 1)$ in $\mathbb{R}^n$.

Let G be some closed, bounded region in the phase space of (7.5.1). Denote by Ω the set of non-wandering trajectories of system (7.5.1) in G. We will assume that $\partial G \cap \Omega = \emptyset$, where ∂G denotes the boundary of G.

Definition 7.9. *System* (7.5.1) *in region G is called a Morse–Smale system if it satisfies the following two axioms*:

Axiom 1. *The non-wandering set Ω consists of a finite number of orbits.*

Axiom 2. *All periodic orbits and equilibrium states in G are structurally stable and any intersection of their stable and unstable invariant manifolds is transverse.*

In fact, it can be shown that periodic orbits and equilibrium states are the only non-wandering trajectories of Morse–Smale systems. Axiom 1 excludes the existence of unclosed self-limit (P-stable) trajectories in view of Birkhoff's Theorem 7.2. The existence of homoclinic orbits is prohibited by Theorems 7.9 and 7.11 below. Next, it is not hard to extract from Theorem 7.12 that an ω-limit (α-limit) set of any trajectory of a Morse–Smale system is an equilibrium state or a periodic orbit.

Recall that an equilibrium state $O(x = x_0)$ is structurally stable if none of its characteristic exponents, i.e. the roots of the characteristic equation

$$\det \left| \frac{\partial X(x_0)}{\partial x} - \lambda I \right| = 0 \,, \tag{7.5.2}$$

lies on the imaginary axis.

A topological type (m, p) is assigned to each equilibrium state, where m is the number of the characteristic exponents in the open left half-plane and p is that in the open right half-plane. Therefore, $m + p = n$. If $m = n$ ($m = 0$), the equilibrium state is stable (completely unstable). An equilibrium state is of saddle type when $m \neq \{0, n\}$.

The set of all points in the phase space whose trajectories converge to x_0 as $t \to +\infty$ ($-\infty$) is called the stable (unstable) manifold of the equilibrium state and denoted by W^s_O and W^u_O, respectively. If O has the type (m, p), then W^s_O is an m-dimensional $\mathbb{C}^r$-manifold, and W^u_O is a p-dimensional $\mathbb{C}^r$-manifold. In the case where $m = n$, the attraction basin of O is W^s_O.

It is also known that W^s_O is diffeomorphic to $\mathbb{R}^m$, and that W^u_O is diffeomorphic to $\mathbb{R}^p$. In a suitable coordinate frame, the system near the saddle

equilibrium state is written in the form

$$\dot{\xi} = A^{-}\xi + f(\xi, \eta)\,,$$
$$\dot{\eta} = A^{+}\eta + g(\xi, \eta)\,,$$

where A^{-} is an $m \times m$-matrix whose spectrum lies to the left of the imaginary axis, A^{+} is a $p \times p$-matrix whose spectrum lies to the right of the imaginary axis, the functions f and g vanish at the equilibrium state O along with first derivatives. In this coordinate frame, the equation of $W^{s}_{\rm loc}(O)$ is

$$\eta = \varphi(\xi)\,,$$

and that of $W^{u}_{\rm loc}(O)$ is

$$\xi = \psi(\eta)\,,$$

where φ and ψ are $\mathbb{C}^{r}$-smooth functions such that $\varphi(0) = 0$, $\varphi'(0) = 0$ and $\psi(0) = 0$, $\psi'(0) = 0$.

Let us suppose next that system (7.5.1) has a periodic trajectory L: $x = \vartheta(t)$, of period τ. The periodic orbit L is structurally stable if none of its $(n-1)$ multipliers lies on the unit circle. Recall that the multipliers of L are the eigenvalues of the $(n-1)\times(n-1)$ matrix A of the linearized Poincaré map at the fixed point which is the point of intersection of L with the cross-section. The orbit L is stable (completely unstable) if all of its multipliers lie inside (outside of) the unit circle. Here, the stability of the periodic orbit may be understood in the sense of Lyapunov as well as in the sense of exponential orbital stability. In the case where some multipliers lie inside and the others lie outside of the unit circle, the periodic orbit is of saddle type.

The set of all points of the phase space whose trajectories converge to L as $t \to +\infty$ $(-\infty)$ is called the stable (unstable) manifold of the periodic orbit. They are denoted by W^{s}_{L} and W^{u}_{L}, respectively. In the case where $m = n$, the attraction basin of L is W^{s}_{L}. In the saddle case, W^{s}_{L} is $(m+1)$-dimensional if m is the number of multipliers inside the unit circle, and W^{u}_{L} is $(p+1)$-dimensional where p is the number of multipliers outside of the unit circle, $p = n - m - 1$. In the three-dimensional case, W^{s}_{L} and W^{u}_{L} are homeomorphic either to two-dimensional cylinders if the multipliers are positive, or to the Möbius bands if the multipliers are negative, as illustrated in Fig. 7.5.1. In the general case, they are either multi-dimensional cylinders diffeomorphic to $\mathbb{R}^{m} \times \mathbb{S}^{1}$, or multi-dimensional Möbius manifolds.

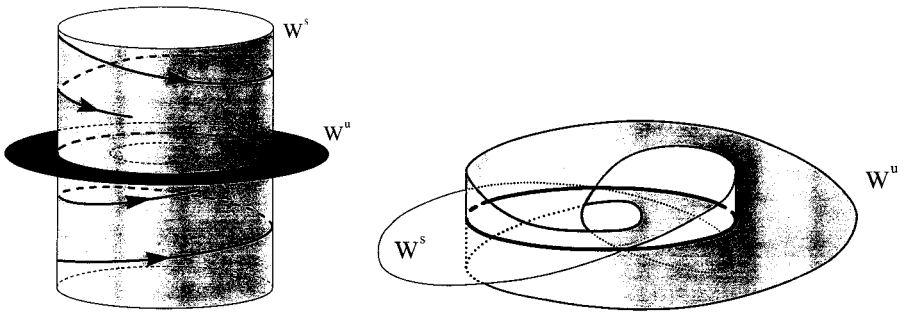

Fig 7.5.1. Saddle periodic orbit in $\mathbb{R}^3$ are distinguished by the topology of the stable and unstable invariant manifolds which may be homeomorphic to: a cylinder (left); or a Möbius band (right).

The stable invariant manifolds of equilibrium states and periodic orbits may have common points with the unstable manifolds. Clearly, if a point x_0 is such a common point of two invariant manifolds, then the trajectory $x = \varphi(t, x_0)$ belongs to both manifolds entirely. In the simplest case, $O = W^s_O \cap W^u_O$, i.e. the stable and unstable manifolds of an equilibrium state intersect at only trajectory, which is the equilibrium state itself.

Analogously, for a periodic orbit L we may have $L = W^s_L \cap W^u_L$. But this is the trivial situation and we are not going to give it our attention. Of interest is the case where x_0 neither is an equilibrium state nor lies on a periodic orbit. Below we will consider equilibrium states and periodic orbits as similar objects which will be denoted as Q.

Let Q_1 and Q_2 be such that $W^s_{Q_1}$ and $W^u_{Q_2}$ have a common point x_0. The trajectory of such point x_0 is called *heteroclinic* if Q_1 and Q_2 are different[5] and it is called *homoclinic* if $Q_1 = Q_2$.

[5]Consider an example

$$\dot{x} = -\mu + x^2\,,$$
$$\dot{y} = -y\,,$$
$$\dot{z} = z\,,$$

which for $\mu > 0$ has two saddle equilibrium states $O_1(-\sqrt{\mu}, 0, 0)$ and $O_2(+\sqrt{\mu}, 0, 0)$ of topological types (2,1) and (1,2), respectively. The invariant manifolds $W^s_{O_1}$ and $W^u_{O_2}$ intersect transversely along a heteroclinic curve ($-\sqrt{\mu} < x < \sqrt{\mu}$, $y = 0$, $z = 0$), as depicted in Fig. 7.5.2.

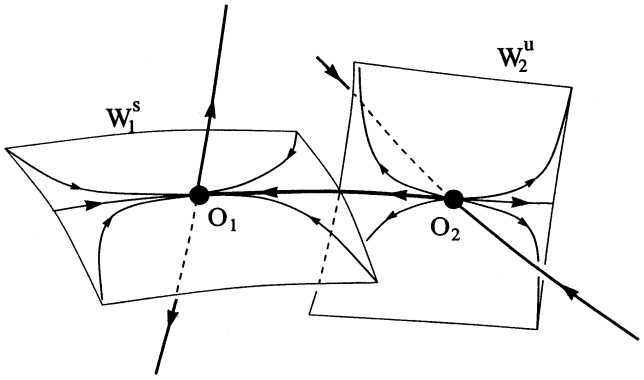

Fig 7.5.2. A structurally stable heteroclinic connection between two saddles in $\mathbb{R}^3$.

Denote the tangent to $W^s_{Q_1}$ at x_0 by $T_{x_0}W^s_{Q_1}$ and the tangent to $W^u_{Q_2}$ at x_0 by $T_{x_0}W^u_{Q_2}$.

Definition 7.10. *We will say that $T_{x_0}W^s_{Q_1}$ and $T_{x_0}W^u_{Q_2}$ intersect transversely if*

$$\dim T_{x_0}W^s_{Q_1} + \dim T_{x_0}W^u_{Q_2} - n = \dim(T_{x_0}W^s_{Q_1} \cap T_{x_0}W^u_{Q_2})\,. \qquad (7.5.3)$$

It is well-known, that if two surfaces intersect transversely at some point, then any two $\mathbb{C}^1$-close surfaces must intersect transversely at a nearby point. On the contrary, a non-transverse intersection can be removed (or made transverse) by a small perturbation.

By Axiom 2, the transversality condition (7.5.3) holds at all intersections of the stable and unstable invariant manifolds of equilibrium states and periodic orbits in system (7.5.1).

We remark that although the definition of transversality is stated at a point x_0, the transversality condition (7.5.3) has nothing to do with the choice of the point x_0, because the corresponding tangents at x_0 and at any other point on the trajectory going through x_0 are mapped onto each other by a non-degenerate linear transformation (the linearization of the time-shift map along the trajectory of x_0).

Since an orbit of the intersection point x_0 lies entirely in both invariant manifolds, it follows that both $T_{x_0}W^s_{Q_1}$ and $T_{x_0}W^u_{Q_2}$ contain the phase velocity vector at x_0, so

$$\dim(T_{x_0}W^s_{Q_1} \cap T_{x_0}W^u_{Q_2}) \geq 1\,.$$

Thus, the transversality condition (7.5.3) implies that in a Morse–Smale flow, only those intersections of invariant manifolds are possible for which

$$\dim W^s_{Q_1} + \dim W^u_{Q_2} \geq n + 1\,. \tag{7.5.4}$$

In particular, we arrive at the following simple result:

Theorem 7.9. *Morse–Smale systems have no homoclinic trajectory to an equilibrium state.*

Proof. For an equilibrium state $\dim W^s_O + \dim W^u_O = n$ which contradicts (7.5.4).

The notion of a Morse–Smale diffeomorphism is introduced in an analogous way. Consider a diffeomorphism

$$\bar{x} = X(x)\,, \tag{7.5.5}$$

where $X(x) \in \mathbb{C}^r$ $(r \geq 1)$ in some bounded, closed sub-region $G \subset \mathbb{R}^n$. Suppose that its non-wandering set has no intersections with the boundary ∂G.

Definition 7.11. *Diffeomorphism* (7.5.5) *in region G is called a Morse–Smale diffeomorphism if*

(1) *its non-wandering set is finite* (*and consists of structurally stable periodic points alone*); *and*
(2) *transversality condition* (7.5.3) *for intersections of the stable and unstable manifolds of each periodic point is satisfied.*

Recall that a fixed point $O(x = x_0)$ is called structurally stable if none of its characteristic multipliers, i.e. the roots of the characteristic equation (7.5.2), lies on the unit circle. A topological type (m, p) is assigned to it, where m is the number of roots inside the unit circle and p is that outside of the unit circle. If $m = n$ $(m = 0)$, the fixed point is stable (completely unstable). The fixed point is of saddle type when $m \neq \{0, n\}$. The set of all points whose trajectories converge to x_0 when iterated positively (negatively) is called the stable (unstable) manifold of the fixed point and denoted by W^s_O (W^u_O). In the case where $m = n$, the attraction basin of O is W^s_O. If the fixed point is a saddle, the manifolds W^s_O and W^u_O are $\mathbb{C}^r$-smooth embeddings of $\mathbb{R}^m$ and $\mathbb{R}^p$ in $\mathbb{R}^n$, respectively.

In the saddle case, the diffeomorphism can be represented locally in the form

$$\bar{\xi} = A^- \xi + f(\xi, \eta)\,,$$
$$\bar{\eta} = A^+ \eta + g(\xi, \eta)\,,$$

where the eigenvalues of A^- lie inside the unit circle, and the eigenvalues of A^+ lie outside of the unit circle; the functions f and g vanish at O along with their first derivatives. Then, the equation of $W^s_{\rm loc}(O)$ is

$$\eta = \varphi(\xi)\,,$$

and that of $W^u_{\rm loc}(O)$ is

$$\xi = \psi(\eta)\,,$$

where φ and ψ are $\mathbb{C}^r$-smooth functions such that $\varphi(0) = 0$, $\varphi'(0) = 0$ and $\psi(0) = 0$, $\psi'(0) = 0$.

Let x_0 be a periodic point of period q for the diffeomorphism (7.5.5). This means that it is a fixed point of the qth power of the diffeomorphism:

$$x_0 = X^{[q]}(x_0) \equiv \underbrace{X(X\cdots(X}_{q\ \text{times}}(x_0)))\,.$$

It seems natural to relate the point x_0 and its cycle $C = (x_0, x_1, \ldots, x_{q-1})$, where $x_k = X(x_{k-1})$, $k = 1, \ldots, q-1$, $x_0 = X(x_{q-1})$. The point x_0 is structurally stable if the roots $\rho_1, \ldots, \rho_n$ of the equation

$$\det \left| \frac{\partial X(x_{q-1})}{\partial x} \frac{\partial X(x_{q-2})}{\partial x} \cdots \frac{\partial X(x_0)}{\partial x} - \rho I \right| = 0$$

do not lie on the unit circle. Note that the characteristic roots of any point of the cycle C coincide with those of the point x_0. The stable (unstable) invariant manifold $W^s_{x_k}$ ($W^u_{x_k}$) of the point x_k is the set of points which tend to x_k under positive iterations of the diffeomorphism $X^{[q]}$. Obviously, $X(W^s_{x_k}) = W^s_{x_{k+1}}$ and $X(W^u_{x_k}) = W^u_{x_{k+1}}$. Thus, the stable manifold of the cycle C is $\bigcup_{i=0}^{q-1} W^s_{x_i}$ and the unstable manifold is $\bigcup_{i=0}^{q-1} W^u_{x_i}$.

Both, the continuous and discrete, Morse–Smale systems on compact smooth manifolds were singled out by Smale in his article "Morse inequalities for a dynamical system" [142]. The title itself reveals that the work deals

with the estimation of the number of equilibrium states and periodic orbits by means of the topological invariants of manifolds. Later, Palis and Smale [106, 102] proved the following theorem.

Theorem 7.10. (Palis and Smale) *Morse–Smale systems are structurally stable.*

This theorem was proven for systems whose phase space is a compact, smooth manifold. It holds for our case as well, if suppose that the boundary ∂G is a smooth $(n-1)$-sphere without contact, through which a trajectory goes inwards of G in the continuous case, or that $X(G) \subset G \backslash \partial G$ in the discrete case.

7.6. Some properties of Morse–Smale systems

Comparing the Andronov–Pontryagin theorem with the definition of Morse–Smale systems, one can see that the last ones are quite similar to rough systems on the plane and are, in essence, their high-dimensional generalization. Like the Andronov–Pontryagin theorem, the Palis–Smale Theorem 7.10 yields sufficient conditions for roughness. Axiom 2 in Definition 7.9 may be viewed as a natural necessary condition. In contrast, Axiom 1 has nothing to do with the problem of structural stability but it restricts rather severely the class of systems under consideration, and suppresses many hidden opportunities which saddle equilibria, and periodic orbits can exhibit in dimensions higher than two.

For example, the following theorem shows that a Morse–Smale system cannot have a homoclinic trajectory to a saddle periodic orbit.

Theorem 7.11. *Let L be a saddle periodic orbit, and let Γ be its homoclinic trajectory along which W^s_L and W^u_L intersect transversely. Then, any small neighborhood of $L \cup \Gamma$ contains infinitely many saddle periodic orbits.*

Proof. Take a small cross-section S to L and consider the local Poincaré map $T_0 : S \to S$. The point $O = S \cap L$ is the saddle fixed point of T_0. Let us introduce the coordinates (x, y) on S near O such that the local unstable manifold of O is $x = 0$ and the local stable manifold is $y = 0$ (thus, $x \in \mathbb{R}^m$, $y \in \mathbb{R}^p$ where $\dim W^s = m$, $\dim W^u = p$). Let $M^-(0, y^-) \in W^u_{\rm loc}$ and $M^+(x^+, 0) \in W^s_{\rm loc}$ be two points of intersection of the homoclinic orbit Γ with S. The flow near the piece of Γ between M^- and M^+ defines a map T_1 from

a small neighborhood Π^- of M^- onto a small neighborhood Π^+ of M^+ on S. This map can be written in the form

$$\begin{aligned} \bar{x}^0 - x^+ &= ax^1 + b(y^1 - y^-) + \cdots , \\ \bar{y}^0 &= cx^1 + d(y^1 - y^-) + \cdots , \end{aligned} \tag{7.6.1}$$

where the ellipsis stand for nonlinear terms; (x^0, y^0) refer to a small neighborhood of M^+ and (x^1, y^1) refer to a small neighborhood of M^-. Observe that the image $T_1 W^u_{\text{loc}}$ is tangent at M^+ to the p-dimensional plane defined by the parametric equation

$$x^0 - x^+ = bu\,, \quad y^0 = du\,,$$

where $u \in \mathbb{R}^p$. By assumption, this hyperplane must be transverse to $y = 0$ which means that

$$|d| \neq 0\,. \tag{7.6.2}$$

It was shown in Sec. 3.7 that for any sufficiently large k there are points in Π^+ whose kth iteration by the local map T_0 lies in Π^-. The set of such points is "a horizontal strip" σ^0_k. As $k \to \infty$, the horizontal strips accumulate at $W^s_{\text{loc}} \cap \Pi^+$. The map T_0^k contracts the strip in the x-direction and stretches it in the y-direction, so that the images $T_0^k \sigma^0_k$ ("the vertical strips" σ^1_k) accumulate at $W^u_{\text{loc}} \cap \Pi^-$. It is geometrically evident (see Fig. 7.5.3) that due to the transversality of $T_1 W^u_{\text{loc}}$ to W^s_{loc}, the image $T_1 T_0^k \sigma^0_k$ intersects σ^0_k "properly" for any sufficiently large k, so that the map $T_1 T_0^k|_{\sigma^0_k}$ is *a saddle map* in the sense of Sec. 3.15. By Theorem 3.28, a saddle map has a saddle fixed point. Since both maps T_1 and T_0 are defined by the orbits of the flow, the fixed point of $T_1 T_0^k$ corresponds to a periodic orbit of the system (it intersects S exactly k times, the first time in Π^+ and the last time in Π^-). Taking different k we will obtain different periodic orbits. Thus, to prove the theorem we must confirm by computation that the maps $T_1 T_0^k$ are of the saddle type for all sufficiently large k.

By Lemmas 3.3 and 3.4, there exist functions ξ_k, η_k which uniformly tend to zero along with their derivatives as $k \to \infty$, such that a point $M^0(x^0, y^0)$ is mapped into a point $M^1(x^1, y^1)$ by T_0^k if, and only if,

$$\begin{aligned} x^1 &= \xi_k(x^0, y^1)\,, \\ y^0 &= \eta_k(x^0, y^1)\,. \end{aligned} \tag{7.6.3}$$

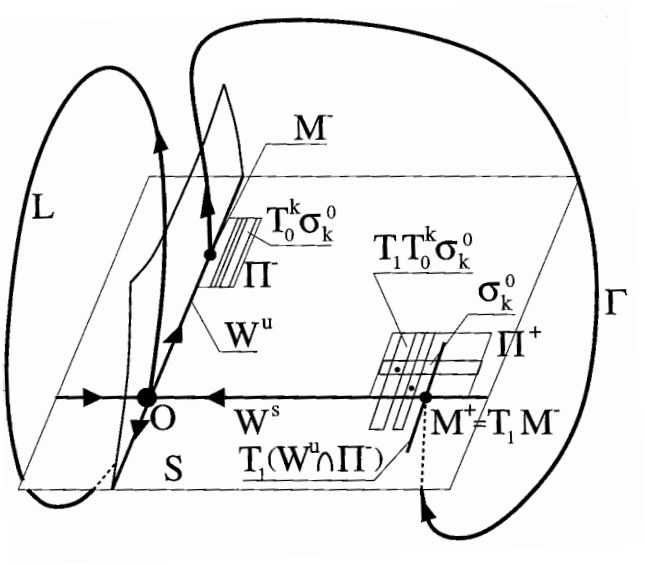

Fig. 7.5.3. The Poincaré map near a transverse homoclinic orbit.

Note that due to (7.6.2), the second equation in (7.6.1) can be solved for y^1, with a sufficiently small x^1 and $\bar{y}^0$:

$$y^1 - y^- = d^{-1}\bar{y}^0 - d^{-1}cx^1 + \cdots ,$$

where the dots stand for small nonlinear terms. Comparing this with the first equation of (7.6.3) we obtain, for sufficiently large k,

$$y^1 = y^- + F_k(\bar{y}^0, x^0) , \tag{7.6.4}$$

where F_k is a smooth function such that $F_k(0,0) = 0$, and the derivative of F_k with respect to x^0 tends uniformly to zero as $k \to \infty$ (we use that $\frac{\partial \xi_k}{\partial(x,y)} \to 0$ as $k \to \infty$).

Now, for all sufficiently large k the map $T_1T_0^k$ can be written as

$$\begin{aligned} \bar{x} &= x^+ + G_k(\bar{y}, x) , \\ y &= \eta_k(x, y^- + F_k(\bar{y}, x)) , \end{aligned} \tag{7.6.5}$$

where we suppress the upper index 0; here G denotes a smooth function such that $G_k(0,0) = 0$, and the derivative of G_k with respect to x tends uniformly to zero as $k \to \infty$. This is a *cross-form* of the map $T_1 T_0^k$ in the sense of Sec. 3.15 (the spaces D_1 and D_2 in Definition 3.6 are small convex neighborhoods of x^+ in the x-space and zero in the y-space, respectively). Since the derivatives of η_k with respect to all variables, and the derivative of G_k with respect to x tend uniformly to zero as $k \to \infty$, it is easy to see that the map $T_1 T_0^k$ fits Definition 3.7 of the saddle map for all sufficiently large k,[6] so Theorem 3.28 on the fixed point is applicable here. This completes the proof.

The above proof can be easily translated into the language of diffeomorphisms with a fixed point having a transverse homoclinic trajectory. It also covers the case of a periodic point with a homoclinic trajectory. In the last case one should consider the qth iteration of the original diffeomorphism, where q is the period.

In essence, the above proof is a close repetition of that suggested by L. Shilnikov [131]. It allows one to liberate from the axiom stipulating the absence of homoclinic trajectories in Morse–Smale systems originally postulated by Smale.

Note that a transverse homoclinic orbit is, obviously, preserved under small smooth perturbations of the system. Therefore, Theorem 7.11 implies that when a transverse homoclinic exists, any close system is away from the Morse–Smale class. This gives us a robust and simple indicator for detecting the complex dynamics. By now, the presence of transverse homoclinics is regarded as a universal criterion of chaos.

As before, we will regard equilibrium states and periodic orbits as equal objects and denote them by Q for uniformity.

---

[6] The condition to check is

$$\|P'_x\|_\circ < 1\,, \quad \|Q'_y\|_\circ < 1\,,$$
$$\|P'_y\|_\circ \|Q'_x\|_\circ < (1 - \|P'_x\|_\circ)(1 - \|Q'_y\|_\circ)\,,$$

where (P, Q) are the right-hand sides of the cross-map:

$$\bar{x} = P(x, \bar{y})\,, \quad y = Q(x, \bar{y})\,.$$

Essentially, this means that the cross-map is contracting in a suitable norm, so the map itself is strongly expanding in the y-direction and strongly contracting in the x-direction.

Let us introduce the following notation: we write $Q_i \le Q_j$ if $W^s_{Q_i} \cap W^u_{Q_j} \neq \emptyset$, in particular $Q_i \le Q_i$. If $(W^s_{Q_i} \setminus Q_i) \cap (W^u_{Q_j} \setminus Q_j) \neq \emptyset$ then we will write $Q_i < Q_j$. We will say that $Q_{k_1}, \ldots, Q_{k_l}$ form *a chain* if

$$Q_{k_1} < \cdots < Q_{k_l}\,. \tag{7.6.6}$$

If the first and the last members of the chain are equal ($Q_{k_1} = Q_{k_l}$), then the chain (7.6.6) is called *a cycle*.

It may be proved that the relation "$\le$" defines a partial order on the set of non-wandering orbits of a Morse–Smale system. An important result is:

Theorem 7.12. *There are no cycles in Morse–Smale systems.*

First of all, observe that there cannot exist cycles like $Q_0 < Q_0$ because homoclinic trajectories are not admissible in Morse–Smale systems. Also, it follows from the transversality condition [see (7.5.4)] that a cycle cannot contain equilibrium states; neither can it include periodic orbits of different topological types.

Thus, only one hypothesis remains; namely when the cycle

$$L_0 < L_1 < \cdots < L_k < L_0$$

is composed of periodic orbits of the same topological type. Consider the chain

$$L_{k-1} < L_k < L_0$$

and let $W^s_{L_{k-1}}$ intersect $W^u_{L_k}$ at a point x_0. By virtue of the λ-lemma (see Sec. 3.7), we may claim that since $W^s_{L_k}$ intersects $W^u_{L_0}$ transversely, in any small neighborhood U of the point x_0, there is a countable set of smooth pieces of $W^u_{L_0}$ converging to $W^u_{L_k} \cap U$. Since $W^s_{L_{k-1}}$ intersects $W^u_{L_k}$ transversely, it follows that $W^s_{L_{k-1}}$ intersects these pieces of $W^u_{L_0}$. Therefore

$$L_{k-1} < L_0\,.$$

Continuing inductively, we obtain

$$L_0 < L_1 < L_0\,,$$

and hence

$$L_0 < L_0\,,$$

i.e. L_0 has a homoclinic trajectory. This contradicts Theorem 7.11.

The fact that there are a finite number of non-wandering trajectories in Morse–Smale systems implies that any chain has a finite length which does not exceed the total number of non-wandering trajectories. Moreover, a maximal chain can end *only* at a stable equilibrium state or a periodic orbit.

It follows from the above arguments that one may introduce an oriented graph for each Morse–Smale system. Its vertices are equilibrium states and periodic orbits, with the topological type assigned. The edges of the graph are oriented in a decreasing way in accordance with the order $<$. Namely, the vertex Q_i is connected with the vertex Q_j by an edge if and only if $Q_i > Q_j$ and there is no Q_k such that $Q_i > Q_k > Q_j$. Such a graded graph is called *a phase diagram*. The phase diagram for a Morse–Smale diffeomorphism can be introduced in an analogous way. The vertices are fixed points and cycles, with their local characteristics specified.

It is clear that the phase diagram is an invariant of topological equivalence of Morse–Smale systems.

However, it is not a complete invariant, generally speaking. For example, it contains no information on the number of orbits of intersection of stable and unstable manifold of saddle trajectories.

Among all heteroclinic trajectories one may select some *special* ones which play a central role.

Definition 7.12. *A heteroclinic trajectory* Γ *is said to be special if there exists a neighborhood* U *of its closure* $\bar{\Gamma}$ *which contains no other heteroclinic trajectories but* Γ.

It is obvious that all heteroclinic trajectories of three-dimensional Morse–Smale flows are that special. This is also true for two-dimensional diffeomorphisms.

The principal feature of Morse–Smale systems which distinguishes them from Andronov–Pontryagin systems is that the former may have infinitely many special heteroclinic trajectories. As an example, let us consider a two-dimensional diffeomorphism with three fixed points of the saddle type denoted by O_1, O and O_2. Suppose that $W^s_{O_1} \cap W^u_O \neq \emptyset$ and $W^s_O \cap W^u_{O_2} \neq \emptyset$, the

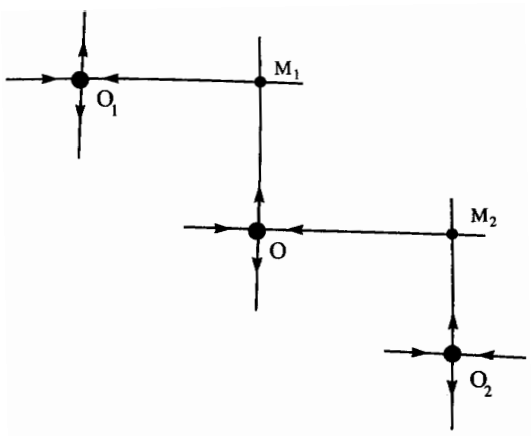

Fig. 7.6.1. Hierarchic intersections of the manifolds of fixed points at the heteroclinic points M_1 and M_2.

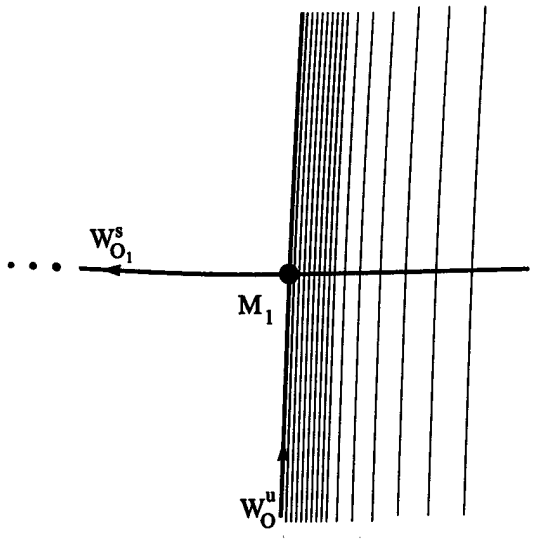

Fig. 7.6.2. A neighborhood of the point M_1: the successive images of $W^u_{0_2}$ accumulate to W^u_0 Fig. 7.6.1.

corresponding scheme is depicted in Fig. 7.6.1. Here, $M_1 \in W^s_{O_1} \cap W^u_O$ and $M_2 \in W^s_O \cap W^u_{O_2}$, i.e. they are heteroclinic points.

Let us now apply the λ-lemma (see Sec. 3.7). Choose a small neighborhood U of the point M_1. It follows that the intersection $U \cap W^u_{O_2}$ consists of a countable set of curves l_k $(k = 1, \ldots, \infty)$ accumulating smoothly to W^u_O, as shown in Fig. 7.6.2. As $W^s_{O_1}$ and W^u_O intersect each other transversely, then $W^s_{O_1}$ intersects each l_k at the points M_k starting from some number k_0. The points M_k are heteroclinic too and correspond to different heteroclinic trajectories which have O_1 and O_2 as an α-limit and an ω-limit points, respectively.

An analogous picture takes place in the case of three-dimensional flows possessing the chain $Q_1 < Q < Q_2$ where Q denotes a saddle periodic orbit, and Q_1 and Q_2 stand for either saddle equilibrium states or periodic orbits.

Heteroclinic trajectories are no longer all special in higher-dimensional case. A heteroclinic trajectory $\Gamma \subset W^s_{Q_1} \cap W^u_{Q_2}$ is special only if the dimension of the forming intersection is equal to 1. We will assign to Γ a type $(\dim W^s_{Q_1}, \dim W^u_{Q_2})$. It is clear that if $\dim W^s_{Q_1} = m+1$, then the type of the special trajectory Γ is $(m+1, n-m)$, where n is the dimension of the phase space.

Let us consider a Morse–Smale flow having two non-wandering motions Q_1 and Q_2. Let $\dim\ W^s_{Q_1} = m+1$ and $\dim\ W^u_{Q_2} = n-m$. Suppose next that $W^s_{Q_1} \cap W^u_{Q_2} \neq \emptyset$, i.e. $Q_1 \leq Q_2$.

Theorem 7.13. (Afraimovich and Shilnikov [2]) *The intersection $W^s_{Q_1} \cap W^u_{Q_2}$ possesses infinitely many heteroclinic trajectories if, and only if the closure $\overline{W^s_{Q_1} \cap W^u_{Q_2}}$ contains a periodic orbit L of type $(m+1, n-m)$, other than Q_1 and Q_2.*

It follows from the proof of this theorem that W^u_L must intersect $W^s_{Q_1}$ transversely and W^s_L must intersect $W^u_{Q_2}$ transversely. Observe also that all trajectories in $W^s_{Q_1} \cap W^u_{Q_2}$ are special.

An analogous statement holds for Morse–Smale diffeomorphisms.

Let us denote by N_{m+1} the set of all special trajectories of type $(m+1,$ $n-m)$ and their limiting non-wandering motions. In the general case, N_{m+1} consists of a finite number of connected components $N^{(1)}_{m+1}, \ldots, N^{(k)}_{m+1}$. It was also shown in [2] that the set of all trajectories $N^{(l)}_{m+1}$, where $1 \leq l \leq k$, is in a one-to-one correspondence with the set of all trajectories of some symbolic system with a finite number of states. Generally speaking, symbolic dynamics was

historically created in connection with the description of systems with complex dynamics. Nevertheless, it has turned out that it can be effectively applied to Morse–Smale systems possessing a countable number of special heteroclinic trajectories as well.

Chapter 8

BIFURCATIONS OF DYNAMICAL SYSTEMS

The *bifurcation* of a dynamical system is understood as a qualitative change of the partitioning of the phase space by trajectories, i.e. as a modification of the qualitative properties of the phase portrait as parameters of the system vary. The notion of "bifurcation" was introduced by Poincaré while studying the equilibrium structures of rotating fluids which change from an ellipsoidal shape of equilibria to a nearby pear shape. Meanwhile Poincaré was investigating the principal bifurcations of equilibrium states of conservative, one degree-of-freedom systems described by a Lagrangian equation. He noticed that variations in parameters may cause the appearance of a multiple equilibrium state, followed by a subsequent decomposition into two equilibria: a center and a saddle. Hence, the word "bifurcation" means precisely a branching in this case.

The modern theory of bifurcations of dynamical system is directly linked to the notion of non-roughness, or structural instability of a system. The main motivation is that the analysis of a system will be rather incomplete if we restrict our consideration to only the regions of structural stability of the system. Indeed, by changing parameters we can move from one structurally stable system to another, a qualitatively different system, upon crossing some boundaries in the parameter space that correspond to non-rough systems.

In the two-dimensional case, rough systems compose an open and dense set in the space of all systems on a plane. The non-rough systems fill the boundaries between different regions of structural stability in this space. This nice structure allows for a mathematical description for transformations of

various oscillatory regimes by bifurcation theory of two-dimensional systems. Even though the space of higher-dimensional systems is not so well organized, the bifurcation theory of multi-dimensional systems still provides an adequate mathematical explanation to such typical phenomena of nonlinear dynamics as transitions between stationary regimes and self-oscillations, synchronization and its loss, various routes to dynamical chaos, etc.

In this book, we concentrate on an in-depth study of equilibrium points and periodic motions because they are the fundamental "bricks" of nonlinear dynamics. For a complete coverage of two-dimensional systems, the reader is referred to the two-volume book by Andronov *et al.* [11, 12]. There, the classification of key bifurcations of periodic orbits by Andronov and Leontovich is based on their theory of two-dimensional systems of a first-degree of non-roughness.

8.1. Systems of first degree of non-roughness

We have already identified the following key elements of any structurally stable dynamical system on the plane which completely determines its entire topological invariant — a scheme. They include special trajectories:

- structurally stable equilibrium states;
- structurally stable periodic orbits; and
- separatrices of saddles.

Any modification of the phase portrait of a system may occur when the system becomes structurally unstable. By the Andronov–Pontryagin theorem, such a system must necessarily possess either:

- an equilibrium state that has one or a pair of characteristic exponents on the imaginary axis; or
- a periodic orbit with a unit multiplier; or
- a separatrix connecting two saddle points; or
- a separatrix loop to a saddle.

We remark that an equilibrium state, or a periodic orbit, may be arbitrarily degenerate. It is therefore logical to begin our study with the simplest structurally unstable systems which Andronov and Leontovich called *systems of first degree of non-roughness*.

Let X and $\tilde{X}$ be some C^r-smooth ($r \geq 3$) systems in a bounded region G on a plane. Introduce a distance between X and $\tilde{X}$ as the $\mathbb{C}^r$-metrics.

Definition 8.1. *The system X is called a system of first-degree of non-roughness if it is not structurally stable and if for any $\varepsilon > 0$ there is $\delta > 0$ such that any structurally unstable system from a δ-neighborhood of X is ε-equivalent*[1] *to it.*

In essence, systems of first degree of non-roughness are structurally stable in the set of structurally unstable systems.

The analysis undertaken by Andronov and Leontovich suggests that the first-degree non-rough systems must have one of the following non-rough trajectories.

(1) An equilibrium state $O(0,0)$ with one zero characteristic exponent and with a non-zero Taylor-series coefficient l_2, called a Lyapunov value or coefficient. The Lyapunov value can be easily calculated from the associated normal form equation

$$\begin{aligned} \dot{x} &= P(x,y)\,, \\ \dot{y} &= \lambda y + Q(x,y)\,, \end{aligned} \tag{8.1.1}$$

where $\lambda \neq 0$, and P and Q vanish at $O(0,0)$ along with their first derivatives. In this case, l_2 is the coefficient of x^2 in the Taylor expansion of $P(x,y)$. The equilibrium state under consideration is called *a* (*simple*) *saddle-node*. Notice that all simple saddle-nodes are locally equivalent to the saddle-node of the system

$$\begin{aligned} \dot{x} &= l_2 x^2\,, \\ \dot{y} &= \lambda y\,, \end{aligned} \tag{8.1.2}$$

where $l_2 > 0$. The behavior of trajectories of the system near $O(0,0)$ is easily described. Let, for example, $\lambda < 0$. Then there is a curve — a strongly stable manifold W^{ss} which separates the node region W^s from the saddle region, as shown in Fig. 8.1.1. The strongly stable manifold consists of O and two trajectories entering O as $t \to +\infty$. The trajectories in W^s converge to O. In the saddle region, there is a single trajectory entering the saddle-node at $t = -\infty$. This trajectory is called *a separatrix*. The other trajectories bypass O.

[1] i.e. topologically equivalent, and the conjugating homeomorphism is ε-close to identity.

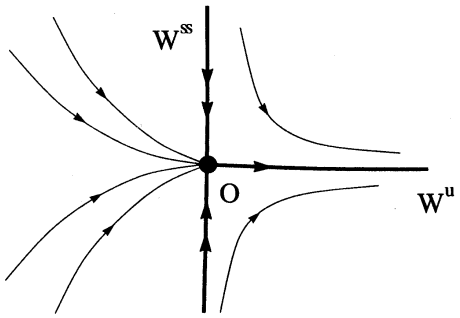

Fig. 8.1.1. A saddle-node corresponding to the case $\lambda < 0$, $l_2 > 0$.

If $\lambda > 0$, then there is a strongly unstable manifold W^{uu} which divides the neighborhood of O into a node region W^u where all trajectories diverge from O, and a saddle region where there is a single stable separatrix entering O as $t \to +\infty$ and the other trajectories bypass O.

(2) An equilibrium state which has a pair of purely imaginary eigenvalues $\lambda_{1,2} = \pm i\omega$ and a Lyapunov (or focal) value $L_1 \neq 0$. Near the bifurcating equilibrium state the system can be represented in the form

$$\begin{aligned} \dot{x} &= -\omega y + (L_1 x - \Omega_1 y)(x^2 + y^2) + \cdots , \\ \dot{y} &= \omega x + (\Omega_1 x + L_1 y)(x^2 + y^2) + \cdots . \end{aligned} \tag{8.1.3}$$

A reduction to this form is possible because in this case all quadratic and cubic terms, other than derived, are non-resonant; the simplest resonant relations here are the two resonances of third degree

$$\begin{aligned} \lambda_1 &= 2\lambda_1 + \lambda_2 , \\ \lambda_2 &= \lambda_1 + 2\lambda_2 \end{aligned}$$

(see Secs. 2.9 and 9.3).

Such equilibrium state is called a weak focus. It is stable if $L_1 < 0$ and unstable if $L_1 > 0$.

(3) A periodic orbit with a real multiplier equal to $+1$. The associated Poincaré map can be represented in the form

$$\bar{u} = u + l_2 u^2 + \cdots .$$

If the Lyapunov value $l_2 \neq 0$ here, then the associated double fixed point corresponds to a double (semi-stable) limit cycle of the original system.

(4) A heteroclinic trajectory Γ connecting two saddles [see Fig. 7.1.1(a)].

(5) A biasymptotic trajectory Γ to a saddle. The simplest case is when the saddle is non-resonant, i.e. when its characteristic exponents satisfy the condition

$$\lambda_1 + \lambda_2 \neq 0\,.$$

In addition, the following conditions must be satisfied by first-degree non-rough systems:

(A) there are no other trajectories of the above types;
(B) there exists no separatrix of a saddle-node going to or from a saddle, as shown in Fig. 8.1.2;
(C) there exists no separatrix of a saddle-node which belongs to its strongly stable manifold, as shown in Fig. 8.1.3;
(D) if there is a semi-stable (double) limit cycle, the system may not have simultaneously an unstable separatrix of a saddle which tends to the cycle as $t \to +\infty$ and a stable separatrix of a saddle which tends to the cycle as $t \to -\infty$, as shown in Fig. 8.1.4; and
(E) there exists no separatrix which tends to a homoclinic loop of a saddle (in forward or backward time), as depicted in Fig. 8.1.5.

Altogether the above requirements comprise the list of necessary and sufficient conditions which a system with first-degree of non-roughness must satisfy.

Structurally stable systems can be identified in the Banach space $\mathcal{B}_G$ of dynamical systems on a plane using conditions involving only inequalities (see Andronov–Pontryagin theorem). However, systems of first-degree of

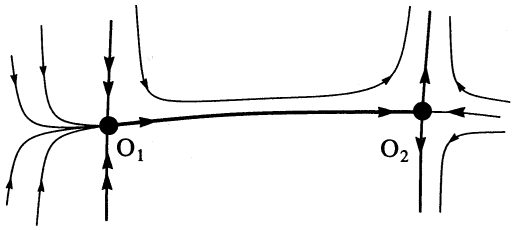

Fig. 8.1.2. A structurally unstable heteroclinic connection between a saddle-node O_1 and a saddle O_2.

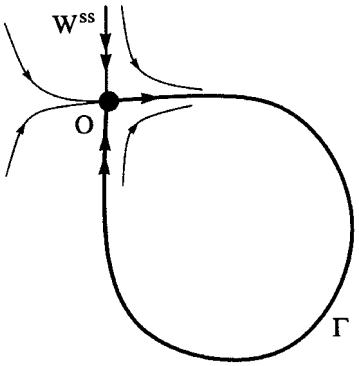

Fig. 8.1.3. A nontransverse homoclinic loop Γ to a saddle-node. The separatrix enters the equilibrium state along its strongly stable manifold.

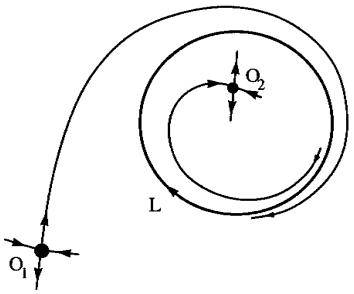

Fig. 8.1.4. The semi-stable periodic orbit L is the ω-limit of the separatrix of the outer saddle O_1, and the α-limit of the separatrix of the inner saddle O_2.

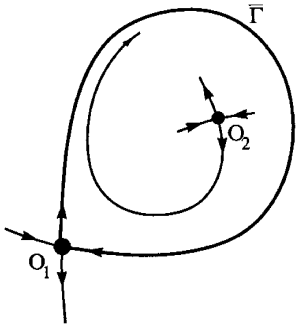

Fig. 8.1.5. The separatrix loop of the saddle O_1 is the ω-limit of the separatrix of another saddle O_2 in the interior region enclosed by the loop emanating from and terminating at O_1.

non-roughness are identified not only by conditions involving inequalities, but also by one additional condition involving equality constrains. In particular, the five conditions of structural instability in the above list assume, schematically, the following form:

(1) $\lambda_1 = 0,\ \lambda_2 \neq 0,\ l_2 \neq 0$;
(2) $\operatorname{Re}\lambda_{1,2} = 0,\ \omega \neq 0,\ L_1 \neq 0$;
(3) $\rho = 1,\ l_2 \neq 0$;
(4) $\Gamma_1 = \Gamma_2$, where Γ_1 and Γ_2 denote, respectively, an incoming and an outgoing separatrix of two connected saddles; and
(5) $\Gamma_1 = \Gamma_2,\ \lambda_1 + \lambda_2 \neq 0$, where Γ_1 and Γ_2 denote an incoming and an outgoing separatrix of one saddle.

The above equality-type conditions can be interpreted as conditions for the vanishing of some functionals defined in a neighborhood of the structurally unstable system. The inequality-type conditions guarantee, in particular, that the zero level of the functional determines a smooth, infinite-dimensional surface $\mathcal{B}^1$ in the Banach space, which divides the neighborhood of the system under consideration into two regions, which we can denote as D^+ and D^-. To avoid saying that this surface has a dimension equal to $\infty - 1$, we simply say that it is of codimension-one. The particular feature of a system of non-roughness of the first-degree is that the regions D^+ and D^- consist of rough systems. All systems in either region have an identical scheme hence they are topologically equivalent by the Leontovich–Mayer theorem.

Therefore, to study the transition from D^- to D^+, it is sufficient to examine a one-parameter family of systems X_μ such that $X_{\mu<0} \in D^-$, $X_{\mu=0} \in \mathcal{B}^1$ and $X_{\mu>0} \in D^+$. Furthermore, since all qualitative changes in the phase portrait must occur in a small neighborhood of some non-rough special trajectory, we can restrict our consideration to the given neighborhood.

Among all bifurcations occurred in systems with first-degree of non-roughness, the bifurcations of limit cycles are of special interest. Andronov and Leontovich have shown that there are four kinds of such bifurcations; namely,

- bifurcation of a limit cycle into (from) a weak focus;
- bifurcation of a double (or semistable) cycle;
- bifurcation of a limit cycle from a separatrix loop to a saddle; and
- bifurcation of a limit cycle from (into) a separatrix loop to a saddle-node.

In the last sections of this book we will discuss in detail these bifurcations whose comprehensive analysis by many researches had taken nearly twenty years; it was initiated by Andronov in the thirties and finished, after a series of exhaustive publications, in the fifties.

To conclude this section, let us elaborate further on the restrictions (D) and (E). In case (D) the surface corresponding to the double cycle is of codimension-one, and therefore, it divides a neighborhood of the non-rough system X_0 into two regions D^- and D^+. Assume that in D^- the double limit cycle is decomposed into two limit cycles, and that it disappears in D^+. The situation in D^- is simple — all systems there are structurally stable and, moreover, of the same type. As for D^+ the situation is less trivial: if (D) is violated, then it is obvious that besides structurally stable systems in D^+ there are structurally unstable ones whose non-roughness is due to the existence of a heteroclinic trajectory between two saddles, as shown in Fig. 8.1.6(a). Moreover, this picture takes place in any neighborhood of X_0. In other words, in the region D^+, there exists a countable number of the associated bifurcation surfaces of codimension-one which accumulate to $\mathcal{B}^1$. In such cases the surface $\mathcal{B}^1$ is said to be *unattainable* from one side.

An analogous situation occurs when the system has a separatrix loop to a non-resonant saddle (i.e. its saddle value $\sigma = \lambda_1 + \lambda_2 \neq 0$) which is the ω-limit of a separatrix of another saddle O_1 (see condition (E) and Fig. 8.1.5). In this case, the bifurcation surface is also unattainable from one side, where close non-rough systems may have a heteroclinic connection, as shown in Fig. 8.1.6(b).

The cases where a bifurcation surface of codimension-one is unattainable from either or both sides are typical for multi-dimensional dynamical systems.

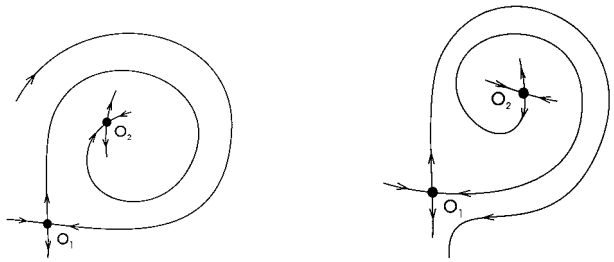

(a) (b)

Fig. 8.1.6. (a) A structurally unstable saddle connection after the disappearance of a saddle-node cycle in Fig. 8.1.4; (b) Phase plane after the splitting of the homoclinic loop in Fig. 8.1.5.

This is the reason why the classification of principal bifurcations in multi-dimensional systems is not stated in terms of the degree of non-roughness, but it rather focuses on bifurcation sets of codimension-one.

8.2. Remarks on bifurcations of multi-dimensional systems

The exploration of bifurcations of systems of higher dimensions, which was launched at the end of the fifties and the beginning of the sixties consists of early attempts to generalize known planar bifurcations results to higher dimensions. The absence of necessary and sufficient conditions for structural stability of high-dimensional systems had played an important (not last) role at that time. But further development of the theory of high-dimensional systems had eventually proven that structurally stable systems are not dense in the space of dynamical systems. First, an example of an open set of structurally unstable systems was given where the structural instability was "concentrated" in heteroclinic trajectories, i.e. on a set of wandering points (Smale), and later the analogous examples with structurally unstable non-wandering orbits had appeared. All proposed examples of "non-removable structural instability" were systems with complex dynamics. In this book we, however, focus on systems with *simple* dynamics, and in particular, on Morse–Smale systems and bifurcations which occur in such systems.

The violation of structural stability in Morse–Smale systems is caused by the bifurcations of equilibrium states, or periodic orbits, by the appearance of homoclinic trajectories and heteroclinic cycles, and by the breakdown of transversality condition for heteroclinic connections. However, we remark that some of these situations may lead us out from the Morse–Smale class; moreover, some of them, under rather simple assumptions, may inevitably cause complex dynamics, thereby indicating that the system is already away from the set of Morse–Smale systems.

The simplest example of such a situation is a homoclinic loop to a saddle-focus in the three-dimensional system

$$\begin{aligned}
\dot{x} &= \rho x - \omega y + f(x, y)\,, \\
\dot{y} &= \omega x + \rho y + g(x, y)\,, \\
\dot{z} &= \lambda z + h(x, y)\,,
\end{aligned}$$

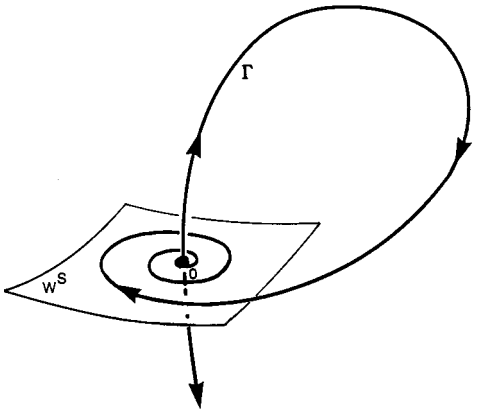

Fig. 8.2.1. A homoclinic loop Γ to a saddle-focus O.

where $\rho < 0$, $\omega \neq 0$, $\lambda > 0$, and f, g, h are smooth functions vanishing at the origin along with their first derivatives. The origin here is a saddle-focus point which is endowed with a homoclinic trajectory Γ, as shown in Fig. 8.2.1. Shilnikov [131, 135] had proved that if the saddle value is positive, i.e.

$$\sigma = \rho + \lambda > 0\,,$$

then any neighborhood of $O \cup \Gamma$ contains infinitely many saddle periodic orbits and transverse homoclinic trajectories. On the contrary, if $\rho + \lambda < 0$, then the structure of the trajectories lying entirely inside a neighborhood of $O \cup \Gamma$ is trivial, namely, besides O and Γ there are no other invariant sets.

Consider next a Banach space $\mathcal{B}$ of dynamical systems X of the Morse–Smale class in a compact region G. Let $\partial\mathcal{B}$ denote the boundary of $\mathcal{B}$. Any system $X_0 \in \partial\mathcal{B}$ is structurally unstable. We will assume then that a system $X_0 \in \partial\mathcal{B}$ is a *boundary* system of the Morse–Smale class, if in any of its neighborhoods there are systems with infinitely many periodic orbits (basically, this means the presence of transverse homoclinic trajectories). The other systems on $\partial\mathcal{B}$ correspond to *internal* bifurcations within the Morse–Smale class.

The boundary system X_0 itself may have a finite number of rough equilibria and periodic orbits, or infinitely many of them. For the latter case an example is given by a period-doubling cascade.

For the former type of boundary system, we consider an example of a homoclinic tangency. Let a $\mathbb{C}^2$-smooth family of diffeomorphisms $T(\mu)$ have, at

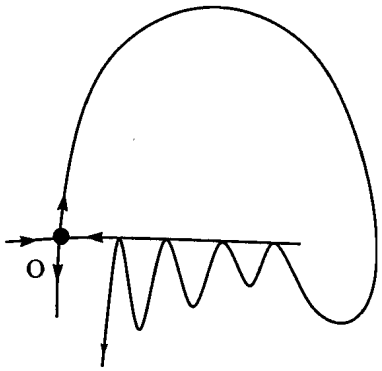

Fig. 8.2.2. A nontransverse homoclinic orbit to a saddle fixed point.

$\mu = 0$, a fixed point O with multipliers $0 < \lambda < 1$ and $\gamma > 1$ such that $\lambda\gamma < 1$. It follows that O remains a saddle point for all small $\mu \neq 0$. Denote by $W^s_O(\mu)$ and by $W^u_O(\mu)$ its stable and unstable manifolds, respectively. Suppose that $W^s_O(\mu) \cap W^u_O(\mu) \backslash O = \emptyset$ when $\mu < 0$, that at $\mu = 0$ the invariant manifolds have a tangency along a homoclinic trajectory Γ. Moreover, assume that the contact is quadratic and that it is the tangency from below, as depicted in Fig. 8.2.2. Finally assume that $W^u_O(\mu)$ and $W^s_O(\mu)$ intersect each other transversely for $\mu > 0$. Thus, the diffeomorphism $T(\mu)$ in the region $\mu > 0$ possesses a transverse homoclinic trajectory and, consequently, all nearby trajectories exhibit complex dynamics (see Theorem 7.11). If $T(\mu)$ at $\mu < 0$ were a Morse–Smale diffeomorphism, then $T(0)$ would have the same non-wandering trajectories, as well as one structurally unstable orbit of the homoclinic tangency. The last statement is due to Gavrilov and Shilnikov [54, 55] who have shown that at $\mu = 0$, any small neighborhood of $\Gamma \cup O$ has no other orbits lying entirely within it but Γ and O.[2]

Another example is a family of two-dimensional $\mathbb{C}^2$-smooth diffeomorphisms whose non-wandering set does not change until the boundary of Morse–Smale diffeomorphisms is reached. The situation is illustrated in Fig. 8.2.3. The two fixed points O_1 and O_2 have positive multipliers, and $W^u_{O_2}$ contacts $W^s_{O_1}$ along a heteroclinic trajectory, and so do $W^u_{O_1}$ and $W^s_{O_2}$. This example

[2]Note that the condition of tangency from below (as in Fig. 8.2.2) is important here: in the case where W^u touches W^s from above the system has inevitably some transverse homoclinics at $\mu = 0$ [54, 55].

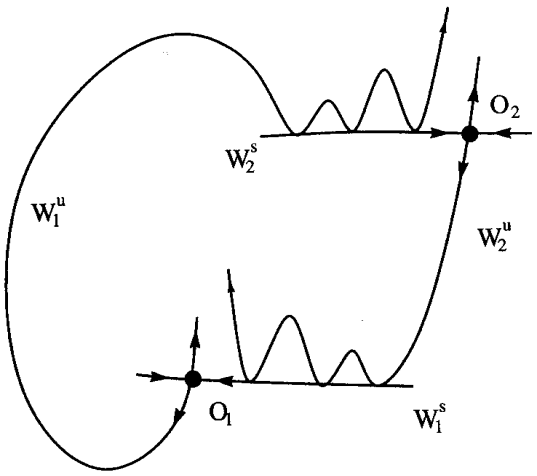

Fig. 8.2.3. A structurally unstable heteroclinic cycle including two saddle fixed points.

is not as simple as the last one because of the presence of two heteroclinic trajectories both of which are wandering.

The primary scope of this book will focus on the analysis of the internal bifurcations within the class of systems with simple dynamics, such as Morse–Smale systems. Furthermore, we will restrict our study mostly to bifurcations of codimension-one. The reason for this restriction is that some bifurcations of higher codimension turn out to be boundary bifurcations in many cases, such as when the normal forms for the equilibrium states are three-dimensional. Nevertheless, we will examine some codimension-two cases which are concerned with equilibrium states and the loss of stability of periodic orbits. Meanwhile, let us start our next section with a discussion of some questions related to structurally unstable heteroclinic connections.

8.3. Structurally unstable homoclinic and heteroclinic orbits. Moduli of topological equivalence

All non-rough two-dimensional systems in a small neighborhood of a system with first-order of non-roughness are now known to form a surface of codimension-one. Moreover, due to Leontovich and Mayer, we know that all of them are identical in the sense that they have an identical topological

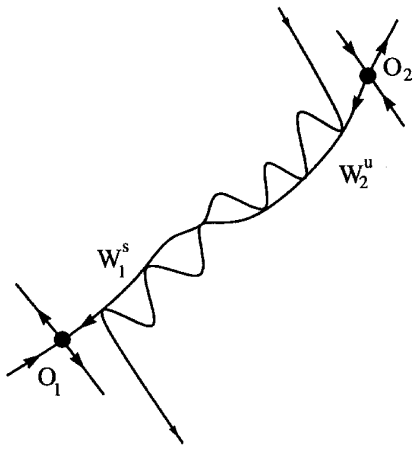

Fig. 8.3.1. A nontransverse heteroclinic trajectory between two saddle fixed points.

invariant — a scheme. In particular, all close systems having a homoclinic loop to a saddle are equivalent to each other; the same holds for close systems with a heteroclinic trajectory which connects two saddles.

However, a similar classification of two-dimensional diffeomorphisms, or of three-dimensional flows, is not that trivial. Let us illustrate this with an example. Consider a diffeomorphism T which has two saddle fixed points O_1 and O_2 with the characteristic roots $|\lambda_i| < 1$ and $|\gamma_i| > 1$ at O_i $(i = 1, 2)$. Suppose that $W^u_{O_1}$ and $W^s_{O_2}$ have a quadratic tangency along a heteroclinic orbit as shown in Fig. 8.3.1. The quadratic tangency condition implies that all similar diffeomorphisms form a surface $\mathcal{B}^1$ of codimension-one in the space of all diffeomorphisms with a $\mathbb{C}^2$-norm.

For the diffeomorphism T we introduce the value

$$\theta = \frac{\ln|\lambda_1|}{\ln|\gamma_2|} \tag{8.3.1}$$

and analogously define

$$\tilde{\theta} = \frac{\ln|\tilde{\lambda}_1|}{\ln|\tilde{\gamma}_2|} \tag{8.3.2}$$

for a close diffeomorphism $\tilde{T} \in \mathcal{B}^1$, where $\tilde{\lambda}_{1(2)}$ and $\tilde{\gamma}_{1(2)}$ are the characteristic roots at the saddle $\tilde{O}_{1(2)}$ of T, which is near the saddle $O_{1(2)}$.

Then, we have the following theorem.

Theorem 8.1. *If the diffeomorphisms T and $\tilde{T}$ are topologically conjugate, then $\theta = \tilde{\theta}$.*

We remark that $\theta = \tilde{\theta}$ is only a necessary condition. It follows from this theorem that $\mathcal{B}^1$ near T is divided into a continuum of topologically different classes of diffeomorphisms. This fact was discovered by Palis [103]; see its proof in [97].

The invariant θ is called *a modulus of topological equivalence* or simply *a modulus*. Because of the fundamental importance of a notion of the modulus let us pause to give its definition.

Definition 8.2. *A system X (continuous or discrete) is said to have a modulus if, in some subspace $\mathcal{B}^*$ of the space of dynamical systems, where $X \in \mathcal{B}^*$, a continuous, locally non-constant functional h is defined such that if X and $\tilde{X}$ are topologically equivalent, then $h(X) = h(\tilde{X})$.*

The condition that the functional is locally non-constant means that in the region of its definition there are no open sets in a neighborhood of X where it might take a constant value. From this point-of-view, the Poincaré rotation number for typical diffeomorphisms of a cycle is not a modulus.

The value θ is also a modulus of topological equivalence in the case of a three-dimensional flow which has two saddle periodic orbits such that an unstable manifold of one periodic orbit has a quadratic tangency with a stable manifold of another orbit along a heteroclinic trajectory.

There are some other occurrences of moduli in structurally unstable three-dimensional systems of codimension-one with simple dynamics. For example, consider a three-dimensional system with a saddle-focus O and a saddle periodic orbit L. Let $\lambda_{1,2} = \rho \pm i\omega$, and λ_3 be the characteristic roots at O such that $\rho < 0$, $\omega > 0$, $\lambda_3 > 0$, i.e. assume the saddle-focus has type (2,1); let $|\nu| < 1$ and $|\gamma| > 1$ be the multipliers of the orbit L. Let one of the two separatrices Γ of O tend to L as $t \to +\infty$, i.e. $\Gamma \in W^s_L$, as shown in Fig. 8.3.2. This condition gives the simplest structural instability. All nearby systems with similar trajectory behavior form a surface $\mathcal{B}^1$ of codimension-one. Belogui [28] had found that the value

$$\tilde{\theta}_1 = \frac{\rho}{\omega} \frac{1}{\ln \gamma} \tag{8.3.3}$$

is a modulus in such systems.

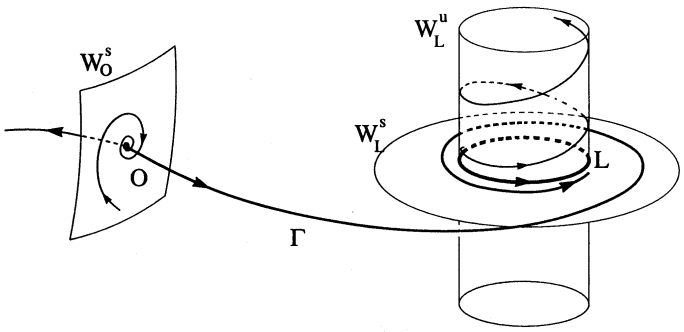

Fig. 8.3.2. A structurally unstable heteroclinic trajectory connecting a saddle-focus and a saddle periodic orbit with positive multipliers, i.e. both manifolds of the saddle cycle are homeomorphic to a cylinder.

Another example is the system shown in Fig. 8.2.1 containing a homoclinic loop Γ to a saddle-focus. If the saddle index

$$\nu = -\frac{\rho}{\lambda_3} < 1\,,$$

then a neighborhood of the loop contains an infinite set of saddle periodic orbits. However, if $\nu > 1$, the dynamics in a neighborhood of Γ is trivial. Moreover, Shilnikov [130] had shown that when $\nu > 1$, no more than one periodic orbit can bifurcate from the homoclinic loop. Thus, it may be classified as an internal bifurcation within the Morse–Smale systems (at least when a small neighborhood of the loop Γ is considered). In this connection Afraimovich and Ilyashenko [21] had noticed that ν is a modulus in this case.

Structurally unstable heteroclinic connections in systems of higher-dimension may require new moduli besides known ones. Moreover, even structurally unstable diffeomorphisms with simple dynamics may require infinitely many moduli for their description. The conditions under which they have either a finite or an infinite number of moduli are presented in [43].

There is no doubt that some subtle aspects of the behavior of homoclinic and heteroclinic trajectories might not be important for nonlinear dynamics since they reflect only fine nuances of the transient process. On the other hand, when we deal with non-wandering trajectories, such as near a homoclinic loop to a saddle-focus with $\nu < 1$, the associated Ω-moduli (i.e. the topological invariants on the non-wandering set) will be of primary importance because they may be employed as parameters governing the bifurcations; see [62, 63].

8.4. Bifurcations in finite-parameter families of systems. Andronov's setup

The mathematical objects of nonlinear dynamics are models — explicitly defined dynamical systems depending on a finite number of parameters. The primary quality of a model is that it must properly, at least qualitatively, describe the nature of the associated physical phenomenon. The primary goal in the study of a model is to give a rigorous mathematical explanation. In this connection let us recall the following remark made by Lyapunov: "... it is not permitted to use dubious arguments as soon we have started to solve a specific problem from mechanics or physics, it does not matter, whatever is set up correctly from the point-of-view of mathematics. As soon as the system is defined it becomes a problem of pure analysis and must be treated as such."[3]

As far as dynamical models are concerned the main requirements for their analysis have been formulated by Andronov. This is why we will call them *Andronov's setup of the problem.* Its principal idea is:

- Partition the phase space into regions of structural stability and identify the bifurcation set.
- Divide this bifurcation set into connected components each of which corresponds to a topologically equivalent structure of trajectories.

It is natural that such a setting of the problem was based on the already known facts and results from the qualitative theory of two-dimensional systems and the theory of bifurcations.

Consider some finite-parameter family of smooth systems X_ε, where $\varepsilon = (\varepsilon_1, \ldots, \varepsilon_p)$ assumes its values from some region $V \in \mathbb{R}^p$. If X_{ε_0} is non-rough, then ε_0 is said to be *a bifurcation parameter value.* The set of all such values in V is called *a bifurcation set.* It is obvious that once we know the bifurcation set, we can identify all regions of structural stability in the parameter space. Hence, the first step in the study of a model is identifying its bifurcation set. This emphasizes a special role of the theory of bifurcations among all tools of nonlinear dynamics.

[3]Lyapunov had uttered these words in connection with Poincaré's investigation where he had applied some non-rigorous methods to a problem on the stability of the equilibrium shapes of rotating fluids, and which had led him to a wrong conclusion in favor of pear shapes. A more rigorous analysis conducted by Lyapunov had revealed that the pear shape is unstable. Lyapunov's proof was later confirmed by Cartan.

The study of a bifurcation means to describe the change in the phase portrait of a non-rough system in transition to an arbitrarily close system (with respect to some $\mathbb{C}^r$-metric; the choice of r depends on the character of non-roughness, and hence must be specified in each concrete case).

In principle, to solve a bifurcation problem we need to consider all systems close to X_{ε_0}. This means that we must consider the Banach space of all small perturbations.[4] On the other hand, when it is possible to reduce the analysis to some appropriate finite-parameter family of systems, the study is simplified significantly.

This idea was proposed by Andronov and Leontovich in their first work [9] which deals with primary bifurcations of limit cycles on the plane.[5] Further developments of the theory of bifurcations, internal to the Morse–Smale class, has also confirmed the sufficiency of using finite-parameter families for a rather large number of problems.

An explicit mathematical formulation to the finite-parameter approach to the local bifurcations was given by Arnold [19], based on the notion of *versal* families. Roughly speaking, versality is a kind of structural stability of the family in the space of families of dynamical systems. Different versions of such stability are discussed in detail in [97].

The main idea of this approach is the following: to a non-rough system X_{ε_0} some codimension k can be assigned. In the case of a finite degeneracy, the codimension k is identified with k equality-like conditions and a finite number of conditions of inequality type. Hence, X_{ε_0} is considered as a point on some Banach submanifold $\mathcal{B}^k$ of codimension k in the space of dynamical systems. In other words, we have k smooth functionals defined in a neighborhood of X_{ε_0} whose zero levels intersect at $\mathcal{B}^k$. In general, the inequality-like conditions secure the smoothness of $\mathcal{B}^k$. In the case of codimension one Sotomayor [144, 145] had proved the smoothness of these functionals, and the smoothness of

[4] Note that in many special cases attention is restricted to the study of the smaller spaces of systems, e.g. systems with some specified symmetries, Hamiltonian systems, etc. In view of that, the notion of structural stability in, say, Hamiltonian systems with one-degree-of-freedom becomes completely meaningful. So, for example, equilibrium states such as centers and saddles of such systems, become structurally stable. Moreover, if there are no heteroclinic cycles containing different saddles, we can naturally distinguish such systems as rough in the set of all systems of the given class.

[5] Nevertheless, in their later works (see also the books [11, 12]) when investigating similar bifurcations they use the Banach space of all small perturbations. Note that the Banach space approach to the bifurcations becomes, in essence, necessary in the case of systems with complex dynamics, due to the persistence of homoclinic tangencies (see [60, 61, 62]).

manifold $\mathcal{B}^1$ in situations where

(1) an equilibrium state becomes structurally unstable;
(2) a periodic orbit loses its structural stability; and
(3) there is a non-transverse intersection of stable and unstable manifolds of saddle equilibrium states and periodic orbits.

Note that all systems from $\mathcal{B}^k$ are non-rough. Moreover, in the general case it is not necessary that they are topologically equivalent to each other. Suppose, however, they are. Next, let us foliate a small neighborhood U of the point $X_{\varepsilon_0} \in \mathcal{B}^k$ into k-parameter families $\tilde{X}_\varepsilon$, where $\tilde{X}_{\varepsilon_0} \in \mathcal{B}^k \cap U$ and $\tilde{X}_\varepsilon$ is transverse to $\mathcal{B}^k$ at $\tilde{X}_{\varepsilon_0}$. If there is a homeomorphism (or, a diffeomorphism, what is better) between the parameters of any two of these families such that the corresponding systems are topologically equivalent, then obviously the study of the bifurcations of the system X_{ε_0} is reduced to the investigation of any k-parameter family $\tilde{X}_\varepsilon$ passing through X_{ε_0} and transverse to $\mathcal{B}^k$.[6] Since U is small, ε assumes its values from a small neighborhood of ε_0 in the parameter space. In such a case, the Andronov's problem can be easily set up.

In essence, this is the case for two-dimensional systems, as well as for a number of high-dimensional systems when, for example, they can be reduced to two-dimensional ones by a center manifold theorem (local or global, see Chaps. 5 and 6).

The situation becomes completely different when moduli of topological equivalence are required to describe systems in $\mathcal{B}^k$, like in the case of heteroclinic tangencies (which correspond to bifurcation sets of codimension one). Although the foliation of a neighborhood U by k-parameter families is still possible, different families will not be topologically equivalent. Thus, from a formal mathematical point-of-view the moduli must be included among the governing parameters and the necessary number of parameters increases up to the codimension of the problem plus the number of moduli. If there is infinitely many independent moduli, then, formally, a reduction to a finite-parameter family is not correct. However, the question of applicability of the finite-parameter approach to these situations remains.

As an example, let us consider the codimension-one bifurcation of three-dimensional systems with a homoclinic loop to a saddle-focus with the negative

[6] Of course, one may consider here families depending on more than k parameters, as well; the only requirement is that the family must be in general position with respect to $\mathcal{B}^k$, for more details see Sec. 11.1.

saddle value (i.e. $\nu > 1$, see the previous section). As explained in the last section, this bifurcation does not bring a system out of the class of systems with trivial dynamics. On the other hand, ν is a modulus in this case. In spite of this fact which means that different systems on the associated bifurcation surface are not topologically equivalent, the bifurcation under consideration can very well be treated in a one-parameter family (see Sec. 13.4) unless we are interested in the behavior of trajectories for which the homoclinic loop is an ω-limit set.

A more complicated example is given by codimension-two problems as those shown in Fig. 8.4.1, which include one or two saddle-foci. The saddle values are assumed to be negative at all equilibrium states. The parameters which govern the bifurcations are introduced in the following way: let $\mu_{1(2)}$ be a deviation of $\Gamma_{12}(\Gamma_{21})$ from $W^s_{O_1}$ ($W^u_{O_2}$) in the case of two saddle-foci, or let it be a deviation of $\Gamma_1(\Gamma_2)$ from W^s_0. As established in [151, 125] not more than one or two periodic orbits can be born in the first and, respectively, second

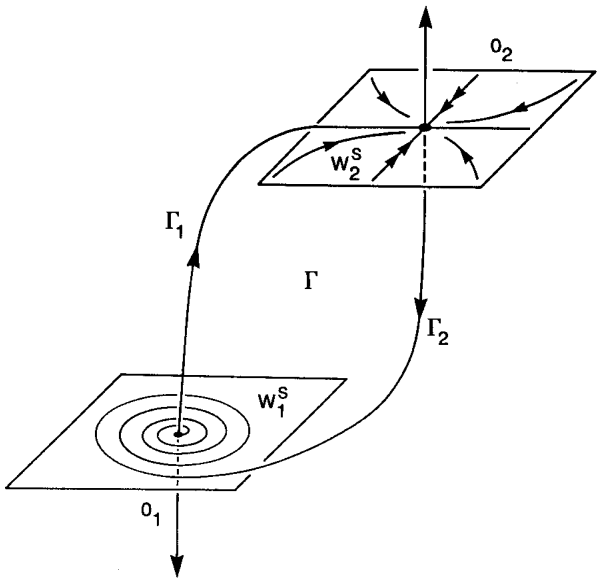

(a)

Fig. 8.4.1. (a) A heteroclinic connection between a saddle O_2 and saddle-focus O_1; (b) a heteroclinic connection between two saddle-foci $O_{1,2}$; (c) a homoclinic figure-eight to a saddle-focus.

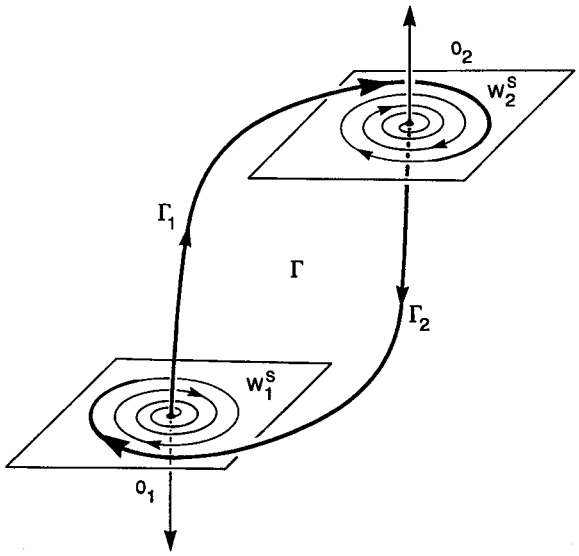

(b)

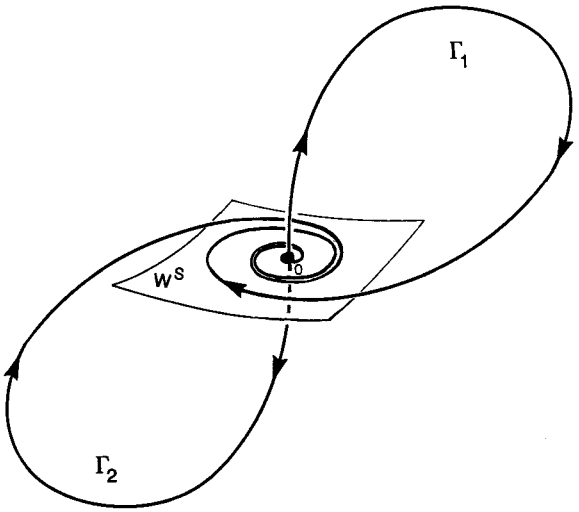

(c)

Fig. 8.4.1. (*Continued*)

bifurcation. Moreover, in the second case, a non-trivial attractor (a stable quasiminimal set composed of the saddle-focus O and two P^+ trajectories having O as their α-limit set, as well as a continuum of other non-closed Poisson-stable trajectories) may appear. Even though the structure of the non-wandering sets here is completely understood, the bifurcation diagrams in the (μ_1, μ_2)-parameter plane look rather non-trivial (as depicted in Fig. 8.4.2), especially for the set of bifurcation values corresponding to secondary heteroclinic and homoclinic trajectories. Presumably, changing the values of the moduli ν at $(\mu_1 = 0, \mu_2 = 0)$ may change the structure of mutual intersections of different bifurcational curves at small (μ_1, μ_2). On the other hand, if we ignore the too subtle fine details, the two-parameter approach is sufficient for a comprehensive understanding of these bifurcations.

An analogous situation also appears in a classical problem on the birth of an invariant torus from a periodic orbit: minor details of the structure of the

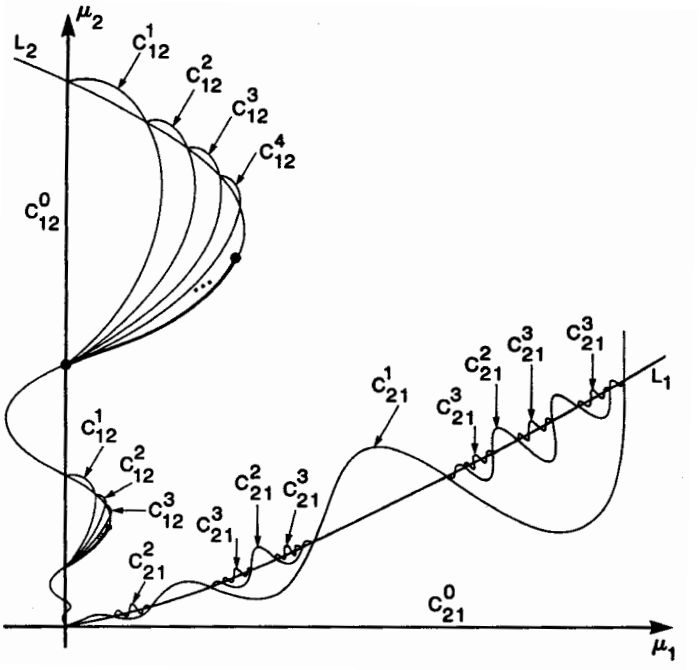

Fig. 8.4.2. A bifurcation diagram corresponding to the case shown in Fig. 8.4.1(a). See Sec. 13.7 for details.

bifurcational set may become extremely sensitive to small perturbation of the family.

We see that in many basic cases the Andronov's problem cannot be solved if it is taken in its full rigor, so in these cases one must determine reasonable bounds to the analysis of the bifurcation set.

In this book we adopt the finite-parameter approach to the bifurcations from the very beginning; the formal scheme is described in Sec. 11.1.

In general, when dealing with a p-parameter family of systems we assume the following natural restrictions:

(1) the structurally stable systems fill out whole regions in the parameter space;
(2) the main bifurcations in the family are of codimensions not greater than p; and
(3) bifurcations of codimension k, such that $k \leq p$, must admit the construction of a reasonable k-parameter unfolding.

Chapter 9

THE BEHAVIOR OF DYNAMICAL SYSTEMS ON STABILITY BOUNDARIES OF EQUILIBRIUM STATES

In this chapter we study *non-rough or structurally unstable equilibrium states* on the stability boundaries, i.e. those which have at least one characteristic exponent on the imaginary axis in the complex plane. As for the rest of the characteristic exponents we will assume that they lie in the open left-half-plane.

The basis of stability theory for systems with structurally unstable equilibrium states was developed by Lyapunov. His works and numerous subsequent studies on various aspects of stability in *critical* cases, as well as of bifurcation phenomena accompanying the loss of stability of equilibrium states had became the foundation on which the principal notions in the theory of nonlinear oscillations had spawned in the twenties and thirties.

The critical equilibrium states have been the subject of a large number of studies. Here, we shall consider only the two most common and simple cases, where the characteristic equation

$$\lambda^n + a_1\lambda^{n-1} + \cdots + a_{n-1}\lambda + a_n = 0$$

(1) has one zero root on the imaginary axis; or
(2) has a pair of complex-conjugate roots on the imaginary axis.

The first case is determined by the condition

$$a_n = 0\,, \quad \Delta_k > 0\,, \quad k = 1, \ldots, n-1\,,$$

where Δ_k is the Routh–Hurwitz determinant (see Sec. 2.1).

The second critical case corresponds to

$$\Delta_{n-1} = 0\,, \quad a_n > 0\,, \quad \Delta_k > 0\,, \quad k = 1, \ldots, n-2\,.$$

Recall that $a_n = (-1)^n \det A$, where A is the matrix of the linearized system at the equilibrium state. Therefore, the condition for crossing the stability boundary in the first case is given by

$$\det A = 0\,.$$

In view of this condition, the equilibrium states associated with the first critical case are also called *degenerate*. Since the implicit function theorem may no longer be applied here, the persistence of such an equilibrium state in a neighboring system is not necessarily guaranteed. Thus, a transition through the stability boundary in the first critical case may result in the disappearance of the equilibrium state.

On the contrary, in the second critical case, the equilibrium state is preserved in all nearby systems and can only lose its stability.

The basic tools for studying critical cases include the method of reduction to the center manifold and the method of normal forms. The latter allows us to calculate *the Lyapunov values* that determine the stability of a critical equilibrium state.

9.1. The reduction theorems. The Lyapunov functions

A system of differential equations near a critical equilibrium state can be written in the form

$$\begin{aligned} \dot{y} &= Ay + f(x, y)\,, \\ \dot{x} &= Bx + g(x, y)\,, \end{aligned} \tag{9.1.1}$$

where $x = (x_1, \ldots, x_m)$ and $y = (y_1, \ldots, y_n)$, $m \neq 0$; the functions $f, g \in \mathbb{C}^r (r \geq 1)$ vanish at the origin along with their first derivatives. The characteristic equation $\det(B - \lambda I) = 0$ has m roots $\lambda_1, \ldots, \lambda_m$ with $\operatorname{Re} \lambda_i = 0\,(i = 1, \ldots, m)$, and the characteristic equation $\det(A - \gamma I) = 0$ has n roots $\gamma_1, \ldots, \gamma_n$ with $\operatorname{Re} \gamma_j < 0$, $(j = 1, \ldots, n)$.

As shown in Chap. 5, the above critical equilibrium state lies in an invariant $\mathbb{C}^r$-smooth *center manifold* W^C defined by an equation of the form $y = \Phi(x)$, where $\Phi(x)$ vanishes at the origin along with its first derivative.

Transversely to the center manifold, another invariant manifold passes through the point $O(0,0)$. It is called *strongly stable* and, as usual, we denote it by W^{ss}. Its equation is given by $x = \Psi(y)$, where $\Psi(y)$ vanishes at the origin along with its first derivative. If the original system is analytic, the manifold W^{ss} is analytic as well. A similar statement for the center manifold is not true in general: even if the system is analytic, the center manifold W^C may be neither analytic nor even $\mathbb{C}^\infty$.

The strongly stable manifold W^{ss} is one of the leaves of a $\mathbb{C}^{r-1}$-smooth foliation which is transverse to the center manifold. As we have shown in Chap. 5 the following reduction theorem holds:

In a neighborhood of the point O there exists a $\mathbb{C}^{r-1}$-smooth change of variables which straightens both the invariant foliation and the center manifold so that the system in the new variables assumes the following **standard form**

$$\dot{x} = Bx + G(x)\,, \tag{9.1.2}$$

$$\dot{y} = [A + F(x,y)]y\,, \tag{9.1.3}$$

where $G(x) \equiv g(x, \Phi(x)) \in \mathbb{C}^r$, $F(x,y) \in \mathbb{C}^{r-1}$ and $F(0,0) = 0$.

In the new variables the equation of the center manifold W^C becomes $y = 0$, and the equation of the strongly stable manifold W^{ss} becomes $x = 0$. The leaves of the strong stable foliation are the surfaces $x = \text{const}$.

The main feature of this theorem is that it reduces significantly the dimension of the problem; namely, instead of studying the original $(n+m)$-dimensional system (9.1.1) we need only to explore the properties of the m-dimensional system (9.1.2), whose dimension does not depend on n, but is equal to the number of critical characteristic exponents. The dynamics in the critical (center) $x-$variable is locally determined by system (9.1.2) and depends in no way on the y-coordinate.

The dynamics in the y-variable is rather simple: if $\|x\|$ is small, the function F in (9.1.3) is also small near the origin. Therefore, the following estimate is valid in an appropriately chosen basis in the y-space:

$$\frac{d}{dt}\|y(t)\| \le -\gamma\|y(t)\|\,,$$

where $0 < \gamma < \max|\operatorname{Re}\gamma_i|$ $(i = 1, \dots, n)$ (see Theorem 2.4). Hence

$$\|y(t)\| < Ce^{-\gamma t}\,, \tag{9.1.4}$$

i.e. *any trajectory tends exponentially to the center manifold W^C.*

All characteristic exponents of the restriction

$$\dot{y} = Ay + f(\Psi(y), y) \tag{9.1.5}$$

of the system (9.1.1) on the strongly stable manifold W^{ss} lie to the left of the imaginary axis. Therefore, the trajectory behavior of the system on W^{ss} is the same as that near a rough stable equilibrium state with the linearization matrix A (see Chap. 2).

It follows from the estimate (9.1.4) that the stability of the equilibrium state of the original system (9.1.1) is equivalent to the stability of the equilibrium state with respect to the associated system reduced to the center manifold.

First, let us recall some definitions. An equilibrium state O is said to be *Lyapunov stable* if for any $\varepsilon > 0$, there exists $\delta > 0$ such that any trajectory which starts from a δ-neighborhood of O never leaves its ε-neighborhood. Otherwise, the equilibrium is said to be unstable.

An equilibrium state O is *asymptotically stable* if any trajectory starting sufficiently close to O tends to it as $t \to +\infty$.

Now, let the equilibrium state $x = 0$ of the reduced system (9.1.2) be stable in the sense of Lyapunov. By definition, this means that for the system (9.1.2 and 9.1.3) in the standard form, the x-coordinate remains small in the norm for all positive times, for any trajectory which starts sufficiently close to O, provided y remains small. At the same time, the smallness of x implies the inequality (9.1.4) for the y-coordinate, i.e. $y(t)$ converges exponentially to zero. Thus, we have the following theorem.

Theorem 9.1. *If the equilibrium state is Lyapunov stable in the center manifold W^C, then the equilibrium state of the original system* (9.1.1) *is Lyapunov stable as well. Moreover, if the equilibrium state is asymptotically stable in the center manifold, then the equilibrium state of the original system is also asymptotically stable.*

If the equilibrium state is unstable in the center manifold W^C, then the equilibrium state of the original system is unstable.[1]

Our investigation of the stability of a critical equilibrium state will make use of Lyapunov functions.

[1] The last statement concerning instability is obvious and requires no proof.

Definition 9.1. *A continuous function $V(x)$ defined in a neighborhood D of O and smooth in $D\backslash O$, is called a Lyapunov function for system* (9.1.2) *if it satisfies the following conditions*

$$(1)\ V(0) = 0\,; \tag{9.1.6}$$

$$(2)\ V(x) > 0 \quad \text{if } x \neq 0\,; \tag{9.1.7}$$

$$(3)\ \frac{dV(x)}{dt} = \langle V'(x), Bx + G(x)\rangle \leq 0 \quad \text{at } x \neq 0\,, \tag{9.1.8}$$

where $\langle \cdot, \cdot \rangle$ denotes the scalar product.

The use of Lyapunov functions to guarantee stability is based upon the following result.

Theorem 9.2. *If there exists a function $V(x)$ satisfying conditions* (9.1.6)–(9.1.8), *then the equilibrium state O is Lyapunov stable. Furthermore, if the inequality* (9.1.8) *is strict for all $x \neq 0$, then all trajectories in D tend to the point O as $t \to +\infty$, i.e. the equilibrium state O is asymptotically stable.*

To prove Lyapunov stability let us surround the point O by a sphere S_ε^{m-1} of radius ε. Let $V_\varepsilon > 0$ be the minimum of the function $V(x)$ on the surface of the sphere (it is strictly positive because all points of the sphere lie at a finite distance from the origin). Since V is continuous and $V(0) = 0$, it follows that for any point x_0 chosen sufficiently close to O the value of the function $V(x)$ is strictly less than V_ε.

Note that (9.1.8) implies that the Lyapunov function cannot increase along a trajectory of system (9.1.2). Hence, for any trajectory $x(t)$ starting close enough to the point O the inequality $V(x(t)) < V_\varepsilon$ holds. This means that such a trajectory cannot intersect the sphere S_ε^{m-1}, and therefore, it must remain within an ε-neighborhood of the equilibrium state O for all $t \geq 0$.

To prove asymptotic stability, let us choose an ε-neighborhood U_ε of the equilibrium state and show that any trajectory from D must enter U_ε after a sufficiently large time and must remain inside there forever. Indeed, if inequality (9.1.8) is strict for all $x \neq 0$, then the minimum

$$\min_{x \in D\backslash U_\varepsilon} \langle V'(x), Bx + G(x)\rangle = -C_\varepsilon$$

is strictly less than zero. If we assume that at time t a representative point on the trajectory $x(t)$ is outside of U_ε, then by virtue of (9.1.8) we have

$$\frac{d}{dt} V(x(t)) \leq -C_\varepsilon$$

(inside U_ε we have at least $\frac{d}{dt}V(x(t)) \le 0$). Hence, for any t

$$V(x(t)) \le V(x(0)) - C_\varepsilon\, T(t)\,, \tag{9.1.9}$$

where T denotes the time during which the trajectory has been outside U_ε. It follows from (9.1.7) and (9.1.9) that this time is finite for any t:

$$T(t) \le V(x_0)/C_\varepsilon \equiv T_\varepsilon(x_0)\,.$$

Hence, for all $t > T_\varepsilon$ the trajectory remains inside the ε-neighborhood of the point O. Since ε may be chosen arbitrarily small, it follows that the trajectory must tend to O as $t \to +\infty$.

Remark. The Lyapunov function is a universal tool of stability theory. Typically, a proof concerning stability consists of either constructing a Lyapunov function, or proving its existence. Moreover, its applicability is not limited to critical equilibria; for example, in our analysis of studying the structurally stable equilibria (Theorem 2.4), we have implicitly shown that the norm of a vector in a Jordan basis is a Lyapunov function.

The Lyapunov function has a simple geometrical meaning, especially in the case of asymptotic stability. Here, the level surfaces $V(x) =$ constant are *surfaces without contact* for system (9.1.1); i.e. the vector field on these surfaces is oriented toward the origin, as shown in Fig. 9.1.1 (to verify this note that the gradient vector $V'(x)$ of the function $V(x)$ is orthogonal to the surface $V =$ constant at the point x and that the strict inequality (9.1.8) means that the angle between the velocity vector $\dot{x}$ and the gradient of the function $V(x)$ is acute). Therefore, all trajectories must flow inside any surface $V =$ constant and converge to the equilibrium state O.

From the practical point of view, stability in the sense of Lyapunov is less important than asymptotic stability. In particular, it follows from simple continuity arguments that if a critical equilibrium state is asymptotically stable, then the trajectories of any nearby system will also converge to a small neighborhood of the origin where they will stay forever. The behavior of trajectories in this small neighborhood may be rather nontrivial. Nevertheless, any deviations from zero of trajectories of a nearby system must remain small because the equilibrium state is asymptotically stable at the critical parameter value.

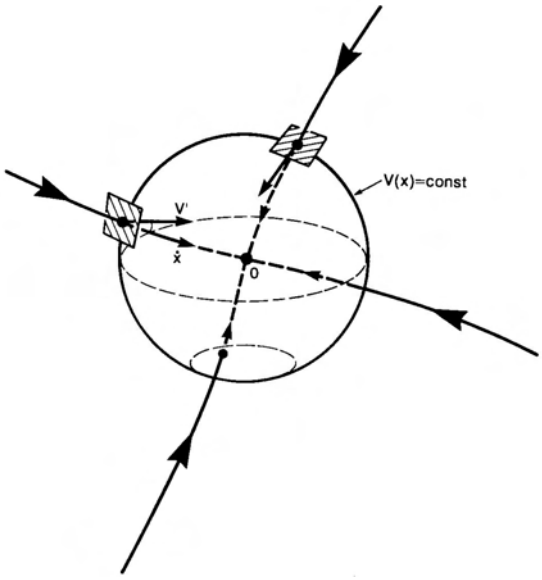

Fig. 9.1.1. Geometrical interpretation of a Lyapunov function. The surface $V(x) =$ constant has no contact with a vector field, i.e. the tangent at any point of the surface is *transverse* to the vector field so that every trajectory goes inwards the sphere.

The above statement is not valid for an equilibrium state which is stable only in the Lyapunov sense. For example, for the linear system

$$\dot{x}_1 = \mu x_1 - \omega x_2 \,,$$

$$\dot{x}_2 = \omega x_1 + \mu x_2 \,,$$

the equilibrium state $O(0,0)$ is a center at $\mu = 0$. It is Lyapunov stable but not asymptotically stable (here, any trajectory is a circumference surrounding the origin). For any $\mu > 0$ arbitrarily small, the equilibrium state becomes an unstable focus and all trajectories leave the origin for infinity as $t \to +\infty$.

The instability of an equilibrium state at a critical parameter value also implies a practically important general conclusion about the trajectory behavior in all nearby systems. Namely, if we fix an arbitrarily small ε_0-neighborhood of such an equilibrium state, then for any system which is sufficiently close to the original system with the unstable equilibrium state there are initial conditions not further from zero than ε_0 such that the corresponding trajectory

will diverge from the origin over a finite distance. Thus, if a critical equilibrium state O of the original system is unstable, then the basin of attraction (provided it does exist) of the corresponding equilibrium state of any neighboring system has to be very small.

To prove that an equilibrium state is unstable one can use some analogies of Lyapunov functions. For example, if there exists a function $V(x)$ satisfying conditions (9.1.6) and (9.1.7) but

$$\langle V'(x), Bx + G(x)\rangle > 0\,, \quad \text{at } x \neq 0\,, \tag{9.1.10}$$

then the corresponding equilibrium state is unstable. Here, the function $V(x)$ is a Lyapunov function for a system obtained from (9.1.2) by a time inversion. Therefore, by virtue of Theorem 9.1 all trajectories tend to O as $t \to -\infty$; i.e. such an equilibrium state is *repelling*, or *completely unstable*.

However, it is possible to have an unstable equilibrium state O such that some trajectories converge to O as $t \to +\infty$. The simplest example is a rough saddle. To prove instability of a saddle in critical cases one can use Chetaev's function where conditions (9.1.6), (9.1.7) and (9.1.10) hold only within some sector adjoining the point O. For details we refer the reader to the book by Khazin and Shnol [75].

9.2. The first critical case

For the case where only one characteristic exponent lies on the imaginary axis, i.e. when $m = 1$, and $\lambda_1 = 0$ in (9.1.1), the system in the standard form is given by

$$\begin{aligned} \dot{x} &= g(x)\,, \\ \dot{y} &= [A + F(x, y)]\, y\,, \end{aligned} \tag{9.2.1}$$

where x is a scalar, and the function $g(x)$ vanishes at the origin along with its first derivative. In this case, the center manifold W^C is one-dimensional and defined by the equation $y = 0$. The system in W^C is

$$\dot{x} = g(x)\,. \tag{9.2.2}$$

Let us investigate the behavior of trajectories of this equation near the equilibrium state. Since $g(0) = g'(0) = 0$,

$$g(x) = l_2 x^2 + l_3 x^3 + \cdots\,, \tag{9.2.3}$$

where the coefficients $l_2, \dots, l_k$ of the Taylor expansion of the function $g(x)$ at O are called *the Lyapunov values.*

Let k be the number of the first non-zero Lyapunov value; i.e. $l_2 = \cdots = l_{k-1} = 0$ and $l_k \neq 0$. Then, Eq. (9.2.2) can be written as

$$\dot{x} = l_k x^k (1 + o(1)) . \tag{9.2.4}$$

Observe that if k is even, then the equilibrium state is unstable. The behavior of the trajectories in a neighborhood of the point O for positive and negative values of l_k is shown in Figs. 9.2.1(a) and (b), respectively. The second case reduces to the other one by change $x \to -x$. There are only three trajectories here: one is the point O, the second is the trajectory coming out from O towards $l_k x > 0$, and the third is the trajectory entering O from the side $l_k x < 0$.

If k is odd ($k = 2p + 1$), the equation assumes the following form

$$\dot{x} = l_{2p+1} x^{2p+1} (1 + o(1)) . \tag{9.2.5}$$

Here, if $l_{2p+1} < 0$, then $\frac{d}{dt}|x| = l_{2p+1}|x|^{2p+1}(1 + o(1)) < 0$ for $x \neq 0$. Hence, the equilibrium state O is stable in this case, as shown in Fig. 9.2.1(c). On the contrary, if $l_{2p+1} > 0$, the equilibrium is unstable, as shown in Fig. 9.2.1(d).

Let us return to the original system (9.2.1) and give a complete description of the trajectories near the point O. The dynamics in the y-variables is

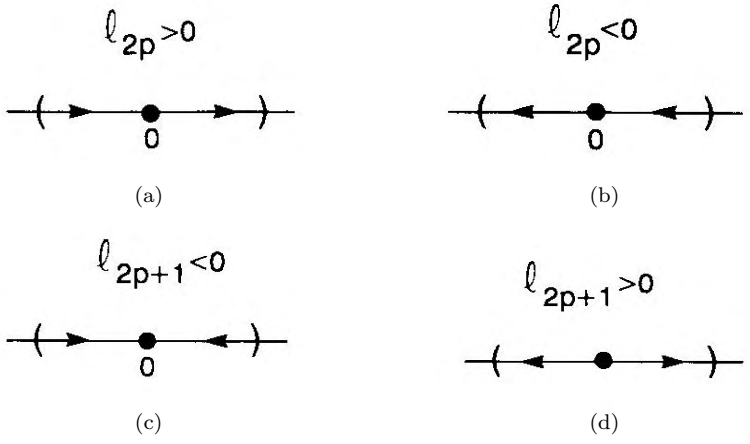

Fig 9.2.1. A saddle-node with different Lyapunov values. See comments in the text.

quite simple — it is dominated by the exponential convergence to zero [see inequality (9.1.4)]. The dynamics in the x-coordinate is described above. Hence, we have:

(1) If the first non-zero Lyapunov value has an even index number, such an equilibrium state is called *a saddle-node*; moreover, it is called *a simple saddle-node* if $l_2 \neq 0$. Here, the strong stable manifold W^{ss} partitions a neighborhood of O into two subregions: a node subregion and a saddle one. In the node subregion all trajectories tend to O along the leading direction $y = 0$. In the saddle subregion all trajectories pass nearby O, except for one trajectory which tends to O as $t \to -\infty$ (Fig. 9.2.2).

In the three-dimensional case all orbits in W^{ss} tend to O exponentially as $t \to +\infty$: if the largest (nearest to the imaginary axis) eigenvalue γ_1 of the matrix A is real, then the point O is a stable node in W^{ss} [see Fig. 9.2.3(a)]; otherwise, if γ_1 is complex, then O is a stable focus in W^{ss} [see Fig. 9.2.3(b)].

(2) If the first non-zero Lyapunov value is negative and has an odd index number, i.e. $l_k < 0$, $k = 2p+1$, then the equilibrium state is stable. All trajectories tend to O as $t \to +\infty$. Moreover, the trajectories which do lie on the strong stable manifold W^{ss} converge to O along W^C as shown

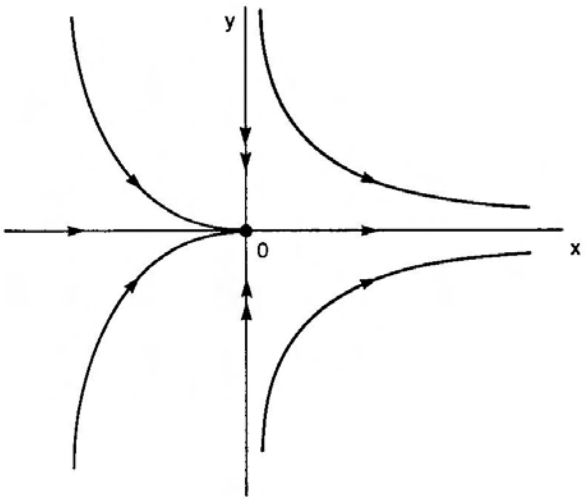

Fig. 9.2.2. A saddle-node in a plane.

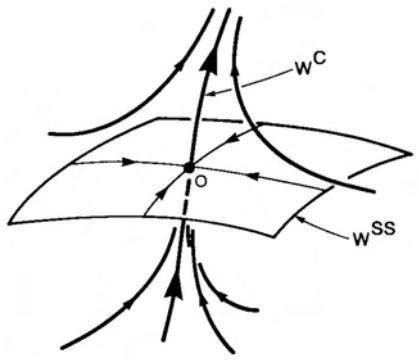

(a)

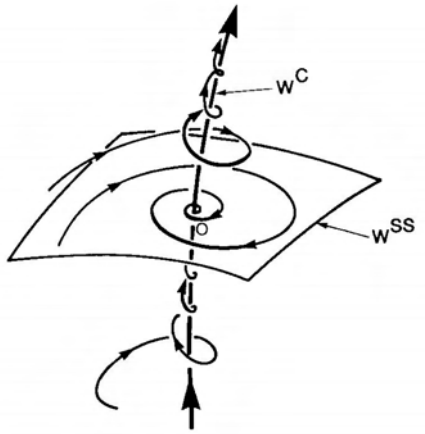

(b)

Fig. 9.2.3. Two R^3-examples of topologically identical saddle-nodes with $l_{2p} \neq 0$; in its restriction to W^{ss} the point O is a stable node (a) or is a stable focus (b).

in Fig. 9.2.4(a). In contrast to the case of a structurally stable node, the convergence here is not exponential.[2]

(3) If the first non-zero Lyapunov value has an odd index number and is positive, i.e. $l_k > 0$, $k = 2p + 1$, then the equilibrium state O has the topological type of a saddle $(n-1, 1)$ (see Sec. 2.5). Here, the unstable

[2]By integrating (9.2.5) we have $x \sim C\|t\|^{-1/2p}$.

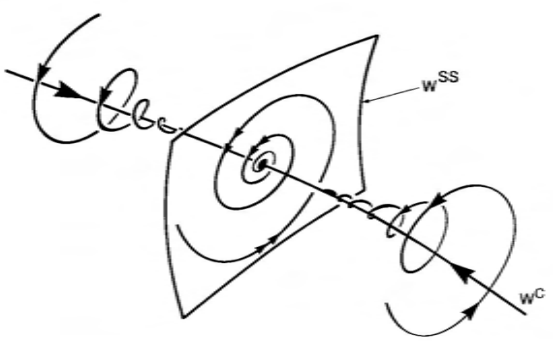

(a)

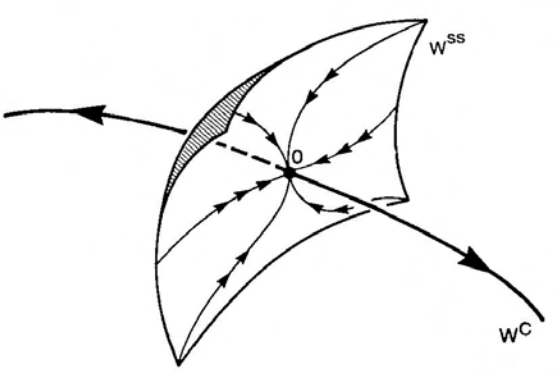

(b)

Fig. 9.2.4. A degenerate equilibrium state with $l_{2p+1} \neq 0$. The center manifold is continued here in both directions. Such a bifurcation called *a pitchfork*, is typical for systems where due to symmetry the first non-zero Lyapunov value at a degenerate equilibrium state is always of an odd order.

manifold of the bifurcating point coincides with W^C, as illustrated in Fig. 9.2.4(b).

Note that in order to calculate the first non-zero Lyapunov value there is no need to reduce the system to the center manifold. If the original system has the form

$$\begin{aligned} \dot{x} &= g(x, y)\,, \\ \dot{y} &= Ay + f(x, y)\,, \end{aligned} \tag{9.2.6}$$

such that $f'(0,0) = 0$ and $g'(0,0) = 0$, the standard routine is as follows. First, write down the system of equations

$$Ay + f(x,y) = 0\,. \tag{9.2.7}$$

As $\det A \neq 0$ and $f(0,0) = 0$, $f'_y(0,0) = 0$, this system can be solved implicitly for y:

$$y = \varphi(x)\,. \tag{9.2.8}$$

The Taylor series of the function $\varphi(x)$ can be found by the method of indeterminate coefficients. Next, one can calculate $g(x,\varphi(x))$. The first non-zero coefficient in the expansion

$$g(x,\varphi(x)) = l_k x^k + \cdots\,, \tag{9.2.9}$$

is the desired first non-zero Lyapunov value.

For the system of second order

$$\begin{aligned}
\dot x = {}& a_{20}x^2 + a_{11}xy + a_{02}y^2 + \cdots = g(x,y),\\
\dot y = {}& -\lambda y + b_{20}x^2 + b_{11}xy + b_{02}y^2 + \cdots = -\lambda y + f(x,y),
\end{aligned}$$

where $\lambda > 0$, the first Lyapunov value is simply equal to a_{20}.

If the linear part is in the general form (with $a\,b \neq 0$)

$$\begin{aligned}
\dot x &= ax + by + g(x,y)\,,\\
\dot y &= cx + dy + f(x,y)\,,
\end{aligned}$$

where $ad - bc = 0$, $a + d < 0$, and the functions f and g start with quadratic terms (as in the previous system), then the formula for calculating l_2 is more complicated:

$$l_2 = a_{20}\cdot bd - a_{11}ad + a_{02}ac - b_{20}b^2 + b_{11}ab - b_{02}a^2$$

Let us show that formula (9.2.9) does give us the Lyapunov value. Indeed, by definition, the Lyapunov value is the first non-zero coefficient of the expansion

$$g(x,\Phi(x)) = l_k x^k + \cdots\,, \tag{9.2.10}$$

where $y = \Phi(x)$ is the equation of the center manifold. The condition of invariance of W^C for the system (9.2.6) is given by

$$A\Phi(x) + f(x, \Phi(x)) = \Phi'(x)g(x, \Phi(x))\,. \tag{9.2.11}$$

By comparing (9.2.7), (9.2.8) and (9.2.11) we find that

$$\varphi(x) - \Phi(x) \sim \Phi'(x)g(x, \Phi(x))\,,$$

i.e. the difference between $\varphi(x)$ and $\Phi(x)$ [and hence the difference between $g(x, \Phi(x))$ and $g(x, \varphi(x))$] is of a higher order of smallness with respect to $g(x, \Phi(x))$. Therefore, the first non-zero terms of the Taylor expansion (9.2.10) and (9.2.9) of the functions $g(x, \Phi(x))$ and $g(x, \varphi(x))$ coincide indeed.

It follows from formula (9.2.9) that if the right-hand side of the system (9.2.6) is analytic, and if all Lyapunov values vanish, then $g(x, \varphi(x)) \equiv 0$. Hence, since $y = \varphi(x)$ is the solution of the system (9.2.7), it follows that the curve $y = \varphi(x)$ is filled out by the equilibrium states of the system (9.2.6). Thus, it is an invariant manifold of this system. Since it is tangent to $y = 0$ at O, it is the center manifold by definition. It follows that for the case under consideration, the system has an analytic center manifold W^C: $y = \varphi(x)$ which consists of equilibrium states as illustrated in Fig. 9.2.5.

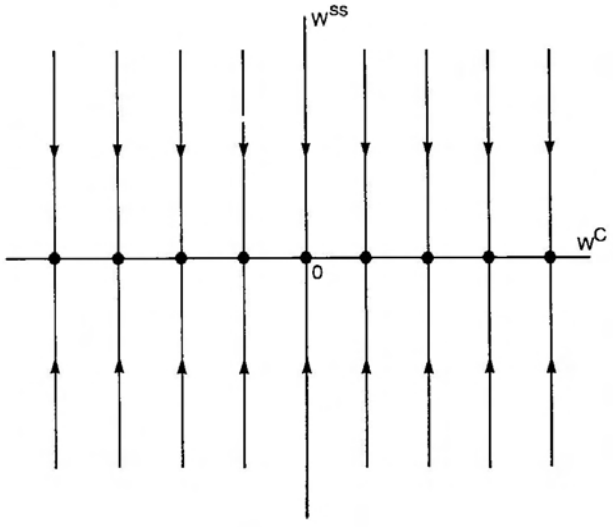

Fig. 9.2.5. A degenerate center manifold composed of equilibrium states.

This is not the case when the system is only smooth but not analytic. For example, a $\mathbb{C}^\infty$-smooth system with the flat right-hand side

$$\begin{aligned}\dot{x} &= \begin{cases} e^{-1/x^2}\,, & x \neq 0\,, \\ 0\,, & x = 0\,, \end{cases} \\ \dot{y} &= -y\,,\end{aligned}$$

has a unique (unstable) equilibrium state all of whose Lyapunov values are zero. Another flat system

$$\begin{aligned}\dot{x} &= \begin{cases} \sin(1/x)\, e^{-1/x^2}, & x \neq 0\,, \\ 0, & x = 0\,, \end{cases} \\ \dot{y} &= -y\,,\end{aligned}$$

has a countable number of isolated equilibrium states accumulating to the origin.

An equilibrium state whose phase portrait cannot be determined by the coefficients of the Taylor expansion (this means that $l_2 = \cdots = l_r = 0$ for $\mathbb{C}^r$-smooth systems, or that all l_i vanish for $\mathbb{C}^\infty$-smooth systems) is called *completely degenerate*, or *infinitely degenerate* in the $\mathbb{C}^\infty$ case.

9.3. The second critical case

Let the equilibrium state at the origin have a pair of purely imaginary eigenvalues $\lambda_{1,2} = \pm i\,\omega$. In this case the restriction of the system on the center manifold W^C is written in the following form

$$\begin{aligned}\dot{x}_1 &= -\omega x_2 + g_1(x_1, x_2)\,, \\ \dot{x}_2 &= \omega x_1 + g_2(x_1, x_2)\,,\end{aligned} \tag{9.3.1}$$

where the functions $g_{1,2}$ vanish at the origin along with their first derivatives.

Let us begin with calculating the normal form for the system (9.3.1). Obviously, there are infinitely many resonant relations of the kind

$$\begin{aligned}\lambda_1 &= (q+1)\,\lambda_1 + q\lambda_2\,, \\ \lambda_2 &= q\lambda_1 + (q+1)\,\lambda_2\,,\end{aligned} \tag{9.3.2}$$

where $q = 1, 2, \dots$. This means that smooth changes of variables cannot, generally speaking, get rid of the monomials $A_q x_1(x_1^2+x_2^2)^q$ and $B_q x_2(x_1^2+x_2^2)^q$ (see Sec. 2.9). Below we show how to nullify the remaining terms up to any finite order.

Lemma 9.1. *For any integer $Q \geq 1$ there exists a polynomial change of variables which transforms the system* (9.3.1) *to*

$$\begin{aligned} \dot{u} &= -\omega v + \sum_{q=1}^{Q} (L_q u - \Omega_q v)(u^2+v^2)^q + o(r^{2Q+1}) \,, \\ \dot{v} &= \omega u + \sum_{q=1}^{Q} (L_q v + \Omega_q u)(u^2+v^2)^q + o(r^{2Q+1}) \,, \end{aligned} \tag{9.3.3}$$

(*where $r = \sqrt{u^2+v^2}$*) *or, in polar coordinates,*

$$\begin{aligned} \dot{r} &= L_1 r^3 + \dots + L_Q r^{2Q+1} + o(r^{2Q+1}) \,, \\ \dot{\theta} &= \omega + \Omega_1 r^2 + \dots + \Omega_Q r^{2Q} + o(r^{2Q}) \,. \end{aligned} \tag{9.3.4}$$

Proof. Let us make the following change of variables

$$z = x_1 + i\, x_2 \,, \quad z^* = x_1 - i\, x_2$$

and rewrite the system in the complex form

$$\begin{aligned} \dot{z} &= \quad i\,\omega z + \sum_{2 \leq p+q \leq 2Q+1} C_{pq} z^p z^{*\,q} + o(|z|^{2Q+1}) \,, \\ \dot{z}^* &= -i\,\omega z^* + \sum_{2 \leq p+q \leq 2Q+1} C^*_{pq} z^{*p} z^q + o(|z|^{2Q+1}) \,, \end{aligned} \tag{9.3.5}$$

where $*$ denotes complex conjugation. This form is more convenient because the matrix of the linear part is diagonal. Moreover, we may neglect the second equation because it follows from the first one.

Let us next make the transformation of variables

$$z = w + \sum_{p,q} \alpha_{pq} w^p w^{*\,q} \,, \qquad 2 \leq p+q \leq 2Q+1 \,, \tag{9.3.6}$$

where α_{pq} are indeterminate coefficients. The equation in the new variables is given by

$$\dot{w} = i\,\omega\,w + \sum_{2\le p+q\le 2Q+1} C'_{pq} w^p w^{*\,q} + o(|w|^{2Q+1})\,. \tag{9.3.7}$$

Let us try to nullify as many coefficients C'_{pq} as possible. By substituting (9.3.6) into (9.3.5) and replacing $\dot{w}$ and $\dot{w}^*$ with their expressions accordingly to (9.3.7), we obtain

$$\begin{aligned}
&\left\{1 + \sum_{p,q} \alpha_{pq}\, p\, w^{p-1} w^{*q}\right\} \cdot \left[i\,\omega w + \sum_{p,q} C'_{pq}\, w^p w^{*q}\right] \\
&\qquad + \quad \sum_{p,q} \alpha_{pq}\, q\, w^p w^{*q-1} \left[-i\ \omega w^* + \sum_{p,q} C'^*_{pq}\, w^{*p} w^q\right] \\
&\qquad = i\,\omega \left[w + \sum_{p,q} \alpha_{pq}\, w^p w^{*q}\right] + \sum_{p,q} C_{pq} (w + \cdots)^p (w^* + \cdots)^q \\
&\qquad + o(|w|^{2Q+1})\,.
\end{aligned}$$

By the coefficients of $w^p\, w^{*q}$ for $p + q = 2$, we obtain

$$i\,\omega\alpha_{pq} p\ w^p w^{*q} + C'_{pq}\, w^p w^{*q} - i\omega\,\alpha_{pq}\, q\ w^p w^{*q} = i\,\omega\,\alpha_{pq} w^p w^{*q} + C_{pq}\, w^p w^{*q}$$

and, consequently

$$C'_{pq} = C_{pq} - i\,\omega\,\alpha_{pq}[p - q - 1]\,. \tag{9.3.8}$$

It is clear that if

$$p \ne q + 1\,, \tag{9.3.9}$$

then letting

$$\alpha_{pq} = \frac{C_{pq}}{i\,\omega(p - 1 - q)} \tag{9.3.10}$$

we have $C'_{pq} = 0$. For $p + q = 2$ the condition (9.3.9) is always fulfilled. Hence, if the coefficients α_{pq} in (9.3.6) are given by (9.3.10), there will be no quadratic terms in the system (9.3.7) when written in the new variables.

By equating the coefficients of $w^p\, w^{*q}$ for $p + q = 3$, we obtain

$$C'_{pq} = C_{pq} - i\,\omega\,\alpha_{pq}[p - q - 1] + \cdots \tag{9.3.11}$$

where the ellipsis denote the terms depending only on those α_{pq} for which $p+q=2$ (we have already found them via (9.3.10)). In this case, for p and q satisfying the condition (9.3.9) we can also find α_{pq} such that in the new variables the coefficients C'_{pq} become zero:

$$\alpha_{pq} = \frac{C_{pq} + \cdots}{i\,\omega(p-1-q)}\,,$$

where the ellipsis has the meaning as above.

The only one "immortal" monomial is the first resonant term $(C_{21}+\cdots)w^2w^*$ $(p=2,\,q=1)$. Since C'_{21} is independent of α_{21}, we can let $\alpha_{21}=0$ in (9.3.6).

For higher values of $(p+q)$, the expression (9.3.11) remains valid, with the understanding that the dots denote the terms depending only on those $\alpha_{p'q'}$ for which $p'+q'<p+q$. Thus, continuing in the same way as above, we can find explicitly the appropriate change of variables that eliminates all monomials with even $(p+q)$, and all non-resonant monomials with odd $(p+q)$. Eventually, only the resonant monomials of type $(C_{q+1,q}+\cdots)w^{q+1}w^{*q}$ survive. Obviously, the procedure can be extended up to any value $(p+q)$.

Finally, Eq. (9.3.7) takes the form

$$\dot w = i\,\omega w + C'_{21}w^2w^* + \cdots + C'_{Q+1,Q}w^{Q+1}w^{*Q} + o(w^{2Q+1})\,. \qquad (9.3.12)$$

Substituting $w = u + i\,v$ yields the desired system (9.3.3) where $L_q = \mathrm{Re}\,C'_{q+1,q}$ and $\Omega_q = \mathrm{Im}\,C'_{q+1,q}$.

The system (9.3.5) or (9.3.4) is *the normal form* for the second critical case. The coefficients L_q are called *the Lyapunov values*. Observe from the above procedure that in order to calculate L_Q one needs to know the Taylor expansion of the Eq. (9.3.1) up to order $p+q=2Q+1$.

Let $L_1=\cdots=L_{k-1}=0$, $L_k\neq 0$. In this case the normal form is given by

$$\dot r = L_k\,r^{2k+1}(1+\varphi(r,\theta))\,,$$
$$\dot\theta = \omega(1+\psi(r,\theta))\,,$$

where φ and ψ tend to zero as $r\to 0$. Having changed the time via

$$dt \to (1+\varphi(r,\theta))^{-1}dt$$

we obtain a new system

$$\begin{aligned} \dot{r} &= L_k\, r^{2k+1}\,, \\ \dot{\theta} &= \omega(1+\cdots)\,, \end{aligned} \tag{9.3.13}$$

which is called *the orbital normal form*.

If $L_k < 0$, then the trajectory spirals to O as $t \to +\infty$, as shown in Fig. 9.3.1. The equilibrium state in this case is called *a stable complex* or *weak focus*. We remark that in contrast to a rough stable focus, here the convergence of the trajectories to O is not exponential. Indeed, it follows from examining system (9.3.13) that

$$r \sim t^{-1/2k}\,, \tag{9.3.14}$$

$$\theta \sim \omega\, t\,. \tag{9.3.15}$$

Here, any trajectory is of the form $r \sim \theta^{-1/2k}$. It is not a logarithmic spiral; in particular, its length tends to infinity as $r \to 0$.

If $L_k > 0$, the origin is an unstable equilibrium state because trajectories starting close to it spiral away as time increases. For the two-dimensional system (9.3.1) the point O is called *an unstable complex* (*weak*) *focus*.

Returning to the original high-order system [see (9.1.1)–(9.1.3)], we observe that if the first non-zero Lyapunov value is negative, then the trajectories

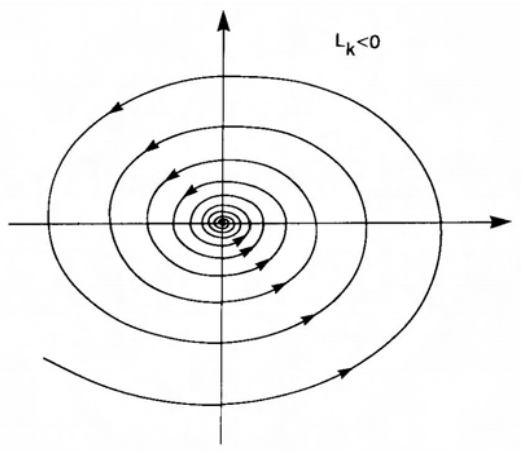

Fig. 9.3.1. A stable ($L_k < 0$) weak focus $\mathbb{R}^2$. When $L_k > 0$, a trajectory leaves a neighborhood of the origin along a counter clock-wise spiral.

behave qualitatively in the same way as those near a rough stable focus as illustrated in Fig. 9.3.2(a).

If the first non-zero Lyapunov value is positive and if all non-critical characteristic exponents $(\gamma_1, \ldots, \gamma_n)$ lie to the left of the imaginary axis in the complex plane, then the equilibrium state is *a complex saddle-focus*, as shown in Fig. 9.3.2(b). Its stable manifold is W^{ss}, and the unstable manifold coincides with the center manifold W^C. The trajectories lying neither in W^{ss} nor W^C pass nearby the equilibrium state.

The formula for the first Lyapunov value expressed in terms of the coefficients of the system (9.3.1) was first derived by Bautin [24]. If we write down the system as

$$\dot{x} = ax + by + P_2(x, y) + P_3(x, y) + \cdots ,$$
$$\dot{y} = cx + dy + Q_2(x, y) + Q_3(x, y) + \cdots ,$$

where $ad - bc > 0$, $a + d = 0$, and

$$P_2(x, y) = a_{20}x^2 + a_{11}xy + a_{02}y^2 ,$$
$$Q_2(x, y) = b_{20}x^2 + b_{11}xy + b_{02}y^2 ,$$
$$P_3(x, y) = a_{30}x^3 + a_{21}x^2y + a_{12}xy^2 + a_{03}y^3 ,$$
$$Q_3(x, y) = b_{30}x^3 + b_{21}x^2y + b_{12}xy^2 + b_{03}y^3 ,$$

then the formula is given by

$$\begin{aligned} L_1 = -\frac{\pi}{4b\omega^3}\{&[ac(a_{11}^2 + a_{11}b_{02} + a_{02}b_{11}) + ab(b_{11}^2 + a_{20}b_{11} + a_{11}b_{20})] \\ &+ c^2(a_{11}a_{02} + 2a_{02}b_{02}) - 2ac(b_{02}^2 - a_{20}a_{02}) - 2ab(a_{20}^2 - b_{20}b_{02}) \\ &- b^2(2a_{20}b_{20} + b_{11}b_{20}) + (bc - 2a^2)(b_{11}b_{02} - a_{11}a_{20})] \\ &- (a^2 + bc)[3(cb_{03} - ba_{30}) + 2a(a_{21} + b_{12}) + (ca_{12} - b_{21}b)]\} , \end{aligned}$$

where $\omega^2 = ad - bc$.

To calculate L_1 in the high-dimensional case one must first derive a system on the center manifold with an accuracy up to terms of third order, and then

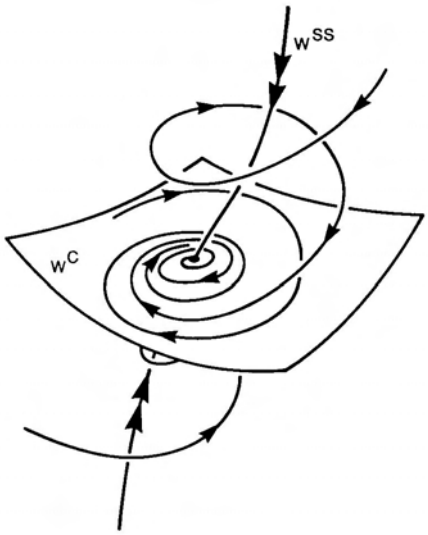

(a)

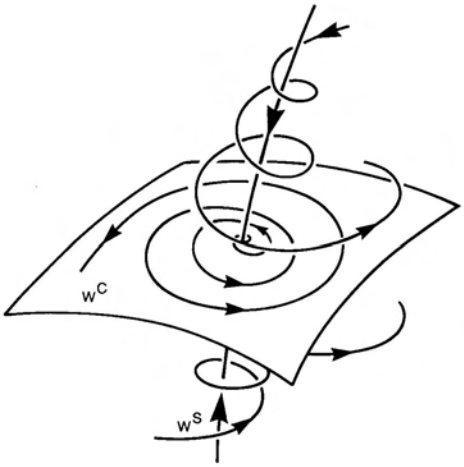

(b)

Fig. 9.3.2. Two opposite situations in $\mathbb{R}^3$ are depicted. When $L_k < 0$ the equilibrium state yet preserves its stability on the stability boundary (a); when $L_k > 0$ the stable equilibrium state becomes an unstable focus on W^C, and, in a global view, a saddle-focus whose stable manifold W^s is W^{ss} (b).

calculate L_1 using the above formula. In cases where L_1 vanishes, the calculation of the second Lyapunov value L_2 requires the reconstruction of the center manifold with an accuracy up to the next subsequent terms of odd order, i.e. of fifth order, etc.

We note that by rescaling the r-variable in (9.3.13), the value L_k can be made equal to one in absolute value. Meanwhile, it is obvious that the sign (as well as the number) of the first non-zero Lyapunov value is not altered by non-singular changes of variables and time. The sign determines whether the given equilibrium state is stable or not, whereas the number determines the speed of convergence of the trajectories to zero [see (9.3.14)].

For the case of all zero Lyapunov values the trajectory behavior can be described only in the analytic case.

Theorem 9.3. *If all Lyapunov values are equal to zero, then the associated analytic system has an analytic invariant (center) manifold which is filled with closed trajectories around the origin, as shown in Fig.* 9.3.3. *On the center manifold the system has a holomorphic integral of the type*

$$U = \frac{x_1^2}{2} + \frac{\omega^2 x_2^2}{2} + V(x_1, x_2)\,,$$

where the function V starts with cubic terms.

Recall that an equilibrium state where all trajectories in its neighborhood are closed, is called *a center*. A center is stable in the sense of Lyapunov but it is not asymptotically stable. An example of a system with a center comes from a rather broad class of systems given by

$$\begin{aligned} \dot{x}_1 &= -\,\omega x_2\,, \\ \dot{x}_2 &= \quad \omega x_1 + f(x_1)\,, \end{aligned} \tag{9.3.16}$$

where $f(0) = f'(0) = 0$. It is easy to see that the system (9.3.16) possesses a first integral (energy integral)

$$U = \frac{x_1^2}{2} + \frac{\omega^2 x_2^2}{2} + \int_0^{x_1} f(\xi) d\xi\,.$$

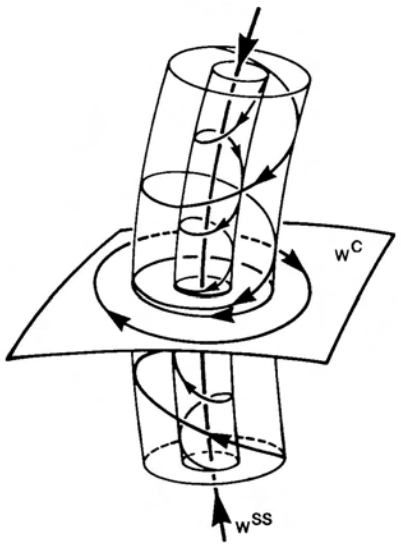

Fig. 9.3.3. When all Lyapunov values vanish in an analytical system, the equilibrium state is a center on W^C. In $\mathbb{R}^3$, its extended neighborhood is foliated by invariant cylinders.

In the $\mathbb{C}^\infty$ case, the origin is not necessarily a center if all Lyapunov values vanish. For example, in the system

$$\dot r = \begin{cases} e^{-1/r^2}, & r \neq 0\,, \\ 0, & r = 0\,, \end{cases}$$

$$\dot\theta = \omega\,,$$

the equilibrium state is asymptotically stable. In contrast, in the system

$$\dot r = \begin{cases} e^{-1/r^2}\sin(1/r), & r \neq 0\,, \\ 0, & r = 0\,, \end{cases}$$

$$\dot\theta = \omega\,,$$

a small neighborhood of the origin contains infinitely many limit cycles.

Chapter 10

THE BEHAVIOR OF DYNAMICAL SYSTEMS ON STABILITY BOUNDARIES OF PERIODIC TRAJECTORIES

10.1. The reduction of the Poincaré map. Lyapunov functions

Unlike the case of equilibrium states, the stability boundaries of periodic trajectories may be of two different types:

(1) The periodic trajectory exists on the stability boundary. Among its multipliers, there is at least one on the unit circle.
(2) The periodic trajectory disappears on the stability boundary.

In this chapter, we will focus on the stability boundaries of the first type[1]. Since the periodic trajectory persists in this case at the critical moment, we can construct a small cross-section and our problem reduces to the study of a Poincaré map. In some suitable coordinates on the cross-section, the Poincaré map can be written in the form

$$\begin{aligned} \bar{x} &= Bx + G(x, y)\,, \\ \bar{y} &= Ay + f(x, y)\,, \end{aligned} \tag{10.1.1}$$

[1]The boundaries of the second type correspond to the merging of a periodic orbit into an equilibrium state (Sec. 11.5) or to a homoclinic loop, or a blue-sky catastrophe (Chaps. 12 and 13).

where $x = (x_1, \ldots, x_m)$, $m \neq 0$, $y = (y_1, \ldots, y_n)$, f and g belong to the class $\mathbb{C}^r$, $r \geq 1$, and vanish at the origin along with their first derivatives. The characteristic equation of the matrix B

$$\det(B - \rho I) = 0$$

has m roots $\rho_1, \ldots, \rho_m$ whose absolute values are all equal to 1. The roots $\rho_{m+1}, \ldots, \rho_{n+m}$ of the characteristic equation

$$\det(A - \rho I) = 0$$

of the matrix A lie strictly inside the unit circle.

In this chapter, we restrict our consideration to the following three principal cases:

(1) Only one multiplier lies on the unit circle and is equal to one $(m = 1,\ \rho_1 = 1)$
(2) Only one multiplier lies on the unit circle and is equal to minus one $(m = 1,\ \rho_1 = -1)$
(3) A pair of multipliers (complex-conjugate) lies on the unit circle $(m = 2,\ \rho_{1,2} = e^{\pm i\,\omega},\ 0 < \omega < \pi)$.

If the characteristic equation

$$\Delta(\rho) = \rho^{m+n} + b_1 \rho^{m+n-1} + \cdots + b_{m+n} = 0$$

associated with the matrix $\begin{pmatrix} B & 0 \\ 0 & A \end{pmatrix}$ is given, then the first and the second critical cases are selected by the conditions $\Delta(1) = 0$ and $\Delta(-1) = 0$, respectively, or

$$1 + b_1 + \cdots + b_{m+n} = 0$$

and

$$(-1)^{m+n} + b_1(-1)^{m+n-1} + \cdots + b_{m+n} = 0\,.$$

In addition one must ensure that the other roots of the characteristic equation lie inside the unit circle.

To derive the condition which corresponds to the third case, let us make a change of variables $\rho = (1 + \lambda)/(1 - \lambda)$. The values of ρ inside the unit circle correspond to the values of λ in the open left-half plane. Those of ρ that lie

on the unit circle correspond to λ on the imaginary axis. Therefore, we have the third critical case when the polynomial

$$\Delta\left(\frac{1+\lambda}{1-\lambda}\right)(1-\lambda)^{m+n} \equiv a_0\lambda^{m+n} + a_1\lambda^{m+n-1} + \cdots + a_{m+n} \qquad (10.1.2)$$

has exactly two purely imaginary roots, and the rest lies to the left of the imaginary axis. The associated conditions for the coefficients a_i are given in Chap. 9 (when $a_0 = 1$). In general, the conditions are

$$\Delta_{n-1} = 0\,, \quad a_0 a_n > 0\,, \quad a_0^k\,\Delta_k > 0\,, \quad k = 1, \ldots, n-2\,,$$

where Δ_k are the Routh–Hurwitz determinants of the polynomial (10.1.2).

For three-dimensional systems (i.e. for two-dimensional Poincaré maps) the characteristic equation is

$$\rho^2 + b_1\rho + b_2 = 0$$

and the stability boundaries are determined as follows:

- 1st critical case ($\rho = 1$)

$$b_1 + b_2 = -1\,, \quad |b_2| < 1\,; \qquad (10.1.3)$$

- 2nd critical case ($\rho = -1$)

$$b_1 = b_2 + 1\,, \quad |b_2| < 1\,; \qquad (10.1.4)$$

- 3rd critical case ($\rho = e^{\pm i\,\omega}$)

$$b_2 = 1\,, \quad |b_1| < 2\,. \qquad (10.1.5)$$

To derive the last condition let us substitute $\rho = e^{i\,\omega}$ into the characteristic equation and obtain

$$e^{2i\,\omega} + b_1 e^{i\,\omega} + b_2 = 0\,,$$

or

$$\begin{cases} \cos 2\omega + b_1 \cos\omega + b_2 = 0 \\ \qquad \sin 2\omega + b_1 \sin\omega = 0\,. \end{cases}$$

We find that $b_1 = -2\cos\omega$, $b_2 = -\cos 2\omega + 2\cos^2\omega$, and (10.1.5) follows.

If a system is represented by differential equations in $\mathbb{R}^3$, then the product of the multipliers of the periodic trajectory must be positive, i.e. $b_2 > 0$. It

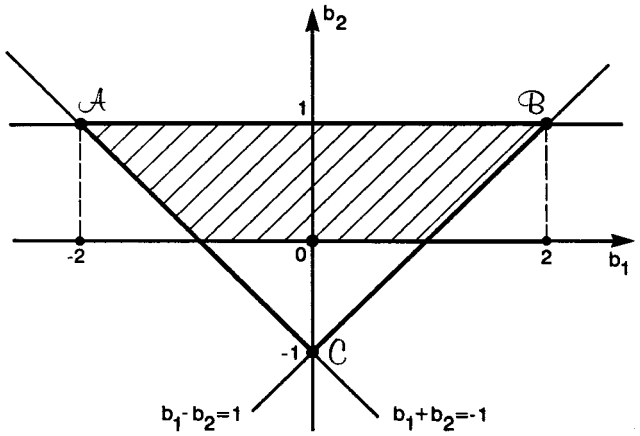

Fig. 10.1.1. The stability region of the two-dimensional diffeomorphism.

follows from (10.1.3)–(10.1.5) that in the (b_1, b_2)-plane the stability region of a periodic trajectory of a three-dimensional system has the form of a trapezoid, in contrast to the stability region of a fixed point of an arbitrary two-dimensional map, which has the form of a triangle, as shown in Fig. 10.1.1. The cases of multiple multipliers $\rho_1 = \rho_2 = 1$ and $\rho_1 = \rho_2 = -1$ correspond to the two apices A and B of the triangle, respectively, and the case $\rho_1 = 1$, $\rho_2 = -1$ corresponds to the apex C.

As shown in Chap. 5, the critical fixed point $O(0, 0)$ lies in an invariant $\mathbb{C}^r$-smooth center manifold W^C defined by the equation $y = \Phi(x)$, where Φ vanishes at the origin along with its first derivative. Moreover, the following reduction theorem holds:

In a neighborhood of the fixed point O there exists a change of variables of class $\mathbb{C}^{r-1}$ such that the Poincaré map in the new variables assumes the standard form

$$\bar{x} = Bx + g(x)\,, \tag{10.1.6}$$

$$\bar{y} = [A + F(x, y)]\, y\,, \tag{10.1.7}$$

where $g(x) \equiv G(x, \Phi(x)) \in \mathbb{C}^r$, $F(x, y) \in \mathbb{C}^{r-1}$, $F(0, 0) = 0$.

In the new variables the center manifold W^C is defined by $y = 0$, and the strong stable manifold W^{ss} is defined by $x = 0$.

The reduction theorem allows us to study the dynamics of the critical variables x independently of the y-variables near the fixed point. As for the y-subspace, the dynamics is relatively simple: since the x-variable is small in the norm, the function F in (10.1.3) is also small, and hence the following estimate holds

$$\|\bar{y}\| \le \rho\|y\|\,,$$

where $1 > \rho > \max|\rho_j|$ $(j = m+1,\dots,m+n)$. This means that every trajectory converges exponentially to the center manifold.

Thus, the stability of the fixed point of the original map (10.1.1) is equivalent to the stability of the fixed point of the map (10.1.6) in the center manifold, which we state formally as follows

Theorem 10.1. *If the fixed point O is Lyapunov stable in the center manifold W^C, then it is also stable for the original map* (10.1.1). *If the fixed point is asymptotically stable in the center manifold, then the fixed point of the original system is also asymptotically stable. If the fixed point is unstable in the center manifold W^C, then it is unstable for the original map.*

The basic tool for studying stability of critical fixed points is the Lyapunov functions.

Definition 10.1. *A continuous function $V(x)$ defined in some neighborhood D of O, is called the Lyapunov function for system* (10.1.6) *if it satisfies the following conditions*

$$(1)\ V(0) = 0\,; \tag{10.1.8}$$

$$(2)\ V(x) > 0\,, \qquad \text{if } x \ne 0\,; \tag{10.1.9}$$

$$(3)\ V(\bar{x}) \le V(x)\,, \quad \text{for } x \ne 0\,. \tag{10.1.10}$$

Theorem 10.2. *If there exists a function $V(x)$ satisfying conditions* (10.1.8)–(10.1.10), *then the fixed point is Lyapunov stable. Furthermore, if the inequality* (10.1.10) *holds strictly for all $x \ne 0$, then all positive semi-trajectories in D tend to O, i.e. the point O is asymptotically stable.*

We omit the proof because it is identical to the proof of Theorem 9.2 on the stability of equilibrium states.

10.2. The first critical case

In the case where the only one multiplier (+1) lies on the unit circle, the Poincaré map has the form

$$\begin{aligned} \bar{x} &= x + g(x)\,, \\ \bar{y} &= [A + F(x,y)]\,y\,, \end{aligned} \tag{10.2.1}$$

where x is a scalar, and

$$g(0) = g'(0) = 0\,, \quad F(0,0) = 0\,.$$

The center manifold W^C is one-dimensional, so the map in W^C can be written in the form

$$\bar{x} = x + g(x) = x + l_2 x^2 + l_3 x^3 + \cdots\,. \tag{10.2.2}$$

The coefficients $l_2, \ldots, l_k$ of the Taylor expansion of the function $g(x)$ at O are called *the Lyapunov values*.

Let us investigate the behavior of trajectories of this map. Let k be the number of the first non-zero Lyapunov value: $l_2 = \cdots = l_{k-1} = 0$, $l_k \neq 0$. Then, the map (10.2.2) assumes the form

$$\bar{x} = x + l_k x^k (1 + o(1))\,. \tag{10.2.3}$$

If k is even, $k = 2p$, then the fixed point O is unstable. The behavior of the trajectories near O is described by the Lamerey diagram in Fig. 10.2.1(a). If $l_k > 0$, then the positive semi-trajectory $\{x_j\}_{j=0}^{j=\infty}$ of a point x_0 to the left of O tends to O as $j \to +\infty$. For any point x_0 to the right of O there exists $J > 0$ such that x_J gets out of a neighborhood of O. If $l_k < 0$ (this case reduces to the previous one by mapping $x \to -x$), then the trajectories starting with positive x tend to O as $j \to +\infty$, but from the side of negative x the point O is unstable, see Fig. 10.2.1(b).

If k is odd, $k = 2p + 1$, then the map has the form

$$\bar{x} = x + l_{2p+1} x^{2p+1} (1 + o(1))\,. \tag{10.2.4}$$

If $l_{2p+1} < 0$, then $|\bar{x}| = |x|(1 - |l_{2p+1}|\, x^{2p}(1 + o(1))) < |x|$ at $x \neq 0$. This means that $|x|$ is a Lyapunov function, so the fixed point O is asymptotically stable, as shown in Fig. 10.2.2(a). On the contrary, if $l_{2p+1} > 0$, then $|\bar{x}| > |x|$, and O is unstable, as shown in Fig. 10.2.2(b).

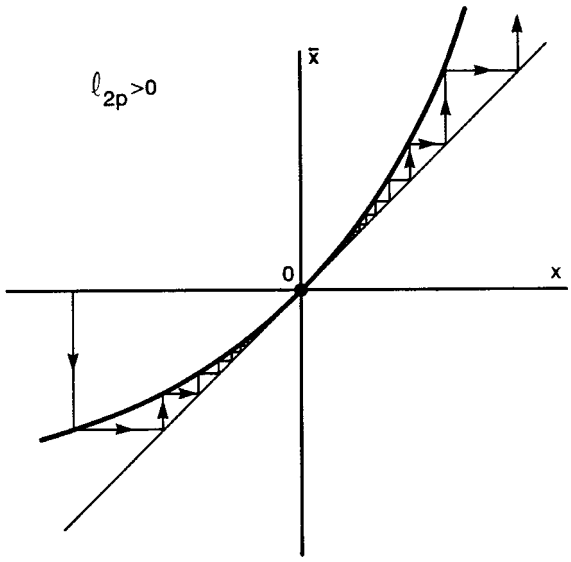

(a)

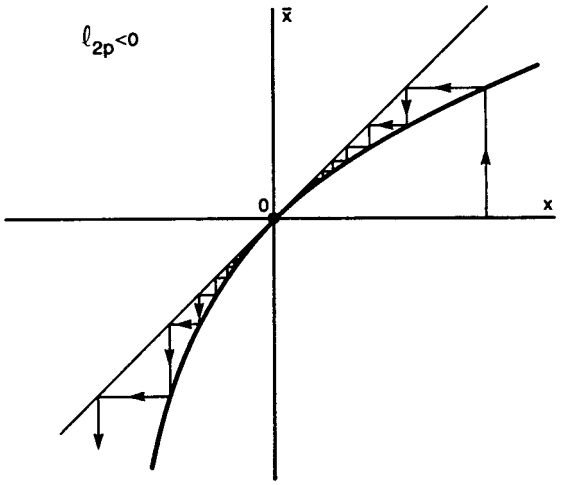

(b)

Fig. 10.2.1. The Lamerey diagrams in the cases where $l_{2p} > 0$ (a) and $l_{2p} < 0$ (b).

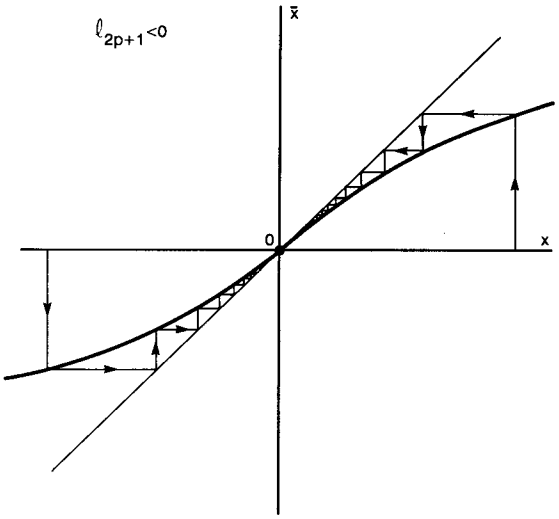

(a)

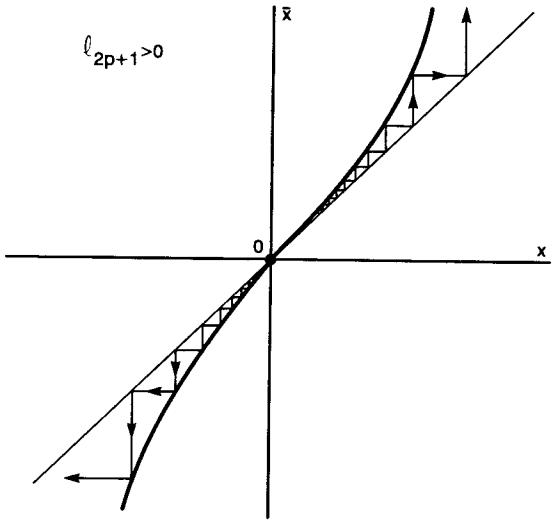

(b)

Fig. 10.2.2. The fixed point at the origin is stable when $l_{2p+1} < 0$ (a) and repelling when $l_{2p+1} > 0$ (b).

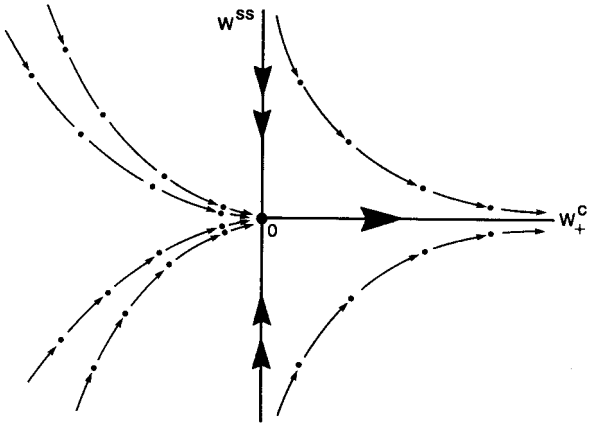

Fig. 10.2.3. An iterated saddle-node of a two-dimensional map.

The trajectory behavior of the original map (10.2.1) is as follows.

Case 1. $l_2 = \cdots = l_{2p-1} = 0$, $l_{2p} \neq 0$.

The strong stable manifold $W^{ss} : x = 0$ subdivides a neighborhood of O into the node region and the saddle region. In the node region all trajectories tend to O along the leading direction $y = 0$ [because the y-coordinate decreases exponentially while the x-coordinate decreases slower than any geometrical progression: $|\bar{x}| > (1-\varepsilon)|x|$ by virtue of (10.2.3)]. In the saddle region all trajectories, except for those on the ray $W_+^C : \{y = 0,\ x \geq 0\}$, leave a neighborhood of O over a finite number of iterations (see Fig. 10.2.3). The trajectories in W_+^C tend to O as $j \to -\infty$. Thus, W_+^C is *the local unstable manifold* of O.[2] Like a corresponding critical equilibrium state in the case of differential equations, the fixed point O under consideration is called *a saddle-node*: *simple* if $p = 1$ (i.e. $l_2 \neq 0$), and *complex* (or *degenerate*) if $l_2 = 0$.

We can now describe the behavior of trajectories in a small neighborhood of the periodic trajectory L to which the fixed point O of the Poincaré map corresponds. In the two-dimensional case the behavior of trajectories is shown in Fig. 10.2.4, and a higher-dimensional case in Fig. 10.2.5. The invariant strongly stable manifold W_L^{ss} (the union of the trajectories which start from the points of W_O^{ss} on the cross-section) partitions a neighborhood of L into a node and a saddle region. In the node region all trajectories wind towards L

[2]Note that this is a manifold with the boundary (which is O).

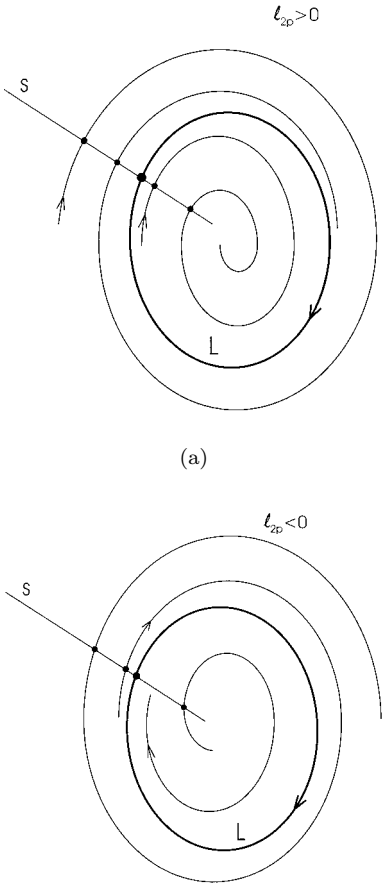

Fig. 10.2.4. Saddle-node periodic orbits in $\mathbb{R}^2$: (a) the cycle L is stable in the interior region and unstable in the exterior region. When $l_{2p} < 0$, it is attractive for the point inside it, and repelling for outer trajectories (b).

as $t \to +\infty$ so that L is orbitally stable in this region. In the saddle region every trajectory leaves the neighborhood of L over a finite time, except for trajectories in the local unstable manifold $W^u_{\text{loc}}(L)$ which tend to L as $t \to -\infty$. Such a periodic trajectory is also called *a saddle-node*. The terms *semi-stable* or *p-multiple* (*double* when $l_2 = 0$) *limit cycle* are more typical for the planar case.

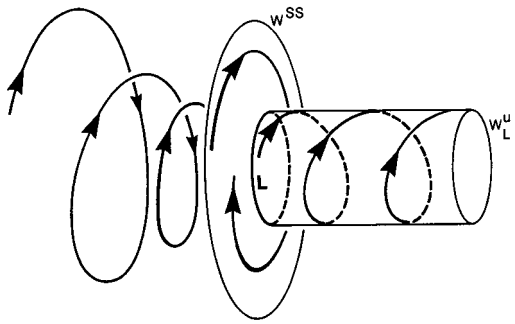

Fig. 10.2.5. A saddle-node periodic orbit in $\mathbb{R}^3$. Its strongly stable invariant manifold separates two domains, a node one where the periodic orbit is stable, and a saddle domain. The unstable manifold W^u_L of the orbit is homeomorphic to a semi-cylinder. We will need this picture many times.

Case 2. $l_2 = \cdots = l_{2p} = 0$, $l_{2p+1} < 0$.

Here the fixed point is asymptotically stable. All trajectories apart belonging to the non-leading manifold W^{ss}: $x = 0$ enter O along the leading direction $y = 0$, as shown in Fig. 10.2.6(a). The behavior of trajectories in a neighborhood of the limit cycle corresponding to the critical fixed point is shown in Fig. 10.2.7(a). The high-dimensional picture looks like a rough stable periodic trajectory but there is no exponential convergence of trajectories to L in the critical case.

Case 3. $l_2 = \cdots = l_{2p} = 0$, $l_{2p+1} > 0$.

Such a critical fixed point is called *a complex* (*degenerate*) *saddle*. Its stable manifold is $W^c : y = 0$, and the unstable manifold W^u is given by $x = 0$, as shown in Fig. 10.2.6(b). Here, in the critical case, the trajectories behave qualitatively identical to those nearby the rough unstable cycle shown in Fig. 10.2.7(b).

If all Lyapunov values vanish and the map is analytic, then the center manifold is analytic too and it consists of fixed points (Fig. 10.2.8). Observe that if the map has the form

$$\begin{aligned} \bar{x} &= x + g(x, y)\,, \\ \bar{y} &= Ay + f(x, y)\,, \end{aligned} \tag{10.2.5}$$

then the first non-zero Lyapunov value is the first non-zero coefficient of the Taylor expansion of $g(x, \phi(x))$, where $y = \phi(x)$ is the solution of the

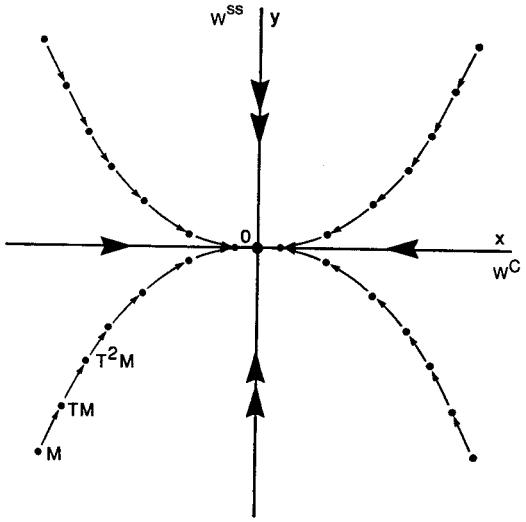

(a)

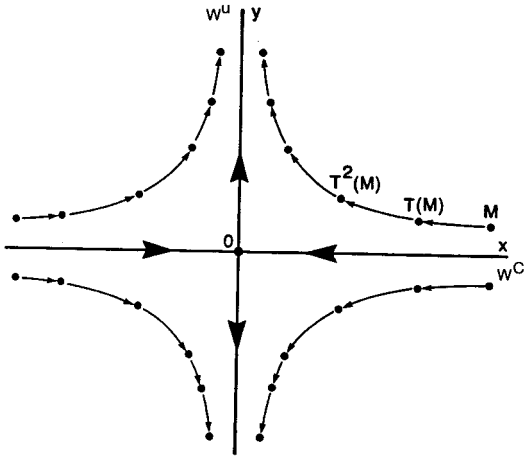

(b)

Fig. 10.2.6. Geometrically, there is no difference between a critical node $l_{2p} < 0$ (a) and a rough stable node. However, a quantitative comparison can be made with respect to the rate of convergence of nearby trajectories to the origin. A similar observation also applies to a rough saddle fixed point and a critical saddle with $l_{2p+1} > 0$ (b).

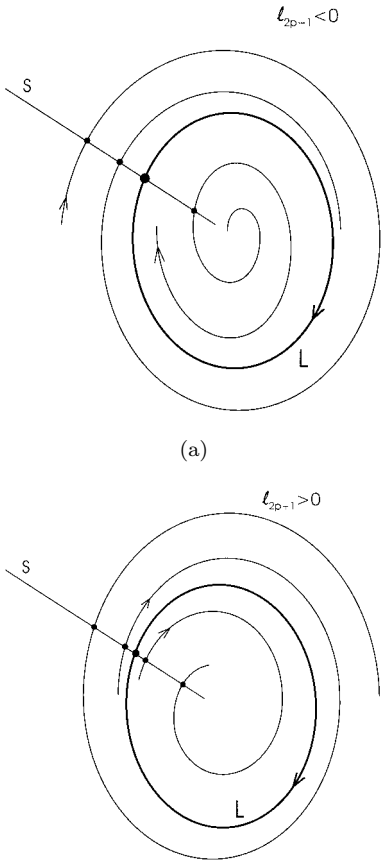

Fig. 10.2.7. In case (a) the bifurcating limit cycle is stable if $l_{2p+1} < 0$ and is repelling if $l_{2p+1} > 0$ (b).

equation

$$Ay + f(x, y) = 0\,. \tag{10.2.6}$$

Hence if all Lyapunov values vanish, then it follows from the analyticity of f that

$$f(x, \phi(x)) \equiv 0\,. \tag{10.2.7}$$

From (10.2.5)–(10.2.7) we can conclude that the analytic curve $y = \phi(x)$ consists entirely of fixed points and, therefore, is an invariant (center) manifold.

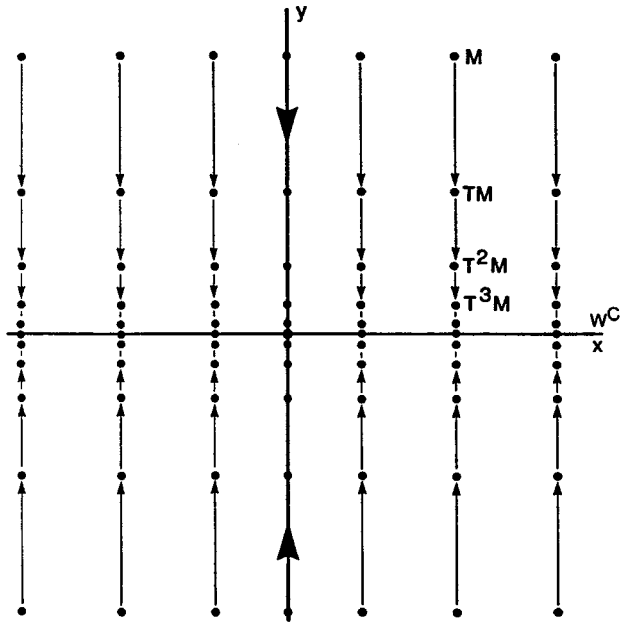

Fig. 10.2.8. The center manifold W^C filled out by fixed points.

A leaf of the stable invariant foliation passes through every fixed point $M \in W^C$ (see Chap. 5). It is obvious that each leaf is the stable manifold W^{ss}_M of the point M; the trajectories in the leaf converge exponentially to M as $j \to +\infty$.

In the non-analytic case, it is hard to make any general statement concerning the dynamics of the map when all Lyapunov values are zero (the fixed point is then said to be *completely degenerate*, or *infinitely degenerate*).[3] For example, for the map

$$\bar{x} = x + \begin{cases} x\, e^{-1/x^2}\,, & x \neq 0\,, \\ 0\,, & x = 0\,, \end{cases}$$

$$\bar{y} = y/2\,,$$

[3]More precisely, a fixed point of a $\mathbb{C}^r$-smooth map is *completely degenerate* if $l_2 = \cdots = l_r = 0$ and a fixed point of a $\mathbb{C}^\infty$-map is called *infinitely degenerate* if the whole set of l_i vanishes.

the origin is a saddle, whereas for the map

$$\bar{x} = x + \begin{cases} \sin(1/x)\, e^{-1/x^2}\,, & x \neq 0\,, \\ 0\,, & x = 0\,, \end{cases}$$
$$\bar{y} = y/2\,,$$

it is stable but not asymptotically.

Finally, we emphasize that infinitely degenerate fixed points are quite common. In fact, (see Gonchenko *et al.* [62] for a survey) in the space of smooth dynamical systems of dimension three or higher there are regions, called Newhouse regions, where systems with infinitely degenerate periodic trajectories are dense everywhere. Note that these regions exist near any system with a single non-degenerate (quadratic) homoclinic tangency, which in turn is a characteristic phenomenon for almost any known model with a complex (chaotic) behaviour. Summarizing, we may conclude that nearly any dynamical model with complex behavior possesses regions in the parameter space where an arbitrarily small perturbation of the system may produce infinitely degenerate periodic orbits (may be of very large periods).

10.3. The second critical case

In this case the Poincaré map in the standard form is given by

$$\begin{aligned} \bar{x} &= -x + g(x)\,, \\ \bar{y} &= [A + f(x,y)]\, y\,, \end{aligned} \tag{10.3.1}$$

where x is a scalar variable, all eigenvalues of A are strictly inside the unit circle, and the functions f and g are such that

$$g(0) = g'(0) = 0\,, \quad f(0,0) = 0\,.$$

Let us consider the map T^C on the center manifold W^C:

$$\bar{x} = -x + a_2 x^2 + a_3 x^3 + \cdots\,. \tag{10.3.2}$$

The multiplier ρ is equal to -1. Therefore, the resonant relations are

$$\rho = \rho^{2p+1}\,.$$

Since the even powers of x are not resonant, it follows that the corresponding terms up to any finite order can be eliminated by a finite number of smooth changes of variables (see Sec. 3.13). As a result the map is led to the normal form

$$\bar{\xi} = -\xi(1 + l_1\xi^2 + \cdots + l_p\xi^{2p} + \cdots)\,, \tag{10.3.3}$$

where the coefficients l_j are the Lyapunov values. The first coefficient is given by the formula

$$l_1 = a_2^2 + a_3\,.$$

The dynamics of trajectories of the map T^C depends on the first non-zero Lyapunov value. If $l_k \neq 0$ and all previous $l_j = 0$ for $j < k$, then the map assumes the form

$$\bar{\xi} = -\xi(1 + l_k\xi^{2k} + \cdots)\,. \tag{10.3.4}$$

It follows that if $l_k < 0$, then the fixed point O at the origin is asymptotically stable (because $|\bar{\xi}| < |\xi|$ for $\xi \neq 0$, i.e. $|\xi|$ is a Lyapunov function). If $l_k > 0$, the point O is unstable. Figures 10.3.1(a) and (b) show the associated Lamerey diagrams for negative and positive values of l_k, respectively.

Observe that the second iteration of the map (10.3.4)

$$\bar{\bar{\xi}} = \xi + 2l_k\xi^{2k+1} + \cdots \tag{10.3.5}$$

has the same form as the map considered in the previous section (Cases 2 and 3).

As for the original map (10.3.1) the fixed point O is asymptotically stable when $l_k < 0$ and is a saddle when $l_k > 0$. In the latter case the stable and unstable manifolds of O are the manifolds W^{ss} and W^C, respectively. In terms of the Poincaré map of the system of differential equations, the corresponding periodic trajectory L is stable when $l_k < 0$, or a saddle when $l_k > 0$. Note that in the saddle case the two-dimensional unstable manifold $W^C(L)$ is, in a neighborhood of the periodic trajectory, a Möbius band.

If all Lyapunov values are equal to zero and the system is analytic, then the center manifold is also analytic, and all points on it, except O, are periodic of period two. This means that for the system of differential equations there exists a non-orientable center manifold which is a Möbius band with the cycle L as its median and which is filled in by the periodic orbits of periods close to the double period of L (see Fig. 10.3.2).

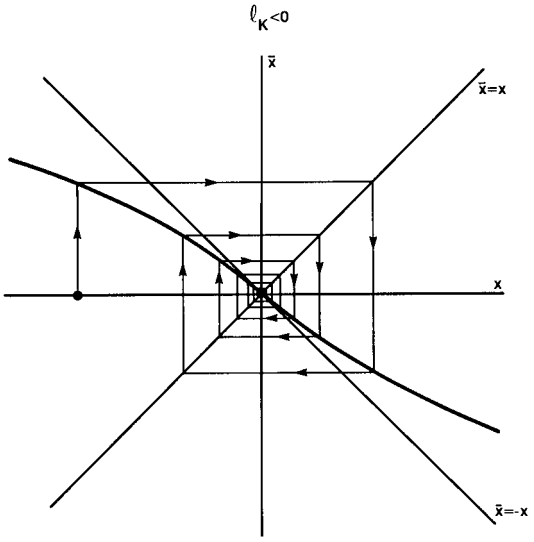

(a)

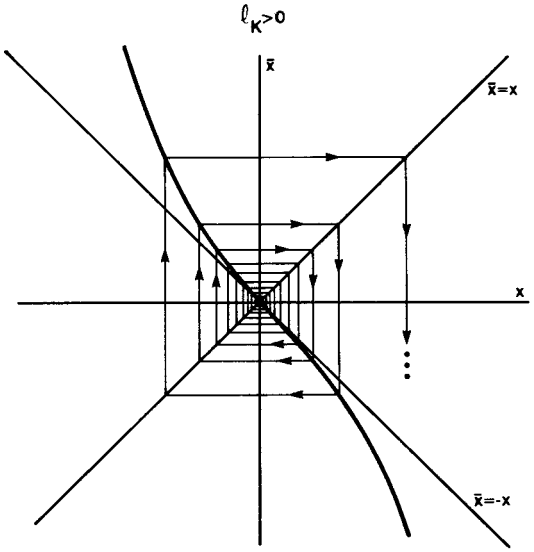

(b)

Fig. 10.3.1. Lamerey spirals: The origin stable when $l_k < 0$ (a) and unstable when $l_k > 0$ (b).

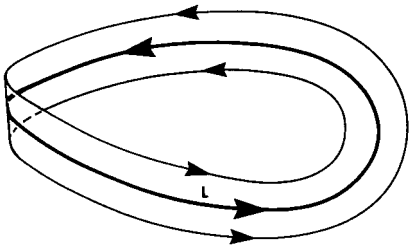

Fig. 10.3.2. The center manifold of the primary periodic orbit L of an analytic system is a Möbius strip filled densely by periodic orbits of double period when all Lyapunov coefficients vanish.

If the map is of class $\mathbb{C}^{2r+1}$, where $1 \leq r \leq \infty$, and if all Lyapunov values $l_1, \ldots, l_r$ vanish, the fixed point O is *completely degenerate* or *infinitely degenerate* when $r = \infty$.

We will now present an algorithm for calculating the first non-zero Lyapunov value for maps which are not reduced to the standard form. First we write the map in the form

$$\begin{aligned} \bar{x} &= -x + g(x, y)\,, \\ \bar{y} &= Ay + f(x, y)\,, \end{aligned} \tag{10.3.6}$$

where

$$f(0,0) = 0\,, \quad f'(0,0) = 0\,, \quad g(0,0) = 0\,, \quad g'(0,0) = 0$$

and then consider its second iteration

$$\begin{aligned} \bar{\bar{x}} &= x + \tilde{g}(x, y)\,, \\ \bar{\bar{y}} &= A^2 y + \tilde{f}(x, y)\,, \end{aligned}$$

where

$$\begin{aligned} \tilde{g}(x, y) &\equiv -g(x, y) + g(-x + g(x, y),\ Ay + f(x, y))\,, \\ \tilde{f}(x, y) &\equiv Af(x, y) + f(-x + g(x, y),\ Ay + f(x, y))\,. \end{aligned}$$

Let us represent y from the implicit equation

$$A^2 y + \tilde{f}(x, y) = 0$$

as $y = \tilde{\psi}(x)$. Then, the desired Lyapunov value is equal to one-half of the first coefficient of the Taylor expansion of the function $\tilde{g}(x, \tilde{\psi}(x))$:

$$\tilde{g}(x, \tilde{\psi}(x)) = 2l_p\, x^{2p+1} + \cdots .$$

10.4. The third critical case. Weak resonances

Let us suppose that two multipliers of the periodic orbit are complex-conjugate and lie on the unit circle. In this case the Poincaré map assumes the form

$$\begin{aligned} \bar{x}_1 &= x_1 \cos\omega - x_2 \sin\omega + g_1(x_1, x_2)\,, \\ \bar{x}_2 &= x_1 \sin\omega + x_2 \cos\omega + g_2(x_1, x_2)\,, \\ \bar{y} &= (A + f(x_1, x_2, y))y\,, \end{aligned} \tag{10.4.1}$$

where $0 < \omega < \pi$, and all eigenvalues of A lie inside the unit circle. The center manifold here is two-dimensional and the map on it is defined by the first two equations in (10.4.1):

$$\begin{aligned} \bar{x}_1 &= x_1 \cos\omega - x_2 \sin\omega + g_1(x_1, x_2)\,, \\ \bar{x}_2 &= x_1 \sin\omega + x_2 \cos\omega + g_2(x_1, x_2)\,, \end{aligned} \tag{10.4.2}$$

where $g_{1,2}$ vanish at the origin along with their first derivatives.

The multipliers of the fixed point at the origin are ($\rho_1 = e^{i\omega}, \rho_2 = e^{-i\omega}$). Like in the case of the equilibrium state with a pair of purely imaginary characteristic exponents (see Sec. 9.3), there exist resonances of the kind:

$$\rho_1 = \rho_1^{p+1}\rho_2^p \ (\rho_2 \equiv \rho_1^* = \rho_2^{p+1}\rho_1^p)\,. \tag{10.4.3}$$

Therefore, one can expect that the following terms will appear in the right-hand side of the normal form:

$$\begin{aligned} &(L_p x_1 - \Omega_p x_2)\ (x_1^2 + x_2^2)^p\,, \\ &(L_p x_2 + \Omega_p x_1)\ (x_1^2 + x_2^2)^p\,. \end{aligned} \tag{10.4.4}$$

We will call the resonant relations (10.4.4) *trivial*. If, an addition, ω is commensurable to 2π, i.e.

$$\omega = \frac{2\pi M}{N}\,,$$

where M and N are positive integers without common divisors, then there are other non-trivial resonant relations. To find them, let us write a resonant relation with unknown p and q:

$$\rho_1 = \rho_1^p \rho_2^q \,,$$

or

$$e^{i\omega(p-q-1)} = 1 \,. \tag{10.4.5}$$

Taking the logarithm of both sides of (10.4.5), we obtain

$$i\omega(p-q-1) = 2\pi i l$$

where l is an integer. Substituting $\omega = 2\pi M/N$, we obtain

$$M(p-q-1) = Nl \,. \tag{10.4.6}$$

For each integer l, the equality (10.4.6) is satisfied if and only if

$$p = q + Ns + 1 \,, \tag{10.4.7}$$

where $s \in \mathbb{Z}$. We will assume that $s \geq 0$ in (10.4.7). Otherwise, for negative s rewrite (10.4.7) in the form

$$q = p + Ns - 1 \,, \tag{10.4.8}$$

where s is now positive. Notice, that plugging $s = 0$ in (10.4.7) gives $p = q+1$ which corresponds to the trivial resonance.

Thus, in the case where ω is commensurable to 2π, the normal form, along with terms of the form (10.4.4), possesses other terms determined by relations (10.4.7) and (10.4.8) for $s > 0$.

To construct the normal form, let us follow in the same way as given in Sec. 9.3, and introduce complex variables so that the linear part becomes diagonal. Let

$$z = x_1 + ix_2 \,,$$

and recast (10.4.2) as follow:

$$\bar{z} = e^{i\omega} z + \sum_{p,q} C_{pq} z^p z^{*q} \,. \tag{10.4.9}$$

Let us next apply the transformation

$$z = w + \sum_{s,t} \alpha_{st} w^s w^{*t} \tag{10.4.10}$$

such that the map in the new variables

$$\bar{w} = e^{i\omega} \left(w + \sum_{p,q} C'_{pq} w^p w^{*q} \right) \tag{10.4.11}$$

has as many zero coefficients C'_{pq} as possible.

By substituting (10.4.10) into (10.4.9) and collecting the coefficients of similar terms $w^p w^{*q}$, we obtain the following relations linking C_{pq} with C'_{pq}:

$$C'_{pq} + \alpha_{pq}[e^{i\omega(p-q-1)} - 1] = e^{-i\omega} C_{pq} \tag{10.4.12}$$

for $p + q = 2$ and

$$C'_{pq} + \alpha_{pq}[e^{i\omega(p-q-1)} - 1] = e^{-i\omega} C_{pq} + S_{pq}(\alpha_{st}) \tag{10.4.13}$$

for $p + q > 2$. Here, $S_{pq}(\alpha_{st})$ is some polynomial which depends only on α_{st} with indices s and t such that $s + t < p + q$. Hence, we can compute the coefficients α_{pq}, starting with $p + q = 2$. Furthermore, if

$$e^{i\omega(p-q-1)} \neq 1\,,$$

then the corresponding coefficient C'_{pq} can be nullified if we let

$$a_{pq} = \frac{e^{-i\omega} C_{pq} + S_{pq}}{e^{i\omega(p-q-1)} - 1}\,.$$

When $p = q + 1$, or if any one of the relations (10.4.7)–(10.4.8) holds, then

$$e^{i\omega(p-q-1)} = 1$$

and hence C'_{pq} cannot, in general, be nullified. In this case, we let $\alpha_{pq} = 0$, and then the resonant coefficient C'_{pq} is connected to C_{pq} via

$$C'_{pq} = e^{-i\omega} C_{pq} + S_{pq}(\alpha_{st})\,,$$

where S_{pq} is the polynomial from (10.4.13).

It is convenient to carry out some further calculations with regard to whether ω is commensurable to 2π or not. The *non-resonant case* where $\omega/2\pi$ is irrational is pretty simple because only trivial resonances occur there. Therefore, a polynomial transformation brings the map to the form

$$\bar{w} = e^{i\omega} w(1 + C'_{21}|w|^2 + \cdots + C'_{p+1,p}|w|^{2p}) + o(|w|^{2p+1}), \tag{10.4.14}$$

for arbitrarily given integer p (not exceeding $(r-1)/2$, where r is the smoothness of the map). In polar coordinates, $w = R\, e^{i\varphi}$ the map (10.4.14) assumes the form

$$\begin{aligned} \bar{R} &= R + L_1 R^3 + \cdots + L_p R^{2p+1} + o(R^{2p+1}), \\ \bar{\varphi} &= \varphi + \omega + \Omega_1 R + \cdots + \Omega_p R^{2p} + o(R^{2p}), \end{aligned} \tag{10.4.15}$$

where the values of L_k and Ω_k are expressed in terms of $C'_{j,j+1}$ with $j \le k$. For example,

$$\begin{aligned} L_1 &= \alpha_1, & \Omega_1 &= \beta_1, \\ L_2 &= \alpha_2 + \beta_1^2/2, & \Omega_2 &= \beta_2 - \beta_1\alpha_1/2, \end{aligned} \tag{10.4.16}$$

where $C'_{k+1,k} \equiv \alpha_k + i\beta_k$.

The values L_k are called *the Lyapunov values.*

Theorem 10.3. *Let L_k be the first non-zero Lyapunov value ($L_k \neq 0$, $L_i = 0$, for $i < k$). Then, the fixed point O is asymptotically stable when $L_k < 0$ and unstable when $L_k > 0$.*

Proof. From (10.4.15) we have

$$\bar{R} = R(1 + L_k R^{2k} + o(R^{2k})). \tag{10.4.17}$$

It follows that if $L_k < 0$, then $\bar{R} < R$; i.e. $V(R, \varphi) \equiv R$ is a Lyapunov function, and therefore the fixed point is asymptotically stable. In the case $L_k > 0$ we have

$$R = \bar{R}(1 - L_k \bar{R}^{2k} + o(\bar{R}^{2k})),$$

whence $\bar{R} > R$. Thus, R is a Lyapunov function for the inverse map and the instability of the fixed point follows. End of the proof.

Remark. It follows from the formulae (10.4.16) that in the general case the stability of the fixed point is determined by the value $\mathrm{Re}C'_{21} \equiv L_1$.

If $\mathrm{Re}C'_{21} < 0$, then the fixed point is stable. Otherwise, when $\mathrm{Re}C'_{21} > 0$, the fixed point is unstable.

One can compute that C'_{21} is given by the following formula:

$$C'_{21} = C_{20}C_{11}\frac{2e^{iw}-1}{1-e^{iw}}e^{-2iw} - 2\frac{|C_{02}|^2}{1-e^{3iw}} - \frac{|C_{11}|^2}{1-e^{iw}} + C_{21}e^{-iw}\,,$$

where C_{pq} are coefficients from (10.4.9). Thus, the first Lyapunov value is given by

$$\begin{aligned} L_1 = {} & \mathrm{Re}(C_{20}C_{11})\frac{\cos 3w - 3\cos 2w + 2\cos w}{2(1-\cos w)} \\ & + \mathrm{Im}(C_{20}C_{11})\frac{\sin 3w - 3\sin 2w + 2\sin w}{2(1-\cos w)} \\ & - |C_{02}|^2 - \frac{1}{2}|C_{11}|^2 + \mathrm{Re}\,C_{21}\cdot\cos w + \mathrm{Im}\,C_{21}\cdot\sin w\,. \end{aligned}$$

The fixed point O under consideration is called either a *complex* (*or weak*) *stable focus* or a *complex* (*weak*) *unstable focus* depending on the sign of the Lyapunov value.

If $L_k < 0$, then for the original multi-dimensional map (10.4.1), the fixed point is also a stable focus. Moreover, its leading manifold coincides with the center manifold W^C. This means that all positive semi-trajectories, excluding those in the non-leading manifold W^{ss}, tend to O along spirals which are tangent to W^C at O. The periodic orbit corresponding to the fixed point O is asymptotically stable as well. The nearby trajectories tend to the periodic orbit by winding around it, as shown in Fig. 10.4.1.

In the case where the Lyapunov value L_k is positive, the fixed point of the original map is *a weak saddle-focus*. Its stable and unstable manifolds are W^{ss} and W^C, respectively, as shown in Fig. 10.4.2.

In *the resonant case*, when $\omega = 2\pi M/N$, there are two groups of non-trivial resonant relations (10.4.7) and (10.4.8), as well as the trivial resonances. For the corresponding values p and q, the coefficient of α_{pq} in formulas (10.4.12) and (10.4.13) vanishes and the monomial $w^p w^{*q}$ survives under the normalizing transformation (10.4.10). Hence, the map (10.4.2) is transformed into

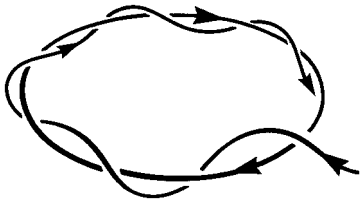

Fig. 10.4.1. A trajectory tends to the periodic orbit winding around it.

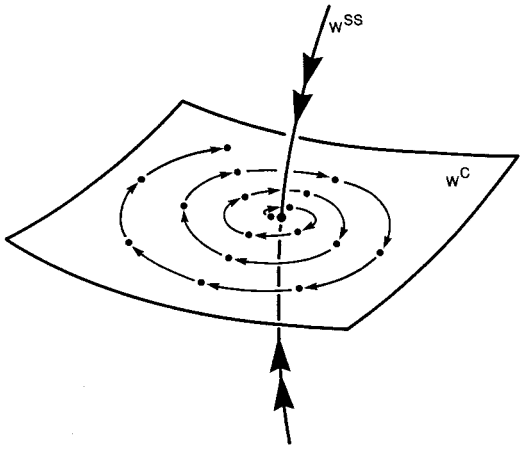

Fig. 10.4.2. An iterated saddle-focus.

the following normal form

$$\begin{aligned}\bar{w} = e^{2\pi iM/N}\Bigg(& w + \sum_{p\geq 1} C'_{p+1,p} w^{p+1} w^{*\,p} + \sum_{p\geq 0, s\geq 1} C'_{p,p+Ns-1} w^{p} w^{*\,p+Ns-1} \\ & + \sum_{q\geq 0, s\geq 1} C'_{q+Ns+1,q} w^{q+Ns+1} w^{*\,q}\Bigg) + o(|w|^{2P+1}) \\ = e^{2\pi iM/N}\Bigg(& w\Bigg(1 + \sum_{p\geq 1} C'_{p+1,p}|w|^{2p}\Bigg) + \sum_{s\geq 1} w^{*\,Ns-1} \sum_{p\geq 1} C'_{p,p+Ns-1}|w|^{2p} \\ & + \sum_{s\geq 1} w^{Ns+1} \sum_{q\geq 1} C'_{q+Ns+1,q}|w|^{2q}\Bigg) + o(|w|^{2P+1})\,, \end{aligned} \tag{10.4.18}$$

where the summation is taken over all indices so that the degrees of the monomials do not exceed $(2P+1)$ for some positive integer P, which can be chosen arbitrarily large but not exceeding $(r-1)/2$, where r is the smoothness of the system.

It follows from formula (10.4.18) that depending on the value N, one of the following three cases takes place:

(1) $N = 3 : \bar{w} = e^{2\pi i/3}(w + C'_{02}w^{*\,2}) + o(|w|^2)\,;$

(2) $N = 4 : \bar{w} = e^{\pi i/2}(w + C'_{21}|w|^2 w + C'_{03}w^{*\,3}) + o(|w|^3)\,;$ and

(3) $N \geq 5 : \bar{w} = e^{2\pi iM/N}(w + C'_{21}|w|^2 w) + o(|w|^3)\,.$

We see that for *strongly resonant* values $\omega = 2\pi/3$ and $\omega = \pi/2$ the normal forms differ *in main order* from the normal forms for other ω's. We will consider strong resonances in the next section, but let us pause first to discuss the *weak* resonances: $\omega = 2\pi M/N$, $N \geq 5$.

For the given case the map (10.4.18) can written in the form

$$\bar{w} = e^{2\pi iM/N}\left(w\left(1 + \sum_{p\geq 1} C'_{p+1,p}|w|^{2p}\right) + C'_{0,N-1}w^{*\,N-1}\right) + o(|w|^{N-1})\,, \tag{10.4.19}$$

where the summation is taken over all p such that $2p + 1 < N - 1$. In polar coordinates

$$\begin{aligned} \bar{R} &= R + L_1R^3 + \cdots + L_PR^{2P+1} + o(R^{N-2})\,, \\ \bar{\varphi} &= \varphi + \omega + \Omega_1R^2 + \cdots + \Omega_PR^{2P} + o(R^{N-3})\,, \end{aligned} \tag{10.4.20}$$

where P is the largest integer less than $(N/2 - 1)$.

Formula (10.4.20) is similar to the formula (10.4.14) for the non-resonant case and the only difference is that in the case of a weak resonance only a finite number of the Lyapunov values $L_1, \ldots, L_P$ is defined (for example, only L_1 is defined when $N = 5$). If at least one of these Lyapunov values is non-zero, then Theorem 10.3 holds; i.e. depending on the sign of the first non-zero Lyapunov value the fixed point is either a stable complex focus or an unstable complex focus (a complex saddle-focus in the multi-dimensional case).

10.5. Strong resonances

Recall that the strong resonances correspond to the values of the frequency $\omega = 2\pi/3$ and $\omega = \pi/2$. In the former case the normal form of the map is

$$\bar{w} = e^{2\pi i/3}(w + C'_{02}w^{*2}) + o(|w|^2)\,. \tag{10.5.1}$$

We will consider only the case where $C'_{02} \neq 0$. Let $C = |C'_{02}|$ and $e^{i\alpha} = C'_{02}/C$. Then, the transformation $w \to we^{i\alpha/3}C^{-1}$ reduces the map to

$$\bar{w} = e^{2\pi i/3}(w + w^{*2}) + o(|w|^2)\,. \tag{10.5.2}$$

Definition 10.2. *An m-fan is a set homeomorphic to the union of m rays emanating from one point (the apex of the fan).*

Definition 10.3. *A fixed point in the plane whose stable manifold W^s and unstable manifold W^u are the m-fans with the apex at the fixed point such that between any two neighboring rays of W^s there is one ray of W^u, and vice versa, is called a saddle with $2m$ separatrices.*

Theorem 10.4. *The fixed point O of map* (10.5.2) *is unstable and is a saddle with six separatrices as shown in Fig.* 10.5.1.

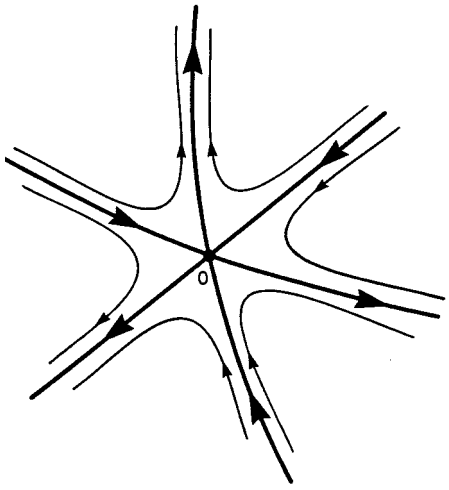

Fig. 10.5.1. A saddle with six separatrices.

Proof. It is more convenient to consider not the map (10.5.2) itself but its third iteration. We have

$$\begin{aligned} \bar{\bar{w}} &= e^{2\pi i/3}(\bar{w} + \bar{w}^{*\,2} + \cdots) = e^{4\pi i/3}(w + 2w^{*\,2} + \cdots)\,, \\ \bar{\bar{\bar{w}}} &= w + 3|w^*|^2 + \cdots\,, \end{aligned} \tag{10.5.3}$$

where the ellipses denote terms of third order and higher.

Let us consider a differential equation

$$\dot{w} = w^{*\,2} \tag{10.5.4}$$

for which the shift map along the trajectories over the time $t = 3$ has the form (10.5.3). To show this, let us rewrite (10.5.4) as

$$w_t = w_0 + \int_0^t w_s^{*\,2} ds\,. \tag{10.5.5}$$

This formula allows us to find a solution of (10.5.4) as the limit of the successive approximations $w_t^{(n)}$:

$$w_t^{(n+1)} = w_0 + \int_0^t (w_s^{(n)*})^2 ds\,. \tag{10.5.6}$$

For the first approximation we have

$$w_t^{(1)} = w_0 + t w_0^{*\,2}\,.$$

For the second one we have

$$w_t^{(2)} = w_0 + t w_0^{*\,2} + t^2 w_0^* w_0^2 + t^3 w_0^4/3\,.$$

It is not hard to see that all approximations coincide up to the terms of second order inclusively, and have the form

$$w_t^{(n)} = w_0 + t w_0^{*\,2} + o(|w|^2)\,.$$

Hence, the solution of Eq. (10.5.4) has the same form.[4] It follows that the shift map along the trajectories of system (10.5.4) over the time $t = 3$ does have the form (10.5.3).

[4]Generally speaking, one must prove that the successive approximations converge; it can be easily checked: if the time interval t is finite and if $|w_0|$ is sufficiently small, we can apply the Banach principle of contraction mappings.

System (10.5.3) can be integrated. To do this let us introduce the polar coordinates $w = R\,e^{i\varphi}$. Then we get

$$\frac{d}{dt}Re^{i\varphi} = R^2 e^{-2i\varphi}\,,$$

$$\dot{R} + iR\dot{\varphi} = R^2 e^{-3i\varphi}$$

or

$$\dot{R} = R^2\cos 3\varphi\,,$$

$$\dot{\varphi} = -R\sin 3\varphi\,.$$

After the change of time $Rdt \to dt$ the system reduces to the form

$$\begin{aligned} \dot{R} &= R\cos 3\varphi\,, \\ \dot{\varphi} &= -\sin 3\varphi\,. \end{aligned} \tag{10.5.7}$$

Observe that the function

$$H = R^3\sin 3\varphi$$

is the first integral of (10.5.7). The level lines of the function H, which are the integral curves of system (10.5.7), are found trivially. The level $H = 0$, which contains the equilibrium state, is given by the equation $\sin 3\varphi = 0$ and is a 6-fan defined by the rays

$$\varphi = \pi n/3\,, \quad (n = 0, \ldots, 5)\,.$$

The equation of motion on the rays with even n is

$$\dot{R} = R\,,$$

and therefore R increases unboundedly along these rays as $t \to +\infty$. The equation of motion on the rays with odd n is

$$\dot{R} = -R,$$

i.e. R tends to zero as $t \to -\infty$. Thus, the rays

$$\varphi = 2\pi n/3$$

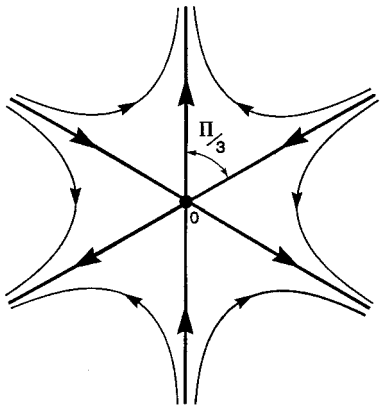

Fig. 10.5.2. A resonant fixed point with six separatrices. The angle between each pair is equal to $\pi/3$.

are the unstable separatrices of the equilibrium state, and the rays

$$\varphi = \pi(2n+1)/3$$

are the stable ones ($n = 0, 1, 2$). The rest of the trajectories have the form of hyperbolas whose asymptotes as $t \to +\infty$ and $t \to -\infty$ are the unstable and stable separatrices respectively, as shown in Fig. 10.5.2.

It is obvious that for the shift map along the trajectories of system (10.5.4) the fixed point also has the same six separatrices; i.e. Theorem 10.4 holds for the given particular case. In order to consider a general case recall that, as in Sec. 3.14, for an arbitrary map near a fixed point some iteration of the map can be approximated up to terms of arbitrarily high order by a shift map along the trajectories of some autonomous system of differential equations.[5] Such a system for the map (10.5.3) has the form

$$\dot{w} = {w^*}^2 + g(w, w^*)\,, \tag{10.5.8}$$

where $g = o(|w|^2)$. To find the function g one may write the Taylor expansion with indeterminate coefficients for the right-hand side of (10.5.8) and then by

[5]One may take an arbitrary non-autonomous time-periodic system such that the map under consideration is a Poincaré map for this system. After that the normalizing procedure described in Sec. 3.14 is applied.

using the method of successive approximations find the Taylor expansion for the time shift map in terms of the Taylor coefficients of g. Comparing the similar terms in the above shift map and in the original map (10.5.3), we get a system of equations from which the desired number of Taylor coefficients of g can be found. The solvability of this system of equations is guaranteed by Theorem 3.23.

The exact representation of the map (10.5.3) is given by the shift map of a non-autonomous system of the form

$$\dot{w} = {w^*}^2 + g(w, w^*) + \tilde{g}(w, w^*, t), \tag{10.5.9}$$

where $\tilde{g}$ is a periodic function with respect to t with period $T = 3$; moreover the terms depending on t can be made arbitrarily small (of order $o(|w|^r)$ where r is the smoothness of the system).

In polar coordinates the system can be written as

$$\begin{aligned} \dot{R} &= R^2 \cos 3\varphi + g_1(R, \varphi) + \tilde{g}_1(R, \varphi, t)\,, \\ \dot{\varphi} &= -R \sin 3\varphi + g_2(R, \varphi) + \tilde{g}_2(R, \varphi, t)\,, \end{aligned} \tag{10.5.10}$$

where $g_1 = O(R^3)$, $g_2 = O(R^2)$ and

$$\tilde{g}_1 = o(R^r)\,, \quad \tilde{g}_2 = o(R^{r-1})\,. \tag{10.5.11}$$

Omitting the non-autonomous terms, we obtain

$$\begin{aligned} \dot{R} &= R^2 \cos 3\varphi + g_1(R, \varphi)\,, \\ \dot{\varphi} &= -R \sin 3\varphi + g_2(R, \varphi)\,. \end{aligned} \tag{10.5.12}$$

After introducing a new time variable

$$d\tau = R\, dt \tag{10.5.13}$$

this system assumes the following form, whose main terms coincide with (10.5.7):

$$\begin{aligned} \dot{R} &= R \cos 3\varphi + O(R^2)\,, \\ \dot{\varphi} &= -\sin 3\varphi + O(R)\,. \end{aligned} \tag{10.5.14}$$

For the moment, let us not identify the points corresponding to $R = 0$ when the values of φ are different. Thus, the phase space of system (10.5.14) becomes a semi-cylinder. On the invariant circle $R = 0$ there are six equilibrium states

$$(R = 0,\ \varphi = \varphi_n \equiv \pi n/3) \quad n = 0, \dots, 5 \tag{10.5.15}$$

determined from the equation $\sin 3\varphi = 0$. The equilibrium states with even n are stable on the circle, and those with odd n are unstable. If we choose a small $\varepsilon > 0$, then the positive semi-trajectory of any trajectory (other than $\varphi = 2\pi n/3$) from the interval $\varphi \in (\pi(2n-1)/3, \pi(2n+1)/3)$ enters the ε-neighborhood of the point $2\pi n/3$ in a finite time; the negative semi-trajectory enters the ε-neighborhood of one of the points $\pi(2n-1)/3$ or $\pi(2n+1)/3$. Due to the continuous dependence on initial data, the trajectories of system (10.5.14) starting with sufficiently small R behave in the same way.

Let us prove that the same holds true for the trajectories of the non-autonomous system (10.5.10). First, let us consider more carefully the rescaling of time given by (10.5.13). The meaning of this formula is that the old time t, which parametrizes the trajectories of (10.5.12), is a function of (R, φ) and of the new time τ, which parametrizes the trajectories of (10.5.14), and it is defined by

$$t(\tau, R, \varphi) = \int_0^\tau \frac{ds}{R^*(s - \tau; R, \varphi)}\,, \tag{10.5.16}$$

where $R^*(s; R, \varphi)$ is the trajectory of system (10.5.14) starting with the point (R, φ) at $s = 0$.

Since $\dot{R}$ is of order R in (10.5.14), it follows that for finite τ the ratio R^*/R is bounded away from zero and infinity for arbitrarily small R. One can also see that $\frac{\partial R^*}{\partial \varphi}$ is of order R. Thus, formula (10.5.16) implies that

$$\frac{\partial t}{\partial \tau} = O\left(\frac{1}{R}\right)\,, \quad \frac{\partial t}{\partial \varphi} = O\left(\frac{1}{R}\right)\,, \quad \frac{\partial t}{\partial R} = O\left(\frac{1}{R^2}\right) \tag{10.5.17}$$

for bounded τ.

Moreover, it is easy to show that

$$\frac{\partial t}{\partial \tau} = \frac{1}{R^*(-\tau; R, \varphi)}\,. \tag{10.5.18}$$

Since this derivative does not vanish, it follows that the formula (10.5.16) defines also τ as a function of t and (R, φ). Consequently, the formula (10.5.13)

can be recast into the form

$$\frac{\partial\tau}{\partial t}+\frac{\partial\tau}{\partial R}\dot{R}+\frac{\partial\tau}{\partial\varphi}\dot{\varphi}=R\,, \tag{10.5.19}$$

where $\dot{R}=O(R^2)$ and $\dot{\varphi}=O(R)$ are given by (10.5.12).

Let us now consider the system (10.5.10) and make the same change of time as in the autonomous system (10.5.12). Namely, let the new time τ be defined by (10.5.16) where R^* is the solution of (10.5.14). The resulting system can be written in the form

$$\begin{aligned}\dot{R}&=\left(R\cos 3\varphi+\frac{1}{R}g_1(R,\varphi)+\frac{1}{R}\tilde{g}_1(R,\varphi,t(\tau,R,\varphi))\right)\chi(\tau,R,\varphi)\,,\\ \dot{\varphi}&=\left(-\sin 3\varphi+\frac{1}{R}g_2(R,\varphi)+\frac{1}{R}\tilde{g}_2(R,\varphi,t(\tau,R,\varphi))\right)\chi(\tau,R,\varphi)\,,\end{aligned} \tag{10.5.20}$$

where

$$\chi=R/\frac{d\tau}{dt}\equiv\frac{R}{\dfrac{\partial\tau}{\partial t}+\dfrac{\partial\tau}{\partial R}\dot{R}+\dfrac{\partial\tau}{\partial\varphi}\dot{\varphi}}$$

with $\dot{R}$ and $\dot{\varphi}$ defined by (10.5.10). These $\dot{R}$ and $\dot{\varphi}$ differ from those in (10.5.19) by the terms $\tilde{g}_1$ and $\tilde{g}_2$ of order $o(R^r)$ and $o(R^{r-1})$, respectively. Therefore,

$$\chi=\frac{1}{1-\dfrac{1}{R\dfrac{\partial t}{\partial\tau}}\left(\dfrac{\partial t}{\partial R}\tilde{g}_1+\dfrac{\partial t}{\partial\varphi}\tilde{g}_2\right)}=1+o(R^{r-2}) \tag{10.5.21}$$

for bounded τ (see (10.5.17) and (10.5.18)).

So, we have that the non-autonomous system (10.5.20) is well-defined at $R=0$ where it assumes the form

$$\dot{\varphi}=-\sin 3\varphi\,,$$

exactly as in the autonomous system (10.5.14). Thus, the non-autonomous system (10.5.20) has the same equilibria at $R=0$ and, moreover, all trajectories starting with a small R enter a small neighborhood of one of these equilibria at a finite time.

Therefore, to study the system (10.5.20) at small R it remains to consider the behavior of trajectories in a small neighborhood of the equilibrium states.

The linear part of system (10.5.20) at the equilibrium state ($R = 0, \varphi = \pi n/3$) is equal to the linear part of system (10.5.14):

$$\dot{R} = R(-1)^n\,,$$

$$\dot{\varphi} = 9(-1)^{n+1}\varphi + k_n R$$

for some k_n. The characteristic exponents are $(-1)^n$ and $9(-1)^{n+1}$. It follows that for the autonomous system (10.5.14) all equilibrium states are saddles. The equilibrium states with even n have an unstable separatrix given by $\varphi = \pi n/3 + Rk_n/10 + O(R^2)$, and the stable separatrices are the arches $\pi(n-1)/3 < \varphi < \pi n/3$ and $\pi n/3 < \varphi < \pi(n+1)/3$ on the circle $R = 0$. The equilibrium states with odd n have a stable separatrix of the form $\varphi = \pi n/3 - Rk_n/10 + O(R^2)$, whereas the arches $\pi(n-1)/3 < \varphi < \pi n/3$ and $\pi n/3 < \varphi < \pi(n+1)/3$ are the unstable separatrices.

We can now construct the phase portrait of system (10.5.14) on a semi-cylinder, as shown in Fig. 10.5.3. Then, by gluing the circle $R = 0$ into one point, the resulting equilibrium state $w = 0$ of (10.5.8) is a saddle with six separatrices as shown in Fig. 10.5.3(a).

To prove the theorem, we must get the same result for the non-autonomous system (10.5.9). Namely, we must prove the existence (and uniqueness) of stable and unstable separatrices for the equilibria ($R = 0, \varphi = \pi n/3$) of system (10.5.20). Due to the symmetry of the problem, it suffices to consider only one equilibrium, say, with $n = 1$.

By the results of Secs. 5.2 and 5.3, to prove the existence and uniqueness of the stable separatrix of the saddle equilibrium state of the non-autonomous system it is sufficient to check that in a small neighborhood of the equilibrium, for all positive times, the non-linearities remain small along with all derivatives. Thus, we must check that the functions $\tilde{g}_{1,2}(R, \varphi, t(R, \varphi, \tau))/R$ and $(\chi - 1)$ in the right-hand side of (10.5.20) are small along with all derivatives, provided that for some small δ

$$0 \le R \le \delta\,, \quad |\varphi - \pi/3| \le \delta\,. \tag{10.5.22}$$

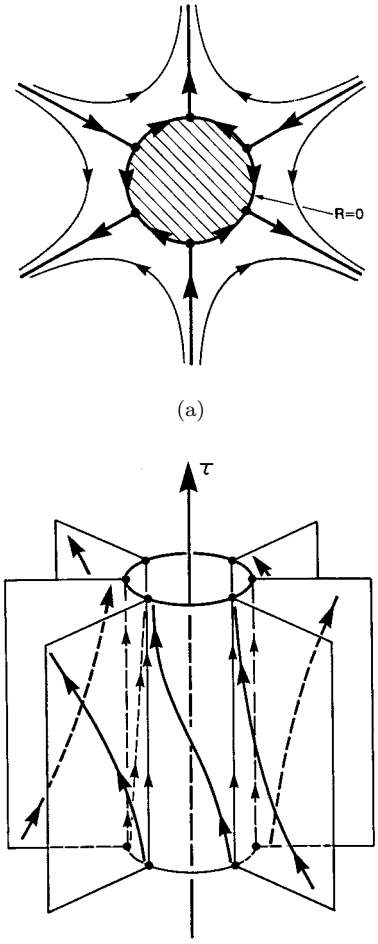

(a)

(b)

Fig. 10.5.3. A cross-section of a cylinder (a) and the behavior of trajectories on the semi-cylinder (b).

In fact, it follows immediately from (10.5.20) that in a small neighborhood of the equilibrium state,

$$R(\tau) \leq e^{-(1-\varepsilon)\tau} R(0)$$

for some sufficiently small $\varepsilon > 0$. Therefore, it is enough to check the smallness of the non-linearities only in that part of the neighborhood of the equilibrium

state where

$$e^{(1-\varepsilon)\tau} \le \frac{1}{R}\,, \quad \tau > 0\,. \tag{10.5.23}$$

Indeed, if the non-linearities are small here, then outside the set defined by (10.5.22) and (10.5.23) the system can be modified such that it becomes globally dichotomic for all (R, φ, τ) (see details in Sec. 5.2). Results of Sec. 5.3 imply the existence and uniqueness of the invariant stable manifold for the modified system. Any positive semi-trajectory in this manifold satisfies (10.5.23) *a priori*; therefore, the obtained invariant manifold lies in the region where the system is not modified. Hence, the intersection of the manifold with a small neighborhood (10.5.22) of the equilibrium state is the sought local invariant manifold of the original system.

Since the functions $\tilde{g}_{1,2}$ are of order at least $o(R^{r-2})$ (see (10.5.11)), as well as their derivatives with respect to time, it is sufficient to prove that the derivatives of the function $t(\tau, R, \varphi)$ in (10.5.20) and (10.5.21) grow not faster than some negative powers of R: when the smoothness r is large enough this would give us the desired smallness of the non-linearities in the right-hand side of (10.5.20). Now note that the spectrum of the linearization of system (10.5.14) at the equilibrium state is bounded from below by $\lambda = -1$. Thus, at $s - \tau \le 0$, we have the following estimates for the solution R^* of the system (10.5.14):

$$\mathrm{Re}^{(1-\varepsilon)(\tau-s)} \le R^*(s-\tau; R, \varphi) \le \mathrm{Re}^{(1+\varepsilon)(\tau-s)}$$

and

$$\frac{\partial^k R^*}{\partial (R, \varphi)^k} = O(e^{(k+\varepsilon)(\tau-s)})$$

for a small $\varepsilon > 0$. Substituting this estimates into the formula (10.5.16) which defines $t(\tau, R, \varphi)$, and using (10.5.18) and (10.5.23) we obtain finally the estimate

$$\frac{\partial^k t}{\partial (\tau, R, \varphi)^k} = O\left(\frac{1}{R^{k+1+\sigma}}\right)$$

with some $\sigma > 0$ which tends to zero as $\varepsilon \to 0$. As explained above, this estimate is good enough to establish the existence and uniqueness of a local stable invariant manifold for the equilibrium state of the non-autonomous system (10.5.20).

Thus, we have established the existence and uniqueness of the invariant manifolds — the surfaces in the space (φ, R, τ) of the form

$$\varphi = \pi n/3 + f_n(R, \tau)$$

which are formed entirely by the solutions $(\varphi(\tau), R(\tau))$ of system (10.5.20) (see Fig. 10.5.3(b)). For odd n these are the stable manifolds: on each the value of R tends to zero as τ grows. For even n these are the unstable manifolds.

Since the solutions of system (10.5.20) are the solutions of system (10.5.10) up to a change of the time variable, we have proven the existence and uniqueness of the invariant stable and unstable manifolds of the stationary states ($R = 0,\ \varphi = \pi n/3$) of system (10.5.10). By construction, the manifolds are the set of trajectories of the system (10.5.10) which emerge at $t = 0$ from the uniquely defined curves $\mathcal{L}_n$ given by

$$\varphi = \pi n/3 + f_n(R, 0)\,. \tag{10.5.24}$$

Since the right-hand side of system (10.5.10) is periodic with respect to t, the set of the trajectories which start at $t = 0$ from the points on the image $\bar{\mathcal{L}}_n$ of the curve $\mathcal{L}_n$ (when mapping along the trajectories of the system over the period) also comprise an invariant manifold. By virtue of uniqueness, this must be the same invariant manifold, and hence $\bar{\mathcal{L}}_n = \mathcal{L}_n$. But the map over the period of the system (10.5.10) is the map (10.5.3). So, we have established the existence of the six invariant manifolds $\mathcal{L}_0, \ldots, \mathcal{L}_5$ (three stable and three unstable) of the fixed point $w = 0$ of the given map, from which the statement of the theorem follows.

Remark. In the multi-dimensional case where besides the central coordinates there are also the stable ones, the unstable set consists of three curves, whereas the stable set is a bunch consisting of three semi-planes intersecting along the non-leading manifold W^{ss}, as shown in Fig. 10.5.4, for the three-dimensional example.

Let us now elaborate on the resonance $\omega = \pi/2$. The map in its normal form is given by

$$\bar{w} = e^{\pi i/2}(w + C'_{21}|w|^2 w + C'_{03} w^{*\,3}) + o(|w|^3)\,. \tag{10.5.25}$$

We will assume that $C'_{03} \neq 0$. Then, after the transformation $w \to e^{\alpha i/4} C^{1/4}$, where $C'_{03} = Ce^{i\alpha}$, the map recasts into the form

$$\bar{w} = e^{\pi i/2}(w + (L + i\Omega)|w|^2 w + w^{*\,3}) + o(|w|^3)\,, \tag{10.5.26}$$

where $L + i\Omega \equiv C'_{21}\sqrt{C}$.

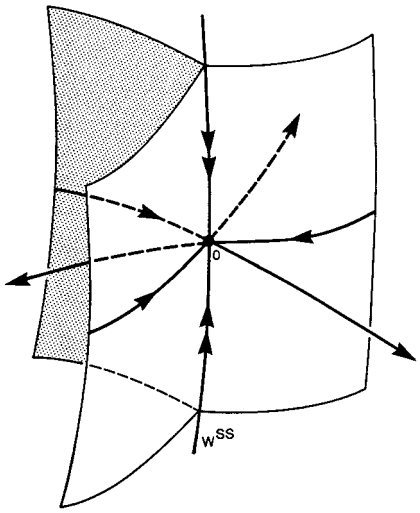

Fig. 10.5.4. Topology of the stable and unstable manifold of a resonant $\pi/3$ fixed point in $\mathbb{R}^3$.

Theorem 10.5. *In the case $L < 0$ and $L^2 + \Omega^2 > 1$ the fixed point is asymptotically stable. In the case $L > 0$ and $L^2 + \Omega^2 > 1$ the fixed point is unstable; when $L^2 + \Omega^2 < 1$ it is a saddle with eight separatrices.*

We will prove the theorem only for the case where the fourth iteration of the map (10.5.26)

$$\bar{w}^{(4)} = w + 4[(L + i\Omega)|w|^2 w + w^{*\,3}] + o(|w|^3) \tag{10.5.27}$$

coincides with the time shift map of some autonomous system (the general case may be treated in basically the same way as in the previous theorem).

Let us write the autonomous system in the form

$$\dot{w} = B_1|w|^2 w + B_2 w^{*\,3} + O(|w|^4) \tag{10.5.28}$$

with yet indeterminate B_1 and B_2. Rewrite (10.5.28) in the form

$$w_t = w_0 + \int_0^t (B_1|w_s|^2 w_s + B_2 w_s^{*\,3} + O(|w_s|^4))ds$$

and construct its solution by the method of successive approximations. On the first step we have

$$w_t = w_0 + (B_1|w_0|^2 w_0 + B_2 w_0^{*\,3})t + O(|w_0|^4)\,.$$

It is easy to see that all approximations have the same form and, therefore, the solution of Eq. (10.5.28) has the same form. If we let $t = 4$, it would follow that the map (10.5.27) coincides, up to the terms of third order, with the shift map along the trajectories of any system in the form

$$\dot{w} = (L + i\Omega)|w|^2 w + {w^*}^3 + g(w, w^*)\,, \tag{10.5.29}$$

where g begins with terms of fourth order. As mentioned above, we assume that the map (10.5.27) coincides exactly with the time $t = 4$ shift map along the trajectories of system (10.5.29) for some g. By introducing the polar coordinates $w = \mathrm{R}\,\mathrm{e}^{i\varphi}$ we obtain

$$\dot{R} = R^3(L + \cos 4\varphi) + O(R^4)\,,$$

$$\dot{\varphi} = R^2(\Omega - \sin 4\varphi) + O(R^3)\,,$$

or after the transformation of time $R^2 dt \to dt$:

$$\begin{aligned} \dot{R} &= R(L + \cos 4\varphi) + O(R^2)\,, \\ \dot{\varphi} &= \Omega - \sin 4\varphi + O(R)\,. \end{aligned} \tag{10.5.30}$$

Without loss of generality, we can assume that $\Omega \geq 0$ because the transformation $\varphi \to -\varphi$ does not alter the form of the system but Ω changes its sign.

At $L = 0$ the shortened system (10.5.30)

$$\dot{R} = R\cos 4\varphi\,,$$

$$\dot{\varphi} = \Omega - \sin 4\varphi$$

possesses a first integral

$$H = R^4(\Omega - \sin 4\varphi)\,.$$

Observe that when $L < 0$ and $\Omega > 1$ the function H is a Lyapunov function for the original system (10.5.30) for sufficiently small R. Indeed, since $\Omega > 1$, it is obvious that $H > 0$ for $R > 0$. Let us check that $\dot{H} < 0$, i.e. $H'_R\dot{R} + H'_\varphi\dot{\varphi} < 0$. The latter inequality can be recast in the form

$$4R^4(\Omega - \sin 4\varphi)(L + \cos 4\varphi) - 4R^4(\Omega - \sin 4\varphi)\cos 4\varphi + O(R^5) < 0$$

or

$$4R^4(\Omega - \sin 4\varphi)L + O(R^5) < 0$$

which is obviously fulfilled for all R sufficiently small if $L < 0$ and $\Omega > 1$.

The existence of a Lyapunov function implies the asymptotic stability, i.e. in this case the theorem holds. One can construct a Lyapunov function for an enlarged parameter region: $\Omega^2 + L^2 > 1$, $L < 0$. To do this let us consider the function $V = R^4(\beta - \sin 4\varphi)$ and show that it is a Lyapunov function for a suitable choice of β. Indeed, one needs $V > 0$ at $R > 0$, i.e.

$$\beta > 1\,, \tag{10.5.31}$$

and $\dot{V} < 0$, i.e. $V'_R\dot{R} + V'_\varphi\dot{\varphi} < 0$. The latter inequality can be recast in the form

$$4R^4(\beta - \sin 4\varphi)(L + \cos 4\varphi) - 4R^4(\Omega - \sin 4\varphi)\cos 4\varphi + O(R^5) < 0\,.$$

To satisfy this inequality for R small enough it is sufficient to have

$$(\beta - \sin 4\varphi)(L + \cos 4\varphi) - (\Omega - \sin 4\varphi)\cos 4\varphi < 0$$

for all φ, or

$$\beta L - L\sin 4\varphi + (\beta - \Omega)\cos 4\varphi < 0\,.$$

It is equivalent (since $\beta L < 0$) to

$$L^2 + (\beta - \Omega)^2 < \beta^2 L^2\,. \tag{10.5.32}$$

One can easily check that the value β satisfying (10.5.31) and (10.5.32) always exists for $L^2 + \Omega^2 > 1$: when $\Omega > 1$ one can let $\beta = \Omega$; when $|L| \geq 1$ any sufficiently large number can be taken as β; in any other case one can let $\beta = \Omega/(1 - L^2)$.

If $L > 0$, then the function V is a Lyapunov function for the system obtained from (10.5.30) by inversion of time. Thus, the equilibrium state of system (10.5.29) and hence the fixed point of the map (10.5.27) is completely unstable here.

Let us consider finally the case where $L^2 + \Omega^2 < 1$. As we have done for the resonance $2\pi/3$, let us assume that the system is defined on a semi-cylinder. Then, it will possess eight equilibrium states

$$(R = 0,\ \varphi = \varphi_n)\,, \quad (n = 0, \ldots, 7)\,,$$

where φ_n is found from the equation

$$\Omega - \sin 4\varphi = 0\,. \tag{10.5.33}$$

The linear part of the system at the equilibrium state has the form

$$\dot{R} = R(L + \cos 4\varphi_n)\,,$$

$$\dot{\varphi} = -(4\cos 4\varphi_n)\varphi + k_n R\,.$$

The determinant of the linearization matrix is equal to

$$\Delta = -4\cos 4\varphi_n(L + \cos 4\varphi_n)\,.$$

It follows from (10.5.33) that $|\cos 4\varphi_n| = (1 - \Omega^2)^{1/2}$, and therefore, $|\cos 4\varphi_n| > |L|$. Hence, both values $\cos 4\varphi_n$ and $(L + \cos 4\varphi_n)$ have the same sign, and the determinant Δ is negative. Thus, we have found that all equilibrium states are saddles as in the case $2\pi/3$. The phase portrait of system (10.5.30) on a semi-cylinder is shown in Fig. 10.5.5. If we identify all points with $R = 0$, the result is going to be a saddle with eight separatrices as shown in Fig. 10.5.6.

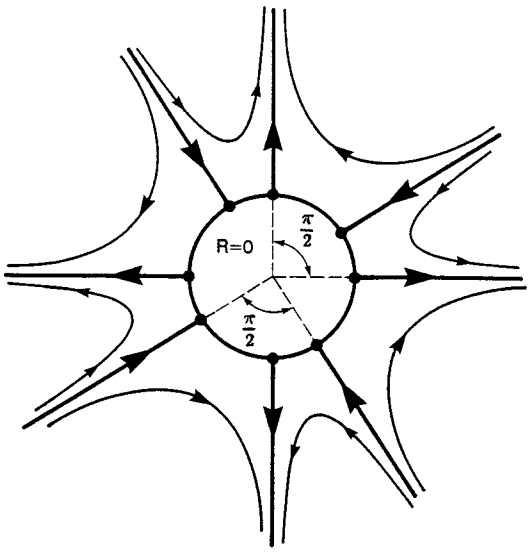

Fig. 10.5.5. Cross-section of a semi-cylinder.

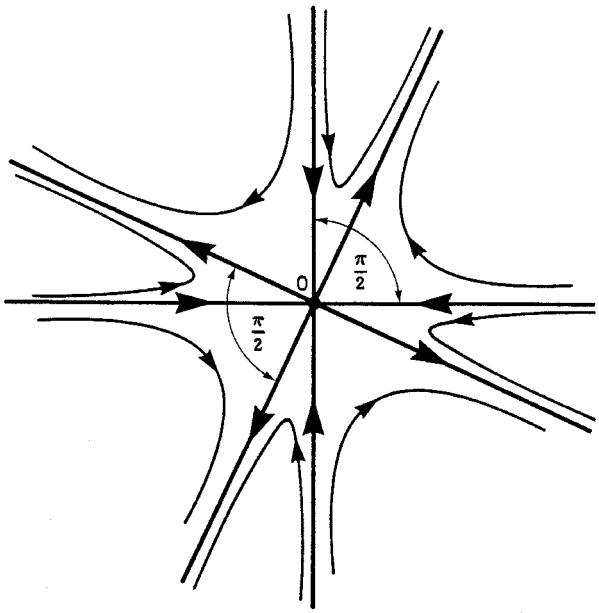

Fig. 10.5.6. Each iteration maps the stable (unstable) manifold through a $\pi/2$ angle.

10.6. Passage through strong resonance on stability boundary

We have seen in the previous sections that the qualitative behavior of a strongly resonant critical fixed point differs essentially from that of a non-resonant or a weakly resonant one. It is therefore natural to ask the question: what happens at a strongly resonant point as the frequency varies? In particular, in the case of the resonance $\omega = 2\pi/3$ the fixed point is a saddle with six separatrices in general, but when an arbitrarily small detuning is introduced the point becomes a weak focus (stable or unstable, depending on the sign of the first Lyapunov value). The question we seek to answer is how does the dynamics evolve before and after the critical moment?

On the stability boundary the map near the fixed point can be written in the following form for ω close to $2\pi/3$

$$\bar{w} = e^{i(2\pi/3+\varepsilon)}(w + w^{*\,2} + C'_{21}|w|^2 w + \cdots)\,, \tag{10.6.1}$$

where the parameter ε measures the deviation from the resonance; the coefficients on the right-hand side of the map, in particular C'_{21}, are assumed to depend continuously on ε. Let us denote the map (10.6.1) as T_ε.

Theorem 10.6. *Let* $\mathrm{Re}C'_{21} < 1$. *Then for any small* $\varepsilon \neq 0$ *the point* $O(w = 0)$ *is stable. Moreover, the map* T_ϵ *possesses a saddle periodic trajectory* (O_1, O_2, O_3) *of period three which lies apart from the point* O *over a distance* $O(\varepsilon)$. *One of the two unstable separatrices of each point* O_i *tends to* O, *the other unstable separatrix leaves a neighborhood of the origin. The stable separatrices of the periodic trajectory form a boundary of the basin of attraction of the point* O (*see Fig.* 10.6.1).

Hence as the parameter approaches a strong resonance, the saddle cycle shrinks continuously to the point O from the outside of a neighborhood of the origin. At the precise moment of resonance it collapses into O so that the latter becomes unstable. Upon passing through the resonance the cycle distances anew from the point O and as ε is further changed the cycle leaves the (small) neighborhood of O. The case where $\mathrm{Re}C'_{21} > 0$ is identical but applied to the inverse map T_ε^{-1}; in this case the point O is completely unstable for $\varepsilon \neq 0$.

We skip the proof of Theorem 10.6 because it is part of a more general problem in the study of bifurcations of strongly resonant critical points (see Arnold [20] and Guckenheimer and Holmes [64]) which is beyond the scope of our book. Instead we restrict ourselves here by considering a modeling example.

Consider the third iteration of map (10.6.1)

$$\overline{\overline{\overline{w}}} = e^{3\varepsilon i} w + (1 + e^{3\varepsilon i} + e^{-3\varepsilon i}) w^{*\,2} + (3C'_{21} e^{3\varepsilon i} + 4 + 2e^{-3\varepsilon i}) |w|^2 w + \cdots , \tag{10.6.2}$$

where the ellipsis denotes the terms of fourth and higher orders with respect to $|w|$. It can be shown that the map (10.6.2) coincides with the shift map over time $t = 3$ of some differential equation of the form

$$\dot{w} = i\varepsilon w + (1 + \alpha_1(\varepsilon)) w^{*\,2} + (C'_{21} - 1 + \alpha_2(\varepsilon)) |w|^2 w + f(w, w^*, t) , \tag{10.6.3}$$

where $\alpha_1(\varepsilon)$ and $\alpha_2(\varepsilon)$ are some functions tending to zero as $\varepsilon \to 0$, and the function f begins with terms of fourth order of smallness (see the previous section for more details).

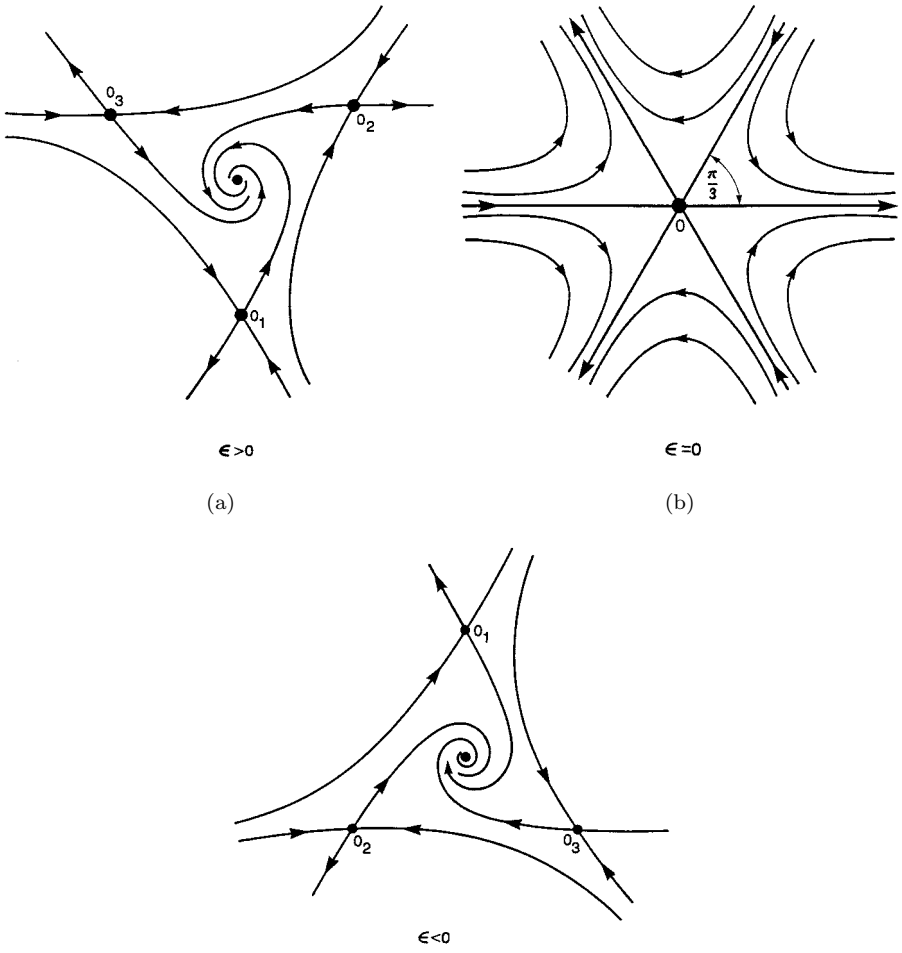

Fig. 10.6.1. Modifications of the phase portrait as ε changes. The fixed point is stable for positive and negative values of ε. The direction of rotation near the origin is changed as the sign of ε is changed.

For definiteness, assume $\varepsilon > 0$ (when $\varepsilon < 0$ the arguments are analogous). Let us make the transformation $w \to \varepsilon w e^{i\arg(1+\alpha_1(\varepsilon))/3}/|1+\alpha_1(\varepsilon)|$ and $t \to t/\varepsilon$. Then, Eq. (10.6.3) can be recast as follow

$$\dot{w} = iw + w^{*\,2} + \varepsilon(C'_{21}(0) - 1)|w|^2 w + o(\varepsilon) \tag{10.6.4}$$

(recall that C'_{21} is also a function of ε whereas $C'_{21}(0)$ is just a constant). Truncate the terms of order $o(\varepsilon)$ and consider the shortened equation

$$\dot{w} = iw + w^{*\,2} + \varepsilon(C'_{21}(0) - 1)|w|^2 w\,. \tag{10.6.5}$$

In the polar coordinates $w = \mathrm{R}\,\mathrm{e}^{i\varphi}$, it is written in the form

$$\begin{aligned} \dot{R} &= R^2 \cos 3\varphi + \varepsilon L R^3\,, \\ \dot{\varphi} &= 1 - R\,\sin 3\varphi + \varepsilon \Omega R^2\,. \end{aligned} \tag{10.6.6}$$

In the Cartesian coordinates $w = x + iy$, (10.6.6) assumes the form

$$\begin{aligned} \dot{x} &= -y + x^2 - y^2 + \varepsilon(Lx - \Omega y)(x^2 + y^2)\,, \\ \dot{y} &= x - 2xy + \varepsilon(\Omega x + Ly)(x^2 + y^2)\,, \end{aligned} \tag{10.6.7}$$

where $C'_{21}(0) - 1 = L + i\Omega$ (recall that for the case under consideration, we have $\mathrm{Re}C'_{21} < 1$, i.e. $L < 0$).

At $\varepsilon = 0$ the system, besides the point O at the origin, has three equilibrium states $O_1(0, -1)$, $O_2(\sqrt{3}/2, 1/2)$ and $O_3(-\sqrt{3}/2, 1/2)$. Observe that the straight lines $y = 1/2$, $y = \sqrt{3}x - 1$, and $y = -\sqrt{3}x - 1$ passing through the points O_2O_3, O_1O_2 and O_1O_3, respectively, are invariant with respect to the system (10.6.7) at $\varepsilon = 0$. Moreover, the function

$$H = (y - 1/2)(y - \sqrt{3}x + 1)(y + \sqrt{3}x + 1)\,,$$

or in polar coordinates

$$H = 3R^2/2 - R^3 \sin 3\varphi - 1/2$$

is a first integral of the system at $\varepsilon = 0$. The level set $H = 0$ is shown in Fig. 10.6.2. So, the point O is a center, and O_1, O_2, O_3 are saddles. The separatrices of the saddles are invariant straight lines. Moreover, the unstable separatrix of the point O_1 coincides with the stable separatrix of the point

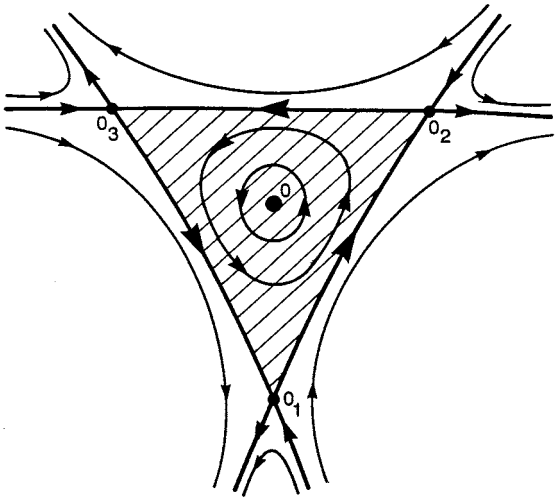

Fig. 10.6.2. The fixed point is a center at $\varepsilon = 0$. The saddle fixed points form a heteroclinic cycle.

O_2, and so on, as depicted in the figure. Thus, all together they comprise the separatrix connection.

When $\varepsilon \neq 0$ the function $(H + 1/2)$ is a Lyapunov function for the equilibrium state at the origin:

$$\dot{H} \equiv H'_R \dot{R} + H'_\varphi \dot{\varphi} = 3\varepsilon L R^4 (1 + O(R)) < 0\,,$$

so the origin is asymptotically stable. The equilibrium states O_1, O_2, O_3 remain as saddles for all small ε. Three variants are *a priori* possible for the behavior of their separatrices: (1) the separatrix connection is preserved; (2) it splits with the unstable branch diverging outwards (see Fig. 10.6.3(a)); or (3) it splits with the unstable branch converging inwards (Fig. 10.6.3(b)). Let us show that the third possibility does occur. Indeed, it is seen from (10.6.7) that the divergence of the right-hand side of the system is negative for $\varepsilon \neq 0$ ($\mathrm{div} \equiv \frac{\partial \dot{x}}{\partial x} + \frac{\partial \dot{y}}{\partial y} = 3\varepsilon L(x^2 + y^2)$). Hence, the area of any region on the plane must decrease after each shift in positive time along the trajectories of the system. On the other hand, one observes from Figs. 10.6.2 and 10.6.3(a) that if the connection is preserved, or it has been split outwards, then we can find a region whose area is not decreasing after a small positive time shift ($S_t \geq S_0$, see the figures).

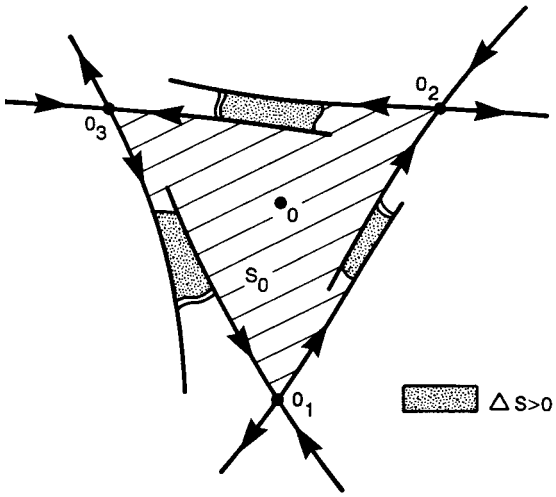

(a)

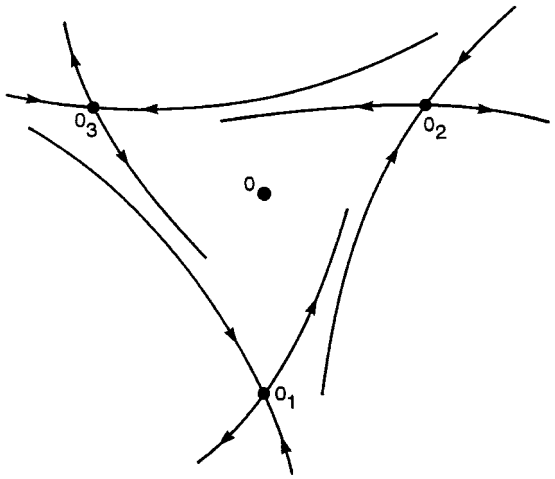

(b)

Fig. 10.6.3. Two ways of how a heteroclinic connection may be broken down. See the discussion in the text.

Therefore, the separatrix connection must split and converge inward for all small ε.

It is obvious that as $t \to +\infty$, the unstable separatrices which converge inwards may in principle tend to either the point O as shown in Fig. 10.6.1, or to some periodic trajectory surrounding the origin, as shown Fig. 10.6.4. In the latter case, however, the area bounded by this trajectory would not decrease when shifted along the trajectories of the system thereby contradicting the negativeness of the divergence. This means that the separatrices must tend to the origin.

The saddle equilibrium states are the saddle fixed points of the shift map, and respectively, their separatrices are the invariant manifolds. Returning to the original (non-rescaled) variables we find that the fixed points must lie apart from the origin at some distance of order ε. If the third iteration (10.6.2) of the map (10.6.1) were the shift map of the reduced system (10.6.5), then the above theorem would follow from our arguments because the fixed points O_1, O_2, O_3 of the third iterations correspond to the cycle of period three of the original map.

However, in general, the map (10.6.2) may not be regarded for all ε as the shift map along the trajectories of an autonomous system. Therefore, to prove that the situation depicted in Fig. 10.6.1 does occur one needs to check (we

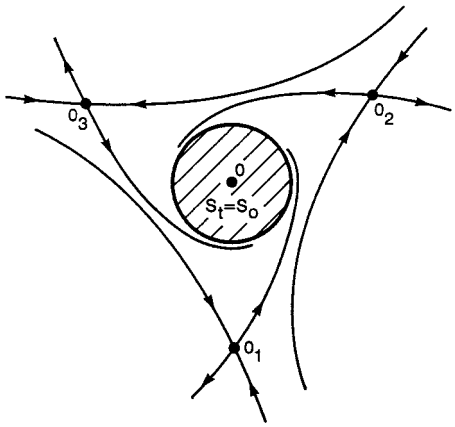

Fig. 10.6.4. A geometrical explanation of the absence of a periodic orbit surrounding the origin; since the *area* of the time shift map is contracting as time increases, the existence of a limit cycle surrounding the origin is not possible.

are not going to) that the whole invariant manifolds of the saddle fixed points of the shift map of the non-autonomous system (10.6.4) lie entirely sufficiently close to the separatrices of the truncated system (10.6.5).

In the case of the second strong resonance $\omega = \pi/2$ the situation is even more subtle. Let us consider the family of maps T_ε defined by

$$\bar{w} = e^{i(\pi/2+\varepsilon)}(w + w^{*\,3} + C'_{21}(\epsilon)|w|^2 w) + o(|w|^3) \tag{10.6.8}$$

which passes through the resonance at $\varepsilon = 0$. Let $C'_{21}(0) = L + i\Omega$.

Theorem 10.7. *Let $L < 0$. Then,*
(1) *if $L < -1$, then for all small ε the fixed point $O(w = 0)$ is asymptotically stable and attracts all trajectories from some small neighborhood which does not depend on ε;*
(2) *if $L^2 + \Omega^2 < 1$, then for any small $\varepsilon \neq 0$, the point O is asymptotically stable. Besides, the map T_ε possesses a saddle cycle (O_1, O_2, O_3, O_4) of period four at a distance of order $O(\sqrt{|\varepsilon|})$ from the point O. One of the two unstable separatrices of each O_i tends to O, the other leaves a neighborhood of the origin. The stable separatrices of the saddle cycle form a boundary of the basin of attraction of the point O (see Fig.* 10.6.5); *and*
(3) *If $0 > L > -1$ and $L^2 + \Omega^2 > 1$, then for all small ε the point O is asymptotically stable, and at $\varepsilon\Omega \geq 0$ it attracts all trajectories from a small neighborhood whose size does not depend on ε. When $\varepsilon\Omega < 0$ the two trajectories of period four bifurcate from the point O : the first is a saddle composed of points (O_1, O_2, O_3, O_4), and the second cycle is stable and consists of (O'_1, O'_2, O'_3, O'_4) as shown in Fig.* 10.6.6. *One of the unstable separatrices of the point O_i tends to O; the other tends to O'_i. The stable separatrices of O_i separate the attraction basins of the point O from that of the cycle (O'_1, O'_2, O'_3, O'_4).*

We replace the proof of this theorem by considering only the dynamics of the reduced system of equations. The fourth iteration of the map (10.6.8) has the form

$$\bar{w}^{(4)} = e^{4i\varepsilon}(w + 4C'_{21}(\varepsilon)|w|^2 w) + w^{*\,3}(e^{4i\varepsilon} + e^{-4i\varepsilon})(1 + e^{-4i\varepsilon}) + o(|w|^3)\,,$$

This map coincides with the shift map over time $t = 4$ of some non-autonomous system of the form

$$\dot{w} = i\varepsilon w + (1 + \alpha_1(\varepsilon))w^{*\,3} + (L + i\Omega + \alpha_2(\varepsilon))|w|^2 w + g(w, w^*, t)\,,$$

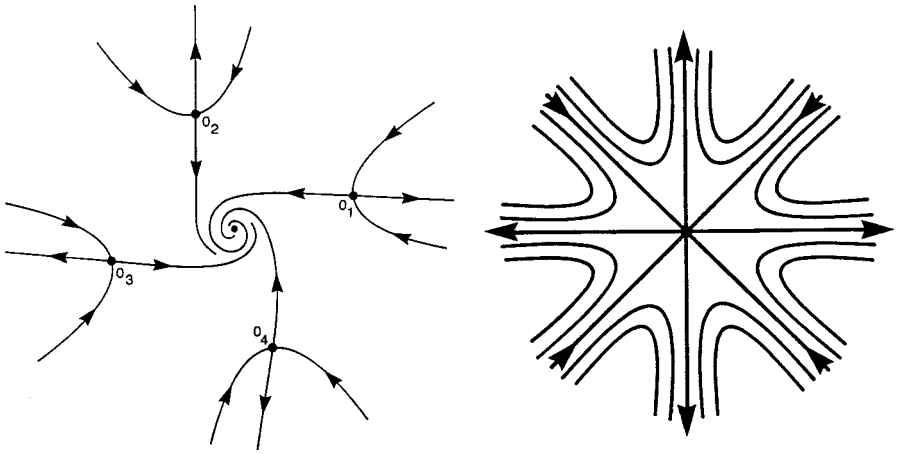

(a) (b)

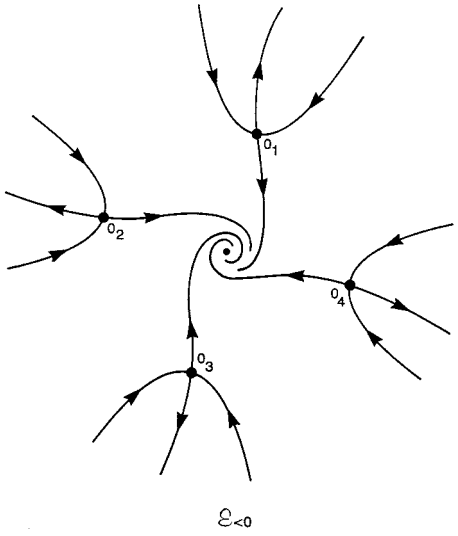

(c)

Fig. 10.6.5. Modifications of the phase portrait as ε changes (here $L^2 + \Omega^2 < 1$).

where $g = o(|w|^3)$. Upon renormalizing w by $\sqrt{|\varepsilon|}$ and the time t by $|\varepsilon|$, and taking the limit $\varepsilon \to 0$, we obtain the reduced system

$$\dot{w} = i\delta w + (L + i\Omega)|w|^2 w + w^{*\,3}\,, \tag{10.6.9}$$

where $\delta = \pm 1 = \operatorname{sign}\varepsilon$.

In Cartesian coordinates this equation is written in the form

$$\begin{aligned} \dot{x} &= -\delta y + (Lx - \Omega y)(x^2 + y^2) + x^3 - 3xy^2\,, \\ \dot{y} &= \delta x + (Lx + \Omega y)(x^2 + y^2) - 3x^2 y + y^3\,. \end{aligned} \tag{10.6.10}$$

In polar coordinates, the corresponding system is given by

$$\begin{aligned} \dot{R} &= R^3(L + \cos 4\varphi)\,, \\ \dot{\varphi} &= \delta + R^2(\Omega - \sin 4\varphi)\,. \end{aligned} \tag{10.6.11}$$

It follows immediately from (10.6.11) that $\dot{R} < 0$ when $L < -1$. Therefore, all trajectories of system (10.6.11) tend to the origin, which confirms the statement of the above theorem.

In order to study the system corresponding to the case $0 > L > -1$, we note that the divergence of the right-hand side is negative and is equal to $4L(x^2 + y^2) < 0$ (see (10.6.10)). It follows (by repeating the corresponding arguments for system (10.6.5)) that the system (10.6.10) has neither closed trajectories nor separatrix connections. As for the equilibrium states, they can be easily found in polar coordinates (see (10.6.11)).

When $L^2 + \Omega^2 > 1$, the system has only one equilibrium state (at the origin) if $\Omega\delta > 0$. This equilibrium state is stable and attracts all trajectories of the system. To show this it is sufficient to check that the function

$$V = R^4(\beta - \sin 4\varphi) + 2\delta R^2 \tag{10.6.12}$$

is a Lyapunov function for $\Omega > 0$ and $\delta = 1$, where β is a value defined from the relations (10.5.25)–(10.5.26) while constructing the Lyapunov function in the previous section; the case where $\Omega < 0$, $\delta = -1$ is reduced to the given one by a change of variable $\varphi \to -\varphi$. When $\Omega\delta < 0$ the system has, besides the zero equilibrium state, eight additional equilibrium states; namely four saddles O_1, O_2, O_3, O_4 and four stable equilibria O_1', O_2', O_3', O_4'. The coordinates of the latter are found from the relations

$$\cos 4\varphi = -L\,, \quad \sin 4\varphi = -\delta\sqrt{1 - L^2}\,, \quad R^2 = \frac{1}{|\Omega| - \sqrt{1 - L^2}}\,,$$

and those of the saddles from

$$\cos 4\varphi = -L\,, \quad \sin 4\varphi = \delta\sqrt{1-L^2}\,, \quad R^2 = \frac{1}{|\Omega| + \sqrt{1-L^2}}\,.$$

Point O is stable; the function $(2R^2 - \delta R^4 \sin 3\varphi)$ is a Lyapunov function for small R. Clearly, the stable separatrices of the saddle points tend to infinity as $t \to -\infty$. Otherwise, they had to tend to a completely unstable periodic trajectory or a completely unstable equilibrium state but there is none. Another possibility is that a stable separatrices of one saddle might coincide with the unstable one of the other saddle thereby forming a separatrix cycle as that shown in Fig. 10.6.2, but with four saddles; however this hypothesis contradicts to the negative divergence condition. The unstable separatrices cannot tend to infinity as $t \to +\infty$. To prove this, check that when R is large, $\dot{V} < 0$ for the function V in (10.6.12). Therefore, all trajectories of the system, as t increases, must get inside some closed curve $V = C$ with C sufficiently large, where they remain forever. The same behavior applies to the separatrices of the saddle. Thus, the only option for the unstable separatrices of the point O_i is that one tends to O and the other to O_i' as shown in Fig. 10.6.6.

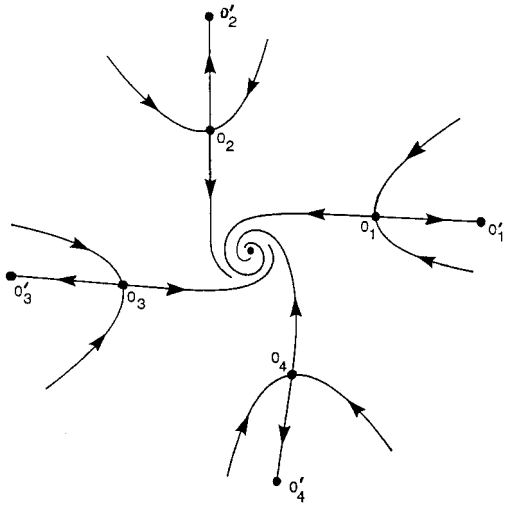

Fig. 10.6.6. The phase portrait at $\varepsilon\Omega < 0$ in the case $-1 < L < 0$, $L^2 + \Omega^2 > 1$. Four pairs of fixed points appear simultaneously through the saddle-node bifurcation.

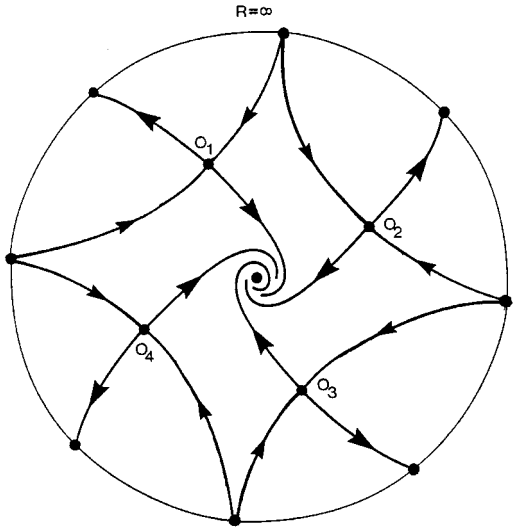

Fig. 10.6.7. This picture illustrates how the separatrices of a saddle point organize the global phase portrait.

At $L^2 + \Omega^2 < 1$, the system has five equilibrium states: one stable trivial at the origin, and four others O_1, O_2, O_3, O_4 which are saddle points for $\delta = 1$ and $\delta = -1$. The coordinates of the equilibrium states are found from the relations:

$$\cos 4\varphi = -L\,, \quad \sin 4\varphi = \delta\sqrt{1-L^2}\,, \quad R^2 = \frac{1}{\sqrt{1-L^2} - \delta\Omega}\,.$$

As in the previous case, the stable separatrices of the saddle points diverge to infinity as $t \to -\infty$. To show that the unstable separatrices of the points O_i behave as they are depicted in Fig. 10.6.7: one tends to infinity as $t \to +\infty$ while the second tends to the origin, we must show that all together they do not go to infinity simultaneously. To do this let us consider system (10.6.11) for large R. Introduce a new variable $z = R^{-2}$ and make the transformation of time $dt \to zdt$. We obtain:

$$\begin{aligned} \dot{z} &= -2z(L + \cos 4\varphi)\,, \\ \dot{\varphi} &= \delta z + \Omega - \sin 4\varphi\,. \end{aligned} \tag{10.6.13}$$

The value $z = 0$ corresponds to $R = +\infty$. System (10.6.13) has at $z = 0$ eight equilibrium states determined from the relation $\Omega = \sin 4\varphi$: four

equilibria are stable and the others are completely unstable. The stable separatrices of the saddles O_i emerge from the completely unstable equilibria at $t = -\infty$, two separatrices from each (because there are eight separatrices to four unstable equilibrium states). It is seen now from Fig. 10.6.7 that only four unstable separatrices enter the stable equilibrium states at infinity as $t \to +\infty$; the remaining ones must stay inside a finite part of the plane and, therefore, must tend to the point O.

10.7. Additional remarks on resonances

We have seen in Sec. 10.4 that in the case of weak resonance $\omega = 2\pi M/N$, $N \geq 5$, the stability of the critical fixed point is, in general, determined by the sign of the first non-zero Lyapunov value. The same situation applies to the critical case of an equilibrium state with a purely imaginary pair of characteristic exponents. However, there is an essential distinction, namely, for a resonant fixed point only a finite number which does not exceed $(N-3)/2$ of the Lyapunov values is defined. The question of the structure of a small neighborhood of the fixed point in the case where all Lyapunov values vanish is difficult, so we do not study it here. Instead, we consider two examples.

The first example is analogous to strong resonances. This is the map

$$\bar{w} = e^{2\pi i M/N} w + (w^*)^{N-1} . \tag{10.7.1}$$

One can see that the Nth iterate of map (10.7.1) coincides up to terms of order N with the shift map over time $t = N$ along the trajectories of the system

$$\dot{w} = (w^*)^{N-1} . \tag{10.7.2}$$

In polar coordinates this system assumes the form

$$\dot{R} = R^{N-1} \cos N\varphi ,$$

$$\dot{\varphi} = -R^{N-2} \sin N\varphi .$$

The function

$$H = R^N \sin N\varphi$$

is a first integral of the system. A trivial reconstruction of the level curves of the function H reveals that the equilibrium state at the origin is a saddle

with $2N$ separatrices. The same holds for the fixed point of the original map (10.7.1) as well.

In fact, resonant fixed points are not restricted to only saddles and stable (completely unstable) points. An example of the other structure is given by the map

$$\bar{w} = e^{2\pi M/N} w + w^{N+1}\,, \tag{10.7.3}$$

whose Nth iterate, up to terms of order $(N+1)$, is the shift map along the trajectories of the system

$$\dot{w} = w^{N+1}\,, \tag{10.7.4}$$

or in the polar coordinates,

$$\dot{R} = R^{N+1} \cos N\varphi\,,$$

$$\dot{\varphi} = R^N \sin N\varphi\,.$$

The latter has a first integral

$$H = \frac{\sin N\varphi}{R^N}\,.$$

The integral curves are given by the formula

$$R = C(\sin N\varphi)^{1/N}\,.$$

We can now construct the phase portrait (see Fig. 10.7.1 for $N = 3$): there are $2N$ invariant rays playing the role of separatrices (stable and unstable) which

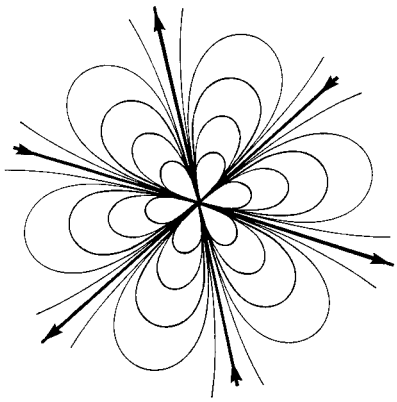

Fig. 10.7.1. A fixed point when $n = 2$. The sectors between the separatrices are called *elliptic*.

partition the phase-plane into $2N$ sectors (so-called *elliptic sectors*): inside each sector any trajectory is biasymptotic to the equilibrium state, i.e. it tends to O as $t \to \pm\infty$. One can verify that a neighborhood of the fixed point of the original map (10.7.3) has a similar structure.

Chapter 11

LOCAL BIFURCATIONS ON THE ROUTE OVER STABILITY BOUNDARIES

The study of critical cases gives rise to a number of questions: why does an equilibrium state, or a periodic orbit, preserves its stability on the boundary in some cases and not in others? What happens beyond the stability boundary?

The answers to these questions are settled by the theory of bifurcations. In this chapter, we consider only *local* bifurcations, i.e. those which occur near critical equilibrium states, and near fixed points of a Poincaré map. We restrict our study to the simplest but key bifurcations which have an immediate connection to the critical cases are discussed in the two last chapters.

The tool kit used for studying bifurcational problems consists of three pieces: the theorem on center manifold, the reduction theorem, and the method of normal forms.

Any study of bifurcations must include choosing appropriate independent parameters that control the bifurcation. In choosing parameters, ideas from the theory of singularities of smooth mappings are applied, based on the notion of transversality. In simple cases, the choice of the governing parameters usually agrees with common sense. For more complicated bifurcations, an appropriate choice of parameters is a non-trivial problem.

11.1. Bifurcation surface and transverse families

A system of differential equations is usually thought of as a mathematical model of a real dynamical system governed by some set of parameters.

Obviously, any statement concerning a real system derived from an analysis of its theoretical idealization, i.e. from its model, must not be too sensible to small uncontrolled variations of the parameters. Hence, it is a standard requirement that one must consider not only a stand-alone system but must also understand what happens with all neighboring systems. This works well for rough (structurally stable) equilibrium states and periodic orbits: in this case the qualitative structure is not modified by small perturbations of the right-hand side of the system. In contrast, for systems on the stability boundary, the analysis of close systems may become a real problem.

Consider a family of systems of differential equations

$$\dot{x} = X(x, \varepsilon)\,,$$

where $x \in \mathbb{R}^n$, and $\varepsilon = (\varepsilon_1, \ldots, \varepsilon_p)$ is a set of parameters. Suppose that for some $\varepsilon = \varepsilon^0$ the system has a critical equilibrium state, or a critical periodic orbit, i.e. it lies on the boundary $\mathfrak{M}$ of the stability region. In general, $\mathfrak{M}$ is a smooth $(p-1)$-dimensional surface in a neighborhood of the point ε^0 and is defined by an equation of the form

$$\Phi(\varepsilon) = 0\,, \tag{11.1.1}$$

where

$$\Phi' = \left(\frac{\partial \Phi}{\partial \varepsilon_1}, \frac{\partial \Phi}{\partial \varepsilon_2}, \ldots, \frac{\partial \Phi}{\partial \varepsilon_p}\right) \neq 0\,. \tag{11.1.2}$$

Since the derivative of Φ with respect to at least one of the parameters does not vanish, we may assume without loss of generality that

$$\frac{\partial \Phi}{\partial \varepsilon_p} \neq 0\,. \tag{11.1.3}$$

It is clear that this condition is not violated by small perturbations of the right-hand side. Moreover, if it is not satisfied, it can be achieved by a small transformation of the family $X(x, \varepsilon)$ under consideration. When the inequality (11.1.2) holds we say that the family $X(x, \varepsilon)$ is *in general position* with respect to $\mathfrak{M}$.

If we let

$$\mu = \Phi(\varepsilon_1, \ldots, \varepsilon_p)\,, \tag{11.1.4}$$

then the surface $\mathfrak{M}$ is simply defined by

$$\mu = 0\,.$$

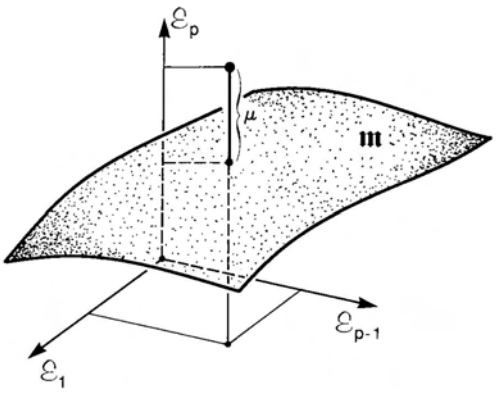

Fig. 11.1.1. Choice of governing parameter in a family transverse to the bifurcation surface $\mathfrak{M}$.

Furthermore, any point near ε^0 in the parameter space can be uniquely identified via the coordinates $\varepsilon_1, \ldots, \varepsilon_{p-1}$ and μ because $\partial\Phi/\partial\varepsilon_p \neq 0$ and ε_p is, therefore, uniquely determined from (11.1.4). If we resolve (11.1.1) for ε_p, i.e. represent $\mathfrak{M}$ in the form

$$\varepsilon_p = \varphi(\varepsilon_1, \ldots, \varepsilon_{p-1}),$$

then we may define

$$\mu \equiv \varepsilon_p - \varphi(\varepsilon_1, \ldots, \varepsilon_{p-1}),$$

and hence

$$\varepsilon_p = \mu + \varphi(\varepsilon_1, \ldots, \varepsilon_{p-1}).$$

The scalar μ is said to be a *governing parameter*. It measures the distance from a point in the parameter space to the surface $\mathfrak{M}$, whereas $\varepsilon_1, \ldots, \varepsilon_{p-1}$ give the projection of the point onto the surface $\mathfrak{M}$, as shown in Fig. 11.1.1.

In the following discussion, we will consider *one-parameter* families recast in the form

$$\dot{x} = X(x, \varepsilon_1(\mu), \ldots, \varepsilon_p(\mu)),$$

where $\varepsilon_i(\mu)$'s are smooth functions, and $\Phi(\varepsilon(\mu)) \equiv \mu$.[1] Such a family is a *transverse* one in the sense that the curve

$$\varepsilon_1 = \varepsilon_1(\mu), \ldots, \varepsilon_p = \varepsilon_p(\mu)$$

[1]To satisfy this equality one may choose $\varepsilon_1(\mu), \ldots, \varepsilon_{p-1}(\mu)$ arbitrarily but find $\varepsilon_p(\mu)$ from (11.1.4).

intersects transversely (without contact) the surface $\mathfrak{M}$. Since such a transverse curve can be defined through any point sufficiently close to ε^0, it is obvious that in order to study all systems close to $\dot{x} = X(x, \varepsilon^0)$ it suffices to analyze the transverse families only. According to the Andronov's setup (Sec. 8.4), this consists of finding the intervals of μ where the trajectories behave in a qualitatively similar way, as well as of detecting what happens at the bifurcation values of μ which correspond to the boundaries of these intervals.

An ideal case (and this is possible sometimes) would be one where all close transverse families are qualitatively equal (such families were called *versal* due to Arnold [20]). Having studied bifurcations in one transverse family, we would have a complete description for all neighboring ones.

For cases having an extra degeneracy (for example an equilibrium state with zero characteristic exponent and zero first Lyapunov value) the boundary of the stability region may lose smoothness at the point ε^0. There may also exist situations where the boundary is smooth but bifurcations in different nearby one-parameter families are different (i.e. there does not exist a versal one-parameter family, for example, such as the case of an equilibrium state with a pair of purely imaginary exponents and zero first Lyapunov value). In such cases the procedure is as follows. Consider a surface $\mathfrak{M}'$ of a smaller dimension (less than $(p-1)$) which passes through the point ε^0 and is a part of the stability boundary, selected by some additional conditions; in the above examples the condition is that the first Lyapunov value be zero. If $(k-1)$ additional conditions are imposed, then the surface $\mathfrak{M}'$ will be $(p-k)$-dimensional and it is defined by a system of the form

$$\begin{cases} \Phi_1(\varepsilon) = 0\,, \\ \vdots \qquad\quad \vdots\,\vdots \\ \Phi_k(\varepsilon) = 0\,. \end{cases} \tag{11.1.5}$$

Let the matrix of derivatives

$$\begin{pmatrix} \dfrac{\partial \Phi_1}{\partial \varepsilon_1} & \cdots & \dfrac{\partial \Phi_1}{\partial \varepsilon_p} \\ \vdots & \ddots & \vdots \\ \dfrac{\partial \Phi_k}{\partial \varepsilon_1} & \cdots & \dfrac{\partial \Phi_k}{\partial \varepsilon_p} \end{pmatrix}$$

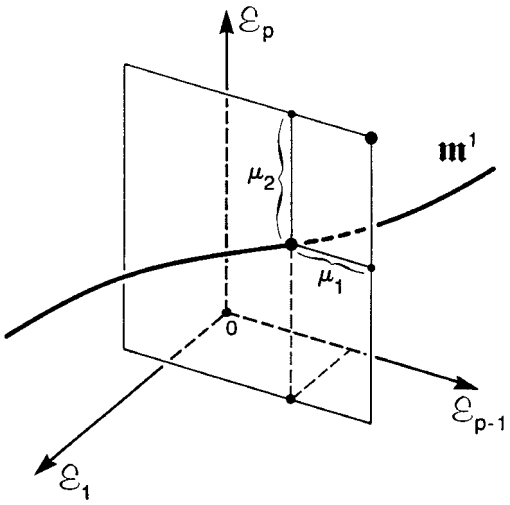

Fig. 11.1.2. The bifurcation surface $\mathfrak{M}'$ of codimension two is a curve in a three-parameter family.

have rank k, i.e. have a maximal rank;[2] where we have assumed that $p \geq k$. In this case, k-parameters can be expressed in terms of the others; namely,

$$\varepsilon_p = \varphi_1(\varepsilon_1, \ldots, \varepsilon_{p-k}), \ldots, \varepsilon_{p-k+1} = \varphi_1(\varepsilon_1, \ldots, \varepsilon_{p-k})\,.$$

Let us introduce the governing parameters (see Fig. 11.1.2 for $k = 2$)

$$\begin{cases} \mu_1 \equiv \varepsilon_p - \varphi_1(\varepsilon_1, \ldots, \varepsilon_{p-k})\,, \\ \quad \vdots \; \vdots \qquad \vdots \\ \mu_k \equiv \varepsilon_{p-k+1} - \varphi_1(\varepsilon_1, \ldots, \varepsilon_{p-k})\,. \end{cases} \tag{11.1.6}$$

If (11.1.5) is not solved for $(\varepsilon_{p-k+1}, \ldots, \varepsilon_p)$, we can still define

$$\begin{cases} \mu_1 \equiv \Phi_1(\varepsilon_1, \ldots, \varepsilon_p)\,, \\ \quad \vdots \; \vdots \qquad \vdots \\ \mu_k \equiv \Phi_k(\varepsilon_1, \ldots, \varepsilon_p)\,. \end{cases} \tag{11.1.7}$$

[2]We will then say that the family is *in general position* with respect to $\mathfrak{M}'$.

Let us now consider a k-parameter family of vector fields, transverse to $\mathfrak{M}'$, represented in the following form

$$\dot{x} = X(x, \varepsilon_1(\mu), \ldots, \varepsilon_p(\mu)),$$

where $\mu = (\mu_1, \ldots, \mu_k)$, and $\varepsilon_i(\mu)$ are some smooth functions satisfying (11.1.6) or (11.1.7).

Such a situation will henceforth be referred to as a *a bifurcation of codimension k*, and the surface $\mathfrak{M}'$ is called *a bifurcation surface of codimension k* (the codimension is equal to the number of the governing parameters).

The procedure for studying a k-parameter family is similar to that for the one-parameter case: firstly, divide the space of the parameters μ into the regions of topologically equivalent behavior of trajectories, and study the system in each of these regions. Secondly, describe the boundaries of these regions (the bifurcation set), and finally study what happens at the bifurcation parameter values. We will see below that in the simplest cases (e.g. an equilibrium state with one zero or a pair of imaginary characteristic exponents, or a periodic orbit with one multiplier equal to 1 or to -1) one can almost always, except for extreme degeneracies, choose a correct bifurcation surface of a suitable codimension and analyze completely the transverse families. Moreover, all of these families turn out to be versal.

It should be noted that constructing the versal families is realistic only in these simple cases, and in a few special cases. For example, a finite-parameter versal family cannot be constructed for the bifurcation of a periodic orbit with one pair of complex multipliers $e^{\pm i\omega}$. Nevertheless, this problem does admit a rather reasonable description within the framework of one- and two-parameter families. In the above example, the birth of an invariant torus can be completely explained and understood in a one-parameter setting, whereas the study of the bifurcations of resonant periodic orbits would require at least two-parameters. Hence, the same bifurcation phenomenon may be treated as a bifurcation of codimension one, or codimension two, depending on which details of dynamics we are focusing on. This indefiniteness is quite typical for the bifurcation theory of dynamical systems.

Moreover, in more complex cases the problem of presenting a complete description, or of proving that a family under consideration is versal, is not even set up. However, the general approach remains the same: a bifurcating system is considered as a point on some smooth bifurcation surface of a finite codimension. Then, a transverse family is constructed and the qualitative

results obtained from studying this concrete transverse family must be proven to hold for all neighboring families as well.

11.2. Bifurcation of an equilibrium state with one zero exponent

Let us consider a family of differential equations of class $\mathbb{C}^r (r \geq 2)$ with respect to both variables and parameters which has an equilibrium state at the origin with one zero characteristic exponent; the other characteristic exponents are assumed to have negative real parts. Near the origin the system can be then written in the form

$$\begin{aligned} \dot{x} &= g(x, y, \varepsilon)\,, \\ \dot{y} &= Ay + f(x, y, \varepsilon)\,, \end{aligned} \tag{11.2.1}$$

where $x \in \mathbb{R}^1$, $y \in \mathbb{R}^n$, the eigenvalues of the matrix A lie to the left of the imaginary axis, f and g are $\mathbb{C}^r$-smooth functions such that both f and g vanish at $x = 0$, $y = 0$, and $\varepsilon = 0$, along with their first derivatives with respect to x and y.

By virtue of the reduction Theorem 5.5, there exist $\mathbb{C}^{r-1}$-coordinates in which the family (11.2.1) reduces to the form

$$\begin{aligned} \dot{x} &= G(x, \varepsilon)\,, \\ \dot{y} &= [A + F(x, y, \varepsilon)]y\,, \end{aligned} \tag{11.2.2}$$

where F is a $\mathbb{C}^{r-1}$ function and G is a $\mathbb{C}^r$ function such that

$$\begin{aligned} F(0, 0, 0) &= 0\,, \\ G(0, 0) &= 0\,, \\ G'_x(0, 0) &= 0\,. \end{aligned} \tag{11.2.3}$$

It follows from (11.2.2) that to investigate the bifurcations of the original system it is sufficient to consider the restriction of the system to the center manifold

$$\dot{x} = G(x, \varepsilon)\,. \tag{11.2.4}$$

It follows from (11.2.3) that the function G at $\varepsilon = 0$ has the form

$$G(x,0) = l_2 x^2 + o(x^2)\,. \tag{11.2.5}$$

Consider first the case where the first Lyapunov value l_2 is non-zero. Following the scheme outlined in the preceding section, we first derive the equation of the boundary $\mathfrak{M}$ of the stability region near $\varepsilon = 0$. Next we will find the conditions under which $\mathfrak{M}$ is a smooth surface of codimension one. Finally, we will select the governing parameter and investigate the transverse families.

The set $\mathfrak{M}$ for small ε is defined by the condition that the system (11.2.4) has an equilibrium state with one zero characteristic exponent. When $\varepsilon \neq 0$ the equilibrium state is not, in general, at the origin. The condition defining $\mathfrak{M}$ is simply that there exists x^* such that

$$G(x^*,\varepsilon) = 0\,, \tag{11.2.6}$$

$$G'_x(x^*,\varepsilon) = 0\,. \tag{11.2.7}$$

Recall that $l_2 \equiv G''_{xx}(0,0)/2 \neq 0$, and therefore by virtue of the implicit function theorem, x^* can be uniquely found from (11.2.7) for all small ε. Hence, we can recast (11.2.6) in the form

$$G(x^*(\varepsilon),\varepsilon) = 0\,. \tag{11.2.8}$$

Denote $\Phi(\varepsilon) = G(x^*(\varepsilon),\varepsilon)$. Since G'_x is a $\mathbb{C}^{r-1}$ function, it follows that $x^*(\varepsilon) \in \mathbb{C}^{r-1}$, and hence $\Phi(\varepsilon) \in \mathbb{C}^{r-1}$. The equation $\Phi(\varepsilon) = 0$ determines, for small ε, a $\mathbb{C}^{r-1}$-smooth surface of codimension one provided that

$$\Phi'_\varepsilon \equiv \left(\frac{\partial\Phi}{\partial\varepsilon_1}, \frac{\partial\Phi}{\partial\varepsilon_2}, \ldots, \frac{\partial\Phi}{\partial\varepsilon_p}\right) \neq 0\,,$$

or

$$\frac{d}{d\varepsilon} G(x^*(\varepsilon),\varepsilon)_{\varepsilon=0} \neq 0\,.$$

The latter inequality may be rewritten as

$$G'_x \frac{dx^*}{d\varepsilon} + G'_\varepsilon \neq 0$$

or, since $G'_x(0,0) = 0$, as

$$G'_\varepsilon(0,0) \neq 0\,. \tag{11.2.9}$$

We will therefore assume that (11.2.9) is satisfied,[3] i.e. the family is in general position. Now, let us introduce a governing parameter

$$\mu \equiv G(x^*(\varepsilon), \varepsilon)\,, \tag{11.2.10}$$

and consider an arbitrary one-parameter family of the form

$$\dot{x} = G(x, \varepsilon(\mu))\,, \tag{11.2.11}$$

which is transverse to $\mathfrak{M}$ (here, $\varepsilon(\mu)$ is some $\mathbb{C}^{r-1}$-smooth function satisfying (11.2.10)).

Let us move the origin to the point $x^*(\varepsilon(\mu))$, i.e. make a change of variable $x = x^* + \xi$. Then (11.2.11) recasts in the form

$$\dot{\xi} = G(x^* + \xi; \varepsilon(\mu)) = G(x^*, \varepsilon(\mu)) + G'_x(x^*, \varepsilon(\mu))\xi + G''_{xx}(x^*, \varepsilon(\mu))\xi^2/2 + o(\xi^2)\,.$$

From (11.2.7) and (11.2.10) we obtain

$$\dot{\xi} = \mu + l_2\xi^2 + \tilde{G}(\xi, \mu)\,, \tag{11.2.12}$$

where $\tilde{G}$ is $\mathbb{C}^r$ with respect to ξ and $\mathbb{C}^{r-1}$ with respect to μ, and

$$\tilde{G}(0, \mu) = 0\,, \quad \tilde{G}'_\xi(0, \mu) = 0\,, \quad \tilde{G}''_{\xi\xi}(0, 0) = 0\,.$$

The value l_2 is equal to $G''_{xx}(x^*(\varepsilon(0)), \varepsilon(0))/2$. It does not depend on μ but on the choice of the transverse family (11.2.11). Since the dependence is continuous, the values of l_2 are close and have the same sign for all close transverse families. Note that the case $l_2 < 0$ is reduced to $l_2 > 0$ by the transformation $\xi \to -\xi$ and $\mu \to -\mu$. Therefore, we will assume that $l_2 > 0$, but also present the corresponding figures for both cases.

Equation (11.2.12) is easily investigated. Observe that $\xi = 0$ is a point of minimum of the right-hand side, and correspondingly μ is a minimal value. Hence, for $\mu > 0$, the value $\dot{\xi}$ is positive for all small ξ, and therefore all trajectories must leave a neighborhood of the origin after a finite time. When $\mu < 0$ the right-hand side vanishes at two points: $O_2(\xi^-(\mu) < 0)$ and $O_1(\xi^+(\mu) > 0)$. The value $\dot{\xi}$ is negative inside the interval $(\xi^-(\mu), \xi^+(\mu))$ and is positive outside

[3]The function G is identically equal to $g(x, \varphi(x, \varepsilon), \varepsilon)$, where $y = \varphi(x, \varepsilon)$ is the equation of the center manifold of system (11.2.1). Since $g'_{(x,y)}(0, 0, 0) = 0$, condition (11.2.9) is equivalent to $g'_\varepsilon(0, 0, 0) \neq 0$.

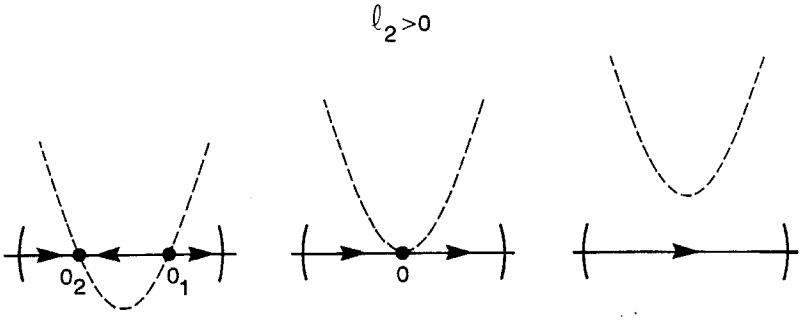

(a) $\mu < 0$ (b) $\mu = 0$ (c) $\mu > 0$

Fig. 11.2.1. A one-dimensional portrait of Eq. (11.2.11) when $G''_{xx} = l_2 > 0$ as a function of the control parameter μ.

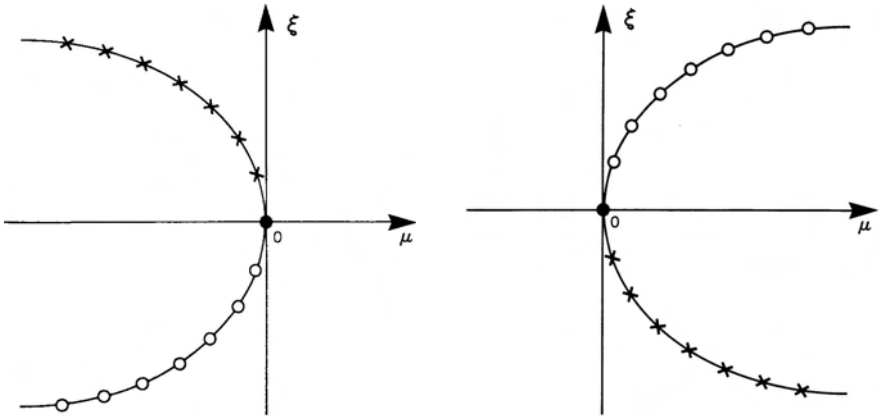

(a) $\ell_2 > 0$ (b) $\ell_2 < 0$

Fig 11.2.2. Dependence of the coordinates of the equilibrium state on μ in the cases $l_2 > 0$ (a) and $l_2 < 0$ (b). The crosses and circles label the unstable and the stable branches, respectively.

of it; so the point $O_2(\xi^-(\mu))$ is a stable equilibrium state, whereas the point $O_1(\xi^+(\mu))$ is an unstable equilibrium state, as shown in Fig. 11.2.1(a). The corresponding scenario for the case $l_2 < 0$ is shown in Fig. 11.2.3.

As μ increases the equilibrium states move closer towards each other, and coalesce at $\mu = 0$. The graph showing the dependence of the coordinate of the equilibrium states on μ is shown in Fig. 11.2.2. The following asymptotic

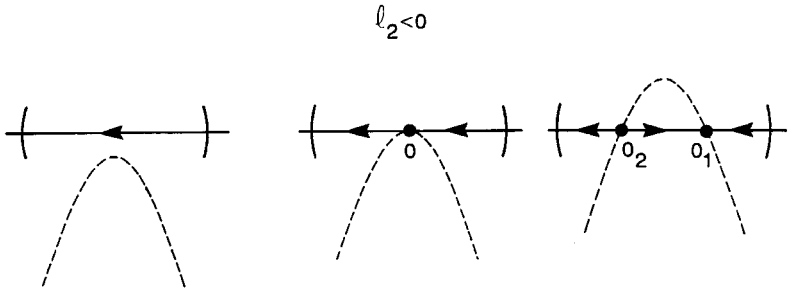

(a) $\mu < 0$ (b) $\mu = 0$ (c) $\mu > 0$

Fig. 11.2.3. Same as Fig. 11.2.1 but with $l_2 < 0$.

expression for the equilibrium states can be derived:

$$\xi^{\pm} \sim \pm\sqrt{|\mu|/l_2}\,. \tag{11.2.13}$$

To prove this let us rescale the ξ-coordinate and the time variable in (11.2.12) by $\sqrt{|\mu|}$: $\xi \to \xi\sqrt{|\mu|}$ and $t \to t/\sqrt{|\mu|}$. Then, (11.2.12) takes the form

$$\frac{d\sqrt{|\mu|}\xi}{dt/\sqrt{|\mu|}} = \mu + l_2(\sqrt{|\mu|}\xi)^2 + \tilde{G}(\sqrt{|\mu|}\xi, \mu)$$

or

$$\dot{\xi} = -1 + l_2\xi^2 + \tilde{G}(\sqrt{|\mu|}\xi, \mu)/|\mu|\,. \tag{11.2.14}$$

Since $\tilde{G} = o(\xi^2)$ and $\tilde{G}'_\xi = o(\xi)$, it follows that $\tilde{G}(\sqrt{|\mu|}\xi, \mu)/|\mu|$ tends to zero as $\mu \to 0$, along with its derivative with respect to ξ. Hence, by virtue of the implicit function theorem, we find that the right-hand side of (11.2.14) vanishes at two points

$$\xi^{\pm} = \pm 1/\sqrt{l_2} + \cdots\,,$$

which gives (11.2.13) upon a return to the original coordinates.

When $l_2 < 0$, the changes in the phase portrait as μ varies are given in Fig. 11.2.3, and the dependence of the coordinates of the fixed points on μ is shown in Fig. 11.2.2(b).

The phase portraits for systems of dimension two and higher are illustrated in Figs. 11.2.4–11.2.7, respectively. Here, when $l_2\mu < 0$, there are two rough equilibrium states: a stable node and a saddle that approach each other as $l_2\mu$

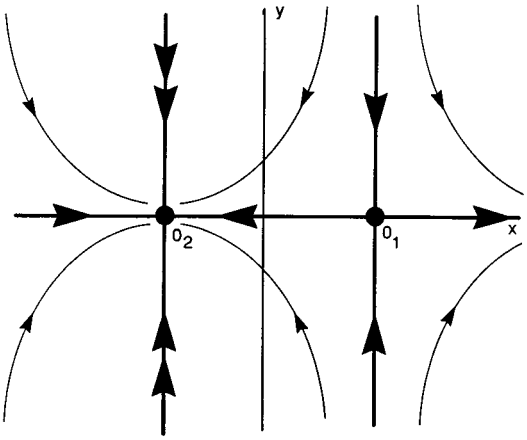

(a) $\mu < 0$

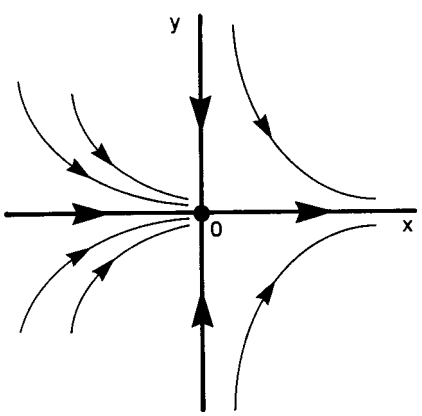

(b) $\mu = 0$

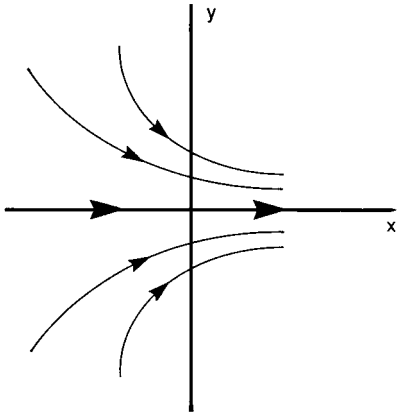

(c) $\mu > 0$

Fig. 11.2.4. Planar bifurcation of a saddle-node equilibrium state with $\ell_2 > 0$.

increases. At $\mu = 0$ they merge thereby forming a saddle-node which disappears as $l_2\mu$ becomes positive; all trajectories move away from a neighborhood of the origin.

Consider next the case $l_2 = 0$. Let k be the index number of the first non-zero Lyapunov value, i.e. at $\varepsilon = 0$, the function $G(x, \varepsilon)$ in (11.2.4) has the

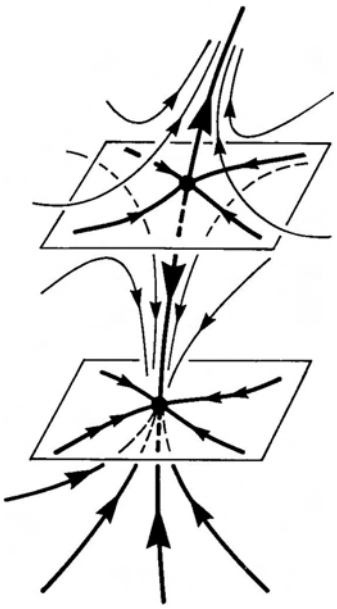

(a) $\mu < 0$

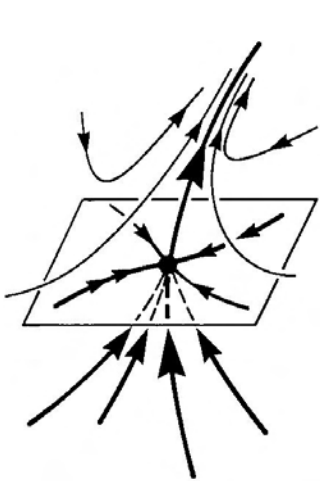

(b) $\mu = 0$

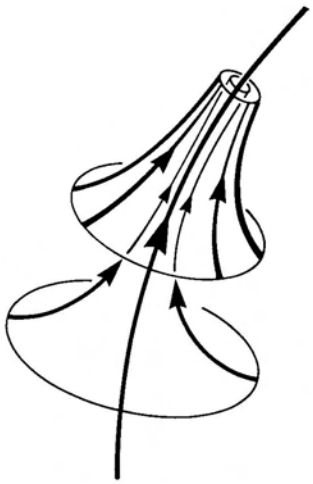

(c) $\mu > 0$

Fig. 11.2.5. Bifurcation of a saddle-node equilibrium state in $\mathbb{R}^3$. Variant I.

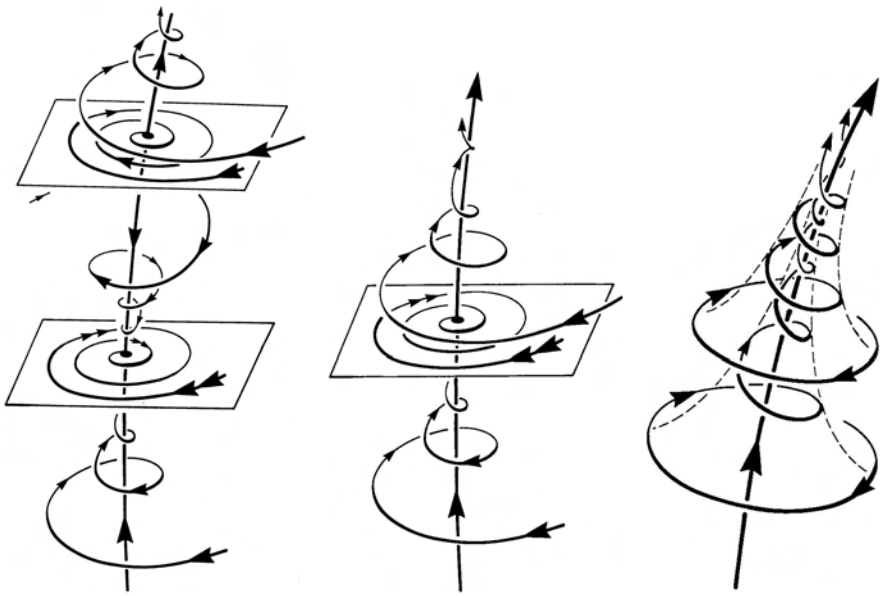

(a) $\mu < 0$ (b) $\mu = 0$ (c) $\mu > 0$

Fig. 11.2.6. Bifurcation of a saddle-node equilibrium state in $\mathbb{R}^3$. Variant II.

form

$$G(x,0) = l_k x^k + o(x^k)$$

(the order of smoothness of the system is assumed to be not less than k). Let us show that if the number p of parameters ε is equal to or greater than $(k-1)$, then the set of points in the parameter space that correspond to the existence of a non-rough equilibrium state with one zero characteristic exponent, and with zero values of $l_2, \ldots, l_{k-1}$ comprises, generically, a smooth surface $\mathfrak{M}'$ of codimension $(k-1)$ such that any family transverse to $\mathfrak{M}'$ may be represented in the following form

$$\dot{x} = \mu_1 + \cdots + \mu_{k-1} x^{k-2} + l_k x^k + o(x^k)\,. \tag{11.2.15}$$

Indeed, the condition under which the system has an equilibrium state x^* with one zero exponent and zero Lyapunov values $l_2, \ldots, l_{k-1}$ is given by

$$G(x^*,\varepsilon) = G'_x(x^*,\varepsilon) = G''_{xx}(x^*,\varepsilon) = \cdots = G^{(k-1)}(x^*,\varepsilon) = 0\,. \tag{11.2.16}$$

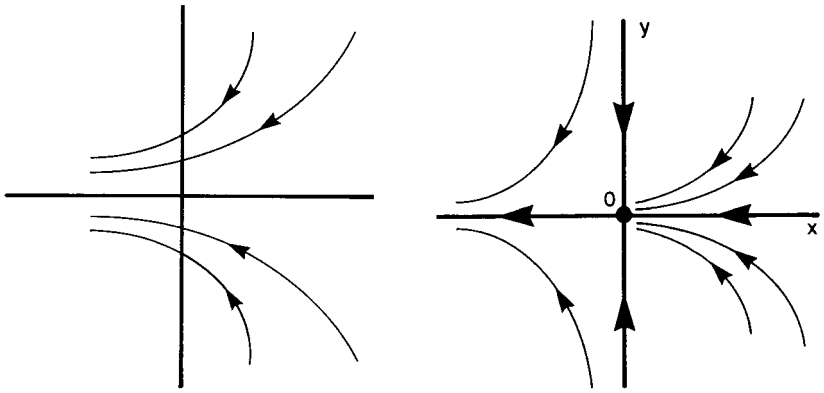

(a) $\mu < 0$ (b) $\mu = 0$

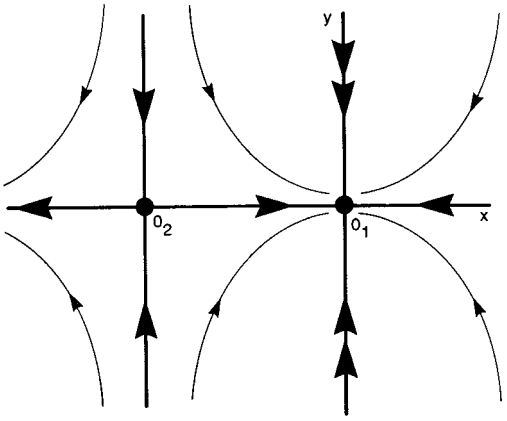

(c) $\mu > 0$

Fig 11.2.7. The case $l_2 < 0$ reduces to that in Fig. 11.2.4 by the transformation $(\mu \to -\mu,\, x \to -x)$.

Since

$$\frac{\partial^k G(0,0)}{\partial x^k} \equiv l_k k! \neq 0\,,$$

the value x^* is uniquely found from the equation

$$G^{(k-1)}(x^*, \varepsilon) = 0 \tag{11.2.17}$$

for small ε. Let $x = x^*(\varepsilon)$ be a solution of (11.2.17); it is clear that x^* is a $\mathbb{C}^{r-k+1}$-smooth function. By substituting $x^*(\varepsilon)$ into the remaining equations in (11.2.16), we obtain the equation of the following surface $\mathfrak{M}'$:

$$G(x^*(\varepsilon),\varepsilon) = 0,\ G'_x(x^*(\varepsilon),\varepsilon) = 0,\dots,G^{(k-2)}(x^*(\varepsilon),\varepsilon) = 0\,.$$

This surface is smooth if the system is in general position, i.e. if the rank of the matrix

$$\left(\begin{array}{ccc} \dfrac{\partial G(x^*(\varepsilon),\varepsilon)}{\partial\varepsilon_1} & \cdots & \dfrac{\partial G(x^*(\varepsilon),\varepsilon)}{\partial\varepsilon_p} \\ \vdots & \ddots & \vdots \\ \dfrac{\partial G^{(k-2)}(x^*(\varepsilon),\varepsilon)}{\partial\varepsilon_1} & \cdots & \dfrac{\partial G^{(k-2)}(x^*(\varepsilon),\varepsilon)}{\partial\varepsilon_p} \end{array}\right)_{\varepsilon=0} \tag{11.2.18}$$

is equal to $(k-1)$ (see preceding section; it follows immediately that the number p of parameters should not be less than $(k-1)$). Since

$$\frac{\partial G^j(x^*(\varepsilon),\varepsilon)}{\partial\varepsilon_i} \equiv \left(\frac{\partial^{j+1}G}{\partial x^{j+1}}\frac{\partial x^*}{\partial\varepsilon_i} + \frac{\partial^{j+1}G}{\partial x^j\partial\varepsilon_i}\right)_{x=x^*(\varepsilon)}$$

and

$$\frac{\partial^j G(0,0)}{\partial x^j} = 0 \quad \text{if} \quad 1 \le j \le k-1\,,$$

it is sufficient for the matrix

$$\left(\begin{array}{ccc} \dfrac{\partial G}{\partial\varepsilon_1} & \cdots & \dfrac{\partial G}{\partial\varepsilon_p} \\ \vdots & \ddots & \vdots \\ \dfrac{\partial^{k-1}G}{\partial\varepsilon_1\partial x^{k-2}} & \cdots & \dfrac{\partial^{k-1}G}{\partial\varepsilon_p\partial x^{k-2}} \end{array}\right)_{(x=0,\varepsilon=0)}$$

to have maximal rank. We will assume that this condition is satisfied. Hence, we can introduce $k-1$ governing parameters $\mu_1,\dots,\mu_{k-1}$:

$$\begin{aligned}
\mu_1 &= G(x^*(\varepsilon),\varepsilon)\,,\\
\mu_2 &= G'_x(x^*(\varepsilon),\varepsilon)\,,\\
&\vdots\ \vdots\ \vdots\\
\mu_i &= G^{(i-1)}(x^*(\varepsilon),\varepsilon)/(i-1)!\,,\\
&\vdots\ \vdots\ \vdots\\
\mu_{k-1} &= G^{(k-2)}(x^*(\varepsilon),\varepsilon)/(k-2)!\,,
\end{aligned} \tag{11.2.19}$$

such that a $(k-1)$-parameter family, transverse to $\mathfrak{M}'$, can be written as

$$\dot x = G(x,\varepsilon(\mu))\,, \tag{11.2.20}$$

where $\varepsilon(\mu)$ is some function of class $\mathbb{C}^{r-k+1}$ which satisfies (11.2.19). Such $\varepsilon(\mu)$ exists in view of maximality of the rank of the matrix (11.2.18): some $(k-1)$ of the ε_i can be uniquely determined from (11.2.19) in terms of $\mu_1,\dots,\mu_{k-1}$, and of the other ε's.

If the origin is shifted to the point x^* (i.e. if we let $x=\xi+x^*$), then Eq. (11.2.20) recasts into the form

$$\begin{aligned}
\dot\xi &= G(x^*+\xi,\varepsilon(\mu))\\
&= G(x^*,\varepsilon(\mu)) + G'_x(x^*,\varepsilon(\mu))\xi + \dots + G^{(k)}(x^*,\varepsilon(\mu))\xi^k/k! + o(\xi^k)\,.
\end{aligned}$$

Using (11.2.17) and (11.2.19), we obtain

$$\dot\xi = \mu_1 + \dots + \mu_{k-1}\xi^{k-2} + l_k\xi^k + \tilde G(\xi,\mu)\,. \tag{11.2.21}$$

The function $\tilde G$ is $\mathbb{C}^r$-smooth with respect to ξ and $\mathbb{C}^{r-k+1}$-smooth with respect to μ; its derivatives up to order $(k-1)$ with respect ξ are $\mathbb{C}^{r-k+1}$-smooth with respect to μ as well. Moreover,

$$\begin{aligned}
\tilde G(0,\mu) = \tilde G'_\xi(0,\mu) = \dots = \tilde G^{(k-1)}(0,\mu) = 0\,,\\
\tilde G^{(k)}(0,0) = 0\,.
\end{aligned} \tag{11.2.22}$$

Finally, changing ξ back to x, we obtain (11.2.15).

We will only consider in detail bifurcations of small codimensions ($k=3,4$). When $l_3\neq 0$, the family (11.2.21) takes the form

$$\dot x = \mu_1 + \mu_2 x + l_3x^3 + \tilde G(x,\mu)\,. \tag{11.2.23}$$

Recall that at $\mu_1 = \mu_2 = 0$, the point $O(x = 0)$ is stable if $l_3 < 0$ or unstable if $l_3 > 0$ (see Sec. 9.2). Notice also that the case $l_3 > 0$ is reduced to the case $l_3 < 0$ by a change of variables: $t \to -t$, $\mu_1 \to -\mu_1$ and $\mu_2 \to -\mu_2$.

It is easy to see that for small μ, Eq. (11.2.23) may have no more than three equilibrium states near the origin. Indeed, if the right-hand side has, for example, four roots (including multiplicity), then its first derivative must have at least three roots, its second derivative must have two roots, and its third derivative must have at least one root. But the third derivative is equal to $(6l_3 + o(1))$ and hence cannot vanish near the origin.

It is obvious that the parameter values for which there are only two equilibrium states are bifurcation points because one of the roots of the right-hand side must then be a multiple root (see Figs. 11.2.8(c) and (d) for $l_3 < 0$ and Figs. 11.2.9(c) and (d) for $l_3 > 0$). This root corresponds to a semi-stable equilibrium state that either disappears, or is split into two equilibria, following an arbitrarily small variation in the parameters.

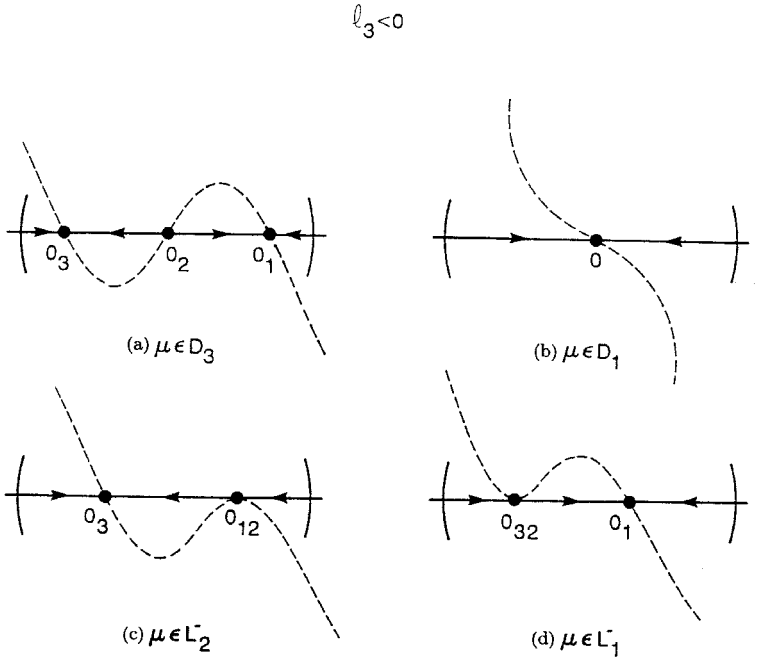

Fig 11.2.8. The case $l_2 = 0$, $l_3 < 0$.

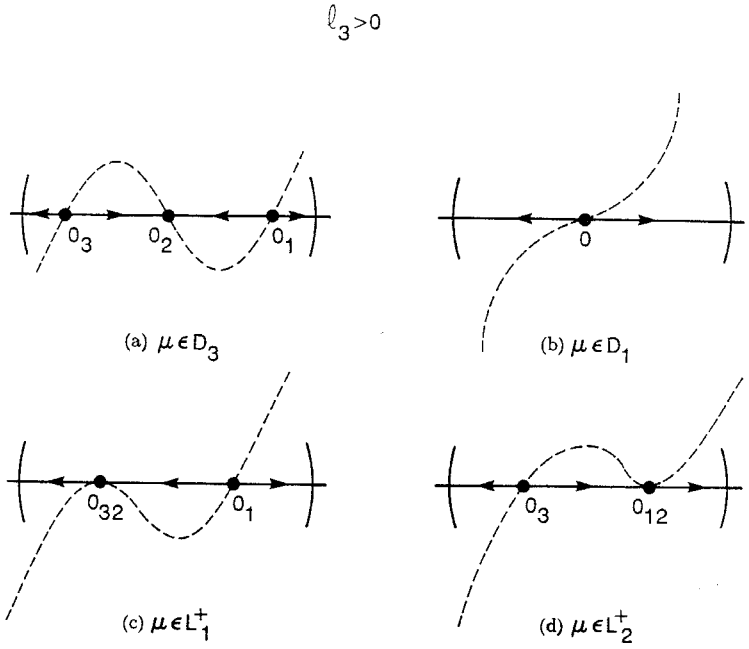

Fig. 11.2.9. The case $l_2 = 0$, $l_3 > 0$.

The point x is a double root if

$$\begin{aligned} \mu_1 + \mu_2 x + l_3 x^3 + \tilde{G}(x, \mu) = 0\,, \\ \mu_2 + 3 l_3 x^2 + \tilde{G}'_x(x, \mu) = 0\,. \end{aligned} \tag{11.2.24}$$

To solve the system (11.2.24), let us rescale x by $\sqrt{|\mu_2|}$ and let $M = \mu_1/(\mu_2\sqrt{|\mu_2|})$. In the new variables the system (11.2.24) becomes

$$\begin{aligned} M + x \pm l_3 x^3 + \tilde{G}(x\sqrt{|\mu_2|}, \mu)/(\mu_2\sqrt{|\mu_2|}) = 0\,, \\ \pm 1 + 3 l_3 x^2 + \tilde{G}'_x(x\sqrt{|\mu_2|}, \mu)|\mu_2| = 0\,, \end{aligned} \tag{11.2.25}$$

where $\pm$ stands for the sign of μ_2. Since $\tilde{G} = o(x^3)$, it follows that the terms with $\tilde{G}$ and $\tilde{G}'$ in (11.2.25) become infinitesimally small as $\mu_1 \to 0$ and $\mu_2 \to 0$. It is seen from the second equation of (11.2.25) that the sign of μ_2 must be opposite to that of l_3. In the limit $\mu_1 = \mu_2 = 0$, the system (11.2.25) reduces

to the form

$$M + x - |l_3|x^3 = 0\,,$$
$$-1 + 3|l_3|x^2 = 0\,.$$

Solving the above system for x, we obtain

$$x = \pm 1/\sqrt{3|l_3|}\,, \quad M = -\frac{2}{3}x\,.$$

It then follows from the implicit function theorem that for small μ_2

$$M = \pm 2/(3\sqrt{3|l_3|}) + \cdots$$

in (11.2.25). Reverting back to non-rescaled variables, we obtain the following equation of the bifurcation curve (Fig. 11.2.10):

$$\mu_1 = \pm 2\mu_2\sqrt{|\mu_2/l_3|}/3\sqrt{3} + \cdots\,, \quad \mu_2 l_3 < 0\,. \tag{11.2.26}$$

We will denote this curve by L^- when $l_3 < 0$ (see Fig. 11.2.10(a)), and by L^+ when $l_3 > 0$ (see Fig. 11.2.10(b)). The point $(\mu_1 = 0, \mu_2 = 0)$ breaks these curves into two branches which we denote as $L_1^{\pm}$ and $L_2^{\pm}$. Both the branches touch each other and the μ_2-axis at the origin.

Due to this particular shape of the bifurcation set, this bifurcation is called *a cusp*. The curve $L^{\pm}$ divides a neighborhood of the origin into two parts: D_3

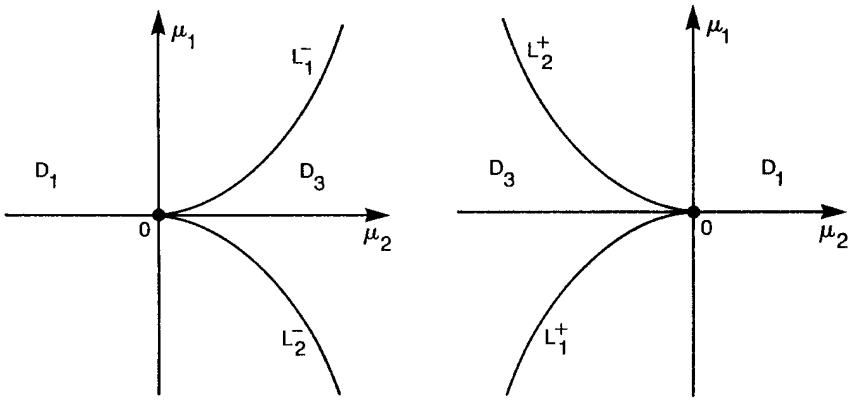

(a) $\ell_3 < 0$ (b) $\ell_3 > 0$

Fig. 11.2.10. Bifurcation unfolding in the cases $l_3 < 0$ (a) and $l_3 > 0$ (b).

is the region inside the wedge (it contains the positive μ_2-semi-axis when $l_3 < 0$ or the negative one when $l_3 > 0$), and D_1 is the region outside. We can easily verify that at each point on the curve $L^{\pm}$, the two-parameter family (11.2.23) satisfies the genericity condition (11.2.9).

It is easy to show that if $l_3 < 0$, then:

(1) inside the wedge D_3, the Eq. (11.2.17) has three equilibrium states: two stable (O_1 and O_3) and one unstable (O_2), as shown in Fig. 11.2.8(a);
(2) outside the wedge, in the region D_1, the Eq. (11.2.17) has only one stable equilibrium state, as shown in Fig. 11.2.8(b);
(3) for $\mu \in L_1^-$ the Eq. (11.2.17) has one stable equilibrium state O_1 and one semi-stable equilibrium state $O_{2,3}$ — the result of the merging of O_3 with O_2, with a negative first Lyapunov value, as shown in Fig. 11.2.8(d); and
(4) for $\mu \in L_2^-$ the Eq. (11.2.17) has one stable equilibrium state O_3 and a saddle-node O_{12} with a negative first Lyapunov value, as shown in Fig. 11.2.8(c).

If $l_3 > 0$, then:

(1) in the region D_3, the Eq. (11.2.17) has three equilibrium states — two unstable (O_1 and O_3) and one stable (O_2), as shown in Fig. 11.2.9(a);
(2) outside the wedge, in D_1, the Eq. (11.2.17) has only one unstable equilibrium state, as shown in Fig. 11.2.9(b);
(3) when $\mu \in L_1^+$ the Eq. (11.2.17) has one unstable equilibrium state O_1 and one semi-stable equilibrium state $O_{2,3}$, with a positive first Lyapunov value, as shown in Fig. 11.2.9(c); and
(4) when $\mu \in L_2^+$ the Eq. (11.2.17) has one unstable equilibrium state O_3 and a semi-stable equilibrium state $O_{1,2}$ as shown in Fig. 11.2.9(d).

The bifurcations in the two-dimensional case are illustrated by Figs. 11.2.11 and 11.2.12 for the cases $l_3 < 0$, and $l_3 > 0$, respectively.

In the case $l_3 > 0$, the central equilibrium state is stable for $\mu \in D_3$. For $l_3 < 0$, the character of the stability region becomes less trivial: namely, it becomes poly-sheeted (see Fig. 11.2.13). It should be noted that the stability boundary is not smooth at the origin.

Suppose next that $l_2 = l_3 = 0$ and $l_4 \neq 0$. Then, the transverse family assumes the form

$$\dot{x} = \mu_1 + \mu_2 x + \mu_3 x^2 + l_4 x^4 + o(x^4)\,. \tag{11.2.27}$$

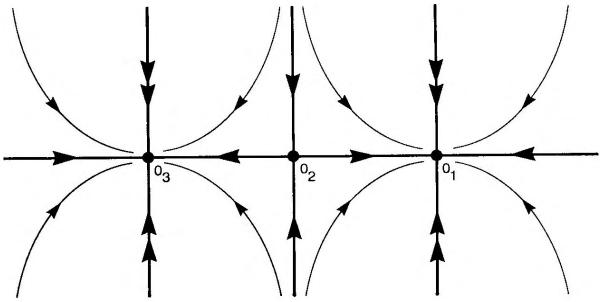

(a) $\mu \epsilon \, \mathrm{D}_3$

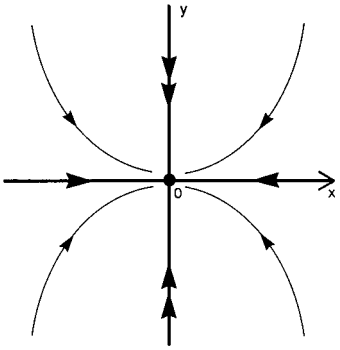

(b) $\mu \epsilon \, \mathrm{D}_1$

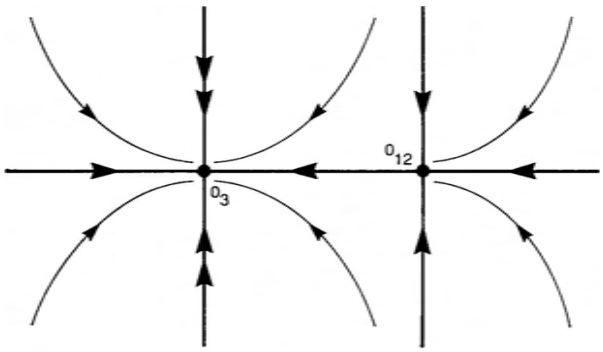

(c) $\mu \epsilon \, \mathrm{L}_2^-$

Fig. 11.2.11. Phase portraits corresponding to the bifurcation diagram in Fig. 11.2.10(a).

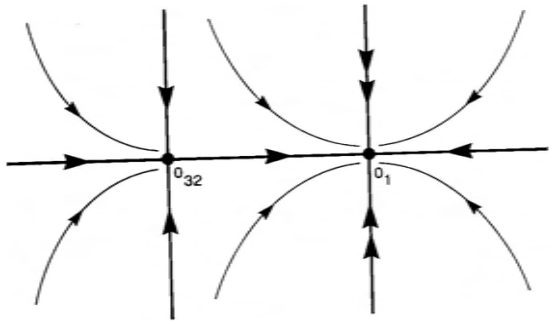

(d) $\mu \in L_1^-$

Fig. 11.2.11. (*Continued*)

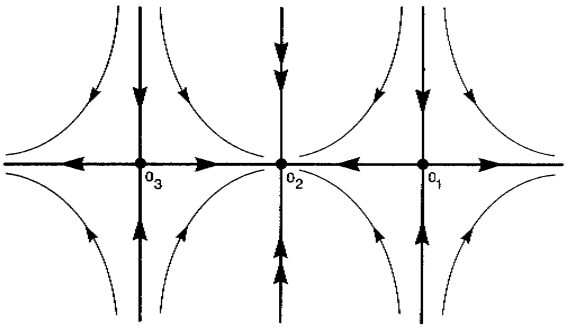

(a) $\mu \in D_3$

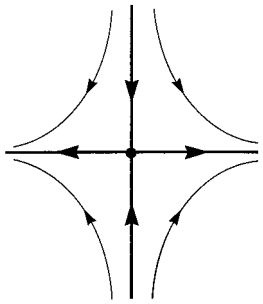

(b) $\mu \in D_1$

Fig. 11.2.12. Phase portraits for the bifurcation diagram in Fig. 11.2.10(b).

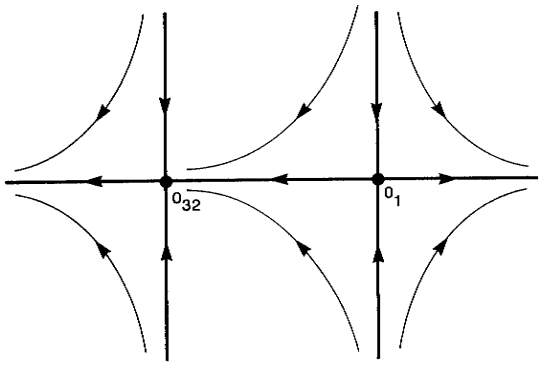

(c) $\mu \in \mathrm{L}_1^+$

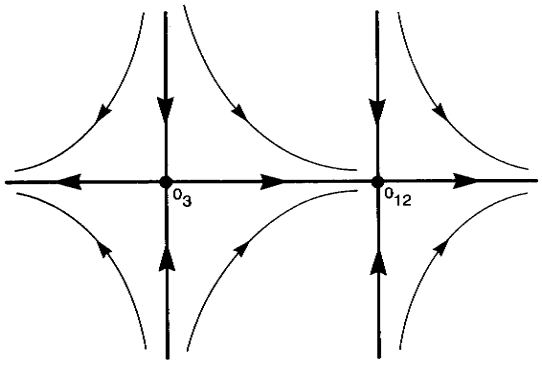

(d) $\mu \in \mathrm{L}_2^+$

Fig. 11.2.12 (*Continued*)

The parameter space here is partitioned into three regions: D_0, D_2 and D_4, joined at the origin. When $\mu \in D_4$, the Eq. (11.2.27) has four rough equilibrium states, two of which are stable and two are unstable; for $\mu \in D_2$, the equation has two rough equilibria, one stable and the other unstable; for $\mu \in D_0$, there is no equilibrium states at all.

The bifurcation surface separating these regions is called *a swallowtail* (see the corresponding picture in Fig. 11.2.14 for $l_4 > 0$). It has a self-intersection line

$$\mu_3 = -2l_4\sqrt{\mu_1/l_4} + o(\sqrt{|\mu_1|})\,, \quad \mu_2 = o(|\mu_1|^{3/4})$$

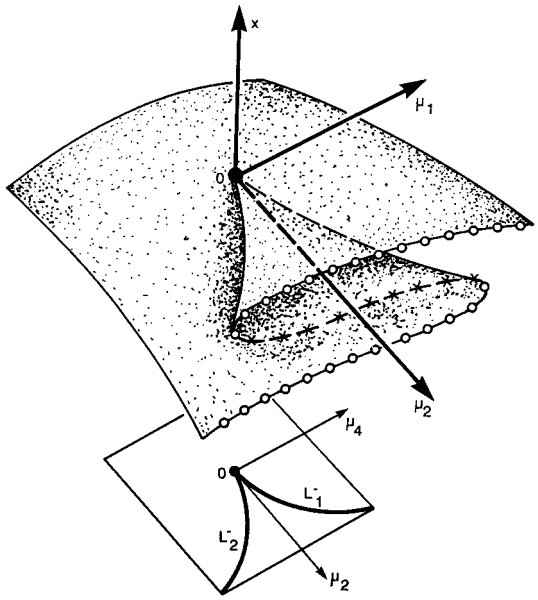

Fig. 11.2.13. Topology of the bifurcation set in the extended phase space.

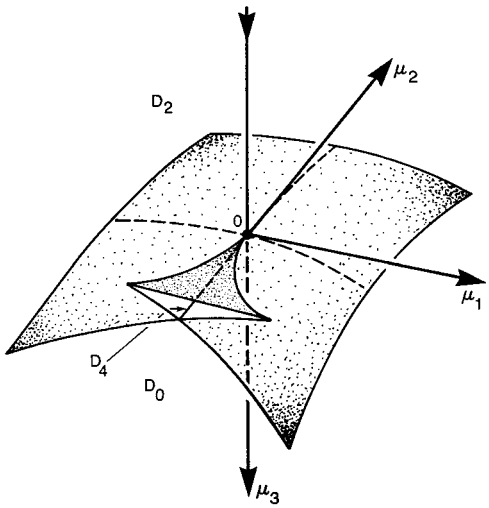

Fig. 11.2.14. The bifurcation surface known as "a swallowtail." See comments in the text.

that corresponds to the existence of a pair of semi-stable equilibrium states in Eq. (11.2.27), and two cusp edges

$$\mu_1 = -\mu_3^2/12l_4 + o(\mu_3^2)\,, \quad \mu_2 = \pm\sqrt{-8\mu_3^3/27l_4} + o(|\mu_3|^{3/2})$$

that correspond to the existence of a triple equilibrium state whose third Lyapunov value is positive if $\mu_2 > 0$ and negative if $\mu_2 < 0$. The parameter values other than those on the line of self-intersection and on the cusp edges on the bifurcation surface correspond to one semi-stable equilibrium state.

The case $l_2 = \cdots = l_{k-1} = 0$, $l_k \neq 0$ may be analyzed in a similar way for any k. It reduces simply to an analysis of the roots of the equation

$$0 = \mu_1 + \cdots + \mu_{k-1}x^{k-2} + l_k x^k + \tilde{G}(x,\mu)\,. \tag{11.2.28}$$

Strictly speaking, the latter problem has to do with the theory of singularities, and we will not consider it in detail. Since the k-th derivative of the right-hand side of (11.2.28) does not vanish when x is small, the number of roots of this equation cannot exceed k (including multiplicity), i.e. the original equilibrium state may not bifurcate into more than k equilibrium states.

The bifurcation set in the space $(\mu_1, \ldots, \mu_{k-1})$ corresponds to equilibrium states of various degrees of degeneracy. The self-intersections of the bifurcation surface correspond to the presence of two or fewer structurally unstable equilibrium states. To find the bifurcation surfaces it is useful to make a renormalization of the coordinates and the parameters. In particular, let

$$\delta = \sum_{i=1}^{k-1} \mu_i^{1/(k+1-i)}\,, \quad M_i = \mu_i/\delta^{k+1-i}\,.$$

Then, after the transformation $x \to \delta x$, Eq. (11.2.28) is recast in the form

$$0 = \sum_{i=1}^{k-1} M_i x^{i-1} + l_k x^k + \cdots\,, \tag{11.2.29}$$

where the ellipsis denote the terms that tend to zero as $\delta \to 0$; x and $M_1, \ldots, M_{k-1}$ are no longer small, and $\sum_{i=1}^{k-1} M_i^{1/(k+1-i)} = 1$.

It can be shown that the analysis of Eq. (11.2.29) is equivalent to analyzing the truncated equation

$$0 = \sum_{i=1}^{k-1} M_i x^{i-1} + l_k x^k \tag{11.2.30}$$

(after reverting to the non-rescaled variables this means that the structure of the bifurcation set as well as the phase portraits of Eq. (11.2.25) are the same as those associated with the polynomial family $\dot{x} = \mu_1 + \cdots + \mu_{k-1}x^{k-2} + l_k x^k$).

Let $(M_1^*, \ldots, M_{k-1}^*)$ be a bifurcation point of (11.2.30), i.e. it corresponds to the existence of one or more multiple roots. At this point the family (11.2.30) is in general position with respect to the given bifurcation. By applying the implicit function theorem one may easily verify that for the Eq. (11.2.29), the curve $\{M_i(\delta) = M_i^* + \cdots\}_{i=1,\ldots,k-1}$ corresponding to the same bifurcation is defined if δ is sufficiently small. Thus, the bifurcation set is composed of curves which have an asymptotic representation

$$\mu_i \sim M_i^* \delta^{k+1-i}\,. \tag{11.2.31}$$

We can probe even deeper; namely, it turns out that for any bifurcation of codimension s at least one of the values M_i^* is non-zero at $i \geq s+1$. This implies that the part of the bifurcation set which corresponds to a bifurcation of codimension s is composed of surfaces (joined at $\mu = 0$) of the form

$$\mu_j = \psi_j(\mu_{s+1}, \ldots, \mu_{k-1}) \quad (j = 1, \ldots, s)\,, \tag{11.2.32}$$

where ψ_j satisfies the relations

$$|\psi_j|^{1/(k+1-j)} \leq C \sum_{i=s+1}^{k-1} |\mu_i|^{1/(k+1-s)} \tag{11.2.33}$$

(here, C is a common constant independent of s and j). So, for example, the swallowtail lies entirely inside the "cone"

$$|\mu_1| \leq C(|\mu_2|^{4/3} + |\mu_3|^2)\,,$$

and the cusp edges and the line of self-intersection on it (they are the curves of codimension two) satisfy the inequalities

$$|\mu_1| \leq C|\mu_3|^2\,, \quad |\mu_2| \leq C|\mu_3|^{3/2}\,.$$

To resume we note that it may often happen in practice that the equation on the center manifold is such that the governing parameters do not come in the generic way. For example, if a system is invariant with respect to the symmetry $x \to -x$, then the equation of the center manifold admits the same symmetry.

Consequently, the right-hand side of the system on the center manifold will contain no terms with even power of x. The associated transverse family can then be represented in the form

$$\dot{x} = \mu x + l_3 x^3 + o(x^3)\,.$$

If $l_3 \neq 0$, one-parameter μ is sufficient. The coordinate dependence on μ for the case $l_3 < 0$ is illustrated in Fig. 12.2.15. When μ becomes positive the trivial equilibrium state loses its stability and gives birth to two new stable ones. Such a bifurcation is called *a pitchfork*.

The other mechanism frequently encountered in applications is when it is known *a priori* that the equilibrium state does not disappear in the bifurcation. If it resides at the origin, then the transverse family has the form

$$\dot{x} = \mu x + l_2 x^2 + o(x^2)\,.$$

If $l_2 \neq 0$, the bifurcation develops in the following manner (see Fig. 11.2.16): as $\mu \to -0$, an unstable equilibrium state approaches the stable one at the origin; when μ goes through zero the trivial equilibrium state becomes unstable whereas the non-trivial one becomes stable, i.e. the so-called exchange of stability takes place. Such bifurcation is called *transcritical*.

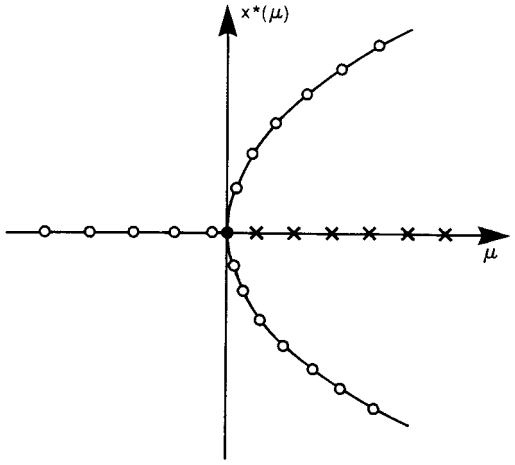

Fig. 11.2.15. The coordinates of the equilibrium state versus the parameter μ at pitchfork bifurcation (typical for symmetric systems).

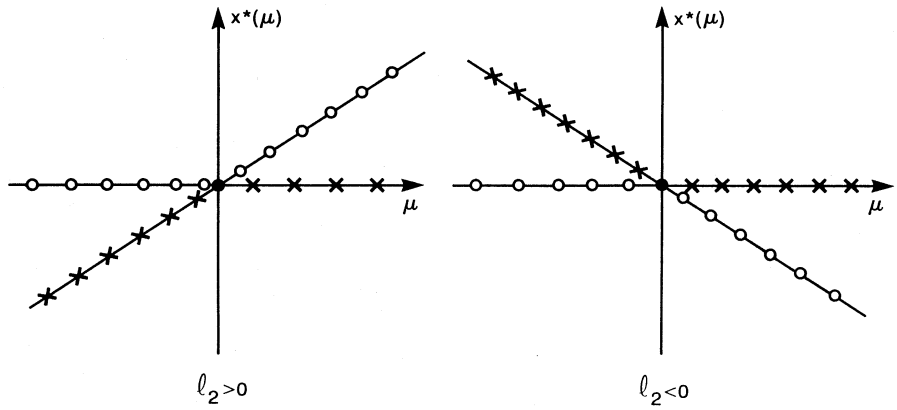

Fig. 11.2.16. Coordinates of equilibrium states at transcritical bifurcations. None of the equilibrium states disappears; they exchange their stability.

11.3. Bifurcations of periodic orbits with multiplier +1

Consider a family of $\mathbb{C}^r$-maps ($r \geq 2$) which has a fixed point with one multiplier equal to $+1$ at zero-parameter value; the rest of the multipliers are assumed to be inside the unit circle. The map near the fixed point in this case is written in the form

$$\begin{aligned} \bar{x} &= x + g(x, y, \varepsilon)\,, \\ \bar{y} &= Ay + f(x, y, \varepsilon)\,, \end{aligned} \tag{11.3.1}$$

where $x \in \mathbb{R}^1$, $y \in \mathbb{R}^n$, the eigenvalues of the matrix A lie inside the unit circle, f and g are $\mathbb{C}^r$-smooth functions such that f and g vanish at $x = 0$, $y = 0$, $\varepsilon = 0$ along with their first derivatives with respect to x and y.

We repeat one more time that by virtue of the reduction theorem there exist some $\mathbb{C}^{r-1}$-coordinates in terms of which the family (11.3.1) is reduced to the form

$$\begin{aligned} \bar{x} &= x + G(x, \varepsilon)\,, \\ \bar{y} &= [A + F(x, y, \varepsilon)]y\,, \end{aligned} \tag{11.3.2}$$

where G is a $\mathbb{C}^r$-function and F is a $\mathbb{C}^{r-1}$-function such that

$$\begin{aligned} F(0,0,0) &= 0\,, \\ G(0,0) &= 0\,, \\ G'_x(0,0) &= 0\,. \end{aligned} \tag{11.3.3}$$

Since the dynamics in the y-variables is trivial — they converge exponentially to the origin, it suffices for us to consider only bifurcations in the restriction of the system (11.3.2) to the center manifold:

$$\bar{x} = x + G(x,\varepsilon)\,. \tag{11.3.4}$$

By (11.3.3), the function G at $\varepsilon = 0$ is at least of second order of smallness with respect to x. If k is the index number of the first non-zero Lyapunov value, then the function G at $\varepsilon = 0$ has the form

$$G(x,0) = l_k x^k + o(x^k)\,, \tag{11.3.5}$$

where $l_k \neq 0$. In the most typical case k is equal to 2, and hence $G(x,0) = l_2 x^2 + o(x^2)$.

Since $G'_x(x,\varepsilon)$ is small when both x and ε are small, the right-hand side of (11.3.4) is a monotonically increasing function of x. The fixed points of the map (11.3.4) are found from the condition $G(x,\varepsilon) = 0$; their stability is determined by the sign of the derivative $G'_x(x,\varepsilon)$: if this derivative is positive at a fixed point, the latter is unstable; if the derivative is negative, the fixed point is stable. In other words, we have a complete analogy with the family of differential equations

$$\dot{x} = G(x,\varepsilon)\,,$$

i.e. a fixed point with a unit multiplier bifurcates in the same way as an equilibrium state with a zero characteristic exponent.

So, we can now simply apply the results of the previous section. Thus, if the family (11.3.4) is in a general position (i.e. the rank of the matrix (11.2.18) is maximal; if $l_2 \neq 0$, this condition reduces to the inequality (11.2.9)), then the set of parameter values which corresponds to the existence of a fixed point with a unit multiplier and zero Lyapunov values $l_2, \ldots, l_{k-1}$, forms a $\mathbb{C}^{r-(k-1)}$-smooth surface $\mathfrak{M}'$ of codimension $(k-1)$ that passes through $\varepsilon = 0$. The families of maps transverse to $\mathfrak{M}'$ can be recast into the form

$$\bar{x} = x + G(x,\mu) = x + \mu_1 + \mu_2 x + \cdots + \mu_{k-1} x^{k-2} + l_k x^k + o(x^k) \tag{11.3.6}$$

(to arrive at this form, one must translate the origin to the point x^* where the derivative $G^{(k-1)}$ vanishes; since the kth derivative of G with respect to x does not vanish, the point x^* is uniquely determined and depends smoothly ($\mathbb{C}^{r-(k-1)}$) on the parameters).

We have already emphasized in the preceding section that the study of zeros of the function G is equivalent to those of the polynomial

$$\mu_1 + \mu_2 x + \cdots + \mu_{k-1} x^{k-2} + l_k x^k \,.$$

We will not discuss further the general case but will henceforth consider only bifurcations of low codimensions.

1. $l_2 \neq 0$. The transverse family of one-dimensional maps in this case assumes the form

$$\bar{x} = x + \mu + l_2 x^2 + o(x^2) \,. \tag{11.3.7}$$

The Lamerey diagrams for the cases $l_2 > 0$ and $l_2 < 0$ are illustrated in Figs. 11.3.1 and 11.3.2, respectively. When $l_2\mu < 0$ there are two fixed points $x^{\pm} = \sqrt{-\mu/l_2} + o(\sqrt{\mu})$; at $\mu = 0$, there is only one structurally unstable point; when $l_2\mu > 0$ there is no fixed point at all, and all trajectories escape from a neighborhood of the origin after a finite number of iterations (of order $\sqrt{\mu/l_2}$).

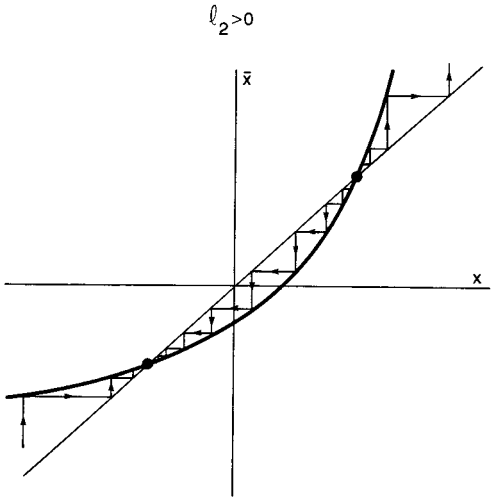

(a) $\mu < 0$

Fig. 11.3.1. Lamerey staircase for the case $l_2 > 0$.

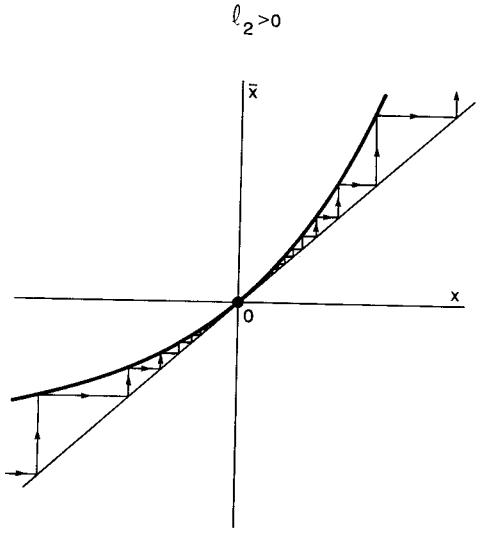

(b) $\mu = 0$

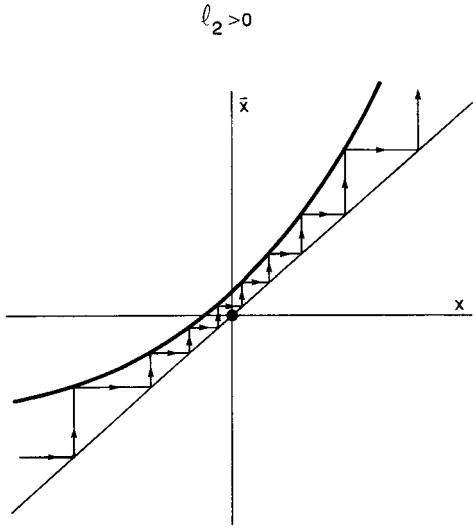

(c) $\mu > 0$

Fig. 11.3.1. (*Continued*)

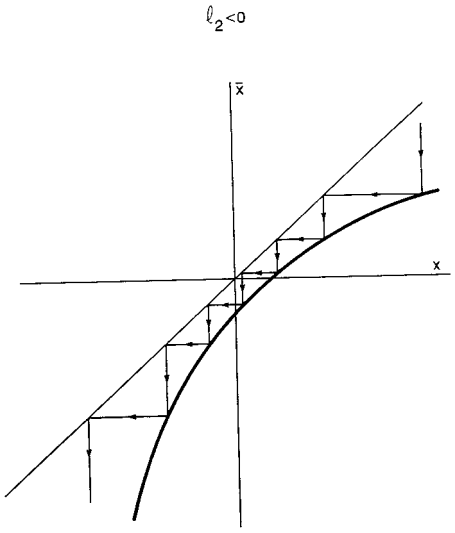

(a) $\mu < 0$

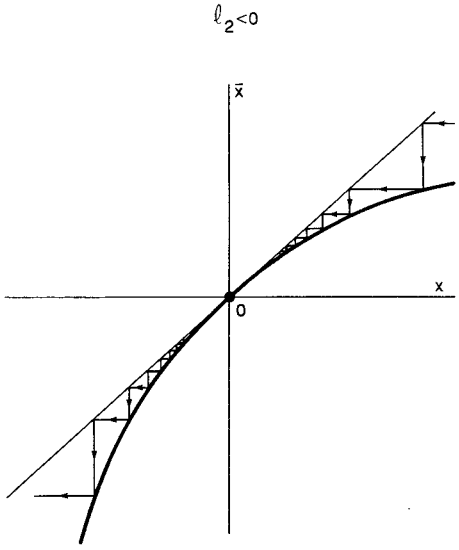

(b) $\mu = 0$

Fig. 11.3.2. Lamerey staircase for the case $l_2 < 0$.

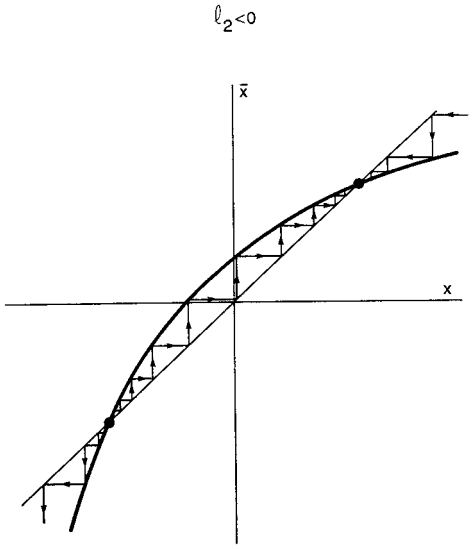

(c) $\mu > 0$

Fig. 11.3.2. (*Continued*)

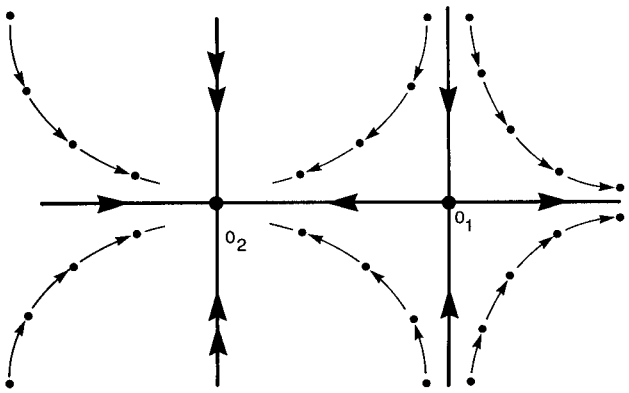

(a) $\mu < 0$

Fig. 11.3.3. Bifurcations of a saddle-node fixed point for the case $l_2 > 0$. Observe that iterations of the points near the ghost of the saddle-node (in (C)) become more dense (the expansion rate in horizontal direction is hardly larger than 1).

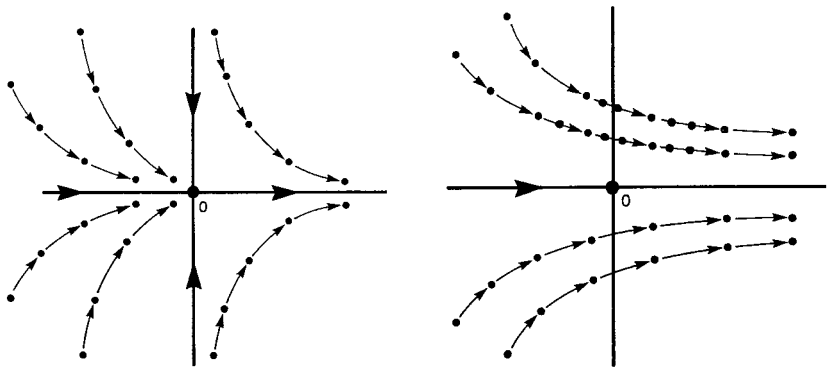

(b) $\mu = 0$ (c) $\mu > 0$

Fig. 11.3.3. (*Continued*)

The dependence of the coordinates of the fixed points on μ is given in Fig. 11.2.2.

For dimensions higher than one, the phase portraits for the initial map (11.3.1) for different μ are shown in Figs. 11.3.3 and 11.3.4.

When the map (11.3.1) is a Poincaré map near a periodic orbit of some system of ODE's, the fixed point under consideration corresponds to a saddle-node periodic orbit (at $\mu = 0$). The phase portraits for this case are shown in Figs. 11.3.5–11.3.7.

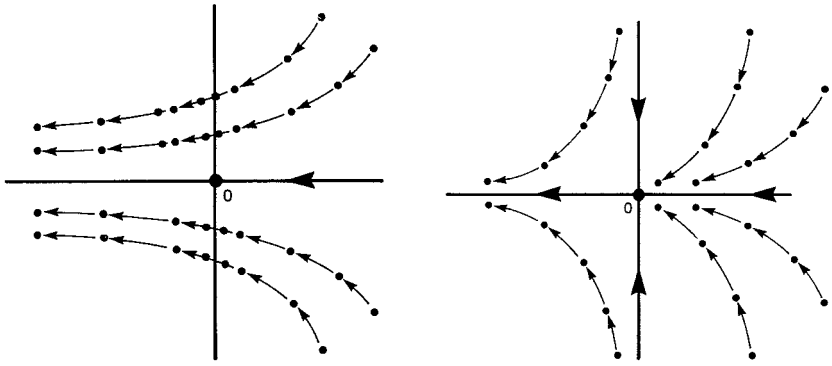

(a) $\mu < 0$ (b) $\mu = 0$

Fig. 11.3.4. Bifurcations of a saddle-node fixed point for the case $l_2 < 0$.

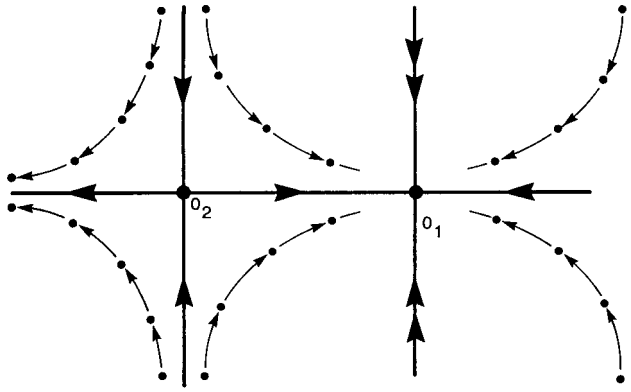

(c) $\mu > 0$

Fig. 11.3.4. (*Continued*)

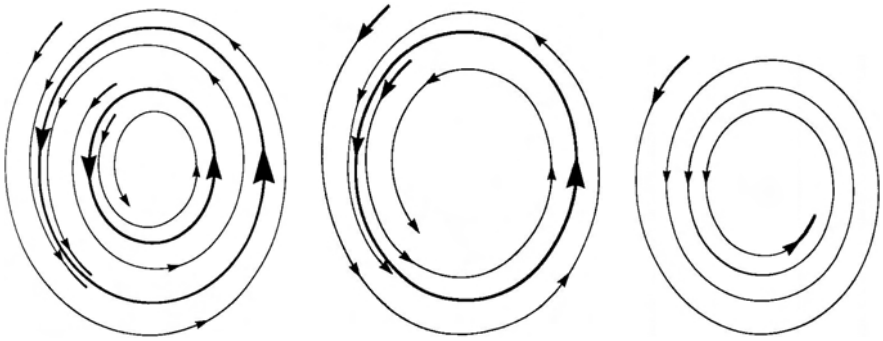

(a) $\mu < 0$ (b) $\mu = 0$ (c) $\mu > 0$

Fig. 11.3.5. Bifurcations of a saddle-node limit cycle in a plane for the case $l_2 > 0$. A semi-stable cycle (b) is attractive in the exterior domain, but repelling in the interior region.

2. $l_2 = 0$, $l_3 \neq 0$. The transverse family in this case assumes the form

$$\bar{x} = x + \mu_1 + \mu_2 x + l_3 x^3 + o(x^3)\,. \tag{11.3.8}$$

The bifurcations are illustrated in Figs. 11.3.8 ($l_3 < 0$) and 11.3.9 ($l_3 > 0$). The bifurcation curves $L^{\pm}$ corresponding to a fixed-point of the saddle-node type [i.e. a multiple root of the equation $G(x, \mu) = 0$] are defined by the

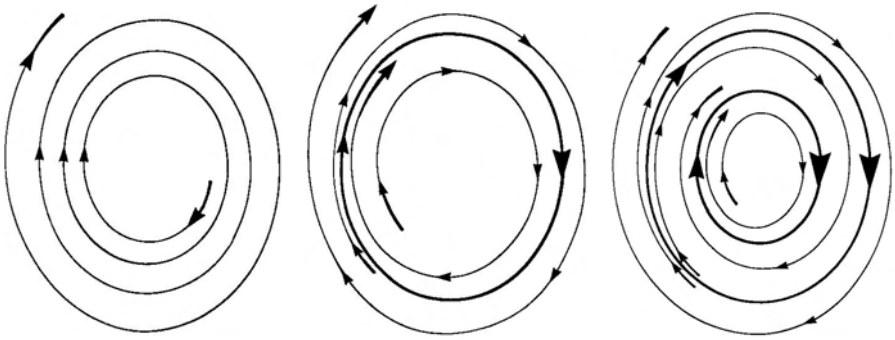

(a) $\mu < 0$ (b) $\mu = 0$ (c) $\mu > 0$

Fig. 11.3.6. Bifurcations of a saddle-node limit cycle in a plane for the case $l_2 < 0$. This is the same as in Fig. 11.3.5 up to a change in $\mu \to -\mu$. The feature of the forward route is the appearance of a saddle-node cycle from condensation of trajectories.

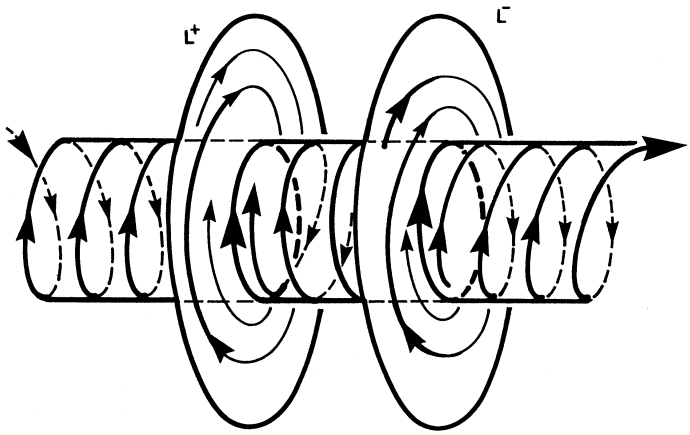

(a)

Fig. 11.3.7. Scenario of a saddle-node bifurcation of periodic orbits in $\mathbb{R}^3$. The stable periodic orbit and the saddle periodic orbit in (a) coalesce at $\mu = 0$ in (b) into a saddle-node periodic orbit, and then vanishes in (c). The unstable manifold of the saddle-node orbit in (c) is homeomorphic to a semi-cylinder. A trajectory following the path in (b) slows down along a transverse direction near the "virtual" saddle-node periodic orbit (i.e., the ghost of the saddle-node orbit in (b)) so that its local segment is similar to a compressed spring.

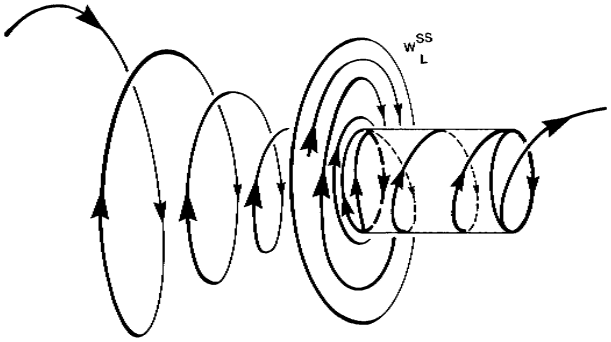

(b)

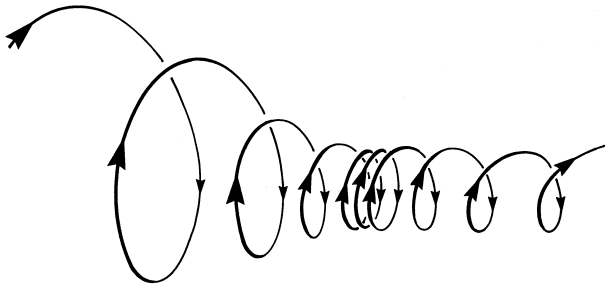

(c)

Fig. 11.3.7. (*Continued*)

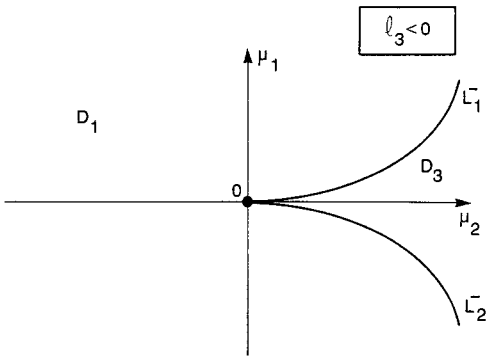

Fig. 11.3.8. Bifurcation diagram for $l_2 = 0$ and $l_3 > 0$.

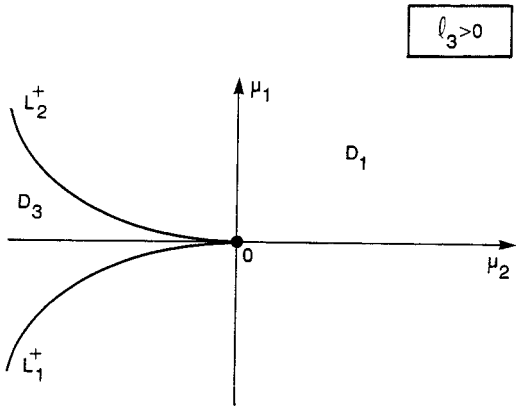

Fig. 11.3.9. Bifurcation diagram for $l_2 = 0$ and $l_3 < 0$.

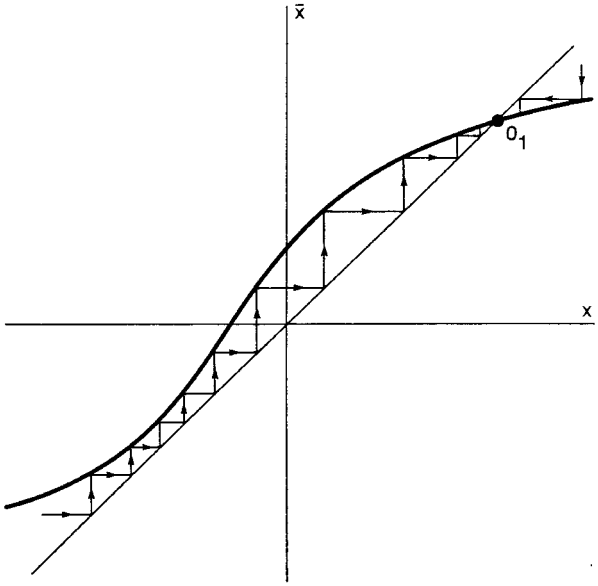

(a) $\mu \epsilon D_1$

Fig. 11.3.10. Bifurcations of the fixed points corresponding to the diagram in Fig. 11.3.8.

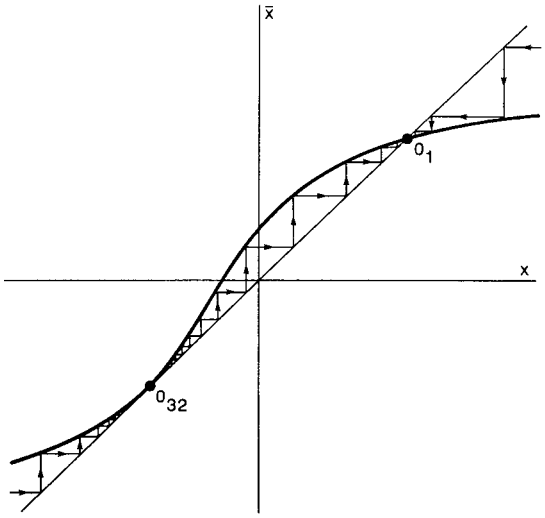

(b) $\mu \epsilon \mathrm{L}_1^-$

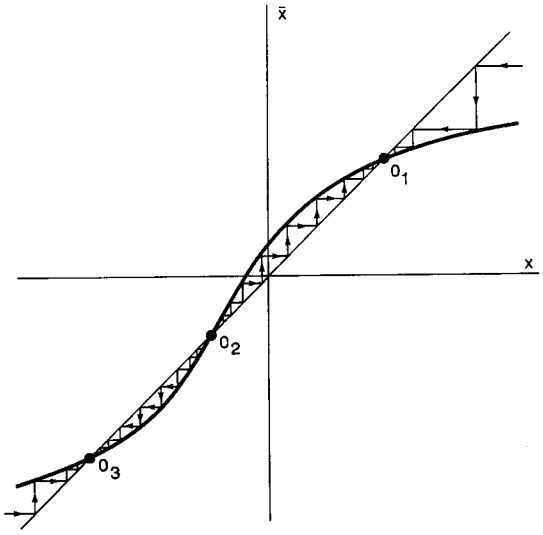

(c) $\mu \epsilon \mathrm{D}_3$

Fig. 11.3.10. (*Continued*)

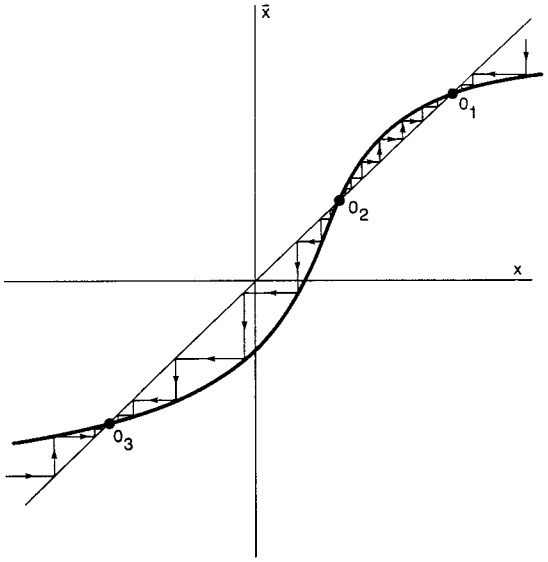

(d) $\mu \in D_3$

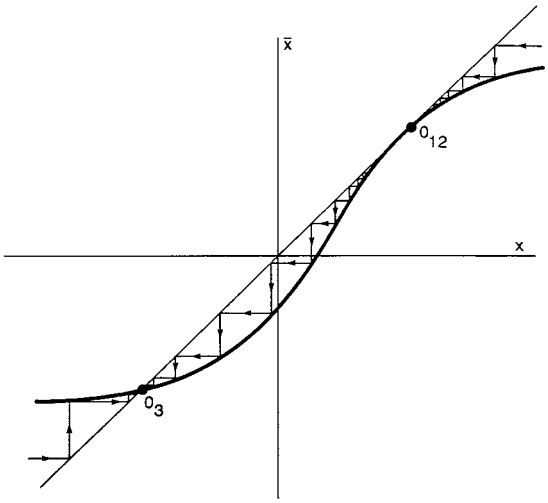

(e) $\mu \in L_2^-$

Fig. 11.3.10. (*Continued*)

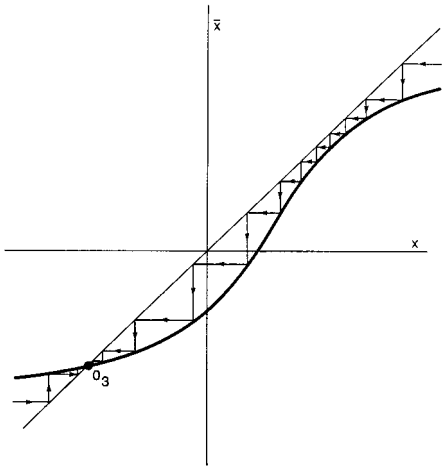

(f) $\mu \epsilon D_1$

Fig. 11.3.10. (*Continued*)

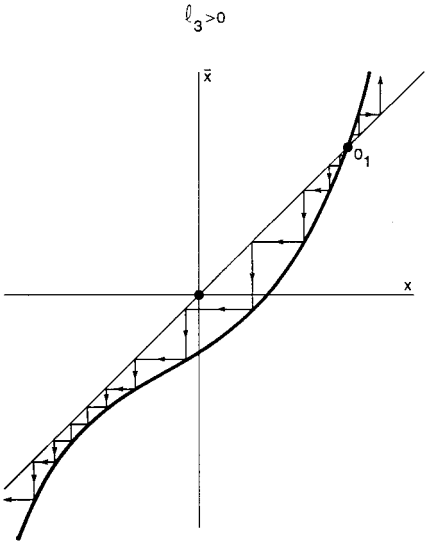

(a) $\mu \epsilon D_1$

Fig. 11.3.11. Bifurcations of the fixed points corresponding to the unfolding in Fig. 11.3.9.

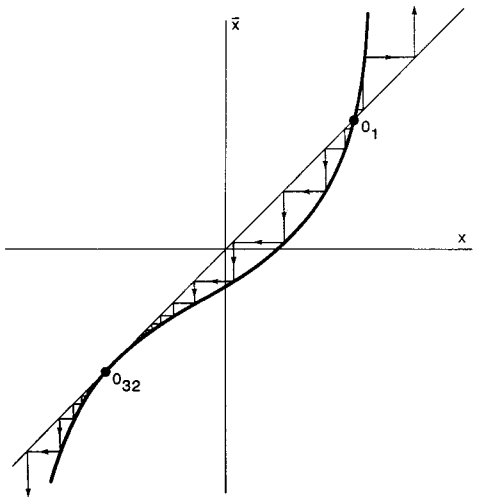

(b) $\mu \in \mathrm{L}_1^+$

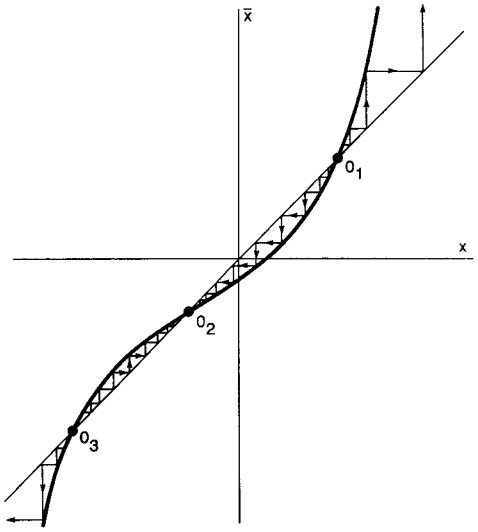

(c) $\mu \in \mathrm{D}_3$

Fig. 11.3.11. (*Continued*)

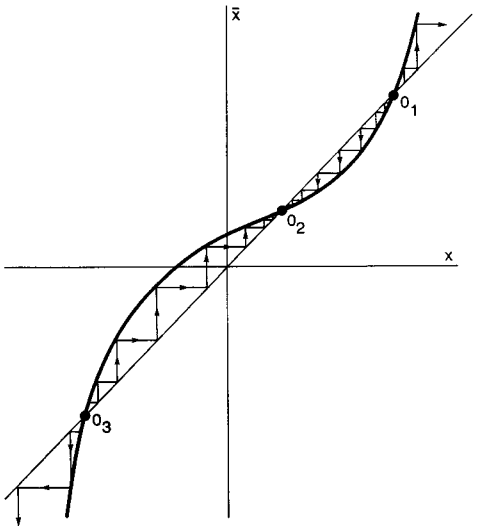

(d) $\mu \epsilon \mathrm{D}_3$

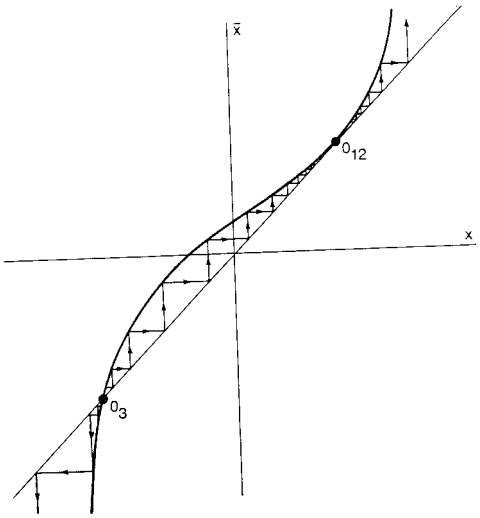

(e) $\mu \epsilon \mathrm{L}_2^+$

Fig. 11.3.11. (*Continued*)

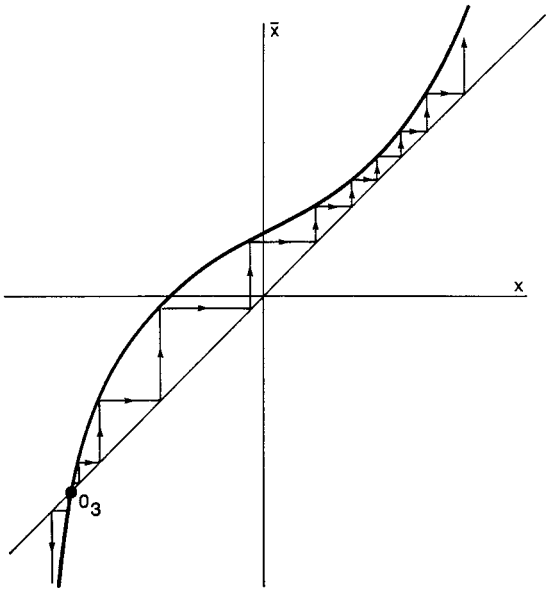

(f) $\mu \in D_1$

Fig. 11.3.11. (*Continued*)

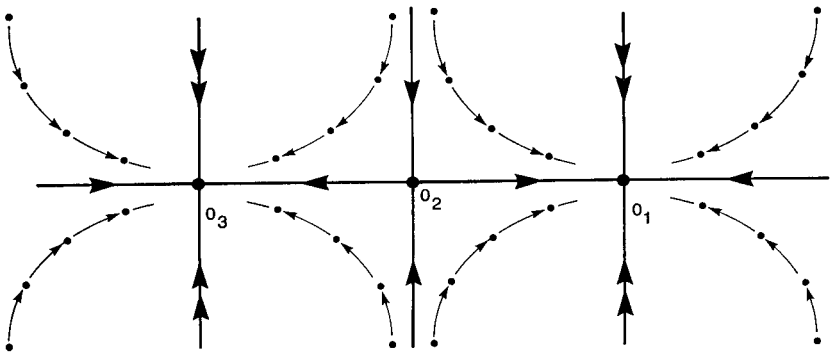

(a) $\mu \in D_3$

Fig. 11.3.12. Bifurcations of the fixed points in a plane for the case $l_2 = 0$ and $l_3 < 0$.

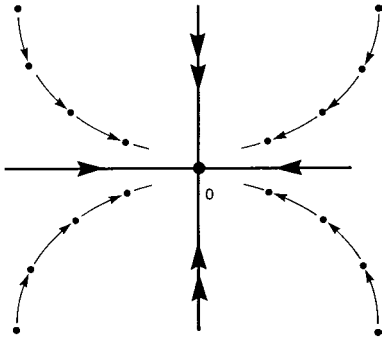

(b) $\mu \in \mathrm{D}_1$

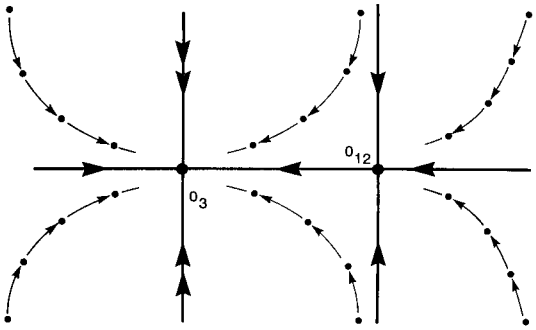

(c) $\mu \in \mathrm{L}_2^-$

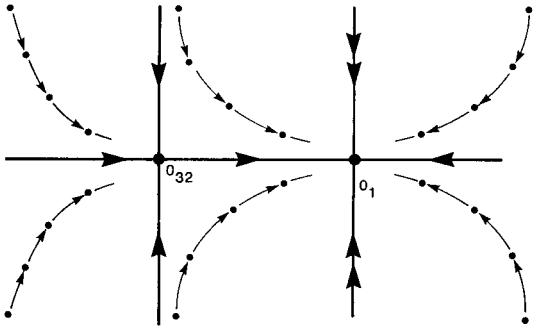

(d) $\mu \in \mathrm{L}_1^-$

Fig. 11.3.12. (*Continued*)

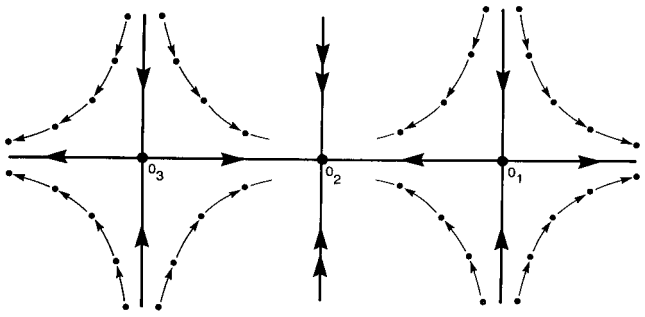

(a) $\mu \epsilon \mathrm{D}_3$

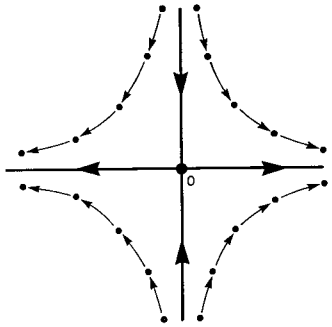

(b) $\mu \epsilon \mathrm{D}_1$

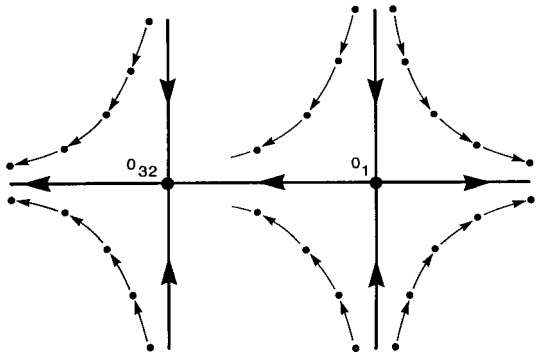

(c) $\mu \epsilon \mathrm{L}_1^+$

Fig. 11.3.13. Bifurcations of the fixed point in a plane for the case $l_2 = 0$ and $l_3 > 0$.

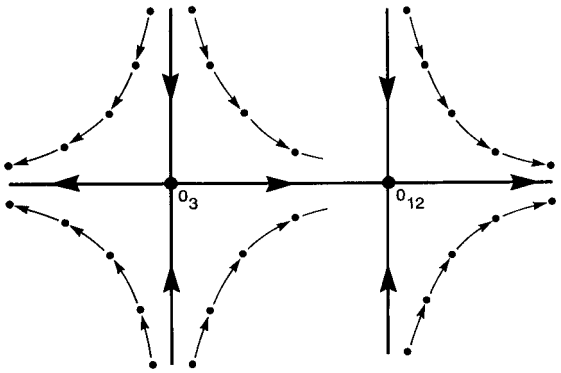

(d) $\mu \in \mathrm{L}_2^+$

Fig. 11.3.13. (*Continued*)

equation

$$27\mu_1^2 + \frac{4\mu_2^3}{l_3} + o(\mu_2^3) = 0\,.$$

In the region D_3, the map (11.3.8) has three rough fixed points: two stable and one unstable if $l_3 < 0$, or two unstable and one stable if $l_3 > 0$. In the region D_1, there is a single rough fixed point: stable if $l_3 < 0$, or unstable otherwise. Figures 11.3.10 and 11.3.11 present the Lamerey diagrams for the transitions over L_1 and L_2 for l_3 of both signs. Figures 11.3.12 and 11.3.13 present the respective two-dimensional cases.

11.4. Bifurcations of periodic orbits with multiplier -1

Consider next a family of maps of class $\mathbb{C}^r (r \geq 3)$ which has a fixed point with one multiplier equal to (-1) at zero-parameter values. Since the rest of the multipliers are supposed to be inside the unit circle, the map near the fixed point assumes the form

$$\begin{aligned} \bar{x} &= -x + G(x, y, \varepsilon)\,, \\ \bar{y} &= (A + F(x, y, \varepsilon))y\,, \end{aligned} \tag{11.4.1}$$

where $x \in \mathbb{R}^1$, $y \in \mathbb{R}^n$, the eigenvalues of the matrix A lie inside the unit circle, G is a $\mathbb{C}^r$-function and F is a $\mathbb{C}^{r-1}$-function such that

$$\begin{aligned} F(0,0,0) &= 0\,, \\ G(0,0) &= 0\,, \\ G'_x(0,0) &= 0\,. \end{aligned} \tag{11.4.2}$$

Let us consider the map on the center manifold

$$\bar{x} = -x + G(x,\varepsilon)\,. \tag{11.4.3}$$

Since the derivative of the right-hand side of the map (11.4.3) does not vanish (it is equal to -1 at $x = 0$, $\varepsilon = 0$), the fixed point persists (and remains single) for all small ε. Without loss of generality let us assume that the fixed point is located at the origin, i.e.

$$G(0,\varepsilon) \equiv 0\,. \tag{11.4.4}$$

It was shown in Sec. 10.6 that at $\varepsilon = 0$, all even powers of x in the Taylor expansion of G are non-resonant. Hence, they can be eliminated up to any order by a polynomial transformation. Obviously, these terms remain non-resonant for small $\varepsilon \neq 0$ as well, i.e. for all small ε they may also be eliminated up to any order by polynomial transformations with coefficients depending smoothly on ε.

Generically, the first Lyapunov value l_1 differs from zero, i.e. the function G at $\varepsilon = 0$ starts with the cubic terms

$$G(x,0) = -l_1 x^3 + o(x^3)\,.$$

Then, by eliminating the x^2-terms for all small ε, the map may be reduced to the form

$$\bar{x} = -x(1 + l_0(\varepsilon) + l_1 x^2) + o(x^3)\,, \tag{11.4.5}$$

where l_0 is a $\mathbb{C}^{r-1}$-smooth function of ε, $l_0(0) = 0$.

The boundary $\mathfrak{M}$ of the stability region of the fixed point is determined by the condition $l_0(\varepsilon) = 0$ and is a $\mathbb{C}^{r-1}$-smooth surface of codimension one provided that the vector $(\partial l_0/\partial\varepsilon_1, \ldots, \partial l_0/\partial\varepsilon_p)_{\varepsilon=0}$ is non-zero. Let us choose $l_0(\varepsilon)$ as the governing parameter μ. Then, any transverse family has the form

$$\bar{x} = -x(1 + \mu + l_1 x^2) + \tilde{G}(x,\mu)\,, \tag{11.4.6}$$

where $\tilde{G} = o(x^3)$; it is a $\mathbb{C}^r$-smooth function of x and a $\mathbb{C}^{r-2}$-smooth function of μ such that

$$\tilde{G}(0,\mu) = \tilde{G}'_x(0,\mu) = \tilde{G}''_{xx}(0,\mu) = \tilde{G}'''_{xxx}(0,0) = 0\,. \tag{11.4.7}$$

For all x and μ sufficiently small, the map (11.4.6) has a unique fixed point. This point (at the origin) is stable when $\mu < 0$ and unstable when $\mu > 0$; when $\mu \neq 0$, it does not undergo bifurcations. Besides this fixed point, the map (11.4.6) may have points of period two. Therefore, to examine the bifurcations one should consider the second iteration of the map. There may not be periodic points of other periods more than two because the second iteration of (11.4.6) is a monotonically increasing one-dimensional map — periodic orbits of such maps are fixed points.

The second iterate is given by

$$\bar{\bar{x}} = x(1 + 2\mu + \mu^2 + 2l_1x^2) + \tilde{\tilde{G}}\,(x,\mu)\,, \tag{11.4.8}$$

where

$$\tilde{\tilde{G}}\,(0,\mu) = \tilde{\tilde{G}}'_x(0,\mu) = \tilde{\tilde{G}}''_{xx}(0,\mu) = \tilde{\tilde{G}}'''_{xxx}(0,0) = 0\,. \tag{11.4.9}$$

The non-zero fixed points of the second iteration are found from the equation

$$\mu(1 + \mu/2) + l_1x^2 + \tilde{\tilde{G}}\,(x,\mu)/2x = 0\,.$$

This equation is analogous to the equation yielding the coordinates of the fixed point which emerge from the saddle-node bifurcation (see (11.2.12)). So, one may verify that the equation has no real roots when $\mu l_1 > 0$, but it has two roots of opposite signs when $\mu l_1 < 0$; namely:

$$x^{\pm}(\mu) = \pm\sqrt{|\mu/l_1|} + o(\sqrt{|\mu|})\,.$$

As for the map (11.4.7), the pair $(x^+,\, x^-)$ comprises an orbit of period two. Its multiplier is found by differentiating the right-hand side of (11.4.8) and is equal to

$$\rho = 1 + 2\mu + 6l_1x^2 + o(\mu) + o(x^2) = 1 - 4\mu + o(\mu)\,.$$

Since in the region of the existence of points of period two the sign of μ is opposite to the sign of l_1, it follows that when $l_1 > 0$, the multiplier is greater than one and the period-two point is unstable. Respectively, when $l_1 < 0$, the multiplier is less than one and the point of period two is stable. Summarizing we conclude that:

(1) If $l_1 < 0$, then the fixed point at the origin is stable for $\mu \leq 0$ and attracts all trajectories from any small neighborhood. When $\mu > 0$, the fixed point becomes unstable and the stable period-two point bifurcates from it; see Fig. 11.4.1 illustrating the corresponding Lamerey diagrams.

(2) If $l_1 > 0$, then for $\mu < 0$, there exists a stable fixed point O at the origin as well as an unstable orbit of period two bounding the attraction basin of O; at $\mu = 0$, the period two orbit merges into O; the latter becomes unstable and all trajectories, except O, leave a neighborhood of the origin for $\mu \geq 0$, see Fig. 11.4.2.

Consider next the original map (11.4.1). For the sake of visualization we restrict ourselves to the two-dimensional case. The map is written in the form

$$\bar{x} = -x(1 + \mu + l_1 x^2) + o(x^2)\,,$$
$$\bar{y} = \gamma(\mu) y + o(y)\,,$$

where $|\gamma(\mu)| < 1$. If we consider the Poincaré map of a three-dimensional flow, then it is to be orientable (orientation preserving). Hence, the product of the multipliers of a periodic orbit must be positive, i.e. $\gamma < 0$.

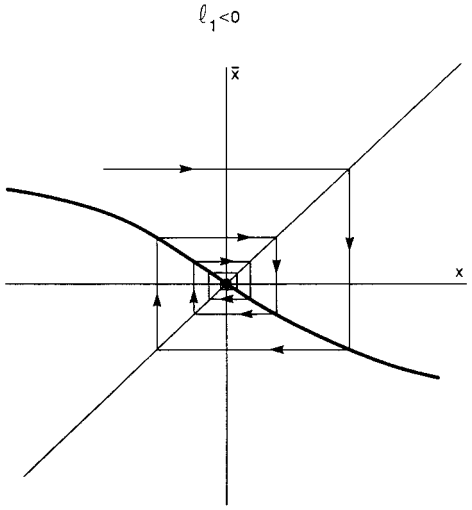

(a) $\mu < 0$

Fig. 11.4.1. Transformations of the Lamerey spiral for the case $l_1 < 0$.

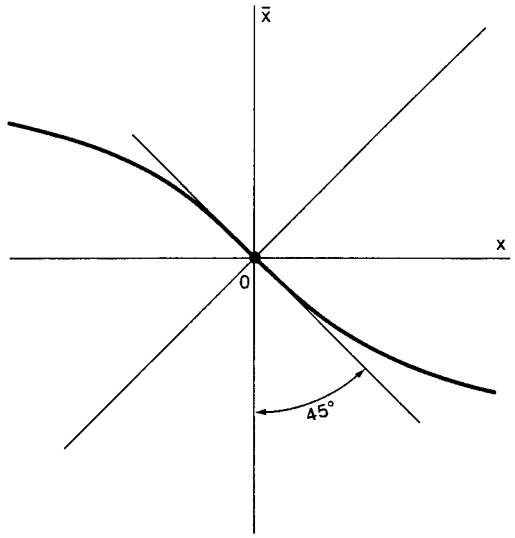

(b) $\mu = 0$

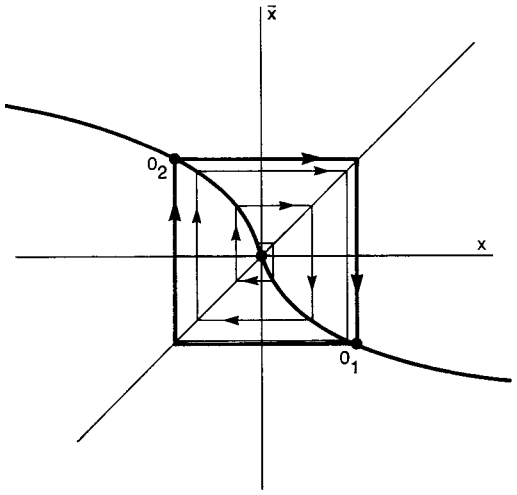

(c) $\mu > 0$

Fig. 11.4.1. (*Continued*)

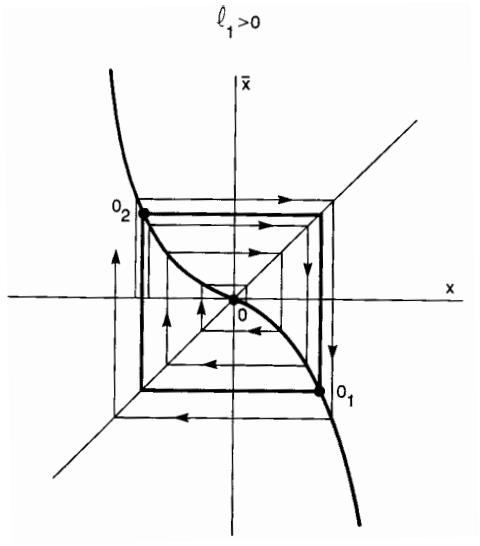

(a) $\mu < 0$

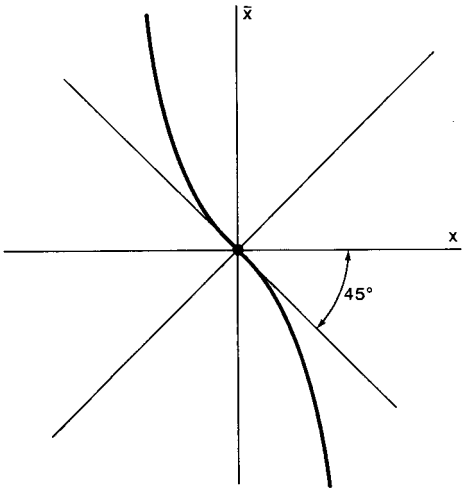

(b) $\mu = 0$

Fig. 11.4.2. Transformations of the Lamerey spiral for the case $l_1 > 0$. The unstable period-two cycle bounds the attraction basin of the origin.

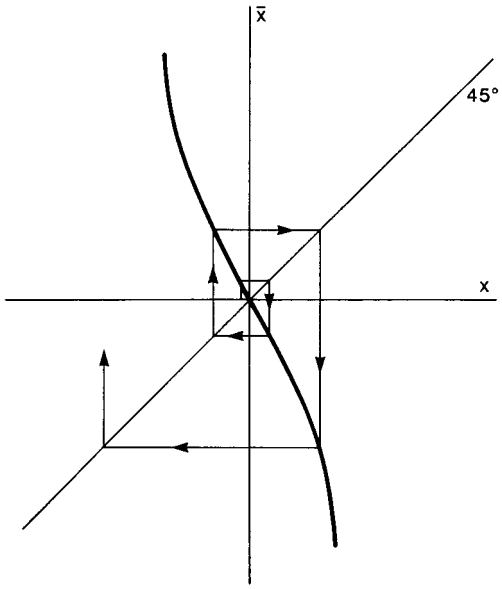

(c) $\mu > 0$

Fig. 11.4.2. (*Continued*)

If $l_1 < 0$, the point O is stable (a node $(-)$) for $\mu \leq 0$. When μ becomes positive the point O loses it stability and transforms into a saddle $(-,-)$; this means that a stable orbit of period two bifurcates from the origin. The phase portraits are shown in Fig. 11.4.3.

If $l_1 > 0$, then for all sufficiently small negative μ, there exists a period-two orbit (O_1, O_3) of saddle $(+,+)$ type. Its invariant stable and unstable manifold separate the attraction basin of the fixed point O_2. As μ tends to zero the orbit of period two approaches O and collapses into it at $\mu = 0$. When $\mu > 0$, the point O becomes a saddle $(-,-)$ (see Fig. 11.4.4).

The remarkable feature of this bifurcation in the case of periodic orbits of autonomous systems of differential equations is that the center manifold of the periodic orbit L corresponding to the fixed point O of the Poincaré map is a Möbius band. The orbit itself is the mean line of the Möbius band, and consequently a new orbit that bifurcates from L must wind twice around L as shown in Fig. 11.4.5. It is quite clear that the period of the new orbit is nearly the double period of L. Consequently, this bifurcation is called

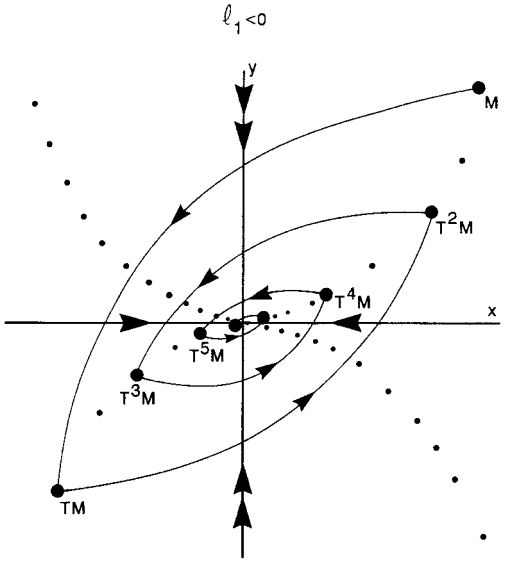

(a) $\mu \leq 0$

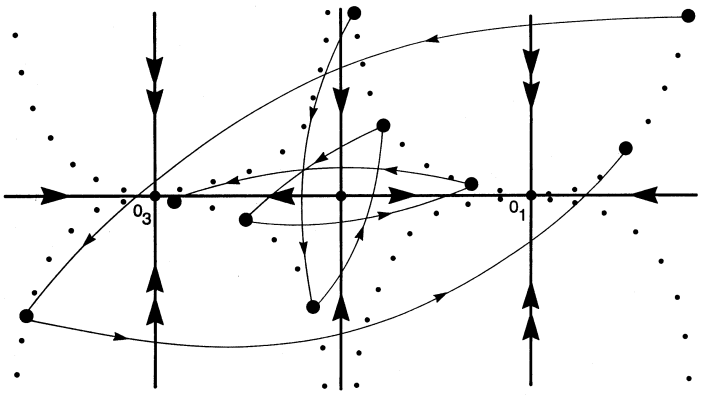

(b) $\mu > 0$

Fig. 11.4.3. The origin is initially a stable node $(-)$. Each point O_1 and O_3 in (b) is periodic of period two. They form a stable cycle of period two bifurcating from the origin which becomes a saddle $(-,-)$.

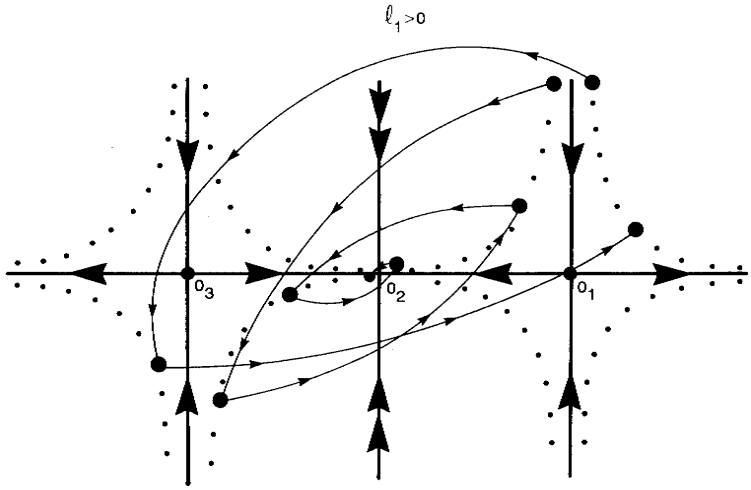

(a) $\mu < 0$

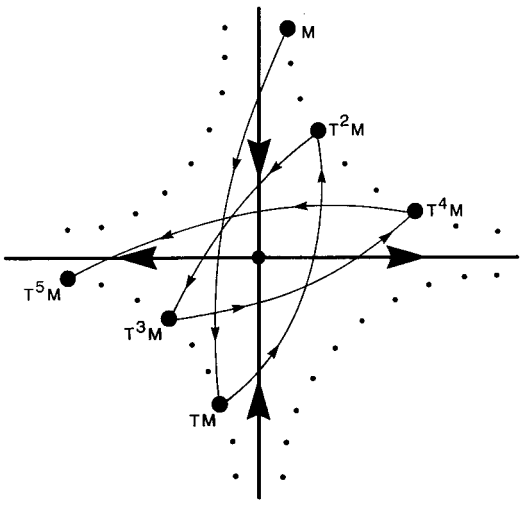

(b) $\mu \geq 0$

Fig. 11.4.4. The case $l_1 > 0$. The stable node $(-)$ at the origin is surrounded by a period-two saddle cycle $(+,+)$. When the cycle collapses at the origin, the latter becomes unstable.

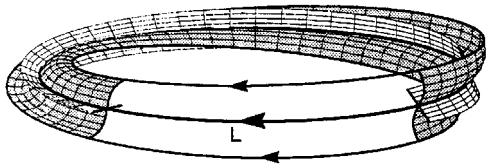

Fig. 11.4.5. Topology of the period-doubling bifurcation. The unstable manifold (dark) of the trivial periodic orbit L is a Möbius strip, whose boundary is a stable orbit of period two that has just bifurcated. The stable manifold of L is shown in white. (Courtesy of B. Krauskopf).

a period-doubling bifurcation. For a non-autonomous system with period τ, the points of period-two in the Poincaré map correspond to two periodic orbits of double period such that one is taken into the other by the phase shift over τ.

The next bifurcation that we will now focus on occurs when the first Lyapunov value vanishes. Here, after getting rid of terms of second and fourth order (the smoothness r of the map is assumed to be not less than five) the map may be reduced to the form

$$\bar{x} = -x(1 + l_0(\varepsilon) + l_1(\varepsilon)x^2 + l_2x^4) + o(x^5)\,,$$

where $l_0(0) = l_1(0) = 0$, $l_2 \neq 0$. The bifurcation surface $\mathfrak{M}$ in this case is defined by the equation

$$l_0(\varepsilon) = l_1(\varepsilon) = 0\,,$$

and assuming that the genericity condition

$$\operatorname{rank} \begin{pmatrix} \dfrac{\partial l_0}{\partial \varepsilon_1} & \cdots & \dfrac{\partial l_0}{\partial \varepsilon_p} \\ \dfrac{\partial l_1}{\partial \varepsilon_1} & \cdots & \dfrac{\partial l_1}{\partial \varepsilon_p} \end{pmatrix}_{\varepsilon=0} = 2\,,$$

holds, it is a $\mathbb{C}^{r-3}$-smooth surface of codimension two. Therefore, the transverse family depends on two-parameters:

$$\bar{x} = -x(1 + \mu_0 + \mu_1x^2 + l_2x^4) + o(x^5)\,. \tag{11.4.10}$$

Here, as above, the fixed point is unique. It is stable when $\mu_0 < 0$ and unstable when $\mu_0 > 0$. For all other small $\mu_0 \neq 0$, it does not undergo bifurcations.

To find points of period two let us consider the second iterate of the map

$$\bar{\bar{x}} = x(1+\mu_0)^2 + \mu_1(1+\mu_0)(2+2\mu_0+\mu_0^2)x^3 + 2l_2x^5 + o(x^5)\,. \qquad (11.4.11)$$

The fixed points, other than $x = 0$, of this map are sought as the roots of the equation

$$2\mu_0 + \mu_0^2 + \mu_1(1+\mu_0)(2+2\mu_0+\mu_0^2)x^2 + 2l_2x^4 + o(x^4) = 0\,. \qquad (11.4.12)$$

Multiple roots must satisfy the additional equation

$$\mu_1(1+\mu_0)(2+2\mu_0+\mu_0^2) + 4l_2x^2 + o(x^2) = 0 \qquad (11.4.13)$$

obtained by differentiating (11.4.12). Solving the system (11.4.12)–(11.4.13) with respect to x, we find that in the (μ_0, μ_1)-parameter plane the curve containing the multiple roots consists of half of the parabola

$$\mu_0 = \mu_1^2/4l_2 + o(\mu_1^2)\,, \quad \mu_1 l_2 < 0\,. \qquad (11.4.14)$$

For the map (11.4.10), this curve corresponds to the presence of a period-two trajectory (x^+, x^-) of saddle-node type. The coordinates of the saddle-node points are found from (11.4.12) and (11.4.13): $x^{\pm} = \pm\sqrt{|\mu_1/2l_2|} + o(\sqrt{|\mu_1|})$. By decomposing the right-hand side of (11.4.11) into a Taylor series at the point x^+ we can verify that the Lyapunov value does not vanish, i.e. the point is a simple saddle-node.

Besides the line $\mu_0 = 0$ and the line (11.4.14), the bifurcation unfolding contains no others (see Fig. 11.4.6). These curves partition a neighborhood of the origin into three regions D_0, D_1 and D_2. The Lamerey diagrams corresponding every region are shown in Figs. 11.4.7 ($l_2 < 0$) and 11.4.8 ($l_2 > 0$). In D_0, there are no trajectories of period-two, in D_1, there is a one period-two trajectory and in D_2, there are two such trajectories. When moving from D_2 to D_0, both period-two orbits merge and disappear.

In conclusion we consider schematically the bifurcations in the general case when a few Lyapunov values vanish simultaneously. Let k be the order number of the first non-zero Lyapunov value at $\varepsilon = 0$. Then, by eliminating the even powers of x up to the order $2k$, the map may be reduced to the form

$$\bar{x} = -x\left(1 + \sum_{i=0}^{k-1} l_i(\varepsilon)x^{2i} + l_k x^{2k}\right) + o(x^{2k+1})\,, \qquad (11.4.15)$$

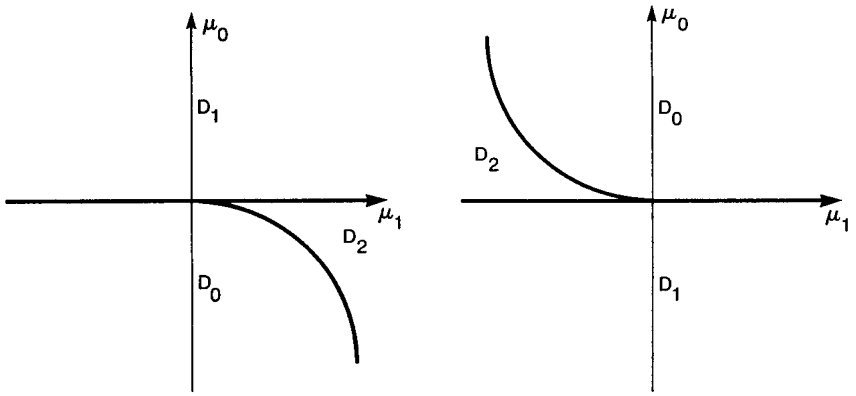

(a) $\ell_2 < 0$ (b) $\ell_2 > 0$

Fig. 11.4.6. Bifurcation unfolding $l_2 < 0$ (a) and $l_2 > 0$ (b).

where l_i is a $\mathbb{C}^{r-(2i+1)}$-smooth function of $\varepsilon (i = 0, \dots, k-1)$; it is supposed that the smoothness r of the map is not less than $(2k+1)$ and $l_0(0) = \cdots = l_{k-1}(0) = 0$, $l_k \neq 0$.

It is obvious that in the case of general position (i.e. when the rank of the matrix

$$\begin{pmatrix} \dfrac{\partial l_0}{\partial \varepsilon_1} & \cdots & \dfrac{\partial l_0}{\partial \varepsilon_p} \\ \vdots & \ddots & \vdots \\ & \ddots & \\ \dfrac{\partial l_{k-1}}{\partial \varepsilon_1} & \cdots & \dfrac{\partial l_{k-1}}{\partial \varepsilon_p} \end{pmatrix}_{\varepsilon=0}$$

is equal to k) the bifurcation surface

$$\mathfrak{M}' : \ l_0(\varepsilon) = \cdots = l_{k-1}(\varepsilon) = 0$$

that passes through the point $\varepsilon = 0$ and corresponds to a fixed point with a multiplier -1 and with $(k-1)$ first zero Lyapunov values, is a $\mathbb{C}^{r-(2k-1)}$-smooth surface of codimension k.[4]

[4]Note that the boundary of the stability region is determined by the condition $l_0(\varepsilon) = 0$ and is a smooth surface of codimension one provided the vector $(\frac{\partial l_0}{\partial \varepsilon_1}, \dots, \frac{\partial l_0}{\partial \varepsilon_p})_{\varepsilon=0}$ is non-zero regardless of whether any Lyapunov values vanish or do not.

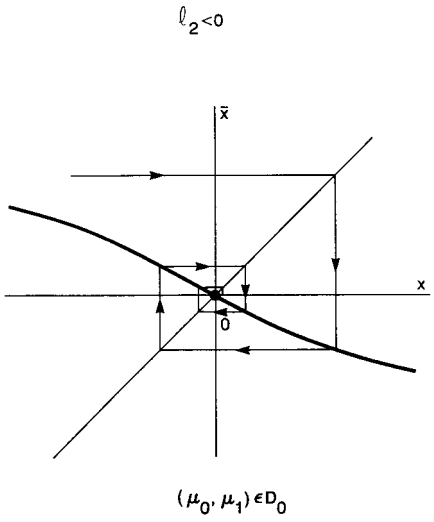

(a)

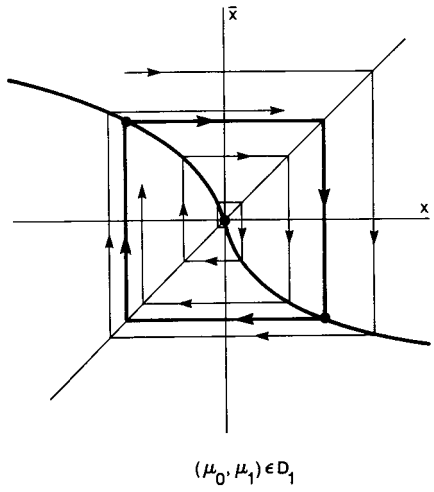

(b)

Fig. 11.4.7. The map for the case $l_2 < 0$ when moving counter-clock-wise in the direction around the origin in the bifurcation diagram in Fig. 11.4.6(a). Two period-two cycles in (c) coalesce on the border separating D_2 and D_0 and disappear in D_0. The semi-stable cycle of period two is shown in (d).

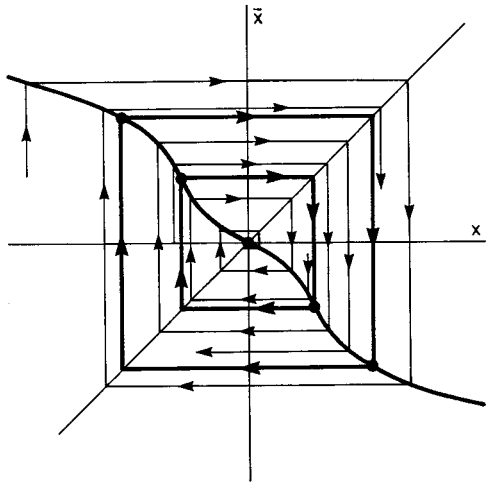

(c)

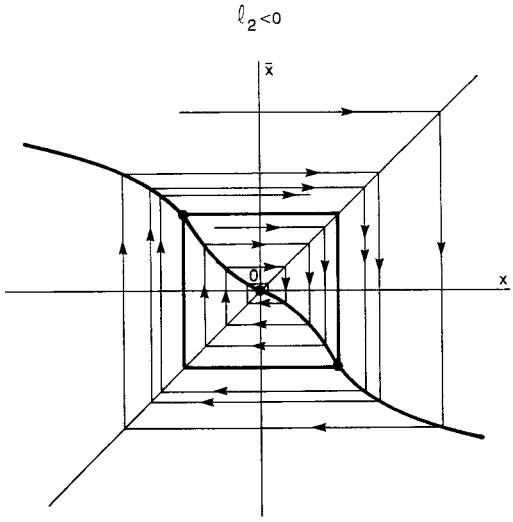

(d)

Fig. 11.4.7. (*Continued*)

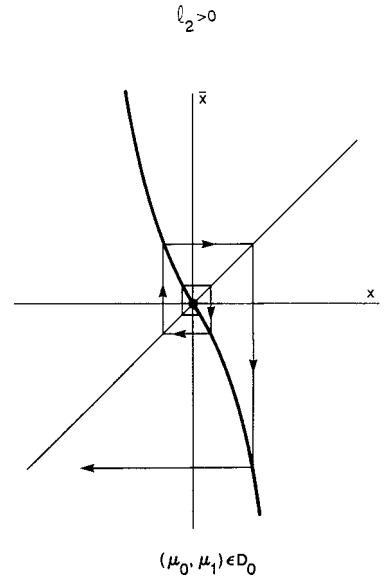

(a)

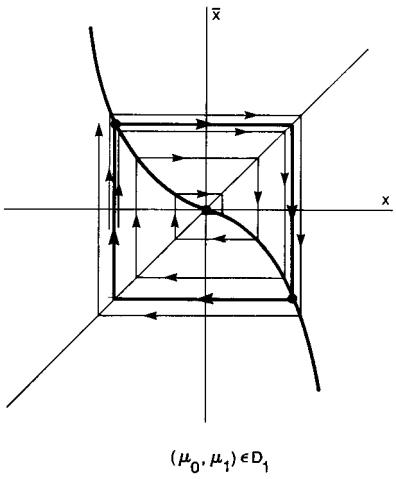

(b)

Fig. 11.4.8. The map corresponding to the bifurcation diagram in Fig. 11.4.6 (b). The semi-stable cycle of period two on the border between D_2 and D_0 is shown in (d).

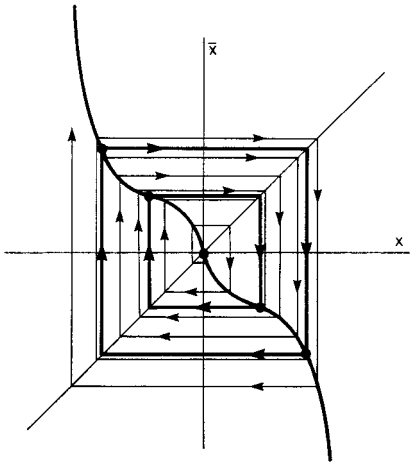

$(\mu_0, \mu_1) \in D_2$

(c)

$\ell_2 > 0$

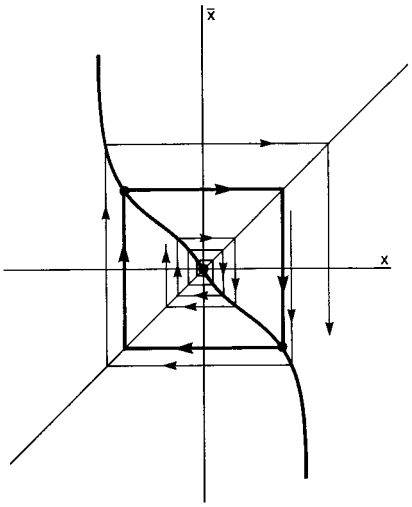

(d)

Fig. 11.4.8. (*Continued*)

Let us choose the values $l_i(\varepsilon)$ as the governing parameters $\mu_0, \dots, \mu_{k-1}$. Then any family transverse to $\mathfrak{M}'$ in this case can be represented in the form

$$\bar{x} = -x(1 + \mu_0 + \mu_1 x^2 + \cdots + \mu_{k-1} x^{2(k-1)} + l_k x^{2k}) + \tilde{G}(x, \mu)\,, \qquad (11.4.16)$$

where $\tilde{G} = o(x^{2k+1})$ is a $\mathbb{C}^r$-smooth function of x and a $\mathbb{C}^{r-2k}$-smooth function of μ such that $\tilde{G}(0,\mu) = \tilde{G}'_x(0,\mu) = \cdots = \tilde{G}^{(2k)}(0,\mu) = 0$ and $\tilde{G}^{(2k+1)}(0,0) = 0$.

The plane $\mu_0 = 0$ corresponds to the loss of stability of the fixed point at the origin. No other bifurcations occur with the fixed point at $\mu_0 \neq 0$. To study the trajectories of period-two we need to examine the second iteration of the map

$$\begin{aligned}\bar{\bar{x}} &= x\left(1 + \sum_{i=0}^{k-1} \mu_i x^{2i} + l_k x^{2k}\right)\left(1 + \sum_{i=0}^{k-1} \mu_i \bar{x}^{2i} + l_k \bar{x}^{2k}\right) \\ &= x(1 + 2\hat{\mu}_0 + 2\hat{\mu}_1 x^2 + \cdots + 2\hat{\mu}_{k-1} x^{2(k-1)} + 2l_k x^{2k}) + o(x^{2k+1})\,,\end{aligned} \qquad (11.4.17)$$

where each $\hat{\mu}_i$ is uniquely expressed in terms of $\mu_0, \dots, \mu_i$:

$$\hat{\mu}_i = \mu_i + \varphi_i(\mu_0, \dots, \mu_i)\,. \qquad (11.4.18)$$

We do not need the concrete form of the functions φ_i. It suffices to notice that

$$\varphi_i = o(\mu_j) \quad (j = 0, \dots, i)\,. \qquad (11.4.19)$$

The non-zero fixed points of the map (11.4.17) are found as the roots of the equation

$$\hat{\mu}_0 + \hat{\mu}_1 x^2 + \cdots + \hat{\mu}_{k-1} x^{2(k-1)} + l_k x^{2k} + o(x^{2k}) = 0\,. \qquad (11.4.20)$$

They correspond to orbits of period two of the map (11.4.16). Moreover each orbit is composed of one positive and one negative root. So, one may then consider the positive roots only; i.e. if we let $u = x^2$, then our problem is reduced to that of a bifurcation analysis of the positive roots of the equation

$$\hat{\mu}_0 + \hat{\mu}_1 u + \cdots + \hat{\mu}_{k-1} u^{k-1} + l_k u^k + o(u^k) = 0\,. \qquad (11.4.21)$$

Similar bifurcations of such roots have been examined in Sec. 11.2 (the difference being that the factor of u^{k-1} is not zero — but this can be always achieved by a translation of the origin; besides this we did not discuss separately the behavior of the positive roots). As in Sec. 11.2, by checking that the k-th derivative of the left-hand side of the equation does not vanish we can show that Eq. (11.4.21) cannot have more than k roots when x and μ are small.

Thus, the bifurcation of a fixed point with one multiplier equal to -1, and with $(k-1)$ zero Lyapunov values, cannot produce more than k orbits of period two. Moreover, it is easy to specify the precise parameter values for which Eq. (11.4.21) has a prescribed number of positive roots, within the range from 0 to k. This implies that in the parameter space of the map (11.4.16), there are regions where the family has any prescribed number (from 0 to k) of period-two orbits.

In order to understand the structure of the bifurcation surface for period-two orbits we must construct a surface $\mathfrak{M}$ of multiple roots of Eq. (11.4.21), and then select the part $\mathfrak{M}^+$ that corresponds to positive multiple roots. The surface $\mathfrak{M}$ is defined by the system

$$\begin{aligned} \hat\mu_0 + \hat\mu_1 u + \cdots + \hat\mu_{k-1} u^{k-1} + l_k u^k + o(u^k) = 0\,, \\ \hat\mu_1 + 2\hat\mu_2 u + \cdots + (k-1)\hat\mu_{k-1} u^{k-2} + k l_k u^{k-1} + o(u^{k-1}) = 0\,. \end{aligned} \tag{11.4.22}$$

It follows from (11.4.22) that the vanishing of the multiple root $u = 0$ corresponds to setting the values $\hat\mu_0$ and $\hat\mu_1$ to zero. Thus, the line defined by $\hat\mu_0 = \hat\mu_1 = 0$ form the boundary of $\mathfrak{M}^+$ in $\mathfrak{M}$. The bifurcation diagram for orbits of period two of the map (11.4.16) coincides with $\mathfrak{M}^+$. Correspondingly, the union of the surface $\mathfrak{M}^+$ and the plane $\mu_0 = 0$ on which the fixed point loses its stability gives a complete bifurcation diagram for the map (11.4.16).

Consider in more detail the question on constructing the set $\mathfrak{M}^+$ (see Fig. 11.4.9 for an example of a bifurcation diagram of the map (11.4.16) for the case $k = 3$, $l_k < 0$). Note that the surface $\mathfrak{M}$ contains the line L corresponding to the existence of a root of multiplicity k. This line is determined from the following system of equations (they require that at some point u the left-hand side of Eq. (11.4.21) as well as its first $(k-1)$ derivatives

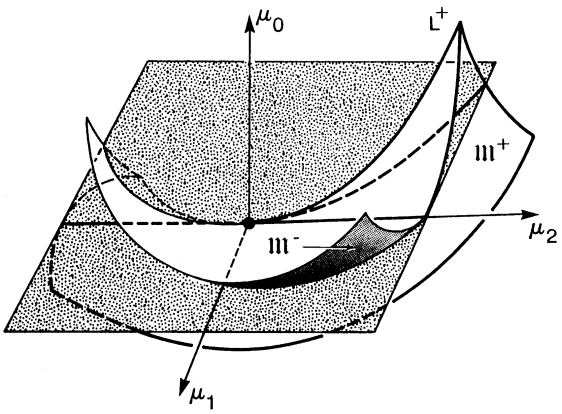

Fig. 11.4.9. The structure of the bifurcation set in the three-parameter family. See comments in the text.

must vanish)

$$
\begin{aligned}
0 &= \hat{\mu}_0 + \hat{\mu}_1 u + \cdots + \hat{\mu}_{k-1} u^{k-1} + l_k u^k + o(u^k)\,,\\
0 &= \hat{\mu}_1 + 2\hat{\mu}_2 u + \cdots + (k-1)\hat{\mu}_{k-1} u^{k-2} + k l_k u^{k-1} + o(u^{k-1})\,,\\
&\vdots \quad\quad \vdots\\
0 &= \hat{\mu}_i + \sum_{j=i+1}^{k-1} C_j^i \hat{\mu}_j u^{j-i} + C_k^i l_k u^{k-i} + o(u^{k-1})\,,\\
&\vdots \quad\quad \vdots\\
0 &= \hat{\mu}_{k-1} + k l_k u + o(u)\,,
\end{aligned}
$$

where C_j^i are binomial factors. By solving the system sequentially, from bottom to top, with respect to $\hat{\mu}_{k-1}$ we find that the curve L can be represented asymptotically in the form

$$\hat{\mu}_i \sim (\hat{\mu}_{k-1})^{k-i} \alpha_i\,, \tag{11.4.23}$$

where α_i are some non-zero coefficients. Moreover, the root of multiplicity k is located at the point

$$u^* \sim -\hat{\mu}_{k-1}/k l_k\,. \tag{11.4.24}$$

The point $\mu = 0$ divides the curve L into two parts: $L^+ : \hat{\mu}_{k-1} l_k < 0$ and $L^- : \hat{\mu}_{k-1} l_k > 0$. Equation (11.4.24) implies that $u^* > 0$ on L^+, i.e. only this branch of L corresponds to period-two orbits of multiplicity k.

By shifting the origin to the point $u = u^*$, the Eq. (11.4.21) is reduced to

$$\nu_0 + \nu_1 u + \cdots + \nu_{k-2} u^{k-2} + l_k u^k + o(u^k) = 0\,,$$

where ν_i are some functions of $\hat{\mu}$. Thus, it follows from Sec. 11.2 that at each cross-section $\hat{\mu}_{k-1} = \text{constant}$, which is transverse to the line L, the surface $\mathfrak{M}$ has the same structure which is (up to a diffeomorphism) a surface of multiple roots of the polynomial $\nu_0 + \nu_1 u + \cdots + \nu_{k-2} u^{k-2} + u^k$ which is restored at the point of intersection of the cross-section and the curve L (the coordinates of this point are found from (11.4.23)).

As explained in Sec. 11.2, this surface is composed of a number of smooth sheets of codimension one, corresponding to double roots. The line $\hat{\mu}_0 = \hat{\mu}_1 = 0$ breaks these sheets into two components corresponding to negative and positive double roots (only the latter part constitutes $\mathfrak{M}^+$): the double root is positive exactly in that part which adjoins L^+ if $\hat{\mu}_{k-1} l_k < 0$ or which does not adjoin L^- if $\hat{\mu}_{k-1} l_k > 0$.

We can also derive asymptotical relations similar to (11.2.31)–(11.2.33), i.e. the surface of multiple roots is foliated into curves represented asymptotically in the form

$$\hat{\mu}_i \sim M_i^* \delta^{k-i}\,, \tag{11.4.25}$$

and all bifurcation sets of codimension s consist of pieces (joined at $\mu = 0$) of surfaces of the form

$$\hat{\mu}_j = \psi_j(\hat{\mu}_s, \ldots, \hat{\mu}_{k-1}) \quad (j = 0, \ldots, s-1)\,, \tag{11.4.26}$$

where the ψ_j's satisfy the relation

$$|\psi_j|^{1/(k-j)} \le C \sum_{i=s}^{k-1} |\hat{\mu}_i|^{1/(k-i)}| \tag{11.4.27}$$

(here, C is a common constant independent of s and j).

It follows from (11.4.18) and (11.4.19) that if we revert to the original parameters $\mu_0, \ldots, \mu_{k-1}$, then each curve (11.4.25) will have the same asymptotic representation with the same set of constants M_i^*. Thus, it is not necessary to express $\hat{\mu}_i$ in terms of μ_i when computing the first order asymptotic relations. We simply let $\hat{\mu}_i = \mu$.

11.5. Andronov–Hopf bifurcation

In this section we discuss what happens when a pair of complex-conjugate characteristic exponents of an equilibrium state crosses over the imaginary axis. The loss of stability here is directly connected to the birth, or vice versa, the disappearance of a periodic orbit. This bifurcation is the simplest mechanism for transition from a stationary regime to oscillations, and it allows one to give a proper interpretation of numerous physical phenomena. For this reason this bifurcation has traditionally played a special role in the theory of bifurcations.

Consider a family of systems of differential equations which is $\mathbb{C}^r$-smooth ($r \geq 3$) with respect to the variables $x \in \mathbb{R}^2$, $y \in \mathbb{R}^m (m \geq 0)$ and parameters $\varepsilon \in \mathbb{R}^p (p \geq 1)$. Let the system have, at $\varepsilon = 0$, an equilibrium state O with a pair of purely imaginary characteristic exponents; the rest are assumed to lie to the left of the imaginary axis. Since the equilibrium state has no zero eigenvalues, it persists in a small neighborhood of $\varepsilon = 0$. Without loss of generality we may suppose that it resides at the origin for all small ε. Let us assume that this is a pair of characteristic exponents closest to the imaginary axis

$$\lambda_{1,2} = \lambda(\varepsilon) \pm i\omega(\varepsilon)$$

where $\lambda(\varepsilon)$ and $\omega(\varepsilon)$ depend $\mathbb{C}^{r-1}$ smoothly on ε, and

$$\lambda(0) = 0\,, \quad \omega(0) > 0\,.$$

By virtue of the reduction theorem the system near the equilibrium state may be reduced to the form

$$\begin{aligned} \dot{x}_1 &= \lambda(\varepsilon)x_1 - \omega(\varepsilon)x_2 + G_1(x_1, x_2, \varepsilon)\,, \\ \dot{x}_2 &= \omega(\varepsilon)x_1 + \lambda(\varepsilon)x_2 + G_2(x_1, x_2, \varepsilon)\,, \\ \dot{y} &= [A + F(x, y, \varepsilon)]y\,, \end{aligned} \tag{11.5.1}$$

where F is a $\mathbb{C}^{r-1}$-function, $G_{1,2}$ are $\mathbb{C}^r$-functions, and

$$\begin{aligned} F(0,0,0) &= 0\,, \\ G(0,0,0) &= 0\,, \\ G'_x(0,0,0) &= 0\,. \end{aligned} \tag{11.5.2}$$

We can verify, as in Sec. 9.3, that at $\varepsilon = 0$, the terms of the Taylor expansion of the functions G, other than $x_1(x_1^2 + x_2^2)$ and $x_2(x_1^2 + x_2^2)$ (e.g. terms in any even power) are non-resonant and may be eliminated by a polynomial (with respect to x) transformation of variables.

The boundary $\mathfrak{M}$ of the stability region of the equilibrium state is given in the parameter space by the equation $\lambda(\varepsilon) = 0$: the equilibrium state O is stable if $\lambda(\varepsilon) < 0$ and unstable if $\lambda(\varepsilon) > 0$. If at least one of the components of the vector $(\frac{\partial\lambda}{\partial\varepsilon_1}, \dots, \frac{\partial\lambda}{\partial\varepsilon_p})_{\varepsilon=0}$ is non-zero, then for all small ε the boundary $\mathfrak{M}$ is a $\mathbb{C}^{r-1}$-smooth surface of codimension one. Choose $\lambda(\varepsilon)$ as the governing parameter μ and consider a one-parameter family transverse to $\mathfrak{M}$. On the center manifold $y = 0$, this family assumes the form

$$\begin{aligned} \dot{x}_1 &= \mu x_1 - \omega(\mu)x_2 + (L_1 x_1 - \Omega_1 x_2)(x_1^2 + x_2^2) + \tilde{G}_1(x_1, x_2, \mu)\,, \\ \dot{x}_2 &= \omega(\mu)x_1 + \mu x_2 + (\Omega_1 x_1 + L_1 x_2)(x_1^2 + x_2^2) + \tilde{G}_2(x_1, x_2, \mu)\,, \end{aligned} \tag{11.5.3}$$

where for all small μ, all quadratic terms in x, as well as cubic terms at $\mu = 0$ other than $x_1(x_1^2 + x_2^2)$ and $x_2(x_1^2 + x_2^2)$, have been eliminated.

This means that in (11.5.3), the functions $\tilde{G}_{1,2}$ (which are $\mathbb{C}^r$-smooth in x and $\mathbb{C}^{r-2}$-smooth in μ) satisfy

$$\begin{aligned} \tilde{G}(0,0,\mu) = 0\,, \qquad \tilde{G}'_x(0,0,\mu) = 0\,, \\ \tilde{G}''_{xx}(0,0,\mu) = 0\,, \quad \tilde{G}'''_{xxx}(0,0,\mu) = 0\,, \end{aligned}$$

i.e. $\tilde{G} = o(R^3)$ where $R = \sqrt{x_1^2 + x_2^2}$.

Theorem 11.1. *If the first Lyapunov value L_1 in* (11.5.3) *is negative, then for small $\mu \le 0$, the equilibrium state O is stable and all trajectories in some neighborhood U of the origin tend to O. When $\mu > 0$, the equilibrium state becomes unstable and a stable periodic orbit of diameter $\sim \sqrt{\mu}$ emerges* (*see Fig.* 11.5.1) *such that all trajectories from U, excepting O, tend to it.*

If the first Lyapunov value L_1 is positive, then for small $\mu \ge 0$, the equilibrium state O is unstable and any other trajectory leaves a small neighborhood U of the origin. When $\mu < 0$, the equilibrium state is stable. Its attraction basin is bounded by an unstable periodic orbit of diameter $\sim \sqrt{-\mu}$ which contracts to O at $\mu = 0$ (*see Fig.* 11.5.2).

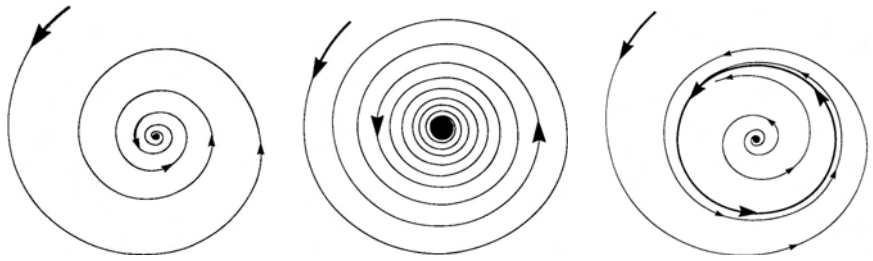

(a) $\mu < 0$ (b) $\mu = 0$ (c) $\mu > 0$

Fig 11.5.1. Soft loss of stability of a stable focus at the origin through a supercritical ($L_1 < 0$) Andronov–Hopf bifurcation.

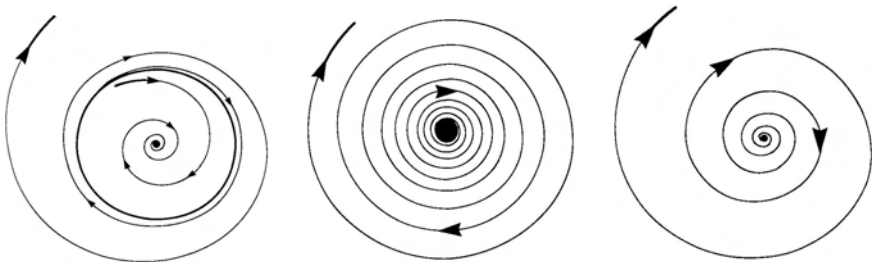

(a) $\mu < 0$ (b) $\mu = 0$ (c) $\mu > 0$

Fig 11.5.2. Rigid loss of stability of a stable focus at the origin through a subcritical ($L_1 > 0$) Andronov–Hopf bifurcation.

Proof. Let us rewrite the system (11.5.3) in polar coordinates

$$\begin{aligned} \dot{R} &= R(\mu + L_1 R^2) + \Phi_1(R, \varphi, \mu)\,, \\ \dot{\varphi} &= \omega(\mu) + \Omega_1(\mu) R^2 + \Phi_2(R, \varphi, \mu)\,, \end{aligned} \tag{11.5.4}$$

where $\Phi_1 = o(R^3)$, $\Phi_2 = o(R^2)$. The claim of the theorem is verified trivially for the truncated system

$$\begin{aligned} \dot{R} &= R(\mu + L_1 R^2)\,, \\ \dot{\varphi} &= \omega(\mu) + \Omega_1(\mu) R^2\,. \end{aligned} \tag{11.5.5}$$

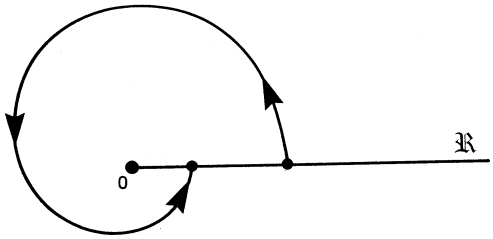

Fig. 11.5.3. Map of the ray R originating from the origin.

Indeed, here the behavior of trajectories is completely governed by the first equation

$$\dot{R} = R(\mu + L_1 R^2)\,. \tag{11.5.6}$$

In particular, the equilibrium states of Eq. (11.5.6) with positive R correspond to the periodic orbits of system (11.5.5). It is easy to find the equilibrium states of (11.5.6); namely, $R = 0$ and $R = \pm\sqrt{-\mu/L_1}$ when $\mu L_1 < 0$. The equilibrium state $R = \sqrt{-\mu/L_1}$ is stable if $L_1 < 0$ and unstable if $L_1 > 0$.

For the general situation, recall that $\omega(\mu) > 0$. Hence $\dot{\varphi}$ in (11.5.4) does not vanish for small R. Thus, any trajectory other than the point O must intersect the ray $\mathfrak{R} : \varphi = 0$, $R > 0$. After one turn in φ it must intersect the ray $\mathfrak{R}$ again and so on, until it leaves a neighborhood of the origin. Thus, it suffices to consider the mapping of the ray $\mathfrak{R}$ into itself along the trajectories of the system, see Fig. 11.5.3.

To compute this mapping let us divide the first equation in (11.5.4) by the second to obtain

$$\frac{dR}{d\varphi} = \frac{R(\mu + L_1 R^2) + \Phi_1(R,\varphi,\mu)}{\omega(\mu) + \Omega_1(\mu)R^2 + \Phi_2(R,\varphi,\mu)} = \frac{R(\mu + L_1 R^2)}{\omega(\mu)} + o(R^3)\,. \tag{11.5.7}$$

Let us look for a solution of the Eq. (11.5.7) that starts from the point $R = R_0$ at $\varphi = 0$. Expand it in the Taylor series with respect to R_0

$$R(\varphi) = \alpha_1(\varphi)R_0 + \alpha_2(\varphi)R_0^2 + \alpha_3(\varphi)R_0^3 + \cdots \tag{11.5.8}$$

(the expansion starts with the linear term because $R(\varphi) \equiv 0$ at $R_0 = 0$). As $R(0) = R_0$, then

$$\alpha_1(0) = 1\,, \quad \alpha_2(0) = 0\,, \quad \alpha_3(0) = 0\,. \tag{11.5.9}$$

Substituting (11.5.8) into (11.5.7) and equating similar terms we obtain

$$\begin{aligned} d\alpha_1/d\varphi &= \mu\alpha_1/\omega(\mu)\,, \\ d\alpha_2/d\varphi &= \mu\alpha_2/\omega(\mu)\,, \\ d\alpha_3/d\varphi &= (\mu\alpha_3 + L_1\alpha_1^3)/\omega(\mu)\,. \end{aligned} \tag{11.5.10}$$

Integrating this system and taking into account the initial data (11.5.9), we obtain

$$\begin{aligned} \alpha_1(\varphi) &= e^{\mu\varphi/\omega(\mu)}\,, \\ \alpha_2(\varphi) &= 0\,, \\ \alpha_3(\varphi) &= L_1 e^{\mu\varphi/\omega(\mu)}(e^{2\mu\varphi/\omega(\mu)} - 1)/2\mu \end{aligned}$$

and

$$R(\varphi) = e^{\mu\varphi/\omega(\mu)}R_0 + L_1 e^{\mu\varphi/\omega(\mu)}\frac{e^{2\mu\varphi/\omega(\mu)} - 1}{2\mu}R_0^3 + \cdots\,.$$

Letting $\varphi = 2\pi$, we obtain the expression for the mapping of the ray $\mathfrak{R}$ into itself: $R \equiv R(0) \mapsto R(2\pi) \equiv \bar{R}$:

$$\bar{R} = e^{2\pi\mu/\omega(\mu)}R + \frac{2\pi}{\omega(0)}L_1R^3 + o(R^3)\,. \tag{11.5.11}$$

The resulting equation

$$(e^{2\pi\mu/\omega(\mu)} - 1)\omega(0)/2\pi + L_1R^2 + o(R^2) = 0 \tag{11.5.12}$$

for non-trivial fixed points of the mapping (11.5.11) can be easily solved (observe that it coincides, up to the leading terms, with the equation for non-trivial equilibrium states of (11.5.6)). It follows that when $L_1\mu \geq 0$, the mapping (11.5.11) has a single fixed point $R = 0$, and, when $L_1\mu < 0$, there appears one more point $R = \sqrt{-\mu/L_1} + o(\sqrt{|\mu|})$ which bifurcates from the former fixed point (recall that the mapping is defined only for $R \geq 0$, its negative roots are not included). From (11.5.11), we obtain the following expression for the multiplier of the non-trivial fixed point

$$\rho(\mu) = 1 - 4\pi\mu/\omega(0) + o(\mu)\,.$$

Observe that the fixed point is stable if $L_1 < 0$ and unstable otherwise. This proves the statement of Theorem 11.1.

Remark. Theorem 11.1 was proven by Andronov and Leontovich via constructing and studying the mapping without using explicitly the theory of normal forms. Figures 11.5.1 and 11.5.2 are copied from the book "Theory of Oscillations" by Andronov, Vitt and Khaikin where they illustrated the phenomena of the soft and the rigid generation of self-oscillations (see Chap. 14).

Let us examine next the bifurcations of the system (11.5.1) in the multidimensional case. If $L_1 < 0$ (Fig. 11.5.4), then when $\mu \le 0$, the equilibrium state O is stable (rough focus when $\mu < 0$, and a weak focus at $\mu = 0$) and it attracts all trajectories in a small neighborhood of the origin. When $\mu > 0$ the point O becomes a saddle-focus with a two-dimensional unstable manifold and an m-dimensional stable manifold. The edge of the unstable manifold is the stable periodic orbit which now attracts all trajectories, except those in the stable manifold of O. One multiplier of the periodic orbit was calculated in Theorem 11.1, this is $\rho_0(\mu) = 1 - 4\pi\mu/\omega(0) + o(\mu)$. To find the others we

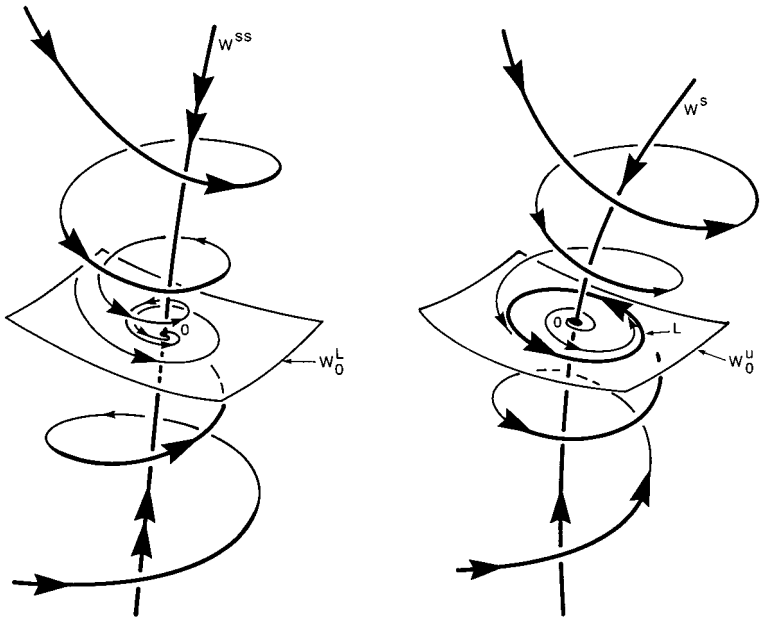

(a) $\mu < 0$ (b) $\mu > 0$

Fig 11.5.4. A supercritical Andronov–Hopf bifurcation in $\mathbb{R}^3$. The stable focus (the leading manifold W^L is two-dimensional) in (a) becomes a saddle-focus in (b). A stable periodic orbit is the edge of the unstable manifold W_0^u.

observe that since the periodic orbit lies in the center manifold $y = 0$, the variational equation in the y-variables is (see (11.5.1)):

$$\frac{\partial \dot{y}}{\partial y_0} = (A + F(x, 0, \varepsilon))\frac{\partial y}{\partial y_0}\,.$$

The absolute value of F is small, hence the time τ shift by this equation is close to $e^{A\tau}$ (where τ is the period of the limit cycle). Hence, the multipliers corresponding to the y-variables are close to $e^{\lambda_j \tau} (j = 1, \ldots, m)$, where the λ_j's are the eigenvalues of the matrix A. Since $\tau = 2\pi/\omega(0) + \cdots$, we have the following formula for the multipliers

$$\rho_j(\mu) = e^{2\pi\lambda_j/\omega(0)}(1 + \cdots) \quad j = 1, \ldots, m\,.$$

The multiplier ρ_0 closest to the unit circle is real, so for all μ sufficiently small the periodic orbit is a node (i.e. the corresponding fixed point of the Poincaré map is a stable node).

If $L_1 > 0$, the phase portraits are depicted in Fig. 11.5.5. Here, when $\mu < 0$, there exists a stable equilibrium state O (a focus) and a saddle periodic orbit whose m-dimensional stable manifold is the boundary of the attraction basin of O. As μ increases, the cycle shrinks towards to O and collapses into it at $\mu = 0$. The equilibrium state O becomes a saddle-focus as soon as μ increases through zero.

We have seen that bifurcations in one-parameter families transverse to the stability boundary $\mathfrak{M}$ may develop in completely different ways depending on the sign of the first Lyapunov value. If the value L_1 vanishes at $\varepsilon = 0$, at the very least we have to consider two-parameter families. To explore such a situation let us reduce the system on the center manifold to the normal form up to the terms of fifth order:[5]

$$\begin{aligned}
\dot{x}_1 &= \lambda(\varepsilon)x_1 - \omega(\varepsilon)x_2 + (L_1(\varepsilon)x_1 - \Omega_1(\varepsilon)x_2)(x_1^2 + x_2^2) \\
&\quad + (L_2 x_1 - \Omega_2 x_2)(x_1^2 + x_2^2)^2 + o(x^5)\,, \\
\dot{x}_2 &= \omega(\varepsilon)x_1 + \lambda(\varepsilon)x_2 + (\Omega_1(\varepsilon)x_1 + L_1(\varepsilon)x_2)(x_1^2 + x_2^2) \\
&\quad + (\Omega_2 x_1 + L_2 x_2)(x_1^2 + x_2^2)^2 + o(x^5)\,,
\end{aligned}$$

[5]The system is assumed to be sufficiently smooth, e.g. $r \geq 5$.

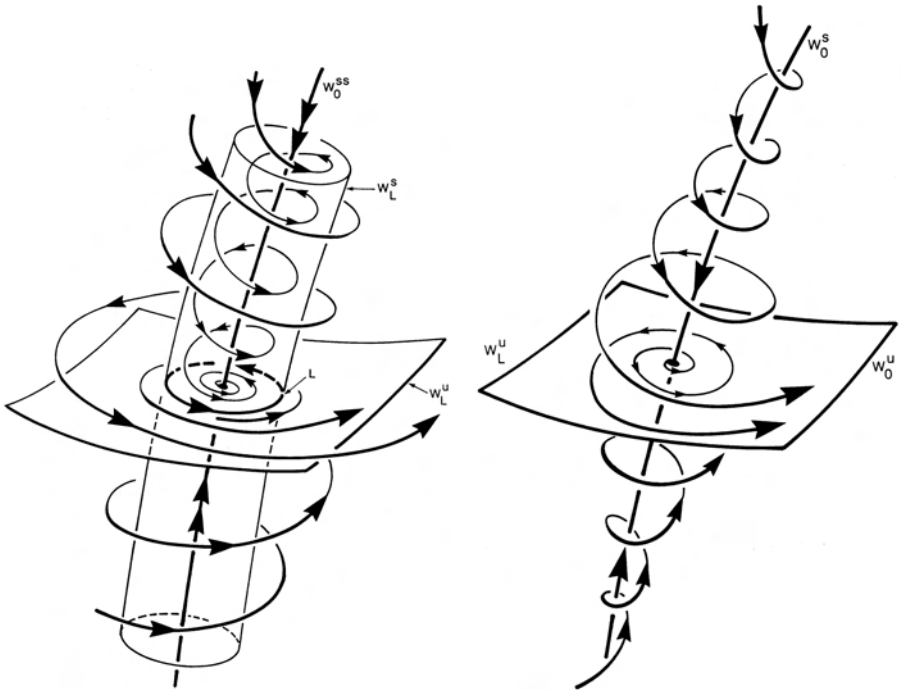

(a) $\mu < 0$ (b) $\mu > 0$

Fig 11.5.5. A subcritical Andronov–Hopf bifurcation. (a) An attraction basin of a stable focus is bounded by a stable manifold of a saddle periodic orbit. (b) The periodic orbit narrows to the stable focus at $\mu = 0$, and the latter becomes a saddle-focus (1,2).

where $L_1(\varepsilon)$, $\Omega_1(\varepsilon)$ are function of class $\mathbb{C}^{r-3}$, $L_1(0) = 0$. Consider the surface $\mathfrak{M}'$ defined by the conditions

$$\lambda(\varepsilon) = 0\,, \quad L_1(\varepsilon) = 0\,.$$

If

$$\operatorname{rank} \begin{pmatrix} \dfrac{\partial \lambda_0}{\partial \varepsilon_1} & \cdots & \dfrac{\partial \lambda_0}{\partial \varepsilon_p} \\ \dfrac{\partial L_1}{\partial \varepsilon_1} & \cdots & \dfrac{\partial L_1}{\partial \varepsilon_p} \end{pmatrix}_{\varepsilon=0} = 2\,,$$

then $\mathfrak{M}'$ is a $\mathbb{C}^{r-3}$-smooth surface of codimension two.

Choose $\lambda(\varepsilon)$ and $L_1(\varepsilon)$ as the governing parameters μ_0 and μ_1, and recast the two-parameter family transverse to $\mathfrak{M}'$ in the form

$$\begin{aligned}\dot{x}_1 &= \mu_0 x_1 - \omega(\mu)x_2 + (\mu_1 x_1 - \Omega_1(\mu)x_2)(x_1^2+x_2^2)\\ &\quad + (L_2 x_1 - \Omega_2 x_2)(x_1^2+x_2^2)^2 + o(x^5)\,,\\ \dot{x}_2 &= \omega(\mu)x_1 + \mu_0 x_2 + (\Omega_1(\mu)x_1 + \mu_1 x_2)(x_1^2+x_2^2)\\ &\quad + (\Omega_2 x_1 + L_2 x_2)(x_1^2+x_2^2)^2 + o(x^5)\,,\end{aligned}$$

or, in polar coordinates as

$$\begin{aligned}\dot{R} &= R(\mu_0 + \mu_1 R^2 + L_2 R^4) + \Phi_1(R,\varphi,\mu)\,,\\ \dot{\varphi} &= \omega(\mu) + \Omega_1(\mu)R^2 + \Omega_2 R^4 + \Phi_2(R,\varphi,\mu)\,,\end{aligned} \tag{11.5.13}$$

where $\Phi_1 = o(R^5)$ and $\Phi_2 = o(R^4)$.

Observe that $\dot{\varphi}$ does not vanish for small R. Therefore, the dynamics near the origin is determined by the mapping of the ray: $\mathfrak{R} : \varphi = 0$, $R \geq 0$ into itself along the trajectories of the system. The map is computed in the same way as above in proving Theorem 11.1, namely by means of expanding the solutions $R(\varphi)$ of the system (11.5.13) into the Taylor series with respect to initial data:

$$R(\varphi) = \alpha_1(\varphi)R_0 + \alpha_2(\varphi)R_0^2 + \alpha_3(\varphi)R_0^3 + \alpha_4(\varphi)R_0^4 + \alpha_5(\varphi)R_0^5 + \cdots\,.$$

Omitting the details the final result is given by

$$\bar{R} = R + \frac{2\pi}{\omega(\mu)}R(\hat{\mu}_0 + \hat{\mu}_1 R^2 + L_2 R^4) + o(R^5)\,, \tag{11.5.14}$$

where:

$$\begin{aligned}\hat{\mu}_0 &= (e^{2\pi\mu_0/\omega(\mu)} - 1)\frac{\omega(\mu)}{2\pi} = \mu_0 + o(\mu_0)\,,\\ \hat{\mu}_1 &= \left(\mu_1 - \frac{\Omega_1(\mu)}{\omega(\mu)}\mu_0\right)e^{2\pi\mu_0/\omega(\mu)}(e^{4\pi\mu_0/\omega(\mu)} - 1)\frac{\omega(\mu)}{4\pi\mu_0}\\ &= \mu_1 - \frac{\Omega_1(0)}{\omega(0)}\mu_0 + o(\mu_0) + o(\mu_1)\,.\end{aligned}$$

Since the right-hand side of the mapping (11.5.14) is a monotonically increasing function, the study of the mapping reduces to the study of its fixed points.

They are sought as the roots of the equation

$$R(\hat{\mu}_0 + \hat{\mu}_1 R^2 + L_2 R^4) + o(R^5) = 0\,.$$

Note that since the map is defined for $R \geq 0$, we need only to look for non-negative roots: $R = 0$ corresponds to an equilibrium state, and the positive roots correspond to periodic orbits of the system (11.5.13). Since we have already examined an equation of this type in the preceding section (Eq. (11.4.12)), when analyzed the period-two orbits emerging from a period-doubling bifurcation in the case of zero Lyapunov value, we can simply reformulate the main results.

No more than two limit cycles may be spawned. If $L_2 < 0$ (see Fig. 11.5.6), then there exists a single limit cycle for $\mu_0 > 0$; inside the sector D_2 bordered by the ray $\mu_0 = 0$, $\mu_1 > 0$ and by the curve $\mathcal{L} : \mu_0 = \mu_1^2/4|L_2| + o(\mu_1^2)$ there exist two limit cycles: one stable and the other unstable; they merge on the curve $\mathcal{L}$, forming one semi-stable cycle; in the region D_0 between $\mathcal{L}$ and the ray $\mu_1 = 0$, $\mu_1 < 0$, there is no periodic orbit. Analogous bifurcations in the case $L_2 > 0$ are shown in Fig. 11.5.7.

Now let the first $(k-1)$ Lyapunov values be zero at $\varepsilon = 0$ (the smoothness of the system under consideration is assumed to be not less than $2k+1$).

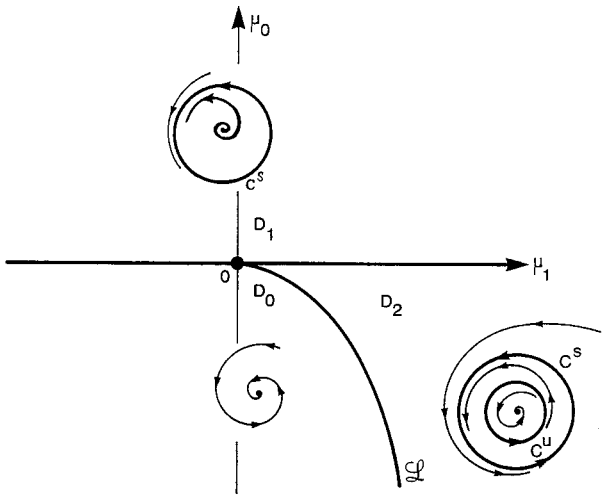

Fig 11.5.6. Bifurcation unfolding for the case $L_1 = 0$, $L_2 < 0$. The curve $\mathcal{L}$ corresponds to the existence of a double cycle.

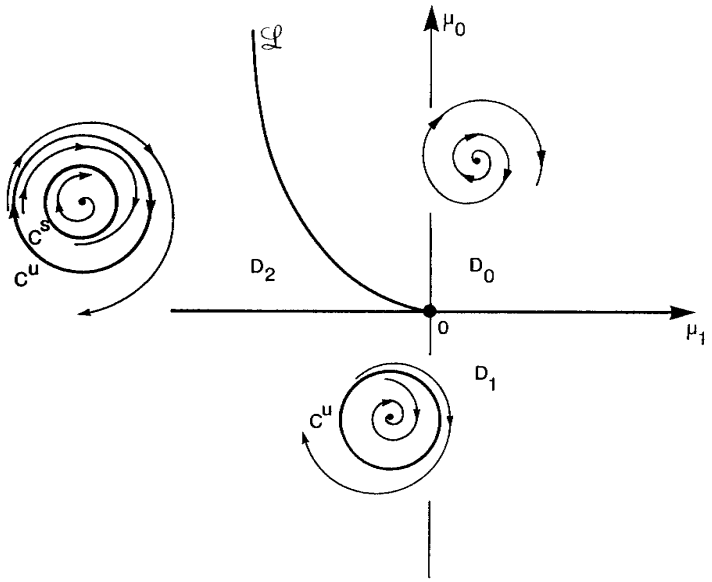

Fig 11.5.7. Bifurcation unfolding for the case $L_1 = 0$, $L_2 > 0$.

Then, in the case of general position the surface $\mathfrak{M}'$ (which corresponds to equilibrium states with a pair of purely imaginary eigenvalues and with the first $(k-1)$ zero Lyapunov values equal to zero) is a $\mathbb{C}^{2k-1}$-smooth surface of codimension k passing through the point $\varepsilon = 0$ in the parameter space. All transverse families in this case depend on k governing parameters $\mu_0, \ldots, \mu_{k-1}$ and may be written in polar coordinates as follows:

$$\begin{aligned} \dot{R} &= R(\mu_0 + \cdots + \mu_{k-1}R^{2k-2} + L_k R^{2k}) + o(R^{2k+1})\,, \\ \dot{\varphi} &= \omega(\mu) + \Omega_1(\mu)R^2 + \cdots + \Omega_k(\mu)R^{2k} + o(R^{2k})\,. \end{aligned} \tag{11.5.15}$$

Analysis of this family can also be reduced to an examination of the map of the ray $\varphi = 0, R \geq 0$ into itself. We may show that this mapping has the form

$$\bar{R} = R + \frac{2\pi}{\omega(\mu)} R(\hat{\mu}_0 + \hat{\mu}_1 R^2 + \cdots + \hat{\mu}_{k-1}R^{2k-2} + L_k R^{2k}) + o(R^{2k+1})\,, \tag{11.5.16}$$

where

$$\begin{aligned}
\hat{\mu}_0 &= \mu_0 + o(\mu_0)\,,\\
\hat{\mu}_1 &= \mu_1 - \hat{\Omega}_1\mu_0 + o(\mu_0) + o(\mu_1)\,,\\
&\vdots\ \vdots \qquad \vdots\\
\hat{\mu}_i &= \mu_i - \hat{\Omega}_1\mu_{i-1} - \cdots - \hat{\Omega}_i\mu_0 + o(\mu_0) + \cdots + o(\mu_i)\,,\\
&\vdots\ \vdots \qquad \vdots\\
\hat{\mu}_{k-1} &= \mu_{k-1} - \hat{\Omega}_1\mu_{k-2} - \cdots - \hat{\Omega}_{k-1}\mu_0 + o(\mu_0) + \cdots + o(\mu_i)\,,
\end{aligned}$$

and the values $\hat{\Omega}_i$ are functions of $\Omega_1(0), \ldots, \Omega_i(0)$ and $\omega(0)$:

$$\begin{aligned}
\hat{\Omega}_1 &= \Omega_1(0)/\omega(0)\,,\\
\hat{\Omega}_2 &= \Omega_2(0)/\omega(0) - \Omega_1^2(0)/\omega^2(0)\,,\\
&\vdots\ \vdots \qquad \vdots\,.
\end{aligned}$$

In the previous section we have reduced the problem of period-two orbits which were spawned from a fixed point with a multiplier -1 to a study of the mapping (11.4.17) analogous to the mapping (11.5.16). Therefore, the bifurcation diagram in this case is the same as in the period-doubling bifurcation with $(k-1)$ zero Lyapunov values: this consists of a union of the plane $\mu_0 = 0$ on which the equilibrium state at the origin loses its stability and that half of the surface of the multiple roots of the polynomial $\hat{\mu}_0 + \cdots + \hat{\mu}_{k-1}u^{k-1} + L_k u^k$ which corresponds to positive u (a positive root of multiplicity s corresponds to an s-multiple limit cycle).

Observe that the mapping (11.5.16) may have no more than k positive fixed points (with multiplicity included) so that an equilibrium state with a pair of purely imaginary characteristic exponents and with first $(k-1)$ zero Lyapunov values can generate a maximum of k limit cycles. Moreover, a region in the parameter space may be identified where the system has a given number, from 0 to k, of limit cycles. They all surround the origin so that an unstable cycle is enclosed between any two consecutive stable ones. The stability of the outermost limit cycle is determined by the sign of the kth Lyapunov value: it is stable if $L_k < 0$ and unstable otherwise.

This theory is due to Andronov and Leontovich who had analyzed the two-dimensional case. Somewhat later Hopf had investigated the families possessing an equilibrium state with a purely imaginary pair of characteristic exponents from a different perspective. His result, using the contemporary approach, may be reformulated as follows: consider a one-parameter family of two-dimensional[6] systems

$$\begin{aligned} \dot{x}_1 &= \lambda(\mu)x_1 - \omega(\mu)x_2 + G_1(x_1, x_2, \mu)\,, \\ \dot{x}_2 &= \omega(\mu)x_1 + \lambda(\mu)x_2 + G_2(x_1, x_2, \mu)\,, \end{aligned} \tag{11.5.17}$$

where $G_{1,2}$ are functions of $\mathbb{C}^r$ $(r \geq 1)$ class such that $G = o(R)$ and $G'_\mu = o(R)$, where $R = \sqrt{x_1^2 + x_2^2}$.

Theorem 11.2. *Let*

$$\lambda(0) = 0\,, \quad \lambda'(0) \neq 0\,, \quad \omega(0) \neq 0\,.$$

Then, in the extended phase space (the direct product of the phase space and the parameter space) near the origin there exists a uniquely defined $\mathbb{C}^r$-smooth invariant surface of the form $\mu = \psi(x)$, $\psi(0) = 0$, such that each its intersection with the plane $\mu =$ constant consists of a set of closed orbits of the system (11.5.17), *lying in a neighborhood of the origin at the given μ.*

Proof. Recast the system (11.5.17) in polar coordinates to obtain

$$\dot{R} = \lambda(\mu)R + \Phi_1(R, \varphi, \mu)\,,$$

$$\dot{\varphi} = \omega(\mu) + \Phi_2(R, \varphi, \mu)\,,$$

where $\Phi_1 = o(R)$, $\partial\Phi_1/\partial\mu = o(R)$, and $\Phi_2 = o(1)$. The mapping of the ray $\varphi = 0$, $R \geq 0$ along the trajectories of the system has the form

$$\bar{R} = e^{2\pi\lambda(\mu)/\omega(\mu)}R + o(R)\,. \tag{11.5.18}$$

The fixed points of this map are found as the zeros of the function

$$\Psi(R, \mu) \equiv e^{2\pi\lambda(\mu)/\omega(\mu)} - 1 + o(R)/R\,. \tag{11.5.19}$$

[6]Hopf had in fact considered the high-dimensional case. However, applying the center manifold theorem, we may restrict our consideration to the two-dimensional case.

The pair $(R = 0, \mu = 0)$ satisfies this equation. Since

$$\frac{\partial \Psi(0,0)}{\partial \mu} = \frac{2\pi\lambda'(0)}{\omega(0)} \neq 0\,,$$

we can apply the implicit function theorem to (11.5.19). Therefore, in the semiplane $(\mu, R \geq 0)$ there is a uniquely defined smooth curve of the form $\mu = \Psi(R)$ that consists of the fixed points of the mapping (11.5.18) at each given μ. Since periodic orbits of the system (11.5.17) correspond to fixed points of the mapping (11.5.18), there exists a surface of the form $\mu = \psi(x)$ in the extended space (μ, x_1, x_2) which is filled out with the closed trajectories of the system. This coincides with the claim of the theorem (checking the smoothness of the surface at $x = 0$ would require additional calculations which we omit here).

Note that the above theorem by itself does not reveal much information about the dynamics of the system (11.5.17). The only information that we can instantly extract from the theorem is that the system has periodic orbits in a small neighborhood of $\mu = 0$ or at $\mu = 0$. But the theorem says nothing about the number of orbits for any fixed μ.

For instance, assuming the conditions of the theorem hold, it may happen that the invariant surface is given by the equation $\mu = 0$. This means that all trajectories near the origin are closed, i.e. the equilibrium state at the origin is a center, whereas the system has no small closed orbits around the origin at $\mu \neq 0$. Thus, the equilibrium state may only lose its stability without giving birth to a limit cycle at the instance how it occurs, for example, in the equation $\ddot{x} + \mu\dot{x} + x + x^3 = 0$.

11.6. Birth of invariant torus

Consider a family of maps of class $\mathbb{C}^r (r \geq 3)$ with respect to the variables $x \in \mathbb{R}^2$, $y \in \mathbb{R}^m (m \geq 0)$ and parameters $\varepsilon \in \mathbb{R}^p (p \geq 1)$. Let the map have, at $\varepsilon = 0$, a fixed point O with a pair of complex-conjugate multipliers whose absolute value is equal to 1:

$$\rho_{1,2} = e^{\pm i\omega_0}$$

where we assume $0 < \omega_0 < \pi$ (the other multipliers are supposed to lie inside the unit circle). Such a fixed point persists also for $\varepsilon \neq 0$. We will assume that the fixed point resides at the origin for all ε. The pair of multipliers closest to

a unit circle is

$$\rho_{1,2}(\varepsilon) = \rho(\varepsilon)e^{\pm i\omega(\varepsilon)}\,, \tag{11.6.1}$$

where $\rho(\varepsilon)$ and $\omega(\varepsilon)$ are $\mathbb{C}^{r-1}$-functions of ε such that

$$\rho(0) = 1\,, \quad 0 < \omega(0) < \pi\,.$$

Since we do not intend to consider the more difficult problem of strong resonances, let us assume that $\omega(0) \neq 2\pi/3, \pi/2$.

By virtue of the reduction theorem, the map near the fixed point can be recast into the form

$$\begin{aligned}
\bar{x}_1 &= \rho(\varepsilon)(x_1\cos\omega(\varepsilon) - x_2\sin\omega(\varepsilon)) + G_1(x_1, x_2, \varepsilon)\,,\\
\bar{x}_2 &= \rho(\varepsilon)(x_1\sin\omega(\varepsilon) + x_2\cos\omega(\varepsilon)) + G_2(x_1, x_2, \varepsilon)\,,\\
\bar{y} &= [A + F(x, y, \varepsilon)]y\,,
\end{aligned} \tag{11.6.2}$$

where F is a $\mathbb{C}^{r-1}$-smooth function, $G_{1,2}$ are of $\mathbb{C}^r$ class,

$$F(0,0,0) = 0\,,$$

$$G(0,0,0) = 0\,,$$

$$G'_x(0,0,0) = 0\,,$$

where we write G for G_i to avoid clutter.

We will assume that the map at $\varepsilon = 0$ is reduced to the normal form up to cubic terms (see Sec. 10.6). Moreover, we can verify that the quadratic terms are non-resonant for all small ε, and hence, they can be eliminated by transformations which are polynomial with respect to x and $\mathbb{C}^{r-2}$-smooth with respect to ε. Then, the map on the center manifold can be recast into the form

$$\begin{aligned}
\bar{x}_1 &= \rho(\varepsilon)(x_1\cos\omega(\varepsilon) - x_2\sin\omega(\varepsilon))\\
&\quad + (\alpha x_1 - \beta x_2)(x_1^2 + x_2^2) + \tilde{G}_1(x_1, x_2, \varepsilon)\,,\\
\bar{x}_2 &= \rho(\varepsilon)(x_1\sin\omega(\varepsilon) + x_2\cos\omega(\varepsilon))\\
&\quad + (\beta x_1 + \alpha x_2)(x_1^2 + x_2^2) + \tilde{G}_2(x_1, x_2, \varepsilon)\,,
\end{aligned}$$

where $\tilde{G}_{1,2}$ are $\mathbb{C}^r$-smooth functions of x and $\mathbb{C}^{r-2}$-smooth functions of ε such that

$$\begin{aligned}
\tilde{G}(0,0,\varepsilon) = 0\,, &\quad \tilde{G}''_{xx}(0,0,\varepsilon) = 0\,,\\
\tilde{G}'_x(0,0,\varepsilon) = 0\,, &\quad \tilde{G}'''_{xxx}(0,0,0) = 0\,.
\end{aligned}$$

Since $\tilde{G}'''_{xxx}$ is small for small ε and $R(R=\sqrt{x_1^2+x_2^2})$, it follows that

$$\tilde{G}''_{xx}=o(R)\,,\quad \tilde{G}'_x=o(R^2)\,,\quad \tilde{G}=o(R^3)\,. \tag{11.6.3}$$

To write the map in polar coordinates we use the formulas $\bar{R}=\sqrt{\bar{x}_1^2+\bar{x}_2^2}$ and $\bar{\varphi}=\operatorname{Im}\ln(\bar{x}_1+i\bar{x}_2)$ to obtain

$$\begin{aligned}
\bar{R}^2 &= \rho^2(x_1^2+x_2^2)[1+2(\alpha\cos\omega+\beta\sin\omega)(x_1^2+x_2^2)/\rho\\
&\quad +2\rho^{-1}(x_1(\tilde{F}_1\cos\omega+\tilde{F}_2\sin\omega)\\
&\quad +x_2(\tilde{F}_2\cos\omega-\tilde{F}_1\sin\omega))/(x_1^2+x_2^2)+\cdots]\,,\\
\bar{\varphi} &= \operatorname{Im}\ln(x_1+ix_2)+\omega+\operatorname{Im}\ln[1+\rho^{-1}e^{-i\omega}(\alpha+i\beta)(x_1^2+x_2^2)\\
&\quad +\rho^{-1}e^{-i\omega}(\tilde{F}_1+i\tilde{F}_2)/(x_1+ix_2)]\,,
\end{aligned}$$

and

$$\begin{aligned}
\bar{R} &= \rho(\varepsilon)R+L_1R^3+\tilde{\Phi}_1(R,\varphi,\varepsilon)\,,\\
\bar{\varphi} &= \varphi+\omega(\varepsilon)+\Omega_1R^2+\tilde{\Phi}_2(R,\varphi,\varepsilon)\,,
\end{aligned} \tag{11.6.4}$$

where $L_1=(\alpha\cos\omega+\beta\sin\omega)$ is the first Lyapunov value, $\Omega_1=(\beta\cos\omega-\alpha\sin\omega)/\rho$, and

$$\begin{aligned}
\tilde{\Phi}_1(R,\varphi,\varepsilon) &= \tilde{F}_1\cos(\omega+\varphi)+\tilde{F}_2\sin(\omega+\varphi)+\cdots=o(R^3)\,,\\
\tilde{\Phi}_2(R,\varphi,\varepsilon) &= \rho^{-1}(\tilde{F}_2\cos(\omega+\varphi)-\tilde{F}_1\sin(\omega+\varphi))/R+\cdots=o(R^2)\,,
\end{aligned} \tag{11.6.5}$$

where the ellipses denote higher order terms.

The boundary $\mathfrak{M}$ of the stability region of the fixed point is defined in the parameter space by the equation $\rho(\varepsilon)=0$: the fixed point O is stable if $\rho(\varepsilon)<0$, and unstable if $\rho(\varepsilon)>0$. If at least one of the component of the vector $(\partial\rho/\partial\varepsilon_1,\ldots,\partial\rho/\partial\varepsilon_p)_{\varepsilon=0}$ differs from zero, then for small ε the boundary $\mathfrak{M}$ is a $\mathbb{C}^{r-1}$-smooth surface of codimension one. Choose the difference $\rho(\varepsilon)-1$ as the governing parameter μ. Hence, the one-parameter families transverse to $\mathfrak{M}$ can be represented in the form

$$\begin{aligned}
\bar{R} &= R+R(\mu+L_1R^2)+\tilde{\Phi}_1(R,\varphi,\mu)\,,\\
\bar{\varphi} &= \varphi+\omega(\mu)+\Omega_1R^2+\tilde{\Phi}_2(R,\varphi,\mu)\,.
\end{aligned} \tag{11.6.6}$$

Theorem 11.3. *Let $L_1 < 0$. Then, for all small $\mu \le 0$ the fixed point O of the map* (11.6.6) *is stable and attracts all trajectories inside a small neighborhood of O.*

At $\mu > 0$, a smooth, invariant closed curve

$$R = \sqrt{\left|\frac{\mu}{L_1}\right|}\psi(\varphi,\mu)\,, \quad \psi_{\mu\to 0} \to 1\,, \tag{11.6.7}$$

bifurcates from O, which attracts all (except for O) neighboring trajectories (see Fig. 11.6.1).

If the first Lyapunov value $L_1 > 0$, then the fixed point of the map (11.6.6) *is unstable for sufficiently small $\mu \ge 0$. When $\mu < 0$ the fixed point is stable; its attraction basin is the inner domain of an unstable smooth invariant curve of the form* (11.6.7). *As $\mu \to -0$, the curve collapses into the fixed point (see Fig.* 11.6.2).

Proof. Observe first that the case $L_1 > 0$ can be reduced to $L_1 < 0$ by using the inverse map to (11.6.6) instead of the original one. So it suffices for us to consider only the situation $L_1 < 0$. The stability of the fixed point for $\mu \le 0$ follows immediately from the fact that $\bar{R} < R$ for $\mu \le 0$, i.e. $V \equiv R$ is a Lyapunov function. Thus, the case left to be analyzed is $\mu > 0$.

Consider the annulus $\mathcal{A}$ defined by

$$\frac{2}{3}\sqrt{|\mu/L_1|} \equiv R_1 \le R \le R_2 \equiv \frac{3}{2}\sqrt{|\mu/L_1|}\,.$$

Observe that given a sufficiently small neighborhood of the origin, for all μ sufficiently small, a trajectory starting outside of the annulus must enter

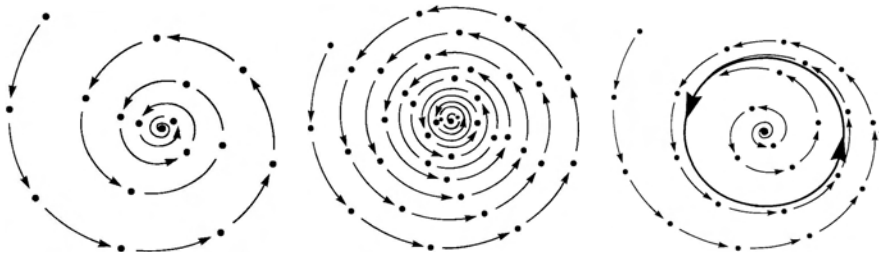

(a) $\mu < 0$ (b) $\mu = 0$ (c) $\mu > 0$

Fig. 11.6.1. Soft generation of an invariant circle.

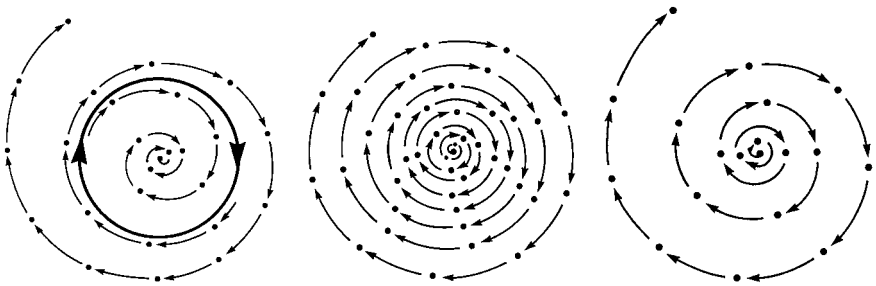

(a) (b) (c)

Fig. 11.6.2. Rigid loss of stability of a stable fixed point.

it after a finite number of iterations: it follows from (11.6.6) that $\bar{R} < R$ when $R > R_2$ and $\bar{R} > R$ when $0 < R < R_1$. To complete the proof we need to apply the annulus principle from Sec. 4.2 to the map (11.6.6) in the annulus $\mathcal{A}$.

In order to do this let us make a renormalization $R \to R\sqrt{|\mu/L_1|}$. In the normalized variables, the annulus is defined by the inequalities

$$\frac{2}{3} \le R \le \frac{3}{2}\,, \tag{11.6.8}$$

and the map assumes the form

$$\begin{aligned} \bar{R} &= R + \mu R(1-R^2) + \Phi_1(R,\varphi,\mu)\,, \\ \bar{\varphi} &= \varphi + \omega(\mu) - \mu\Omega_1 R^2/L_1 + \Phi_2(R,\varphi,\mu)\,, \end{aligned} \tag{11.6.9}$$

where

$$\begin{aligned} \Phi_1 &= \tilde{\Phi}_1(R\sqrt{|\mu/L_1|},\varphi,\mu)/\sqrt{|\mu/L_1|}\,, \\ \Phi_2 &= \tilde{\Phi}_2(R\sqrt{|\mu/L_1|},\varphi,\mu)\,. \end{aligned} \tag{11.6.10}$$

One can see from the formulas (11.6.10), (11.6.5), and (11.6.3) that

$$\Phi_{1,2} = o(\mu)\,. \tag{11.6.11}$$

If we denote, as in Sec. 4.2,

$$\begin{aligned} \bar{R} &= f(R,\varphi)\,, \\ \bar{\varphi} &= g(R,\varphi)\,, \end{aligned}$$

then the map (11.6.9) in the annulus satisfies the following relations

$$\begin{aligned} \|(g'_\varphi)^{-1}\|_\circ &= 1 + o(\mu)\,, \\ \|g'_R\|_\circ &= O(\mu)\,, \\ \|f'_R\|_\circ &= 1 - \mu/3 + o(\mu)\,, \\ \|f'_\varphi\|_\circ &= o(\mu)\,, \end{aligned}$$

where $\|\cdot\|_\circ \equiv \sup\|\cdot\|$. Observe that for sufficiently small μ the following inequality holds

$$\begin{aligned} &\sqrt[r+1]{(\|f'_R\|_\circ + \|g'_R\|_\circ \|f'_\varphi (g'_\varphi)^{-1}\|_\circ)\cdot \|(g'_\varphi)^{-1}\|_\circ^r} \\ &\quad + \sqrt{\|(g'_\varphi)^{-1}\|_\circ \|g'_R\|_\circ \|f'_\varphi (g'_\varphi)^{-1}\|_\circ} < 1\,. \end{aligned} \tag{11.6.12}$$

It follows from the annulus principle (Theorems 4.2 and 4.5) that there exists a smooth stable invariant curve C of the form

$$R = \psi(\varphi, \mu)$$

to which all trajectories from $\mathcal{A}$ converge.

It follows from the proof of the annulus principle that the curve C is a limit of a sequence of the curves obtained as iterations of an arbitrary initial curve $R = \text{const.}$, for example, $R = 1$. Observe from (11.6.9) that for any small $\delta > 0$, all iterations of this curve lie inside the annulus $|R - 1| \le \delta$ provided that μ is small enough. Indeed, if μ is sufficiently small, then for $R = 1 + \delta$, we have

$$\bar{R} = 1 + \delta - \mu\delta(1 + \delta)(2 + \delta) + o(\mu) < 1 + \delta\,;$$

and for $R = 1 - \delta$, we have

$$\bar{R} = 1 - \delta + \mu\delta(1 - \delta)(2 - \delta) + o(\mu) < 1 - \delta\,.$$

Hence, the limit curve C lies inside this annulus too. Since δ may be made arbitrarily small as $\mu \to 0$, we obtain that $\psi(\varphi, \mu) \to 1$ as $\mu \to 0$. End of the proof.

Remark. Since the smoothness of the invariant curve cannot, in general, exceed the smoothness of the map itself, the function ψ in (11.6.7) is only $\mathbb{C}^r$-smooth with respect to φ and C^{r-2}-smooth with respect to μ. In fact, the

loss of smoothness with respect to parameters is caused only by the loss of smoothness when reducing the original map to the form (11.6.6). By a more careful normal form reduction the $\mathbb{C}^r$-smoothness with respect to parameters can be restored. These smoothness results are concerned only with non-zero values of μ (the annulus principle is not applicable at $\mu = 0$ to the map (11.6.9)). However, we can show that the right-hand side of the Eq. (11.6.7) which defines the invariant curve is sufficiently smooth with respect to φ and $\sqrt{\mu}$ for all $L_1\mu \le 0$. For example, let us check that all derivatives of ψ with respect to φ tend to zero as $\mu \to 0$. Indeed, note that the invariance of the curve C implies that if $R = \psi(\varphi, \mu)$, then $\bar{R} = \psi(\bar{\varphi}, \mu)$. By differentiating this equality and using (11.6.9) we obtain

$$\bar{u} = \frac{(1 + \mu(1 - 3R^2) + \Phi'_{1R})u + \Phi'_{1\varphi}}{1 + \Phi'_{\varphi} - (2\mu\Omega_1 R/L_1 - \Phi'_{2R})u}\,, \tag{11.6.13}$$

where $u \equiv \partial\psi/\partial\varphi$ and $\bar{u} = u(\bar{\varphi})$. The right-hand side in (11.6.13) is computed by letting $R = \psi(\varphi, \mu)$. The Eq. (11.6.13) along with the second equation in (11.6.9) can be treated as a mapping of the cylinder $\mathbb{R}^1 \times \mathbb{S}^1$ into itself: $(u, \varphi) \mapsto (\bar{u}, \bar{\varphi})$. Taking into account that $R = \psi(\varphi, \mu) \to 1$ as $\mu \to 0$, we can recast (11.6.13) into the form

$$\bar{u} = (1 - 2\mu)u + o(\mu)\,. \tag{11.6.14}$$

Observe that (11.6.14) maps the annulus

$$|u| \le \delta$$

into itself, where δ may be arbitrarily small due to the smallness of μ. The derivative $u = \partial\psi/\partial\varphi$ is sought as the invariant curve of this map. It follows from the proof of the annulus principle that this curve is a limit of iterations of any curve $u = \text{const}$. Since all iterations of the circle $u = 0$ lie inside the annulus $|u| \le \delta$, the limit curve must also lie inside the annulus. Thus, it follows that $\partial\psi/\partial\varphi \to 0$ as $\mu \to 0$, i.e. ψ at $\mu = 0$ is a smooth function of φ.

Differentiating (11.6.13), we find that as in (11.6.14), the second derivative $\bar{u}^{(2)} = \partial u/\partial\varphi$ satisfies the relation

$$\bar{u}^{(2)} = (1 - 2\mu)u^{(2)} + o(\mu)$$

similar to (11.6.14). Repeating the above arguments we find that the second derivative exists and is continuous for all $\mu \ge 0$. We can iterate this procedure to obtain all derivatives with respect to φ.

The above theorem is related to the map on the center manifold. Reconstructing the behavior of trajectories of the original map (11.6.2) is relatively simple. Here, if $L_1 < 0$, then the fixed point is stable when $\mu \le 0$. When $\mu > 0$ it becomes a saddle-focus with an m-dimensional stable manifold (defined by $x = 0$) and with a two-dimensional unstable manifold which consists of a part of the plane $y = 0$ bounded by the stable invariant curve C.

If $L_1 > 0$, then when $\mu \ge 0$, the fixed point is a saddle-focus of the above type, but its unstable manifold is the whole plane $y = 0$. Upon entering the region $\mu < 0$, the fixed point becomes stable. Meanwhile a saddle invariant curve C bifurcates from the fixed point; its unstable manifold W^u_C is $(m+1)$-dimensional and consists of the layers $x =$ constant, restored at the points of the invariant curve. The stable manifold W^s_C separates the attraction basin of the point O: all trajectories from the inner region tend to O, and all those from outside of W^s_C leave a neighborhood of the origin.

If the mapping (11.6.2) is the Poincaré map of an autonomous system of differential equations, then the invariant curve corresponds to a two-dimensional smooth invariant torus (see Fig. 11.6.3). It is stable if $L_1 < 0$, or it is saddle with a three-dimensional unstable manifold and an $(m+2)$-dimensional stable manifold if $L_1 > 0$. Recall from Sec. 3.4, that the motion on the torus is determined by the Poincaré rotation number: if the rotation number ν is irrational, then trajectories on the torus are quasiperiodic with a frequency rate ν; otherwise, if the rotation number is rational, then there are resonant periodic orbits on a torus.

We postpone our study of bifurcations on the torus until the next paragraph, and consider first what happens if the first Lyapunov value L_1 vanishes.

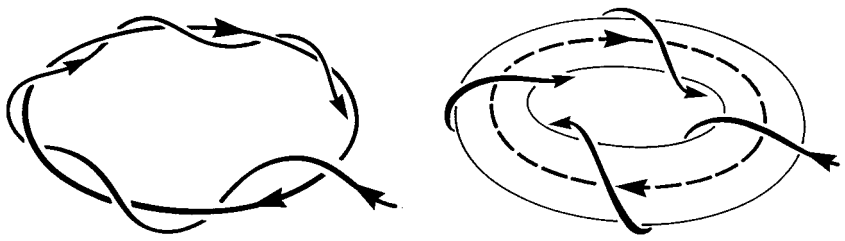

(a) (b)

Fig. 11.6.3. (a) The birth of an invariant torus: in $\mathbb{R}^3$ the cycle lost its skin. (b) The unstable cycle is the dash line inside the solid torus.

Let $\omega(0)$ in (11.6.1) be other than $2\pi/3$, $\pi/2$, $2\pi/5$, $4\pi/5$ or $\pi/3$. Then, after reduction to the normal form, and accounting up to terms of fifth order, the map in polar coordinates is written in the form

$$\begin{aligned} \bar{R} &= R + R(\mu_0 + \mu_1 R^2 + L_2 R^4) + \tilde{\Phi}_1(R, \varphi, \mu)\,, \\ \bar{\varphi} &= \varphi + \omega(\mu) + \Omega_1(\mu) R^2 + \Omega_2 R^4 + \tilde{\Phi}_2(R, \varphi, \mu)\,. \end{aligned} \tag{11.6.15}$$

Here, $\tilde{\Phi}_1 = o(R^5)$, $\tilde{\Phi}_2 = o(R^4)$; $L_2 \neq 0$ is the second Lyapunov value, and the governing parameters are $\mu_0 = \rho(\varepsilon) - 1$ and $\mu_1 = L_1(\varepsilon)$.

Theorem 11.4. *Let $L_2 < 0$. Then, a pair of curves $\mathcal{L}_1$ and $\mathcal{L}_2$ defined by*

$$\mu_0 = -\mu_1^2/4|L_2| \pm o(\mu_1^2)\,, \quad \mu_1 \geq 0$$

can be identified in the parameter plane such that in the region D_0 between the curve $\mathcal{L}_1$ and the ray $\mu_0 = 0$, $\mu_1 \leq 0$ (see Fig. 11.6.4) the fixed point O at the

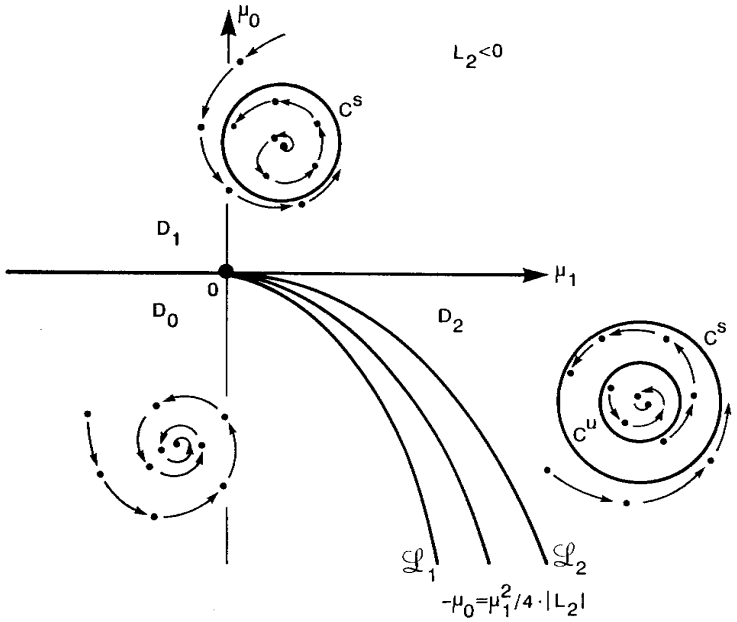

Fig. 11.6.4. Bifurcation unfolding for $L_2 > 0$.

origin is stable and attracts all trajectories from some of its neighborhood; in the region $D_1 : \mu_0 > 0$*, the fixed point is unstable and all trajectories tend to a* $\mathbb{C}^r$*-smooth invariant closed curve* C^s *surrounding the origin; in the region* D_2 *between the curve* $\mathcal{L}_2$ *and the ray* $\mu_0 = 0$, $\mu_1 \geq 0$*, the fixed point becomes stable and, in addition to* C^s*, an unstable* $\mathbb{C}^r$*-smooth invariant closed curve* C^u *is born which separates the basins of* O *and* C^s*.*

In the case $L_2 > 0$*, there exist curves* $\mathcal{L}_1$ *and* $\mathcal{L}_2$ *in the parameter plane defined respectively by*

$$\mu_0 = \mu_1^2/4|L_2| \pm o(\mu_1^2)\,, \quad \mu_1 \leq 0\,,$$

such that in the region D_0 *between the curve* $\mathcal{L}_1$ *and the ray* $\mu_0 = 0$, $\mu_1 \geq 0$ (*see Fig.* 11.6.5)*, the fixed point is unstable and repels all nearby trajectories from a small neighborhood of the origin; in the region* $D_1 : \mu_0 < 0$*, the fixed point is stable but its attraction basin is bounded by an unstable* $\mathbb{C}^r$*-smooth invariant closed curve* C^u*; in the region* D_2 *bordered by* $\mathcal{L}_2$ *and the ray* $\mu_0 = 0$, $\mu_1 \leq 0$*, the fixed point loses its stability and becomes unstable; a stable* $\mathbb{C}^r$*-smooth invariant curve bifurcates from it which now attracts all trajectories in the inner region bounded by* C^u*.*

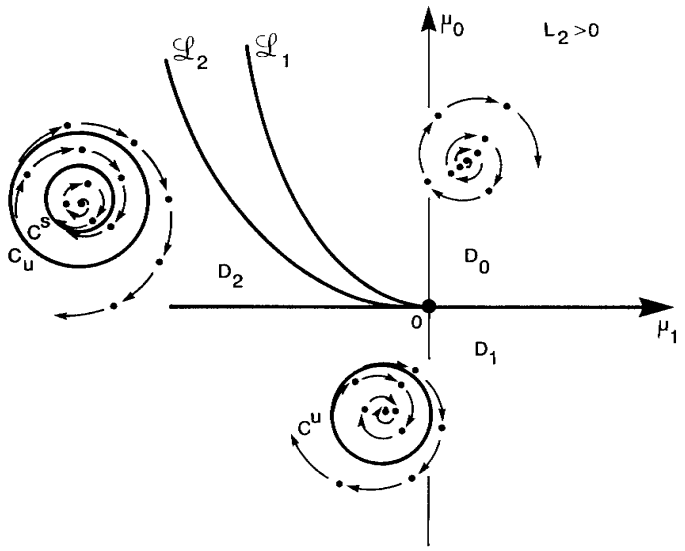

Fig. 11.6.5. Bifurcation unfolding for $L_2 < 0$.

To avoid lengthy calculations we present an outline of the proof. We will consider only the case $L_2 < 0$ (because the case $L_2 > 0$ is reduced to the above one if instead of the map (11.6.15) its inverse is used). Observe, first of all, that the statement of the theorem can be easily verified for the truncated map

$$\begin{aligned} \bar{R} &= R + R(\mu_0 + \mu_1 R^2 + L_2 R^4)\,, \\ \bar{\varphi} &= \varphi + \omega(\mu) + \Omega_1(\mu) R^2 + \Omega_2 R^4\,. \end{aligned} \tag{11.6.16}$$

Here, the invariant curves are the circles $R =$ constant and the problem is reduced to that of finding the positive roots of the equation

$$\mu_0 + \mu_1 R^2 + L_2 R^4 = 0\,.$$

This equation has one positive root

$$R_s^2 = (\mu_1 + \sqrt{\mu_1^2 + 4|L_2|\mu_0})/2|L_2|$$

if $\mu_0 > 0$, no positive roots if $\mu_0 < 0$ and $\mu_1 < 2\sqrt{L_2\mu_0}$, two positive roots

$$R_s^2 = (\mu_1 + \sqrt{\mu_1^2 + 4|L_2|\mu_0})/2|L_2|\,,$$

$$R_u^2 = (\mu_1 - \sqrt{\mu_1^2 + 4|L_2|\mu_0})/2|L_2|$$

if $0 > \mu_0 > -\mu_1^2/4|L_2|$ and $\mu_1 > 0$.

For the map (11.6.15) both curves $\mathcal{L}_1$ and $\mathcal{L}_2$ coalesce ($\mathcal{L}_1 = \mathcal{L}_2 = \mathcal{L}$) and are defined by the equation

$$\mu_0 = -\mu_1^2/4|L_2|\,, \quad \mu_1 \geq 0\,.$$

Below the curve $\mathcal{L}$, the map has no invariant curves. Above $\mu_0 = 0$, it has only one invariant curve $R = R_s$, and between $\mathcal{L}$ and the ray $\mu_0 = 0$, $\mu_1 \geq 0$, the map has two invariant curves $R = R_s$ and $R = R_u$. We can easily derive

$$\frac{\partial \bar{R}}{\partial R} = 1 - 2R_s^2\sqrt{\mu_1^2 + 4|L_2|\mu_0} < 1$$

at $R = R_s$ and

$$\frac{\partial \bar{R}}{\partial R} = 1 + 2R_u^2\sqrt{\mu_1^2 + 4|L_2|\mu_0} > 1$$

at $R = R_u$; i.e. the invariant circle $R = R_s$ is stable, and the invariant curve $R = R_u$ is unstable. On the curve $\mathcal{L}$, the truncated map (11.6.16) has a semi-stable invariant circle $R^2 = \mu_1/2|L_2|$.

As for the initial map (11.6.15) one can arrange the curves $\mathcal{L}_1$ and $\mathcal{L}_2$ in the parameter plane in such a way ($\mathcal{L}_1$ goes slightly above and $\mathcal{L}_2$ goes slightly below $\mathcal{L}$), that for all sufficiently small μ taken outside of the sector between these curves, the behavior of trajectories near the origin inherits the behavior of trajectories of the truncated map (11.6.16). The curve $\mathcal{L}_1$ is chosen so that the value $\bar{R}$ in (11.6.15) is strictly smaller than R for a sufficiently small $\mu \in D_0$ and a small R. This means that R is a Lyapunov function for the map in neighborhood of the origin, so every trajectory converges to the stable fixed point. In the same way as we have done in the proof of Theorem 11.6.1, we can check for the region D_1: $\mu_0 > 0$ that if we surround the circle $R = R_s$ by a small annulus $\mathcal{A}$, then for all small μ the trajectories from a small neighborhood of the origin will converge towards the $\mathcal{A}$; then the annulus principle may be applied to the restriction of the map on $\mathcal{A}$. It follows that $\mathcal{A}$ contains a smooth invariant curve which attracts all trajectories near the origin. As for the curve $\mathcal{L}_2$, it can be chosen so that in the region D_2, if we surround the circles $R = R_s$ and $R = R_u$ with two narrow annuli which we denote by $\mathcal{A}_s$ and $\mathcal{A}_u$ respectively, then all trajectories from the part of the phase-plane which lie outside of $\mathcal{A}_u$ will move toward $\mathcal{A}_s$. Those trajectories that start from the inner part of the phase-plane will tend to the fixed point (see Fig. 11.6.6). Since the annulus principle is also applied here to the restriction of the map on $\mathcal{A}_s$, it implies the existence of a stable invariant closed curve inside $\mathcal{A}_s$. Analogous reasoning concerning the inverse map proves the existence of an unstable closed invariant curve inside $\mathcal{A}_u$ which separates the attraction basins of the stable invariant curve and the fixed point.

Theorem 11.4 shows essentially that outside the narrow sector bounded by $\mathcal{L}_1$ and $\mathcal{L}_2$, the bifurcation behavior does not differ from that of equilibrium states (see Sec. 11.5): fixed points correspond to equilibrium states, and the invariant curves correspond to periodic orbits. However, the transition from the region D_2 to the region D_0 occurs here in a more complicated way. In the case of equilibrium states the regions D_2 and D_0 are separated by a line on which a stable and an unstable periodic orbits coalesce thereby forming a semi-stable cycle. In the case of invariant closed curves, the existence of a line corresponding to a semi-stable invariant closed curve is possible only in very degenerate cases (for example, when the value of $\bar{R}$ does not depend on φ, as

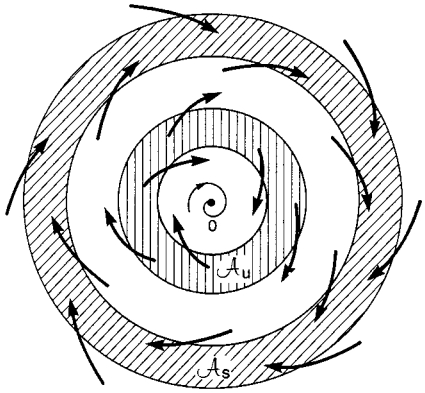

Fig. 11.6.6. At $\mu\epsilon D_2$, the inner ring is unstable and the outer ring is stable.

in the truncated map (11.6.16)). In the general case invariant closed curves do not coalesce into a semi-stable invariant closed curve but are instead destroyed. Their breakdown may be accompanied by the appearance of a non-trivial set containing infinitely many unstable (saddle) periodic orbits of different periods; see more details in [37].

11.7. Bifurcations of resonant periodic orbits accompanying the birth of invariant torus

In this section we continue our study of the bifurcation of a pair of complex-conjugate multipliers of the periodic orbit over and beyond the unit circle

$$\rho_{1,2} = \rho(\varepsilon)e^{\pm i\omega(\varepsilon)}\,, \tag{11.7.1}$$

where $\rho(0) = 1$ and $0 < \omega(0) < \pi$. We do not consider the strong resonances, i.e. $\omega(0) \neq 2\pi/3,\ \pi/2$.

We have already established in the last section that when the first Lyapunov value does not vanish, the passage over the stability boundary $\mathfrak{M} : \rho(\varepsilon) = 0$ is accompanied by the appearance of an invariant two-dimensional torus (in the associated Poincaré map this corresponds to the appearance of an invariant closed curve). If we are not interested in the behavior of the trajectories on the torus, we can restrict our consideration to the study of one-parameter families transverse to $\mathfrak{M}$. In this case Theorem 11.4 in Sec. 11.6, gives a complete description of the bifurcation structure. In order to examine the

bifurcations on the torus itself, we need, however, to examine two-parameter families. The first governing parameter is still $\mu = \rho(\varepsilon) - 1$. As for the second independent governing parameter we chose $\omega(\varepsilon)$; namely, the argument of the multiplier (11.7.1). The Poincaré map on the center manifold when recast in polar coordinates assumes the form

$$\begin{aligned} \bar{R} &= R + R(\mu + L_1 R^2) + \tilde{\Phi}_1(R, \varphi, \mu, \omega)\,, \\ \bar{\varphi} &= \varphi + \omega + \Omega_1 R^2 + \tilde{\Phi}_1(R, \varphi, \mu, \omega) \end{aligned} \tag{11.7.2}$$

[see (11.6.4); from a formal point of view, we have derived a codimension two family transverse to the surface $\mathfrak{M}' : \rho(\varepsilon) = 1$, $\omega(\varepsilon) = \omega(0)$]. The map on the invariant curve $R = \sqrt{\mu}\psi(\varphi, \mu, \omega)$ has the form

$$\bar{\varphi} = \varphi + \omega + \Omega_1 \mu \psi^2(\varphi, \mu, \omega) + \tilde{\Phi}_2(\sqrt{\mu}\psi(\varphi, \mu, \omega), \varphi, \mu, \omega)\,. \tag{11.7.3}$$

It follows from the annulus principle (see the proof of Theorem 11.4) that the function ψ depends smoothly on ω for $\mu > 0$. Moreover, as we have done with the derivatives of ψ with respect to φ we can verify that the derivatives of ψ with respect to ω tend to zero as $\mu \to 0$. This implies that ψ is a smooth function of ω for all $\mu \geq 0$.

The map (11.7.3) at $\mu = 0$ transforms into a rotation over the constant angle ω; its rotation number is equal to $\omega/2\pi$. Therefore, if we choose two different values $\omega = \omega_1$ and $\omega = \omega_2$, then by virtue of the continuous dependence of rotation number on parameters, when μ is small the rotation number ν of the map (11.7.3) is close to $\omega_1/2\pi$ at $\omega = \omega_1$, and is close to $\omega_2/2\pi$ at $\omega = \omega_2$.

Since the derivative $\partial\bar{\varphi}/\partial\omega$ is equal to $1 + O(\mu) > 0$, $\bar{\varphi}$ increases monotonically as ω increases. Therefore, at each fixed small μ, the rotation number ν changes monotonically as ω changes from ω_1 to ω_2, assuming all values from those close to $\omega_1/2\pi$ to those close to $\omega_2/2\pi$. Consequently, as in the problem of a periodic orbit forced by small periodic perturbations (Sec. 4.4), we have (see Fig. 11.7.1) for each rational $\nu = M/N$ from the interval $[\omega_1/2\pi; \omega_2/2\pi]$, a resonance zone emanating from the point $(\mu = 0, \omega = 2\pi M/N)$. Each resonant zone corresponds to the existence of periodic trajectories with frequency $M : N$ on the torus. If ν is an irrational number within the given interval, then there exists a Lipschitz curve of the form $\omega = h(\mu)$ originating from the point $(\mu = 0, \omega = 2\pi\nu)$ that corresponds to a quasiperiodic regime with the frequency ratio ν.

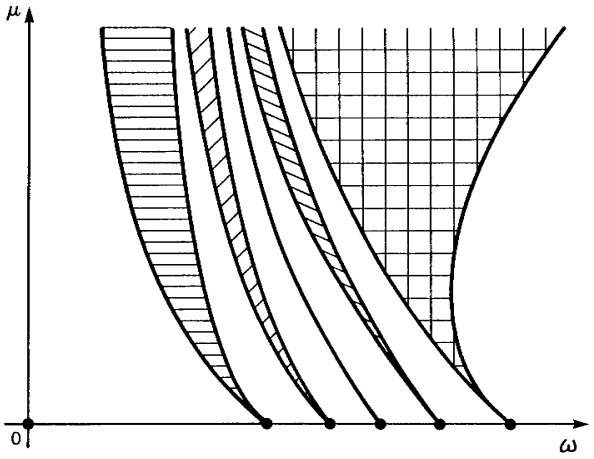

Fig. 11.7.1. The graph μ versus the frequency ω illustrating the resonance wedges originating at rational values of ω.

Let us consider in detail what occurs inside the resonance zone when μ is small enough. Let us choose some $\omega_0 = 2\pi M/N$ and reduce the map to the normal form up to terms of order $N-1$. Assuming that the values of μ are small and ω is close to ω_0, we can derive an expression analogous to formula (10.4.19):

$$\bar{w} = (1+\mu)e^{i\omega}\left(w\left(1+\sum_{p\geq 1}^{2p\leq N-2} C'_{p+1,p}|w|^{2p}\right)+C'_{0,N-1}(w^*)^{N-1}\right) + o(|w|^{N-1})\,, \tag{11.7.4}$$

where $w = x_1 + ix_2$. In polar coordinates the above map can be recast in the form

$$\begin{aligned} \bar{R} &= (1+\mu)(R + L_1R^3 + \cdots + L_PR^{2P+1} \\ &\quad + AR^{N-1}\cos(N\varphi+\alpha)) + o(R^{N-1})\,, \\ \bar{\varphi} &= \varphi + \omega + \Omega_1R^2 + \cdots + \Omega_PR^{2P} \\ &\quad - AR^{N-2}\sin(N\varphi+\alpha) + o(R^{N-2})\,, \end{aligned} \tag{11.7.5}$$

where $C'_{0,N-1} = Ae^{i\alpha}$, P is the largest integer not exceeding $[(N/2)-1]$, L_i and Ω_i are smooth functions of μ and ω.

Theorem 11.5. *Let $L_1 \neq 0$ and $A \neq 0$. Then, for small μ the resonance zone corresponding to a rotation number M/N has the form of a wedge of width $\sim |\mu|^{(N-2)/2}$ tangent to the straight-line $\omega = \omega_0 + \mu\Omega_1/L_1$ at the point $(\mu = 0, \omega = \omega_0)$. If μ is sufficiently small, then the map inside the wedge has exactly two orbits of period N: one orbit is of the saddle type and the other orbit is stable if $L_1 < 0$, or unstable if $L_1 > 0$ (see Fig. 11.7.2(a), 11.7.3(a) for $N = 5$).*

Proof. Let us suppose, for definiteness, that the first Lyapunov value L_1 is negative. Then, the invariant curve exists when $\mu > 0$. The resonance zone adjoining at the point $(\mu = 0, \omega = \omega_0)$ corresponds to periodic orbits of period-N. To find these orbits let us derive the N-th iteration of the map (11.7.5)

$$\begin{aligned} \bar{R} &= (1+\mu)^N (R + \tilde{L}_1 R^3 + \cdots + \tilde{L}_P R^{2P+1} \\ &\quad + NAR^{N-1}\cos(N\varphi + \alpha)) + o(R^{N-1}), \\ \bar{\varphi} &= \varphi + N\omega + \tilde{\Omega}_1 R^2 + \cdots + \tilde{\Omega}_P R^{2P} \\ &\quad - NAR^{N-2}\sin(N\varphi + \alpha) + o(R^{N-2}), \end{aligned} \tag{11.7.6}$$

where $o(R^{N-1})$ and $o(R^{N-2})$ stand for terms which tend to zero faster than R^{N-1} and R^{N-2}, respectively, as $\mu \to 0$, $\omega \to \omega_0$ and $R \to 0$; and $\tilde{L}_i$ and $\tilde{\Omega}_i$ are

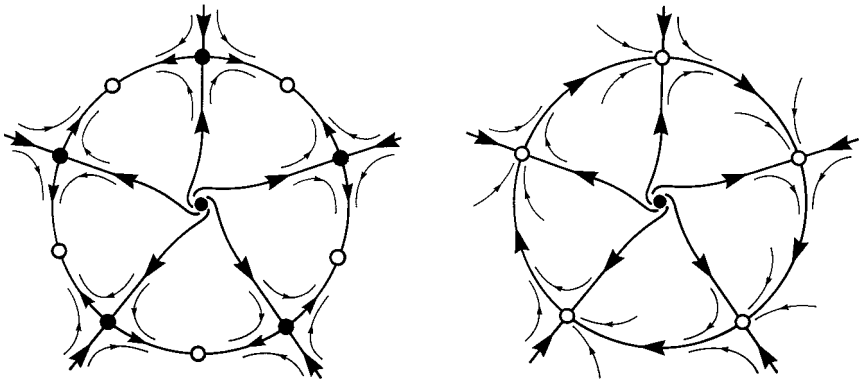

(a) (b)

Fig 11.7.2. An example of a stable resonant torus with five pairs of periodic orbits on it. The torus becomes non-resonant when the periodic orbits coalesce in pairs and disappear.

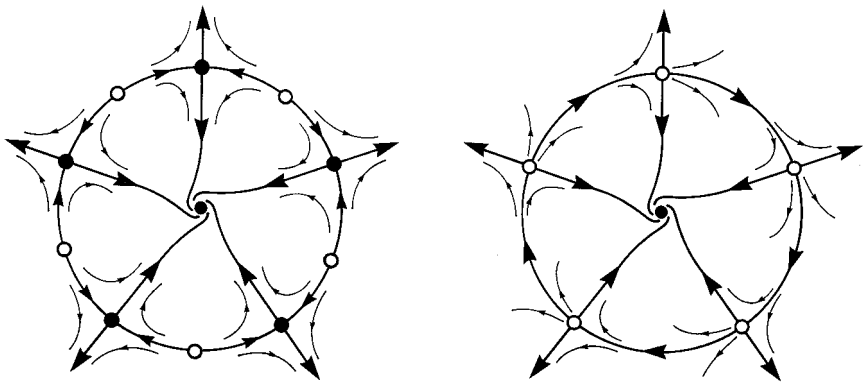

(a) (b)

Fig 11.7.3. An example of an unstable torus with five pairs of periodic orbits in a resonant zone (a) and on its boundary.

some functions of $\{L_1, \dots, L_i\}$ and $\{\Omega_1, \dots, \Omega_i\}$, respectively. In particular,

$$\tilde{\Omega}_1 = \Omega_1(1 + (1+\mu)^2 + \cdots + (1+\mu)^{2(N-1)}) = N\Omega_1(1 + O(\mu))\,,$$

$$\tilde{L}_1 = L_1(1 + (1+\mu)^2 + \cdots + (1+\mu)^{2(N-1)}) = NL_1(1 + O(\mu)) < 0\,.$$

The fixed points of the map (11.7.6) are found from the condition

$$\bar{R} = R\,, \tag{11.7.7}$$

$$\bar{\varphi} = \varphi \mod 2\pi\,. \tag{11.7.8}$$

From (11.7.6) we find the following equation defining the coordinates of the fixed points:

$$R = \Psi(\mu, \omega) + \frac{A}{2|L_1|}(\sqrt{\mu/|L_1|})^{N-3}\cos(N\varphi + \alpha) + o(\mu^{(N-3)/2})\,,$$

where $\Psi = \sqrt{\mu/|L_1|} + o(\sqrt{\mu})$ does not depend on φ. Substituting this expression into (11.7.8) we obtain

$$N\omega + \tilde{\Omega}_1\Psi^2 + \cdots + \tilde{\Omega}_P\Psi^{2P} = \frac{NA}{|L_1|}\left(\sqrt{\frac{\mu}{|L_1|}}\right)^{N-2}(\Omega_1\cos(N\varphi + \alpha) + L_1\sin(N\varphi + \alpha)) + o(\mu^{(N-2)/2}) \mod 2\pi\,.$$

Since ω is close to ω_0, it follows that $N\omega$ is close to $2\pi M$, and hence the last equation can be rewritten in the form

$$\delta = D\mu^{(N-2)/2}\sin(N\varphi+\gamma) + o(\mu^{(N-2)/2})\,, \tag{11.7.9}$$

where:

$$\begin{gathered} D = A\sqrt{L_1^2+\Omega_1^2}/|L_1|^{N/2}\,, \quad \gamma = \alpha+\pi-\arctan|\Omega_1/L_1|\,, \\ \delta = \omega - 2\pi M/N + (\tilde\Omega_1\Psi^2+\cdots+\tilde\Omega_p\Psi^{2P})/N = \omega-\omega_0+\mu\Omega_1/|L_1| + o(\mu)\,. \end{gathered} \tag{11.7.10}$$

Since $A\neq 0$, by assumption, the value D in (11.7.9) is non-zero. Under this assumption, the Eq. (11.7.10) is easily analyzed if μ is sufficiently small. Indeed, the right-hand side of the equation for small μ has exactly N maximums and N minimums in the interval $\varphi\in[0,2\pi]$. Hence this equation cannot have more than $2N$ roots. On the other hand, this equation defines the period-N orbits of the map (11.7.5): each such orbit gives exactly N roots of Eq. (11.7.9). It follows from here that the number of roots must be a multiple of N. Thus, either the equation has no roots at all (in this case the value δ is larger than the maximum or smaller than the minimum of the right-hand side) or the equation has $2N$ roots if δ is between the maximum and the minimum; or it has N roots if δ is equal to either the maximum, or the minimum (all maximal (minimal) values of the right-hand side are equal in this critical case).

By equaling δ to the maximum and then to the minimum of the right-hand side of (11.7.9) we find that the critical case is realized when (μ,ω) belongs to some curves K_1 and K_2 of the form

$$\delta = \pm D\mu^{(N-2)/2} + o(\mu^{(N-2)/2})\,. \tag{11.7.11}$$

It follows from (11.7.10) that both curves are tangent to the straight line $\omega=\omega_0-\mu\Omega_1/|L_1|$. They bound the wedge of width $\sim 2D\mu^{(N-2)/2}$.

The Eq. (11.7.9) has no solutions for parameter values outside of this wedge, but it has exactly $2N$ solutions inside:

$$N\varphi+\gamma = 2\pi n + \arcsin(\delta/D\mu^{(N-2)/2}) + \cdots \tag{11.7.12}$$

and

$$N\varphi+\gamma = 2\pi n + \pi - \arcsin(\delta/D\mu^{(N-2)/2}) + \cdots \tag{11.7.13}$$

(here $n = 0, \dots, N-1$). These solutions correspond to the fixed points of the map (11.7.6). Since the N fixed points of the map (11.7.6) correspond to an orbit of period N, it follows that the map inside the wedge has exactly two orbits of period N — one orbit defined by formula (11.7.12) and the second orbit defined by (11.7.13).

Differentiating (11.7.6) we obtain the multipliers of these orbits:

$$\rho_1 = 1 - 2\mu N + o(\mu) < 1\,,$$

$$\rho_2 = 1 - \frac{AN^2}{|L_1|}\left(\sqrt{\frac{\mu}{|L_1|}}\right)^{N-2}\sqrt{L_1^2+\Omega_1^2}\cos(N\varphi+\gamma) + o(\mu^{(N-2)/2})\,.$$

Observe that the trajectory (11.7.12) is stable, whereas the trajectory (11.7.13) is of saddle type.

We have obtained a complete correspondence to the statement of Theorem 11.7.1. The case $L_1 > 0$ can be carried out in the same way. End of the proof.

Note that both the saddles and nodes appearing inside the resonant wedge (called "Arnold tongue," sometimes) lie on the invariant curve (stable if $L_1 < 0$ or unstable if $L_1 > 0$). Since the only stable invariant curve that can go through a saddle is its unstable manifold, and since the only unstable curve that can also go through a saddle is its stable manifold, it follows that inside the resonance zone the invariant curve is the union of the separatrices of saddles (unstable separatrices if $L_1 < 0$, or stable separatrices if $L_1 > 0$) that terminate at the nodes.[7]

On the curves (11.7.11) which bound a resonant wedge, the saddle and the unstable periodic orbit coalesce. In this case the separatrix (attractive if $L_1 > 0$, or repelling if $L_1 < 0$) of each saddle-node tends to a neighboring saddle-node, and together they comprise the invariant curve shown in Figs. 11.7.2 and 11.7.3. Upon exiting from resonance all saddle-nodes disappear; the invariant curve is preserved but the rotation number is no longer equal to $2\pi M/N$.

Inside the resonant wedge all trajectories on the invariant torus tend to a stable periodic orbit, which means that the dominating regimes here is a periodic one. Outside the wedge either a quasiperiodic regime or a periodic one of a very long period is established on the torus. Both are "practically" indistinguishable. Therefore, a transition over the boundary of a resonant

[7] Observe that near each node point the invariant curve coincides with its leading manifolds. It follows that the invariant curve has a finite smoothness, generally speaking.

wedge may be interpreted as a transition from a synchronization regime to "beating" modulations. An explanation of this phenomenon was first given within the framework of the "averaging method" by Andronov and Vitt when they studied a closely related problem on detecting the synchronization region in the Van der Pol equation under an external force

$$\ddot{x} - \mu(1 - x^2)\dot{x} + \omega_0^2 x = \mu A \sin \omega t \,,$$

where $\mu \ll 1$ and $\omega_0 - \omega \sim \mu$ (see Sec. 12.1 for further details).

As μ increases within a resonant zone other periodic orbits with the same rotation number M/N may appear. In some cases, the boundary of the resonant zone can lose its smoothness at some points, like in the example shown in Fig. 11.7.4: here, the resonant zone consists of the union of two regions D_1 and D_2 corresponding to the existence of, respectively, one and two pairs of periodic orbits on the torus. The points C_1 and C_2 in Fig. 11.7.4 correspond to a cusp-bifurcation. At the point S corresponding to the existence of a pair of saddle-node periodic orbits the boundary of the resonant zone is non-smooth.

Theorem 11.7.1 prohibits the above behavior when μ is small. However, the value of overcriticality, beyond which the theorem is no longer valid, is different for different zones. Moreover, it may tend to zero as the denominator N of the rotation number increases (i.e. when the value of the rotation number approaches an irrational number).

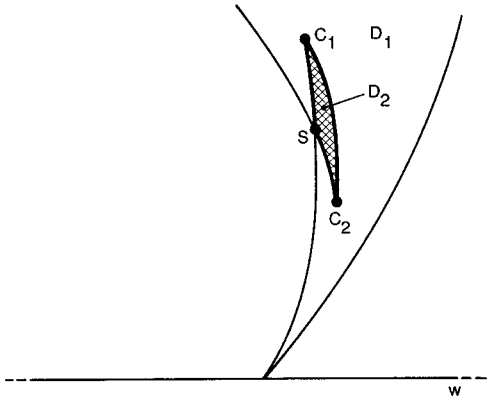

Fig. 11.7.4. Sketch of the local structure of stability regions of periodic orbits near the boundary of a resonant zone far beyond the critical threshold.

In fact, no common upper bound exists on the number of the periodic orbits which can be generated from a fixed point of a smooth map through the given bifurcation. If the smoothness r of the map is finite, the absence of this upper estimate is obvious because it follows from the proof of the last theorem that to estimate the number of the periodic orbits within the resonant zone $\nu = M/N$ the map must be brought to the normal form containing terms up to order $(N-1)$. In this case the smoothness of the map must not be less than $(N-1)$. Hence, we can estimate only a finite number of resonant zones if the smoothness is finite.

A similar result for maps of infinite smoothness is given by the following theorem.

Theorem 11.6. *Let a smooth annulus map have a smooth invariant curve and let the rotation number on the invariant curve be irrational. Then, by an arbitrarily small smooth perturbation, infinitely many periodic orbits may be born.*

Proof. Let us introduce on the annulus an angular variable φ and a radial variable R as coordinates. We can always choose the coordinates so that the invariant curve becomes the circle $R = 1$ so that the map takes the form

$$\begin{aligned} \bar{R} &= (1-R)F(R,\varphi)\,, \\ \bar{\varphi} &= \varphi + g(\varphi) + (1-R)G(R,\varphi) \mod 2\pi\,. \end{aligned} \tag{11.7.14}$$

Let us embed this map into the family

$$\begin{aligned} \bar{R} &= (1-R)F(R,\varphi)\,, \\ \bar{\varphi} &= \delta + \varphi + g(\varphi) + (1-R)G(R,\varphi) \mod 2\pi\,, \end{aligned} \tag{11.7.15}$$

where δ is a small parameter. Since the circle $R = 1$ remains invariant for all δ, the map on it has the form

$$\bar{\varphi} = \delta + \varphi + g(\varphi) \mod 2\pi\,. \tag{11.7.16}$$

Since the rotation number is irrational at $\delta = 0$ and since $\partial\bar{\varphi}/\partial\varphi > 0$, then (see Sec.4.4) the rotation number ν of the map (11.7.16) is, at $\delta = 0$, a strictly monotonic function of δ. This means that as δ varies the value $\nu(\delta)$ assumes all values close to $\nu(0)$.

Let us choose δ small enough such that the rotation number $\nu(\delta)$ is irrational and cannot be well approximated by "short" rational numbers. We will use the following result proven by Hermann [68]:

If the rotation number of the circle map is irrational and is not well approximated by rational numbers, then there exists a smooth transformation of variables which brings the map to a rotation with a constant angle:

$$\bar{\varphi} = \varphi + 2\pi\nu \mod 2\pi\,.$$

If we make such a transformation on the φ-variable of the map (11.7.15) (without affecting R), then the map in the new variables assumes the form

$$\begin{aligned} \bar{R} &= (1-R)\tilde{F}(R,\varphi)\,, \\ \bar{\varphi} &= 2\pi\nu + \varphi + (1-R)\tilde{G}(R,\varphi) \mod 2\pi\,. \end{aligned} \tag{11.7.17}$$

Hence, by a small perturbation of the original map (11.7.14) we can transform (in some new variables) the map of an invariant circle into a rotation with a constant angle. If we change a little bit the value ν in (11.7.17) so that it becomes a rational number $\nu = M/N$, then the map on the circle $R = 1$ assumes the form

$$\bar{\varphi} = \varphi + 2\pi M/N \mod 2\pi\,,$$

and the N-th iteration of this map is

$$\bar{\varphi} = \varphi + 2\pi M \mod 2\pi\,.$$

The latter is just the identity map, all points of which are fixed; i.e. we have infinitely many periodic orbits here. Recall that (11.7.17) is a small perturbation of the original map, so the theorem is proven.

Observe that if the N-th iteration of the circle map is an identity, then all points on the circle are structurally unstable with a multiplier equal to one. Moreover, all Lyapunov values of each point are equal to zero. This is an infinitely degenerate case. We saw in Sec. 11.3 that to investigate the bifurcations of structurally unstable periodic orbits with $k-1$ first zero Lyapunov values it is necessary to consider at least k-parameter families. It is now clear that to study bifurcations in this case one has to introduce infinitely many parameters. Moreover, it is seen from the proof of Theorem 11.5 that such maps can be obtained by applying a small perturbation to an arbitrary circle map

with an irrational rotation number. Hence, we can conclude that a complete finite-parameter description of bifurcations of periodic trajectories for maps close to a circle map with an irrational rotation number is unrealistic.

Consequently, the bifurcation of the birth of an invariant torus differs significantly from other bifurcations discussed in preceding sections. Here, an arbitrarily small modification of a finite-parameter family passing through a bifurcation point can always change the structure of the bifurcation set. Moreover, increasing the number of governing parameters will only make the bifurcations even more degenerate: in two-parameter families such degenerate points are cusps and "breaking" points on the boundaries of resonant zones (see Fig. 11.7.4). In three-parameter families they are swallowtails, etc.

Finally, we note an obvious analogy between the bifurcation of the birth of a cycle from an equilibrium state, and that of a two-dimensional invariant torus from a periodic orbit. We can go even further and imagine the next bifurcation of a three-dimensional torus from a two-dimensional one, a four-dimensional torus from a three-dimensional one and so on. In principle a dynamical system with a stable equilibrium state may evolve as follows: the equilibrium state loses its stability through a supercritical ($L_1 < 0$) Andronov–Hopf bifurcation as a parameter changes, so that a stable periodic orbit bifurcates from it, i.e. the stationary regime is replaced by a periodic one. Next, as the parameter varies further, the periodic orbit loses its stability again and a two-frequency regime (a quasiperiodic trajectory on a two-dimensional torus) appears, which, in turn, loses and transfer its stability to a three-frequency regime, and so on. Some time ago such a scenario of sequential evolution in the complexity of the dynamics (Landau–Hopf scenario) was proposed as a possible mechanism for the development of turbulence, where a well-developed turbulent process was interpreted as a quasiperiodic one with a gigantic set of independent frequencies. However, such a sequence of bifurcations is in fact far from being typical. This rarity can be explained by observation that an equilibrium state, or a periodic orbit, engaged in various bifurcation routes, always represents a "stand alone" single trajectory. This is no longer the case for an invariant torus. For example, within a resonant zone there are at least two periodic orbits on the torus, a saddle type and a stable orbit. Therefore, we must have some additional special conditions in order that they may simultaneously bifurcate to give birth to a three-dimensional torus.

In reality a similar bifurcation chain often ends at the two- (rarely three-) frequency regime, which as the parameter varies transforms into chaotic one

with a continuous frequency spectrum. In the phase space such an onset of chaos originates through the following stages [7]: the invariant curve of the Poincaré map first becomes non-smooth, and then gets "annihilated" (see Fig. 11.7.5 where the destruction of the invariant curve is accomplished with the appearance of homoclinic trajectories, i.e. with the intersections of the stable and unstable manifolds of the saddle periodic orbit). As soon as the invariant curve disappears its place in the phase space is filled out by a non-trivial set containing a countable number of periodic orbits with rotation numbers within some interval. In the parameter plane this occurs inside the regions where the resonant zones overlap with each other, as it is illustrated in Fig. 11.7.6. Note that in the non-resonant or weakly resonant cases, the overlapping of

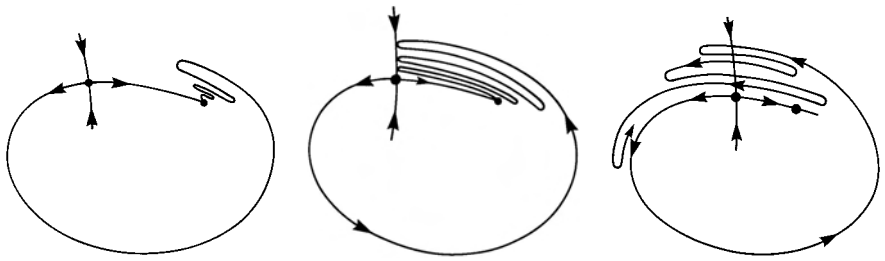

Fig. 11.7.5. The typical scenario of the breakdown of a two-dimensional torus due to a loss of its smoothness.

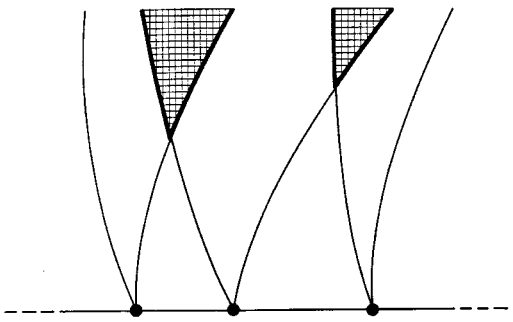

Fig. 11.7.6. As μ increases to finite values, the resonant zones in Fig. 11.7.1 may overlap.

resonant zones occurs at finite magnitudes of overcriticality, i.e. quite far away from the primary torus bifurcation. On the other hand, overlapping of the resonant zones may occur near the strong resonances $\omega_0 = 2\pi/3$ and $\omega_0 = \pi/2$ just after the bifurcation of the torus, i.e. resonant zones may start overlapping even for arbitrarily small μ.

Chapter 12

GLOBAL BIFURCATIONS AT THE DISAPPEARANCE OF SADDLE-NODE EQUILIBRIUM STATES AND PERIODIC ORBITS

We have already remarked that the problem concerning the loss of stability of periodic orbits in autonomous systems cannot always be reduced to a study of bifurcations of fixed points of the Poincaré map. It may happen that the periodic orbit does not exist on the stability boundary and, therefore, the Poincaré map is not defined at the critical parameter value.

To study such bifurcations one should understand the structure of the limit set into which the periodic orbit transforms when the stability boundary is approached. In particular, such a limit set may be a homoclinic loop to a saddle or to a saddle-node equilibrium state. In another bifurcation scenario (called the "blue sky catastrophe") the periodic orbit approaches a set composed of homoclinic orbits to a saddle-node periodic orbit. In this chapter we consider homoclinic bifurcations associated with the disappearance of the saddle-node equilibrium states and periodic orbits. Note that we do not restrict our attention to the problem on the stability boundaries of periodic orbits but consider also the creation of invariant two-dimensional tori and Klein bottles and discuss briefly their routes to chaos.

12.1. Bifurcations of a homoclinic loop to a saddle-node equilibrium state

Consider a one-parameter family of $\mathbb{C}^r$ $(r \geq 2)$ smooth dynamical systems in $\mathbb{R}^{n+1}$ $(n \geq 1)$. Suppose that when the parameter vanishes the system possesses a non-rough equilibrium state at the origin with one characteristic exponent equal to zero and the other n exponents lying to the left of the imaginary axis. We suppose also that the equilibrium state is a simple saddle-node, namely the first Lyapunov value l_2 is not zero (see Sec. 11.2). Without loss of generality we assume $l_2 > 0$.

We also assume that the family is transverse to the surface of the systems with a simple saddle-node. Therefore, near the origin such system is written as

$$\begin{aligned} \dot{x} &= \mu + l_2 x^2 + G(x, \mu)\,, \\ \dot{y} &= [A + h(x, y, \mu)]y \end{aligned} \tag{12.1.1}$$

(see Sec. 11.2, formulas (11.2.2) and (11.2.12)), where μ is a scalar parameter, $x \in \mathbb{R}^1$, $y \in \mathbb{R}^n$. Here, $G = o(x^2)$ is a function of class $\mathbb{C}^r$ with respect to x and of class $\mathbb{C}^{r-1}$ with respect to μ; h is a $\mathbb{C}^{r-1}$-smooth function vanishing at $(x = 0,\, y = 0,\, \mu = 0)$; the eigenvalues of the matrix A lie strictly to the left of the imaginary axes.

Recall from Sec. 11.2 that at $\mu = 0$, a neighborhood of the origin of system (12.1.1) is partitioned by the non-leading manifold W^{ss}, which is locally defined by the equation $x = 0$, into two regions — node and saddle. All trajectories in the node region converge to the point O as $t \to +\infty$. All trajectories, except one, in the saddle region leave a neighborhood of the origin as $t \to \pm\infty$. The single trajectory which enters O as $t \to -\infty$ is the unstable separatrix Γ. As t increases, Γ leaves a neighborhood of O as well.

Let us suppose that *as t increases further, the separatrix Γ returns to a neighborhood of the saddle-node O from the node region, as shown in* Fig. 12.1.1(b).

It follows from our assumption that Γ tends to O bi-asymptotically, i.e. as $t \to \pm\infty$. In other words, the trajectory Γ is *homoclinic* to O. The union $\Gamma \cup O$ is a closed curve which is called *a homoclinic loop* of the saddle-node.

We will show below that one can choose a small neighborhood V of the homoclinic loop so that for all small μ the forward trajectories of points in V remain in it forever. Moreover, at $\mu = 0$, all trajectories in V come into the

node region as t increases, and in the limit $t \to +\infty$, they converge to the saddle-node.

When $\mu < 0$, the saddle-node is decomposed into a saddle $O_1(x = x^+(\mu), y = 0)$ and a node $O_2(x = x^-(\mu), y = 0)$, where $x^\pm \sim \pm\sqrt{|\mu|/l_2}$ (see Sec. 11.2). The stable invariant manifold $W^s_{O_1}$ of the saddle is locally defined by the equation $x = x^+$. The unstable manifold $W^u_{O_1}$ is locally defined by the equation $y = 0$. The point O_1 divides the unstable manifold into two separatrices, one of which lies entirely in the neighborhood of the origin (it is the segment of the axis $y = 0$ which connects the points O_1 and O_2). The other separatrix comes out of the neighborhood. Due to continuous dependence on parameters, the separatrix follows along the loop Γ and returns to the origin from the side of the node O_2. It is clear that all trajectories in V, other than those in the stable manifold $W^s_{O_1}$ of the saddle O_1, converge to O_2, as shown in Fig. 12.1.1(a). The behavior of trajectories for $\mu > 0$ is described by the following theorem.

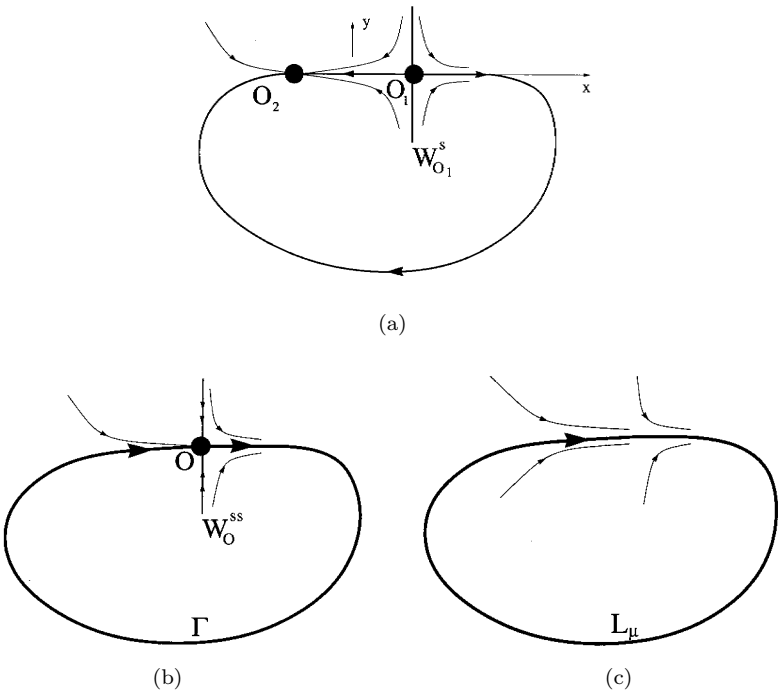

Fig 12.1.1. Bifurcation sequence of a saddle-node equilibrium with a homoclinic trajectory: (a) before, (b) at, and (c) after the bifurcation.

Theorem 12.1. *The disappearance of the saddle-node equilibrium with the homoclinic loop results in the appearance of a stable periodic orbit L_μ of period $\sim \pi/\sqrt{\mu l_2}$, which attracts all trajectories in V (see* Fig. 12.1.1(c)).

Proof. Let us construct two cross-sections (Fig. 12.1.2) transverse to the trajectories of the system:

$$S_0 : \; x = -d\,, \quad \|y\| \le d\,,$$

and

$$S_1 : \; x = d\,, \quad \|y\| \le d\,,$$

where d is chosen appropriately small, such that at $\mu = 0$, the separatrix Γ in its return to the point O intersects S_0 (this can always be achieved because Γ enters O tangentially to the axis $y = 0$).

Due to continuity, all trajectories starting on S_1 sufficiently close to the point $M_1(x = d,\, y = 0)$ at which Γ intersects S_1, come back to the neighborhood of the origin and hit S_0 near the point $M_0 = \Gamma \cap S_0$. Let us choose a small $\delta > 0$ and construct a tube V_1 composed of the segments of the trajectories which originate on S_1 at $|y| \le \delta$ and terminate on S_0. Consider a set V consisting of V_1 and of a frustum of cone V_0 bounded by the surfaces S_0, $S_1 \cap \{\|y\| \le \delta\}$ and $\{|x| \le d,\, \|y\| = d - (x + d)(d - \delta)/2d\}$, as shown in Fig. 12.1.3. We will assume that the y-coordinates are introduced

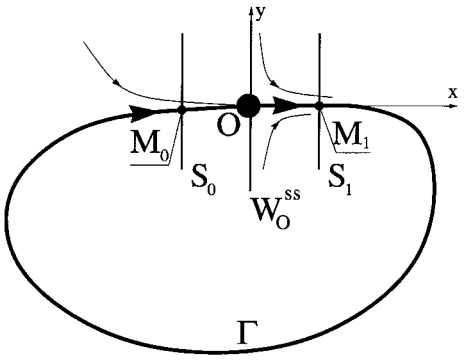

Fig. 12.1.2. Two cross-sections S_0 and S_1 to the homoclinic loop Γ are chosen near the saddle-node equilibrium O.

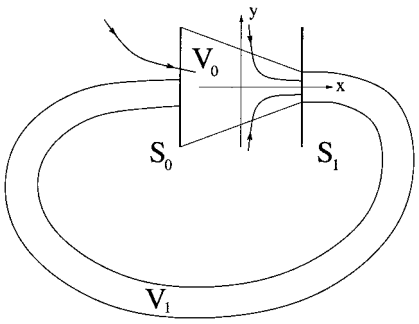

Fig. 12.1.3. Due to a strong contraction along W^{ss} (in the y-direction), for all small μ, the trajectories near a saddle-node leave the frustum of cone V_0 through the cross-section S_1. Therefore, the union of V_0 and the tube V_1 (composed of the whole segments of orbits starting on S_1) confines all forward semi-orbits starting nearby.

so that the matrix A in (12.1.1) is in the Jordan form and, moreover, the off-diagonal entries, if there are any, are sufficiently small. If d is small, then the function h in (12.1.1) is also sufficiently small elsewhere in V_0. Hence, the following estimate for the trajectories in V_0 is valid:

$$\frac{d}{dt}\|y(t)\| \le -\lambda\|y(t)\|\,, \tag{12.1.2}$$

where $0 < \lambda < \max|\mathrm{Re}\,\lambda_j|$, $\lambda_1, \ldots, \lambda_n$ are the eigenvalues of the matrix A (see Theorem 2.4). By using (12.1.2), one can show that if δ is small enough, then for all μ small, the vector field of system (12.1.1) everywhere on the boundary of V_0 is oriented either inward V_0 or inward V_1 (on S_1). Since V_1 consists of entire trajectories, the vector field of the system is everywhere tangent to the boundary of the set V_1. Thus, at each point on the boundary the vector field either touches the boundary tangentially, or is directed inward V. Hence all trajectories originating near V must enter V and never leave it.

The value $\dot{x}$ vanishes nowhere in V_0 for $\mu > 0$. Therefore, any trajectory which starts on S_0 will necessarily reach S_1 as time increases. It will then enter the tube V_1 and return to V_0. It follows that a map $T:\ S_0 \to S_0$ is defined for all small $\mu > 0$: this map is a superposition of two maps along the trajectories of the system: $T_0:\ S_0 \to S_1$ and $T_1:\ S_1 \to S_0$. We will call T_0 *the local* (*through*) *map* and T_1 *the global map*.

Let y_0 stand for the coordinates on S_0 and let y_1 stand for the coordinates on S_1. Obviously, the global map is well defined for all (not necessarily positive)

small μ. Since the flight time from S_1 to S_0 is bounded, the derivative of $T_1 y_1$ with respect to y_1 remains bounded for all small μ.

Let us show that the local map is contracting, and that the contraction becomes unboundedly strong, as $\mu \to 0$. Let $\{x(t;\mu),\ y(t;y_0,\mu)\}$ be the trajectory of system (12.1.1) passing through the point $(x = -d, y_0)$ on S_0 at $t = 0$. Note that since $\dot{x}$ in (12.1.1) does not depend on y, it follows that $x(t,\mu)$ does not depend on y_0 either. Therefore, the flight time t^* from S_0 to S_1 defined by the condition

$$x(t^*;\mu) = d \tag{12.1.3}$$

is a function of μ only. At $\mu = 0$, any trajectory starting on S_0 tends to the saddle-node, i.e. it remains in V_0 infinitely long. Hence, $t^*(\mu)$ tends to infinity as $\mu \to +0$.

To obtain a more precise estimate for t^* note that it follows from (12.1.1) and (12.1.3) that

$$t^* = \int_{-d}^{+d} \frac{dx}{\mu + l_2 x^2 + o(x^2)}$$

from which

$$t^*(\mu) = \pi/\sqrt{\mu l_2} + o(1/\sqrt{\mu})\,. \tag{12.1.4}$$

The map T_0 is defined by the formula

$$T_0 : \quad y \mapsto y(t^*(\mu); y_0, \mu)\,. \tag{12.1.5}$$

Let us show that

$$\left\| \frac{\partial y}{\partial y_0} \right\| \le e^{-\lambda t^*}\,. \tag{12.1.6}$$

Indeed, by differentiating (12.1.1) we find that

$$\frac{\partial \dot{y}(t)}{\partial y_0} = [A + h(x(y), y(t), \mu) + h'_y(x(t), y(t), \mu) y(t)] \frac{\partial y(t)}{\partial y_0}\,.$$

Since both h and $h'_y y$ are small everywhere in V_0 and since A is in the Jordan form with small off-diagonal entries, we have an estimate analogous to (12.1.2):

$$\frac{d}{dt} \left\| \frac{\partial y}{\partial y_0} \right\| \le -\lambda \left\| \frac{\partial y}{\partial y_0} \right\|\,.$$

By integrating the last inequality we find

$$\left\| \frac{\partial y}{\partial y_0} \right\| \le e^{-\lambda t} \left\| \frac{\partial y}{\partial y_0} \right\|_{t=0}\,,$$

or, since $(\partial y/\partial y_0)|_{t=0}$ is the identity matrix, we have

$$\left\| \frac{\partial y}{\partial y_0} \right\| \leq e^{-\lambda t} .$$

By substituting $t = t^*(\mu)$, we obtain the inequality (12.1.6) for the map (12.1.5). Because $t^* \to \infty$ as $\mu \to 0$, this inequality means that the map T_0 is strongly contracting if μ is small.

Since the contraction in the local map can be made arbitrarily strong and the derivative of the global map is bounded, the superposition $T = T_0 \circ T_1$ inherits the contraction of the local map for all small μ as well. It then follows from the Banach principle of contracting mappings (Sec. 3.15) that the map T has a unique stable fixed point on S_0. As this is a map defined along the trajectories of the system, it follows that the system has a stable periodic orbit in V which attracts all trajectories in V. The period of this orbit is the sum of two times: the "dwelling" time t^* of local transition from S_0 to S_1 and the flight time from S_1 to S_0. The latter is always finite for all small μ. It now follows from (12.1.4) that the period of the stable periodic orbit increases asymptotically of order $\sim \pi/\sqrt{\mu l_2}$. This completes the proof.

The proof of Theorem 12.1 is also applicable to the case of a degenerate saddle-node:[1] indeed nowhere in the proof have we invoked $l_2 \neq 0$. The only important property employed here is that while approaching the stability boundary the transition time from one cross-section to the other increases unboundedly, which follows from the fact that on the boundary itself all trajectories starting from S_0 converge to the saddle-node and, hence, must remain inside V_0 infinitely long. The bifurcation diagram for the degenerate saddle-node with a homoclinic loop is the same as it is for local bifurcations (for example, in the case where $l_4 \neq 0$, this is *a swallowtail*, as shown Fig. 11.2.14), where a stable periodic orbit appears in the region D_0.

The bifurcation of a limit cycle from the homoclinic loop to the saddle-node was first discovered by Andronov and Vitt in their study of the Van der Pol equation with a small periodic force at a $1:1$ resonance:

$$\ddot{x} - \mu(1 - x^2)\dot{x} + \omega_0^2 x = \mu A \sin \omega t \,, \tag{12.1.7}$$

where $\mu \ll 1$ and $|\omega_0 - \omega| \sim \mu$ (at $\mu = 0$, this equation describes a harmonic oscillator with the frequency ω_0; at zero frequency detuning, this is an exact

[1] The asymptotic relation for the period of the cycle will be different in this case as it includes the dependence on not one but many governing parameters.

1 : 1 resonance). In polar coordinates ($R\cos\varphi = \omega_0 x, R\sin\varphi = \dot{x}$) Eq. (12.1.7) assumes the form

$$\dot{R} = \mu \sin\varphi(A\sin\omega t - R(1 - R^2\cos^2\varphi/\omega_0^2)\sin\varphi)\,,$$
$$\dot{\varphi} = -\omega_0 + \mu\cos\varphi\left(\frac{A}{R}\sin\omega t - (1 - R^2\cos^2\varphi/\omega_0^2)\sin\varphi\right).$$

Let $\Phi = \varphi + \omega t$. Then by making a change of the time variable $t \to t/\mu$ we obtain

$$\begin{aligned}\dot{R} &= \frac{A}{2}\cos(\Phi - 2\omega t/\mu) - \frac{A}{2}\cos\Phi \\ &\quad - R\left(1 - \frac{R^2}{\omega_0^2}\cos^2(\Phi - \omega t/\mu)\right)\sin^2(\Phi - \omega t/\mu)\,, \\ \dot{\Phi} &= -\delta + \frac{A}{2R}\sin\Phi - \frac{A}{2R}\sin(\Phi - 2\omega t/\mu) \\ &\quad - \left(1 - \frac{R^2}{w_0^2}\cos^2(\Phi - \omega t/\mu)\right)\sin(\Phi - \omega t/\mu)\cos(\Phi - \omega t/\mu)\,,\end{aligned} \tag{12.1.8}$$

where $\delta = (\omega_0 - \omega)/\mu$ is the frequency detuning normalized by the small parameter.

Andronov and Vitt analyzed the averaged system

$$\dot{R} = -\frac{A}{2}\cos\Phi - \frac{R}{2}\left(1 - \frac{R^2}{4\omega_0^2}\right),$$
$$\dot{\Phi} = -\delta + \frac{A}{2R}\sin\Phi\,, \tag{12.1.9}$$

which is obtained from (12.1.8) by replacing the fast (with frequency $\geq \omega/\mu$) oscillatory terms by their averaged magnitudes. When $A = 0$, this system is easily analyzed: it has a repelling equilibrium state at the origin, and all trajectories tend to the stable limit cycle $R = 2\omega_0$; at $\delta = 0$, the limit cycle degenerates into a single invariant circle filled densely by equilibrium states. For small $A > 0$, the repelling equilibrium state persists, whereas only two points among all others on the circle survive: they are a saddle and a node, both existing in the region $D:\ 4|\delta|\omega_0 < A$. By expanding in a series of powers of A, one can show that for small A, the system still has an invariant curve surrounding the origin — outside the resonant zone D, the invariant curve is the limit cycle; inside D it consists of a connection of the separatrices of the

saddle which go to the stable node. On the boundary of the zone D, the system possesses a saddle-node with a separatrix loop.

In terms of the original variable $\varphi = \Phi - \omega t$, the stationary value of Φ (the equilibrium state of system (12.1.9)) corresponds to an oscillatory regime with the same frequency as that of the external force. The periodic oscillations of Φ (the limit cycle in (12.1.9)) correspond to a two-frequency regime. Hence, the above bifurcation scenario of a limit cycle from a homoclinic loop to a saddle-node characterizes the corresponding route from synchronization to beat modulations in Eq. (12.1.7).

The generalization of this bifurcation for second-order systems was studied by Andronov and Leontovich. Their proof uses essentially the features of systems on a plane. Our proof of Theorem 12.1 is close to that suggested by L. Shilnikov in [130] for the high-dimensional case with the difference that we have simplified calculations by reducing the system near the origin to the form (12.1.1).

We remark that Theorem 12.1 remains valid also in the case where the separatrix enters an edge of the node region, i.e. $\Gamma \subset W^{ss}$. However, a complete bifurcation analysis in this case requires an additional governing parameter. It is introduced in the following way. Let us build a cross-section S_0 to the on-edge homoclinic loop Γ, i.e. we define $S_0 = \{\|y\| = d, |x| \le d/2\}$, as depicted in Fig. 12.1.4. At the bifurcation point, the separatrix Γ intersects S_0 at some

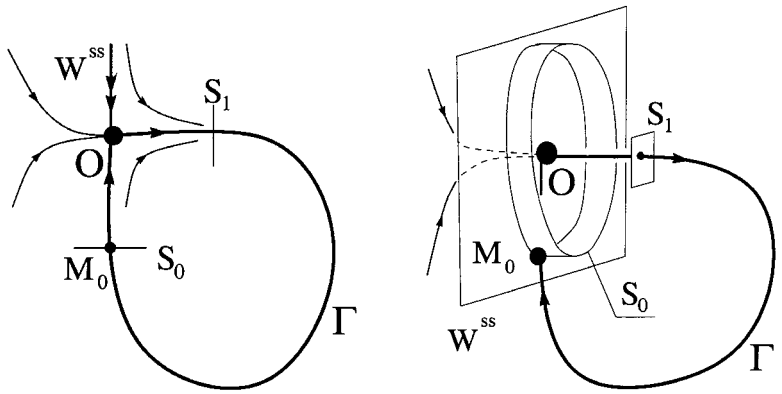

(a) (b)

Fig 12.1.4. The choice of cross-sections to the nontransverse homoclinic loop Γ in the two-dimensional (a) and multi-dimensional (b) cases.

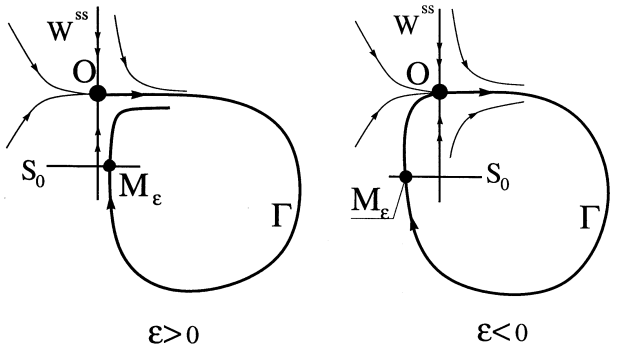

Fig. 12.1.5. Behavior of the unstable separatrix before ($\varepsilon < 0$) and after ($\varepsilon > 0$) on-edge bifurcation.

point $M_0 \in W^{ss}$. Thus, for any nearby system, the global map T_1 is defined by trajectories which start from $S_1 : \{x = d, \|y\| \le \delta\}$ and intersect S_0 near M_0. Let ε be the x-coordinate of the point $M_\varepsilon = T_1(y_1 = 0)$ on the cross-section S_0. We will treat ε as an additional bifurcation parameter. It is obvious that at $\mu = 0$, when the saddle-node still exists, the point M_ε is the intersection of the separatrix Γ with S_0. Thus, $\varepsilon = 0$ corresponds to the on-edge homoclinic loop; at $\varepsilon < 0$, the separatrix enters the node region and a generic homoclinic loop persists, as illustrated in Fig. 12.1.5.

As before, the parameter μ governs the local bifurcations of the saddle-node O: at $\mu > 0$, it disappears whereas it disintegrates into the saddle $O_1(\mu, \varepsilon)$ and the node $O_2(\mu, \varepsilon)$ at $\mu < 0$.

As in Theorem 12.2, it is easy to construct a small neighborhood V of the on-edge homoclinic loop $\Gamma \cup O$ such that for all small μ and ε, the forward trajectory of any point in V stays there forever.

Theorem 12.2. (Lukyanov [88]) *On the (ε, μ)-plane, in the region $\mu < 0$, there is a curve $\varepsilon = h_{hom}(\mu) \sim \sqrt{|\mu|/l_2}$ which corresponds to the existence of a homoclinic loop to the saddle O_1. In the region $\{\mu > 0\} \cup \{\varepsilon > h_{hom}(\mu)\}$, the system has a unique stable periodic orbit L. As $t \to +\infty$, the trajectories in V which do not tend to the equilibrium points tend to L (see the bifurcation diagram in Fig.* 12.1.6).

Proof. As in Theorem 12.2, the problem can be reduced to a study of the map $T = T_1 \circ T_0$ where $T_1 : S_1 \to S_0$ is the global map and T_0 is the local map. The map T_0 is defined at all points of S_0 for $\mu > 0$; it is easy to see that

for $\mu \le 0$, the local map is defined at $x > x^+(\mu, \varepsilon)$ (trajectories starting from $x = x^+$ lie in the stable manifold of O_1 and those starting from $x < x^+$ tend to O_2; recall that $x^+(\mu, \varepsilon)$ is the coordinate of the saddle O_1).

Let us prove that the map T_0 is strongly contracting. Indeed, represent the system (12.1.1) in the form

$$\frac{dy}{dx} = \frac{A + h(x, y, \mu, \varepsilon)}{g(x, \mu, \varepsilon)}\, y \tag{12.1.10}$$

where we denote

$$\dot{x} = g(x, \mu, \varepsilon)\,. \tag{12.1.11}$$

Obviously, $g > 0$ at $\mu > 0$ or at $x > x^+$, therefore (12.1.10) is well defined in the region we are interested in. Let $y(x; x_0, y_0, \mu, \varepsilon)$ be the trajectory of (12.1.10) which starts with $y = y_0$ at $x = x_0$. We must prove that $\frac{\partial y}{\partial(x_0, y_0)}$ is small at $x = d$ provided μ and x_0 both are small.

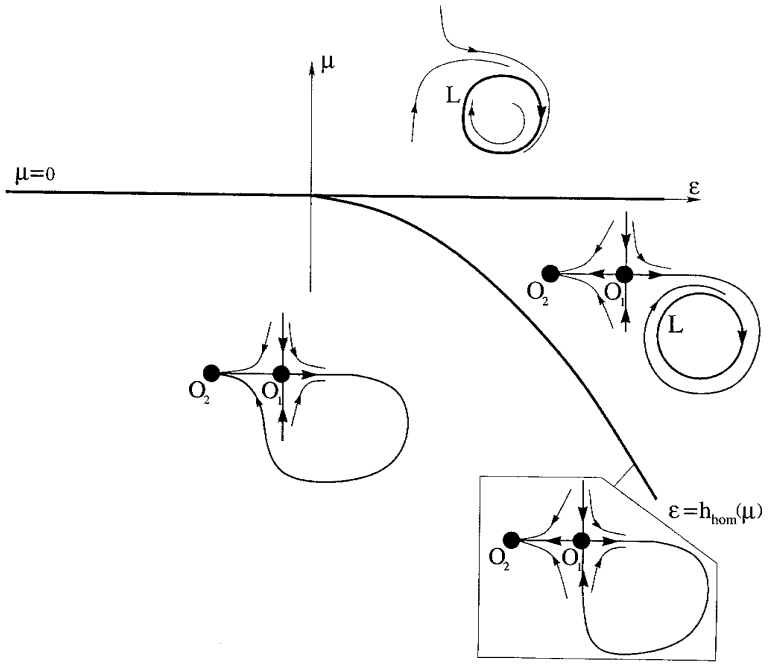

Fig. 12.1.6. Bifurcation diagram for the on-edge homoclinic loop to a saddle-node equilibrium.

Denote $u = \frac{\partial y}{\partial(x_0,y_0)}$. By differentiation of (12.1.10), we have

$$\frac{du}{dx} = \frac{A + h + h'_y y}{g}\, u\,,$$

or

$$\frac{d}{dx}\|u\| \le -\frac{\lambda}{g}\,\|u\|$$

(we use the fact that the spectrum of A lies to the left of the imaginary axis and that h and y are small). Finally,

$$\|u\| \le e^{-\lambda \int_{x_0}^{x} \frac{ds}{g(s,\mu,\varepsilon)}} = e^{-\lambda t^*(x_0,x;\mu,\varepsilon)}$$

where t^* is the flight time in (12.1.11) from x_0 to x. For fixed $x = d$, this time obviously goes to infinity as $\mu \to 0$, $x_0 \to 0$. Thus, $\frac{\partial y}{\partial(x_0,y_0)} \to 0$. This means that T_0 is strongly contracting indeed.

As before, since the map T_0 is strongly contracting, the map $T = T_1 \circ T_0$ is also strongly contracting. When $\mu > 0$, the map T is defined everywhere on S_0. Hence, it follows from the contraction mapping principle that the map T has a unique stable fixed point. The fixed point of the map T corresponds to a periodic orbit of the system, which gives the theorem for the case $\mu > 0$. When $\mu \le 0$, the domain of definition of T is bounded by the surface $\Sigma : \{x = x^+\}$, i.e. by the stable manifold of the saddle point O_1 (the strong stable manifold of the saddle-node O at $\mu = 0$). When a point $M \in S_0$ approaches Σ from the side $x > x^+$, the image TM tends to the point M_ε (the point of intersection of the separatrix of O_1 with S_0). Thus, by continuity, we may assume that the image of the surface Σ by the map T is the single point M_ε.

This situation is completely analogous to that we have in the study of a homoclinic loop to a saddle, which is considered in detail in Sec. 13.4. There (Lemma 13.4.1) we prove that the contracting map of the kind under consideration has a stable fixed point if and only if the single point of the image of the boundary of the domain of definition lies inside the domain. Thus, our system has a stable periodic orbit if and only if the point M_ε lies in the region $x > x^+$.

We have found that the region of existence of the stable periodic orbit is given by the condition $\varepsilon > x^+(\mu,\varepsilon)$, which can obviously be rewritten in the form $\varepsilon > h_{hom}(\mu)$ where the smooth function h_{hom} behaves asymptotically as $\sqrt{|\mu|/l_2}$. The boundary of the region corresponds to the point M_ε on Σ, i.e. to a homoclinic loop of O_1. End of the proof.

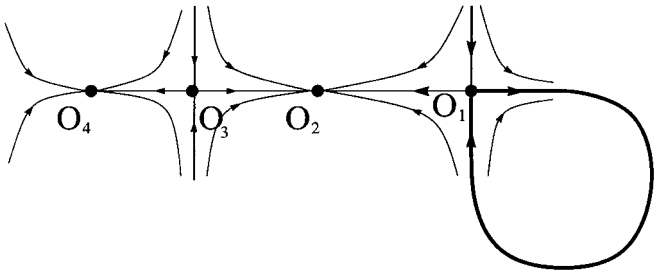

Fig. 12.1.7. The boundary of the stability region of the periodic orbit born at the bifurcation of the on-edge homoclinic loop to a degenerate saddle-node corresponds to the homoclinic loop of the "border" saddle equilibrium state O_1.

Remark. This statement remains valid (with obvious modifications) also in the case of the on-edge homoclinic loop to a degenerate saddle-node. In this case, μ is a vector of parameters (of dimension equal to the number of zero Lyapunov values plus one), and an additional bifurcation parameter ε is introduced as before. A stable periodic orbit exists when the saddle-node disappears (the region $\mu \in D_0$ in our notations), or when $\varepsilon > h_{hom}(\mu)$ at $\mu \notin D_0$. Here, the surface $\varepsilon = h_{hom}(\mu)$ corresponds to the homoclinic loop of the "border" saddle equilibrium O_1, as illustrated in Fig. 12.1.7.

12.2. Creation of an invariant torus

Let us consider a one-parameter family of n-dimensional $\mathbb{C}^r$-smooth ($r \geq 2$) systems having a saddle-node periodic orbit L at $\mu = 0$. We assume that μ is the governing parameter for local bifurcations. Thus (recall Fig. 11.3.7), for $\mu < 0$, there exist stable and saddle periodic orbits which collapse into one orbit L at $\mu = 0$. The local unstable set $W^u_{L,\mathrm{loc}}$ is homeomorphic to a half-cylinder $\mathbb{R}^+ \times \mathbb{S}^1$. The orbit L also has a strong-stable manifold W^{ss}_L which divides a neighborhood of L into a saddle region and a node region. When $\mu > 0$, the saddle-node disappears and all orbits leave its small neighborhood. Note that the time necessary to pass through the neighborhood tends to infinity as $\mu \to +0$.

Our standing assumption is that at $\mu = 0$, *all trajectories in* W^u_L *return to the node region*[2], *and tend to* L *as* $t \to +\infty$.

[2]In particular, $W^u_L \cap W^{ss}_L = \emptyset$.

Thus, W^u_L is a compact set (it contains L by definition). Let U be a small neighborhood of W^u_L. It is obvious that at $\mu = 0$, all trajectories in U tend to L as $t \to +\infty$. When $\mu < 0$, the trajectories in U tend to one of the stable periodic orbits appearing as L disintegrates. The problem we are interested in is what happens in U when $\mu > 0$?

As already mentioned, problems of this nature had appeared as early as in the twenties in connection with the phenomenon of transition from synchronization to an amplitude modulation regime. A rigorous study of this bifurcation was initiated in [3], under the assumption that the dynamical system with the saddle-node is either non-autonomous and periodically depending on time, or autonomous but possessing a global cross-section (at least in that part of the phase space which is under consideration). Thus, the problem was reduced to the study of a one-parameter family of $\mathbb{C}^r$-diffeomorphisms ($r \geq 2$) on the cross-section, which has a saddle-node fixed point O at $\mu = 0$ such that all orbits of the unstable set of the saddle-node come back to it as the number of iterations tends to $+\infty$ (see Fig. 12.2.1(a) and (b)).

Recall that a saddle-node fixed point or periodic orbit has one multiplier equal to $+1$ and the rest of the multipliers lies inside the unit circle. The diffeomorphism (the Poincaré map) near the fixed point may be represented

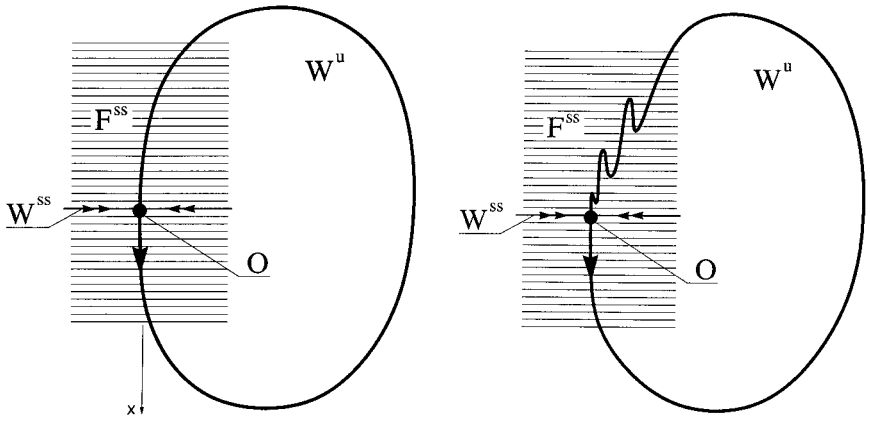

(a) (b)

Fig 12.2.1. The unstable manifold W^u of the saddle-node fixed point may be a smooth curve (a) or a non-smooth curve (b). In the latter case the tangent vector oscillates without a limit when a point on W^u reaches O from the side of node region.

in the standard form:

$$\begin{aligned} \bar{y} &= [A + h(x, y, \mu)]y\,, \\ \bar{x} &= x + g(x, \mu)\,, \end{aligned} \tag{12.2.1}$$

where $x \in \mathbb{R}^1$, $y \in \mathbb{R}^{n-2}$, A is a matrix whose eigenvalues lie strictly inside the unit circle, and

$$h(0,0,0) = 0\,, \quad g(0,0) = 0\,, \quad g'_x(0,\mu) = 0\,.$$

Here, the center manifold W^C is defined by the equation $y = 0$. The surfaces $\{x = \text{constant}\}$ are the leaves of the strong-stable invariant foliation $\mathcal{F}^{ss}$. In particular, $x = 0$ is the equation of the strong-stable manifold of O. At $\mu = 0$, the function g (nonlinear part of the map on W^C) has a strict extremum at $x = 0$. For more definiteness, we assume that it is a minimum, i.e. $g(x, 0) > 0$ when $x \neq 0$. Thus, the saddle region on the cross-section corresponds to $x > 0$, and the node region corresponds to $x < 0$. Since the saddle-node disappears when $\mu > 0$, it follows that $g(x, \mu) > 0$ for all sufficiently small x and for all small positive μ.

The saddle-node is *simple* if $g''_{xx}(0,0) \neq 0$. In this case the second equation of (12.2.1) may be written in the form

$$\bar{x} = x + \mu + l_2 x^2 + \cdots\,, \tag{12.2.2}$$

where $l_2 = g''(0)/2 \neq 0 > 0$.

By assumption, the global unstable manifold W^u_O returns to the node region, i.e. it forms a closed invariant curve. This curve is smooth everywhere, except possibly at the point O. Indeed, since the rate of contraction along the x-direction in the node region is less than exponential, it is much weaker than the contraction in the y-direction. Therefore, any piece of a curve transverse to the strong-stable foliation, when iterated forward, becomes tangent to $y = 0$ as it approaches the point O. At the same time, if the invariant curve is tangent to a leaf of the strong-stable foliation at some point, it will be tangent to the foliation at all forward iterations of this point (because the foliation is invariant). Therefore, arbitrarily close to O, the invariant curve will have points where the angle between the tangent to the curve and $\{y = 0\}$ remains bounded away from zero.

Thus,

the global unstable manifold W^u is smooth everywhere (including O) if it is transverse to the strong-stable foliation in the node region, as depicted in

Fig. 12.2.1(a), *and it is non-smooth at O if it is tangent to the strong-stable foliation at the points of some orbit, as depicted in Fig.* 12.2.1(b).

The smooth case corresponds, in particular, to a small time-periodic perturbations of an autonomous system possessing a homoclinic loop to a saddle-node equilibrium (see the previous section). Indeed, for a constant time shift map along the orbits of the autonomous system the equilibrium point becomes a saddle-node fixed point and the homoclinic loop becomes a smooth closed invariant curve, but the transversality of W^u to $F^{ss}_{\rm loc}$ is, obviously, preserved under small smooth perturbations.

The non-smooth case appears, for example, when W^u_O touches the strong-stable manifold W^{ss}_O, as shown in Fig. 12.2.2. The latter, in turn, may be detected via a small time-periodic perturbation of a system with an on-edge homoclinic loop to a saddle-node (see the previous section). Generically, the non-transversality of W^u with respect to $\mathcal{F}^{ss}_{\rm loc}$ is also preserved under small smooth perturbations (say, if the tangency between W^u and the corresponding leaf of $\mathcal{F}^{ss}_{\rm loc}$ is quadratic).

The closed invariant curve W^u_O for the Poincaré map on the cross-section is the loci of intersection of an invariant two-dimensional torus W^u_L with the cross-section. The torus is smooth if the invariant curve is smooth, and it is non-smooth otherwise. If the original non-autonomous system does *not* have a global cross-section, then other configurations of W^u_L are also possible, as

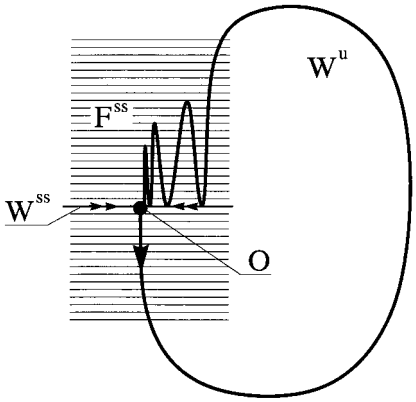

Fig. 12.2.2. A nontransverse tangency of the unstable and strong-stable manifolds of a saddle-node fixed point may be obtained by a small time-periodic perturbation of the system with an on-edge homoclinic loop to a saddle-node equilibrium state, as shown in Fig. 12.1.4.

we will discuss below. For example, it may be a Klein bottle, smooth or non-smooth as well [6].

Theorem 12.3. (Afraimovich–Shilnikov [3, 6]) *If the global unstable set of the saddle-node L is a smooth compact manifold (a torus or a Klein bottle) at $\mu = 0$, then a smooth closed attractive invariant manifold $\mathcal{T}_\mu$ (a torus or a Klein bottle, respectively) exists for all small μ.*

The invariant manifold depends continuously on μ. At $\mu = 0$, it coincides with W^u_L. When $\mu < 0$, it is the union of the unstable manifold of the saddle periodic orbit $L^-(\mu)$ with the stable periodic orbit $L^+(\mu)$ (where $L^\pm(\mu)$ are the periodic orbits into which the saddle-node bifurcates[3]). In the case of torus, for $\mu > 0$, the Poincaré rotation number on $\mathcal{T}_\mu$ tends to zero as $\mu \to +0$. Thus, on the μ-axis there are infinitely many (practically indistinguishable as $\mu \to +0$) resonant zones which correspond to periodic orbits on $\mathcal{T}_\mu$ with rational rotation numbers, as well as an infinite set (typically, a Cantor set) of irrational values of μ for which the motion on $\mathcal{T}_\mu$ is quasiperiodic.

Before we proceed to the proof of Theorem 12.3, let us study the global structure of the W^u_L in more detail. Introduce normal coordinates (see Sec. 3.10) in a small neighborhood of L, such that near L, the system takes the form

$$\dot y = \mathcal{A}(\mu)y + H(x, y, \varphi; \mu)\,, \tag{12.2.3}$$

$$\dot x = G(x, y, \varphi; \mu)\,, \quad \dot\varphi = 1\,, \tag{12.2.4}$$

where H and G vanish at $(y = 0, x = 0, \mu = 0)$ along with their first derivatives with respect to (x, y); the eigenvalues of the matrix $\mathcal{A}$ lie strictly to the left of the imaginary axis. Here $\varphi \in [0, 1]$ is the angular variable, the surfaces $\varphi = 0$ and $\varphi = 1$ are assumed to be glued by some involution, namely, by changing the sign of a number of components of the vector y (an appropriate choice of this involution allows one to make the linear part of the system independent of φ, without loss of smoothness; see details in Sec. 3.11).

We also assume that the center manifold W^C is locally straightened so that it has the form $\{y = 0\}$. Correspondingly,

$$H\,|_{y=0} \equiv 0\,. \tag{12.2.5}$$

[3]If the saddle-node is not simple, then there may be more saddle and stable periodic orbits when $\mu < 0$; in this case $\mathcal{T}_\mu$ is the union of all of them and all their unstable manifolds.

Next, let us straighten the strong stable invariant foliation. The leaves of the foliation are given by $\{x = Q(y; \varphi, x', \mu),\ \varphi = \text{constant}\}$ where x' is the coordinate of intersection of a leaf with the center manifold; Q is a $\mathbb{C}^{r-1}$-function (it is $\mathbb{C}^r$-smooth with respect to y). The straightening is achieved via a coordinate transformation $x \mapsto x'$ which brings the invariant foliation to the form $\{x = \text{constant}, \varphi = \text{constant}\}$. Thus, Eq. (12.2.4) becomes independent of y and the system can be recast as follows:

$$\dot{y} = \mathcal{A}(\mu)y + H(x, y, \varphi; \mu)\,, \tag{12.2.6}$$

$$\dot{x} = G(x, \varphi; \mu)\,, \quad \dot{\varphi} = 1\,. \tag{12.2.7}$$

By construction, the new function G which coincides with the original one at $\{y = 0\}$ is still a $\mathbb{C}^r$-function.

In the new coordinates, the strong-stable invariant manifold W^{ss}_L is the surface $\{x = 0\}$; the node region U_- now corresponds to small negative x and the saddle region U_+ corresponds to small positive x.

Already we have stated that the invariant foliation is $\mathbb{C}^{r-1}$-smooth; moreover, it can be shown for the case of the saddle-node that the foliation is, in fact, $\mathbb{C}^r$-smooth everywhere except on W^{ss}_L at $\mu = 0$ [140]. The coordinate transformation that reduces (12.2.4) to (12.2.7) has the same smoothness.

Choose small positive d^+ and d^-. Consider two cross-sections (both are $(n-1)$-dimensional solid tori) $S_0 : \{x = -d^-\}$ and $S_1 : \{x = d^+\}$ to the flow. By assumption, at $\mu = 0$ (and, hence, at all small μ), a trajectory of W^u_L returns to the node region $U_- = \{x < 0\}$ in a finite time. Therefore, the flow defines a diffeomorphism T_1 (*the global map*) by which a small neighborhood of the intersection line $l^- : \{y = 0\} = W^u_L \cap S_1$ is mapped into S_0. This map has the form

$$\begin{aligned} y_0 &= p(\varphi_1, y_1; \mu)\,, \\ \varphi_0 &= q(\varphi_1, y_1; \mu) \mod 1\,, \end{aligned} \tag{12.2.8}$$

where the coordinates on S_0 and S_1 are denoted by (φ_0, y_0) and (φ_1, y_1) respectively; the two $\mathbb{C}^r$-smooth functions p and q (mod 1) are both period 1 in φ.

The closed curve

$$l^+ = T_1 l^- : \{y_0 = p(\varphi_1, 0; 0)\,, \quad \varphi_0 = q(\varphi_1, 0; 0) \mod 1\}$$

is the intersection of W^u_L and S_0. Note that the function q can be written in the form:

$$q(\varphi, y; \mu) = m\varphi + q_0(\varphi, y; \mu)\,, \tag{12.2.9}$$

where q_0 is periodic in φ. The integer m defines the homotopy class of l^+ in S_0 (the sign of m determines the orientation of l^+ with respect to l^-). If the dimension n of the phase space is greater than three, then S_0 is at least three-dimensional and the integer m may be of arbitrary value. In $\mathbb{R}^3$, the cross-section S_0 is a two-dimensional annulus. Since l^+ cannot have self-intersections, it follows that it is possible to have $m = 1$ and $m = 0$ only in this case (if $m = -1$, then W^u_L is a Klein bottle, so this case cannot occur in $\mathbb{R}^3$).

Note that the structure of the set W^u_L is completely determined by the way W^u_L adjoins to L from the side of the node region. Since the intersection $l^+ = W^u_L \cap S_0$ is an $|m|$-winding curve in S_0, the intersection of $W^u_L \cap U_-$ with any cross-section of the kind $\{\varphi = \text{constant}\}$ consists, at $m \neq 0$, of $|m|$ pieces glued at the point $\{x = 0, y = 0\} = L_0 \cap \{\varphi = \text{constant}\}$, as depicted in Fig. 12.2.3. At $m = 0$, this intersection is a sequence of circles accumulating at $\{x = 0, y = 0\}$, see Fig. 12.4.1. Thus, samples of W^u_L corresponding to different values of m are mutually non-homeomorphic to each other. Moreover, at $|m| \neq 1$, for

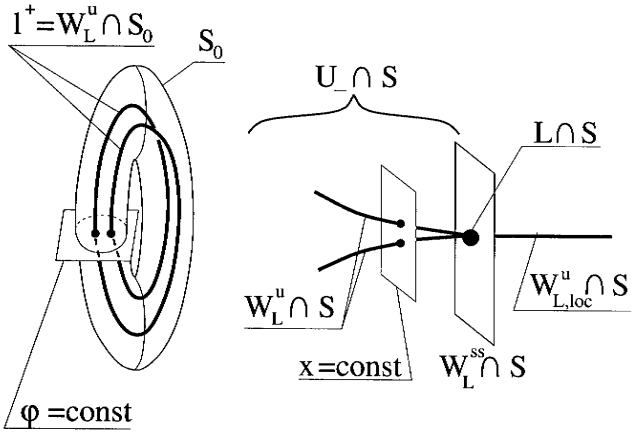

Fig. 12.2.3. The structure of intersection of the unstable manifold W^u_L of a saddle-node periodic orbit L with a solid-torus-like cross-section S_0 in the case $m = 2$. A trace of the intersection is a doubly-twisted curve l^+. Consequently, it has at least two intersections with each level $\varphi = \text{constant}$ in S_0, and with each level $x = \text{constant}$ in the cross-section $S : \{\varphi = 0\}$.

any point of L, its small neighborhood in W^u_L is not homeomorphic to a disk, i.e. W^u_L is not a manifold in this case.

We will study the case $m = 0$ in Sec. 12.4 in connection with the problem of the "blue sky catastrophe". In the case $|m| \geq 2$, infinitely many saddle periodic orbits are born (see Theorem 12.5) when the saddle-node disappears; moreover, even hyperbolic attractors may arise here (see [139]). We do not discuss such kind of bifurcations in this book.

If $m = \pm 1$, then W^u_L is a manifold. It is homeomorphic to a torus if $m = 1$ and to a Klein bottle if $m = -1$. As already mentioned, this manifold may be smooth or non-smooth, depending on whether W^u_L intersects the strong-stable foliation F^{ss} transversely everywhere or not. When $\dot{x}$ and $\dot{\varphi}$ are independent of y (see (12.2.7)), the leaves of $\mathcal{F}^{ss}$ on the cross-section S_0 are the (hyper)planes $\varphi_0 = \text{constant}$. The intersection $l^+ = W^u_L \cap S_0$ is represented as $\{y_0 = p(\varphi_1, 0, 0), \varphi_0 = q(\varphi_1, 0, 0)\}$ where (p, q) is the right-hand side of the global map $T_1 : S_1 \to S_0$ (see (12.2.8)). Thus, the transversality of W^u_L to $\mathcal{F}^{ss}$ holds if, and only if,

$$\left.\frac{\partial q}{\partial \varphi}\right|_{y=0,\mu=0} \neq 0\,. \tag{12.2.10}$$

This inequality, along with the requirement $|m| = 1$, is the analytical form of the condition of Theorem 12.3.

The proof of this theorem is based on the reduction of the problem to a study of some map ("the essential map" below) of a circle. In fact, this reduction works independently of the value of m or of the smoothness of W^u_L, and our two next sections are based on it.

As explained in Sec. 12.5, we may assume that in (12.2.7)

$$\left.\frac{\partial G}{\partial \varphi}\right|_{\mu=0} \equiv 0\,. \tag{12.2.11}$$

In other words, at $\mu = 0$, the right-hand side of Eq. (12.2.7) can be made independent on φ (by an appropriate change of variables), so it assumes the following autonomous form

$$\begin{aligned} \dot{x} &= \tilde{g}(x)\,, \\ \dot{\varphi} &= 1\,, \end{aligned} \tag{12.2.12}$$

where $\tilde{g}(0) = 0$, $\tilde{g}'(0) = 0$. If $x \neq 0$, then $\tilde{g}(x) > 0$. Note that the function $\tilde{g}(x)$ is *uniquely defined* by the nonlinear part $g(x, 0)$ of the Poincaré map on the center manifold [see (12.2.1)]. It is shown in [140] that the transformation

which brings the system (12.2.7) to the autonomous form (12.2.12) at $\mu = 0$, is $\mathbb{C}^r$ at $x \neq 0$. Thus, the system (12.2.6) and (12.2.7) is $\mathbb{C}^{r-1}$-smooth at $x \neq 0$ after the transformation, whereas the flow map between any two cross-sections which did not intersect $\{x = 0\}$ remains $\mathbb{C}^r$-smooth.

Once we fix coordinates such that the system on the center manifold is in the autonomous form (12.2.12) at $\mu = 0$, we can then define *the essential map*

$$\varphi \mapsto f(\varphi) \equiv m\varphi + q_0(\varphi, 0; 0)\,. \tag{12.2.13}$$

By construction, it is obtained as follows: apply the map T_1 to the intersection line of the local unstable manifold $W^u_{\rm loc} = W^C \cap U_+$ with the cross-section S_1 and then project the image onto the center manifold along the leaves of the strong-stable foliation. The projection is done in S_0 which lies in the node region where the foliation is uniquely defined (see Chap. 5). Thus, once the cross-sections S_0 and S_1 are fixed, the essential map is defined uniquely, modulo coordinate transformations on the center manifold which keep the system autonomous (the center manifold in the node region is not unique but systems on different center manifolds are smoothly conjugate by their projection along the strong-stable invariant foliation. Therefore, the choice of another center manifold is equivalent to a coordinate transformation on the given one).

In fact, the set of coordinate transformations which keeps the system at $\mu = 0$ in the form (12.2.12) is rather poor. Indeed, a new coordinate φ must satisfy $\frac{d}{dt}(\varphi_{\rm new} - \varphi) = 0$, hence the difference $\varphi_{\rm new} - \varphi$ must be constant along a trajectory of the system. In particular, it is constant on L. Now, since any orbit on the center manifold tends to L either as $t \to +\infty$ or as $t \to -\infty$, it follows that $\varphi_{\rm new} - \varphi =$ constant everywhere on W^c. Furthermore, since the equation for x in (12.2.12) must remain autonomous, one can show that only autonomous (independent of φ) transformations of the variable x are allowed. Indeed, consider first a transformation which is identical at $\varphi = 0$. By definition, it does not change the Poincaré map of the local cross-section $S : \{\varphi = 0\}$. Therefore, by the uniqueness of the embedding into the flow (Lemma 12.4), if such transformation keeps the system autonomous, it cannot change the right-hand side $\tilde{g}$. It follows that if $x_{\rm new} \equiv x$ at $\varphi = 0$, then the time evolution of $x_{\rm new}$ and the time evolution of x are governed by the same equation which immediately implies that $x_{\rm new} \equiv x$ for all φ in this case. Since an arbitrary transformation is a superposition of an autonomous

transformation and a transformation of the kind we have just considered, this proves the claim.

Thus, the only possible coordinate transformation is

$$\varphi \mapsto \varphi + \text{const}\,, \quad x \mapsto X(x)\,. \tag{12.2.14}$$

For the essential map, the effect of such a transformation of x is equivalent to a shift of the cross-sections S_0 and S_1 to $x = X^{-1}(-d^-)$ and $x = X^{-1}(d^+)$, respectively. Since the evolution of x is autonomous, the flight time from a cross-section $\{x = \text{constant}\}$ to any other cross-section of this form depends only on the position of the cross-sections but not on the initial point on the cross-section. Thus, any shift of S_0 or S_1 is equivalent to a rigid rotation of φ_0 or φ_1, respectively. We have finally arrived at

Lemma 12.1. *The essential map is uniquely defined by the system at $\mu = 0$, modulo an arbitrary additive constant and a shift of the origin*:

$$f(\varphi) \to c_0 + f(\varphi + c_1)\,.$$

The essential map carries most of the information on the global saddle-node bifurcations. As already mentioned, its degree m defines the topological type of W^u_L. If $|m| = 1$, then W^u_L is smooth if, and only if, $f(\varphi)$ does not have critical points (see (12.2.10) and (12.2.13)). Below (Theorem 12.4), we give a precise formulation to the following *reduction principle*:
the bifurcations in $U(W^u_L)$ as $\mu \to +0$ follow the bifurcations in the family of one-dimensional maps

$$\bar\varphi = \omega(\mu) + f(\varphi)\,, \tag{12.2.15}$$

where $\omega(\mu) \to +\infty$ as $\mu \to +0$.

The above reduction principle was applied explicitly in [151] for the case $|m| = 1$. An earlier study in [97] was essentially based on the same idea.

Let us consider the Poincaré map $T = T_0 \circ T_1$ of the cross-section S_1 which is defined by the trajectories of the system for all small $\mu > 0$. Here, T_1 is a global map defined by (12.2.8) and $T_0 : S_0 \to S_1$ is a through map defined locally near L for $\mu > 0$.

As in the previous section, the behavior of the trajectories in U for $\mu > 0$ is completely determined by the behavior of the map T.

Since the Eq. (12.2.7) for $\dot{x}$ and $\dot{\varphi}$ are independent of y, the local through map $T_0 : (y_0, \varphi_0) \mapsto (y_1, \varphi_1)$ is written in the form (for some $\mathbb{C}^r$-function Y)

$$\begin{aligned} y_1 &= Y(\varphi_0, y_0, \mu)\,, \\ \varphi_1 &= \varphi_0 + \tau(\varphi_0, \mu) \mod 1\,. \end{aligned} \tag{12.2.16}$$

The function τ is *the flight time* from S_0 to S_1. It is a smooth function periodic in φ_0. Clearly, $\tau(\varphi_0, \mu) \to \infty$ as $\mu \to +0$.

Lemma 12.2. *When* (12.2.11) *is satisfied at* $\mu = 0$*, then* $\partial\tau/\partial\varphi$ *tends uniformly to zero as* $\mu \to +0$*, in the* $\mathbb{C}^{r-1}$*-topology.*

In its full generality, this lemma is proven in [140] and it implies almost immediately the basic Theorem 12.4 below. The proof is based on a lengthy calculations and we omit them here. A simple proof of an analogous statement is given in Sec. 12.5 under some additional assumptions. Namely, it is assumed there that the system is sufficiently smooth with respect to all variables and μ, and that the saddle-node L is simple. Moreover, instead of proving that all of the derivatives tend to zero, the vanishing of only a sufficiently large number of derivatives is established. Of course, all this does not represent a severe restriction.

By denoting $\omega(\mu) = \tau(0, \mu)$, we get from Lemma 12.2 that

$$\tau(\varphi_0, \mu) = \omega(\mu) + o(1)\,. \tag{12.2.17}$$

If the saddle-node is simple, then

$$\omega(\mu) \sim \frac{\pi}{\sqrt{\mu l_2}}\,. \tag{12.2.18}$$

Note also that since the eigenvalues of the matrix $\mathcal{A}(\mu)$ in (12.2.3) lie strictly to the left of the imaginary axis and since, by (12.2.5), $\dot{y} = (\mathcal{A} + \tilde{h})y$ for some $\mathbb{C}^{r-1}$-function $\tilde{h}$, it is easy to show that

$$\| Y \|_{\mathbb{C}^{r-1}} \leq O(e^{-\lambda\omega}) \tag{12.2.19}$$

for some positive λ. In fact, it may be shown [140] that

$$\| Y \|_{\mathbb{C}^r} \to 0 \text{ as } \mu \to 0\,. \tag{12.2.20}$$

Collecting formulas (12.2.8), (12.2.9), (12.2.10), (12.2.16), (12.2.17), and (12.2.20) gives the following result [140].

Theorem 12.4. (Reduction principle) *The Poincaré map $T = T_0 \circ T_1$ is written as*

$$\begin{aligned} \bar{y} &= \psi(\varphi, y; \mu)\,, \\ \bar{\varphi} &= \omega + f(\varphi) + \xi(\varphi, y; \mu) \mod 1\,, \end{aligned} \tag{12.2.21}$$

where $\omega(\mu) \to \infty$ and ψ, ξ tend to zero (along with all derivatives) as $\mu \to +0$.

It follows immediately from this theorem that if the essential map (12.2.15) has a rough stable (unstable) periodic orbit at some ω^*, then there is a sequence of intervals δ_k of values of μ which accumulate at $+0$, such that the difference $(\omega(\mu) - k)$ remains close to ω^* at $\mu \in \delta_k$, and the system has, respectively, a rough stable or saddle periodic orbit at $\mu \in \delta_k$ for all sufficiently large k.

In fact, Theorem 12.4 holds also when the system depends on μ smoothly: we assume in this case that
the first derivatives of the right-hand sides of (12.2.3) *and* (12.2.4) *with respect to the phase variables (y, z, φ) are $\mathbb{C}^{r-1}$-smooth with respect to all variables and μ.*
Assume also that the local Poincaré map near L depends monotonically on μ; i.e.

$$g'_\mu(0; 0) > 0 \tag{12.2.22}$$

in (12.2.1).[4] In this case one can prove that

$$\partial\omega/\partial\mu \neq 0\,, \tag{12.2.23}$$

i.e. ω can be viewed as a new parameter, and μ may then be considered as a function of ω which tends to zero as $\omega \to \infty$. It can be proved that all the derivatives of μ with respect to ω tend to zero too. Lemma 12.1 when restated for the derivatives of τ'_φ with respect to both ω and φ_0 remains valid. Theorem 12.4 provides absolutely the same; namely "all derivatives" include now the derivatives with respect to ω (see [140]).

Note that the above trick of letting the flight time be a new parameter is necessary only in the case of low smoothness: upon proving Lemma 12.3 which corresponds to the case where the smoothness is high (and the saddle-node is

[4] When the saddle-node is simple, (12.2.22) is just a condition of transversality of the one-parameter family under consideration to the bifurcation surface of systems with the saddle-node, which allows the Poincaré map on W^C_{loc} to be written in the form (12.2.2).

simple), we show the vanishing of an arbitrarily large number of derivatives with respect to μ itself.

Now, Theorem 12.3 follows immediately from formula (12.2.21): by the conditions of the theorem we have $|m| = 1$ and $f'(\varphi) \neq 0$, so the map $\varphi \mapsto \omega + f(\varphi) + \xi(\varphi, 0; \mu)$ is a diffeomorphism and it is easy to see that the annulus principle (Sec. 4.2) is applicable here. Thus, the existence of a uniquely defined $\mathbb{C}^r$-smooth closed invariant curve

$$y = \eta(\varphi; \mu) \tag{12.2.24}$$

which attracts all orbits in S_1 is established for the map T for any $\mu > 0$. Since this map is defined by the orbits of the system under consideration, this proves the theorem.

Due to the annulus principle, the invariant curve depends continuously on μ (or smoothly, when the system is smooth with respect to μ). By fixing any value of $\nu = \omega(\mu) \bmod 1$ so that $\omega = \nu + k$, where $k \in \mathbb{Z}$ such that $k \to \infty$ as $\mu \to +0$, the map (12.2.21) has a limit (in smooth topology) as $k \to \infty$

$$\begin{aligned} &\bar{y} = 0\,, \\ &\bar{\varphi} = \nu + f(\varphi) \mod 1\,. \end{aligned} \tag{12.2.25}$$

Thus, the invariant curve of the map T has the invariant curve $\{y = 0\}$ of the map (12.2.25) as a limit, i.e. the function η in (12.2.24) vanishes (along with all derivatives) as $\mu \to +0$.

On the invariant curve, the map T can be represented as

$$\bar{\varphi} = \omega(\mu) \pm \varphi + f_0(\varphi) + f_1(\varphi; \mu) \mod 1\,, \tag{12.2.26}$$

where "+" (the orientable case) corresponds to the case of a torus and "−" (the non-orientable case) to a Klein bottle; f_0 and f_1 are periodic functions of φ and $f_1 \to 0$ along with all derivatives as $\mu \to +0$. If the system depends smoothly on μ (and the monotonicity condition (12.2.22) holds), then it follows from (12.2.23) that this map (when lifted onto $\mathbb{R}^1$) is strictly monotonic with respect to μ.

Therefore, in the orientable case, the Poincaré rotation number on the torus depends monotonically on μ (see Sec. 4.4). Typically, each rational rotation number corresponds to an interval of values of μ (a resonant zone). In the simplest case, there exist only two periodic orbits on the torus in the

resonant zone, one stable and the other unstable (for example, there may be only two fixed points if $f_0(\varphi) = \sin\varphi$). The unstable periodic orbit on the invariant curve is a saddle orbit for the map T of the annulus (the solid torus) S_1; the invariant curve is the closure of the unstable manifold of this saddle periodic orbit. In general, for different functions f_0, there may be arbitrarily many periodic orbits in the resonant zone (with an equal number of stable and saddle orbits on the torus). In this case the invariant curve is the closure of the unstable manifolds of all saddle periodic orbits.

The boundary of the resonant zone corresponds to a coalescence of the stable and unstable periodic orbits on the invariant circle, i.e. to the saddle-node bifurcation of the same type we consider here. Besides, if there were more than two periodic orbits, saddle-node bifurcations may happen at the values of parameters inside the resonant zone. By the structure of the Poincaré map (12.2.26) on the invariant curve,
if some value ν^* corresponds to a codimension-one bifurcation (a simple saddle-node) in the essential map

$$\bar\varphi = \nu + \varphi + f_0(\varphi)\,,$$

then there is a sequence of values $\mu_k \to +0$, such that $\omega(\mu_k) - k \to \nu^*$, and the map (12.2.26) *undergoes the same bifurcation at $\mu = \mu_k$ for all sufficiently large k.*

Let us now consider the question concerning what happens when W^u_L is non-smooth. For the first time, this question was studied in [3] where it was discovered that the possibility of *the breakdown of the invariant manifold causes an onset of chaos* at such bifurcations. In particular, sufficient conditions (the so-called "big lobe" and "small lobe" conditions) were given in [3] for the creation of infinitely many saddle periodic orbits upon the disappearance of a saddle-node in the non-smooth case. Subsequent studies have shown that these conditions may be further refined so we may reformulate them as follows.

Recall that in the smooth case, the manifold W^u_L intersects the strong-stable foliation $\mathcal{F}^{ss}$ transversely, and each leaf has only one point of intersection with W^u_L. In the generic non-smooth case, some of the leaves have one-sided tangencies to W^u_L. Therefore, there must be leaves in the node region where each leaf has several intersections with W^u_L.

Definition 12.1. *The set W^u_L satisfies the (refined) big lobe condition if each leaf of $\mathcal{F}^{ss}$ intersects W^u_L at least twice in the node region* (*Fig.* 12.2.4).

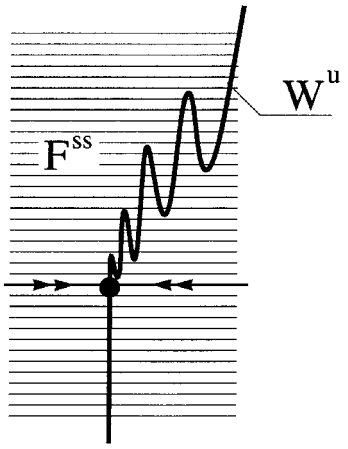

Fig. 12.2.4. Geometrical interpretation of the big lobe condition — each leaf of the strong stable foliation F^{ss} must cut W^u through not fewer than two points.

In terms of the essential map this condition translates into a condition for the existence of at least two pre-images for any value of $\bar{\varphi}$, with respect to the map

$$\bar{\varphi} = f(\varphi)\,.$$

The following result is a stronger version of the corresponding theorem in [3].

Theorem 12.5. *If the big lobe condition is satisfied, then the system has infinitely many saddle periodic orbits for all small* $\mu > 0$.

Note that this theorem holds independently of the type of the topological structure of W^u_L (i.e. independently of the degree m of the essential map). Obviously, the big lobe condition is always satisfied when $|m| > 2$, so the disappearance of the saddle-node always implies chaos in this case. Therefore, for the rest of this chapter we will be focusing on the cases $m = 1, 0, -1$.

The small lobe condition was originally introduced for the case where W^u_L is a torus ($m = 1$), but it makes sense at $m = 0$ and $m = -1$ as well. In terms of the essential map, the small lobe condition is satisfied if
there exist φ_1 *and* φ_2 *such that*

$$f(\varphi_1) = f(\varphi_2)$$

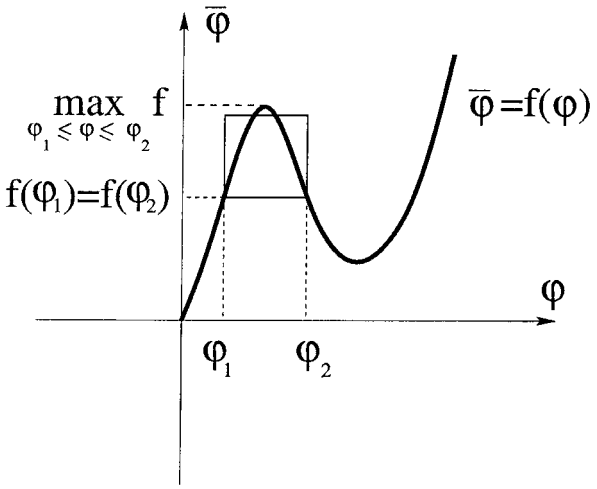

Fig. 12.2.5. A form of $f(\varphi)$ satisfying the small lobe condition.

and

$$\max_{\varphi\in[\varphi_1,\varphi_2]} |f(\varphi) - f(\varphi_1)| > |\varphi_2 - \varphi_1|$$

(see Fig. 12.2.5).

Theorem 12.6. *If the small lobe condition is satisfied, then on the μ-axis there is a sequence of intervals Δ_i which accumulate at $\mu = +0$, such that the system has infinitely many saddle periodic orbits for any $\mu \in \Delta_i$.*

Note the difference between the transition to chaos under the big lobe condition and without it: in the second case the intervals Δ_i of chaotic dynamics may, in principle, interchange with the intervals where the system has only finitely many saddle and stable periodic orbits [151]. According to the reduction principle (Theorem 12.4), this occurs if, within some interval of ω, the essential map

$$\bar{\varphi} = \omega + f(\varphi)$$

has only a finite number of periodic orbits.

For example, if $f(\varphi) = \varphi + \frac{C}{2\pi}\sin 2\pi\varphi$, then the manifold W^u_L is non-smooth for $C \ge 1$, whereas the big lobe condition is satisfied if

$$\sqrt{C^2-1} > \pi + \arccos\frac{1}{C}\,,$$

and the small lobe condition is fulfilled with $\varphi_2 = 1/2$ if

$$\sqrt{C^2-1} > \pi + \arccos\frac{1}{C} - u\,,$$

where $u \in (0,\pi)$ is the root of the equation $\pi = u + C\sin u$. It is obvious that when $(C-1)$ is sufficiently small, then the essential map has only one stable and one unstable fixed point in the interval $|2\pi\omega| < 1$, and no other periodic orbits. Therefore, if $(C-1)$ is sufficiently small, on the μ-axis there exist intervals of simple dynamics; in fact, the existence of such intervals may be easily checked, for example, when

$$\sqrt{C^2-1} > \frac{3\pi}{4} + \arccos\frac{1}{C}\,.$$

Note that both theorems above give only sufficient conditions for chaotic dynamics following the disappearance of the saddle-node. These conditions may be further refined. The most important improvement (essentially due to Newhouse, Palis and Takens [97]) can be made in the case $m = 1$ where the unstable manifold W^u_L of the saddle-node is a torus.

Theorem 12.7. *Generically, if W^u_L is a non-smooth torus, then on the μ-axis there is a sequence of intervals Δ_i which accumulate at $\mu = +0$, such that the system has infinitely many saddle periodic orbits for any $\mu \in \Delta_i$.*

The genericity condition of this theorem may be explicitly formulated: for each $\varphi_0 \in \mathbb{S}^1$, check that either there is another φ such that $f(\varphi) = f(\varphi_0)$, or at least some of the derivatives $f'(\varphi_0), f''(\varphi_0), \ldots, f^{(r)}(\varphi_0)$ are non-zero. It is not clear whether this condition is essential, or it is just a technical restriction. In any case, the simultaneous vanishing of all derivatives of the essential map at some point is an extremely rare situation.

So, the results of Theorems 12.3, 12.5 and 12.7 are summarized as follows: *If W^u_L is a smooth torus, then a smooth attracting invariant torus persists after the disappearance of the saddle-node L. If W^u_L is homeomorphic to a torus but it is non-smooth, then chaotic dynamics appears after the disappearance of L. Here, either the torus is destroyed and chaos exists for all small $\mu > 0$ (the big lobe condition is sufficient for that), or chaotic zones on the parameter axis alternate with regions of simple dynamics.*

Theorem 12.7 uses heavily that the degree m of the essential map is equal to 1. It has no analogues for the cases $m = 0$ and $m = -1$ where the scenario of the onset of chaos is rather vague.

12.3. The formation of a Klein bottle

Let us consider next the bifurcation of the saddle-node periodic orbit L in the case where the unstable manifold W^u_L is a Klein bottle, as depicted in Fig. 12.3.1, i.e. when the essential map has degree $m = -1$. By virtue of Theorem 12.3, if W^u_L is smooth, then a smooth invariant attracting Klein bottle persists when L disappears. In its intersection with a cross-section S_0, the flow on the Klein bottle defines a Poincaré map of the form (see (12.2.26))

$$\bar{\varphi} = \omega(\mu) - \varphi + f_0(\varphi) + f_1(\varphi, \mu) \mod 1\,, \tag{12.3.1}$$

where $\omega \to \infty$ as $\mu \to +0$; f_0 and f_1 are smooth 1-periodic functions, f_1 vanishes at $\mu = 0$ along with all derivatives, $-\varphi + f_0(\varphi)$ is the essential map defined uniquely by the system at $\mu = 0$. As shown in the last section, the manifold W^u_L is smooth if, and only if,

$$-1 + f_0'(\varphi) \neq 0 \tag{12.3.2}$$

for all φ. In this case, the Poincaré map (12.3.1) is a (non-orientable) diffeomorphism of the circle.

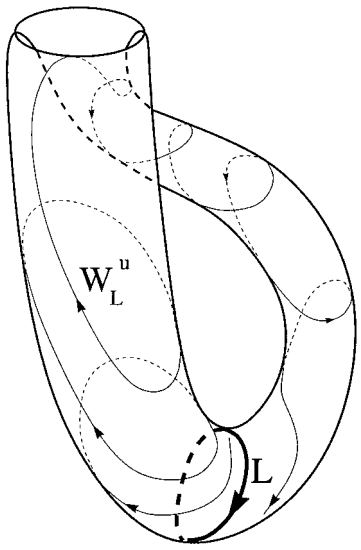

Fig. 12.3.1. A saddle-node periodic orbit on the Klein bottle.

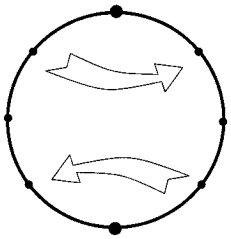

Fig. 12.3.2. The non-orientable circle map in action.

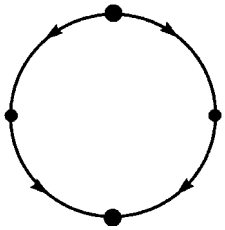

Fig. 12.3.3. A possible saddle-node bifurcation of a period-two orbit of a non-orientable circle map.

Such maps are known to have exactly two fixed points. They partition the circle into two arcs, each one cycles into another under the action of the map. On these arcs there may also be a number of period-two points, as shown in Fig. 12.3.2. Generically, the following bifurcations are possible: a period-two orbit collapses into, or emerges from a fixed point (whose multiplier passes through -1), or two orbits of period two may coalesce into a saddle-node orbit of period two, as depicted in Fig. 12.3.3. It follows immediately from (12.3.1) that if the essential map

$$\bar{\varphi} = \nu - \varphi + f_0(\varphi) \mod 1 \tag{12.3.3}$$

undergoes one of these bifurcations at some $\nu = \nu^*$, then
there exists a sequence $\mu_k \to +0$ *such that* $(\omega(\mu_k) - k) \to \nu^*$ *and the Poincaré map* (12.3.1) *undergoes the same bifurcation at each* $\mu = \mu_k$.

The fixed points of the map (12.3.1) are found from the equation

$$\begin{aligned} \varphi_0 &= \frac{1}{2}\omega(\mu) + \frac{1}{2}(f_0(\varphi_0) + f_1(\varphi_0, \mu))\,, \\ \varphi_1 &= \frac{1}{2}\omega(\mu) + \frac{1}{2}(f_0(\varphi_1) + f_1(\varphi_1, \mu)) + \pi\,. \end{aligned} \tag{12.3.4}$$

Since f_0 and f_1 are periodic functions, they are bounded. So, it follows from (12.3.4) and (12.3.2) that as $\omega \to \infty$, the coordinates φ_0 and φ_1 corresponding to the fixed points increase unboundedly. In other words, as $\mu \to +0$, both fixed points move around along the circle infinitely many times.

The multiplier of the fixed point is equal to $-1 + f_0'(\varphi_{0,1}) + f_1'(\varphi_{0,1}, \mu)$. Since $f_1' \to 0$ as $\mu \to +0$, it follows that if $f_0(\varphi) \not\equiv 0$, then the multiplier of each fixed point oscillates back and forth around -1. We arrive at the following result (first noticed in [6] with the detailed proof first published in [86]):

Theorem 12.8. *For all $\mu > 0$, the system on the Klein bottle has exactly two periodic orbits with negative multipliers. If $f_0(\varphi)$ does not vanish identically, each of these two periodic orbits undergoes a period-doubling bifurcation infinitely many times as $\mu \to +0$.*

In the simplest case (say, when $f_0(\varphi) = \frac{C}{2\pi} \sin 2\pi\varphi$ with $C < 1$), the bifurcations proceed as follows (see Fig. 12.3.4): on some interval of μ one of the fixed points (φ_0) is stable and another (φ_1) is unstable. Then at some value of μ, the fixed point φ_0 loses its stability and a stable orbit of period two is born. After that, in some interval of μ, there exist two unstable fixed points and a stable orbit of period two; then the stable orbit collapses into the fixed point φ_1 which becomes stable now, and then the bifurcation process is repeated: the stable fixed point again loses its stability via period-doubling, and so on, infinitely many times without ever ending.

Since the recurrent time of a nearby orbit to a cross-section is about $\omega(\mu)$ (see the last section), it follows that the period of the orbits of the flow which corresponds to the fixed points of the Poincaré map tends to infinity as $\mu \to +0$ (typically, it is $\sim \pi/\sqrt{\mu l_2}$). Before the orbits return to the cross-section, each must make $\omega(\mu)$ rotations in a small neighborhood of the just disappeared saddle-node L. Accordingly, the length of these periodic orbits is also increasing to infinity. Thus, Theorem 12.8 gives a positive answer to the following

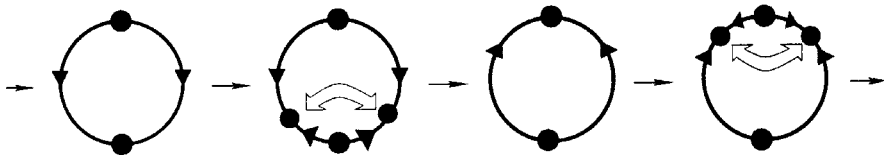

Fig. 12.3.4. The simplest cycle of bifurcations on the Klein bottle for the Poincaré map (12.3.1) as $\mu \to +0$.

question posed by Palis and Pugh [105]: can a periodic orbit disappear at a finite distance from the equilibrium states such that the period and the length of the orbit increase to infinity when approaching the moment of bifurcation?

Virtual bifurcations of such kind were named "the blue sky catastrophes" by R. Abraham. The first example of a blue sky catastrophe was constructed by Medvedev [95] for the saddle-node bifurcation on a Klein bottle. The most important feature of Medvedev's example is that the periodic orbit whose length and period are constantly increasing as $\mu \to +0$ remains stable and does not undergo any bifurcation for all small $\mu > 0$. Theorem 12.8 shows that this is only possible in the case $f_0(\varphi) \equiv 0$, which means that all points (except for the two fixed points) of the essential map are of period two.

Since the essential map is highly degenerate in this case, it does not reveal much information concerning the structure of the Poincaré map (12.3.1). To find out the ways on how the stable periodic orbit survives, let us choose

$$f_1(\varphi, \mu) = \mu \cos \pi\omega(\mu) \sin 2\pi\varphi - \mu \sin \pi\omega(\mu) \cos 2\pi\varphi \,.$$

The Poincaré map is then written as

$$\bar{\varphi} = \omega(\mu) - \varphi + \mu \sin(2\pi\varphi - \pi\omega(\mu)) \mod 1 \,.$$

Observe that this map has a fixed point $\varphi_0 = \omega(\mu)/2$ with a multiplier equal to $-1 + 2\pi\mu$, i.e. this point is stable for all $\mu > 0$.

We see that Medvedev's example describes an extremely degenerate situation. A generic example of the blue sky catastrophe for a stable periodic orbit (when the degree m of the essential map is equal to zero) is given in the next section.

Let us now consider briefly the question on what may happen if W^u_L is a non-smooth Klein bottle. Since Theorems 12.5 and 12.6 are applicable in this case, it follows that when $\mu > 0$, chaos may appear when the big lobe or the small lobe condition is satisfied. However, a direct analogue of Theorem 12.7 does not exist here because of the following possibility:
even if W^u_L is non-smooth, the system may nevertheless exhibit simple dynamics for all small positive values of μ.

The above situation can occur if the essential map (12.3.3) has only finitely many periodic orbits for all ν. For example, when $f_0(\varphi) = \frac{C}{2\pi} \sin 2\pi\varphi$, one can show that the essential map has only a finite number of fixed points, and points of period-two, but no other periodic orbits for all ν if, for instance, $C < \sqrt{2}$.

12.4. The blue sky catastrophe

Let us now consider the case where the global unstable set W_L^u of the saddle-node periodic orbit L is not a manifold, but has the structure like shown in Fig. 12.4.1. This means that the integer m which determines the homotopy class of the curve $l^+ = W_L^u \cap S_0$ in the cross-section $S_0 : \{x = -d^-\}$ is equal to zero. In other words, the essential map of Sec. 12.2 in this case has

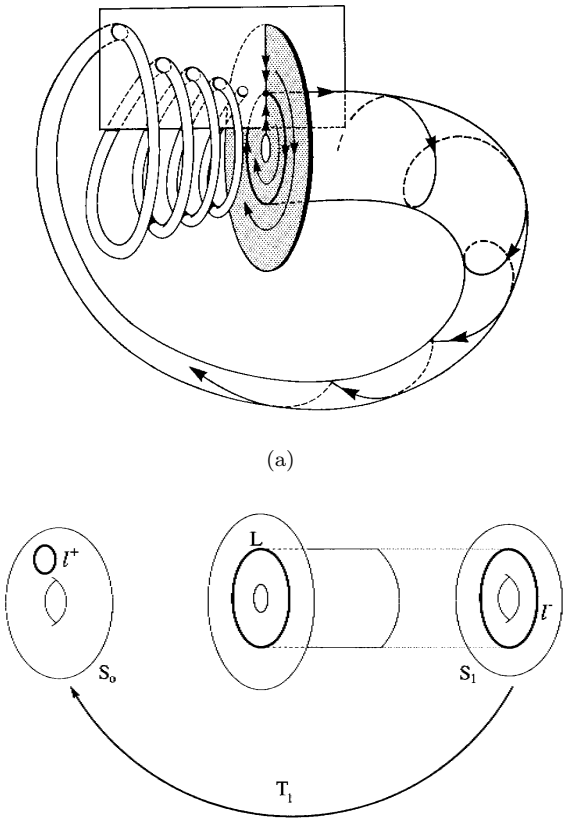

Fig. 12.4.1. (a) Illustrates the mechanism of a blue-sky catastrophe. The unstable manifold W_L^u returns to the saddle-node from the node region so that the circles of its intersection with the cross-section S tighten with each subsequent iterate. (b) The return map along W_L^u.

the form

$$\bar{\varphi} = \omega + f_0(\varphi) \mod 1\,, \tag{12.4.1}$$

where f_0 is a 1-periodic smooth function.

Theorem 12.9. *Consider a one-parameter family of dynamical systems which has a saddle-node periodic orbit L at $\mu = 0$ such that all orbits in the global unstable set W^u_L tend to L as $t \to +\infty$, but do not lie in W^{ss}_L. Let the essential map satisfy $m = 0$ and $|f_0'(\varphi)| < 1$ for all φ. Then, after disappearance of the saddle-node for $\mu > 0$, the system has a stable periodic orbit L_μ (non-homotopic to L in U) which is the only attractor for all trajectories in U.*

Proof. By Theorem 12.4, the Poincaré map T of a cross-section $S_1 : \{x = d^+\}$ is close (in smooth topology) to the following map

$$\begin{aligned} \bar{y} &= 0\,, \\ \bar{\varphi} &= \omega(\mu) + f_0(\varphi) \mod 1 \end{aligned} \tag{12.4.2}$$

for small $\mu > 0$. By assumption, $|f_0'(\varphi)| < 1$. Hence, the map (12.4.2) is a contraction, and has a unique attractor for any ω; namely, it has a unique stable fixed point. The same result clearly holds for all close maps; in particular, for the map T for small $\mu > 0$. Since the map T is defined by the orbits of the flow, the fixed point corresponds to an attracting periodic orbit L_μ. End of the proof.

Since the return time from/to the cross-section S_1 (i.e. the period of L_μ) grows proportionally to $\sim \omega(\mu)$, it must tend to infinity as $\mu \to +\infty$ (see Sec. 12.2; if L is a simple saddle-node, then the period grows as $\sim \pi/\sqrt{\mu l_2}$). Since the vector field vanishes nowhere in U, it follows that the length of L_μ must tend to infinity also. Since L_μ, does not bifurcate when $\mu > 0$, we have an example of the blue sky catastrophe [152].

If the saddle-node L is simple, then all neighboring systems having a saddle-node periodic orbit close to L constitute a codimension-one bifurcational surface. By construction (Sec. 12.2), the function f_0 depends continuously on the system on this bifurcational surface. Thus, if the conditions of Theorem 12.9 are satisfied by a certain system with a simple saddle-node, they are also satisfied by all nearby systems on the bifurcational surface. This implies that Theorem 12.9 is valid for any one-parameter family which intersects the surface transversely. In other words, our blue sky catastrophe *occurs generically*

in one-parameter families. The corresponding bifurcation surface is a new stability boundary for periodic orbits (the orbit L_μ here), which has no analogues in two-dimensional systems.

Note that the specific topological structure of W^u_L is not yet sufficient for realizing a blue sky catastrophe: there exists also a quantitative condition in Theorem 12.9 which is needed to ensure contraction. If this condition is violated, i.e. if $|f_0'(\varphi)| > 1$ at some φ, then *infinitely many bifurcations occur in the region* $\mu > 0$, just like the cases considered in the preceding sections. Indeed, consider the lift of the map (12.4.1) onto $\mathbb{R}^1$:

$$\bar{\varphi} = \omega + f_0(\varphi)\,. \tag{12.4.3}$$

The fixed points of this map correspond to the fixed points of the essential map (12.4.1). Since f_0 is periodic, it is bounded. Thus, (12.4.3) always has at least one fixed point and the corresponding value of φ becomes arbitrarily large as ω grows. In the region where $f_0'(\varphi) < 1$, the coordinate of the fixed point is a monotonically increasing function of ω, but it is a decreasing one in the region $f_0'(\varphi) > 1$. Thus, if $|f_0'(\varphi)| > 1$ at certain intervals of φ, then we inevitably have the sequence of values of ω for which either a stable and an unstable fixed points coalesce into a saddle-node, or a stable fixed point undergoes a period doubling, changing its stability. Since $\omega \to \infty$ corresponds to $\mu \to +0$ and the Poincaré map T approaches the essential map arbitrarily closely (Theorem 12.4), it follows that the fixed points of map T must undergo the same bifurcations infinitely many times as $\mu \to +0$.

Moreover, it follows from Theorems 12.5 and 12.6 that chaotic behavior may also be possible if the condition $|f_0'(\varphi)| < 1$ of Theorem 12.9 is not met. In particular, the big lobe condition (Sec. 12.2) is here equivalent to the existence of a leaf of the strong-stable foliation which intersects at least two connected components of the intersection of W^u_L with the local cross-section $S : \{\varphi = \text{constant}\}$ (see Fig. 12.4.2). In terms of the essential map this condition is written as

$$\max f_0 \geq \min f_0 + 1\,, \tag{12.4.4}$$

i.e. this inequality will guarantee chaos at all small $\mu > 0$.

To make it clear that the configuration of W^u_L shown in Fig. 12.4.1(a) is indeed possible for the flows in $\mathbb{R}^n$ with $n \geq 3$, let us consider the following geometrical construction. Let a *two*-parameter family of three-dimensional

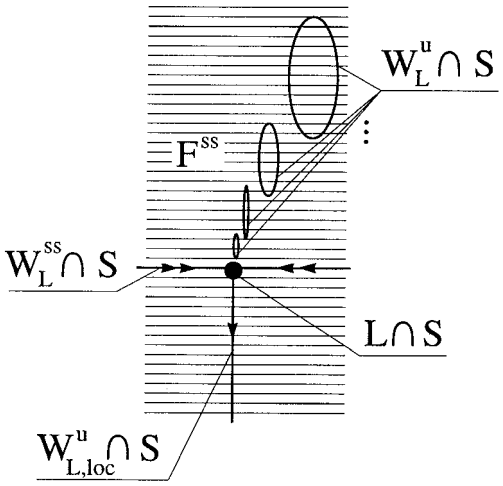

Fig. 12.4.2. The option of chaotic behavior resulted from the disappearance of a saddle-node fixed point of the corresponding Poincaré map, assuming the contraction condition is not satisfied but the big lobe condition holds: each leaf of the foliation $\mathcal{F}^{ss}$ must intersect at least two of the connected components of $W^s \cap S$.

vector fields have, for some parameter values, a saddle-node periodic orbit L and a saddle-node equilibrium state O. Suppose that all orbits of W^u_L tend to O as $t \to +\infty$ and that the one-dimensional separatrix of O goes to L, as shown in Fig. 12.4.3. If one of the parameters of the system is introduced in a way such that O disappears but L does not when it is slightly tuned, then the set W^u_L will have the desired configuration.

By following this recipe, a family of three-dimensional systems with analytically defined right-hand side has been explicitly designed which realizes the blue sky catastrophe [53]. This family is as follows

$$\begin{aligned} \dot{x} &= x(2+\mu - B(x^2+y^2)) + z^2 + y^2 + 2y \equiv P\,, \\ \dot{y} &= -z^3 - (1+y)(z^2+y^2+2y) - 4x + \mu y \equiv Q\,, \\ \dot{z} &= (1+y)z^2 + x^2 - \varepsilon \equiv R\,, \end{aligned} \tag{12.4.5}$$

where μ, ε and B are some parameters. At $\mu = \varepsilon = 0$ it has a closed integral curve ($x = 0$, $z^2 + y^2 + 2y = 0$). There are two equilibrium states on it (see Fig. 12.4.5(a)). The first one $O'(0, -2, 0)$ is a simple saddle-node with one zero $\lambda_1 = 0$ and two negative characteristic exponents found from

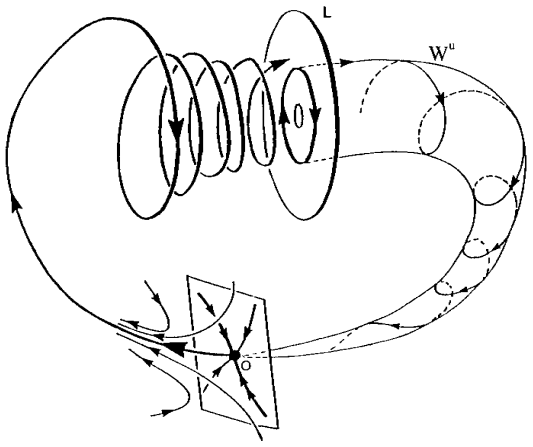

Fig. 12.4.3. A phemenological scenario of development of the blue sky catastrophe: when the saddle-node equilibrium O disappears, the unstable manifold of the saddle-node periodic orbit L has the desired configuration, as the one shown in Fig.12.4.1(a).

the equation $\lambda^2 + 4B\lambda + 8B - 12 = 0$. The second equilibrium state $O(0,0,0)$ also has one zero exponent $\lambda_1 = 0$, but along with a pair of purely imaginary characteristic exponents $\lambda_{1,2} = \pm 2i$. The point O' is of codimension one (a simple saddle-node), whereas the point O is of codimension three because the two-dimensional divergence $\sigma(z) = P'_x + Q'_y = -z^2 + \cdots$ at O starts with a quadratic term in z. This means that a double (semi-stable) cycle may emerge from O in the (x, y)-plane [51].

The bifurcation diagram is presented in Fig. 12.4.4. When $\varepsilon > 0$, the saddle-node O' disappears, while the equilibrium state O is decomposed into two ones O_1 and O_2 (region b in Fig. 12.4.4.), where $z_{O_{1,2}} = \mp\sqrt{2\varepsilon} + \cdots$. In this region the point O_1 is stable and O_2 is a saddle-focus of type (2,1) whose one-dimensional separatrices tend to O_1 as $t \to +\infty$ (Fig. 12.4.5(b)). As μ increases, the point O_1 loses its stability through a super-critical Andronov–Hopf bifurcation on the curve AH_1 in Fig. 12.4.4 and becomes a saddle-focus (1,2), and the unstable separatrices of the saddle-focus O_2 tend now to the new-born stable periodic orbit as shown in Fig. 12.4.5(c). The equilibrium state O_2 bifurcates on the curve AH_2. It also undergoes a supercritical Andronov–Hopf bifurcation, so that it becomes totally repelling. The unstable manifold of the saddle periodic orbit L_2, continues to tend to L_1 as $t \to +\infty$, as sketched in Fig. 12.4.5(d). On the bifurcation curve labeled SN

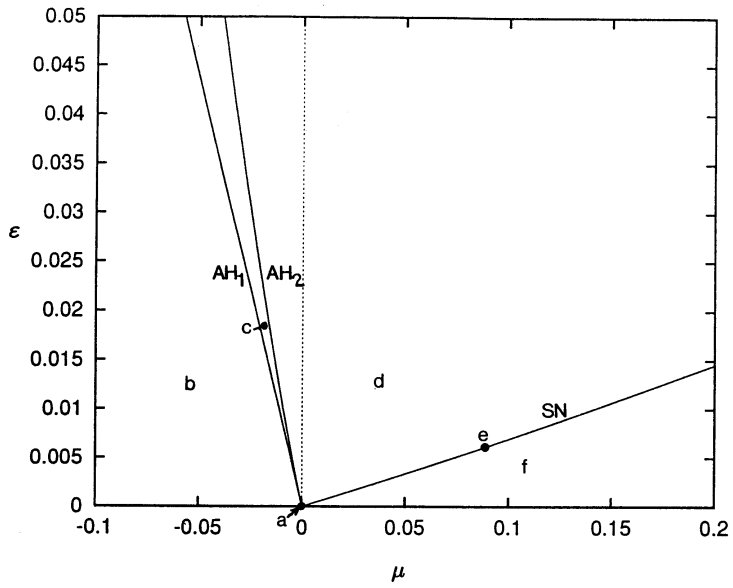

Fig. 12.4.4. The (μ, ε)-bifurcation diagram of system (12.4.5).

both cycles coalesce thereby composing a saddle-node cycle L^* whose unstable manifold is biasymptotic to L^*, as shown in Fig. 12.4.5(e). To the right of the curve SN, the cycle L^* disappears and in accordance with Theorem 12.9, the global stability is inherited by a new, large amplitude, stable periodic orbit L_{bs} which is not homotopic to either L_1 or L_2.

Another kind of examples where our blue sky catastrophe may appear naturally is given by *singularly perturbed systems*, i.e. the systems of the form

$$\begin{aligned} \dot{x} &= g(x, y, \varepsilon)\,, \\ \varepsilon\dot{y} &= h(x, y, \varepsilon)\,, \end{aligned} \tag{12.4.6}$$

where ε is a small parameter. This system may be regularized by rescaling the time $t = \varepsilon\tau$. In the new time τ, (12.4.6) becomes

$$\begin{aligned} x' &= \varepsilon g(x, y, \varepsilon)\,, \\ y' &= h(x, y, \varepsilon)\,, \end{aligned} \tag{12.4.7}$$

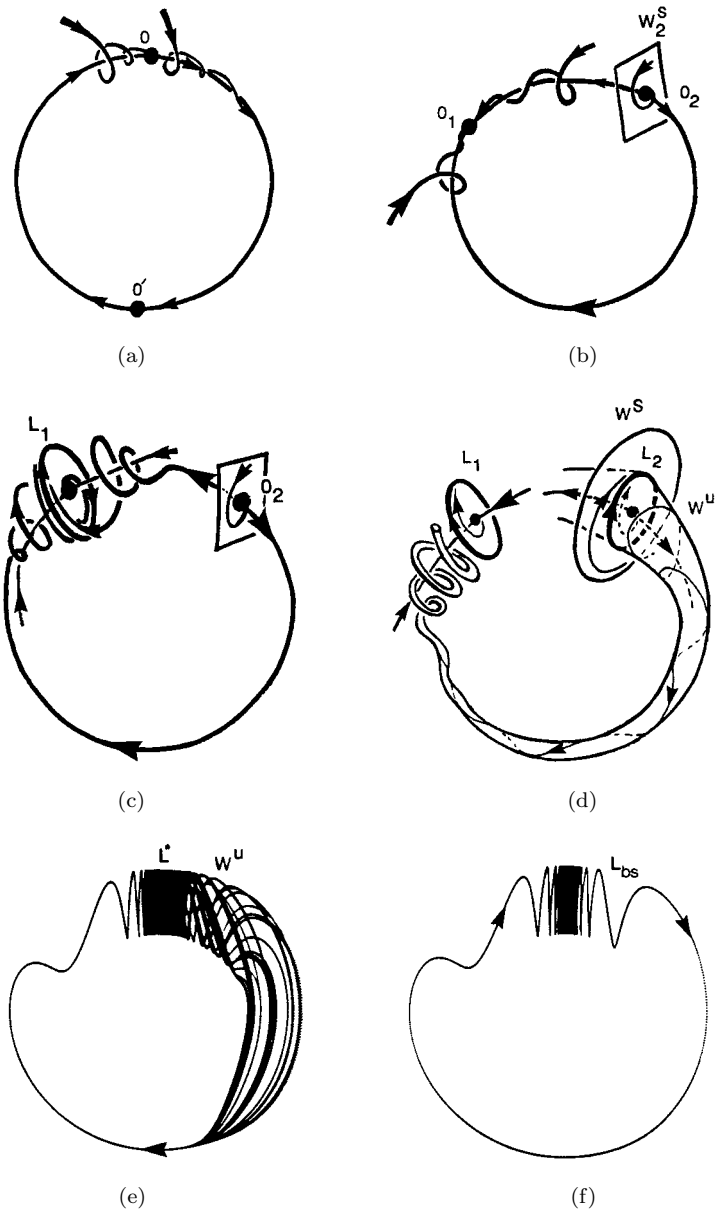

Fig. 12.4.5. Route to the blue sky catastrophe in (12.4.5) as μ, ε vary from (a) to (f) in Fig. 12.4.4.

where the prime denotes differentiating with respect to τ. Taking the limit $\varepsilon = 0$ here, we obtain

$$\begin{aligned} x' &= 0\,, \\ y' &= h(x, y, 0)\,. \end{aligned} \tag{12.4.8}$$

The second equation here is called the *fast* system. For simplicity, we assume that $x \in \mathbb{R}^1$. The variable x may be considered as a parameter which governs the motion of the fast y-variable.

Starting with any (x, y), a trajectory of system (12.4.8) converges typically to an attractor of the fast system corresponding to the chosen value of x. This attractor may be a stable equilibrium, or a stable periodic orbit, or of a less trivial structure — we do not explore this last possibility here. When an equilibrium state or a periodic orbit of the fast system is structurally stable, it depends smoothly on x. Thus, we obtain smooth attractive invariant manifolds of system (12.4.8): equilibrium states of the fast system form curves $M_{\rm eq}$ and the periodic orbits form two-dimensional cylinders $M_{\rm po}$, as shown in Fig. 12.4.6. Locally, near each structurally stable fast equilibrium point, or periodic orbit, such a manifold is a center manifold with respect to system (12.4.8). Since the center manifold exists in any nearby system (see Chap. 5), it follows that the smooth attractive invariant manifolds $M_{\rm eq}(\varepsilon)$ and $M_{\rm po}(\varepsilon)$ exist for all small ε in the system (12.4.7) [48].

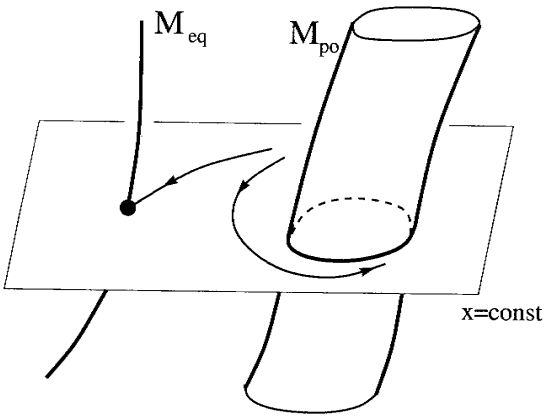

Fig. 12.4.6. Structurally stable equilibria and structurally stable limit cycles of the fast system compose invariant manifolds as x varies: respectively, curve $M_{\rm eq}$ and two-dimensional cylinder $M_{\rm po}$.

Thus, a trajectory of the system (12.4.7) for small ε behaves in the following way: during some finite time it comes to a small neighborhood of one of the invariant manifolds $M_{\rm eq}$ or $M_{\rm po}$, so that its x-coordinate is nearly fixed. Then, it drifts along the invariant manifold so that it corresponds to a slow change of x. As for the initial system (12.4.6) one observes a jump of the y-variables to the invariant manifold followed by a finite speed motion in the x-variable. In addition, if this is a manifold of a fast periodic orbit, then we have a fast circular motion of the y-variables on the manifold, as depicted in Fig. 12.4.7.

The equilibrium states of the fast system are found from the condition $h(x, y, 0) = 0$, which gives the equation of $M_{\rm eq}$. If $y = y_{\rm eq}(x)$ is a stable branch of $M_{\rm eq}$, then the evolution of x along it is, to first order in ε, given by the equation

$$\dot{x} = g(x, y_{\rm eq}(x), 0)\,. \tag{12.4.9}$$

This is a one-dimensional system which may have stable and unstable equilibrium states corresponding to stable and saddle equilibrium states of the entire system (12.4.6) or (12.4.7). The evolution along $M_{\rm eq}$ is either limited to one of the stable points, or it reaches a small neighborhood of the critical values of x. Recall, that we consider x as a governing parameter for the fast system and critical values of x are those ones which correspond to bifurcations of the fast system. In particular, at some x^* two equilibrium states (stable and saddle) of the fast system may coalesce into a saddle-node. This corresponds to a maximum (or a minimum) of x on $M_{\rm eq}$, so the value of x cannot further

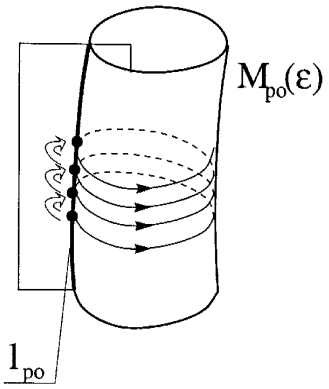

Fig. 12.4.7. The fast circular motion along an invariant cylinder $M_{\rm po}(\varepsilon)$ defines the Poincaré map on the intersection line $l_{\rm po}(\varepsilon)$ with a cross-section.

increase (respectively decrease) along the stable branch of $M_{\rm eq}$ when it reaches a small neighborhood of x^*. Instead, the orbit jumps to a new attractor, which is the ω-limit set of the separatrix of the saddle-node for the fast system at $x = x^*$, as shown in Fig. 12.4.8.

To find the evolution of x along the cylinder $M_{\rm po}$ we must find the equation $y = y_{\rm po}(\tau; x)$ of the corresponding fast periodic orbits, then substitute $y = y_{\rm po}(t\varepsilon; x)$ into the right-hand side of the first equation of (12.4.6) and average it over one period. The result of the averaging gives a first order approximation for the x-motion along a stable branch of $M_{\rm po}$; namely:

$$\dot{x} = \phi(x) \equiv \frac{1}{T(x)} \int_0^{T(x)} g(x, y_{\rm po}(\tau; x))\, d\tau\,, \tag{12.4.10}$$

where $T(x)$ is the period of the fast periodic orbit corresponding to the given value x. By chopping the cylinder by a cross-section transverse to the fast motion, one finds a Poincaré map on the intersection line $l_{\rm po}(\varepsilon)$, as shown in Fig. 12.4.7, whose first approximation is given by

$$\bar{x} = x + \varepsilon\phi(x)T(x)\,. \tag{12.4.11}$$

This is a one-dimensional map which may have stable and unstable fixed points (at the zeros of $\phi(x)$). They correspond to stable and saddle periodic orbits of the system (12.4.6). The evolution along $l_{\rm eq}$ either converges to one of the

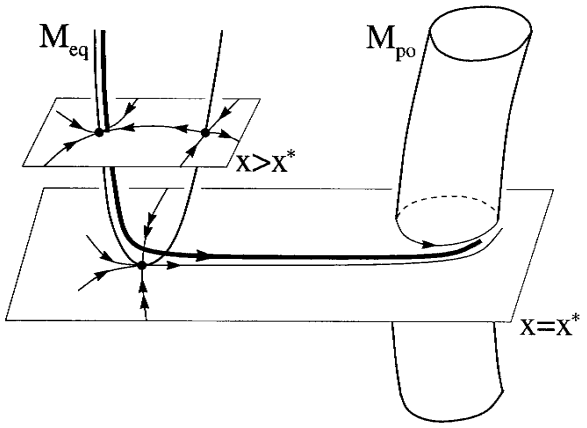

Fig. 12.4.8. A moment of the disruption occurs when an evolving stable node merges with a saddle and disappears. The representative point jumps onto a stable cylinder.

stable fixed points, or it reaches a small neighborhood of a critical value of x. In particular, if at some x^*, the stable fast periodic orbit coalesces with a saddle periodic orbit at a saddle-node, then the orbit must jump to an ω-limit set of the unstable manifold of the saddle-node for the fast system at $x = x^*$.

Let us now suppose that a singularly perturbed system has a curve $M_{\rm eq}$ of stable equilibria of the fast system along which the x-variable decreases until it reaches a critical value x_1^*. At $x = x_1^*$, the trajectories jump to a cylinder $M_{\rm po}$ of stable periodic orbits of the fast system. Assume that x increases along $M_{\rm po}$ and that $x = x_2^*$ is the critical value on $M_{\rm po}$ where the orbits jump to $M_{\rm eq}$, as depicted in Fig. 12.4.9 (note that y must be at least three-dimensional to make this particular picture possible). Let the Poincaré map on the curve $l_{\rm po}(\varepsilon)$ have a saddle-node fixed point. This corresponds to a saddle-node periodic orbit L on the cylinder $M_{\rm po}(\varepsilon)$. The unstable manifold of this periodic orbit coincides with the $M_{\rm po}(\varepsilon)$ above L. After the jump at $x = x_2^*$, the manifold W_L^u shrinks to an extremely thin tube which goes along the curve $M_{\rm eq}$ until it makes a new jump at $x = x_1^*$, after which it returns to L from below, winding around $M_{\rm po}$. This gives exactly the configuration of W_L^u required by Theorem 12.9; moreover, it can be computed that the contraction condition required by the theorem also holds here. Thus, the blue sky catastrophe occurs in the singularly perturbed system under consideration.

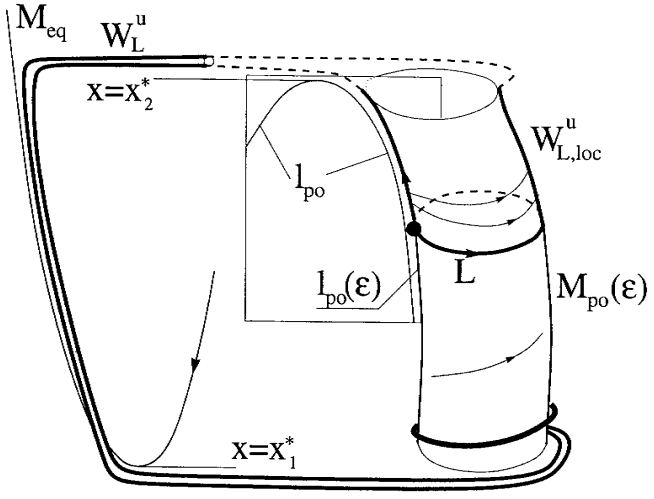

Fig. 12.4.9. Mechanism of a blue sky catastrophe in fast–slow systems.

In fact, the triggering from one stable branch to another is the most typical phenomenon in singularly perturbed systems, so one may encounter for our blue sky catastrophe every time when jumps between the branches of fast periodic orbits and fast equilibrium states are observed.

To conclude we remark that the mechanism suggested above may be helpful for a qualitative explanation of the frequently observed transitions from low-amplitude (spiking) oscillations to large bursting ones in models of neuronal activity, or to flow surges in jet engines.

12.5. On embedding into the flow

This section addresses the question on the local behavior of the flow near a saddle-node periodic orbit. Since the dynamics in the directions transverse to the center manifold is trivial (it is a strong contraction), we restrict our consideration to the system on the center manifold:

$$\dot{x} = G(x, \varphi, \mu), \qquad \dot{\varphi} = 1\,, \tag{12.5.1}$$

where $x \in \mathbb{R}^1$, $\varphi \in \mathbb{S}^1$, and G is a smooth function, 1-periodic in φ, such that $G(0, \varphi, 0) \equiv 0$. We assume that $L : \{x = 0\}$ is a saddle-node periodic orbit at $\mu = 0$, which disappears for $\mu > 0$.

The main result which we establish here is that the evolution of the x-variable in this system at $\mu \geq 0$ is well described by an *autonomous* equation (i.e. independent on the angular variable φ). An immediate advantage of this is that such equations are easily integrated (since x is one-dimensional) which allows for obtaining long-time asymptotics for the local dynamics near a saddle-node.

Let G be sufficiently smooth with respect to (x, φ, μ). It follows from Theorem 3.23 (see Sec. 3.14) that we may always assume that some sufficiently long finite segment of the Taylor expansion of G in powers of x and μ is independent of φ.

We assume also that L is a simple saddle-node. Thus, the function G can be represented in the form

$$G(x, \varphi, \mu) = \mu + x^2 + O(x^2 + \mu) \tag{12.5.2}$$

for $\mu \geq 0$. As mentioned, the order of φ-dependent terms in G can be made arbitrarily high. It follows that we may take an arbitrarily large k such that

under an appropriate choice of the variable x, we will have

$$\lim_{\mu\to+0,x\to 0}\frac{1}{G^k}\,\frac{\partial G}{\partial\varphi}=0\,. \tag{12.5.3}$$

We can also add

$$\lim\frac{1}{G^k}\,\frac{\partial^2 G}{\partial\varphi^2}=0\,,\quad \lim\frac{1}{G^k}\,\frac{\partial^3 G}{\partial\varphi^3}=0,\cdots \tag{12.5.4}$$

for an arbitrary fixed number of derivatives.

Lemma 12.3. *For $\mu\geq 0$, there exists a smooth transformation of the angular variable $\varphi\mapsto\Phi$ and a rescaling of time which reduce the system to the autonomous form*

$$\dot{x}=\tilde{g}(x,\mu)\,,\qquad \dot{\Phi}=1\,. \tag{12.5.5}$$

As we mentioned, the importance of this result is that the flight time from any cross-section $x=$ constant to any other cross-section of this form *is independent on the initial point on this cross-section*. Thus, when the system is brought to the form (12.5.5), Lemma 12.2 is valid which, in turn, implies the reduction principle of Theorem 12.4.

Note that when the system is in the form (12.5.5), the local Poincaré map on the cross-section $\Phi=0$ coincides with the time 1 shift by the autonomous flow given by $\dot{x}=\tilde{g}(x,\mu)$. In such cases, it is said that *the map is embedded into the flow*. Strictly speaking, we did not prove yet that the local Poincaré map of the original system (12.5.1) is embedded into the flow: original Poincaré map is defined on a different cross-section $\varphi=0$. However, the change of cross-section is equivalent to a change of variables on the cross-section (see Sec. 3.1), but the fact that a map can be embedded into a flow is valid independently on the choice of coordinates.

Let us now prove the lemma. Let $\tau(x;x_0,\varphi_0,\mu)$ be the time at which the orbit of (12.5.1) starting with $(x=x_0,\varphi=\varphi_0)$ attains the given value of x. Since $\dot{x}>0$ for $\mu>0$, and since $\dot{x}\neq 0$ at $\mu=0$, it follows that the function τ is well-defined and smooth for $\mu>0$ at all small x and x_0, as well as at $\mu=0$ for x_0 and x of the same sign. Denote

$$u\equiv\frac{\partial\tau}{\partial\varphi_0}\,.$$

Let us show that *as $\mu \to +0$, the function u has a finite limit, in smooth topology, uniformly for all φ_0 and for all small x_0 and x such that $x_0 \neq 0$ and $x \cdot x_0 \geq 0$*[5].

Indeed, integrating the system (12.5.1) gives:

$$\varphi = \varphi_0 + \tau(x; x_0, \varphi_0, \mu)\,, \tag{12.5.6}$$

$$\tau(x; x_0, \varphi_0, \mu) = \int_{x_0}^{x} \frac{ds}{G(s, \varphi_0 + \tau(s; x_0, \varphi_0, \mu), \mu)}\,. \tag{12.5.7}$$

Differentiating (12.5.7) with respect to φ_0, we find that

$$u(x) = -\int_{x_0}^{x} \frac{1}{G^2} \frac{\partial G}{\partial \varphi}\bigg|_{(s, \varphi_0 + \tau(s), \mu)} [1 + u(s)] ds \tag{12.5.8}$$

(we do not indicate the dependence of τ on (x_0, φ_0, μ) for the sake of brevity). By (12.5.3), we have

$$\frac{G'_\varphi}{G^2} \to 0 \quad \text{as} \quad \mu \to +0,\ x \to 0\,, \tag{12.5.9}$$

so the integral operator on the right-hand side of (12.5.8) is contracting. Thus, by the Banach contraction mapping principle, the function u can be found by the successive approximation method as a unique continuous solution of the integral Eq. (12.5.8).

By the contraction mapping principle, the solution $u(x; x_0, \varphi_0, \mu)$ depends continuously on (x_0, φ_0, μ) when the integral operator on the right-hand side of (12.5.8) depends on these data continuously. Note that the function τ entering expression (12.5.8) has a finite limit at $\mu = 0$ only if $x \cdot x_0 > 0$. Nevertheless, by virtue of (12.5.9), the integral in (12.5.8) has a finite limit at $x = 0$. Thus, the function $u(x;\, x_0, \varphi_0, \mu)$ has a finite limit at $\mu = 0$ uniformly in the region $\{x \cdot x_0 \geq 0,\ x_0 \neq 0\}$.

Using estimates (12.5.4), we can repeat these arguments for any given number of derivatives of u with respect to φ_0, x_0 and μ (this number can be made arbitrarily large by increasing the value of k in the estimates). This completes the proof of the claim.

[5] It is important here that we have the convergence at $x = 0$, despite the function τ tends to infinity as $\mu \to +0,\ x \to 0$.

Now, since the right-hand side of Eq. (12.5.8) for the function u is small for small x, x_0 and μ, it follows that the function u is small itself. Moreover, observe that it tends to zero uniformly as $x - x_0 \to 0$. The same conclusion holds for the derivatives of u (because they are found from the integral equations of the same type). Now we see that the function $u(0; x_0, \varphi_0, \mu)$ is well defined and smooth for all $\mu \geq 0$ (*a priori*, it might happen here that, as $\mu \to +0$, the function u, or some of its derivatives, had different limits at $x_0 = +0$ and $x_0 = -0$, but all these limits are zero as we just have shown).

Let us now introduce a new angular variable

$$\Phi = \varphi + \int_0^{\varphi} u(0; x, \phi, \mu) d\phi \,. \tag{12.5.10}$$

This is a correct transformation of variables because u is small. Moreover, u is a derivative of a 1-periodic function ($u = \frac{\partial \tau}{\partial \varphi_0}$) — hence the integral in the right-hand side defines a 1-periodic function indeed.

Let, in the old variables, an orbit which starts with (x_0, φ_0), reach a point (x_1, φ_1) at the moment of time $\tau(x_1; x_0, \varphi_0, \mu)$. By differentiating the obvious identity

$$\tau(x_1; x_0, \varphi_0, \mu) = \tau(0; x_0, \varphi_0, \mu) - \tau(0; x_1, \varphi_1, \mu)$$

(the flight time from x_0 to x_1 is equal to the flight time from x_0 to 0 plus the flight time from 0 to x_1), we obtain

$$\frac{\partial \varphi_1}{\partial \varphi_0} = \frac{1 + u(0; x_0, \varphi_0, \mu)}{1 + u(0; x_1, \varphi_1, \mu)} \,.$$

Comparing this formula with (12.5.10), we see that in the new variables

$$\frac{\partial \Phi_1}{\partial \Phi_0} \equiv 1 \,. \tag{12.5.11}$$

Let us rescale the time variable so that $\dot{\Phi} = 1$. Now, the difference between Φ_1 and Φ_0 is the flight time from $x = x_0$ to $x = x_1$. By (12.5.11), this time is independent of the initial value Φ_0 but depends only on (x_0, x_1, μ). This means that $\frac{dx}{d\Phi}$ is now independent of Φ, which gives the lemma.

As we mentioned, Lemma 12.3 may be reformulated as a possibility to embed a sufficiently smooth one-dimensional map near a simple saddle-node fixed point into a smooth one-dimensional flow for $\mu \geq 0$. An analogous result was proved in [74] in connection with the problem on the appearance of

separatrix connections between saddles at the disappearance of a semi-stable cycle on the plane (see Sec. 8.1) and in [45] in connection with the problem of appearance of strange attractors at the disappearance of a saddle-node periodic orbit on a non-smooth torus. The embedding into a flow at $\mu = 0$ is due to Takens (see [97]). Our proof is based on the method from [152, 139]. In [140], the existence of smooth embedding into the flow at $\mu = 0$ was shown without the high-smoothness assumption and without the assumption that the saddle-node is simple.

While defining the essential map in Sec. 12.2, we used the following property of *rigidity* of the embedding into the flow:

Lemma 12.4. *Let the $\mathbb{C}^r$-smooth ($r \geq 2$) map*

$$\bar{x} = x + g(x) \tag{12.5.12}$$

have a saddle-node at $x = 0$, i.e. *$g(0) = 0$, $g'(0) = 0$, and $g(x) > 0$ for $x \neq 0$. Let this map coincide with the time-1 map of the smooth flow*

$$\bar{x} = x + \tilde{g}(x) \tag{12.5.13}$$

Then the function $\tilde{g}$ is defined uniquely by g.

Proof. Map (12.5.12) coincides with the time-1 map of flow (12.5.13) if and only if

$$\int_x^{\bar{x}} \frac{ds}{\tilde{g}(s)} = 1\,. \tag{12.5.14}$$

Since $x = 0$ must be the fixed point of the time shift of (12.5.13) with the multiplier equal to 1, it follows that $\tilde{g}$ must vanish at zero along with $\tilde{g}'$. Taking then the limit $x \to 0$ in (12.5.14) gives

$$\lim_{x\to 0} \frac{\tilde{g}(x)}{g(x)} = 1 \tag{12.5.15}$$

(for a proof, note that

$$\int_x^{\bar{x}} \frac{ds}{\tilde{g}(s)} = \frac{\bar{x} - x}{\tilde{g}(x) + \frac{1}{2}\tilde{g}'(x)(\bar{x} - x) + o(\bar{x} - x)} \sim \frac{g(x)}{\tilde{g}(x)}\,;$$

here we use smoothness of $\tilde{g}$ at zero).

Differentiating (12.5.14), we obtain

$$\frac{1+g'(x)}{\tilde{g}(\bar{x})} - \frac{1}{\tilde{g}(x)} = 0\,. \tag{12.5.16}$$

Therefore, if there exist two functions $\tilde{g}_1$ and $\tilde{g}_2$ which provide the embedding of the map (12.5.12) into the flow, then (12.5.16) implies

$$\frac{\tilde{g}_1(\bar{x})}{\tilde{g}_2(\bar{x})} = \frac{\tilde{g}_1(x)}{\tilde{g}_2(x)}\,.$$

In other words, the ratio $\tilde{g}_1/\tilde{g}_2$ is invariant with respect to map (12.5.12). Since any orbit of (12.5.1) tends to zero either at forward or at backward iterations, we obtain that

$$\frac{\tilde{g}_1(x)}{\tilde{g}_2(x)} = \lim_{x\to 0}\frac{\tilde{g}_1(x)}{\tilde{g}_2(x)}\,.$$

By virtue of (12.5.15) we have that $\tilde{g}_1 \equiv \tilde{g}_2$ which completes the proof of Lemma 12.4.

Chapter 13

BIFURCATIONS OF HOMOCLINIC LOOPS OF SADDLE EQUILIBRIUM STATES

The problem of the birth of a limit cycle from a separatrix loop to a saddle had already been solved in the two-dimensional case by Andronov and Leontovich at the end of the thirties, even though the corresponding publications appeared years later. Their investigation on this subject embraced both the generic case and the case of an arbitrarily high degeneracy. In the latter case, their theory was related to the work of Dulac concerning the stability of the separatrix loop. We present these results in the first three sections of this chapter. Our proof of the main theorem differs from the classical treatment in [12]. Namely, we explicitly reduce the problem to a study of the Poincaré map near the loop. Such an approach allows one to extend the result naturally to the multi-dimensional case. Moreover, by applying the center manifold theorem near a homoclinic loop (Chap. 6), one may, in some cases, reduce the multi-dimensional problem directly to a two-dimensional problem.

We should, however, stress that such a reduction to the two-dimensional case is not *always* possible. In particular, it cannot be performed when the equilibrium state is a saddle-focus. Moreover, under certain conditions, we run into an important new phenomenon when infinitely many saddle periodic orbits coexist in a neighborhood of a homoclinic loop to a saddle-focus. Hence, the problem of finding the stability boundaries of periodic orbits in multi-dimensional systems requires a complete and incisive analysis of all cases of homoclinic loops of codimension one, both with simple and complex dynamics. This problem was solved by L. Shilnikov in the sixties.

We prove the main theorem on the birth of a stable periodic orbit from a homoclinic loop to a saddle with the negative saddle value in Sec. 13.4.

We also show in Secs. 13.4 and 13.5 (the latter deals with the case where the dimension of the unstable manifold of the saddle is greater than one) that in other cases either a saddle periodic orbit is born from the loop, or a system exhibits complex dynamics (the case of a saddle-focus).

We study some homoclinic bifurcations of codimension two in Secs. 13.6. In Sec. 13.7, we review the results on the bifurcations of a homoclinic-8, and on the simplest heteroclinic cycles.

13.1. Stability of a separatrix loop on the plane

Suppose that a smooth two-dimensional system

$$\dot{x} = X(x)\,,$$

has a structurally stable equilibrium state $O(0,0)$ of the saddle type. Recall that in this case the saddle has two one-dimensional local invariant manifolds: the stable manifold

$$W^s_O = O \cup \Gamma^+_1 \cup \Gamma^+_2\,,$$

and the unstable manifold

$$W^u_O = O \cup \Gamma^-_1 \cup \Gamma^-_2\,,$$

where $\Gamma^+_{1,2}$ denote the stable separatrices and $\Gamma^-_{1,2}$ denote the unstable separatrices of the saddle O.

If Γ^+_1 and Γ^-_1 coincide, then $\Gamma = \Gamma^+_1 = \Gamma^-_1$ is called *a separatrix loop* (*or a homoclinic loop*). The closure $\bar{\Gamma}$ of the separatrix loop is an invariant closed set $\bar{\Gamma} = O \cup \Gamma$. Our goal of this section is to describe the behavior of trajectories in a sufficiently small neighborhood of $\bar{\Gamma}$ (the bifurcations of the separatrix loop will be analyzed in the following section).

A sufficiently small neighborhood of $\bar{\Gamma}$ is an annulus, partitioned by $\bar{\Gamma}$ into two regions which we denote by U and V, as shown in Fig. 13.1.1. Let V be the outer region within which there are two small pieces passing through O which belong to the separatrices Γ^+_2 and Γ^-_2. It is clear that all other trajectories from V must leave V both as $t \to -\infty$ and $t \to +\infty$. Hence, we can define the stability of $\bar{\Gamma}$ from one side only, i.e. from the side of the inner region U. In this context we say that the separatrix loop is asymptotically one-side stable if it is the ω-limit of all trajectories starting from U.[1] On the

[1] It may turn out that $\bar{\Gamma}$ is one-side stable, but not asymptotically. For example, in the case of Hamiltonian systems the region U may be filled by periodic orbits.

contrary, the separatrix loop is unstable if it is the α-limit of all trajectories from U.

A basic method for studying the homoclinic loop is to construct a Poincaré map T via a superposition of two maps: a local map T_0 and a global map T_1. To do this let us choose two cross-sections S_0 and S_1 near the saddle, which are both transverse to Γ, as shown in Fig. 13.1.2. The map $T_1 : S_1 \to S_0$ is

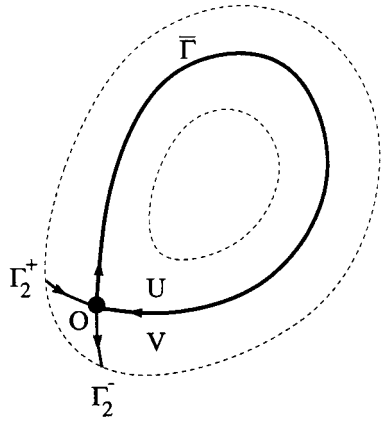

Fig. 13.1.1. A separatrix loop $\bar{\Gamma}$ is within an annulus consisting of an outer neighborhood V and an inner neighborhood U.

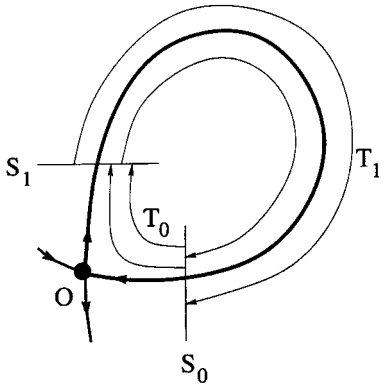

Fig. 13.1.2. The Poincaré map T is represented as the local map T_0 by the orbits of the system from the cross-section S_0 to S_1 along with the global map T_1 from S_1 to S_0.

defined as follows: let us take any point on S_1; then its image by T_1 is the point of intersection of its trajectory with S_0. Since the flight time from S_1 to S_0 is bounded, it follows that T_1 is a diffeomorphism and it is well approximated by the Taylor expansion near the point of intersection of Γ with S_1. As for the map $T_0 : S_0 \to S_1$, the situation here is less obvious because the trajectories come arbitrarily close to the saddle. Therefore, the flight time from S_0 to S_1 is not bounded from above.

Hence, the first problem in studying homoclinic loops is to obtain appropriate/suitable estimates for the local map T_0. To do this we will reduce the system in a neighborhood of O to a special form (see Appendix A in Part I of this book).

The problem of stability of a separatrix loop on a plane is easily solved when the so-called saddle value

$$\sigma_0 = \operatorname{div} X|_O$$

is non-zero at the saddle. In this case, we have the following result:

Theorem 13.1. *If $\sigma_0 < 0$, the homoclinic loop $\bar{\Gamma}$ is asymptotically one-side stable. If $\sigma_0 > 0$, the homoclinic loop $\bar{\Gamma}$ is unstable.*

Here we prove this theorem for the case where the system is $\mathbb{C}^r$-smooth with $r \geq 2$. In the $\mathbb{C}^1$-case the theorem is still true (see the next section).

Let us straighten the local stable and unstable invariant manifolds. Then the system near O takes the form (see Sec. 2.7)

$$\dot{x} = (\lambda + f(x, y))x\,, \quad \dot{y} = (\gamma + g(x, y))y\,, \tag{13.1.1}$$

where $\lambda < 0 < \gamma$, and the $\mathbb{C}^{r-1}$-smooth functions f and g vanish at the origin. Observe that $\sigma_0 = \lambda + \gamma$. Recall, that we can make an additional $\mathbb{C}^{r-1}$-smooth transformation of coordinates such that the system will retain its form (13.1.1) and such that the functions f and g will satisfy the following identities (see Theorem 2.17)

$$f(x, 0) \equiv 0\,, \quad f(0, y) \equiv 0\,, \tag{13.1.2}$$

$$g(x, 0) \equiv 0\,, \quad g(0, y) \equiv 0\,. \tag{13.1.3}$$

It is known (see, for example, [27]) that a $\mathbb{C}^r$-system ($r \geq 2$) near a saddle on the plane can be reduced to the linear form by a $\mathbb{C}^1$-transformation, and

finding the map T_0 in that case would be very easy. However, the form (13.1.1)–(13.1.3) suffices for our purposes because there is no essential loss of smoothness in this case. Moreover, the method we will develop can be generalized directly to the multi-dimensional case.

Let us rescale the time $dt \to (\gamma + g(x,y))^{-1}dt$. The system then assumes the form

$$\dot{x} = (-\nu + f(x,y))x, \quad \dot{y} = y \tag{13.1.4}$$

with some new function f which still satisfies (13.1.2). Here, the ratio $\nu = |\lambda/\gamma|$ is called *the saddle index*. Note that $\nu > 1$ corresponds to a negative saddle value σ_0, and $\nu < 1$ corresponds to $\sigma_0 > 0$, respectively.

Let us choose a small $d > 0$ and let $x = d$ be the cross-section S_0 and $y = d$ be the cross-section S_1 (we assume that the separatrices Γ_1^+ and Γ_1^- adjoin the saddle point O from the side of positive x and y, respectively). If the system were locally linear (i.e., if f were identically zero in (13.1.4)), the solution with the initial point (d, y_0) on S_0 would be

$$x = e^{-\nu t}d\,, \quad y = y_0 e^t\,.$$

The flight time τ from S_0 to S_1 can be found from the condition

$$d = y_0 e^{\tau}\,.$$

Hence,

$$\tau = -\ln \frac{y_0}{d}$$

(it is evident that the trajectory starting from $y_0 \le 0$ never reaches S_1). Thus, in the linear case, the point (x_1, d) of the intersection of the trajectory with the cross-section S_1 is found as

$$x_1 = e^{-\nu t}d = y_0^{\nu}\, d^{1-\nu}\,.$$

In the general case, where f is non-zero, this formula for the local map T_0 does not change significantly.

Lemma 13.1. *If the function f satisfies identity* (13.1.2)*, then the local map for the system* (13.1.4) *assumes the form*

$$x_1 = y_0^{\nu} d^{1-\nu} + o(y_0^{\nu})\,. \tag{13.1.5}$$

Proof. One may show that a solution of (13.1.4) which starts from S_0 at $t = 0$ and hits S_1 at $t = \tau$ satisfies

$$\begin{aligned} y(t) &= e^{t-\tau} d\,, \\ x(t) &= e^{-\nu t} d + \int_0^t e^{-\nu(t-s)} f(x(s), y(s))\; x(s) ds\,. \end{aligned} \tag{13.1.6}$$

Here, $y(0) \equiv y_0$ is the coordinate of the initial point on S_0 and $x(\tau) \equiv x_1$ is the coordinate of the point of intersection of the trajectory with S_1.

As shown in Sec. 2.8, the integral equation (13.1.6) is solved by the method of successive approximations, i.e. the solution $x(t)$ is the limit of a sequence $x_n(t)$ defined inductively by

$$x_{n+1}(t) = e^{-\nu t} d + \int_0^t e^{-\nu(t-s)} f(x_n(s), e^{s-\tau} d) x_n(s) ds\,, \tag{13.1.7}$$

where we take $x_1(t) = e^{-\nu t} d$ as the first approximation. It is easy to see that all further approximations satisfy

$$|x_n(t)| \le 2de^{-\nu t} \tag{13.1.8}$$

for $t \in [0, \tau]$. Indeed, by induction, it is enough to show that

$$\int_0^t |f(x_n(s), e^{s-\tau} d)| ds \le \frac{1}{2}\,,$$

provided (13.1.8) is satisfied. Since f is a smooth function vanishing at $y = 0$, it follows that $|f(x, y)| \le C|y|$ for some constant C. Thus, the above integral can be estimated by

$$Cde^{-\tau} \int_0^t e^s ds \le Cd\,.$$

Obviously, this integral is less than $\frac{1}{2}$ provided d is sufficiently small. This proves the inequality (13.1.8). Taking the limit $n \to +\infty$, we have found that the solution $x(t)$ of the system satisfies the same estimate, i.e.

$$x(t) \le 2de^{-\nu t}\,. \tag{13.1.9}$$

By assumption [see (13.1.2)], the function f vanishes at $y = 0$. Therefore,

$$|f(x, y)| \le |y| \max |f'_y|\,,$$

where the maximum is taken over $|y| \le d$ and for a fixed value of x. Since f vanishes at $x = 0$ as well, we have $f'_y(0, y) \equiv 0$. Hence, the inequality above gives us the following estimate

$$|f(x, y)| \le |y|\, o(1)_{x\to 0}\,.$$

Thus, in (13.1.6), we have

$$|f(x(s), y(s))| \le e^{-\tau} o(e^s)\,.$$

Hence, taking into account (13.1.9), we obtain

$$\left| \int_0^t e^{-\nu(t-s)} f(x(s), y(s)) x(s) ds \right| \le e^{-\nu t} e^{-\tau} o(e^t)\,.$$

At $t = \tau$, we have from (13.1.6) that

$$x_1 \equiv x(\tau) = e^{-\nu\tau} d + o(e^{-\nu\tau})\,. \tag{13.1.10}$$

The flight time τ is found from the first equation of (13.1.6) at $t = 0$:

$$y_0 = e^{-\tau} d\,.$$

Substituting this expression into (13.1.10) we obtain Lemma 13.1.

Remark. By rescaling variables $x_0 \to x_0 d$ and $y_1 \to y_1 d$ one can always assume (and we will henceforth do so) that $d = 1$ in (13.1.5). Note also that one can differentiate the formula (13.1.5): the sth ($s = 1, \dots, r-1$) derivative of the $o(y_0^\nu)$-term in (13.1.5) can be easily estimated as $o(y_0^{\nu-s})$. We skip the proof of this estimate for the derivatives because it goes absolutely along the same lines as the proof of an analogous statement (Lemma 3.6) presented in Appendix B in Part I of this book. A close statement will be also proven in Sec. 13.8 [see (13.8.30)–(13.8.33)]. By applying these estimates to our situation we find that if the system is $\mathbb{C}^r$-smooth with $r \ge 3$, then after a reduction to the form (13.1.1)–(13.1.3), the local map can be written in the form

$$x_1 = y_0^\nu + o(y_0^{\tilde\nu}) \tag{13.1.11}$$

for any $\tilde\nu$ such that $\nu < \tilde\nu < \nu + \min(1, \nu)$. Moreover, the sth ($s = 1, \dots, r-2$) derivative of the $o(y_0^{\tilde\nu})$ term is estimated by $o(y_0^{\tilde\nu - s})$.

Let us now consider the global map $T_1 : S_1 \to S_0$ defined by the orbits close to the piece of Γ that lies outside of a small neighborhood of O. Recall that this global map is a diffeomorphism. The fact that there is a homoclinic loop to the saddle O means that the point $x_1 = 0$ on S_1 is mapped by T_1 into $y_0 = 0$ on S_0. Thus, the map T_1 can be written in the form

$$\bar{y}_0 = Ax_1 + h(x_1)\,,$$

where $A \neq 0$, and $h(x)$ tends to zero along with its first derivative. Observe that since the problem under consideration is planar, we have $A > 0$ (the case $A < 0$ is possible for systems on a non-orientable two-dimensional surface).

Finally, we arrive at the following formula for the map $T = T_1 \circ T_0$:

$$\bar{y}_0 = Ay_0^\nu + o(y_0^\nu)\,. \tag{13.1.12}$$

It is immediately seen from the above formula that $\bar{y}_0 < y_0$ for any sufficiently small positive y_0, provided $\nu > 1$ (or, provided that $\nu = 1$ and $A < 1$). Therefore, in this case, the iterations of any point by the map T converge to the fixed point $y_0 = 0$. The latter is the point of intersection of the separatrix loop Γ with S_0. It follows that any trajectory starting from the side of a positive y_0 must converge to the loop Γ as $t \to +\infty$. This means that the separatrix loop is asymptotically one-side stable if $\sigma_0 < 0$, or if $\sigma_0 = 0$ and $A < 1$.

If $\nu < 1$ (i.e. $\sigma_0 > 0$), or if $\nu = 1$ (i.e. $\sigma_0 = 0$), but $A > 1$, we have $y_0 < \bar{y}_0$ in (13.1.12). Therefore, the backward iterations of any point by the map T converge to the fixed point $y_0 = 0$ in this case. This means that the homoclinic loop is one-side unstable here. This completes the proof.

Observe also that we have meanwhile proven the following result.

Theorem 13.2. *Let $\sigma_0 = 0$. Then, the separatrix loop is stable if $A < 1$, and unstable if $A > 1$.*

Remark. As noted above, Theorem 13.1 holds even for $\mathbb{C}^1$-smooth systems. However, Theorem 13.2 does not hold in the $\mathbb{C}^1$-case. To show this let us consider the following counterexample. Assume that a system near the saddle is represented in the following form

$$\dot{x} = -x\,, \quad \dot{y} = y\left[1 + \frac{1}{|\ln y| + 1}\right]\,,$$

where $|x| \le 1$ and $|y| \le 1$. Its solution, starting from the cross-section $S_0 : \{x = 1\}$ with a positive y_0, is given by

$$x = e^{-t}\,, \quad y(|\ln y| + 2) = e^t y_0(|\ln y_0| + 2)\,.$$

Hence, the local map T_0 from S_0 to $S_1 : \{y = 1\}$ is given by

$$x_1 = \frac{1}{2} y_0(|\ln y_0| + 2)\,.$$

Assume also the global map T_1 is linear, i.e. $\bar{y}_0 = Ax_1$. Then, the Poincaré map $T = T_1 \circ T_0$ near the loop is given by

$$\bar{y}_0 = \frac{1}{2} A y_0(|\ln y_0| + 2)\,.$$

Obviously, since $\bar{y}_0 > y_0$ for all small y_0, it follows that the homoclinic loop is unstable here, no matter what the value of A is.

The above counterexample shows that Theorem 13.2 is valid only if the system is $\mathbb{C}^r$-smooth with $r \ge 2$. Note that in this case the integral

$$s_1 = \int_{-\infty}^{+\infty} \operatorname{div} X(\varphi(t))dt$$

is convergent [where $(x, y) = \varphi(t)$ is a parametric equation of the separatrix loop Γ; recall that $\sigma_0 = 0$ implies $\operatorname{div} X(\varphi(t)) \to 0$ as $t \to \pm\infty$]. The real number s_1 is called *the first separatrix value*. It is obvious that it is invariant with respect to smooth coordinate transformations.

One can show that when $\sigma_0 = 0$, the derivative A of the global map $T_1 : S_1 \to S_0$ at the point $x_1 = 0$ can be found[2] as follows:

$$A = e^{s_1}\,,$$

provided that W^s and W^u are locally straightened [i.e. the system is in the form (13.1.1)] and the identities (13.1.2) and (13.1.3) hold. Therefore, the value A is also an invariant in this case.

Let us now elaborate on the case where $\sigma_0 = 0$, and $s_1 = 0$. First of all, we will need to reduce the system (13.1.1) near the saddle to some normal form.

[2]Independent of the choice of the constant d which defines the position of the cross-sections S_0 and S_1.

Observe that since $\sigma_0 \equiv \lambda + \gamma = 0$, there emerge the following resonances

$$\lambda = (m+1)\lambda + m\gamma\,,$$
$$\gamma = m\lambda + (m+1)\gamma\,,$$

where m is any positive integer. These resonances are the same ones we met in the case of a weak focus. In order to analyze this situation, we need to introduce a more refined form of the system which is called *a canonical normal form*.

Lemma 13.2. *A $\mathbb{C}^{r-(2n+1)}$-transformation, where $(r \geq 2n+2)$, reduces a $\mathbb{C}^r$-smooth system near a resonant saddle with $\sigma_0 = 0$ to the following form*:

$$\begin{aligned} \dot{x} &= -x(1 - \sigma_1 xy - \cdots - \sigma_n (xy)^n - (xy)^n f(x,y))\,, \\ \dot{y} &= y\,, \end{aligned} \tag{13.1.13}$$

where the $\mathbb{C}^{r-(2n+1)}$-smooth function f vanishes identically at both $x = 0$ and $y = 0$ (see (13.1.2)).

The above coefficients $\sigma_i, \ldots, \sigma_n$ are called *saddle values*. Although they are not all invariant with respect to smooth coordinate transformations, however the number of the first non-zero saddle value is defined by the system uniquely (because it is the coefficient of the first non-zero resonant term), and is therefore invariant.

The above canonical normal form was first constructed by Dulac [47] in the analytic case. The smooth case was considered by E.A. Leontovich [85]. Below we briefly review the proof by Leontovich.

Note that we have already included the result of Lemma 13.2 for $n = 0$ [see (13.1.4)] as part of a more general statement (Theorem 2.17). Thus, we can proceed further by induction. Namely, let us assume that the system has already been reduced to the form (13.1.13) for some $n = k$. Then, if $r \geq 2k+4$, the $\mathbb{C}^{r-(2k+1)}$-smooth function f is, at least, $\mathbb{C}^3$-smooth, and, since f vanishes at both $x = 0$ and $y = 0$, it can be written in the form

$$f(x,y) = xyF(x,y)\,,$$

where F is a $\mathbb{C}^{r-(2k+3)}$-smooth function. Denote

$$F(x,y) = \sigma_{k+1} + \phi_1(x) + \phi_2(y) + \tilde{f}(x,y)\,,$$

where ϕ_1 and ϕ_2 vanish at $x = 0$ or $y = 0$, respectively, and $\tilde{f}$ vanishes at both $x = 0$ and $y = 0$. By construction, since

$$\sigma_{k+1} = F(0,0) = f''_{xy}(0,0)\,,$$
$$\phi_1(x) = F(x,0) - F(0,0)\,,$$
$$\phi_2(y) = F(0,y) - F(0,0)\,,$$

it follows that the functions $\phi_{1,2}$ and $\tilde{f}$ possess the same smoothness as that of F.

Thus, the system can be rewritten as

$$\dot{x} = -x\left(1 - \sum_{i=1}^{k+1}\sigma_i(xy)^i - (xy)^{k+1}\tilde{f}(x,y)\right) + x(xy)^{k+1}(\phi_1(x) + \phi_2(y))\,,$$
$$\dot{y} = y\,.$$

Now note that the transformation

$$x_{\text{new}} = x(1 + \alpha(x)(xy)^{k+1} - \beta(y)(xy)^{k+1})$$

brings the system to the form (13.1.13) for $n = k + 1$ if

$$\alpha(x) = \int_0^1 \phi_1(xs)\frac{ds}{s}\,, \quad \beta(y) = \int_0^1 \phi_2(ys)\frac{ds}{s}\,. \tag{13.1.14}$$

Since $\phi_{1,2}$ are smooth functions vanishing at zero, the above integrals are well-defined. Moreover, α and β have the same smoothness as $\phi_{1,2}$; i.e. the coordinate transformation is $\mathbb{C}^{r-(2n+1)}$-smooth as required. Continuing further by induction, we obtain the result of the lemma.

Observe that Leontovich's result is much broader. Namely, while deriving estimates for the solution of the system in the canonical form, she had shown that after an additional smooth change of coordinates a system of the form (13.1.13) becomes integrable. Explicitly, it was shown in [22] that in the $\mathbb{C}^\infty$-smooth case with $\sigma_1 = \cdots = \sigma_{n-1} = 0$ and $\sigma_n \neq 0$, the system near a saddle can be reduced by a $\mathbb{C}^\infty$-transformation to the following integrable form

$$\dot{x} = -x(1 - \sigma_n(xy)^n - \sigma_{2n}(xy)^{2n})\,,$$
$$\dot{y} = y\,.$$

It also follows that when all saddle values vanish (i.e. in the infinitely degenerate case) the system is locally reduced to the linear form.

Let us now proceed further and evaluate the local map $T_0 : S_0 \to S_1$ for the system in the canonical form (13.1.13). Let σ_n be the first non-zero saddle value in (13.1.13), i.e. the system assumes the form

$$\begin{aligned} \dot{x} &= -x(1 - \sigma_n(xy)^n - (xy)^n f(x,y))\,, \\ \dot{y} &= y\,. \end{aligned} \tag{13.1.15}$$

As before, we assume that the homoclinic loop Γ adjoins the saddle from the side of positive x and y. Note that this assumption fixes the direction of the x and y axes and, therefore, it holds the sign of the nth saddle value σ_n fixed. Let us choose a small $d > 0$ and define the cross-sections S_0 and S_1 by $\{x = d\}$ and $\{y = d\}$, respectively.

The solution of (13.1.15) which starts from S_0 at $t = 0$ and reaches S_1 at $t = \tau$ satisfies

$$\begin{aligned} &y(t) = e^{t-\tau} d\,, \\ &x(t) = e^{-t} d + \int_0^t e^{-(t-s)} x(s)\ (x(s)y(s))^n (\sigma_n + f(x(s), y(s)))ds\,. \end{aligned} \tag{13.1.16}$$

This integral equation can be solved by the successive approximation method (see Sec. 2.8). Let us choose

$$x(t) = e^{-t} d$$

as our first approximation. Substituting this expression into the right-hand side of the integral equation, we obtain the second approximation

$$x(t) = e^{-t} d + d^{2n+1} \sigma_n t e^{-t} e^{-n\tau} + e^{-t} o(e^{-n\tau})$$

(here we must make use of the observation that since f is smooth and vanishes at both $x = 0$ and $y = 0$, it satisfies the sublinear estimate $|f| \le |y| o(1)_{x \to 0}$; see the proof of Lemma 13.1).

It is easy to see that all further approximations will have the same form, and so does the solution $x(t)$. Hence, we obtain

$$y(0) = e^{-\tau} d\,, \quad x(\tau) = e^{-\tau} d + d^{2n+1} \sigma_n \tau e^{-(n+1)\tau} + o(e^{-(n+1)\tau})\,.$$

Thus, denoting by $y_0 (\equiv y(0)/d)$, the coordinate of the initial point on S_0 and by $x_1 (\equiv x(\tau)/d)$, the coordinate of the point of intersection of the trajectory with S_1, we obtain the following formula for the *local map* T_0:

$$x_1 = y_0 + d^{2n} \sigma_n y_0^{n+1} |\ln y_0| + o(y_0^{n+1})\,.$$

A Taylor expansion for the global map $T_1 : S_1 \to S_0$ near the separatrix loop Γ can be written in the form

$$\bar{y}_0 = x_1 + s_2 x_1^2 + \cdots + s_m x_1^m + \cdots$$

(recall that we have assumed the first saddle value $s_1 = 0$, which is equivalent to $A \equiv \frac{d\bar{y}_0}{dx_1} = 1$). Let $s_2 = \cdots = s_{m-1} = 0$ and $s_m \neq 0$ for some m. In this case the Poincaré map $T = T_1 \circ T_0$ assumes the form

$$\bar{y}_0 = y_0 + \tilde{\sigma}_n y_0^{n+1} |\ln y_0| + s_m y_0^m + \cdots , \tag{13.1.17}$$

where $\tilde{\sigma}_n$ has the same sign as σ_n; the ellipsis denote terms of order higher than at least one of the two leading terms. Finally, if $m \leq n$ in (13.1.17), then $\bar{y}_0$ can be represented by:

$$\bar{y}_0 = y_0 + s_m y_0^m + \cdots ; \tag{13.1.18}$$

or by

$$\bar{y}_0 = y_0 + \tilde{\sigma}_n y_0^{n+1} |\ln y_0| + \cdots \tag{13.1.19}$$

if $n < m$.

It follows that the fixed point $y_0 = 0$ is stable if $s_m < 0$ in (13.1.18), or if $\tilde{\sigma}_n < 0$ in (13.1.19) (the latter condition is equivalent to $\sigma_n < 0$). Vice versa, the fixed point is unstable if s_m or, respectively, σ_n, is positive.

Thus, we arrive at the following result. Consider the series

$$\sigma_0, s_1, \sigma_1, \ldots, s_n, \sigma_n, s_{n+1}, \ldots . \tag{13.1.20}$$

called *a Dulac sequence*. Suppose that not all entries in the sequence are vanishing. Then, the following theorem takes place:

Theorem 13.3. *The stability of a separatrix loop is determined by the first non-zero entry in a Dulac sequence*: *if the first non-zero entry is negative*, *then the loop is stable. Otherwise*, *if it is positive*, *then the loop is unstable.*

This theorem in the analytic case is due to Dulac. He had also shown that if the system is analytic and all entries of the sequence (13.1.20) are zero, then the system is integrable (Hamiltonian), and a small neighborhood U of the separatrix loop is filled by periodic orbits. These results had enabled Dulac to show that in the nondegenerate case of polynomial vector fields limit cycles cannot accumulate to a separatrix loop.

13.2. Bifurcation of a limit cycle from a separatrix loop of a saddle with non-zero saddle value

Two-dimensional systems having a separatrix loop to a saddle with non-zero first saddle value σ_0 form a bifurcation set of codimension one. Therefore, we can study such homoclinic bifurcations using one-parameter families.

Consider a continuous one-parameter family X_μ of $\mathbb{C}^r$-smooth ($r \geq 1$) systems on a plane which have a saddle equilibrium state O_μ. Suppose that at $\mu = 0$, the system has a separatrix loop of the saddle; i.e. the separatrix Γ_1^- coincides with the separatrix Γ_1^+ at $\mu = 0$.

We assume that the family X_μ is defined in such a way that for $\mu \neq 0$, the loop may be broken and split so that if $\mu > 0$, the unstable separatrix $\Gamma_1^-(\mu)$ goes inwards the loop and enters the inner neighborhood U as $t \to +\infty$; and if $\mu < 0$, it goes outwards, i.e. it gets into the outer neighborhood V.

Theorem 13.4. (Andronov and Leontovich) *Let $\sigma_0 \neq 0$.*

(1) *If $\sigma_0 < 0$, then for sufficiently small $\mu > 0$, there exists a unique stable limit cycle $L(\mu)$ in U which as $\mu \to +0$ gets closer to the saddle and becomes the separatrix loop at $\mu = 0$ (see Fig. 13.2.1). When $\mu < 0$, there are no limit cycles.*

(2) *If $\sigma_0 > 0$, then for sufficiently small $\mu < 0$ there exists a unique unstable cycle $L(\mu)$ in U which becomes the separatrix loop $\bar{\Gamma}$ as $\mu \to -0$ (see Fig. 13.2.2). When $\mu > 0$, there are no limit cycles.*

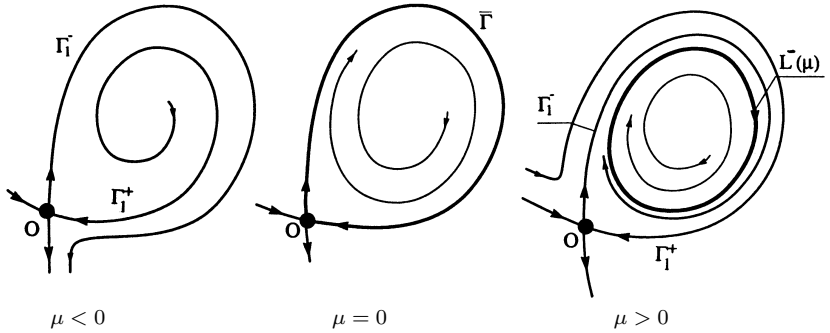

Fig. 13.2.1. Planar bifurcation of a stable separatrix loop of a saddle with $\sigma_0 < 0$.

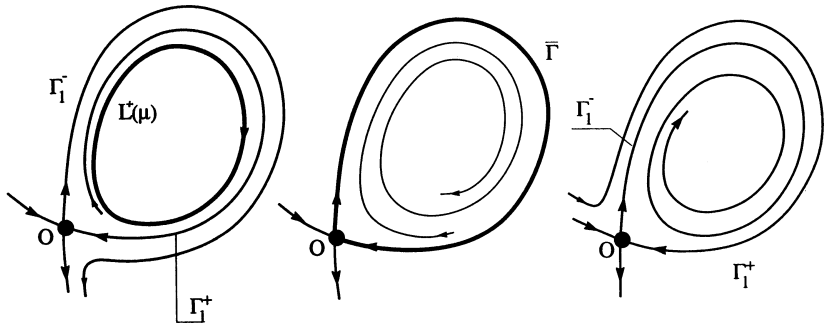

Fig. 13.2.2. Bifurcation of an unstable separatrix loop of a saddle with $\sigma_0 > 0$ in $\mathbb{R}^2$.

Remark 1. It is obvious that the case $\sigma_0 > 0$ reduces to the case $\sigma_0 < 0$ by a reversion of the time variable $t \to -t$. Therefore, the second part of the above theorem follows immediately from its first part.

Remark 2. The proof by Andronov and Leontovich was given under the assumption that the system is $\mathbb{C}^1$-smooth. This was in fact the first example where the vector fields had been required to possess only a minimal degree of smoothness. We will see later that the possibility to work with the case of low smoothness will become especially relevant for the analysis of the multi-dimensional case.

The original proof of the Andronov-Leontovich theorem assumes that the system is defined on the plane. We choose here a somewhat different approach which can be easily adopted to the case of systems defined on non-orientable two-dimensional surfaces as well.

Let us introduce coordinates (x, y) near the saddle O. Without loss of generality we may assume that the saddle resides at the origin for all μ. We may also assume that the unstable separatrices are tangent at O to the y-axis and the stable separatrices are tangent to the x-axis. Thus, the system can be written in the following form

$$\begin{aligned} \dot{x} &= \lambda(\mu)x + p(x, y, \mu) \equiv P(x, y, \mu) \\ \dot{y} &= \gamma(\mu)y + q(x, y, \mu) \equiv Q(x, y, \mu) \end{aligned} \tag{13.2.1}$$

where p and q vanish at the origin along with their derivatives with respect to (x, y); the characteristic exponents $\lambda(\mu)$ and $\gamma(\mu)$ are such that

$\lambda(\mu) < 0 < \gamma(\mu)$. By definition, the saddle value is given by

$$\sigma_0(\mu) = \lambda(\mu) + \gamma(\mu)\,.$$

Let the separatrix Γ_1^+ enter the saddle from the half-plane $x > 0$, and let the separatrix Γ_1^- leave O towards positive values of y. Since we have not yet straightened the invariant manifolds, the local equations of Γ_1^+ and Γ_1^- are given by, respectively,

$$y = \varphi(x,\mu)\,, \quad x > 0\,, \quad \text{and} \quad x = \psi(y,\mu)\,, \quad y > 0\,,$$

where φ and ψ vanish at the origin along with their derivatives with respect to x and y.

Let us choose a small positive d and consider two cross-sections $S_0 : \{x = d\}$ and $S_1 : \{y = d\}$. Just like in the previous section, we are going to reduce our problem to a study of the Poincaré map $T : S_0 \to S_0$ formed by a composition of the local map $T_0 : S_0 \to S_1$ and the global map $T_1 : S_1 \to S_0$, both defined by the trajectories of the system.

As in the preceding section, the flight time of a nearby trajectory from S_1 to S_0 along the separatrix loop is bounded. Therefore, the global map T_1 is a diffeomorphism of a small neighborhood of the point $M^- = \Gamma_1^- \cap S_1$ into a small neighborhood of the point $M^+ = \Gamma_1^+ \cap S_0$. By our assumption, $T_1 M^- = M^+$ at $\mu = 0$. Thus, the map T_1 is written as

$$\bar{y}_0 - y^+ = a(\mu) + A(\mu)(x_1 - x^-) + o(x_1 - x^-)\,. \tag{13.2.2}$$

Here we denote the coordinate on S_1 by x_1 and the coordinate on S_0 by y_0; then, the x-coordinate of M^- is $x^- = \psi(d,\mu)$ and the y-coordinate of M^+ is $y^+ = \varphi(d,\mu)$. The coefficient $A(\mu)$ is non-zero because T_1 is a diffeomorphism. Moreover, $A > 0$ (always) for systems defined on the plane.

The term $a(\mu)$ governs the splitting of the separatrix loop (see Fig. 13.2.3): it follows from (13.2.2) that $a(\mu)$ is equal to the difference between the y-coordinates of the points M^+ and $T_1 M^-$ (the latter is the point where the unstable separatrix Γ_1^- first intersects S_0). By assumption, the separatrix splits inwards for $\mu > 0$, and outwards for $\mu < 0$. Thus, sign $a(\mu) =$ sign μ.

Let us now study the local map T_0. It maps the interval $y_0 > y^+$ on the cross-section S_0 into the interval $x_1 > x^-$ on S_1. Let us represent this map as

$$x_1 - x^- = \eta(y_0 - y^+, \mu)\,. \tag{13.2.3}$$

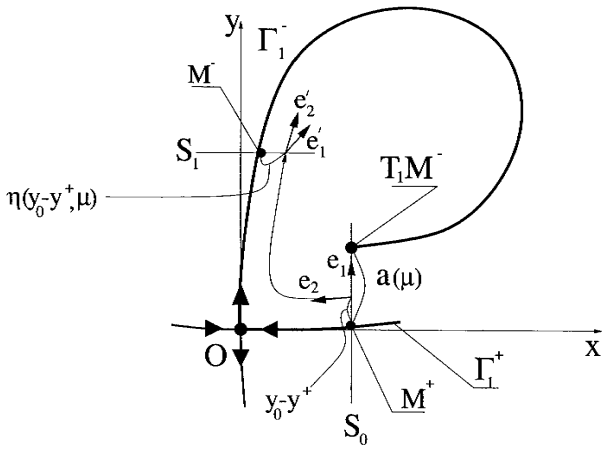

Fig. 13.2.3. An illustration to Theorem 13.4.

We also denote by $\tau(y_0, \mu)$ the flight time from the point (d, y_0) on S_0 to the point $(\eta(y_0 - y^+, \mu), d)$ on S_1. Obviously, $\eta(y_0 - y^+, \mu) \to 0$ and $\tau(y_0, \mu) \to +\infty$ as $y_0 \to y^+$.

Lemma 13.3. *The map T_0 is contracting if $\sigma_0 = \lambda + \gamma < 0$ and expanding if $\sigma_0 = \lambda + \gamma > 0$. Furthermore,*

$$\lim_{y_0 \to y^+} \frac{\partial \eta}{\partial y_0} = \begin{cases} 0 & \text{for } \sigma_0 < 0 \\ +\infty & \text{for } \sigma_0 > 0 \end{cases} \tag{13.2.4}$$

uniformly for all small μ.

Proof. It suffices to consider the case $\sigma_0 < 0$ (the case $\sigma_0 < 0$ is reduced to this one by a reversion of time). The idea of the proof is relatively simple: since we assume that the divergence of the vector field at O is negative, it is also negative in a small neighborhood of O. This implies that the flow near O contracts areas. The latter immediately implies that the Poincaré map between any two cross-sections is indeed a contraction.

Let us be more precise. Denote by $u(t)$ the derivative of the solution $(x(t), y(t))$ of the system (13.2.1) with respect to initial conditions (x_0, y_0). This is a matrix which satisfies the variational equation

$$\dot{u} = \begin{pmatrix} P_x & P_y \\ Q_x & Q_y \end{pmatrix}_{\substack{x=x(t) \\ y=y(t)}} u$$

with the initial condition $u(0) = I$. Therefore, the determinant of u satisfies the following equation

$$\frac{d}{dt}\det u = \operatorname{tr}\begin{pmatrix} P_x & P_y \\ Q_x & Q_y \end{pmatrix}\det u$$

which yields

$$\det u(t) = e^{\int_0^t (\lambda+\gamma+P_x(x(s),y(s))+Q_y(x(s),y(s)))ds}\,.$$

Since we assume that $\lambda+\gamma < 0$ and that the derivatives of P and Q vanish at O, it follows that the determinant of u decreases exponentially all the time until the trajectory $(x(t), y(t))$ stays in a small neighborhood of O:

$$\det u(t) \le e^{\bar\sigma t} \tag{13.2.5}$$

for some $\bar\sigma < 0$. This means indeed that the flow defined by system (13.2.1) contracts areas exponentially; namely, for any two vectors e_1 and e_2

$$[u(t)e_1, u(t)e_2] = \det u(t)[e_1, e_2] \le e^{\bar\sigma t}[e_1, e_2]\,, \tag{13.2.6}$$

where $[e_1, e_2]$ denotes the area of the parallelogram spanned by e_1 and e_2, and $[u(t)e_1, u(t)e_2]$ is the area of the parallelogram spanned by the images of e_1 and e_2 by the linearized flow.

Another fact we need is (see Sec. 3.11) that the matrix $u(t)$ takes the phase velocity vector at the point (x_0, y_0) into the phase velocity vector at the point $(x(t), y(t))$:

$$\begin{pmatrix} P(x(t),y(t)) \\ Q(x(t),y(t)) \end{pmatrix} = u(t)\begin{pmatrix} P(x_0,y_0) \\ Q(x_0,y_0) \end{pmatrix}. \tag{13.2.7}$$

Let us now choose a point $(x_0 = d, y_0)$ on the cross-section S_0. Its orbit hits S_1 at a point $(x(\tau) = \eta(y_0 - y^+)\,, y(\tau) = d)$ at some time $\tau(y_0)$. The derivative $\eta'(y_0 - y^+)$ is given by

$$\eta'(y_0 - y^+) = \frac{\partial x(\tau)}{\partial y_0} + \dot x(\tau)\tau'(y_0)\,,$$

where $\tau'(y_0)$ is found from the condition

$$\frac{\partial y(\tau)}{\partial y_0} + \dot y(\tau)\tau'(y_0) = 0\,.$$

Hence it follows that

$$\eta'(y_0 - y^+)\dot{y}(\tau) = [e_1', e_2'] = [u(\tau)e_1, u(\tau)e_2] \le e^{\bar{\sigma}\tau}|\dot{x}(0)|\,, \tag{13.2.8}$$

where $e_1 = (0,1)$ (the unit vector parallel to S_0), $e_1' = (\frac{\partial x(\tau)}{\partial y_0}, \frac{\partial y(\tau)}{\partial y_0})$ [recall that it is equal to $u(\tau)e_1$ by definition of $u(t)$) and e_2 and e_2' are the phase velocity vectors at the points (x_0, y_0) and $(x(\tau), y(\tau)]$, respectively:

$$e_2 = (\dot{x}(0), \dot{y}(0)) \equiv (P(x_0, y_0), Q(x_0, y_0))\,,$$

and

$$e_2' = (\dot{x}(\tau), \dot{y}(\tau)) \equiv (P(x(\tau), y(\tau)), Q(x(\tau), y(\tau)))\,,$$

where we have used relations (13.2.6) and (13.2.7) in deriving (13.2.8).

Observe now that since $y(\tau) = d$, it follows that $\dot{y}(\tau)(= \gamma d + q(x(\tau), d))$ is bounded away from zero. Hence, by (13.2.8)

$$\eta'(y_0 - y^+) = O(e^{\bar{\sigma}\tau})\,,$$

which gives the lemma because $\tau(y_0) \to +\infty$ as $y_0 \to y^+$, and because $\bar{\sigma} < 0$ due to the assumption $\lambda + \gamma < 0$. End of the proof.

Thus, denoting $v = y_0 - y^+$ we have from (13.2.2) and (13.2.3) that the Poincaré map $T : S_0 \to S_0$ can be written in the form

$$\bar{v} = a(\mu) + A(\mu)\eta(v, \mu) + o(\eta)\,, \quad v > 0\,, \tag{13.2.9}$$

where $a(\mu)$ is the splitting parameter of the separatrices Γ_1^- and Γ_1^+ and η is an increasing function which is either strongly contracting ($\lambda + \gamma < 0$) or strongly expanding ($\lambda + \gamma > 0$). Recall that $a(\mu)$ has the same sign as μ (in general, $a(\mu)$ is proportional to μ, but we do not use this property).

The analysis of such maps is obvious. The associated Lamerey diagrams are shown in Figs. 13.2.4 ($\lambda + \gamma < 0$) and 13.2.5 ($\lambda + \gamma > 0$). When $\lambda + \gamma < 0$, the fixed point $v^*(\mu)$ of the map exists for $\mu \ge 0$ only. It corresponds to the limit cycle $L^-(\mu)$ for $\mu > 0$ and to the separatrix loop at $\mu = 0$ [formally, the map T is not defined at $v = 0$, but we define it by continuity, assuming $T(M^+) = T_1(M^-)$]. Since the map T is a contraction, the fixed point is stable (one-side stable at $\mu = 0$). Correspondingly, $L^-(\mu)$ is a stable cycle and the loop Γ is also stable (this generalizes Theorem 13.1.1 of the preceding section

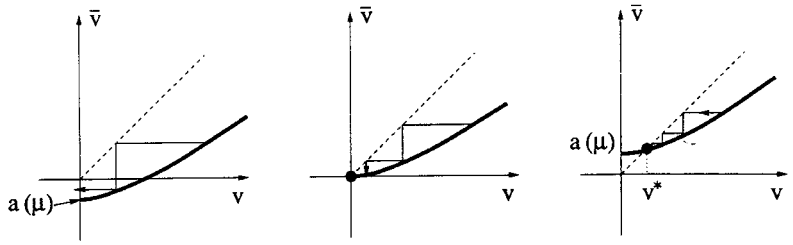

$\mu < 0$ $\mu = 0$ $\mu > 0$

Fig. 13.2.4. Lamerey diagram of the Poincaré map corresponding to the bifurcation in Fig. 13.2.1.

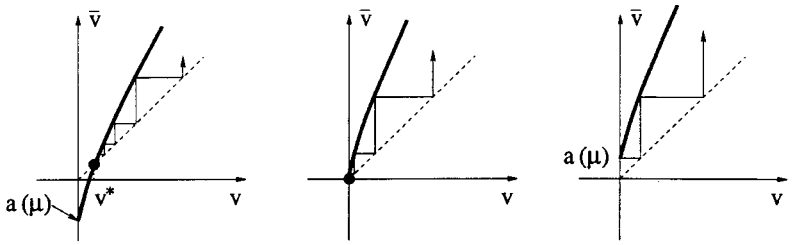

$\mu < 0$ $\mu = 0$ $\mu > 0$

Fig. 13.2.5. Lamerey diagram of the Poincaré map corresponding to the bifurcation in Fig. 13.2.2.

for the $\mathbb{C}^1$-case). Note that for $\mu > 0$, the separatrix $\Gamma_1^-(\mu)$ tends to $L^-(\mu)$ as $t \to +\infty$.

In the case $\lambda + \gamma > 0$, the fixed point $v^*(\mu)$ is unstable and exists for $\mu \le 0$ only. It corresponds to the unstable limit cycle $L^+(\mu)$ for $\mu < 0$ and to the separatrix loop at $\mu = 0$, respectively.

Remark 3. When the system is at least $\mathbb{C}^2$-smooth one may introduce local coordinates near O (see Lemma 13.1) so that

$$\eta(v) = v^{\nu(\mu)} + o(v^{\nu(\mu)}),$$

where $\nu = |\lambda/\gamma|$ is the saddle index. In this case the fixed point of the map (13.2.9) satisfies the following relation:

$$v^* = a(\mu) + A(\mu)(v^*)^{\nu(\mu)} + \cdots,$$

whence we have

$$v^*(\mu) \sim \begin{cases} a(\mu) & \text{for } \lambda + \gamma < 0 \\ \left(-\dfrac{a(\mu)}{A(\mu)}\right)^{\frac{1}{\nu(\mu)}} & \text{for } \lambda + \gamma > 0\,. \end{cases} \tag{13.2.10}$$

Remark 4. The above proof can be easily adopted to the case of a separatrix loop on a general two-dimensional surface, regardless whether it is orientable or non-orientable. In both cases the map will have the form (13.2.9). Note, however, that if a small neighborhood of the separatrix loop is homeomorphic to an annulus, then $A > 0$; and if a neighborhood of $\bar{\Gamma}$ is a Möbius band, then $A < 0$ (the latter corresponds, obviously, to the non-orientable case). In the case $A > 0$, the Andronov-Leontovich theorem holds without changes.

Let us now consider the case $A < 0$ in more detail. First, let us examine the associated Lamerey diagram (Fig. 13.2.6) with $A < 0$ when $\nu > 1$ ($\lambda + \gamma < 0$). Just as in the orientable case, a stable fixed point exists for $\mu > 0$: indeed, the map T is decreasing and contracting, so the interval $[0, a(\mu) = T(0)]$ is mapped into the inside itself by T, which implies the existence of a unique stable fixed point on this interval by virtue of the Banach contraction mapping principle.

The Lamerey diagram corresponding to the case $\nu(\mu) < 1$ is shown in Fig. 13.2.7. Here, in contrast to the orientable case, an unstable fixed point $v^*(\mu)$ exists for $\mu > 0$.

Note that in the orientable case ($A > 0$), the separatrix loop at $\mu = 0$ is a limit trajectory (ω-limit if $\nu > 1$, or α-limit if $\nu < 1$) for nearby trajectories from the inner neighborhood U. On the contrary, in the non-orientable case

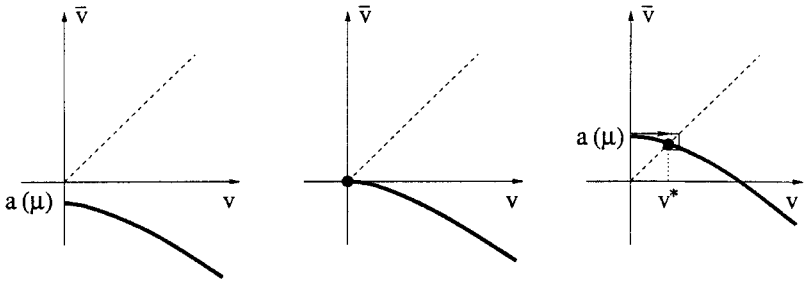

$\mu < 0$ $\mu = 0$ $\mu > 0$

Fig. 13.2.6. Lamerey diagram of the Poincaré map for the non-orientable separatrix loop with $\sigma_0 < 0$.

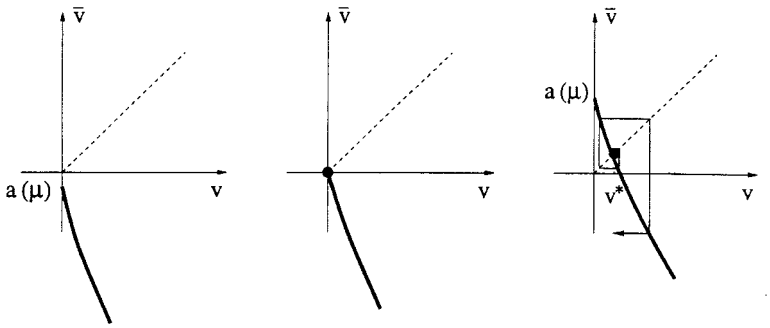

Fig. 13.2.7. Lamerey diagram for the non-orientable separatrix loop to a saddle with $\sigma_0 > 0$.

($A < 0$), each point of Γ is non-wandering but it cannot be a limit point. This shows that while limit points are non-wandering (see Chap. 8), the converse is not true.

Remark 5. The splitting parameter $a(\mu)$ may be an arbitrary continuous function of μ satisfying the above sign condition. When the system depends on μ smoothly, the family X_μ is transverse to the bifurcation surface if $a'(0) \neq 0$. In this case, one can always assume that $a(\mu) \equiv \mu$.

Remark 6. It follows from the above analysis that all properties of the Poincaré map of the transverse family X_μ are exhibited by the simplified map

$$\bar{y} = \mu \pm y^\nu \,, \tag{13.2.11}$$

where $\nu \neq 1$. The sign "+" corresponds to the orientable case, and the sign "−" corresponds to the non-orientable case. In essence, the map (13.2.11) is a kind of a normal form of the Poincaré map near a separatrix loop with non-zero saddle value.

We can now discuss the bifurcation of an equilibrium state with two zero characteristic exponents. This bifurcation is worth being distinguished because its analysis includes nearly all bifurcations of codimension one.

In general, system on the center manifold near an equilibrium state $(0, 0)$ with a couple of zero characteristic exponents can be represented by

$$\begin{aligned} \dot{x} &= y + g(x, y) \,, \\ \dot{y} &= f(x, y) \,, \end{aligned}$$

where f and g vanish at the origin along with their first derivatives. Note that we assume that the linearization matrix at the origin has a Jordan box. In this case, we may introduce $y + g(x, y)$ as a new y-variable and recast the system into the form

$$\begin{aligned} \dot{x} &= y\,, \\ \dot{y} &= ax^2 + bxy + h(x, y)\,, \end{aligned} \tag{13.2.12}$$

where $h(x, y)$ is of third order of smallness.

Let us suppose that the coefficients a and b do not vanish. One can now rescale the phase and time variables so that the system assumes the form

$$\begin{aligned} \dot{x} &= y\,, \\ \dot{y} &= x^2 \pm xy + \tilde{h}(x, y)\,, \end{aligned} \tag{13.2.13}$$

where the sign "+" corresponds to $b > 0$, and the sign "−" corresponds to $b < 0$. Observe that the transformation $t \to -t,\ y \to -y$ reduces the first case to the second one. Let us choose the sign "−" in front of xy in (13.2.13).

The behavior of trajectories of system (13.2.13) near $O(0, 0)$ is shown in Fig. 13.2.8. To investigate the bifurcations near this point let us consider a two-parameter family which can be written in the following form:

$$\begin{aligned} \dot{x} &= y\,, \\ \dot{y} &= \mu_1 + \mu_2 x + x^2 - xy + \tilde{h}(x, y, \mu)\,. \end{aligned} \tag{13.2.14}$$

The bifurcation diagram and the corresponding phase portraits are shown in Fig. 13.2.9. The bifurcational curves $L_1, \ldots, L_4$ partition the (μ_1, μ_2)-plane into four regions $D_1, \ldots, D_4$. Since there are no equilibrium states in the region D_1, all trajectories leave a neighborhood of the origin in the phase space as $t \to \pm\infty$. When moving from D_1 across the curves $L_1 : \{\mu_1 = \mu_2^2/4 + \cdots, \mu_2 > 0\}$, or $L_4 : \{\mu_1 = \mu_2^2/4 + \cdots, \mu_2 < 0\}$, there arises a saddle-node equilibrium state. This saddle-node is simple in the sense that the first Lyapunov value l_2 is non-zero on L_1 and L_4. However, there is a difference in the trajectory behavior on these curves: on L_1 the saddle-node is unstable in the node region, whereas on L_4 it is stable in the node region. Upon crossing L_1, the saddle-node is decomposed into an unstable node and a saddle. As the parameter varies further, the node becomes an unstable focus, as shown in Fig. 13.2.9 (region D_2). On the curve $L_2 : \{\mu_1 = -6/25\mu_2^2 + o(\mu_2^2),\ \mu_2 < 0\}$ the system has a stable separatrix loop. Therefore, in the region D_3, there is a

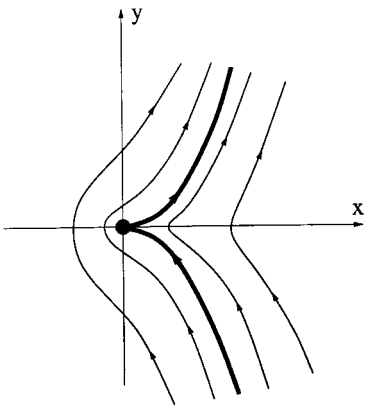

Fig. 13.2.8. Behavior of trajectories near an equilibrium state with two zero characteristic exponents.

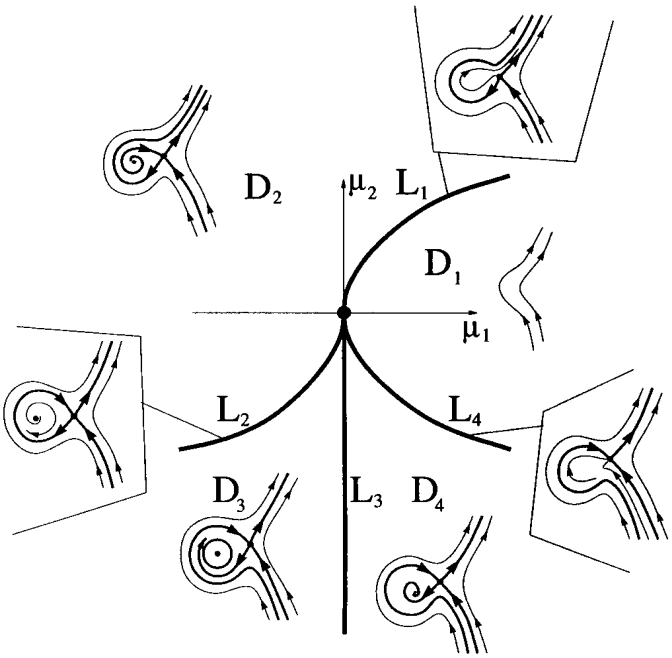

Fig. 13.2.9. Bifurcation diagram of the Bogdanov-Takens point in the (μ_1, μ_2)-parameter plane.

stable limit cycle born from the separatrix loop. The focus becomes weak on the curve $L_3 : \{\mu_1 = 0,\ \mu_2 < 0\}$; it has a pair of purely imaginary eigenvalues. The associated Lyapunov value is negative on L_3. When moving from D_3 to D_4, the stable cycle collapses into a weak focus and disappears via a supercritical Andronov-Hopf bifurcation on the curve L_3, so that the focus inherits the stability of the stable limit cycle. Near the curve L_4, the stable focus transforms into a stable node, and merges with the saddle on the curve L_4. Both equilibrium states disappear in region D_1.

The asymptotics of curves L_1, L_3, L_4 come from the analysis of the linearization of system (13.2.14) at the equilibrium states. The existence of the curve L_2 corresponding to the separatrix loop is necessary for the completeness of the bifurcation puzzle; the stable cycle generating from the weak focus on the curve L_3 must disappear in the loop (when moving towards L_2).

The asymptotics for the curve L_2 may be found as follows. Assume $\mu_1 < 0$ in (13.2.14). Upon rescaling variables and time: $x \to x\sqrt{|\mu_1|}$, $y \to y|\mu_1|^{3/4}$, $t \to t/|\mu_1|^{1/4}$, the system takes the form

$$\begin{aligned} &\dot{x} = y\,, \\ &\dot{y} = -1 + Cx + x^2 - \varepsilon xy + o(\varepsilon)\,, \end{aligned} \tag{13.2.15}$$

where $C = \mu_2/\sqrt{|\mu_1|}$ and $\varepsilon = |\mu|^{1/4}$. At $\varepsilon = 0$, this system becomes a Hamiltonian system with the first integral

$$H = \frac{y^2}{2} + x - \frac{1}{2}Cx^2 - \frac{1}{3}x^3\,.$$

It has a saddle equilibrium at $x = x_0 = -\frac{1}{2}C + \frac{1}{2}\sqrt{C^2+4}$ (and $y = 0$) with a separatrix loop which is a component of the level set of the integral H; namely, $\Gamma = \{H(x,y) = H(x_0,0),\ x < x_0\}$. For arbitrarily small non-zero ε, this system is no longer Hamiltonian, and H is no longer its first integral because $\dot{H} \neq 0$ at $\varepsilon = 0$. The loop is split, in general. It is sufficiently obvious that if for some C

$$\frac{\partial}{\partial\varepsilon}\int_{-\infty}^{+\infty}\frac{d}{dt}H(x(t),y(t))dt\bigg|_{\varepsilon=0} \neq 0\,,$$

then the loop is split for sufficiently small $\varepsilon \neq 0$ (here, $(x = x(t), y = y(t))$ yields the homoclinic trajectory at $\varepsilon = 0$). By virtue of system (13.2.15), this inequality can be rewritten as

$$\int_{x_1}^{x_0} xy(x)dx \neq 0\,,$$

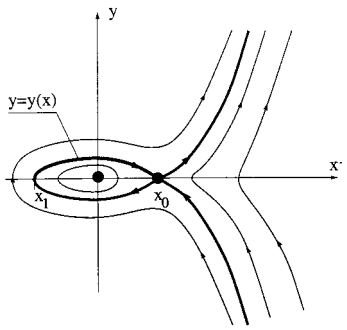

Fig. 13.2.10. The phase portrait of the associated Hamiltonian system with the loop at the level $H(x,y) = H(x_0,0)$.

where x_1 is the point of intersection of the loop Γ with the x-axis, $H(x_0,0) = H(x_1,0)$; and $y = y(x)$ is the equation of Γ, i.e. $H(x,y(x)) = H(x_0,0)$, see Fig. 13.2.10. Thus, the above inequality reduces to

$$\int_{x_1}^{x_0} x(x_0 - x)\sqrt{x - x_1}dx \neq 0\,,$$

which can be easily solved, thereby giving $C \neq C^* = -5/\sqrt{6}$. These values of C correspond to splitting the loop for non-zero ε. On the other hand, one may prove that there is a curve $C = C^* + O(\varepsilon)$ which corresponds to the existence of a separatrix loop for $\varepsilon \neq 0$. Returning to the (μ_1,μ_2)-plane gives the required asymptotic for the curve L_2: $\{\mu_2 = -5/\sqrt{6}\sqrt{|\mu_1|}\}$.

This bifurcation diagram for the equilibrium state with two zero characteristic exponents had been known for a long time. However, there remained a problem of proving *the uniqueness* of the limit cycle. In other words, one must prove additionally that there are no other bifurcational curves besides $L_1,\ldots,L_4$ (namely, curves corresponding to semi-stable limit cycles). This problem was independently solved by Bogdanov [33] and Takens [146] with whom this bifurcation is often named after.

13.3. Bifurcations of a separatrix loop with zero saddle value

The question of the bifurcations of a separatrix loop to a saddle with zero saddle value σ_0 was first considered by E. Leontovich. She had proven the following theorem:

Theorem 13.5. (Leontovich) *If*

$$\sigma_0 = s_1 = \cdots = s_{n-1} = \sigma_{n-1} = 0\,, \quad s_n \neq 0$$

in the Dulac sequence, then no more than $2n$ *limit cycles can bifurcate from a separatrix loop of the saddle.*
If

$$\sigma_0 = s_1 = \cdots = s_n = 0\,, \quad \sigma_n \neq 0\,,$$

then the number of limit cycles which can be spawned from the separatrix loop does not exceed $2n+1$. *These estimates are sharp*, i.e., *one may perturb the system so that the resulting system will have, respectively,* $2n$ *or* $2n+1$ *limit cycles.*

In her proof of the above theorem, Leontovich had assumed $\mathbb{C}^r$-smoothness for the system, where $r \geq 4n+6$. First of all, she proved that when the first saddle value is close to zero, a system near the saddle can be transformed into

$$\begin{aligned} &\dot{x} = -x(1+\varepsilon - \sigma_1 xy - \cdots - \sigma_n (xy)^n - (xy)^{n+1} F(x,y))\,, \\ &\dot{y} = y\,, \end{aligned} \tag{13.3.1}$$

where $1+\varepsilon = \nu$ is the saddle index, σ_i are the saddle values, F is a smooth function. It is assumed that $n|\varepsilon| < 1$. The coordinate transformation is constructed in the same way as in the case $\varepsilon = 0$ (see Lemma 13.2); the only difference is that the formulas (13.1.14) are modified as follows:

$$\begin{aligned} \alpha(x) &= \frac{1}{1+\varepsilon}\int_0^1 \phi_1(xs)\frac{ds}{s^{1-(k+1)\varepsilon}}\,, \\ \beta(y) &= \int_0^1 \phi_2(ys)\frac{ds}{s^{1+(k+1)\varepsilon}}\,. \end{aligned} \tag{13.3.2}$$

One can trace through the proof of Lemma 13.2 that the coordinate transformation is $\mathbb{C}^{r-(2n+1)}$ and the function F is $\mathbb{C}^{r-(2n+3)}$-smooth.

On the next step of the proof Leontovich had evaluated the local map. She considered, in fact, the map from the cross-section $S_1 : \{y = d\}$ to $S_0 : \{x = d\}$, i.e. the inverse of the local map T_0 in our notations. Note that by assumption of the theorem only the last saddle value σ_n is bounded away from zero, whereas $\sigma_1, \ldots, \sigma_{n-1}$ are small. Therefore, by rescaling time variable the system may

be rewritten in the form

$$\begin{aligned} \dot{x} &= -x\,, \\ \dot{y} &= y(1+\tilde{\varepsilon}+\tilde{\sigma}_1 xy+\cdots+\tilde{\sigma}_n(xy)^n+(xy)^{n+1}\tilde{F}(x,y))\,, \end{aligned} \tag{13.3.3}$$

where the coefficients $\tilde{\varepsilon}$ and $\tilde{\sigma}_1,\dots,\tilde{\sigma}_{n-1}$ are small and $\tilde{\sigma}_n$ is bounded away from zero. Leontovich showed that the map T_0^{-1} for the system (13.3.3) has the form[3]

$$y_0 = x_1+\tilde{\varepsilon}[\theta x_1+\psi_1(x_1)]+\tilde{\sigma}_1[\theta x_1^2+\psi_2(x_1)]+\cdots+\tilde{\sigma}_n[\theta x_1^{n+1}+\psi_{n+1}(x_1)]\,, \tag{13.3.4}$$

where

$$\theta = \frac{x_1^{\tilde{\varepsilon}}-1}{\tilde{\varepsilon}}\,,$$

and $\psi_k = O(x_1^{k+\delta})$ for some $\delta > 0$ (moreover, the jth derivative of ψ_k is estimated as $O(x_1^{k-j+\delta})$ for $j = 1,\dots,2n+1$).

The Taylor expansion for the global map $T_1 : S_1 \to S_0$ is represented by

$$\bar{y}_0 = \mu + x_1 e^{s_1} + s_2 x_1^2 + \cdots + s_n x_1^n + O(x_1^{n+1})\,, \tag{13.3.5}$$

where μ is the small splitting parameter and $s_1,\dots,s_n$ are the separatrix values. By assumption of the theorem, $s_1,\dots,s_{n-1}$ are small. The nth separatrix value s_n is bounded away from zero in the first case of the theorem and it is small in the second case.

If the system has a limit cycle, the x_1-coordinate of its intersection with S_1 satisfies $T_0^{-1}(x_1) = T_1(x_1)$. Therefore, the problem of the number of limit cycles is reduced here to the problem on the number of zeros of the smooth (at least $\mathbb{C}^{2n+1}$) quasi-polynomial

$$\begin{aligned} G(x_1) = &-\ \mu\ +[\tilde{\varepsilon}(\theta x_1+O(x_1^{1+\delta}))-x_1(e^{s_1}-1)] \\ &+\ [\tilde{\sigma}_1(\theta x^2+O(x^{2+\delta}))-s_2x^2] \\ &+\ [\tilde{\sigma}_{n-1}(\theta x_1^n+O(x_1^{n+\delta}))-s_nx_1^n]+\tilde{\sigma}_n[\theta x^{n+1}+O(x^{n+1})]\,. \end{aligned} \tag{13.3.6}$$

(where δ is not necessarily an integer). While proving the theorem, Leontovich developed a calculus of quasi-polynomials of the above kind which allowed her to show that for small μ, $\tilde{\varepsilon}$, $s_1,\dots,\tilde{\sigma}_{n-1}$, the function G cannot have more than

[3]This formula can be derived by applying the boundary-value problem method as in the proof of Theorem 13.3.

$2n$ zeros for small x_1 if s_n is bounded away from zero, or more than $2n+1$ zeros if s_n is small.

To finish the proof, one must also prove the "sharpness" of this estimate. To do this, Leontovich presented a very detailed construction of the perturbed system with the given number of limit cycles.

Note that she did not use finite-parameter families. Nevertheless, it is understood that an appropriate transverse family can be found such that the governing parameters are $\mu, \varepsilon, s_1, \sigma_1, \dots, \sigma_{n-1}$ in the first case of Theorem 13.5, or $\mu, \varepsilon, s_1, \sigma_1, \dots, s_n$ in the second case.

Our review of the proof of this theorem is, of course, too narrative. The original proof by Leontovich, consisting of two large parts, had been stored at the VINITI archive in Moscow, and was therefore available only to researchers from the Soviet Union. More than thirty years later, Roussarie had published an independent proof of the above estimate for the number of bifurcating periodic orbits but without proving its "sharpness". The reader interested in further details is referred to the review [73]. In the spirit of this review, the Leontovich theorem can be rephrased as follows: *in a generic p-parameter family of smooth vector fields on the plane the number of limit cycles bifurcating from a separatrix loop to a rough saddle does not exceed p. Moreover, this estimate is sharp.*

Let us now consider the case of codimension two in more detail. Recall that this case is distinguished by two conditions: the first is the existence of a separatrix loop, and the second condition is the vanishing of the first saddle value σ_0 while the first separatrix value s_1 is non-zero. The latter is equivalent to $A \neq 1$. We will assume that $A < 1$ because the case $A > 1$ follows directly by a reversion of time.

It follows from the results of Sec. 13.8 (see formulas (13.8.30)–(13.8.32)) that the local map T_0 can be written as

$$\bar{x}_1 = y_0^{\nu} + \varphi(y_0)$$

in some $\mathbb{C}^{r-1}$-coordinates; here ν is the saddle index which equals to 1 at the bifurcation point. The function φ satisfies the estimates

$$\begin{aligned} \varphi(y) &= o(y^{1+\delta})\,, \\ \varphi^{(s)}(y) &= o(y^{1-s+\delta}) \quad (s = 1, \dots, r-2)\,, \\ \varphi^{(r-1)}(y) &= o(y^{\nu-(r-1)}) \end{aligned} \tag{13.3.7}$$

for some positive δ bounded away from zero.

Combining the above formula for the local map with the formula (13.3.5) (at $n = 1$) for the global map T_1, we obtain the equation

$$\bar{y} = \mu + A(\mu, \varepsilon)y^{1+\varepsilon} + \varphi(y), \quad y > 0\,, \tag{13.3.8}$$

for the Poincaré map $T = T_1 \circ T_0$, where $\nu = 1 + \varepsilon$, and φ is a new function which still satisfies (13.3.7). We will assume that the system is at least $\mathbb{C}^3$-smooth, so that the Poincaré map (13.3.8) is to be at least $\mathbb{C}^2$-smooth.

This map is a monotonically increasing (since $A > 0$ for systems on the plane) one-dimensional map. The only possible bifurcation occurring in such maps is the bifurcation of a fixed point with a multiplier equal to $+1$. The y-coordinate of such a point must satisfy

$$\begin{aligned} y &= \mu + A(\mu, \varepsilon)y^{1+\varepsilon} + o(y^{1+\delta})\,, \\ 1 &= (1 + \varepsilon)A(\mu, \varepsilon)y^{\varepsilon} + o(y^{\delta})\,. \end{aligned} \tag{13.3.9}$$

The right-hand side of the second equation is at least $\mathbb{C}^1$-smooth. So, the y-coordinate can be uniquely found from this equation when $\varepsilon < 0$:

$$y = e^{-1}A^{1/|\varepsilon|} + o(A^{(1+\delta)/|\varepsilon|})\,. \tag{13.3.10}$$

The second derivative of the map at this point is equal to

$$(1 + \varepsilon)A(\mu, \varepsilon)\varepsilon y^{\varepsilon-1} + o(y^{\varepsilon-1})\,,$$

and, obviously, it is non-zero. Therefore, the saddle-node fixed point is simple. By substituting (13.3.10) into the first equation in (13.3.9), we obtain the equation of the corresponding bifurcation curve L_1

$$\mu = \varepsilon e^{-1}A(0, \varepsilon)^{1/|\varepsilon|}[1 + o(1)]\,. \tag{13.3.11}$$

The bifurcation diagram is shown in Fig. 13.3.1. The curve L_1 corresponds to a semi-stable limit cycle. The curve L_2 (the negative ε-semi-axis) corresponds to a separatrix loop with a positive saddle value, whereas L_3 (the positive ε-semi-axis) corresponds to a separatrix loop with a negative saddle value. These curves divide a neighborhood of the origin on the parameter plane into three regions. In the region D_1, there are two limit cycles. Upon crossing L_1, they coalesce and disappear, so in the region D_2, there are no limit cycles. Upon moving from D_1 to D_3, a stable limit cycle bifurcates from

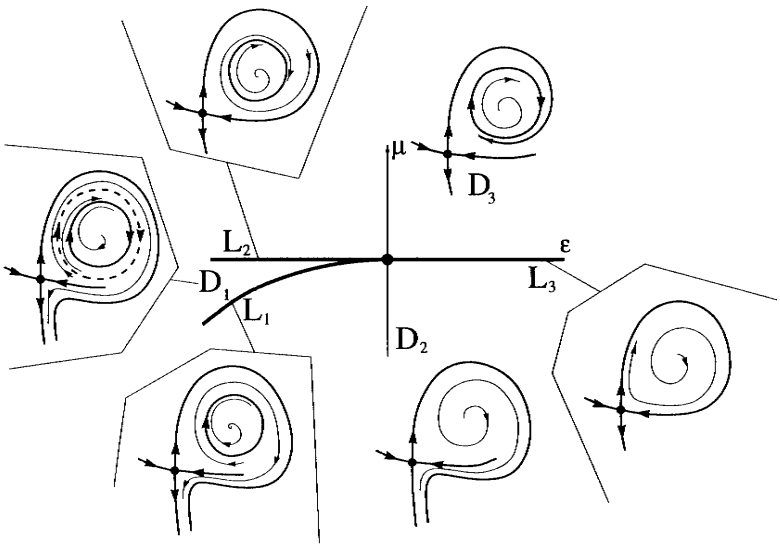

Fig. 13.3.1. Bifurcation diagram for the homoclinic loop to a saddle with zero saddle value ($\lambda + \gamma = 0$) in the orientable case ($0 < A < 1$). Parameter μ governs the splitting of the loop; the sign of ε is opposite to the sign of the saddle value.

the homoclinic loop on the curve L_3 ($\sigma_0 < 0$). The stable limit cycle exists for the parameter values from D_3, L_2 and D_1. Upon crossing the curve L_2 towards D_3, one more limit cycle, this time unstable, bifurcates from the homoclinic loop ($\sigma_0 > 0$). This bifurcation diagram is due to Nozdracheva [99].

Let us consider next the case where $-1 < A < 0$ which corresponds to a separatrix loop Γ on a non-orientable surface (the case $A < -1$ follows similarly by a reversion of time). A neighborhood of $\bar{\Gamma}$ is then a Möbius band whose median is $\bar{\Gamma}$. The Poincaré map in this case also has the form (13.3.8) with the function φ satisfying estimates (13.3.7). However, now we need more smoothness. So we assume that the system is at least $\mathbb{C}^4$-smooth, i.e. $r \geq 4$ in (13.3.7).

Since $A < 0$, the Poincaré map is decreasing. The new feature in this case is that such maps may have orbits of period two, which correspond to the so-called double limit cycles. They may appear via a period-doubling bifurcation (a fixed point with a multiplier equal to -1) or via a bifurcation of a double homoclinic loop. The latter corresponds to the period-two point of the Poincaré map at $y = 0$ (see Fig. 13.3.2).

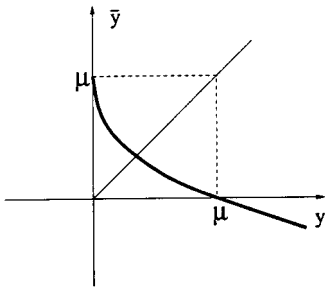

Fig. 13.3.2. Lamerey diagram corresponding to the double separatrix loop.

Since $T(0) = \mu$, the double loop occurs when

$$0 = \mu + A(\mu, \varepsilon)\mu^{1+\varepsilon} + o(\mu^{1+\delta})\,.$$

From this constraint we obtain the following equation for the bifurcational curve L_2 corresponding to a double loop:

$$\mu = |A(0, \varepsilon)|^{1/|\varepsilon|}[1 + o(1)]\,, \quad \varepsilon < 0\,. \tag{13.3.12}$$

Since $\varepsilon < 0$, the saddle value is positive, and hence the periodic orbit bifurcating from the separatrix loop is unstable here.

Observe that the curve L_2 lies above the curve L_1 defined by the system (see Fig. 13.3.3)

$$\begin{aligned} y &= \mu + A(\mu, \varepsilon)y^{1+\varepsilon} + o(y^{1+\delta})\,, \\ -1 &= (1+\varepsilon)A(\mu, \varepsilon)y^{\varepsilon} + o(y^{\delta}) \end{aligned} \tag{13.3.13}$$

which corresponds to the period-doubling bifurcation. Eliminating y from (13.3.13), we find that the curve L_1 is given by

$$\mu = \frac{2}{e}|A(0, \varepsilon)|^{1/|\varepsilon|}[1 + o(1)]\,, \quad \varepsilon < 0\,. \tag{13.3.14}$$

The bifurcation diagram (proposed in [38]) for this case is shown in Fig. 13.3.3. It includes the following four bifurcation curves:

- L_1 corresponds to a period-doubling bifurcation, i.e. to a structurally unstable limit cycle with one multiplier equal to -1 and a positive first Lyapunov value[4]

[4]To compute the Lyapunov value we need at least three derivatives of the function in the right-hand side of (13.3.8), and that is why we require $r \geq 4$ in (13.3.7).

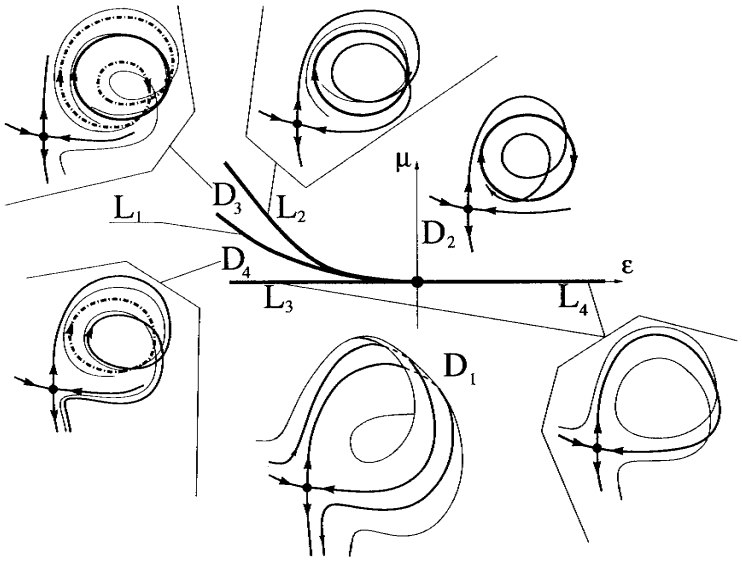

Fig. 13.3.3. Bifurcation diagram of the homoclinic loop to a saddle with zero saddle value in the non-orientable case ($-1 < A < 0$). The governing parameters are the same as in Fig. 13.3.1.

- L_2 corresponds to a "double" separatrix loop on the Möbius band. The saddle value σ_0 is positive on this curve;
- L_3 (the negative ε-semi-axis) corresponds to a simple separatrix loop with a positive saddle value σ_0; and
- L_4 (the positive ε-semi-axis) corresponds to a simple separatrix loop with a negative saddle value σ_0.

In the (μ, ε)-parameter plane thsese curves separate four regions of the structurally stable behavior of trajectories.

In the region D_1, there are no limit cycles. On the curve L_4, upon moving from D_1 towards D_2, a stable limit cycle is born from a simple separatrix loop. An unstable double-loop limit cycle bifurcates from a double separatrix loop with $\sigma_0 > 0$ on L_2. Thus, in the region D_3, there are two limit cycles: one stable and the other is unstable. The unstable double limit cycle merges with the stable limit cycle on the curve L_1. After that only one single-circuit unstable limit cycle remains in region D_4. It adheres into the homoclinic loop on the curve L_3.

Note that one must also prove that there are no other bifurcational curves in this bifurcation diagram; namely, that there may not be any saddle-node orbits of period two. An orbit (y_1, y_2) of period two of the map (13.3.8) must satisfy the equation

$$\begin{aligned} y_2 &= \mu + A(\mu,\varepsilon)y_1^{1+\varepsilon} + \varphi(y_1)\,, \\ y_1 &= \mu + A(\mu,\varepsilon)y_2^{1+\varepsilon} + \varphi(y_2)\,. \end{aligned} \tag{13.3.15}$$

If (y_1, y_2) is a solution of this system, then (y_2, y_1) is a solution as well. There is also the solution $y_1 = y_2 = y_0$ where y_0 is the unique fixed point of the map (13.3.8), which always exists for $\mu > 0$. Therefore, to prove that there are no saddle-node orbits of period two, it suffices to check that system (13.3.8) has no more than three solutions, including multiplicity. This verification will be performed in Sec. 13.6 for a more general system (see (13.6.26)), corresponding to the bifurcation of a homoclinic loop of a multi-dimensional saddle with $\sigma_0 = 0$.

13.4. Birth of periodic orbits from a homoclinic loop (the case dim W^u=1)

Let us now study the bifurcations of homoclinic loops in dimensions higher than two. Consider a continuous one-parameter family X_μ of $\mathbb{C}^r$-smooth ($r \geq 1$) systems in $\mathbb{R}^{m+1}$ (or, more generally, on an $(m+1)$-dimensional smooth manifold) having a saddle equilibrium state O_μ. With no loss of generality we may assume that the equilibrium state is at the origin for all μ. Assume also that only one characteristic exponent of O is positive and that the others lie to the left of the imaginary axis. We denote the characteristic exponents as γ and $\lambda_1, \ldots, \lambda_m$, respectively, so that

$$\gamma > 0 > \operatorname{Re}\lambda_i\,, \quad i = 1, \ldots, m\,.$$

By this assumption, the unstable manifold W^u of the saddle O is one-dimensional and the stable manifold W^s of O is m-dimensional. The unstable manifold consists of three orbits: the saddle O itself and two separatrices: Γ_1 and Γ_2. We suppose that at $\mu = 0$, the system has a separatrix loop of the saddle O; i.e. Γ_1 tends to O as $t \to +\infty$. Thus,

$$\Gamma_1 \subset W^s\,.$$

Besides, we suppose that the loop splits for $\mu \neq 0$: inwards (above W^s) if $\mu > 0$ and outward (below W^s) if $\mu < 0$.

Let us consider first the case of *a negative saddle value* σ

$$\sigma = \gamma + \max \operatorname{Re} \lambda_i < 0\,. \tag{13.4.1}$$

Geometrically, this means that the linearized flow near the saddle *contracts two-dimensional areas*. This implies, in turn, that the local map between any two cross-sections is a contraction (see the proof of Lemma 13.3). By this reason, the dynamics of the system near such homoclinic loop remains simple.

Theorem 13.6. (Shilnikov [130]) *When the saddle value σ is negative at the saddle, a single stable periodic orbit L is born from the homoclinic loop for $\mu > 0$. The separatrix Γ_1 tends to L as $t \to +\infty$. For $\mu \leq 0$, there are no periodic orbits in a small neighborhood U of the homoclinic loop. The trajectories of X_μ tend either to L (or, to the loop Γ at $\mu = 0$), or to O, or leave U as $t \to +\infty$.*

The qualitative behavior described by the theorem is illustrated in Fig. 13.4.1.

Originally, this theorem was proved for $\mathbb{C}^2$-smooth systems. We stress here that our proof includes the $\mathbb{C}^1$-case which allows for a direct use of this theorem in the situation where the system is defined on a $\mathbb{C}^1$-smooth invariant manifold (see Theorem 13.9).

The proof of the above theorem is based on the study of the Poincaré map $T = T_1 \circ T_0$. As usual, the local map by the trajectories near O between some cross-sections S_0 and S_1 is denoted by T_0, and the global map from S_1 to S_0 by the trajectories close to the homoclinic loop Γ is denoted by T_1, respectively.

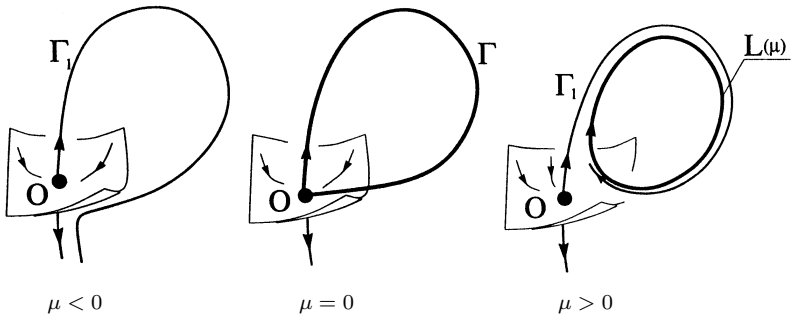

Fig. 13.4.1. Birth of a stable periodic orbit from a separatrix loop to the saddle with $\sigma_0 < 0$.

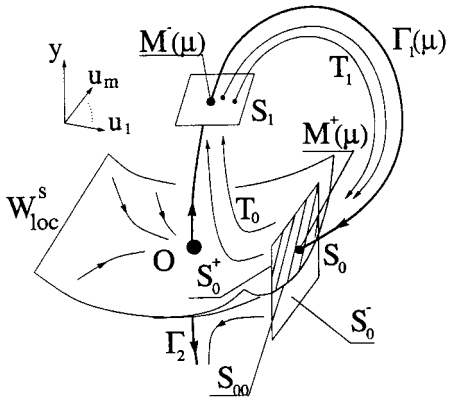

Fig. 13.4.2. An illustration to the proof of Theorem 13.6.

Let us introduce coordinates (u, y), $u \in \mathbb{R}^m$, $y \in \mathbb{R}^1$, near O such that the unstable manifold is tangent to the y-axis at O and the stable manifold is tangent to the u-space. Thus, the system near O can be written in the following form

$$\begin{aligned} \dot{u} &= B(\mu)u + p(u, y, \mu)\,, \\ \dot{y} &= \gamma(\mu)y + q(u, y, \mu)\,, \end{aligned} \tag{13.4.2}$$

where p and q vanish at the origin along with their first derivatives with respect to (u, y); the eigenvalues $\lambda_1(\mu), \ldots, \lambda_m(\mu)$ of the matrix B have negative real parts by assumption, and the characteristic exponent $\gamma(\mu)$ is real and positive.

Let M^+ be some point of the homoclinic loop Γ on W^s_{loc}, and let M^- be a point of Γ on W^u_{loc}. We choose these points sufficiently close to O so that we can construct two cross-sections transverse to Γ_1: the cross-section S_0 goes through the point M^+, and the cross-section S_1 goes through M^- (Fig. 13.4.2). Since the stable manifold is tangent to the u-space, it follows that if M^+ is sufficiently close to O, then $\dot{u} \neq 0$ at M^+. Recall that u is the vector of coordinates $u_1, \ldots, u_m$. Since their choice is arbitrary, let us assume that $\dot{u}_1 \neq 0$ at M^+. Hence, we can choose the cross-section S_0 as a small area through M^+ at $u_1 = \text{constant}$. The other cross-section S_1 through M^- is a small area at $y = \text{constant}$.

Thus, $u^1 = (u_1, \ldots, u_m)$ serve as the coordinates on S_1 and $(y^0, u^0) = (y, u_2, \ldots, u_m)$ are the coordinates on S_0. It was proved in Sec. 6.2 of the first

part of the book (Lemma 6.1) that

$$\left\| \frac{\partial u^1}{\partial (y^0, u^0)} \right\| \le C e^{(\sigma+\delta)\tau}\,, \tag{13.4.3}$$

where $u^1 = T_0(y^0, u^0)$ (i.e. the orbit starting from (u^0, y^0) on S_0 hits S_1 at the point u^1) and τ is the flight time between corresponding points. The quantity δ can be made as small as necessary by moving the cross-sections closer to O.

The orbits on the stable manifold stay in a small neighborhood of O for all positive times. Therefore, for the points on S_0 close to $W^s_{\rm loc}$, the flight time τ is large. Thus, the meaning of the formula (13.4.3) is that the map T_0 is strongly contracting (recall that $\sigma < 0$ by assumption). As mentioned previously, this contraction is a direct consequence of the contraction of areas by the linearized flow (in Lemma 6.1 the proof of the estimates like (13.4.3) is based on a more general approach).

Observe that the stable manifold divides the cross-section S_0 into two parts, and that the map T_0 is defined only on the upper part S_0^+ (all trajectories starting from the lower part S_0^- leave a small neighborhood of O close to the other separatrix Γ_2, and, therefore, do not intersect S_1).

Just like in the two-dimensional case, the global map T_1 from S_1 to S_0 by the trajectories of the system near the homoclinic loop is a diffeomorphism of a small neighborhood of the point M^- into a small neighborhood of the point M^+. Thus, its derivative is bounded.

Hence, the Poincaré map $T = T_1 \circ T_0$ is a strongly contracting map from S_0^+ to S_0. Obviously, as the point $M \in S_0^+$ approaches the boundary $S_{00} = W^s_{\rm loc} \cap S_0$, its image $T_0 M$ tends to the point $M^-(\mu) = \Gamma_1(\mu) \cap S_1$. Therefore, by continuity, we can define

$$TS_{00} = M^+(\mu) \equiv T_1 M^-(\mu)\,.$$

By assumption, the loop is split inward (above $W^s_{\rm loc}$) for $\mu > 0$ and outward (below $W^s_{\rm loc}$) for $\mu < 0$. This is equivalent to the following condition:

$$M^+(\mu) \in \begin{cases} S_0^+ & \text{for } \mu > 0\,, \\ S_{00} & \text{at } \mu = 0\,, \\ S_0^- & \text{for } \mu < 0\,. \end{cases}$$

Lemma 13.4. *Let V be a closed convex set in $\mathbb{R}^m$ and U be a closed subset of V. Let T be a contracting map $T:\ U \to V$. Assume also that the boundary*

∂U of U in V is mapped by T into a single point M^+. Then, if $M^+ \in U$, the map has a unique fixed point M^* in U which is the limit of the iterations of M^+ by T. All trajectories which do not enter $V\backslash U$ tend to the fixed point in U. On the contrary, if $M^+ \in V\backslash U$, then there is no fixed point in U; moreover any orbit leaves U after a finite number of iterations of the map.

Note that Theorem 13.6 follows immediately from this lemma. Here $V = S_0$, $U = S_0^+$, $\partial U = S_{00}$, $V\backslash U = S_0^-$, and since T is the Poincaré map, its stable fixed point in S_+ corresponds to a stable limit cycle (the fixed point on $S_{00} = W^s_{\rm loc} \cap S_0$ corresponds to the homoclinic loop Γ by construction).

To prove the above lemma, let us continue the map T on $V\backslash U$ so that $TM = M^+$ for all $M \in V\backslash U$. This extended map remains contracting and takes V into V. Thus, it has a unique fixed point M^* which attracts forward orbits of all points of V. This fixed point is a fixed point of the original map T provided it belongs to U; otherwise, it is "a virtual fixed point" if it lies in $V\backslash U$. In the latter case, $M^* = TM^* = M^+$ by construction. Vice versa, if $M^+ \in V\backslash U$, then $TM^+ = M^+$. This means that $M^+ = M^*$ (by uniqueness of the fixed point). Thus, $M^* \notin U$ if and only if $M^+ \notin U$. We have almost proven the lemma. The final step to be proven is to show that the iterations of M^+ never leave U if $M^* \in U$ (this implies that these iterations converge to M^*). To do this we must observe that by virtue of the contraction property we have the following relationship

$$\text{dist } (T^k M^+, M^*) = \text{dist } (T^{k+1}(\partial U), T^{k+1} M^*) < \text{dist } (\partial U, M^*)$$

which proves our claim, and hence completes the proof of Lemma 13.4 and Theorem 13.6.

This result gives us the last known principal (codimension one) stability boundary for periodic orbits. We will see below (Theorems 13.9 and 13.10) that the other cases of bifurcations of a homoclinic loop lead either to complex dynamics (infinitely many periodic orbits), or to the birth of a single saddle periodic orbit.

So, let us consider the case of the positive saddle value, i.e.

$$\gamma + \max_{i=1,\dots,m} \text{Re } \lambda_i > 0$$

(where, as before, we denote the only positive characteristic exponent as γ and $\lambda_1, \dots \lambda_m$ stand for the characteristic exponents with negative real parts). We assume that the characteristic exponent nearest to the imaginary axis is simple

and real, i.e.

$$0 > \lambda_1 > \max_{i=2,\dots,m} \operatorname{Re} \lambda_i \,.$$

The case where λ_1 is complex will be discussed later (Theorem 13.8).

Let us make the following *nondegeneracy assumptions*[5]:

(1) $\Gamma \not\subset W^{ss}$.

(2) *The extended unstable manifold* W^{uE} *is transverse to the stable manifold* W^s *at the points of* Γ (Fig. 13.4.3).

Traditionally, this condition is written as

$$A \neq 0 \,.$$

We will define below the quantity A in terms of the Poincaré map. It is an analogue of the separatrix value A introduced in Secs. 13.1 and 13.2 for the two-dimensional case. Recall that A is always non-zero in dimension two. However, in the multi-dimensional case the non-vanishing of A is an essential assumption.

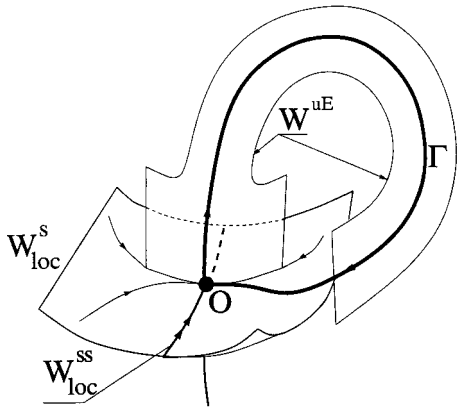

Fig. 13.4.3. Illustration of the non-degeneracy condition of Theorem 13.7: the homoclinic loop enters the saddle along the leading direction; the two manifolds W^{uE} and W^s intersect transversely to each other.

[5]Recall that the strong stable invariant manifold W^{ss} is tangent at O to the eigenspace of the linearization matrix which corresponds to the non-leading characteristic exponents $\lambda_2, \dots, \lambda_m$. It is $(m-1)$-dimensional and it partitions W^s into two components. The orbits of W^s which do not belong to W^{ss} tend to O along the leading direction as $t \to +\infty$. The extended unstable manifold is a smooth invariant one which is tangent at O to the eigenspace corresponding to the characteristic exponents γ and λ_1.

The situation which we consider here is a particular case of Theorem 13.9 of the next section.[6] It follows from this theorem (applied to the system in the reversed time) that a single saddle periodic orbit L is born from a homoclinic loop; it has an m-dimensional stable manifold and a two-dimensional unstable manifold. This result is similar to Theorem 13.6. Note, however, that in the case of a negative saddle value the main result (the birth of a unique stable limit cycle) holds without any additional non-degeneracy requirements (the leading stable eigenvalue λ_1 is nowhere required to be simple or real). On the contrary, when the saddle value is positive, a violation of the non-degeneracy assumptions (1) and (2) leads to more bifurcations. We will study this problem in Sec. 13.6.

Let us assume further that the system is $\mathbb{C}^r$ with $r \geq 2$.[7] In this case, the system near O may be written in the form [see Sec. 13.8 and formula (13.8.28)]

$$\begin{aligned} \dot{x} &= -\lambda_1 x + f_{11}(x,y)x + f_{12}(x,u,y)u\,, \\ \dot{u} &= B_2 u + f_{21}(x,y)x + f_{22}(x,u,y)u\,, \\ \dot{y} &= \gamma y\,, \end{aligned} \tag{13.4.4}$$

where $x \in \mathbb{R}^1$ and $y \in \mathbb{R}^1$ are the leading coordinates, $u \in \mathbb{R}^{m-1}$ is the vector of stable non-leading coordinates, the eigenvalues $(\lambda_2, \ldots, \lambda_m)$ of B_2 lie to the left of the line $\mathrm{Re}(\cdot) = \lambda_1$. The functions f_{ij} satisfy

$$f_{i1}(x,0) \equiv 0\,, \quad f_{1j}(0,0,y) \equiv 0\,. \tag{13.4.5}$$

In these coordinates, the stable manifold is locally defined by $y = 0$, the local unstable manifold is defined by $\{x = 0, u = 0\}$, and the strong stable manifold is defined by $\{x = 0, y = 0\}$.

The extended unstable manifold W^{uE}_{loc} is tangent to the plane $u = 0$ at the points of the unstable manifold. Indeed, the equation for $\dot{u}$ linearized at $\{x = 0, u = 0\}$ is (here, we have made use of $f_{21} = 0$ at $x = 0$)

$$\dot{u} = (B_2 + f_{22}(0,0,y(t)))u\,.$$

Hence it follows that the plane $u = 0$ is invariant with respect to the linearized flow along W^u_{loc}, and transverse to W^{ss} at O. Therefore, it is indeed the uniquely defined tangent to W^{uE}_{loc} at W^u_{loc} (see Sec. 5.3 of Part I).

[6] Consider the case of the one-dimensional stable manifold in Theorem 13.9 and make a reversal of time. After that, the conditions (1) and (2) of the theorem will coincide with the two nondegeneracy assumptions above.

[7] The picture we obtain here remains valid in the $\mathbb{C}^1$-case as well; however when the system is at least $\mathbb{C}^2$, the analysis becomes much more explicit.

By assumption, the loop Γ enters O as $t \to +\infty$ along the x-axis. Meanwhile, it coincides locally with the y semi-axis when it leaves O at $t = -\infty$. We assume that Γ adjoins O from the side of positive x and y, respectively.

Choose two cross-sections transverse to Γ; namely $S_0 : \{x = d\}$ and $S_1 : \{y = d\}$ for some small $d > 0$. Denote the coordinates on S_0 by (y_0, u_0) and the coordinates on S_1 by (x_1, u_1). We are interested in what happens in a small neighborhood of Γ, and therefore let us assume $\|u_0 - u^+\| \le \delta$ on S_0 and $\|x_1, u_1\| \le \delta$ on S_1 for some small $\delta > 0$. Here, u^+ is the u-coordinate of the point $M^+(0, u^+) = \Gamma \cap S_0$.

The local map $T_0 : S_0 \to S_1$ in the given coordinates can be recast as (see formula (13.8.30) in Sec. 13.8)

$$x_1 = y_0^\nu d^{1-\nu} + o(y_0^\nu)\,, \quad u_1 = o(y_0^\nu)\,, \tag{13.4.6}$$

where $\nu = |\lambda_1/\gamma|$ is the saddle index. Note that only the $o(y_0^\nu)$-like terms depend on u_0 in the right-hand sides of (13.4.6). The local map T_0 is defined on the upper part $S_0^+ : \{y_0 \ge 0\}$ of S_0 (the orbits starting from $y_0 < 0$ leave a small neighborhood of O along the other unstable separatrix which coincides locally with the negative y semi-axis). It is immediately seen from (13.4.6) that the image $T_0 S_0^+$ on S_1 is a curvilinear triangle (Fig. 13.4.4) with the apex at

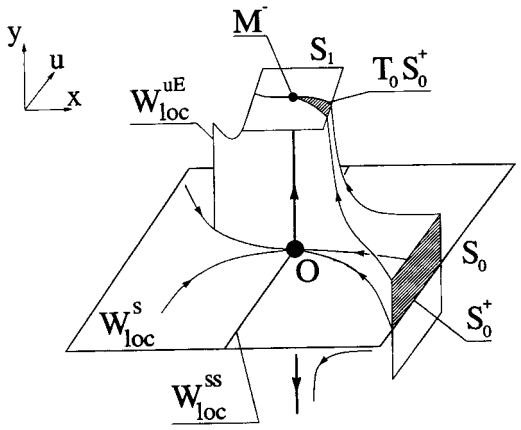

Fig. 13.4.4. The local Poincaré map T_0 transforms the upper part S_0^+ of the cross-section S_0 into a curvilinear rectangle on the cross-section S_1. The points in $S_0 \cap W^s_{\rm loc}$ are mapped into a single point M^-.

the point $M^-(0,0) = \Gamma \cap S_1$ and with both boundary sides at M^- tangent to $W^{uE}_{\rm loc} \cap S_1$ (the x_1-axis in our coordinates).

One can see that the map T_0 is strongly contracting in the u-directions and, since $\nu < 1$, (equiv. $\sigma = \gamma + \lambda_1 > 0$), it is expanding in y;[8] i.e.

$$\frac{\partial x_1}{\partial y_0} \gg 1\,.$$

The flow outside a small neighborhood of O defines the global map $T_1 : S_1 \to S_0$ by the trajectories close to Γ. In a small neighborhood of the origin M^- on S_1, the map T_1 can be written in the form

$$\begin{aligned} \bar y_0 &= \mu + a_{11}x_1 + a_{12}u_1 + \cdots\,, \\ \bar u_0 &= u^+(\mu) + a_{21}x_1 + a_{22}u_1 + \cdots\,, \end{aligned} \tag{13.4.7}$$

where μ is the splitting parameter of the loop. If we denote $M^+(\mu) = \Gamma_1(\mu) \cap S_0 = T_1 M^-$, then $(\mu, u^+(\mu))$ are the coordinates of this point. By definition, $M^+ \in W^s_{\rm loc} \cap S_0$ at $\mu = 0$. When $\mu > 0$, the point $M^+(\mu)$ lies in S_0^+, i.e. the loop is split inward. When $\mu < 0$, the point $M^+(\mu)$ lies in S_0^-, i.e. the loop splits outward.

Since T_1 is a diffeomorphism, we have

$$\Delta = \begin{vmatrix} a_{11} & a_{12} \\ a_{21} & a_{22} \end{vmatrix} \neq 0$$

(moreover, $\Delta > 0$ when the flow is defined in $\mathbb{R}^{n+1}$ or on an orientable manifold). It also follows that both a_{11} and a_{12} cannot vanish simultaneously.

[8] We have already presented this picture in Sec. 2.4 for the case where the system near the saddle is linear. In the case of a $\mathbb{C}^1$-smooth nonlinear system, this picture follows from the estimates proven in Sec. 6.2. Indeed, it follows from Lemma 6.3 that in our case the image by T_0 of any line $\{u_0 = \text{constant}, y_0 \geq 0\}$ from S_0 is the curve

$$u_1 = w_{\rm loc}(d, x_1, u_0),\ x_1 \geq 0$$

on S_1 where $w_{\rm loc}$ is a smooth function which vanishes identically at $x_1 = 0$ along with the first derivative with respect to x_1. Thus, for any fixed u_0 this curve is tangent to the x_1-axis at the point M^-, and hence the whole set $T_0 S_0^+$ is a curvilinear wedge tangent to the x_1-axis. The contraction in the u-directions and the expansion in the y-direction are due to Lemma 6.1. Note that our notations here and those in Sec. 6.2 are different. To establish the correspondence with Lemmas 6.1–6.3, one must make the following substitution: the map $T_{\rm loc}$ of Sec. 6.2 is the inverse of our map T_0, our cross-sections S_0 and S_1 are, respectively, $S^{\rm out}$ and $S^{\rm in}$ in Sec. 6.2. Finally, the coordinates (u^0, y^0, w^0) on $S^{\rm in}$ and (u^1, w^1) on $S^{\rm out}$ in Lemma 6.3 correspond to our coordinates $(y = d, x_1, u_1)$ on S_1 and, respectively, (y_0, u_0) on S_0.

Nevertheless, the coefficient a_{11} alone may vanish. We will denote $a_{11} \equiv A$. By definition,

$$A = \left.\frac{\partial \bar{y}_0}{\partial x_1}\right|_{M^-} . \tag{13.4.8}$$

Observe that the transversality of W^{uE} and W^s on Γ is indeed equivalent to the condition $A \neq 0$. Note that the choice of the coordinates on the cross-sections is important here: since we take the x_1-axis tangent to the line $W^{uE}_{\rm loc} \cap S_1$, the image of this line $T_1(W^{uE}_{\rm loc} \cap S_1)$ is transverse to $\{y_0 = 0\} = W^s_{\rm loc} \cap S_0$ if, and only if $\frac{\partial \bar{y}_0}{\partial x_1} \neq 0$.

Combining formulas (13.4.6) and (13.4.7), we obtain the following representation for the Poincaré map T:

$$\begin{aligned} \bar{y} &= \mu + Ay^\nu + o(y^\nu)\,, \\ \bar{u} &= u^+(\mu) + a_{21}y^\nu + o(y^\nu) \end{aligned} \tag{13.4.9}$$

(we drop the sub-index "0" and rescale variables to make $d = 1$ in (13.4.6); the dependence on u in the right-hand side is concealed in the $o(y^\nu)$ terms). Observe that the separatrix value A appears as a coefficient in front of the leading term y^ν of the asymptotics for $\bar{y}$ in the Poincaré map.

Hence, if $A \neq 0$, then the map $T = T_1 \circ T_0$ has the same property as the local map T_0, namely: it is contracting in the u-directions and expanding in the y-direction, i.e. it is *a saddle map* (see Sec. 3.15). The image TS_0^+ on S_0 will have a form similar to that shown in Fig. 13.4.5 at $\mu = 0$. Observe that $TS_0^+ \cap S_0^+ = \emptyset$ for $A < 0$, i.e. any orbit from a small neighborhood of the homoclinic loop must leave the neighborhood after one iteration performed near the loop in this case. On the contrary, in the case $A > 0$, the intersection $TS_0^+ \cap S_0^+$ is non-empty. For any vertical line $u_0 = \text{constant}$ in S_0^+, its iterations by the map T will lie in S_0^+ and converge to the smooth invariant curve l_0^+ of T emanating from the point $M^+ = \Gamma \cap S_0$.

Figures 13.4.6 ($A\mu > 0$) and 13.4.7 ($A\mu < 0$) show how the image of S_0^+ by the map T moves when the loop is split. In any case, since the map T is contracting in the u-variables and expanding in y, it follows that it has a smooth attracting invariant curve $l_0(\mu)$, transverse to $\{y_0 = 0\}$ in S_0.

The trajectories starting from $l_0(\mu)$ compose a two-dimensional attracting invariant manifold $\mathcal{M}_\mu$ of the flow. The proof of the existence of such a manifold in a small neighborhood of the homoclinic loop is given by Theorem 6.2

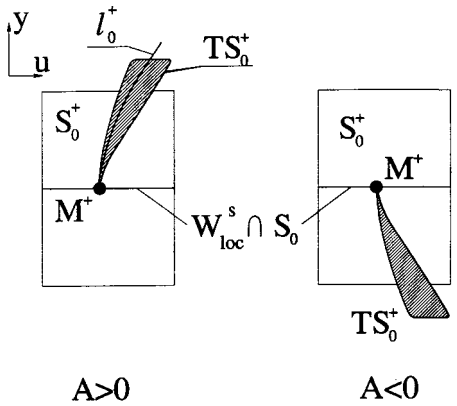

Fig. 13.4.5. The image TS_0^+ of S_0^+ on S_0 is a wedge which is mapped to S_0^+ if $A > 0$, or it is mapped upside down about $W^s_{\rm loc} \cap S_0$ if $A < 0$. When $A > 0$, there exists an invariant curve l_0^+ of the map.

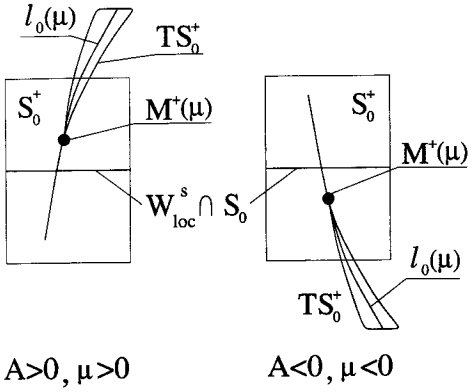

Fig. 13.4.6. The map after the spliting of the separatrix loop.

in Sec. 6.1 under assumptions which coincide with our conditions (1) and (2) in the case under consideration.

The manifold $\mathcal{M}_\mu$ contains all trajectories staying in a small neighborhood U of Γ for all negative times. Near O, the manifold $\mathcal{M}_\mu$ coincides with an extended unstable manifold $W^{uE}_{\rm loc}$ (not unique). Thus, if we denote $l_1(\mu) = \mathcal{M}_\mu \cap S_1$, then $l_1(\mu)$ is tangent to the x_1-axis at the point M^-. Since $\mathcal{M}_\mu$ is an

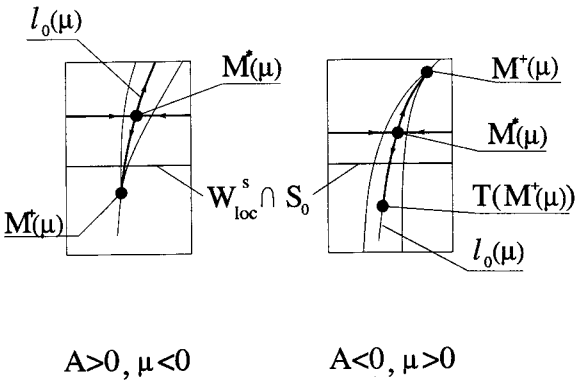

Fig. 13.4.7. The fixed point M^* corresponds to a saddle periodic orbit that emerges from the homoclinic loop. Its unstable multiplier is positive when $A > 0$, and it is negative in the case $A < 0$.

invariant manifold, the orbits starting from $l_1(\mu)$ must intersect S_0 at the points of $l_0(\mu)$, i.e. $T_1 l_1(\mu) = l_0(\mu)$. It follows from (13.4.7) and (13.4.8) that at the points of $l_0(\mu)$, the manifold $\mathcal{M}_\mu$ is glued to itself with a reversal of orientation if $A < 0$, or with the same orientation if $A > 0$. So, $\mathcal{M}_\mu$ is an annulus if $A > 0$, or a Möbius band if $A < 0$ (see Fig. 13.4.8).

When restricted onto the invariant curve $l_0(\mu)$, the map T is an expanding one-dimensional map, monotonically increasing when $A > 0$, or monotonically decreasing when $A < 0$. The Lamerey diagrams for such maps are shown in Figs. 13.2.5 and 13.2.6 in Sec. 13.2. Thus, one can see that all trajectories leave S_0^+ upon iterations of T if $A\mu > 0$. If $A\mu < 0$, then the map T has an unstable fixed point $M^*(\mu)$ on $l_0(\mu)$. Due to contraction in directions transverse to $l_0(\mu)$, the point $M^*(\mu)$ is a saddle in S_0^+.

The following coordinates of the fixed point are easily found from (13.4.9):

$$u \sim u^+(\mu)\,, \quad y \sim \left(\frac{-\mu}{A}\right)^{\frac{1}{\nu}}\,.$$

Since a fixed point of the Poincaré map T corresponds to a periodic orbit of the flow, we may formulate the following result (see Fig. 13.4.9).

Theorem 13.7. *If a homoclinic loop* Γ *to a saddle with a positive saddle value satisfies both conditions* (1) *and* (2), *then a single saddle periodic orbit* $L(\mu)$ *is born from the loop for* $A\mu < 0$. *The unstable manifold of* $L(\mu)$ *is two-dimensional and orientable when* $A > 0$ (*then there is only one positive*

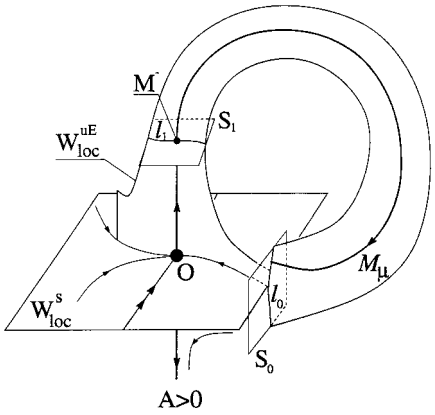

(a)

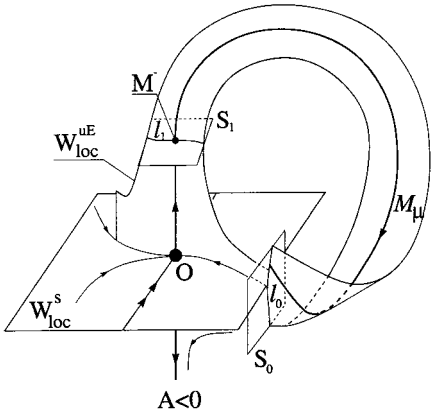

(b)

Fig. 13.4.8. The invariant manifold $\mathcal{M}_\mu$ is an orientable surface when $A > 0$ (a), or it is a Möbius band if $A > 0$ (b).

multiplier greater than one), *or non-orientable when* $A < 0$ (*then the multiplier greater than one in absolute value is negative*). *For* $A\mu > 0$, *there are no orbits* (*besides the equilibrium state* O) *staying in a small neighborhood* U *of* Γ *for all times. For* $A\mu < 0$, *almost all orbits leave* U. *The exceptions are* O, L *and one heteroclinic orbit which is* α*-limit to* L *and* ω*-limit to* O.[9]

[9]This orbit is the stable separatrix of O on the invariant manifold $\mathcal{M}_\mu$.

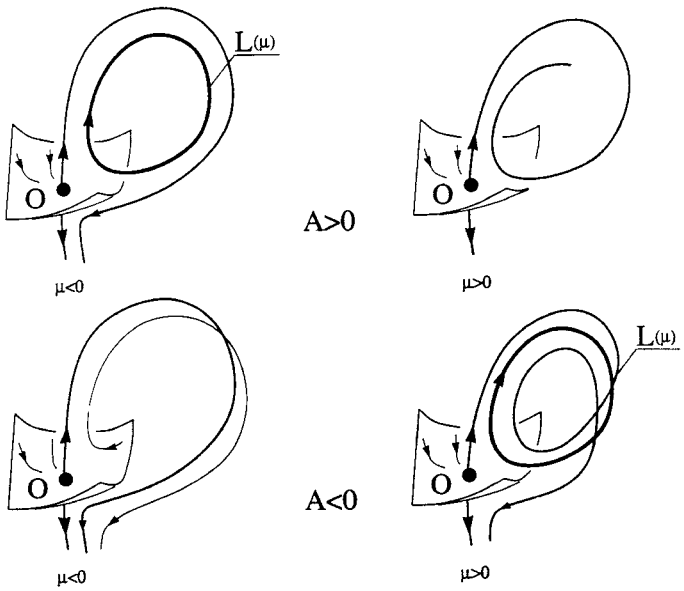

Fig. 13.4.9. The birth of a saddle periodic orbit from a homoclinic loop to a saddle with the positive saddle value.

On the cross-section S_0, the local unstable manifold of the fixed point $M^*(\mu)$ is a small piece of the invariant curve $l_0(\mu)$ through this point. The entire unstable manifold of $M^*(\mu)$ on S_0 can be obtained by iterating the local unstable manifold under the action of the map T. Since the domain S_0^+ of the map T is bounded by the surface $\{y_0 = 0\} = W^s_{\rm loc}(O) \cap S_0$, the unstable manifold of $M^*(\mu)$ is bounded by the images of this surface. Thus, it is a part of $l_0(\mu)$ bounded by the point $M^+(\mu) = T_1 M^- = \Gamma_1(\mu) \cap S_0$ if $A > 0$, or a part of $l_0(\mu)$ between the points $M^+(\mu)$ and $T(M^+(\mu))$ when $A < 0$ (see Fig. 13.4.7). As $\mu \to 0$, the unstable manifold of $M^*(\mu)$ tends to the invariant curve l_0^+ for $A > 0$, or shrinks to the point M^+ for $A < 0$; the stable manifold of $M^*(\mu)$ tends to $\{y_0 = 0\}$.

By construction, the curve l_0^+ is the intersection of the invariant manifold $\mathcal{M}_0$ with S_0^+. If $A > 0$, the backward orbits of the points of l_0^+ tend to the point $M^+ = \Gamma \cap S_0$ at $\mu = 0$. Thus, in the case $A > 0$, all orbits from the upper part ($y_0 > 0$) of the invariant manifold $\mathcal{M}_0$ are α-limit to the homoclinic loop Γ (see also Remark 4 in Sec. 13.2). Since the manifold $\mathcal{M}_0$ is attracting, it must repel backward semi-trajectories. Therefore, there may not be other

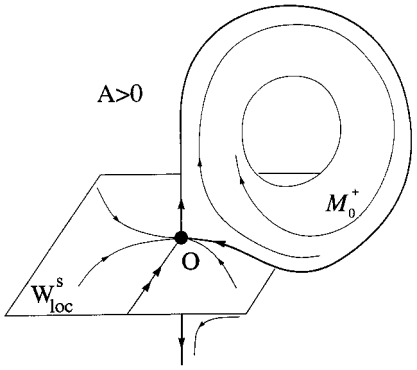

Fig. 13.4.10. The orientable homoclinic loop ($A > 0$) to a saddle with the positive saddle value has unstable invariant manifold.

orbits which are α-limit to Γ. It follows that the upper half of $\mathcal{M}_0$ is a uniquely defined *unstable manifold* of the loop Γ for $A > 0$ (Fig. 13.4.10).

When $\mu \neq 0$, the fixed point $M^*(\mu)$ of the Poincaré map corresponds to the saddle periodic orbit $L(\mu)$ of the flow. The unstable manifold of $L(\mu)$ intersects the stable manifold of O, and therefore it is bounded by the unstable separatrices $\Gamma_{1,2}$. It follows from the above analysis that, when $A > 0$, the unstable manifold of $L(\mu)$ is a two-dimensional cylinder which tends to the unstable manifold of Γ as $\mu \to -0$. When $A < 0$, the unstable manifold of $L(\mu)$ is a Möbius band which shrinks to Γ as $\mu \to +0$.

As $\mu \to 0$, the stable manifold of $L(\mu)$ approaches the component W^s_+ of $W^s(O)\backslash W^{ss}(O)$ which contains Γ. The characteristic form of W^s_+ in the small neighborhood U of Γ is sketched in Fig. 13.4.11. Here, the local stable manifold can be continued along Γ in backward time so that it returns to the small neighborhood of O. Since $A \neq 0$, the manifold W^s is transverse to $W^{uE}_{\rm loc}$, and therefore it is limited to the manifold W^{ss} as $t \to -\infty$. This geometry of W^s is a direct consequence of the non-vanishing of the value of A. We remark, however, that in some cases, even if $A = 0$, the manifold W^s may be still limited to W^{ss} in backward time.

Observe also that in the case $\sigma < 0$, we have the same geometrical behavior provided that the following three conditions hold:

(1) the leading eigenvalue λ_1 is simple and real,

(2) the homoclinic loop Γ does not belong to the strong stable manifold, and $A \neq 0$.

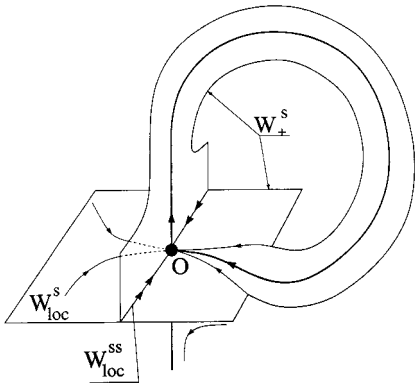

Fig. 13.4.11. Behavior of the stable manifold W_+^S in backward time near a homoclinic loop to the saddle with real λ_1, provided the non-degeneracy assumptions hold.

Here the map T will still have an attracting invariant curve $l_0(\mu)$, but (in the case $\sigma < 0$) the map T is a contraction on $l_0(\mu)$. It follows that the homoclinic loop Γ possesses *a stable manifold* when $A > 0$, i.e. the set of points which are ω-limit to Γ. This set consists from all trajectories passing through the upper part S_0^+ of the cross-section S_0 and is bounded by the closure of W_+^s. Note that the possible existence of stable or unstable manifolds for homoclinic loops opens the way for the appearance of the so-called superhomoclinic (homoclinic to homoclinic) orbits which could enrich dynamics essentially. We refer the reader to [69, 157, 159].

As we have seen above, the dynamics near the homoclinic loop to a saddle with real leading eigenvalues is essentially two-dimensional. New phenomena appear when we consider the case of a saddle-focus. Namely, we take a $\mathbb{C}^r$-smooth ($r \geq 2$) system with an equilibrium state O of the saddle-focus saddle-focus $(2,1)$ type (in the notation we introduced in Sec. 2.7). In other words, we assume that the equilibrium state has only one positive characteristic exponent $\gamma > 0$, whereas the other characteristic exponents $\lambda_1, \lambda_2, \ldots, \lambda_m$ are with negative real parts. Besides, we also assume that the leading (nearest to the imaginary axis) stable exponents consist of a complex conjugate pair λ_1 and λ_2:

$$\lambda_{1,2} = -\rho \pm i\omega\,, \quad \text{Re}\ \lambda_j < -\rho < 0 \quad (j = 3, \ldots, m)\,.$$

By time rescaling we can always make $\gamma = 1$, which we will assume to be throughout this section. So, the case $\rho > 1$ corresponds here to the negative

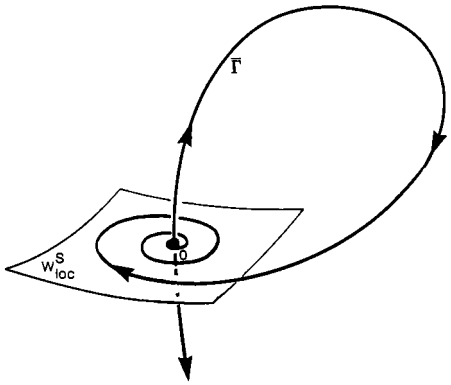

Fig. 13.4.12. A homoclinic loop to a saddle-focus.

saddle value (and it is hence covered by Theorem 13.6). Thus, we will mainly be focused here on the case $\rho < 1$ (positive saddle value).

The unstable W^u and stable manifold W^s of O are one-dimensional and n-dimensional, respectively. The unstable manifold is the union of O and two separatrices, Γ_1 and Γ_2. By definition, the separatrices $\Gamma_{1,2}$ tend to O as $t \to -\infty$. Suppose that one of the separatrices (Γ_1) tends to O as $t \to +\infty$ thereby forming a homoclinic loop $\bar{\Gamma}$ (Fig. 13.4.12).

The structure of the phase space in a small neighborhood of $\bar{\Gamma}$ depends on the sign of the saddle index ρ. We will see that the behavior of the trajectories in a neighborhood of $\bar{\Gamma}$ differs essentially in the two cases $\rho > 1$ (simple dynamics) and $\rho < 1$ (complex dynamics).

Our study is based on the construction of a Poincaré map T via a superposition of a local map $T_0 : S_0 \to S_1$ and a global map $T_1 : S_1 \to S_0$, where S_0 and S_1 are appropriately matching cross-sections to Γ.

It follows from the result of Appendix A in Part I (see also formula (13.8.28) in Sec. 13.8) that a system near O can be recast into the form

$$\begin{aligned} \dot{x}_1 &= -\rho x_1 - \omega x_2 + f_{11}(x,y)x + f_{12}(x,u,y)u\,, \\ \dot{x}_2 &= \omega x_1 - \rho x_2 + f_{21}(x,y)x + f_{22}(x,u,y)u\,, \\ \dot{u} &= Bu + f_{31}(x,y)x + f_{32}(x,u,y)u\,, \\ \dot{y} &= y\,, \end{aligned} \tag{13.4.10}$$

by some $\mathbb{C}^{r-1}$-transformation of coordinates and time. Here, $u \in \mathbb{R}^{m-2}$ is the vector of non-leading coordinates, and the eigenvalues of the matrix B are

$(\lambda_3, \dots, \lambda_m)$. The $\mathbb{C}^{r-1}$-functions f_{ij} satisfy

$$f_{i1}(x,0) \equiv 0\,, \quad f_{1j}(0,0,y) \equiv 0\,, \quad f_{2j}(0,0,y) \equiv 0\,. \tag{13.4.11}$$

In these coordinates the invariant manifolds are locally straightened: their equations are $W^u_{\rm loc} = \{x = 0, u = 0\}$ and $W^s_{\rm loc} = \{y = 0\}$, respectively. Moreover, the system in the leading coordinates (x_1, x_2) is linear on the stable manifold.

We will assume that Γ leaves O at $t = -\infty$ towards positive y, i.e. it coincides locally with the positive y semi-axis. Therefore, we may chose the cross-section S_1 as $y = d$ for some small $d > 0$.

When the separatrix returns to O, it lies in the stable manifold $y = 0$. If the system has order more then three, we will assume that Γ *does not belong to the strong stable manifold* W^{ss}. Recall that W^{ss} is a smooth invariant manifold which is tangent at O to the u-space; and when (13.4.11) is satisfied, $W^{ss} = \{x = 0, y = 0\}$. Recall from Secs. 2.6 and 2.7 that any trajectory from $W^s \backslash W^{ss}$ (and hence the separatrix Γ too) tends to O along the leading plane $u = 0$, so that its projection onto this plane is a spiral which intersects, say, the positive x_1 semi-axis infinitely many times. Let $M^+(x^+ > 0, 0, u^+, 0)$ be a corresponding point on Γ. Let us take the cross-section $S_0 : \{x_2 = 0\}$ through this point.

It follows from Sec. 13.8 [see (13.8.30)–(13.8.33)] that the solution $(x(t), u(t), y(t))$ which starts from $x = (x_0, 0)$, $u = u_0$ at $t = 0$ and ends at $y = d$ at $t = \tau$ must satisfy the relation

$$\begin{aligned} &y(0) = e^{-\tau} d\,, \\ &x(\tau) = \exp\left[\tau \begin{pmatrix} -\rho & -\omega \\ \omega & -\rho \end{pmatrix}\right] \begin{pmatrix} x_0 \\ 0 \end{pmatrix} + o(e^{-\rho\tau})\,, \\ &u(\tau) = o(e^{-\rho\tau})\,, \end{aligned} \tag{13.4.12}$$

where the $o(e^{-\rho\tau})$-terms denote some $\mathbb{C}^{r-1}$-smooth functions of (x_0, u_0, τ) which decay to zero faster than $e^{-\rho\tau}$ along with all their derivatives up to the order $(r-1)$.

We can now evaluate the flight time τ from the point $(x_0, u_0, y_0) \in S_0$ to S_1

$$\tau = -\ln \frac{y_0}{d}\,.$$

Substituting this expression into (13.4.12), we obtain the following formula for the local map $T_0 : (x_0, u_0, y_0) \mapsto (x_1, x_2, u_1) \in S_1$[10] by the trajectories of the flow near O:

$$\begin{aligned} x_1 &= x_0 \left(\frac{y_0}{d}\right)^{\rho} \cos \omega \ln \frac{d}{y_0} + o(y_0^{\rho}) \,, \\ x_2 &= x_0 \left(\frac{y_0}{d}\right)^{\rho} \sin \omega \ln \frac{d}{y_0} + o(y_0^{\rho}) \,, \\ u_1 &= o(y_0^{\rho}) \,. \end{aligned} \tag{13.4.13}$$

Here, the derivatives of the $o(y_0^{\rho})$-terms with respect to (x_0, u_0, y_0) up to the order $(r-1)$ are estimated as $o(y_0^{\rho-q})$ where q is the number of differentiations with respect to y_0.

Observe that the map T_0 is defined only for $y_0 > 0$. Choose a small $\delta > 0$ and let S_0^+ be the rectangle $\{|x_0 - x^+| \le \delta, \|u_0 - u^+\| \le \delta, 0 \le y_0 \le \delta\}$ on S_0 (recall that $(x^+, u^+, 0)$ are the coordinates of the point $M^+ = \Gamma \cap S_0$). We can see from formulas (13.4.13) that the image $T_0 S_0^+$ in S_1 looks like a "snake" (Fig. 13.4.13) which spirals onto the point $M^-(0,0,0) = \Gamma \cap S_1$ along

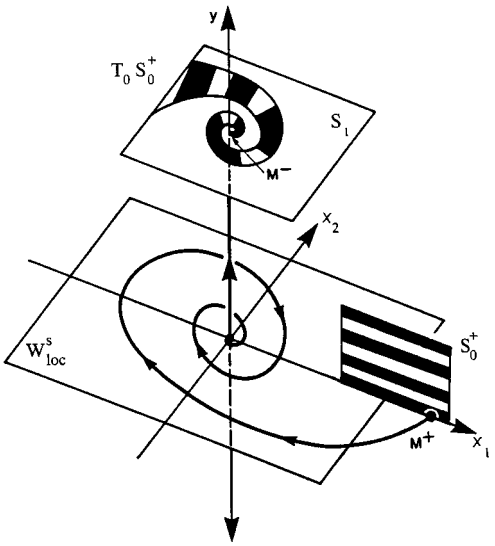

Fig. 13.4.13. The local Poincaré map T_0 near a saddle-focus.

[10] We denote the u-coordinates of a point on S_1 by u_1 and that on S_0 by u_0.

the plane $u_1 = 0$ (we have already described this shape in more detail in Sec. 2.4). By continuity, let us define the map T_0 at $y_0 = 0$ by $T_0(W^s_{\rm loc} \cap S_0) = M^-$.

The global map $T_1 : S_1 \to S_0$ is defined by the trajectories close to that piece of Γ which lies outside a small neighborhood of O. The map T_1 is a diffeomorphism which takes the point M^- to M^+, and can be therefore represented by

$$\begin{aligned} \bar{x}_0 &= x^+ + a_{11}x_1 + a_{12}x_2 + a_{13}u_1 + \cdots , \\ \bar{y}_0 &= a_{21}x_1 + a_{22}x_2 + a_{23}u_1 + \cdots , \\ \bar{u}_0 &= u^+ + a_{31}x_1 + a_{32}x_2 + a_{33}u_1 + \cdots . \end{aligned} \tag{13.4.14}$$

We will require that

$$A \equiv \sqrt{a_{21}^2 + a_{22}^2} \neq 0 . \tag{13.4.15}$$

Note that this condition is automatically satisfied for three-dimensional systems, where there is no non-leading u-coordinates. In this case the global map assumes the form

$$\begin{aligned} \bar{x}_0 &= x^+ + a_{11}x_1 + a_{12}x_2 + \cdots , \\ \bar{y}_0 &= a_{21}x_1 + a_{22}x_2 + \cdots . \end{aligned}$$

Since the global map must be a diffeomorphism, it follows that $\left|\begin{smallmatrix} a_{11} & a_{12} \\ a_{21} & a_{22} \end{smallmatrix}\right| \neq 0$, which indeed implies (13.4.15).

In dimensions higher than three, the condition $A \neq 0$ is an essential non-degeneracy condition. It is important that we use the coordinates in which the system has locally the form (13.4.10) and that the identities (13.4.11) are hold. In these coordinates the intersection of $W^s_{\rm loc}$ with S_0 is the straightline $y_0 = 0$, and the intersection of the extended unstable manifold $W^{uE}_{\rm loc}$ with S_1 is tangent to the space $u_1 = 0$ (the extended unstable manifold is a smooth invariant manifold which is transverse to $W^{ss}_{\rm loc}$ at O). Thus, one can see from (13.4.14) that the condition $A \neq 0$ is equivalent to the condition of transversality of $T_1(W^{uE}_{\rm loc} \cap S_1)$ to $W^s_{\rm loc} \cap S_0$ at the point M^+, i.e. to *the transversality condition of the extended unstable manifold W^{ue} to the stable manifold W^s at the points of the homoclinic loop* Γ.

Formulas (13.4.13) and (13.4.14) yield the following expression for the Poincaré map $T = T_1 \circ T_0$:

$$\begin{aligned}
\bar{y} &= Axy^\rho \cos\left(\omega \ln \frac{1}{y} + \theta\right) + o(y^\rho)\,, \\
\bar{x} &= x^+ d^{-1} + A_1 xy^\rho \cos\left(\omega \ln \frac{1}{y} + \theta_1\right) + o(y^\rho)\,, \\
\bar{u} &= u^+ d^{-1} + A_2 xy^\rho \cos\left(\omega \ln \frac{1}{y} + \theta_2\right) + o(y^\rho)\,,
\end{aligned} \tag{13.4.16}$$

where $(x, u, y) = (x_0, u_0, y_0)d^{-1}$, and A_1, A_2, θ, θ_1, θ_2 are some constants.

The image of $T_0 S_0^+$ by the diffeomorphism T_1 also has a spiraling shape. It intersects W^s_{loc} infinitely many times near M^+. Indeed, it is immediately seen from (13.4.16)[11] that the preimage $T^{-1}(W^s_{\text{loc}} \cap S_0)$ of $y = 0$ consists of an infinite sequence of surfaces

$$l_k : y = y_k(x, u) \equiv Ce^{-\pi k/\omega}(1 + o(1)_{k\to+\infty})\,, \tag{13.4.17}$$

where $C = e^{(\theta - \frac{\pi}{2})/\omega}$ and k runs through all sufficiently large positive integer values. As $k \to +\infty$, these surfaces accumulate on $y = 0$. By construction, they are intersections of the (global) stable manifold of O with S_0. Thus, the stable manifold is self-limiting here (it has the helicoid-like shape shown in Fig. 13.4.14).

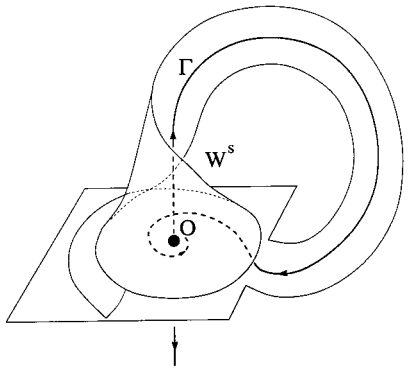

Fig. 13.4.14. The stable manifold of the saddle-focus continued along the homoclinic loop in backward time has a helicoid form.

[11] Note that $A > 0$ by assumption, and that $x > 0$ because x is close to x^+ (the coordinate of the point $M^+ = \Gamma \cap S_0$) which is positive. Recall that $x^+ \neq 0$ because Γ does not lie in the strong stable manifold by assumption.

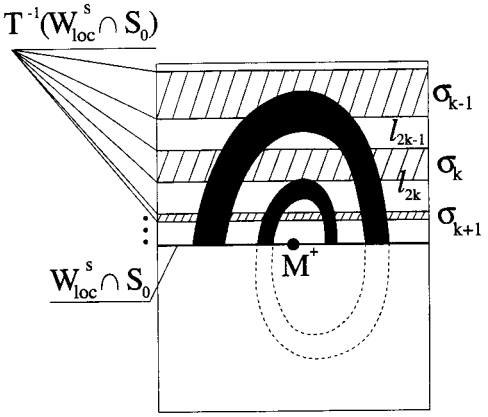

Fig. 13.4.15. The structure of the Poincaré map near a homoclinic loop to the saddle-focus.

Let σ_k be the region in S_0^+ bounded by l_{2k-1} and l_{2k}. By construction, the images by the Poincaré map T of those points on S_0^+ which do not belong to the union of the "strips" σ_k fall into the region $y < 0$. Thus, their orbits leave a neighborhood of the loop. Let us therefore restrict our consideration to the strips σ_k.

The image $T\sigma_k$ of each strip is one half of a single curl of the "snake" located on the surface $y = 0$ (see Fig. 13.4.15). Observe that it has a distinguishable horseshoe-like form. It follows from (13.4.16) and (13.4.17) that the top of the kth horseshoe corresponds to

$$y \sim y_{2k}^{\rho} \sim e^{-2\pi\rho k/\omega}\,.$$

Thus, when $\rho > 1$, there is no intersection between σ_k and $T\sigma_k$. On the contrary, when $\rho < 1$, the intersection $T\sigma_k \cap \sigma_k$ is non-empty and consists of two connected components (Fig. 13.4.16). It is geometrically evident that there is a fixed point of T at each of the components.[12]

The fixed points of the Poincaré map T correspond to the periodic orbits of the system. Thus, we have almost proved the following theorem.

Theorem 13.8. *If $\rho < 1$, then there exists infinitely many saddle periodic orbits in any neighborhood of the loop $\bar{\Gamma}$.*

[12] What we see is analogous to the famous *Smale horseshoe*.

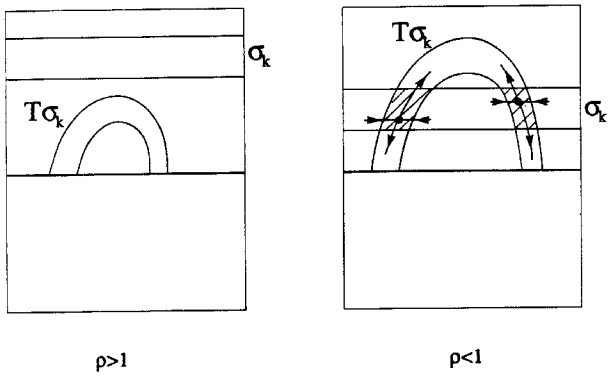

Fig. 13.4.16. Location of the strip σ_k and its image $T\sigma_k$ under the Poincaré mapping for $\rho > 1$ and $\rho < 1$.

This theorem is a part of a more general assertion [including also the case of a multi-dimensional unstable manifold as well as saddle-foci of types $(2,1)$ and $(2,2)$] on complex dynamics near the homoclinic loop of a saddle-focus [136]. Condition $\rho < 1$ also known as the Shilnikov condition is very important here, because the structure of the phase space near the homoclinic loop is drastically changed in comparison to the case $\rho > 1$ covered by Theorem 13.6. The main bifurcations in the boundary case $\rho = 1$, when a small perturbation trigging the system into a homoclinic explosion from simple dynamics ($\rho > 1$) to complex dynamics ($\rho < 1$) were first considered in [29].

Proof. The fixed points of the Poincaré map T given by (13.4.16) are found from the equation

$$\begin{aligned} y &= Axy^\rho \cos\left(\omega \ln \frac{1}{y} + \theta\right) + o(y^\rho)\,, \\ x &= x^+ d^{-1} + A_1 xy^\rho \cos\left(\omega \ln \frac{1}{y} + \theta_1\right) + o(y^\rho)\,, \\ u &= u^+ d^{-1} + A_2 xy^\rho \cos\left(\omega \ln \frac{1}{y} + \theta_2\right) + o(y^\rho)\,. \end{aligned} \tag{13.4.18}$$

The values of x and u are uniquely determined from the second and third equations:

$$x = x^+ d^{-1} + O(y^\rho)\,, \quad u = u^+ d^{-1} + O(y^\rho)\,. \tag{13.4.19}$$

Substituting these expressions into the first equation of (13.4.18), we obtain the following equation for the y-coordinate of a fixed point:

$$y = A\frac{x^+}{d}y^\rho \cos\left(\omega \ln\frac{1}{y} + \theta\right) + o(y^\rho)\,. \tag{13.4.20}$$

The graph of the right-hand side of this equation is shown in Fig. 13.4.17. When $\rho < 1$ [Fig. (13.4.17(b)], there are infinitely many roots accumulating to zero:

$$y_k^* = Ce^{-\pi k/\omega}(1 + o(1)_{k\to+\infty})\,, \tag{13.4.21}$$

where $C = e^{(\theta-\frac{\pi}{2})/\omega}$.

The Jacobian matrix of the map T at the corresponding fixed point is given by [see (13.4.16), (13.4.19) and (13.4.21)]

$$\begin{pmatrix} (-1)^{k+1}A\dfrac{x^+}{d}\omega\ (y_k^*)^{\rho-1}(1+o(1)) & O((y_k^*)^\rho) & O((y_k^*)^\rho) \\ O((y_k^*)^{\rho-1}) & O((y_k^*)^\rho) & O((y_k^*)^\rho) \\ O((y_k^*)^{\rho-1}) & O((y_k^*)^\rho) & O((y_k^*)^\rho) \end{pmatrix}. \tag{13.4.22}$$

Since $y_k^* \to 0$ as $k \to +\infty$, it follows that $(y_k^*)^\rho \to 0$ and $(y_k^*)^{\rho-1} \to +\infty$ (recall that $\rho < 1$). It is easy to see now that the matrix (13.4.22) has only one eigenvalue

$$\left(\text{estimated as} \quad \sim (-1)^{k+1}A\frac{x^+}{d}\omega(y_k^*)^{\rho-1}\right)$$

which is greater than 1 in absolute value, while all other eigenvalues tend to zero as $k \to +\infty$.

We have shown the existence of infinitely many saddle fixed points of the map T which correspond to saddle periodic orbits (with two-dimensional unstable and m-dimensional stable manifolds) of the system. Those with *even* k's have a negative unstable multiplier, and their unstable manifolds are non-orientable. The periodic orbits corresponding to *odd* k's have a positive unstable multiplier, and hence, orientable unstable manifolds.

The y-coordinate of the kth fixed point tends to zero as $k \to +\infty$, which implies that the x-coordinate tends to x^+, and the u-coordinate tends to u^+

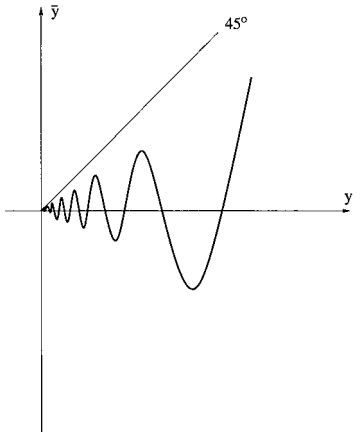

(a)

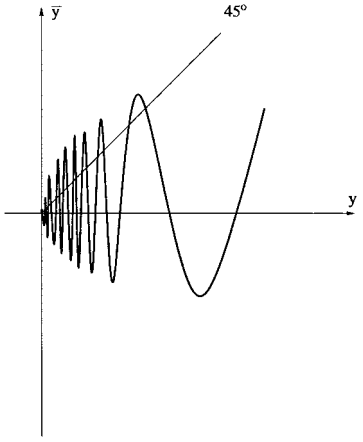

(b)

Fig. 13.4.17. Modelling one-dimensional Poincaré map for $\rho > 1$ (a) and $\rho < 1$ (b).

[see (13.4.19)]. Thus, these periodic orbits do accumulate to the homoclinic loop Γ. End of the proof.

Remark. Note that the problem on the fixed points of the Poincaré map near the homoclinic loop to a saddle-focus is reduced to the study of the fixed point

of the one-dimensional map

$$\bar{y} = Ay^\rho \cos\left(\omega \ln \frac{1}{y} + \theta\right) + o(y^\rho)\,.$$

In fact, this map indeed captures many (not all, though) features of the dynamics near such homoclinic loop.

13.5. Behavior of trajectories near a homoclinic loop in the case dim $W^u > 1$

Let us consider next the general case where the dimension of the unstable manifold of O is $n \geq 1$. Let $\gamma_1, \ldots, \gamma_n$ be the characteristic exponents with positive real parts, ordered so that

$$0 < \operatorname{Re}\,\gamma_1 \leq \operatorname{Re}\,\gamma_2 \leq \cdots \leq \operatorname{Re}\,\gamma_n\,.$$

Let us assume that the saddle value is negative:

$$\sigma = \operatorname{Re}\,\lambda_1 + \operatorname{Re}\,\gamma_1 < 0\,, \tag{13.5.1}$$

i.e. *the characteristic exponent nearest to the imaginary axis has a positive real part.*

It is obvious that if $\sigma > 0$, we can always make it negative by a reversion of time.

Generically, we may assume that if the leading exponent γ_1 is real, then

$$\gamma_1 < \operatorname{Re}\,\gamma_i \qquad (i = 2, \ldots, n)\,, \tag{13.5.2}$$

and if γ_1 is complex, then

$$\operatorname{Re}\,\gamma_1 = \operatorname{Re}\,\gamma_2 < \operatorname{Re}\,\gamma_i \quad (i = 3, \ldots, n)\,. \tag{13.5.3}$$

To distinguish between these two cases, we will call the equilibrium state *a saddle* in the first case, and *a saddle-focus* in the second case, for the sake of brevity. Note that this terminology differs from what we have used throughout the first part of this book. Namely, in this section we do not take into account whether the leading characteristic exponent λ is real or complex. Thus, in this particular section, we call O a saddle if (13.5.1) and (13.5.2) are satisfied, even if λ_1 is complex.

Let us now make two more non-degeneracy assumptions. Namely, we assume that

(1) *the homoclinic loop* Γ *does not belong to the strongly unstable manifold* W^{uu}. Recall (Secs. 2.6 and 2.7) that the unstable manifold of a saddle has a special subset — an invariant smooth strong unstable manifold W^{uu}. It is tangent at O to the eigenspace of the linearization matrix which corresponds to the non-leading characteristic exponents $\gamma_2, \dots, \gamma_n$ in the case of a saddle, or to $\gamma_3, \dots, \gamma_n$ in the case of a saddle-focus. The trajectories of W^u which do not belong to W^{uu} tend to O as $t \to -\infty$ along the leading direction (the eigenvector corresponding to the leading characteristic exponent γ_1) in the case of saddle, or they spiral toward O along the two-dimensional leading plane (the eigenplane corresponding to the leading characteristic exponents γ_1 and γ_2) in the case of a saddle-focus.

In other words, we assume that the homoclinic loop behaves in one of the two ways described above as it approaches O as $t \to -\infty$. In principle, this is not a strong restriction since it defines an open and dense subset on the bifurcation surface: if Γ lies in W^{uu} for some system, then by an arbitrarily small smooth perturbation it may be pushed into $W^u \backslash W^{uu}$.

(2) *The extended stable manifold* W^{sE} *is transverse to the unstable manifold* W^u *at the points lying on* Γ. Recall (Sec. 2.7) that a two-dimensional local invariant manifold W^{sE} is tangent at O to the eigenspace of the linearization matrix corresponding to the stable characteristic exponents $\lambda_1, \dots, \lambda_m$ and the leading unstable exponents γ_1 (in the case of the saddle), or $\gamma_{1,2}$ (in the case of the saddle-focus), respectively. Since it contains the local stable manifold, it also contains the homoclinic loop Γ. Continuation along the backward orbits near Γ defines the invariant manifold W^{sE} globally. The local (hence, global) extended stable manifolds are not unique, but any two such manifolds are tangent to each other at any point on the stable manifold. Therefore, our transversality condition is well-posed.

Note that in the case of a saddle (γ_1 is real) the tangent to the unstable manifold at any point which does not belong to the strong unstable manifold W^{uu} is spanned onto the phase velocity vector and the tangent to a leaf of the strong-unstable foliation F^{uu} through the given point.[13] Since W^{sE} is an invariant manifold, it consists of whole trajectories. Therefore, its tangent contains the phase velocity vector as well. Hence, in the case of a saddle the

[13] This is the uniquely defined invariant foliation of W^u transverse to the leading direction near O; see Sec. 6.1.

transversality of W^{sE} to W^u is equivalent to the transversality of W^{sE} to the foliation F^{uu}.

One can now notice that in the case of a saddle, the above assumptions coincide with the conditions of Theorem 6.1 in Sec. 6.1 of Part I of this book. This theorem constitutes the existence (for the system with a homoclinic loop itself, and for all nearby systems) of *a repelling smooth* ($\mathbb{C}^1$) *invariant* $(m+1)$*-dimensional manifold* $\mathcal{M}$ which contains all orbits staying in a small neighborhood U of Γ for all positive times. It follows that our problem on the bifurcations of Γ can be reduced here to that on the bifurcations on $\mathcal{M}$.

In a small neighborhood of the saddle O, this invariant manifold coincides with some extended stable manifold $W^{sE}_{\rm loc}$. Thus, the latter manifold is tangent at O to the eigenspace corresponding to the characteristic exponents γ_1 and $\lambda_1, \dots, \lambda_m$. Hence, the saddle equilibrium state of the system restricted on $\mathcal{M}$ has a one-dimensional (corresponding to γ_1) unstable manifold and an m-dimensional stable manifold (corresponding to $\lambda_1, \dots, \lambda_m$). The associated saddle value is negative. The bifurcations of the homoclinic loop in this situations are described by Theorem 13.6. Now, recall that $\mathcal{M}$ is *a repelling manifold*, i.e. flow is expanding in directions transverse to $\mathcal{M}$. Therefore, the stable periodic orbit bifurcating from the saddle on $\mathcal{M}$ (according to Theorem 13.6) is indeed a *saddle* periodic orbit with an n-dimensional unstable manifold for the whole system. Thus, we arrive at the following result.

Theorem 13.9. (Shilnikov [134]) *Let a saddle O with saddle value $\sigma < 0$ have a homoclinic loop Γ which satisfies the non-degeneracy conditions* (1) *and* (2). *Let U be a small neighborhood of Γ. If the homoclinic loop splits inward on the invariant manifold $\mathcal{M}$, then a single periodic orbit L with an n-dimensional unstable manifold will be born. Furthermore, the only orbits which stay in U for all times are the saddle O, the cycle L and a single heteroclinic orbit*[14] *which is α-limit to O and ω-limit to L.*
When the loop splits outward, there are no periodic orbits in U; moreover, the only entire orbit in U is the saddle O. When there exists the separatrix loop Γ, there are no other entire orbits in U, except for Γ and O.

This theorem was originally proved without a reduction onto the invariant manifold (although the original formulation was somewhat different from the present one, both are equivalent). Its proof was based on a direct analysis

[14] This is the unstable separatrix Γ_1 for the system on $\mathcal{M}$.

of the $(m+n-1)$-dimensional Poincaré map near the homoclinic loop. This map was shown to be a saddle map in the sense similar to our definition in Sec. 3.15 of Part I, and after that a fixed point theorem was applied, analogous to Theorem 3.28 in Sec. 3.15. In order to obtain suitable estimates on the Poincaré map, the system was assumed to be analytical in [134]. Note that the present proof needs only $\mathbb{C}^1$-smoothness.

In the case of a saddle-focus the following result holds.

Theorem 13.10. (Shilnikov [136]) *Let a saddle-focus O have a homoclinic loop Γ which satisfies the non-degeneracy conditions* (1) *and* (2). *Then, in an arbitrarily small neighborhood of Γ, there exist infinitely many saddle periodic orbits.*

We do not give its proof here because it is beyond the scope of this book. A partial case (Theorem 13.8) was discussed in the preceding section. In fact, the main theorem of [136] contains much more detailed information on the structure of the phase space in a neighborhood of the homoclinic loop of the saddle-focus; namely, a description of hyperbolic subsets in terms of symbolic dynamics.

In the original proof the system under consideration was assumed to be analytic. Later on, other simplified proofs have been proposed which are based on a reduction to a non-local center manifold near the separatrix loop (such a center manifold is, generically, 3-dimensional if the stable characteristic exponent λ_1 is real, and 4-dimensional if $\lambda_1 = \lambda_2^*$ is complex) and on a smooth linearization of the reduced system near the equilibrium state (see [120, 147]). The existence of the smooth invariant manifold of low dimension is important here because it effectively reduces the dimension of the problem.[15]

13.6. Codimension-two bifurcations of homoclinic loops

In this and the following sections we will review some codimension-two bifurcations of homoclinic loops and heteroclinic cycles which occur in various models.

[15] We should however stress that conditions (1) and (2) alone are not sufficient for the existence of any smooth invariant manifold near the loop in the case of a saddle-focus (what one really needs for such manifold to exist is the tranversality condition of W^{sE} to F^{uu}; see [150]). Therefore, the reduction to an invariant manifold cannot give Theorem 13.10 in its full generality.

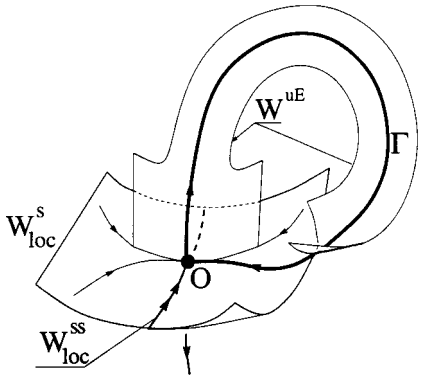

Fig. 13.6.1. The inclination-flip bifurcation ($A = 0$) is due to a violation of the transversality of the intersection of W^{uE} and W^s at the points of the homoclinic loop Γ.

Consider an $(n+1)$-dimensional $\mathbb{C}^r$-smooth ($r \geq 4$) system with a saddle equilibrium state O. Let O have only one positive characteristic exponent $\gamma > 0$; the other characteristic exponents $\lambda_1, \lambda_2, \ldots, \lambda_n$ are assumed to have negative real parts. Moreover, we want the leading stable exponent λ_1 to be real:

$$\lambda_1 > \mathrm{Re}\ \lambda_j\,, \quad j = 2, \ldots, n\,.$$

The unstable manifold W^u of O is one-dimensional, and the stable manifold W^s is n-dimensional. Suppose that one of the unstable separatrices (Γ_1) tends to O as $t \to +\infty$, thereby forming a homoclinic loop, as shown in Fig. 13.6.1.

We will analyze the following three cases of codimension-two bifurcations of such homoclinic loops.

Case A.

(1) $\nu = 1$;
(2) $\Gamma \not\subset W^{ss}$; and
(3) $A \neq 0$.

Case B.

(1) $A = 0$,
i.e. W^{uE} is tangent to W^s at the points of Γ (see Fig. 13.6.1);
(2) $\Gamma \not\subset W^{ss}$,
i.e. Γ enters O as $t \to +\infty$ along the leading direction; and
(3) $\frac{1}{2} < \nu < 1$, $\nu_j > 1$ $(j = 2, \ldots, n)$.

Case C.

(1) $\Gamma \subset W^{ss}$,
i.e. Γ enters O as $t \to +\infty$ along a non-leading direction (see Fig. 13.6.2);
(2) The extended unstable manifold W^{uE} is transverse to the stable manifold W^s at points on Γ; and
(3) $\nu < 1$, $\nu_j > 1$ $(j = 2, \dots, n)$.
$\Big($Here: $\nu = \left|\frac{\lambda_1}{\gamma}\right|$, $\quad \nu_j = \left|\frac{\mathrm{Re}\lambda_j}{\gamma}\right|$.$\Big)$

Case A corresponds to the boundary between positive and negative saddle values. Cases B and C correspond to a violation of the non-degeneracy conditions (1) and (2) of Theorem 13.4.2, respectively (the birth of a saddle periodic orbit from a homoclinic loop with positive saddle value). Condition (3) in the last two cases is necessary to exclude the transition to complex dynamics via these bifurcations (some of the cases with complex dynamics were studied in [44, 70, 78, 96, 79, 71, 72]).

Codimension-two bifurcations of homoclinic loops are essential for studying bifurcation phenomena in the Lorenz equation

$$\dot{x} = -\sigma(x - y)\,, \quad \dot{y} = rx - y + xz, \quad \dot{z} = -bz + xy\,.$$

When $\sigma = 10$, $b = 8/3$ and $r \approx 13.926$, both of the one-dimensional unstable separatrices Γ_1 and Γ_2 of the saddle $O(0, 0, 0)$ return to the saddle, along the same direction (the positive z semi-axis). They form a geometrical configuration called a homoclinic butterfly (Fig. 13.6.3). Note that a homoclinic butterfly may only occur in $\mathbb{R}^n$ with $n \geq 3$.

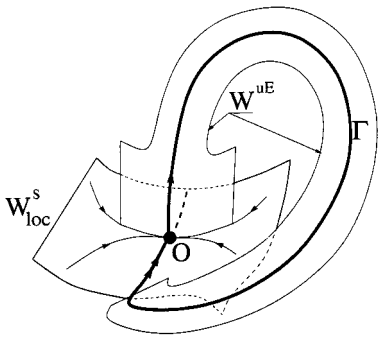

Fig. 13.6.2. The orbit-flip bifurcation — the homoclinic loop Γ gets closed along the non-leading submanifold at the moment of bifurcation.

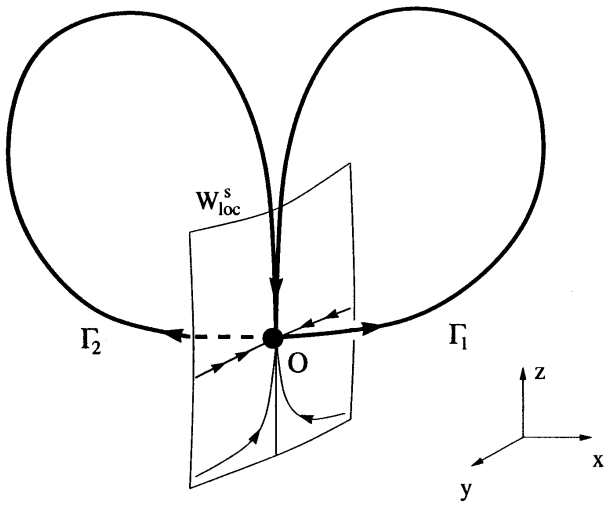

Fig. 13.6.3. A homoclinic butterfly. Both separatrices return to the saddle tangentially to each other.

In general, the bifurcation of a homoclinic butterfly is of codimension two. However, the Lorenz equation is symmetric with respect to the transformation $(x, y, z) \leftrightarrow (-x, -y, z)$. In such systems the existence of one homoclinic loop automatically implies the existence of another loop which is a symmetrical image of the other one. Therefore, the homoclinic butterfly is a codimension-one phenomenon for the systems with symmetry.

In the Lorenz model, the saddle value is positive for the parameter values corresponding to the homoclinic butterfly. Therefore, upon splitting the two symmetric homoclinic loops outward, a saddle periodic orbit is born from each loop. Furthermore, the stable manifold of one of the periodic orbits intersects transversely the unstable manifold of the other one, and vice versa. The occurrence of such an intersection leads, in turn, to the existence of a hyperbolic limit set containing transverse homoclinic orbits, infinitely many saddle periodic orbits and so on [1]. In the case of a homoclinic butterfly without symmetry there is also a region in the parameter space for which such a rough limit set exists [1, 141, 149]. However, since this limit set is unstable, it cannot be directly associated with the strange attractor — a mathematical image of dynamical chaos in the Lorenz equation.

In order to resolve this problem, it was proposed in [138] to study the homoclinic butterflies in the Cases A, B and C above. Namely, it was established that the bifurcation of a homoclinic butterfly results in the immediate appearance of a Lorenz attractor when

(a) the saddle value $\sigma = 0$ with the additional condition that $|A| < 2$ on both loops; or when
(b) $A = 0$ on both loops with $\sigma > 0$ and condition 3 of Case B is satisfied; or when
(c) both loops belong to the non-leading manifold (with $\sigma > 0$ and condition 3 satisfied, as well).

Case (a) corresponds to a codimension-three bifurcation, while Cases (b) and (c) are of codimension four. However, if the system exhibits some symmetry, then all of the above three bifurcations reduce to codimension two. It was established in [126, 127, 129] that a symmetric homoclinic butterfly with either $\sigma = 0$ or $A = 0$ appears in the so-called extended Lorenz model, and in the Shimizu–Morioka system, as well as in some cases of local bifurcations of codimension three in the presence of certain discrete symmetries [129].

We will not consider here the birth of the Lorenz attractor (see [114, 115, 117, 126, 127, 129] for that), but we consider the codimension-two bifurcations of a single homoclinic loop. The bifurcation diagrams for Case A are the same as in the two-dimensional case (see Fig. 13.3.1 when $0 < A < 1$ and Fig. 13.3.3 for $-1 < A < 0$, respectively; the situation where $|A| > 1$ reduces to that of $|A| < 1$ upon a reversion of time). This was established in [38], although the proof of the completeness of the diagrams (the absence of other bifurcational curves) was not done. We close this problem here (Subsec. 13.6.3).

The bifurcation unfoldings for Cases B and C are identical and shown in Fig. 13.6.4. Here, μ is the splitting parameter of the homoclinic loop, and A is the separatrix value. Since in Sec. 13.4 the separatrix value A was defined only when the loop does not belong to W^{ss}, we must specify its meaning for Case C.

Recall that the non-leading manifold $W^{ss}_{\rm loc}$ is $(n-1)$-dimensional. It partitions $W^{s}_{\rm loc}$ into two components. If the loop Γ lies in W^{ss}, then a small perturbation may make it miss $W^{ss}_{\rm loc}$ so that it enters the saddle from either component of $W^{s}_{\rm loc}$. We will show (Subsec. 13.6.2) that when the loop is moved from one component to the other, it is accompanied by a change in the sign of the separatrix value A.

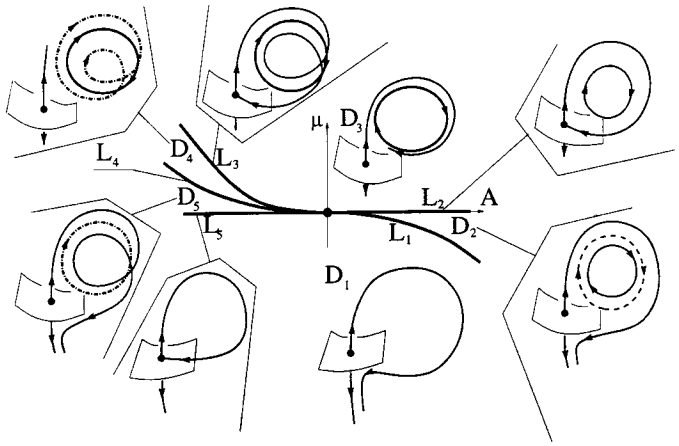

Fig. 13.6.4. The bifurcation unfoldings for an orbit- and an inclination-flip bifurcation are identical in the simplest case.

The bifurcation diagram for Case B was proposed, independently, in [126] (see also [127, 129]) and in [77], for Case C — in [119]. Here, we give a unified and self-consistent proof for both cases, including the proof of the completeness of the bifurcational diagram. In the West, the Case B is called the *inclination-flip* bifurcation and the Case C is called the *orbit-flip*.

Let us introduce coordinates near the saddle so that the system assumes, locally, the following form [see Sec. 13.8, formula (13.8.28)]

$$\begin{aligned} \dot{x} &= -\nu x + f_{11}(x,y)x + f_{12}(x,u,y)u\,, \\ \dot{u} &= Bu + f_{21}(x,y)x + f_{22}(x,u,y)u\,, \\ \dot{y} &= y\,, \end{aligned} \tag{13.6.1}$$

where $x \in \mathbb{R}^1$ and $y \in \mathbb{R}^1$ are the leading coordinates, $u \in \mathbb{R}^{n-1}$ is the vector of stable non-leading coordinates; $\nu = |\lambda_1/\gamma|$ is the saddle index, and the eigenvalues of matrix B are $-\nu_2, \ldots, -\nu_n$, where $\nu_j = |\mathrm{Re}\,\lambda_j/\gamma|$. Recall that $1 < \nu_j$, $j = 2, \ldots, n$. In Case B we have $\frac{1}{2} < \nu < 1$, and $\nu < 1$ in Case C. In Case A, $\nu = 1$ at the bifurcation point, so we can let $\nu = 1 + \varepsilon$ here, where ε is a small parameter. The $\mathbb{C}^{r-1}$-functions f_{ij} satisfy

$$f_{i1}(x,0) \equiv 0\,, \quad f_{1j}(0,0,y) \equiv 0\,. \tag{13.6.2}$$

In these coordinates, the stable manifold is locally given by $y = 0$, the local unstable manifold is given by $\{x = 0, u = 0\}$. The equation of the strong stable manifold is $\{x = 0, y = 0\}$.

By assumption, the loop Γ coincides locally with the y semi-axis when it leaves O at $t = -\infty$. Since $\Gamma \not\subset W^{ss}$ in Cases A and B, it enters O as $t \to +\infty$ along the x-axis. In Case C, the separatrix Γ lies locally in $\{x = 0, y = 0\}$ as it returns to the saddle. We assume also that the loop adjoins O from the side of positive y as $t \to -\infty$ and, in the first two cases, from the side of positive x as $t \to +\infty$.

Let us choose two cross-sections S_0 and S_1 transverse to the loop Γ. Let S_1 be given by $\{y = d\}$ and S_0 be given by $\{\|u\| = d\}$ in Case C, or by $\{x = d\}$ in Cases A and B, where $d > 0$ is small. Denote the coordinates on S_1 by (x_1, u_1) and the coordinates on S_0 by (y_0, u_0) in Cases A and B, or by (y_0, x_0, u_0) in Case C.

On the upper part $S_0^+ : \{y_0 \geq 0\}$ of S_0, the local map $T_0 : S_0^+ \to S_1$ is defined by the orbits of the system. It follows from the last equation in (13.6.1) that the flight time from S_0^+ to S_1 is

$$\tau = -\ln \frac{y_0}{d}\,. \tag{13.6.3}$$

It was shown in Sec. 13.8 [see formulas (13.8.30)–(13.8.36)] that the fulfillment of identities (13.6.2) implies the following estimates for the solution of the system starting from a point (x_0, u_0) at $t = 0$ and ending on $\{y = d\}$ at $t = \tau$:

$$\begin{aligned} x(\tau) &= e^{-\nu\tau} x_0 + \xi_1(x_0, u_0, \tau) + \bar{\xi}_1(u_0, \tau)\,, \\ u(\tau) &= \xi_2(x_0, u_0, \tau) + \bar{\xi}_2(u_0, \tau)\,, \end{aligned} \tag{13.6.4}$$

where

$$\begin{gathered} \xi_{1,2}(0, u_0, \tau) \equiv 0\,, \\ \|\xi_{1,2}\|_{C^{r-2}} = o(e^{-\tilde{\nu}\tau}), \quad \|\bar{\xi}_{1,2}\|_{C^{r-2}} = o(e^{-(1+\delta)\tau})\,, \\ \|\xi_{1,2}\|_{C^{r-1}} + \|\bar{\xi}_{1,2}\|_{C^{r-1}} = o(e^{-\nu\tau})\,, \end{gathered} \tag{13.6.5}$$

where $\tilde{\nu}$ may be taken arbitrarity close from below to $\min\{2\nu, 1+\nu, \nu_2, \ldots, \nu_n\}$ (so $\tilde{\nu} > \nu$ and, moreover, $\tilde{\nu} > 1$ in Case A and B where we have $2\nu > 1$) and δ is such that $0 < \delta < \min\{\nu, \nu_2 - 1, \ldots, \nu_n - 1\}$.

Substituting formula (13.6.3) for the flight time into (13.6.6) and (13.6.5), we obtain the following estimate for the local map $T_0 : S_0^+ \to S_1$ in Case C

(where the cross-section S_0 is $\|u_0 = d\|$)

$$x_1 = x_0 y_0^\nu d^{-\nu} + \varphi_1(x_0, y_0, u_0)\,, \quad u_1 = \varphi_2(x_0, y_0, u_0)\,, \tag{13.6.6}$$

where

$$\begin{gathered}
\varphi = o(|x_0| y_0^{\tilde\nu} + y_0^{1+\delta})\,, \\
\frac{\partial^{p+q}\varphi}{\partial u_0^p \partial y_0^q} = o(|x_0| y_0^{\tilde\nu - q} + y_0^{1+\delta-q}) \quad (p+q \le r-3)\,, \\
\frac{\partial^{r-2}\varphi}{\partial u_0^p \partial y_0^q} = o(y_0^{\tilde\nu-q}), \quad \frac{\partial^{s+p+q}\varphi}{\partial x_0^s u_0^p \partial y_0^q} = o(y_0^{\tilde\nu-q}) \quad (s+p+q \le r-2)\,, \\
\frac{\partial^{p+q}\varphi}{\partial (x_0,u_0)^p \partial y_0^q} = o(y_0^{\nu-q}) \quad \text{at } p+q = r-1\,.
\end{gathered} \tag{13.6.7}$$

In both Cases A and B, where $x_0 = d$ on S_0, we have the following formula for T_0:

$$x_1 = y_0^\nu d^{1-\nu} + \varphi_1(y_0, u_0)\,, \qquad u_1 = \varphi_2(y_0, u_0)\,, \tag{13.6.8}$$

where the functions $\varphi_{1,2}$ satisfy

$$\begin{gathered}
\varphi = o(y_0^{\tilde\nu})\,, \\
\frac{\partial^{p+q}\varphi}{\partial u_0^p \partial y_0^q} = o(y_0^{\tilde\nu-q}) \quad (p+q \le r-2), \quad \frac{\partial^{r-1}\varphi}{\partial u_0^p \partial y_0^q} = o(y_0^{\nu-q})\,.
\end{gathered} \tag{13.6.9}$$

Recall that $\tilde\nu > 1$ here, contrary to (13.6.7) where we have only $\tilde\nu > \nu$.

13.6.1. The case A = 0 — inclination-flip

The flow outside a small neighborhood of O defines the global map $T_1 : S_1 \to S_0$ by the orbits close to Γ. In Case B the map T_1 in a small neighborhood of the point $M^-(0,0) = W^u_{\rm loc} \cap S_1$ can be represented by

$$\begin{aligned}
\bar y_0 &= \mu + Ax_1 + a_{12}u_1 + \cdots\,, \\
\bar u_0 &= u^+ + a_{21}x_1 + a_{22}u_1 + \cdots\,,
\end{aligned} \tag{13.6.10}$$

where A is the separatrix value which is assumed to vanish at the bifurcation point. In this formula, $(\mu, u^+(\mu, A))$ are the coordinates of the point $M^+ = T_1 M^-$ where the separatrix Γ_1 first intersects S_0. The homoclinic loop exists at $\mu = 0$ (since $M^+ \in W^s_{\rm loc} \cap S_0$ in this case).

Combining formulas (13.6.8) and (13.6.10), we obtain the following representation for the Poincaré map T in Case B:

$$\begin{aligned} \bar{y} &= \mu + Ay^{\nu} + \varphi_1(y,u)\,, \quad y \geq 0\,, \\ \bar{u} &= u^{+} + a_{21}y^{\nu} + \varphi_2(y,u) \end{aligned} \tag{13.6.11}$$

(we drop here the sub-index "0" and also rescale variables to make $d = 1$ in (13.6.8); the modified functions $\varphi_{1,2}$ still satisfy estimates (13.6.7) — note that the second-order terms in the Taylor expansion for the global map T_1 make a contribution of order $O(y^{2\nu})$ in the new functions $\varphi_{1,2}$, but it is negligible in comparison with (13.6.7) because $\nu > 1/2$).

Let α be the root of the equation

$$\left(\frac{\mu}{\alpha}\right)^2 + \left(\frac{A}{\alpha^{1-\nu}}\right)^2 = 1\,. \tag{13.6.12}$$

Observe that α, which is uniquely defined by (13.6.12), converges to zero as $\mu, A \to 0$. One can see from (13.6.11) that $\bar{y} < y$ for $y > \alpha/(1-\nu)$. Thus, upon iterating the map T, the value of y decreases until it becomes of size $O(\alpha)$. Therefore, it is reasonable to rescale the variables and parameters via:

$$y \mapsto \alpha y\,, \quad u \mapsto u^{+} + \alpha^{\nu} u, \quad \mu = \alpha \sin\phi, \quad A = \alpha^{1-\nu}\cos\phi\,,$$

where (α, ϕ) are a kind of polar coordinates on the (μ, A)-plane. We can then recast this map into the form

$$\begin{aligned} \bar{y} &= \sin\phi + \cos\phi\; y^{\nu} + \cdots\,, \\ \bar{u} &= a_{21}y^{\nu} + \cdots\,, \end{aligned} \tag{13.6.13}$$

where the ellipsis stand for the terms which vanish along with the first derivatives with respect to y^{ν} and u as $\alpha \to +0$; moreover, all their derivatives up to order $(r-1)$ tend to zero uniformly on any interval of values of y bounded away from zero. This type of convergence is sufficient for one to show that the map (13.6.13) undergoes the same bifurcations as the limiting one-dimensional map

$$\bar{y} = \sin\phi + \cos\phi\; y^{\nu}\,, \quad y \geq 0\,. \tag{13.6.14}$$

The Lamerey diagrams for this map are shown in Fig. 13.6.5. The right-hand side of the map is either monotonically increasing (when $-\pi/2 < \phi < \pi/2$), or monotonically decreasing (when $\pi/2 < \phi < 3\pi/2$). Such maps may have only

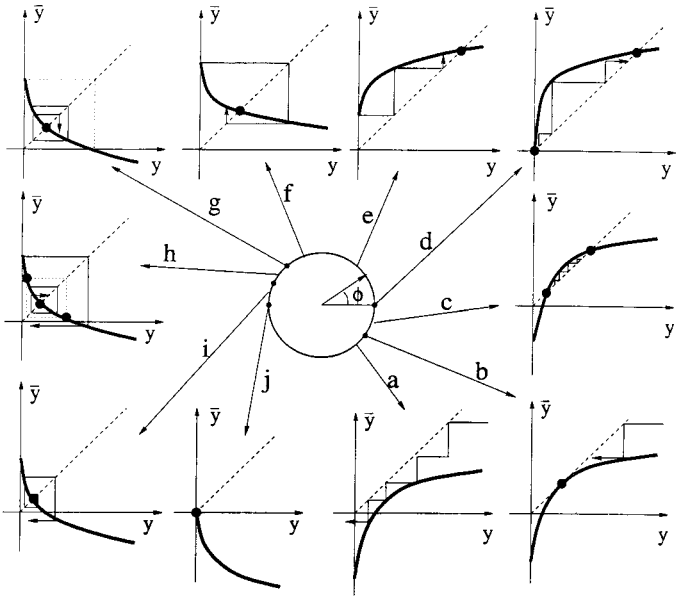

Fig. 13.6.5. The Lamerey diagrams for the map (13.6.14).

fixed points and orbits of period two, respectively. Moreover, the only possible bifurcations occurring in such maps are saddle-node bifurcations and primary period-doubling's ("primary" is applied to fixed points only). In addition, a fixed point or a period-two orbit may vanish on the boundary (given by $y = 0$) of the domain of definition of the map. This corresponds to the bifurcation of a homoclinic loop (simple or double, respectively) in the original system. The bifurcation values of ϕ are found from the system

$$\begin{aligned} y &= \sin\phi + y^{\nu}\cos\phi\,, \\ \pm 1 &= \nu y^{\nu-1}\cos\phi\,, \end{aligned} \tag{13.6.15}$$

where "+" corresponds to a saddle-node bifurcation of a fixed point, and "-" corresponds to a period-doubling of a fixed point. This system can be recast as

$$\begin{aligned} y &= -\frac{\nu}{1-\nu}\sin\phi\,, \\ \frac{(1-\nu)^{1-\nu}}{\nu^{\nu}} &= \frac{\cos\phi}{(-\sin\phi)^{1-\nu}} \end{aligned} \tag{13.6.16}$$

for the saddle-node bifurcation case, or as

$$\begin{aligned} y &= \frac{\nu}{1+\nu}\sin\phi\,, \\ -\frac{(1+\nu)^{1-\nu}}{\nu^{\nu}} &= \frac{\cos\phi}{(\sin\phi)^{1-\nu}} \end{aligned} \tag{13.6.17}$$

for the period-doubling case. Here, y is the coordinate of the bifurcating fixed point. One can see that these equations define a unique value of ϕ for each bifurcation. Moreover, both bifurcations are non-degenerate: the Lyapunov value is non-zero at a saddle-node bifurcation, and is non-zero and positive at a period-doubling bifurcation.

Thus, the saddle-node bifurcation leads to the appearance of a pair of fixed points, stable and unstable, whereas the period-doubling leads to the appearance of an unstable orbit of period two. An unstable fixed point vanishes at $y = 0$ (corresponding to a single-circuit homoclinic loop) when $\phi = 0$ and $\phi = \pi$. An unstable orbit of period two approaches $y = 0$ (a double homoclinic loop) when

$$0 = 1 + \frac{\cos\phi}{(\sin\phi)^{1-\nu}}\,. \tag{13.6.18}$$

To make sure that there are no other bifurcation values (which might also give rise to saddle-node bifurcations of period-two orbits), just note that the third derivative of the second iterate of the map (13.6.14) never vanishes. This means that the second iteration of the map cannot have more than three fixed points, including their multiplicity. Hence, this guarantees the absence of other orbits of period two in the map.

We have completed our analysis of the one-dimensional map (13.6.14). The phase portraits for the degenerate multi-dimensional map $\tilde{T}$

$$\bar{y} = \sin\phi + \cos\phi\; y^{\nu}\,, \quad \bar{u} = a_{21}y^{\nu} \tag{13.6.19}$$

can be easily constructed. Since the Poincaré map T is close to the above map [see (13.6.13)], every orbit which does not escape from the region $0 \le y \le 2/(1-\nu)$ must come to a small neighborhood of $\alpha-$ or $\omega-$ limit sets of the map $\tilde{T}$ given by (13.6.19). As the analysis above shows, these limit sets are fixed points or periodic orbits of period two. When they are not close to $y = 0$, the map T is close to $\tilde{T}$ along with at least three derivatives [for this purpose we have assumed above that the system under consideration is C^r-smooth with $r \ge 4$; see comments after the formula (13.6.13)]. This guarantees

that the two maps have the same phase portraits when all periodic points of (13.6.19) are rough, and that these maps undergo the same bifurcations near the values of ϕ for which the map $\tilde{T}$ undergoes a non-degenerate saddle-node or period-doubling bifurcation. Near the values of ϕ for which a fixed point or a period-two orbit of $\tilde{T}$ comes close to $y = 0$ [these values are, given, respectively, by the equations $\sin\phi = 0$ and (13.6.18)], this fixed point or period-two orbit is always of a saddle type. Moreover, the first or, respectively, second iteration of the map $\tilde{T}$ is a saddle map near $y = 0$ in the sense of Sec. 3.15. The same is true for the map T: since its first derivative with respect to y^ν is uniformly close to that of $\tilde{T}$, one can find y as a function of $\bar{y}$ and u and check, for the obtained cross-map, that conditions (3.15.10) of Definition 3.7 are fulfilled. Since a saddle map can have only a single saddle fixed point, it follows that the map T may have only a single saddle periodic orbit close to $y = 0$, and this periodic orbit is close to that of the map $\tilde{T}$.

Thus, the map T undergoes (for small α) the same bifurcations as the one-dimensional map (13.6.14). Returning to the original parameters (μ, A) we obtain the following asymptotics for the bifurcational curves (13.6.16)–(13.6.18):

- $\mu \sim -\dfrac{\nu^{\frac{\nu}{1-\nu}}}{1-\nu} A^{\frac{1}{1-\nu}}$, $A > 0$ — a saddle-node;
- $\mu \sim \dfrac{\nu^{\frac{\nu}{1-\nu}}}{1+\nu} (-A)^{\frac{1}{1-\nu}}$, $A < 0$ — a period-doubling bifurcation; and
- $\mu \sim (-A)^{\frac{1}{1-\nu}}$, $A < 0$ — a double loop.

Recall also that the line $\mu = 0$ corresponds to the primary homoclinic loop.

Summarizing, we have obtained the following description of the bifurcations on the (A, μ)-plane in Case B (see Fig. 13.6.4):
in the region D_1 there is no orbit (except the saddle) staying inside a small neighborhood U of the homoclinic loop Γ for all times. Upon crossing the curve L_1 corresponding to a saddle-node bifurcation, a stable and a saddle single-circuit periodic orbits are born. The saddle periodic orbit adheres to a homoclinic loop with $A > 0$ on the curve L_2. After this, the single stable periodic orbit exists in the region D_3. Upon crossing the line L_3, a saddle double periodic orbit bifurcates from a double homoclinic loop. This double-circuit periodic orbit coalesces with the single-circuit periodic orbit on the line L_4, so that the latter periodic orbit looses its stability (the reverse period-doubling bifurcation) and becomes of the saddle type. The new saddle periodic orbit disappears

in a single non-orientable/twisted ($A < 0$) homoclinic loop on the bifurcation curve L_5.

13.6.2. The case $\Gamma \subset W^{ss}$ — orbit-flip

Let us show next that the bifurcations in Case C ($\Gamma \subset W^{ss}$) proceed in the exactly same way. Here, the cross-section S_0 is given by $\{|u| = d\}$. The global map $T_1 : S_1 \to S_0$ defined by the orbits close to Γ is now represented by

$$\begin{aligned} \bar{y}_0 &= \mu + a_{11}x_1 + a_{12}u_1 + \cdots , \\ \bar{x}_0 &= \eta + a_{21}x_1 + a_{22}u_1 + \cdots , \\ \bar{u}_0 &= u^+ + a_{31}x_1 + a_{32}u_1 + \cdots , \end{aligned} \tag{13.6.20}$$

where $(\mu, \eta, u^+(\mu, \eta))$ are the coordinates of the point $M^+ = T_1 M^- = \Gamma_1 \cap S_0$. At $(\mu, \eta) = (0, 0)$, the system has a homoclinic loop lying in W^{ss} (since $M^+ \in W^{ss}_{\rm loc} \cap S_0$ in this case). Thus, we must consider bifurcations for small η and μ.

Note that the assumed transversality of W^{uE} to W^s is equivalent to the condition $a_{11} \neq 0$ (see Sec. 13.4).

Combining formula (13.6.20) with formula (13.6.6) for the local map, we obtain the following representation for the Poincaré map T in Case C:

$$\begin{aligned} \bar{y} &= \mu + a_{11}xy^\nu + \varphi_1(x, y, u) , \quad y \geq 0 , \\ \bar{x} &= \eta + a_{21}xy^\nu + \varphi_2(x, y, u) , \\ \bar{u} &= u^+ + a_{31}xy^\nu + \varphi_3(x, y, u) \end{aligned} \tag{13.6.21}$$

(we omit here the sub-index "0" and also rescale variables to let $d = 1$ in (13.6.6); the functions $\varphi_{1,2,3}$ satisfy estimates (13.6.7), i.e. $\varphi_{1,2,3} = o(|x|y^{\tilde{\nu}} + y^{1+\delta})$).

Let us define the separatrix value as

$$A = \eta a_{11} .$$

Note that at $\mu = 0$ and $\eta \neq 0$, the separatrix Γ_1 forms a homoclinic loop, approaching one of the two components of $W^s_{\rm loc} \backslash W^{ss}_{\rm loc}$ depending on the sign of η. Since the non-degeneracy conditions of Theorem 13.7 are satisfied for $\eta \neq 0$, the Poincaré map T has a smooth invariant curve through the point $M^+(0, \eta, u^+)$, transverse to the stable manifold. When restricted to this curve, the map T assumes the form

$$\bar{y} = a_{11}\eta y^\nu + o(y^\nu) ,$$

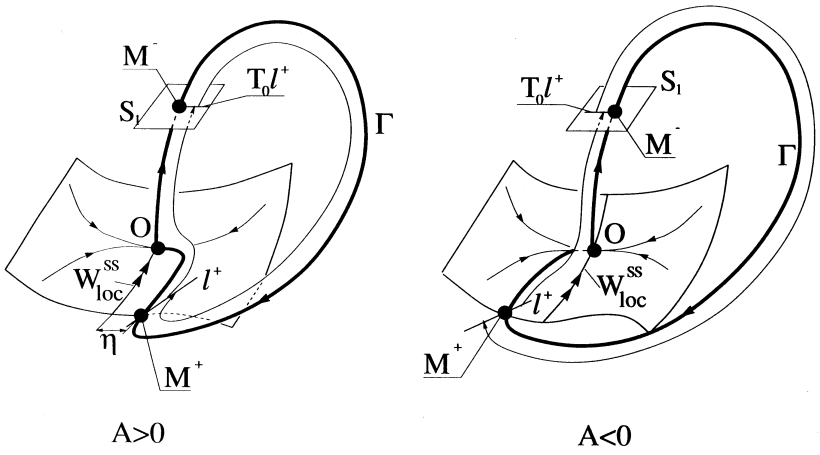

Fig. 13.6.6. Orbit-flip homoclinic bifurcation: the change of the way the separatrix Γ tends to the saddle results in the change of sign of separatrix A.

i.e. our definition of the separatrix value A is consistent with the definition in Sec. 13.4 for the case of a non-degenerate (codimension one) homoclinic loop. Observe that when the homoclinic loop moves from one component of $W^s_{\rm loc}\backslash W^{ss}_{\rm loc}$ to the other, the separatrix value changes its sign as shown in Fig 13.6.6.

Let us transform the x-variable: $x \to x+\eta$. The map T can then be recast as

$$\begin{aligned}
&\bar y = \mu + Ay^\nu + a_{11}xy^\nu + \varphi_1(x+\eta, y, u)\,, \quad y \ge 0\,,\\
&\bar x = a_{21}\eta y^\nu + a_{21}xy^\nu + \varphi_2(x+\eta, y, u)\,,\\
&\bar u = u^+ + a_{31}\eta y^\nu + a_{31}xy^\nu + \varphi_3(x+\eta, y, u)\,.
\end{aligned}$$

After rescaling $y \mapsto y\alpha$, $x \mapsto \alpha x$, $u \mapsto u^+ + \alpha u$ (where α is taken from (13.6.12)) the map is brought to a form analogous to (13.6.13). After this point, all considerations may now proceed in the same way as in Case B and leading to the exactly same result.

13.6.3. The case $\sigma = 0$

Let us now examine Case A — bifurcations of a homoclinic loop with $\sigma = 0$. Here, the local map from S_0 to S_1 is given by the formula (13.6.8) where $\nu = 1+\varepsilon$. The global map from S_1 to S_0 is defined by formula (13.6.10)

(where A is no longer assumed small; moreover, it depends now on the small parameters (μ, ε)). We also assume that $|A| < 1$ (the case $|A > 1$ can be similarly obtained by reversing of time). Combining formulas (13.6.8) and (13.6.10), we can write the Poincaré map T in the form

$$\begin{aligned} \bar{y} &= \mu + A(\mu, \varepsilon) y^{1+\varepsilon} + \varphi_1(y, u)\,, \quad y \geq 0\,, \\ \bar{u} &= u^+ + a_{21} y^{1+\varepsilon} + \varphi_2(y, u)\,, \end{aligned} \tag{13.6.22}$$

where $\varphi_{1,2}$ satisfy the estimates (13.6.7) (in which the dependence on x must be suppressed).

Note that conditions 2 and 3 in Case A coincide with the conditions of Theorem 6.2 (see detailed explanations in Sec. 13.4) which guarantees the existence of a smooth attracting two-dimensional invariant manifold $\mathcal{M}$ for all small μ. It is only $\mathbb{C}^1$, in general. Therefore, we cannot apply the two-dimensional results from Sec. 13.3 directly to our case because the former requires a higher order of smoothness. Nonetheless, the intersection of the invariant manifold $\mathcal{M}$ with S_0 is a smooth attracting invariant curve l_0 (transverse to $y = 0$) for the Poincaré map T. The Poincaré map, when restricted to this curve, is a one-dimensional map with either a monotonically increasing (when $A > 0$), or a monotonically decreasing (when $A < 0$) right-hand side. This gives us an important qualitative information on the anticipated bifurcations of the original map T: they may include only a saddle-node and a period-doubling bifurcation of a fixed point when $A > 0$ and, virtually, a saddle-node bifurcation of an orbit of period two when $A < 0$. In addition, a fixed point, or an orbit of period two when $A < 0$, may migrate to the boundary $\{y = 0\}$ of the domain of definition of the map (this corresponds to a homoclinic loop, simple or double, respectively).

A simple homoclinic loop corresponds to $\mu = 0$. A double homoclinic loop exists for $A < 0$ if $TM^+ \in W^s_{\rm loc}$, i.e.

$$0 = \mu + A(\mu, \varepsilon)\mu^{1+\varepsilon} + \varphi_1(\mu, u^+)$$

(see (13.6.22)). This gives the following asymptotics for the corresponding bifurcational curve:

$$\mu = |A(0, \varepsilon)|^{1/|\varepsilon|}[1 + o(1)]\,, \quad \varepsilon < 0\,.$$

The bifurcations of the fixed point are found from the system (compare with (13.6.22)):

$$\begin{aligned} &y = \mu + Ay^{1+\varepsilon} + \varphi_1(y,u), \quad y \geq 0\,, \\ &u = u^+ + a_{21}y^{1+\varepsilon} + \varphi_2(y,u)\,, \\ &\pm\begin{pmatrix}1\\ z\end{pmatrix} = \begin{pmatrix} A(1+\varepsilon)y^\varepsilon + \varphi'_{1y} & \varphi'_{1u} \\ a_{21}(1+\varepsilon)y^\varepsilon + \varphi'_{2y} & \varphi'_{2u}\end{pmatrix}\begin{pmatrix}1\\ z\end{pmatrix}. \end{aligned} \tag{13.6.23}$$

Here, "+" corresponds to a saddle-node bifurcation and "−" corresponds to a period-doubling bifurcation; (y,u) are the coordinates of the bifurcating fixed point, and $(1,z)$ is the eigenvector corresponding to the multiplier ±1.

Since $\varphi'_{(1,2)y} = o(y^\delta)$ and $\varphi'_{(1,2)u} = o(y^{1+\delta})$, one can easily express z and u in terms of y:

$$z \sim \pm a_{21}(1+\varepsilon)y^\varepsilon, \quad u \sim u^+\,.$$

Thus, the system takes the form

$$\begin{aligned} &y = \mu + Ay^{1+\varepsilon} + o(y^{1+\delta}), \quad y \geq 0\,, \\ &\pm1 = A(1+\varepsilon)y^\varepsilon + o(y^\delta)\,, \end{aligned} \tag{13.6.24}$$

which is analogous to systems (13.3.9) and (13.3.13) which define the bifurcation curves of the fixed points of the map T in the two-dimensional case (Sec. 13.3). This system gives the following asymptotics for the bifurcation curves ($\varepsilon < 0$):

- $\mu = \dfrac{1}{e}A(0,\varepsilon)^{\frac{1}{\varepsilon}}(1+o(1))$ — a saddle-node fixed point ($A > 0$); and
- $\mu = \dfrac{2}{e}|A(0,\varepsilon)|^{\frac{1}{\varepsilon}}(1+o(1))$ — period-doubling ($A < 0$).

It can also be shown that these bifurcations are non-degenerate, i.e. the first Lyapunov value is non-zero in both cases. Moreover, at the period-doubling bifurcation the Lyapunov value is positive. Therefore, a saddle orbit of period two is born at this bifurcation.

All of these results coincide with those we have obtained in the two-dimensional case. Therefore the bifurcation diagrams are the same. The remaining final step is to verify that there may not be saddle-node bifurcations of the orbits of period two for $A < 0$. A period-two orbit $\{(y_1,u_1),(y_2,u_2)\}$

must satisfy the equation

$$\begin{aligned} y_2 &= \mu + A(\mu,\varepsilon)y_1^{1+\varepsilon} + \varphi_1(y_1,u_1)\,,\\ y_1 &= \mu + A(\mu,\varepsilon)y_2^{1+\varepsilon} + \varphi_1(y_2,u_2)\,,\\ u_2 &= u^+ + a_{21}y_1^{1+\varepsilon} + \varphi_2(y_1,u_1)\,,\\ u_1 &= u^+ + a_{21}y_2^{1+\varepsilon} + \varphi_2(y_2,u_2)\,, \end{aligned} \tag{13.6.25}$$

where $y_1 \geq 0$ and $y_2 \geq 0$.

Since φ'_{2u} is small for small y, one can find (u_1,u_2) as functions of (y_1,y_2) from the two last equations in (13.6.25). The equations for $y_{1,2}$ can be written as

$$\begin{aligned} y_2 &= \mu + A(\mu,\varepsilon)y_1^{1+\varepsilon} + \varphi(y_1,y_2)\,,\\ y_1 &= \mu + A(\mu,\varepsilon)y_2^{1+\varepsilon} + \varphi(y_2,y_1)\,, \quad y_1 \geq 0,\ y_2 \geq 0\,. \end{aligned} \tag{13.6.26}$$

Here, the function φ is estimated as follows:

$$\begin{aligned} \varphi(y_1,y_2) &= o(y_1^{1+\delta})\,,\\ \frac{\partial^q \varphi}{\partial y_1^q} &= o(y_1^{1-q+\delta}) \qquad (q = 1,\dots,r-2)\,,\\ \frac{\partial^{r-1}\varphi}{\partial y_1^{r-1}} &= o(y_1^{2-r+\varepsilon})\,,\\ \frac{\partial^{q+p}\varphi}{\partial y_1^q \partial y_2^p} &= o(y_1^{1-q+\delta}y_2^{1-p+\varepsilon}) \quad (1 \leq p \leq r-2-q)\,,\\ \frac{\partial^{p+q}\varphi}{\partial y_1^q \partial y_2^p} &= o(y_1^{1-q+\varepsilon}y_2^{1-p+\varepsilon}) \quad \text{at } p+q = r-1, p \geq 1\,. \end{aligned} \tag{13.6.27}$$

Recall that we have assumed $-1 < A < 0$. Therefore, for $\varepsilon \geq 0$, the right-hand side of (13.6.26) is a contraction. Hence, the system may have only one solution for $\varepsilon \geq 0$. By symmetry, we have $y_1 = y_2$ at this solution; i.e. it corresponds to a fixed point of the map T. Thus, the map T does not have orbits of period two for $\varepsilon \geq 0$ and we will now restrict our consideration to negative ε.

Since $A < 0$, the right-hand side of the first equation in (13.6.26) decreases as y_1 increases. Therefore, $y_2 \leq \mu$. Analogously, $y_1 \leq \mu$ as well. Thus, we may

rescale variables: $y_1 \to y_1\mu$, $y_2 \to y_2\mu$. The resulting system takes the form

$$\begin{aligned} y_2 &= 1 - Cy_1^{1+\varepsilon} + \frac{1}{\mu}\varphi(\mu y_1, \mu y_2)\,, \\ y_1 &= 1 - Cy_2^{1+\varepsilon} + \frac{1}{\mu}\varphi(\mu y_2, \mu y_1)\,, \end{aligned} \tag{13.6.28}$$

where

$$C = \frac{|A|}{\mu^{|\varepsilon|}}\,, \tag{13.6.29}$$

and both rescaled variables $y_{1,2}$ belong to the interval [0, 1]. With no loss of generality we may assume that $y_1 \geq y_2$, and y_1 is bounded away from zero for bounded C.

It is easy to see, that if C remains bounded away from $C = 1$, then system (13.6.28) has a unique solution for small μ and ε. Observe that the symmetry of the system implies $y_1 = y_2$ in this case, which means that the map T cannot have orbits of period two when C is not close to 1.

Thus, the only relevant region in the parameter plane corresponds to $\mu^{|\varepsilon|} \sim |A|$. Since $|A| < 1$ by assumption, it follows that μ is exponentially small with respect to ε; namely,

$$\mu < e^{-K/|\varepsilon|}$$

for some positive K. It follows that the φ-terms in (13.6.28) are negligible and it can be easily checked that solving y_1 in terms of y_2 from the second equation of (13.6.28) and substituting the resulting expression into the first equation, the third derivative of the right-hand side of the resulting equation will never vanish for small $\varepsilon < 0$.

This implies that the system cannot have more than three solutions. Each orbit of period two gives two solutions [(y_1, y_2) and (y_2, y_1)]. Therefore, the map T cannot have more than one period-two orbit, even accounting for multiplicity, i.e. there may not be saddle-node orbits of period two either.

13.7. Bifurcations of the homoclinic-8 and heteroclinic cycles

In this section, we will review the bifurcations of a homoclinic-8, as well as of heteroclinic cycles including a pair of saddles such that they do not induce complex dynamics. We skip all proofs here just because our goal is only to

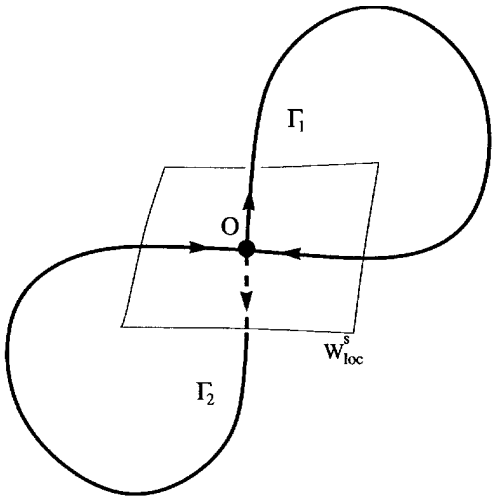

Fig. 13.7.1. A homoclinic-8 — the separatrices leave the saddle from opposite directions.

acquaint the readers with the results obtained in [148, 149, 151] and [50] for the homoclinic-8, and in [121–125] and in [34–35] for heteroclinic cycles of various kinds which have not yet been widely known.

The homoclinic-8 consists of a pair of homoclinic loops to a saddle such that the unstable separatrices Γ_1 and Γ_2 come out from the saddle in the opposite directions at $t = -\infty$ (Fig. 13.7.1). We will consider the case where the unstable manifold of the saddle O is one-dimensional; i.e. the saddle has only one positive characteristic exponent $\gamma > 0$; all other exponents are assumed to have negative real parts: $\operatorname{Re}\lambda_j < 0$, $j = 1, \ldots, n$. Moreover, we assume that *the saddle value σ is negative*:

$$\sigma = \gamma + \max \operatorname{Re} \lambda_j < 0\,.$$

We assume also that the system is $\mathbb{C}^r$-smooth with $r \geq 1$, and can hence examine its bifurcations under $\mathbb{C}^r$-smooth perturbations. Consider a sufficiently small neighborhood U of the homoclinic-8 $\Gamma_1 \cup \Gamma_2 \cup O$. Denote by N the set of all orbits lying entirely in U. The following theorem asserts that the set N contains no other orbits except for the two homoclinic loops and O at the bifurcation point. It also describes the structure of this set in any nearby system.

Theorem 13.11. *For any system sufficiently close to the system with a homoclinic-8 with $\sigma < 0$, the set N is the closure of the union of the separatrices $\Gamma_1 \cup \Gamma_2$ and may be of the following six possible types*:

(1) *$N\backslash O$ contains two stable periodic orbits, one of which is the ω-limit set of Γ_1 and the other is the ω-limit set of Γ_2;*
(2) *$N\backslash O$ contains one stable periodic orbit which is the ω-limit set of both separatrices Γ_1 and Γ_2;*
(3) *$N\backslash O$ contains a stable periodic orbit which is the ω-limit set of one of the separatrices, and the second separatrix forms a homoclinic loop;*
(4) *$N = \Gamma_1 \cup \Gamma_2 \cup O$, where one of the separatrices forms a homoclinic loop and the second separatrix is ω-limit to this loop;*
(5) *$N = \Gamma_1 \cup \Gamma_2 \cup O$, where both separatrices form homoclinic loops (thereby forming a homoclinic-8); and*
(6) *N is an attracting quasiminimal set which contains two P^+-stable separatrices Γ_1 and Γ_2, one P^--orbit in $W^s(O)$ and a continuum of unclosed Poisson-stable trajectories.*

Note that only cases (1) and (2) correspond to structurally stable systems; the other cases are non-rough. In essence, a bifurcation of a homoclinic-8 with a negative saddle value is an internal bifurcation in the Morse-Smale class.

Of special consideration are systems with symmetry where both separatrix loops approach together the saddle point. Such a situation is rather trivial; namely: when the loops split inwards, each gives the birth to a single stable limit cycle, in view of Theorem 13.4.1. When the loops split outwards, the stability migrates to a large-amplitude symmetric stable periodic orbit that bifurcates from the homoclinic-8 as shown in Fig. 13.7.2. And that is it. This is the reason why the theory below focuses primarily on non-symmetric systems.

Introduce a neighborhood U of the homoclinic-8 as a small ball U_0 with two handles U_1 and U_2 glued to U_0 containing the saddle O and the separatrices inside. Thus, for any orbit lying entirely in U, there exists a natural *code* — a sequence of symbols 1 and 2 which describes an itinerary according to which the orbit cruises along inside the handles U_1 and U_2. The codes for homoclinic loops are finite; furthermore we will also assign the codes of a finite length to the limit cycles, defined modulo a cyclic permutations of the symbols. To describe the possible codes for periodic orbits, as well as for homoclinic loops, which can be born from the homoclinic-8, let us construct a binary tree analogous to the Farey tree from number theory. We will assign the symbol pair $(1, 2)$ at the

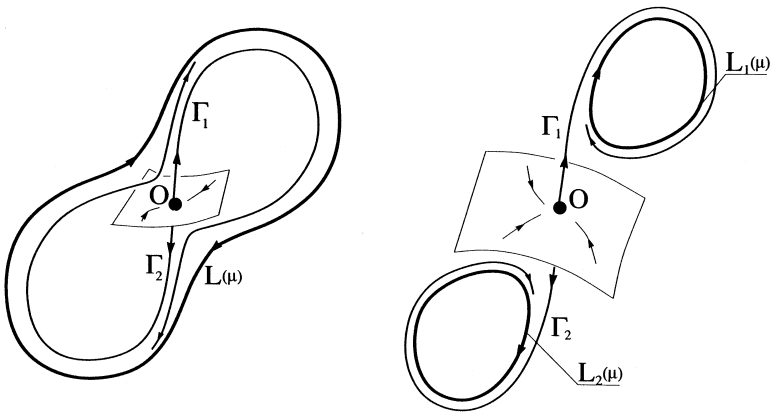

Fig. 13.7.2. The bifurcations of the homoclinic-8 in the symmetric case. An "outward" breakdown of both homoclinic loops gives birth to a large symmetric periodic orbit. When the loops split inwards, a periodic orbit bifurcates from each of the loops.

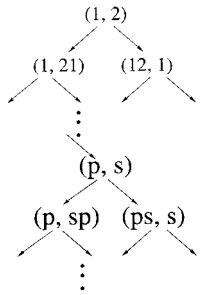

Fig. 13.7.3. A binary tree describing possible types of periodic orbits and homoclinic loops which can be born from the homoclinic-8 in the asymmetric case.

first vertex; from which two arrows descend to the vertices $(1, 21)$ and $(12, 1)$, and so on by following the rule that from a vertex (p, s), there are arrows going to the vertices (p, sp) and (ps, s) (as depicted in Fig. 13.7.3), where p and s denote finite words made up from the alphabet $\{1, 2\}$. We call a pair (p, s) *admissible* if it is at one of the vertices of the tree so constructed. A pair of infinite sequences (p, s) of symbols 1 and 2 is admissible if there exists an infinite path formed by the edges of the tree which passes through the vertices (p_i, s_i) such that $p_i \to p$ and $s_i \to s$ as $i \to +\infty$. A word is called admissible if it is an element of an admissible pair.

Theorem 13.12. *For any system sufficiently close to a system with the homoclinic-8 with a negative saddle value, the periodic orbits or homoclinic loops in U must have admissible codes. If there is a pair of periodic orbits, or a pair of homoclinic loops, or a limit cycle and a homoclinic loop, their codes must form an admissible pair. If the separatrices Γ_1 and Γ_2 are P^+-stable (i.e. N is a quasi-minimal set), then their codes form an admissible pair of infinite sequences.*

The local structure of the quasiminimal sets here is completely determined by the codes of the separatrices. Let us introduce *a rotation number* $\beta(s)$ for an infinite sequence $s = \{s_i\}_{i=0}^{+\infty}$ of symbols 1 and 2 by the formula:

$$\beta(s) = \lim_{n\to+\infty} \frac{1}{n}\{\text{number of } 1'\text{s in the sequence } \{s_i\}_{i=0}^{n}\}\,, \qquad (13.7.1)$$

assuming that this limit exists. It is easy to show that if a pair of infinite sequences (p, s) is admissible, then the rotation numbers $\beta(p)$ and $\beta(s)$ indeed exist; moreover, they are equal to each other:

$$\beta(p) = \beta(s)\,,$$

and are irrational. For any irrational number β from the interval $[0, 1]$, there exists a unique admissible pair of infinite sequences with a rotation number equal to β.

Thus, one can assign a rotation number β to each quasiminimal set born from bifurcations of a homoclinic-8.

Theorem 13.13. *If the set N of Theorem* 13.11 *is quasiminimal with a rotation number β, then the flow on N is topologically conjugate to a special Cherry flow (restricted to its quasiminimal set) with a rotation number β.*

The Cherry flow is a flow on a two-dimensional torus with two equilibrium states: a saddle and an unstable node; both unstable separatrices are P^+-stable; one stable separatrix is α-limit to a node and the other lies in the closure of the unstable separatrices and it is P^--stable [see Fig. 13.7.4(a)]. The closure of the unstable separatrices is a quasiminimal set which contains the saddle O and a continuum of unclosed P-stable trajectories. The rotation number for such flows is defined in the same way as for flows on a torus without equilibrium states. Since there is no periodic orbits in a Cherry flow,

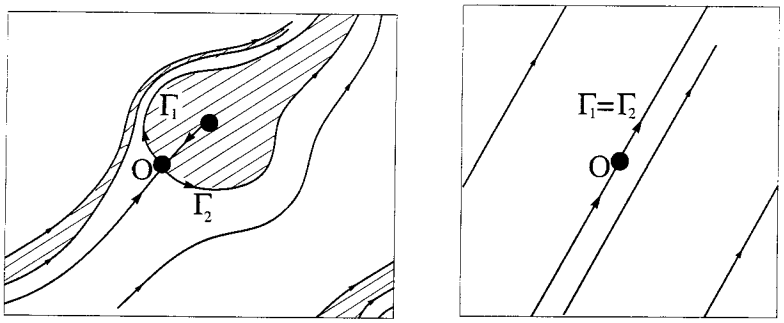

(a) (b)

Fig. 13.7.4. (a) The Cherry flow on a torus. (b) A quasiperiodic flow obtained from the Cherry flow by identifying the separatrices of the saddle.

its rotation number is irrational. The Cherry flow is *special*, if it contracts areas everywhere except for a small neighborhood of the unstable node. Two special Cherry flows are topologically conjugate, if and only if, their rotation numbers coincide (see more details in [104, 16]). We see that Theorem 13.13 gives a complete characterization of quasiminimal attractors which can be born from a homoclinic-8 with a negative saddle value. Note that one can glue the unstable separatrices Γ_1 and Γ_2 together so that the flow on the quasiminimal set after this "gluing" operation becomes topologically conjugate to the system

$$\dot{x} = x^2 + y^2\,, \quad \dot{y} = (x^2 + y^2)\beta$$

on the torus $\{|x| \le 1,\ |y| \le 1\}$ [see Fig. 13.7.4(b)].

Generically, one must distinguish between the following two cases:

Case 1. *saddle-focus*: $\lambda_{1,2}$ are complex and

$$0 > \mathrm{Re}\ \lambda_1 = \mathrm{Re}\ \lambda_2 > \mathrm{Re}\ \lambda_j \quad (j = 3, \dots, n)\,.$$

Case 2. *saddle*: λ_1 is real and

$$0 > \lambda_1 > \mathrm{Re}\ \lambda_j \quad (j = 2, \dots, n)\,.$$

In both cases, let us assume that at the bifurcation point,

- the homoclinic loops $\Gamma_{1,2}$ do not lie in the strong stable manifold W^{ss}, and
- the separatrix values $A_{1,2}$ do not vanish on both loops.

The latter condition can be interpreted as the transversality of the two-dimensional extended unstable manifold W^{uE} to the stable manifold along both loops. The separatrix values are defined by formula (13.4.8) in the case of a saddle, and by formula (13.4.15) in the case of a saddle-focus.

Consider a smooth two-parameter family $X_{\mu_1\mu_2}$ which is transverse to the codimension-two bifurcation set of systems with a homoclinic-8 with a negative saddle value, and which satisfy the above non-degeneracy conditions. The governing parameters $\mu_{1,2}$ are the splitting parameters for the homoclinic loops: when $\mu_i > 0$, the loop Γ_i is assumed to split inwards.

Let C_s denote the bifurcation set on the (μ_1, μ_2)-plane that corresponds to the existence of a homoclinic loop with a code s. By definition, $\{\mu_1 = 0\}$ defines the curve C_1 and $\{\mu_2 = 0\}$ corresponds to the curve C_2. For the other codes in the cases below, C_s is either a curve defined by an equation $\mu_1 = h_s(\mu_2)$ (if the last symbol in the word $\{s\}$ is 1) or $\mu_2 = h_s(\mu_1)$ (if the last symbol in $\{s\}$ is 2) where h_s is a smooth function defined for $\mu < 0$ whose first derivative tends to zero as $\mu \to -0$ (uniformly for all possible codes $\{s\}$), or it is an infinite set of open arcs (intervals) of such a curve.

In the case of a saddle-focus, all possibilities allowed by Theorems 13.11 and 13.12 are encountered in any transverse family $X_{\mu_1\mu_2}$. The bifurcation diagram for this case is shown in Fig. 13.7.5. Observe that the bifurcation curves which correspond to the homoclinic loops whose codes are ending by "1" are close to the negative μ_2 semi-axis and, therefore, they all lie in the sector $|\mu_1| < |\mu_2|$. The curves that correspond to the homoclinic loops whose codes are ending by "2" lie within the sector $|\mu_2| < |\mu_1|$. Since the picture in both sectors is symmetric here, it suffices to describe only the configuration of the bifurcational curves corresponding to homoclinic loops with the codes ending by "1".

Here, $\mu_1 = 0$ corresponds to the curve C_1; the curve C_{21} also leaves the point $(0, 0)$ towards negative values of μ_2; the curves C_{21} and L_1 intersect at infinitely many points. Then, one may continue inductively according to this rule: let (p, s) be an admissible pair of words ended by 1; then C_p and C_s intersect at infinitely many points, and if P and Q are neighboring points of intersection of C_p and C_s such that $h_p > h_s$ on the interval between P and Q, then P and Q are further connected by arcs of C_{ps} and C_{sp} which intersect C_s and, respectively, C_p infinitely many times, etc. In the region bounded by these arcs of C_{ps} and C_{sp}, a stable limit cycle exists with the code $\{ps\}$. On the contrary, if $h_p < h_s$ on the interval between P and Q, then for these values

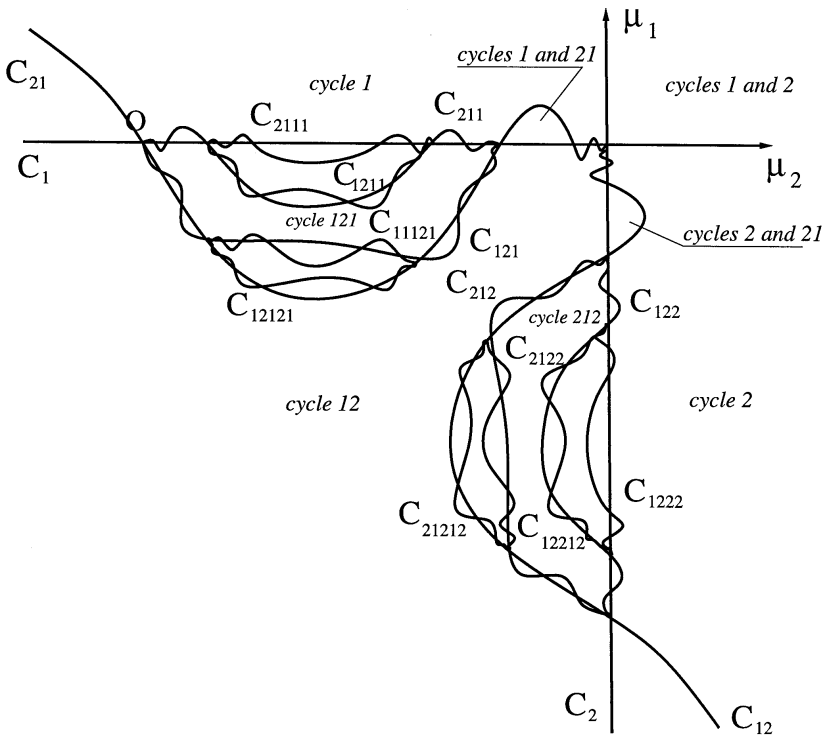

Fig. 13.7.5. A bifurcation diagram for a homoclinic-8 of a saddle-focus with a negative saddle value.

of μ_2 there cannot be homoclinic loops with the codes composed of the words p and s. Moreover, if $h_p < h_s$, then everywhere in the region bounded by the segments of the curves C_p and C_s from P to Q, there exists a pair of stable limit cycles with the codes $\{p\}$ and $\{s\}$.

The quasiminimal attractors correspond to the limit points of the union of the curves C_s.

In the case of a saddle (the leading characteristic exponent λ_1 is real), the bifurcation diagram depends on the signs of the separatrix values A_1 and A_2, as well as on the way the homoclinic loops Γ_1 and Γ_2 enter the saddle at $t = +\infty$. Let us consider first the case where Γ_1 and Γ_2 enter the saddle tangentially to each other, i.e. bifurcations of the stable homoclinic butterfly.

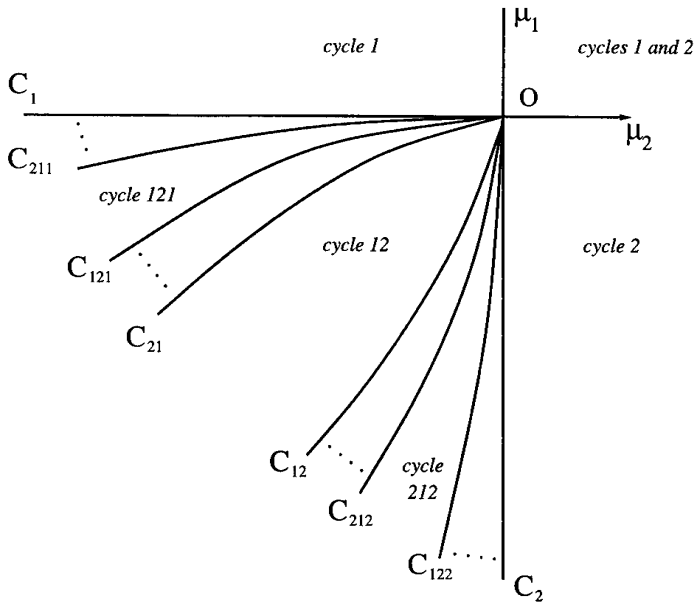

Fig. 13.7.6. A bifurcation diagram for an orientable ($A_{1,2} > 0$) homoclinic butterfly of the saddle with a negative saddle value.

Here, if $A_1 > 0$ and $A_2 > 0$ (see Fig. 13.7.6), the region ($\mu_1 > 0$, $\mu_2 > 0$) corresponds to the existence of a pair of cycles with the codes $\{1\}$ and $\{2\}$, and the region $\mu_1 > 0, \mu_2 < 0$ corresponds to the existence of a unique cycle with the code $\{1\}$. The region ($\mu_1 < 0$, $\mu_2 > 0$) corresponds to the existence of a unique cycle with the code $\{2\}$. In the region ($\mu_1 < 0$, $\mu_2 < 0$), the bifurcation set is a Cantor pencil of curves emanating from the origin, and composed of a countable number of curves corresponding to homoclinic loops and a continuum of curves corresponding to quasiminimal sets. This region has the following structure: for any admissible pair of finite words (p, s) there exist curves C_p and C_s; in the region bounded by C_p and C_s, the curves C_{ps} and C_{sp} are positioned in such a way that C_{sp} lies between C_p and C_{ps}. The region bounded by the curves C_{ps} and C_{sp} corresponds to the existence of a single stable limit cycle with the code $\{ps\}$. On each curve C_s, one of the unstable separatrices forms a homoclinic loop with the code s whereas the second separatrix tends to this homoclinic loop (i.e. it belongs to the stable manifold of the homoclinic loop; see the end of Sec. 13.4).

For each admissible pair (p, s) of infinite sequences, there exists a curve $C(p, s)$ corresponding to the existence of a quasiminimal attractor with the rotation number $\beta(p) = \beta(s)$. The curve $C(p, s)$ is found from

$$\lim C_{s_i} = \lim C_{p_i} ,$$

where (p_i, s_i) is a sequence of admissible pairs of finite words approximating (p, s).

In the other remaining cases, quasiminimal attractors do not appear. In the case $A_1 > 0$ and $A_2 < 0$ (see Fig. 13.7.7), there exist cycles only with the codes $\{1\}$, $\{2\}$ and $\{21^k\}$, $k = 1, 2, \ldots$ (here $\{1^k\}$ denotes the word consisting of k "ones"), and the parameter plane is partitioned into a countable number of regions by the curves C_1, C_2, C_{12}, C_{21^k} and C_{121^k} $(k = 1, 2, \ldots)$. Note that these curves accumulate onto the negative μ_2 semi-axis where the separatrix Γ_1 forms a simple homoclinic loop and the separatrix Γ_2 tends to the loop as $t \to +\infty$.

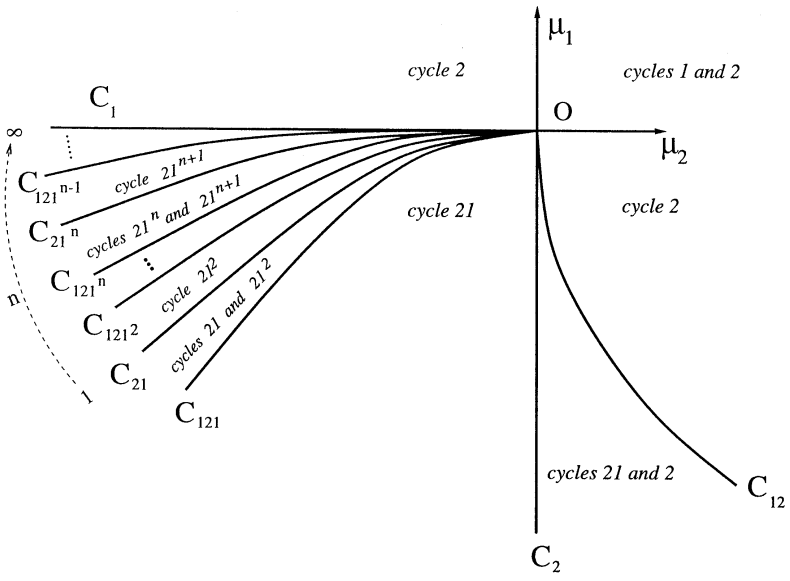

Fig. 13.7.7. A bifurcation diagram for a semi-orientable ($A_1 > 0$ and $A_2 < 0$) homoclinic butterfly of the saddle with a negative saddle value.

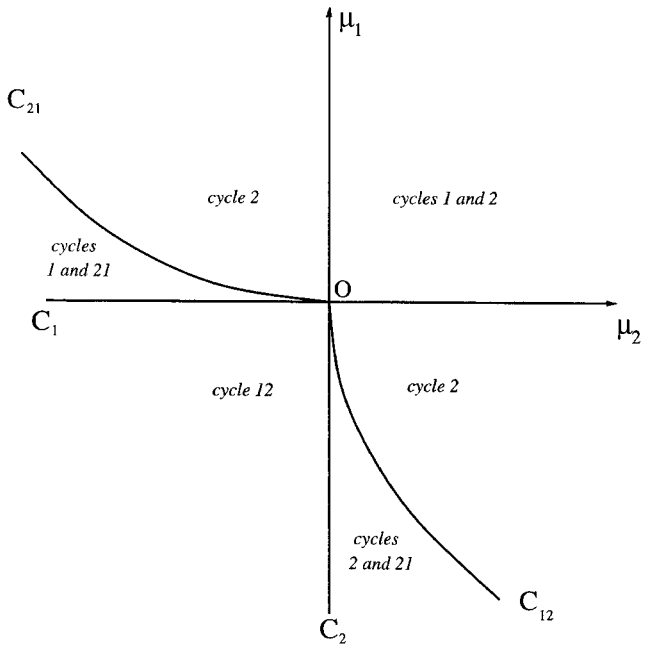

Fig. 13.7.8. A bifurcation diagram for a non-orientable ($A_{1,2} < 0$) homoclinic butterfly of the saddle with a negative saddle value.

In the case $A_1 < 0$ and $A_2 < 0$ (see the diagram shown in Fig. 13.7.8) there exist cycles only with codes $\{1\}$, $\{2\}$ and $\{12\}$; the parameter plane is partitioned into 6 regions.

The bifurcation diagrams for the case where Γ_1 and Γ_2 arrive at the saddle from opposite directions are shown in Figs. 13.7.9–13.7.11. In this case there cannot be quasiminimal attractors and the codes of the limit cycles can only be $\{1\}$, $\{2\}$, $\{12\}$, $\{1(21)^k\}$ and $\{2(12)^k\}$ $(k = 1, 2, \ldots)$. In the cases $A_1 > 0$, $A_2 > 0$ and $A_1 < 0$, $A_2 > 0$, the bifurcation set consists of a finite number of curves. In the case $A_1 < 0$, $A_2 < 0$, it consists of a countable number of curves which accumulate at the curves C_{12} and C_{21}. On these curves, one of the unstable separatrices forms a double-circuit homoclinic loop and the other separatrix converges to it as $t \to +\infty$.

We remark that a systematic study of the bifurcations of a homoclinic loop which is a limit set for the other separatrix was undertaken in [69].

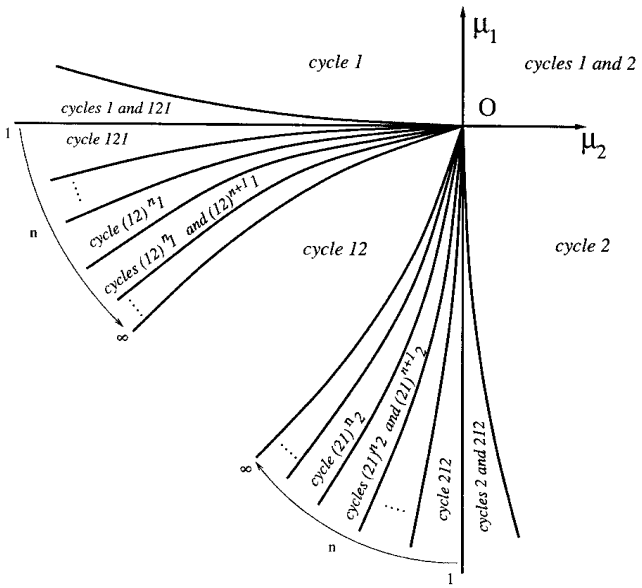

Fig. 13.7.9. A bifurcation diagram for a non-orientable ($A_{1,2} < 0$) homoclinic-8 of the saddle with a negative saddle value.

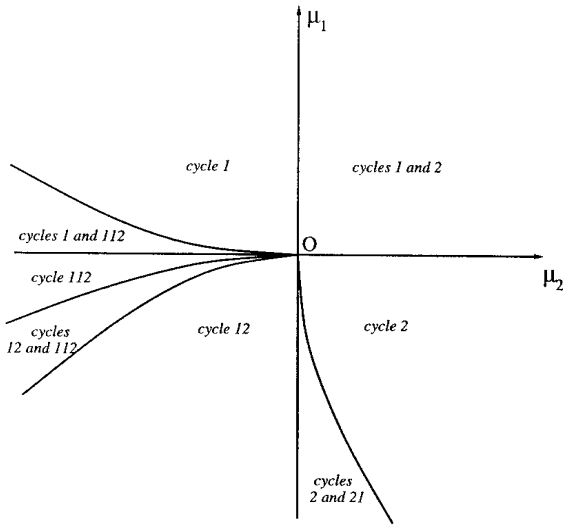

Fig. 13.7.10. A bifurcation diagram for a semi-orientable ($A_1 > 0$ and $A_2 < 0$) homoclinic-8 of the saddle with a negative saddle value.

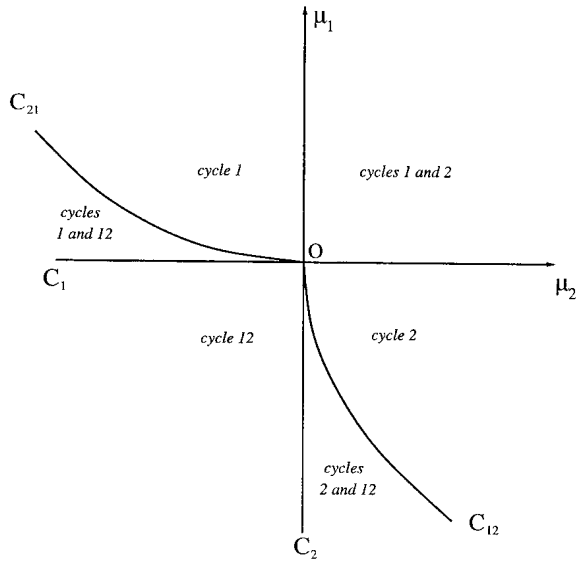

Fig. 13.7.11. A bifurcation diagram for an orientable ($A_{1,2} > 0$) homoclinic-8 of the saddle with a negative saddle value.

Note also that these results can be extended immediately to the case of a saddle with a multi-dimensional unstable manifold. Namely, if O has several characteristic exponents with positive real parts but the leading characteristic exponent γ_1 is real, i.e. if

$$\gamma_1 < \operatorname{Re} \gamma_j \,,$$

and if both the homoclinic loops do not belong to the strong unstable manifold W^{uu} and leave the saddle in opposite directions, and if the extended stable manifold is transverse to the unstable manifold on both loops, then Theorem 6.3 can be applied to guarantee the existence of a repelling $(n+1)$-dimensional $\mathbb{C}^1$-smooth invariant manifold. Since the system on the invariant manifold has only one positive characteristic exponent at O, it follows that all of the above results can be used here with the only difference that the limit cycles and the quasiminimal sets will no longer remain attracting but have become a saddle instead.

Let us now consider the case of a heteroclinic cycle with two saddles O_1 and O_2. Let the unstable manifolds of both saddles be one-dimensional and let an unstable separatrix Γ_1 of O_1 tend to O_2 as $t \to +\infty$ and an unstable

separatrix Γ_2 of O_2 tend to O_1 as $t \to +\infty$. The union $\Gamma_1 \cup \Gamma_2 \cup O_1 \cup O_2$ is a heteroclinic cycle. The question of bifurcations in a small neighborhood U of such a cycle was considered in detail in [121].

We assume throughout this section that the saddle values are negative in both saddles. In this case, *no more than one periodic orbit can bifurcate* from the heteroclinic cycle. Moreover, this unique orbit is stable (attracting).

When the system has a symmetry such that O_1 is symmetric with respect to O_2 and the separatrix Γ_1 is symmetric with respect to the separatrix Γ_2, then the bifurcations are rather simple: a stable periodic orbit is born when the separatrices split inwards; when the separatrices split outwards, all trajectories (next to $O_{1,2}$) leave U.

In the general case the picture may be more involved due to the appearance of multi-circuit heteroclinic connections.

Let us take a smooth two-parameter family $X_{\mu_1\mu_2}$ transverse to the codimension two-bifurcational surface of $\mathbb{C}^r$-smooth ($r \geq 1$) systems with a heteroclinic cycle of the type under consideration. Let μ_1 and μ_2 be the splitting parameters governing the heteroclinic orbits Γ_1 and Γ_2 so that the heteroclinic connection Γ_i splits inward for $\mu_i > 0$.

On the plane (μ_1, μ_2), there exist two curves L_1 and L_2, corresponding to the homoclinic loops of the saddles O_1 and O_2 respectively. These curves are the graphs of some smooth functions $\mu_1 = h_1(\mu_2)$ and $\mu_2 = h_2(\mu_1)$, respectively, which are defined for positive μ and such that $h(0) = 0$, $h'(0) = 0$. A stable periodic orbit exists in the region between L_1 and L_2. Note that multi-circuit homoclinic loops cannot appear when the saddle values are negative.

The bifurcation diagram for the family $X_{\mu_1\mu_2}$ may also contain the curves C^k_{12} and C^k_{21} ($k = 1, \ldots$) such that at $\mu \in C^k_{ij}$ the unstable separatrix Γ_i of O_i ($i = \{1\,2\}$) makes k complete rotations along U and enters the saddle Q_j ($i \neq j$), thereby forming a heteroclinic connection. The curves C^k_{ij} are defined by the equations $\mu_j = h_{kij}(\mu_i)$, where h_{kij} is some smooth function defined on an open subset of the positive μ_i-axis such that the first derivative of h_{kij} tends uniformly (with respect to k) to zero as $\mu_i \to 0$. The exact structure of the bifurcation set corresponding to heteroclinic connections is quite different depending on whether the equilibria O_i are saddles or saddle-foci.

The bifurcation diagrams for the case where both O_1 and O_2 are saddles are shown in Figs. 13.7.12–13.7.15. Here, if both the separatrix values are positive, the only possible heteroclinic connections are the original ones which exist at

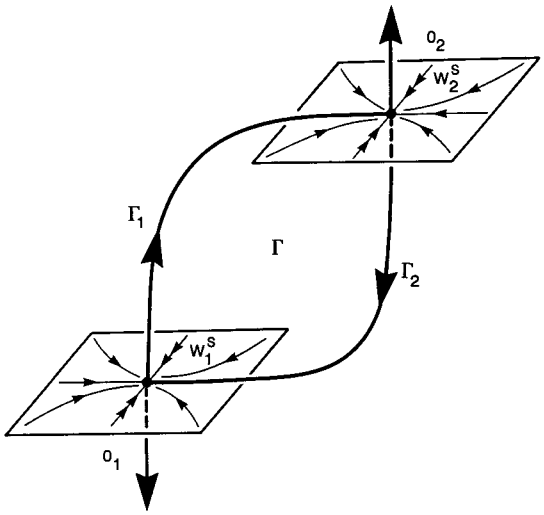

Fig. 13.7.12. A one-dimensional two-way heteroclinic connection between two saddles.

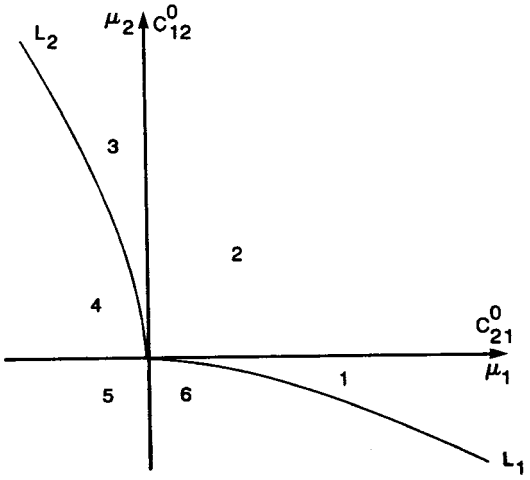

Fig. 13.7.13. The (μ_1, μ_2)-plane for the bifurcation of the heteroclinic cycle in Fig. 13.7.12 for the case $A_1 > 0$, $A_2 > 0$, and $\nu_{1,2} > 1$. Only one stable periodic orbit exists in regions 1,2 and 3.

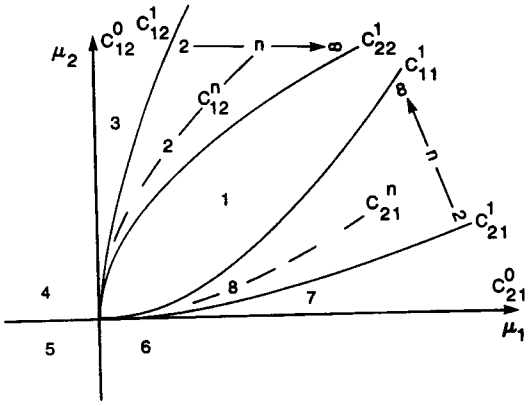

Fig. 13.7.14. Same as in Fig. 13.7.13, but $A_1 < 0$, $A_2 < 0$. The system has one stable periodic orbit in region 1, and has no periodic orbits elsewhere.

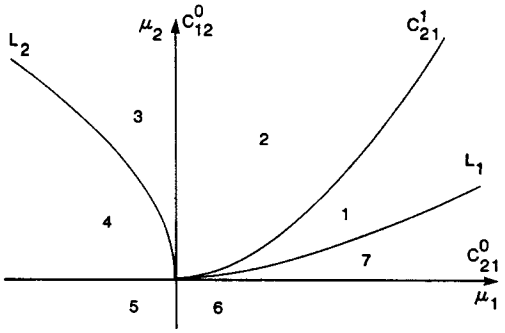

Fig. 13.7.15. Same as in Fig. 13.7.13, but $A_1 > 0$, $A_2 < 0$. The system has one stable periodic orbit in regions 1-3, and has no periodic orbits elsewhere.

$\mu_1 = 0$ or at $\mu_2 = 0$. When $A_1 > 0$ and $A_2 < 0$, the only new bifurcation curve is that labeled by C_{21}^1. In the case where $A_1 < 0$ and $A_2 < 0$, there exist infinitely many bifurcational curves corresponding to all possible heteroclinic connections. The curves C_{ij}^k accumulate to the curve C_j such that, for $\mu \in C_j$, the separatrix Γ_j forms a simple homoclinic loop to O_j and the separatrix Γ_i of O_i tends to the loop as $t \to +\infty$.

The separatrix values $A_{1,2}$ on the heteroclinic orbits are defined in the same way as in the case of homoclinic loops. Note that both cases $\{A_1 > 0,\ A_2 > 0\}$

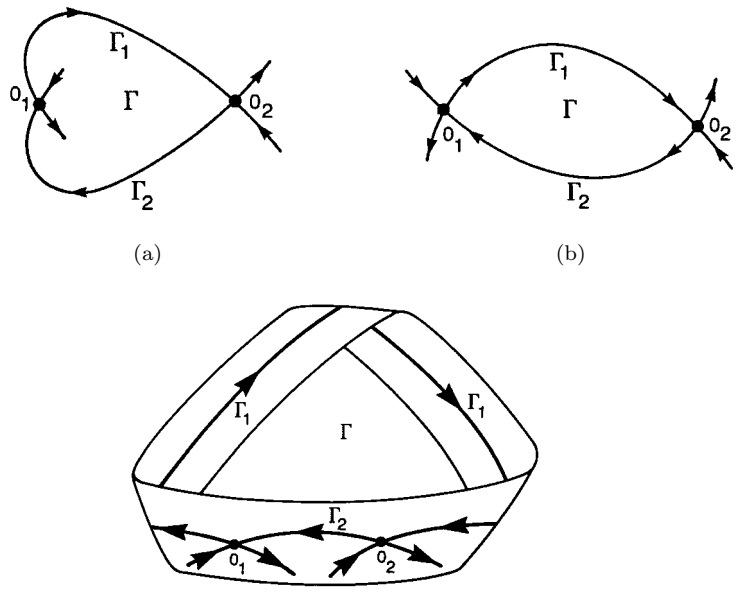

Fig. 13.7.16. Three types of heteroclinic cycles: (a) $A_{1,2} > 0$; (b) $A_{1,2} < 0$; (c) A semiorientable heteroclinic connection between two saddles on a Möbius band $A_1 < 0$, $A_2 > 0$.

and $\{A_1 < 0,\ A_2 < 0\}$ are possible in systems defined on the plane (see Fig. 13.7.16) but in the latter case both orbits Γ_1 and Γ_2 are wandering.

The bifurcation diagram for the case where both O_1 and O_2 are saddle-foci is shown in Fig. 13.7.17. Here, the curves L_1 and L_2 which correspond to the homoclinic loops intersect the curves $C_{21}^0 : \{\mu_1 = 0\}$ and $C_{12}^0 : \{\mu_2 = 0\}$ infinitely many times. Next, for each $k = 0, 1, 2, \ldots$, for any two neighboring points of intersection of L_1 with a connected component of C_{21}^k (L_2 with a connected component of C_{12}^k) such that the inequality $h_1(\mu_2) > h_{k12}(\mu_2)$ (respectively, $h_2(\mu_1) > h_{k21}(\mu_)$) holds between these points, there is a component of the curve C_{21}^{k+1} (respectively C_{21}^{k+1}) which connects these points. In turn, this component intersects L_1 (respectively L_2) infinitely many times, etc.

The limit points of this process correspond to the existence of a homoclinic loop which is the ω-limit set for a separatrix of the other saddle-focus.

The bifurcation diagrams for the case where O_1 is a saddle-focus and O_2 is a saddle are shown in Figs. 13.7.18 and 13.7.19. Here, the picture depends on

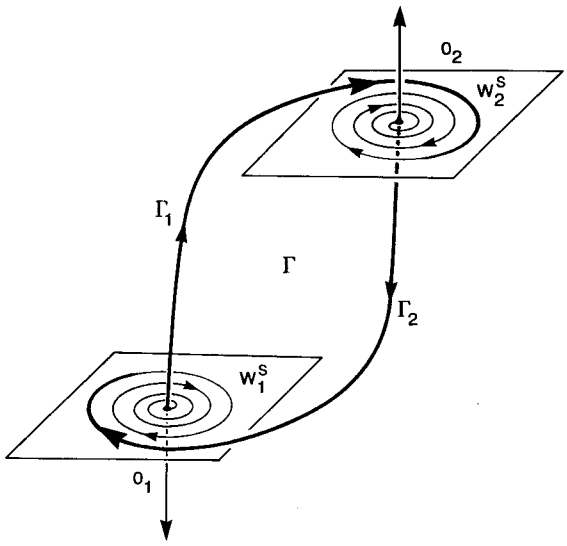

(a)

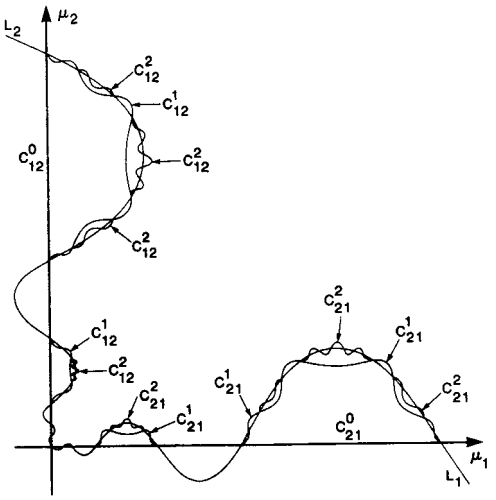

(b)

Fig. 13.7.17. (a) A one-dimensional two-way heteroclinic connection between a pair of saddle-foci. (b) The corresponding bifurcation diagram.

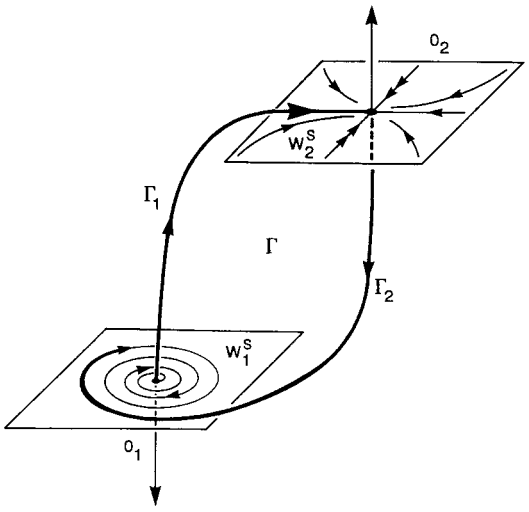

(a)

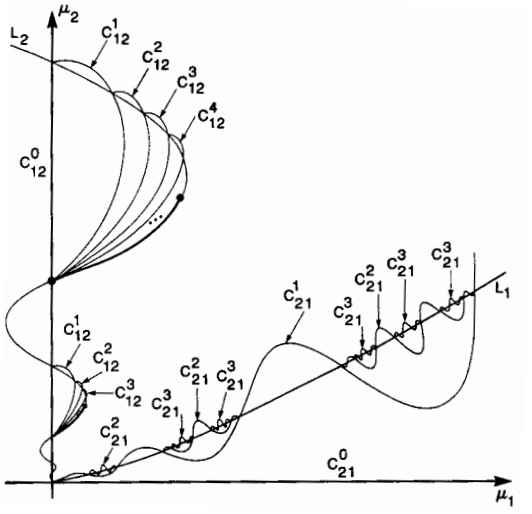

(b)

Fig. 13.7.18. (a) A two-way heteroclinic connection between a saddle-focus and a saddle. The corresponding bifurcation diagrams for the case $A_2 < 0$ (b) and $A_2 > 0$ (c).

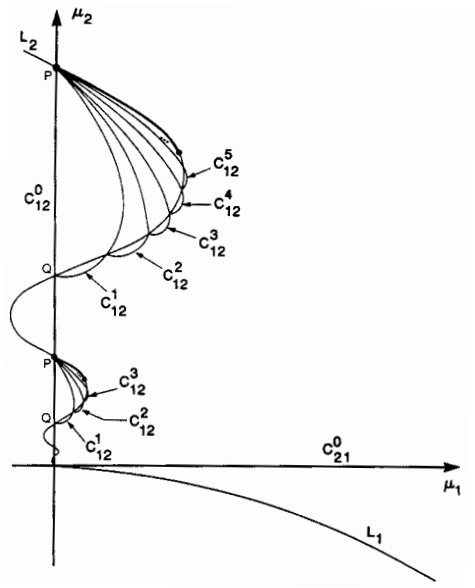

(c)

Fig. 13.7.18. (*Continued*)

the sign of the separatrix value A_2 computed along the heteroclinic orbit Γ_2. There are no curves like C_{21}^k with $k \geq 1$ for $A_2 > 0$. When $A_2 < 0$, the curve C_{21}^1 intersects L_1 infinitely many times and the structure of the set of curves C_{21}^k for $A_2 < 0$ is the same as in the case where both $O_{1,2}$ are saddle-foci.

The set of curves C_{12}^k is organized as follows. Observe that the curve $L_2 : \mu_2 = h_2(\mu_1)$ intersects the line $C_{12}^0 : \{\mu_2 = 0\}$ infinitely many times. Let $P(\mu_1', 0)$ and $Q(\mu_1'', 0)$ be two neighboring points of the intersection such that $h_2 > 0$ between these points. Let $\mu_1' > \mu_1''$. Then, infinitely many curves C_{12}^k emanate from the point P when $A_2 > 0$ (or from the point Q when $A_2 < 0$) each of which intersects L_2 at one point. The curve C_{12}^1 ends at Q (at P if $A_2 < 0$), the curve C_{12}^2 ends at the point of intersection $C_{12}^1 \cap L_2$, etc: the curve C_{12}^{k+1} ends at the point $C_{12}^k \cap L_2$.

All these intersection points correspond to a *non-orientable* homoclinic loop of O_2 (the separatrix value on the loop is negative), and they accumulate at the point where the separatrix value vanishes on the loop. The segment of L_2 between this point and the point P (the point Q at $A_2 < 0$) corresponds to

an orientable homoclinic loop onto which the separatrix Γ_1 of O_1 winds around as $t \to +\infty$. The curves C_{12}^k accumulate to this segment from the left.

We must note that this picture is proven to hold only if the system is at least $\mathbb{C}^3$ and providing

$$2\rho\nu < \rho\bar{\nu} + 2\,.$$

Here ρ is the saddle index at the saddle-focus O_1, and ν is the saddle index at the saddle O_2 and $\bar{\nu} = |\mathrm{Re}\,\lambda_2/\gamma|$, where γ denotes the positive characteristic exponents of O_2, and λ_2 is the *non-leading* characteristic exponent of O_2 nearest to the imaginary axis (λ_1 is the leading exponent so $\nu = |\lambda_1/\gamma|$ and $1 < \nu < \bar{\nu}$; recall also that $\rho > 1$ by assumption — the saddle values are negative).

If this inequality is not satisfied, then the structure of the set of curves C_{12}^k may differ: there will be still infinitely many curves C_{12}^k starting from P or Q but, in some cases, only a finite number of them will have an intersection with L_2 and the rest of the curves will end at the last intersection point.

Note that all of these results (except for the subtle structure of the set of curves C_{12}^k in the case where O_1 is a saddle-focus and O_2 is a saddle) are proven for $\mathbb{C}^1$-smooth systems. Therefore, just like in the case of a homoclinic-8, these results can be directly extended to the case where the unstable manifolds of O_1 and O_2 are multi-dimensional (but they must have equal dimensions in this case), provided that the conditions of Theorem 6.4 in Part I of this book, which guarantee the existence of an invariant $\mathbb{C}^1$-manifold near the heteroclinic cycle, are satisfied.

Another case studied in [121] corresponds to the bifurcations of a heteroclinic cycle when the saddle values have opposite signs at equilibrium state O_1 and O_2 (the case where both saddle values are positive leads either to complex dynamics, if O_1 and O_2 are both saddle-foci, or reduces to the preceding one by a reversal of time and reduction to the invariant manifold). The main assumption here is that both O_1 and O_2 are simple saddles (not saddle-foci).

In particular, let the dimension of the unstable manifold of O_1 be equal to the dimension of the unstable manifold of O_2. Besides, let both the stable and unstable leading characteristic exponents at both O_1 and O_2 be real. Assume also that both heteroclinic orbits $\Gamma_{1,2}$ enter and leave the saddles along the leading directions. We also assume that the extended unstable manifold of one saddle is transverse to the stable manifold of the other saddle along every orbit $\Gamma_{1,2}$, and that the extended stable manifold of one saddle is transverse to the unstable manifold of the other saddle along $\Gamma_{1,2}$ as well. Under

these assumptions, Theorem 6.4 constitutes the existence of a two-dimensional invariant manifold which captures all orbits staying in a small neighborhood of the heteroclinic cycle for all times. Thus, the dynamics here is essentially two-dimensional. Note once again that because the invariant manifold is, in general, only $\mathbb{C}^1$-smooth, in order to study the problem one has to perform computations for the original multi-dimensional system.

Let ν_1 and ν_2 be the saddle indices at O_1 and O_2, respectively. Assume that $\nu_1 \neq 1$, $\nu_2 \neq 1$ and $\nu_1\nu_2 \neq 1$. Then, *no more than two periodic orbits* can bifurcate from the heteroclinic cycle under consideration.

The bifurcation diagrams are shown in Figs. 13.7.20–13.7.23. The separatrix values A_1 and A_2 are defined as derivatives of the global maps near the heteroclinic orbits Γ_1 and Γ_2 on the two-dimensional invariant manifold. Note that the other cases of combinations of the signs of $A_{1,2}$ and of saddle values can be obtained similarly by a reversal of time and a permutation of the sub-indices "1" and "2".

One may see that the peculiarity of this case, in contrast to the case where the saddle values have the same sign, is the possibilities of a saddle-node

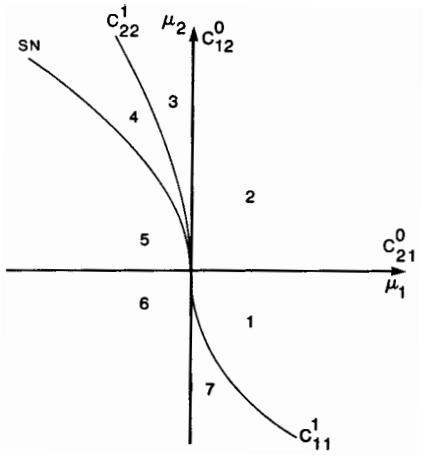

Fig. 13.7.20. The bifurcation diagram for the case where both equilibrium states of the heteroclinic cycle are saddles (see Fig. 13.7.12) provided $A_{1,2} > 0$, $\nu_1 > 1$, $\nu_2 < 1$ and $\nu_1\nu_2 > 1$. The system has one limit cycle in regions 1-3, two limit cycles in region 4, none in regions 5–7. A pair of limit cycles are born from a saddle-node on the curve SN; the unstable one becomes a homoclinic loop on the curve L_2, whereas the stable limit cycle terminates on L_1.

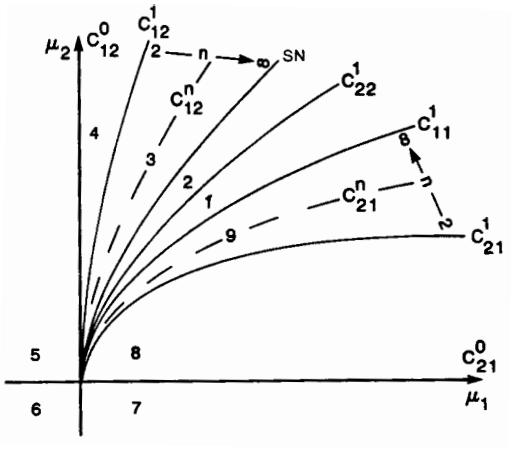

Fig. 13.7.21. The bifurcation diagram for the heteroclinic cycle in Fig. 13.7.12 for the case $A_{1,2} < 0$, $\nu_1 > 1$, $\nu_2 < 1$ and $\nu_1\nu_2 > 1$. This system has one limit cycle in region 1, two limit cycles in region 2, none elsewhere.

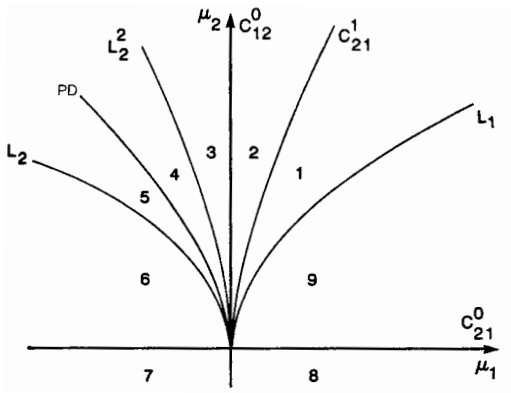

Fig. 13.7.22. The bifurcation diagram for the heteroclinic connection in Fig. 13.7.12 when $A_1 > 0$, $A_2 < 0$, $\nu_1 > 1$, $\nu_2 < 1$ and $\nu_1\nu_2 > 1$. The system has one simple periodic orbit in regions 1, 2, 3 and 5, two periodic orbits (one simple and one of double period) in region 4, and no periodic orbits elsewhere. The stable periodic orbit loses stability on the curve PD corresponding to a period-doubling (flip) bifurcation. The unstable limit cycle of double period becomes a double-circuit separatrix loop on L_2^2. The stable simple limit cycle terminates on L_1.

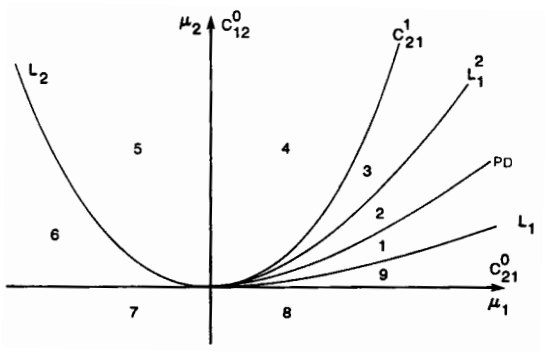

Fig. 13.7.23. The bifurcation diagram for the heteroclinic connection in Fig. 13.7.12 when $A_1 > 0$, $A_2 < 0$, $\nu_1 < 1$, $\nu_2 > 1$ and $\nu_1\nu_2 > 1$. This system has one simple periodic orbit in regions 1, 2, 3 and 5, two periodic orbits (one simple and one of double period) in region 4, and no periodic orbits elsewhere.

bifurcation and a period-doubling bifurcation of single-circuit periodic orbits, as well as of the appearance of double-circuit homoclinic loops.

The heteroclinic cycles including the saddles whose unstable manifolds have *different* dimensions were first studied in [34, 35]. This study mostly focused on systems with complex dynamics. Let us, however, discuss here a case where the dynamics is simple. Let a three-dimensional infinitely smooth system have two equilibrium states O_1 and O_2 with real characteristic exponents, respectively, $\gamma > 0 > \lambda_1 > \lambda_2$ and $\eta_2 > \eta_1 > 0 > \xi$ (i.e. the unstable manifold of O_1 is one-dimensional and the unstable manifold of O_2 is two-dimensional). Suppose that the two-dimensional manifolds $W^s(O_1)$ and $W^u(O_2)$ have a *transverse* intersection along a heteroclinic trajectory Γ_0 (which lies neither in the corresponding strongly stable manifold, nor in the strongly unstable manifold). Suppose also that the one-dimensional unstable separatrix of O_1 coincides with the one-dimensional stable separatrix of O_2, so that a structurally unstable heteroclinic orbit Γ exists (Fig. 13.7.24). The additional non-degeneracy assumptions here are that the saddle values are non-zero and that the extended unstable manifold of O_1 is transverse to the extended stable manifold of O_2 at the points of the structurally unstable heteroclinic orbit Γ.

This bifurcation has codimension two: the governing parameters (μ_1, μ_2) are chosen here to be the coordinates of the point of intersection of the one-dimensional unstable separatrix of O_1 with some cross-section transverse to the one-dimensional stable separatrix of the other saddle O_2. Since the

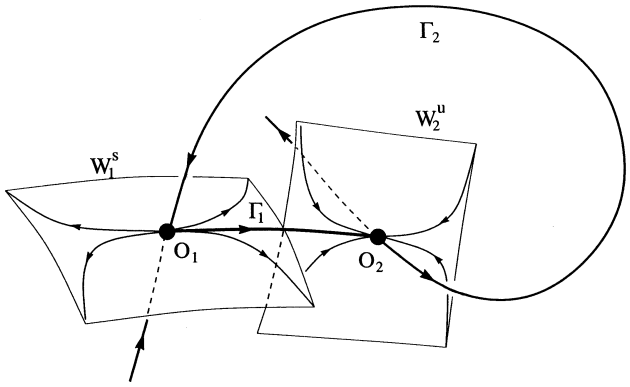

Fig. 13.7.24. A heteroclinic cycle between two saddles. Notice that the heteroclinic trajectory Γ_1 connecting O_1 with O_2 is structurally stable.

corresponding bifurcation diagrams are rather complicated, we do not present them here but refer the interested reader to the original works [34, 35]. Nonetheless, in this case *no more than two periodic orbits* (*always saddle*) bifurcate from such a heteroclinic connection.

13.8. Estimates of the behavior of trajectories near a saddle equilibrium state

In this section, we prove our estimates of the solutions near a saddle equilibrium state which we used throughout this chapter.

Consider a $\mathbb{C}^r$-smooth ($r \geq 3$) system in a neighborhood of a saddle equilibrium state with m-dimensional stable and n-dimensional unstable invariant manifolds.

Let the characteristic exponents of the saddle be $(\lambda_1, \dots, \lambda_m)$ and $(\gamma_1, \dots, \gamma_n)$, where $\operatorname{Re}\lambda_i < 0$ $(i = 1, \dots, m)$ and $\operatorname{Re}\gamma_i > 0$ $(i = 1, \dots, n)$. Assume that the real parts of $(\lambda_1, \dots, \lambda_{m_1})$ are equal to some $-\lambda < 0$ and the rest of the stable characteristic exponents $(\lambda_{m_1+1}, \dots, \lambda_m)$ lie strictly to the left of the line $\operatorname{Re}(\cdot) = -\lambda$. Concerning the unstable characteristic exponents we assume that $\operatorname{Re}\gamma_1 = \dots = \operatorname{Re}\gamma_{n_1} = \gamma > 0$ and $\operatorname{Re}\gamma_i > \gamma$ for $i > n_1$.

As shown in Appendix A of the Part I of this book, a system in $\mathbb{R}^{n+m}$, satisfying to the above assumptions, can be reduced by a $\mathbb{C}^{r-1}$-transformation

of variables to the form

$$\begin{aligned}
\dot{x} &= B_1 x + f_{11}(x,y,v)x + f_{12}(x,u,y,v)u\,,\\
\dot{u} &= B_2 u + f_{21}(x,y,v)x + f_{22}(x,u,y,v)u\,,\\
\dot{y} &= C_1 y + g_{11}(x,u,y)y + g_{12}(x,u,y,v)v\,,\\
\dot{v} &= C_2 v + g_{21}(x,u,y)y + g_{22}(x,u,y,v)v\,,
\end{aligned} \tag{13.8.1}$$

where the eigenvalues of B_1 are $(\lambda_1,\dots,\lambda_{m_1})$, the eigenvalues of B_2 are $(\lambda_{m_1+1},\dots,\lambda_m)$, those of C_1 are $(\gamma_1,\dots,\gamma_{n_1})$ and those of C_2 are $(\gamma_{n_1+1},\dots,\gamma_n)$. Moreover, the $\mathbb{C}^{r-1}$-smooth functions f_{ij} and g_{ij} satisfy

$$\begin{aligned}
f_{11}(x,0,0) &\equiv 0\,, \quad & g_{11}(0,0,y) &\equiv 0\,,\\
f_{12}(x,u,0,0) &\equiv 0\,, \quad & g_{12}(0,0,y,v) &\equiv 0\,,\\
f_{j1}(0,y,v) &\equiv 0\,, \quad & g_{j1}(x,u,0) &\equiv 0\,,\\
f_{22}(0,0,0,0) &= 0\,, \quad & g_{22}(0,0,0,0) &= 0\,.
\end{aligned} \tag{13.8.2}$$

Let $\lambda_0 > 0$ and $\gamma_0 > 0$ be such that for all $t \geq 0$

$$\|e^{B_1 t}\| \leq e^{-\lambda_0 t}\,, \quad \|e^{-C_1 t}\| \leq e^{-\gamma_0 t}\,. \tag{13.8.3}$$

For example, when there is only one stable leading characteristic exponent ($m_1 = 1$ and $\lambda_1 = -\lambda$ is real), or if there is a pair of complex-conjugate stable leading characteristic exponents ($m_1 = 2$ and $\lambda_1 = \lambda_2^* = -\lambda + i\omega$ with $\omega \neq 0$), then $\lambda_0 = \lambda$. Analogously, $\gamma_0 = \gamma$ if $n_1 = 1$, or if $n_1 = 2$ and $\gamma_1 = \gamma_2^*$ is not real.

Let us also choose some quantities λ' and γ', satisfying

$$0 < \lambda_0 < \lambda' < \min\{2\lambda_0, \lambda''\} \quad \text{and} \quad 0 < \gamma_0 < \gamma' < \min\{2\gamma_0, \gamma''\}\,, \tag{13.8.4}$$

where λ'' and γ'' are such that for all $t \geq 0$

$$\|e^{B_2 t}\| \leq e^{-\lambda'' t}\,, \quad \|e^{-C_2 t}\| \leq e^{-\gamma'' t}\,. \tag{13.8.5}$$

We also take some $\tilde{\lambda}$ and $\tilde{\gamma}$ such that

$$0 < \lambda_0 < \tilde{\lambda} < \min\{\lambda', \lambda_0 + \gamma_0\} \quad \text{and} \quad 0 < \gamma_0 < \tilde{\gamma} < \min\{\gamma', \gamma_0 + \lambda_0\}\,. \tag{13.8.6}$$

Let two points $M_0(x_0,u_0,y_0,v_0)$ and $M_1(x_1,u_1,y_1,v_1)$ be in a small neighborhood of the saddle, and let the orbit of M_0 reach M_1 at the time $t = \tau$,

without leaving the neighborhood of the saddle. It is shown in Sec. 2.8 that (x_1, u_1) and (y_0, v_0) are uniquely defined for any small (x_0, u_0, y_1, v_1) and $\tau \geq 0$. Moreover, (x_1, u_1, y_0, v_0) depends smoothly on $(x_0, u_0, y_1, v_1, \tau)$.

Lemma 13.5. (Ovsyannikov-Shilnikov [101]) *Denote*

$$\begin{aligned} x_1 &= e^{B_1\tau}x_0 + \xi_1(x_0, u_0, y_1, v_1, \tau)\,, \\ y_0 &= e^{-C_1\tau}y_1 + \eta_1(x_0, u_0, y_1, v_1, \tau)\,, \\ u_1 &= \xi_2(x_0, u_0, y_1, v_1, \tau)\,, \\ v_0 &= \eta_2(x_0, u_0, y_1, v_1, \tau)\,. \end{aligned} \tag{13.8.7}$$

If identities (13.8.2) *hold, then the following estimates are valid*:

$$\|\xi_1\|_{\mathbb{C}^{r-2}} = o(e^{-\tilde{\lambda}\tau})\,, \quad \|\eta_1\|_{\mathbb{C}^{r-2}} = o(e^{-\tilde{\gamma}\tau})\,, \tag{13.8.8}$$

$$\|\xi_2\|_{\mathbb{C}^{r-2}} = o(e^{-\lambda'\tau})\,, \quad \|\eta_2\|_{\mathbb{C}^{r-2}} = o(e^{-\gamma'\tau})\,, \tag{13.8.9}$$

where $\|\cdot\|_{\mathbb{C}^{r-2}}$ *denotes the maximum of the norm of the function itself and the norms of all of its derivatives up to the order* $(r-2)$.

Proof. Let us denote

$$f_i = f_{i1}x + f_{i2}u \quad \text{and} \quad g_i = g_{i1}y + g_{i2}v\,. \tag{13.8.10}$$

It is sufficient to show (see Sec. 2.7) that, given small (x_0, u_0, y_1, v_1), the solution $(x(t), u(t), y(t), v(t))$ of the system

$$\begin{aligned} x(t) &= e^{B_1 t}x_0 + \int_0^t e^{B_1(t-s)}f_1(x(s), u(s), y(s), v(s))ds\,, \\ u(t) &= e^{B_2 t}u_0 + \int_0^t e^{B_2(t-s)}f_2(x(s), u(s), y(s), v(s))ds\,, \\ y(t) &= e^{-C_1(\tau-t)}y_1 - \int_t^\tau e^{-C_1(s-t)}g_1(x(s), u(s), y(s), v(s))ds\,, \\ v(t) &= e^{-C_2(\tau-t)}v_1 - \int_t^\tau e^{-C_2(s-t)}g_2(x(s), u(s), y(s), v(s))ds \end{aligned} \tag{13.8.11}$$

satisfies the following estimates

$$\begin{aligned}
&\|x(t) - e^{B_1 t}x_0\| \le K_1 e^{-\lambda_0 t}e^{-(\tilde\lambda-\lambda_0)\tau}\,,\\
&\|u(t)\| \le K_2 e^{-\lambda' t}\,,\\
&\|y(t) - e^{-C_1(\tau-t)}y_1\| \le K_1 e^{-\gamma_0(\tau-t)}e^{-(\tilde\gamma-\gamma_0)\tau}\,,\\
&\|v(t)\| \le K_2 e^{-\gamma'(\tau-t)}
\end{aligned} \tag{13.8.12}$$

for $t \in [0,\tau]$; here $K_{1,2}$ are some constants.[16]

Moreover, analogous estimates must hold for all derivatives of the expressions in the left-hand side of (13.8.12) with respect to (x_0, u_0, y_1, v_1) while the values of K's may depend on the order of the derivatives. Note that there is no need to evaluate the derivatives with respect to t and τ because they are related to the other derivatives by simple identities (see Lemma 5.1 and explanations in Sec. 5.2).

As shown in Sec. 2.8, the solution of (13.8.11) is the limit of successive approximations $(x^{(k)}(t), u^{(k)}(t), y^{(k)}(t), v^{(k)}(t))$ $(k \to +\infty)$ computed as

$$\begin{aligned}
x^{(k+1)}(t) &= e^{B_1 t}x_0 + \int_0^t e^{B_1(t-s)} f_1(x^{(k)}(s), u^{(k)}(s), y^{(k)}(s), v^{(k)}(s))ds\,,\\
u^{(k+1)}(t) &= e^{B_2 t}u_0 + \int_0^t e^{B_2(t-s)} f_2(x^{(k)}(s), u^{(k)}(s), y^{(k)}(s), v^{(k)}(s))ds\,,\\
y^{(k+1)}(t) &= e^{-C_1(\tau-t)}y_1 - \int_t^\tau e^{-C_1(s-t)} g_1(x^{(k)}(s), u^{(k)}(s), y^{(k)}(s), v^{(k)}(s))ds\,,\\
v^{(k+1)}(t) &= e^{-C_2(\tau-t)}v_1 - \int_t^\tau e^{-C_2(s-t)} g_2(x^{(k)}(s), u^{(k)}(s), y^{(k)}(s), v^{(k)}(s))ds
\end{aligned} \tag{13.8.13}$$

starting with the initial guess $(x^{(1)}(t), u^{(1)}(t), y^{(1)}(t), v^{(1)}(t)) = 0$.

Thus, to prove some estimates of the solution of (13.8.11), we may assume that the kth successive approximation satisfies these estimates and then, based on this assumption, we must check that the $(k+1)$th approximation satisfies them too; of course, the estimators must be independent of k.

[16] Strictly speaking, this gives $O(\cdot)$-type estimates in the right-hand side of (13.8.8) and (13.8.9), but the O-symbol can be replaced by o by just moving $\tilde\lambda$, λ', $\tilde\gamma$, γ' slightly closer to zero.

Let us now assume that the kth approximation satisfy (13.8.12) for some $K_{1,2}$. It follows that

$$\|x^{(k)}(t)\| \le 2\varepsilon e^{-\lambda_0 t}\,, \quad \|y^{(k)}(t)\| \le 2\varepsilon e^{-\gamma_0(\tau-t)}\,, \tag{13.8.14}$$

independently of the value of K_1, provided τ is large enough; here ε is the size of the neighborhood of the saddle under consideration (so $\|x_0\| \le \varepsilon$, $\|y_1\| \le \varepsilon$).

Based on identities (13.8.2), the function f_1 can be estimated as

$$\|f_1\| \le \sup \|f''_{11x(y,v)}\| \cdot \|x\|^2 \|y,v\| + \sup \|f'_{12(y,v)}\| \cdot \|u\| \cdot \|y,v\|\,. \tag{13.8.15}$$

Thus, it follows from (13.8.14) and from the assumed validity of (13.8.12), that for sufficiently small ε

$$\begin{aligned} &\|f_1(x^{(k)}(s), u^{(k)}(s), y^{(k)}(s), v^{(k)}(s))\| \\ &\qquad \le e^{-2\lambda_0 s} e^{-\gamma_0(\tau-s)} + K_0 K_2^2 e^{-\lambda' s} e^{-\gamma_0(\tau-s)} \\ &\qquad \le (1 + K_0 K_2^2) e^{-\tilde{\lambda} s} e^{-\gamma_0(\tau-s)}\,, \end{aligned} \tag{13.8.16}$$

where K_0 is some constant; note that we use here the relations (13.8.4) and (13.8.6) between the λ's.

Analogously, if ε is sufficiently small, then

$$\|f_2(x^{(k)}(s), u^{(k)}(s), y^{(k)}(s), v^{(k)}(s))\| \le (\varepsilon + \delta K_2) e^{-\lambda' s}\,, \tag{13.8.17}$$

where $\delta \equiv \sup \|f_{22}\|$ may be choosen as small as necessary by decreasing the size of the neighborhood of the saddle.

By (13.8.16) and (13.8.17) we obtain, respectively,

$$\begin{aligned} &\left\| \int_0^t e^{\lambda_0 s} f_1(x^{(k)}(s), u^{(k)}(s), y^{(k)}(s), v^{(k)}(s)) ds \right\| \\ &\qquad \le (1 + K_0 K_2^2) e^{-\gamma_0 \tau} \int_0^\tau e^{(\gamma_0 + \lambda_0 - \tilde{\lambda}) s} ds \end{aligned}$$

and

$$\begin{aligned} &\left\| \int_0^t e^{\lambda'' s} f_2(x^{(k)}(s), u^{(k)}(s), y^{(k)}(s), v^{(k)}(s)) ds \right\| \\ &\qquad \le (\varepsilon + \delta K_2) \int_0^t e^{(\lambda'' - \lambda') s} ds\,. \end{aligned}$$

Thus [see (13.8.13), (13.8.3) and (13.8.5)], $(x,u)^{(k+1)}$ satisfy (13.8.12) *with the same* K_1 *and* K_2 if

$$K_1 \geq (1 + K_0 K_2^2) \frac{1}{\lambda_0 + \gamma_0 - \tilde{\lambda}}$$

and

$$K_2 \geq \varepsilon + (\varepsilon + \delta K_2) \frac{1}{\lambda'' - \lambda'} \,.$$

By the symmetry of the problem, we obtain immediately the inequalities on $K_{1,2}$ which are sufficient for $(y,v)^{(k+1)}$ to satisfy (13.8.12). Altogether, this gives

$$\begin{aligned} K_1 &\geq (1 + K_0 K_2^2) \frac{1}{\lambda_0 + \gamma_0 - \max\{\tilde{\gamma}\,, \tilde{\lambda}\}} \,, \\ K_2 &\geq \varepsilon + (\varepsilon + \delta K_2) \max\left\{ \frac{1}{\gamma'' - \gamma'}, \frac{1}{\lambda'' - \lambda'} \right\} \,, \end{aligned} \tag{13.8.18}$$

where δ tends to zero as the size ε of the neighborhood of the saddle is diminished.

These inequalities are easy to satisfy for $K_2 = O(\varepsilon)$ and $K_1 = O(1)$. Thus, one can indeed choose appropriate constants $K_{1,2}$ such that the estimates (13.8.12) are satisfied. To complete the proof of our lemma we must show that analogous estimates hold for all derivatives of the solution $(x(t), u(t), y(t), v(t))$ of (13.8.11).

It is shown in Sec. 2.8 that the successive approximations converge to the solution of the boundary-value problem along with all derivatives. Thus, we may *assume* that the kth approximation satisfies[17]

$$\begin{aligned} &\| D_p x^{(k)}(t) - D_p \left(e^{B_1 t} x_0 \right) \| \leq K_1^{(p)} e^{-\lambda_0 t} e^{-(\tilde{\lambda} - \lambda_0)\tau} \,, \\ &\| D_p u^{(k)}(t) \| \leq K_2^{(p)} e^{-\lambda' t} \,, \\ &\| D_p y^{(k)}(t) - D_p \left(e^{-C_1(\tau - t)} y_1 \right) \| \leq K_1^{(p)} e^{-\gamma_0(\tau - t)} e^{-(\tilde{\gamma} - \gamma_0)\tau} \,, \\ &\| D_p v^{(k)}(t) \| \leq K_2^{(p)} e^{-\gamma'(\tau - t)} \,, \end{aligned} \tag{13.8.19}$$

for some $K_{1,2}$ which are independent of k but may depend on the order p of the derivative. Then, based on this assumption, we must show that the derivatives

[17] We use the notation $D_p = \frac{\partial^p}{\partial (x^0, u^0, y^1, v^1)^p}$.

of the next approximation $(x^{(k+1)}(t), u^{(k+1)}(t), y^{(k+1)}(t), v^{(k+1)}(t))$ satisfy the same estimates.

In fact, it suffices to make computations only for $x^{(k+1)}(t)$ and $u^{(k+1)}(t)$; the formulas concerning $y^{(k+1)}(t)$ and $v^{(k+1)}(t)$ will follow from the symmetry of the problem.

The differentiation of (13.8.13) gives

$$\begin{aligned} D_p x^{(k+1)}(t) &= D_p\left(e^{B_1 t}x_0\right) + \int_0^t e^{B_1(t-s)} \\ &\quad \times D_p f_1(x^{(k)}(s), u^{(k)}(s), y^{(k)}(s), v^{(k)}(s))ds\,, \\ D_p u^{(k+1)}(t) &= D_p(e^{B_2 t}u_0) + \int_0^t e^{B_2(t-s)} \\ &\quad \times D_p f_2(x^{(k)}(s), u^{(k)}(s), y^{(k)}(s), v^{(k)}(s))ds\,. \end{aligned}$$

By (13.8.3) and (13.8.5), we have

$$\begin{aligned} &\|D_p x^{(k+1)}(t) - D_p(e^{B_1 t}x_0)\| \\ &\quad \le e^{-\lambda_0 t}\int_0^t e^{\lambda_0 s}\left\|D_p f_1(x^{(k)}(s), u^{(k)}(s), y^{(k)}(s), v^{(k)}(s))\right\| ds\,, \\ &\|D_p u^{(k+1)}(t)\| \\ &\quad \le e^{-\lambda'' t}\left[1 + \int_0^t e^{\lambda'' s}\left\|D_p f_2(x^{(k)}(s), u^{(k)}(s), y^{(k)}(s), v^{(k)}(s))\right\| ds\right]. \end{aligned} \tag{13.8.20}$$

Now, in the same way as done earlier in proving our lemma we must check that the estimates analogous to (13.8.16) and (13.8.17) hold for the derivatives $D_p f_{1,2}$ for any p:

$$\|D_p f_1(x^{(k)}(s), u^{(k)}(s), y^{(k)}(s), v^{(k)}(s))\| \le \tilde{K}_1 e^{-\gamma_0(\tau-s)}e^{-\tilde{\lambda}s} \tag{13.8.21}$$

and

$$\|D_p f_2(x^{(k)}(s), u^{(k)}(s), y^{(k)}(s), v^{(k)}(s))\| \le (\tilde{K}_2 + \delta K_2^{(p)})e^{-\lambda' s}\,, \tag{13.8.22}$$

where δ may be chosen arbitrarily small by decreasing the size of the neighborhood of the saddle under consideration; $\tilde{K}_2$ is independent of the specific

choice of the constants $K_{1,2}^{(p)}$ in (13.8.19), and $\tilde{K}_1$ is independent of $K_1^{(p)}$ (nevertheless, $\tilde{K}_{1,2}$ may depend on $K_{1,2}$ corresponding to the derivatives of lower orders).

By the chain rule, the derivatives

$$D_p f_i(x^{(k)}(s), u^{(k)}(s), y^{(k)}(s), v^{(k)}(s))$$

can be estimated by the sum

$$\begin{aligned}\text{const} \cdot \sum_{q_1,q_2} \left\| \frac{\partial^p f_i}{\partial(x,u)^{q_1}\partial(y,v)^{q_2}}(x^{(k)}(s), u^{(k)}(s), y^{(k)}(s), v^{(k)}(s)) \right\| \\ \times \|D_{l_1}(x^{(k)}(s), u^{(k)}(s))\| \cdots \|D_{l_{q_1}}(x^{(k)}(s), u^{(k)}(s))\| \\ \times \|D_{l_{q_1+1}}(y^{(k)}(s), v^{(k)}(s))\| \cdots \|D_{l_{q_1+q_2}}(y^{(k)}(s), v^{(k)}(s))\|\,, \qquad (13.8.23)\end{aligned}$$

where $q_{1,2}$ are non-negative integers such that $1 \le q_1 + q_2 \le p$, and l's are positive integers such that $l_1 + \cdots + l_{q_1+q_2} = p$.

By assumption, the estimates for the derivatives $\|D_l u^{(k)}(s)\|$ and $\|D_l v^{(k)}(s)\|$ are given by (13.8.19). For large τ, the estimates (13.8.19) imply

$$\|D_l x^{(k)}(s)\| \le 2e^{-\lambda_0 s}\,, \quad \|D_l y^{(k)}(s)\| \le 2e^{-\gamma_0(\tau-s)}\,. \qquad (13.8.24)$$

Thus, the estimate (13.8.23) can be rewritten as

$$\begin{aligned}\text{const} \cdot \sum_{q_1,q_2} \left\| \frac{\partial^p f_i}{\partial(x,u)^{q_1}\partial(y,v)^{q_2}}(x^{(k)}(s), u^{(k)}(s), y^{(k)}(s), v^{(k)}(s)) \right\| \\ \times e^{-q_1\lambda_0 s} e^{-q_2\gamma_0(\tau-s)}\,. \qquad (13.8.25)\end{aligned}$$

Obviously, in the estimate for f_1, the terms with $q_1 \ge 2$ and $q_2 \ge 1$ fit (13.8.21), and all terms with $q_1 \ge 2$ in the estimate for f_2 fit (13.8.22). Note also, that

$$\frac{\partial^{q_2} f_i}{\partial(y,v)^{q_2}} \equiv \frac{\partial^{q_2} f_{i1}}{\partial(y,v)^{q_2}} \cdot x^{(k)}(s) + \frac{\partial^{q_2} f_{i2}}{\partial(y,v)^{q_2}} \cdot u^{(k)}(s) = O(e^{-\lambda' s})\,. \qquad (13.8.26)$$

Here, we use (13.8.12), (13.8.14), (13.8.4) and the identities (13.8.2) which give $\frac{\partial^{q_2} f_{i1}}{\partial(y,v)^{q_2}} = 0$ at $x = 0$. Since $q_2 \le r-2$ and $f_{i1} \in \mathbb{C}^{r-1}$, the derivative of order q_2 of f_{i1} is a smooth function. Thus, once it vanishes at $x = 0$, it can be estimated by $\frac{\partial^{q_2} f_{i1}}{\partial(y,v)^{q_2}} = O(x)$.

Hence, it follows from (13.8.26) that the terms with $q_1 = 0$ and $q_2 \geq 1$ in the estimate (13.8.25) for f_1, and all terms with $q_1 = 0$ in the estimate for f_2 also fit (13.8.21) and (13.8.22), respectively.

Analogously, since f_1 vanishes identically at $(y, v) = 0$, it follows that

$$\frac{\partial^{q_1} f_1}{\partial (x,u)^{q_1}} = O(e^{-\gamma_0(\tau - s)}) .$$

Hence, all terms with $q_1 \geq 2$ in the estimate (13.8.25) for f_1 fit (13.8.21).

The last remaining terms to examine in (13.8.25) are ($q_1 = 1$)

$$\left\| \frac{\partial}{\partial x} \frac{\partial^{q_2} f_i}{\partial (y,v)^{q_2}} \right\| \cdot e^{-q_2 \gamma_0 (\tau - s)} e^{-\lambda_0 s}$$

and

$$\left\| \frac{\partial}{\partial u} \frac{\partial^{q_2} f_i}{\partial (y,v)^{q_2}} \right\| \cdot e^{-q_2 \gamma_0 (\tau - s)} e^{-\lambda' s} .$$

Note that $f'_{ix} = 0$ at $(x, u) = 0$ [see (13.8.2)]. Hence, it is of order $O(x, u)$ along with all of its derivatives with respect to (y, v) up to the order $q_2 \leq r-3$. Thus, it follows from (13.8.12), (13.8.14) and (13.8.4) that both terms above can be estimated by constant $\cdot\, e^{-q_2 \gamma_0 (\tau - s)} e^{-\lambda' s}$; i.e. they fit (13.8.22), and if $q_2 \geq 1$, they fit (13.8.21).

It remains to consider the case $q_1 = 1, q_2 = 0$ for f_1. To satisfy (13.8.21) we have to show that

$$e^{-\lambda_0 s} \frac{\partial f_1}{\partial (x,u)} = O(e^{-\gamma_0(\tau - s)} e^{-\tilde{\lambda} s}) ,$$

but this obviously follows from (13.8.14) and (13.8.12) because $f_1 = f_{11} x + f_{12} u$ and both f_{1i} vanish at $(y, v) = 0$ [see (13.8.2)].

We have proven that the derivatives $D_p f_i(x^{(k)}(s), u^{(k)}(s), y^{(k)}(s), v^{(k)}(s))$ satisfy estimates (13.8.21) and (13.8.22). Note that for the derivatives of $x^{(k)}(s)$ and $y^{(k)}(s)$, we used only estimates (13.8.24) which are independent of the choice of $K_{1,2}$ in (13.8.19). Thus, the estimator $\tilde{K}_1$ in (13.8.21) is indeed independent of $K_1^{(p)}$. The only terms in (13.8.23) which might give a contribution in (13.8.22) depending on $K_{1,2}^{(p)}$ are

$$\|f'_{2u}\| \cdot \|D_p u^{(k)}(s)\| \quad \text{and } \|f'_{2v}\| \cdot \|D_p v^{(k)}(s)\| .$$

The first term here can be estimated by $\delta K_2^{(p)} e^{-\lambda' s}$ where δ may be chosen arbitrarily small by diminishing the size ε of the neighborhood of the saddle

under consideration. The second term can be estimated [see (13.8.14), (13.8.12) and (13.8.18)] by

$$K_2^{(p)} e^{-\gamma'(\tau-s)} \cdot (\|f'_{21v}\| \|x^{(k)}(s)\| + \|f'_{22v}\| \|u^{(k)}(s)\|) \\ = K_2^{(p)} \cdot O(\|x^{(k)}(s)\|^2 + \|u^{(k)}(s)\|) = K_2^{(p)} \cdot O(\varepsilon e^{-\lambda' s}) .$$

All this is in complete agreement with (13.8.22).

Now, the validity of estimates (13.8.19) for the next approximation $(x^{(k+1)}(t),\ u^{(k+1)}(t),\ y^{(k+1)}(t),\ v^{(k+1)}(t))$ follows from (13.8.21), (13.8.22) exactly in the same way as the validity of (13.8.12) follows from (13.8.16), and (13.8.17).
This completes the proof of the Lemma 13.5.

Remark 1. Following exactly the same procedure as in Appendix B of Part I for the trajectories near a saddle fixed point of a diffeomorphism, one may show also that

$$\|\xi_{1,2}\|_{\mathbb{C}^{r-1}} = o(e^{-\lambda_0 \tau}) , \quad \|\eta_{1,2}\|_{\mathbb{C}^{r-1}} = o(e^{-\gamma_0 \tau}) , \tag{13.8.27}$$

and this estimate is valid at $r = 2$ as well.

Remark 2. Recall that when the system depends smoothly ($\mathbb{C}^r$) on some parameters, the coordinate transformation which brings the system to the form (13.8.1) and (13.8.2) depends on the parameters $\mathbb{C}^{r-2}$-smoothly (precisely, it has continuous derivatives with respect to all variables and parameters up to the order $(r-1)$, except for the last $(r-1)$th derivative with respect to the parameters alone which may not exist). In this case the matrices $B_{1,2}$ and $C_{1,2}$ are $\mathbb{C}^{r-2}$-smooth functions of the parameters.

The estimates of Lemma 13.5 remain valid in this case. Indeed, it is easy to trace throughout our proof (compare also with the analogous statement in Appendix B of Part I) that an additional q-times ($q \le r-2$) differentiation with respect to the parameters may only lead to the appearance of a factor τ^q in the right-hand side of the estimates (13.8.8) and (13.8.9), but this factor can be absorbed by the $o(e^{-\lambda\tau})$ and $o(e^{-\gamma\tau})$ terms by pushing the λ's and γ's closer to zero.

The derivatives of the order $(r-1)$ of the functions ξ and η can now be estimated by $o(\tau^q e^{-\lambda_0 \tau})$ and $o(\tau^q e^{-\gamma_0 \tau})$, respectively (the proof follows exactly the same procedure as in Appendix B). Here $q = 0, \dots, r-2$ is the number of the differentiations with respect to the parameters; λ_0 and γ_0 depend now

on the parameters in such a way that the estimates (13.8.3) for the matrix exponents are always satisfied.

Remark 3. Let us draw more attention to the case where the unstable manifold of the saddle is one-dimensional. There is no v-variables here and $y \in \mathbb{R}^1$. By rescaling time, the system (13.8.1) can be reduced to the form

$$\begin{aligned} \dot{x} &= B_1 x + f_{11}(x,y)x + f_{12}(x,u,y)u\,, \\ \dot{u} &= B_2 u + f_{21}(x,y)x + f_{22}(x,u,y)u\,, \\ \dot{y} &= y\,, \end{aligned} \tag{13.8.28}$$

where all eigenvalues $(\nu_1, \dots, \nu_{m_1})$ of B_1 have the same real part $-\nu < 0$, and all eigenvalues $(\nu_{m_1+1}, \dots, \nu_m)$ of B_2 lie to the left of the line $\operatorname{Re}(\cdot) = -\nu'' < -\nu$. The $\mathbb{C}^{r-1}$-smooth functions f_{ij} must satisfy

$$f_{i1}(x,0) \equiv 0\,, \quad f_{1j}(0,0,y) \equiv 0\,. \tag{13.8.29}$$

Lemma 13.5 asserts here that the solution of the boundary-value problem is given by

$$\begin{aligned} y_0 &= e^{-\tau} y_1\,, \\ x_1 &= e^{B_1 \tau} x_0 + \xi_1(x_0, u_0, y_1, \tau)\,, \\ u_1 &= \xi_2(x_0, u_0, y_1, \tau)\,, \end{aligned} \tag{13.8.30}$$

where

$$\|\xi_1\|_{\mathbb{C}^{r-2}} = o(e^{-\tilde{\nu}\tau})\,, \quad \|\xi_2\|_{\mathbb{C}^{r-2}} = o(e^{-\nu'\tau})\,. \tag{13.8.31}$$

Here,

$$\nu < \nu' < \min\{2\nu, \nu''\}\,, \quad \nu < \tilde{\nu} < \min\{\nu', \nu+1\}\,. \tag{13.8.32}$$

The estimates (13.8.27) can be written as follows

$$\|\xi_{1,2}\|_{\mathbb{C}^{r-1}} = o(e^{-\nu\tau})\,. \tag{13.8.33}$$

Remark 4. One may obtain slightly refined estimates for the functions $\xi_{1,2}$ in (13.8.30). Namely, let

$$\bar{\xi}_{1,2}(u_0, y_1, \tau) = \xi_{1,2}(0, u_0, y_1, \tau)\,. \tag{13.8.34}$$

Then the functions $\bar{\xi}_{1,2}$ satisfy some better estimates than those for $\xi_{1,2}$ respectively. Indeed, we have

$$\|\bar{\xi}_1\|_{C^{r-2}} = o(e^{-\bar{\nu}\tau}), \quad \|\bar{\xi}_2\|_{C^{r-2}} = o(e^{-\hat{\nu}\tau})\,, \tag{13.8.35}$$

for any $\bar\nu$ and $\hat\nu$ such that

$$\nu < \hat\nu < \min\{\nu'', 2(1+\nu)\}, \quad \nu < \bar\nu < \min\{\nu'', 1+\nu\}\,. \tag{13.8.36}$$

For a proof note that $\bar\xi_1 = x(\tau)$ and $\bar\xi_2 = u(\tau)$, where $(x(t), u(t), y(t))$ is the solution of the boundary value problem $\{x(0) = 0, u(0) = u_0, y(\tau) = y_1\}$ for system (13.8.28). It satisfies the system of integral equations (see (13.8.11)):

$$\begin{aligned} x(t) &= \int_0^t e^{B_1(t-s)} f_1(x(s), u(s), y_1 e^{s-\tau}) ds\,, \\ u(t) &= e^{B_2 t} u_0 + \int_0^t e^{B_2(t-s)} f_2(x(s), u(s), y_1 e^{s-\tau}) ds\,, \end{aligned} \tag{13.8.37}$$

which can be solved by successive approximations, starting with $(x, u)(t) = 0$. One can check (in the same way as Lemma 13.5 was proved) that every successive approximation satisfies the inequalities

$$\|x(t)\|_{C^{r-2}} \le K_1 e^{-\bar\nu t}, \quad \|u(t)\|_{C^{r-2}} \le K_2 e^{-\hat\nu t} \tag{13.8.38}$$

for all $t \in [0, \tau]$, with some constant K, the same for every approximation step. Thus, the limit of approximations satisfies the same inequalities, and this gives (13.8.35) (see comments on the inequalities (13.8.12)).

Chapter 14

SAFE AND DANGEROUS STABILITY BOUNDARIES

The material presented so far in this book covers the theoretical foundation for the analysis of two non-transient phenomena: stationary states and self (auto)-oscillations. The mathematical image of the former is a stable equilibrium state, and that of the latter is a stable periodic orbit. Theoretically, the observable state of a system that is associated with the position of a representative point in the phase space is not necessarily located precisely at an equilibrium state, or on a periodic orbit but can be only infinitesimally close to it.[1] One must also take into account possible variations of the parameters of the system. If a parameter varies sufficiently slowly, then the representative point is able to follow the evolution of the limit regime within the stability region. However, while studying a concrete dynamical system and choosing parameter values, one must care not only about the requirements concerning the stability of regimes but also about other problems. For instance, it may turn out that the optimal working conditions of a device can be achieved only near the threshold of its stability region. Another matter is that the parameters of the system may evolve in a quasistationary way towards the stability boundary. Any further trespassing beyond this boundary may lead to rather non-trivial dynamics.[2] To analyze such situations, we now arrive at

[1] The process of convergence of a representative point to a limiting state is called the *transient* regime. Formally, the limit regime and a nearby transient process cannot be clearly distinguished. Nevertheless, the intuitive understanding of these processes in each specific field of nonlinear dynamics and their separation in time usually cause no difficulties.

[2] Such a situation is literally called "on the edge of chaos."

the main topic of this final chapter: how does the representative point behave while cruising over the boundary of the stability region?

14.1. Main stability boundaries of equilibrium states and periodic orbits

To answer the question raised in the preceding paragraph, we must first itemize the main types of boundaries of stability regions of equilibrium states and periodic orbits. To do this we must undertake a systematic classification of the information we have presented in all previous chapters. We will pay special attention to the features that distinguish each type of boundaries.

Consider a p-parameter family of n-dimensional systems described by

$$\dot{x} = X(x, \varepsilon)\,, \quad \varepsilon = (\varepsilon_1, \ldots, \varepsilon_p)\,. \tag{14.1.1}$$

Let us assume that the system has an equilibrium state (in the origin, for simplicity, i.e. $X(0, \varepsilon) = 0$). The principal boundaries of the stability region of the equilibrium in the parameter space $\mathbb{R}^p$ are two codimension-one surfaces defined by the conditions given below, on which the equilibrium states becomes

(1) A saddle-node

$$X(0, \varepsilon) = 0\,, \quad \Delta_n(\varepsilon) = 0\,,$$

$$\Delta_1(\varepsilon) > 0, \ldots, \Delta_{n-1}(\varepsilon) > 0\,, \quad l_2(\varepsilon) \neq 0\,,$$

where $\Delta_i(\varepsilon)$ is the ith Routh-Hurwitz minor, and $l_2(\varepsilon)$ is the first Lyapunov value.

(2) A weak focus

$$X(0, \varepsilon) = 0\,, \quad \Delta_{n-1}(\varepsilon) = 0\,,$$

$$\Delta_1(\varepsilon) > 0, \ldots, \Delta_{n-2}(\varepsilon) > 0\,, \quad \Delta_n(\varepsilon) > 0\,, \quad L_1(\varepsilon) \neq 0\,,$$

where $L_1(\varepsilon)$ is the first Lyapunov (focal) value.

Suppose next that system (14.1.1) possesses a stable periodic orbit in some parameter region. Here, the boundaries of the stability region may be of two principally different types depending on whether the periodic orbit exists on the

boundary or not. If the periodic orbits exists on the stability boundary, then the problem reduces to the study of stability conditions of the corresponding fixed point of the Poincaré map.

Let

$$\Xi(\rho,\varepsilon) \equiv \rho^{n-1} + a_1(\varepsilon)\rho^{n-1} + \cdots + a_{n-1}(\varepsilon) = 0 \tag{14.1.2}$$

be the characteristic equation of the linearized map at the fixed point. Then the stability boundaries of the first type are given by the following conditions corresponding to

(1) A saddle-node periodic orbit (fold bifurcation) $\Xi(+1,\varepsilon) = 0$, $l_2(\varepsilon) \neq 0$. Moreover, except for $\rho = +1$, all other roots of the characteristic Eq. (14.1.1) must lie strictly inside the unit circle.

(2) A period-doubling bifurcation (flip bifurcation) $\Xi_n(-1,\varepsilon) = 0$, $l_3(\varepsilon) \neq 0$. Except for $\rho = -1$, the remaining roots of (14.1.1) must lie strictly inside the unit circle.

(3) A birth of an invariant torus $\Xi(e^{\pm i\omega}, \varepsilon) = 0$, $\omega \neq \{0, \pi/2, 2\pi/3, \pi\}$, $L_1(\varepsilon) \neq 0$. Except for $\rho_{1,2} = e^{\pm i\omega}$, all other roots of (14.1.1) must lie strictly inside the unit circle.

There are also four known types of the principal stability boundaries on which the periodic orbit no longer exists.

(4) A periodic orbit collapses into a weak focus (the length of the periodic orbit shrinks to zero while it approaches the bifurcation point). This condition coincides with the condition defining the boundary of an equilibrium state with a single pair of pure imaginary eigenvalues provided that the Lyapunov value $L_1(\varepsilon) < 0$.

(5) A periodic orbit merges with a homoclinic loop $\Gamma(\varepsilon)$ to a saddle-node equilibrium state O_ε, where $\Gamma(\varepsilon) \notin W^{ss}(O_\varepsilon)$.

(6) A periodic orbit merges with a homoclinic loop $\Gamma(\varepsilon)$ to a saddle equilibrium state O_ε whose characteristic exponents $\lambda_1(\varepsilon), \ldots, \lambda_n(\varepsilon)$ satisfy the following conditions:

$$\operatorname{Re}\lambda_i(\varepsilon) < 0\,, \quad (i = 1, \ldots, n-1)\,, \quad \lambda_n(\varepsilon) > 0$$

$$\max_{1\le i\le n-1} \lambda_i(\varepsilon) + \lambda_n(\varepsilon) < 0\,.$$

The period of the periodic orbits in this case, and in the previous one, increases unboundedly whereas its length remains finite.

(7) The fourth and last situation corresponds to the "blue sky catastrophe", i.e. when both period and length of the periodic orbit $\mathcal{L}_\varepsilon$ go to infinity upon approaching the stability boundary. This boundary is distinguished by the existence of a saddle-node periodic orbit $\mathcal{L}^*$ under the assumption that all trajectories of the unstable set $W^u(\mathcal{L}^*)$ return to $\mathcal{L}^*$ as $t \to +\infty$, where $W^u(\mathcal{L}^*) \cap W^{ss}(\mathcal{L}^*) = \emptyset$. The trajectories in $W^u(\mathcal{L}^*)$ define the so-called essential map f (see details in Chap. 12). It is the map of a circle and the blue sky catastrophe emerges upon crossing that part of the saddle-node boundary where the degree of f is zero and, $\max|f'| < 1$.

The computing algorithms of most of these bifurcations have been well developed and can therefore be implemented in software; we mention here the packages designed to settle these bifurcation problems: LOCBIF [76], AUTO [46] and CONTENT [83]. The exception is the "blue sky catastrophe." Despite the fact that it is a codimension-one boundary, this bifurcation has not yet been found in applications of nonlinear dynamics although an explicit mathematical model does exist [53].

14.2. Classification of codimension-one boundaries of stability regions

The notion of safe and dangerous boundaries of stability was suggested by Bautin [24] who studied the stability boundaries for equilibrium states.

Safe boundaries are such that crossing over them leads to only small quantitative changes of the system's state. Dangerous boundaries are such that arbitrarily small perturbations of the system beyond them cause significant and irreversible changes in the system's behavior.

We should notice here that in the case of safe boundaries, a slow drift of the parameters back into the stability region brings a system back into the original response, whereas in the dangerous case this is generally impossible.

Obviously, safe and dangerous boundaries are distinguished mainly by the stability or instability of the corresponding equilibrium state, or periodic trajectory, on the boundary.

Definition 14.1. *A point ε_0 on the stability boundary of an equilibrium state O_ε is said to be safe if O_{ε_0} is asymptotically stable.*

Definition 14.2. *A point ε_0 on the stability boundary of a periodic trajectory L_ε is said to be safe if L_{ε_0} is asymptotically orbitally stable.*

In the latter case the corresponding fixed point of the Poincaré map is asymptotically stable.

On such a stability boundary, a bifurcating equilibrium state O_{ε_0} (or periodic trajectory L_{ε_0}) still possesses a basin of attraction. Therefore, after crossing the boundary, a small attracting "cloud" (whose size depends on how far away we are from the boundary) will inherit the stability of O_{ε_0} (or L_{ε_0}). A reverse evolution of the parameters which returns to the stability boundary will make the spot shrink back to a point (or periodic trajectory).

In such a case we have the so-called *soft* loss of stability. The newly established regime inside the attracting spot may be either a new equilibrium state, a periodic trajectory, a non-resonant torus, or even a strange attractor (a situation generally referred as instant chaos). The latter option is possible when O_{ε_0} has three zero eigenvalues (see [18], or [129] for systems with symmetry).

Definition 14.3. *A point ε_0 on the stability boundary of an equilibrium state O_ε is said to be dangerous if O_{ε_0} is unstable in the sense of Lyapunov.*

Definition 14.4. *A point ε_0 of the stability boundary of a periodic trajectory L_ε is said to be dangerous if the corresponding fixed point of the Poincaré map is unstable in the sense of Lyapunov.*

Remark that Definitions 14.2 and 14.4 apply only to the cases where the periodic orbit exists on the stability boundary.

Here, the following scenarios is played when approaching the stability boundary: the attraction basin of $O_\varepsilon(L_\varepsilon)$ is getting smaller and smaller, and in the limit at $\varepsilon = \varepsilon_0$, it degenerates into a stable set $W^s(O_{\varepsilon_0})(W^s(L_{\varepsilon_0}))$. This set is not empty because, by definition, $O_{\varepsilon_0} \in W^s(O_{\varepsilon_0})(L_{\varepsilon_0} \subseteq W^s(L_{\varepsilon_0}))$. However, it may also consist of one point O_{ε_0} only: this, for example, occurs on a plane when an unstable cycle collapses into a stable focus. In the general case, $W^s(O_{\varepsilon_0})(W^s(L_{\varepsilon_0}))$ is non-trivial. Moreover, it may have a full dimension (the dimension of the phase space) in some cases: if O_{ε_0} is a saddle-node, for example.

After the dangerous point has passed, the behavior of the representative point may be as follows:

(1) If no new limit set appears in a small neighborhood of $O_{\varepsilon_0}(L_{\varepsilon_0})$, then the representative points diverges from the neighborhood. In such case we have the so-called *rigid* loss of stability.
(2) If new attractors do appear, there still exists the possibility that a representative point can escape from the neighborhood, rather than choose one of the stable regimes which has emerged. Hence, one can also refer to this case as a rigid loss of stability.

The latter comment is only heuristic. It reflects the influence of small noise, which always persists in real systems (moreover, it is well-known that fluctuations near bifurcational thresholds are amplified). Therefore, a representative point may break loose from an old regime even before the system reaches the dangerous boundary.

It follows from the above reasoning that the question concerning the dynamics of a system while crossing a stability boundary depends on the system's behavior in the critical cases. This is why the study of critical cases is very important even without a further investigation of the associated bifurcation phenomena. Moreover, a complete bifurcation analysis in a number of cases (e.g. an equilibrium state with at least three characteristic exponents on the imaginary axis, or a periodic trajectory with three multipliers on the unit circle) is unrealistic in principle (see [60]).

For the case of the safe/dangerous points on a stability boundary where periodic trajectories do not exist (the case of global bifurcations), the situation becomes less definite and cannot yet be well specified in general. However, it is well understood in the main cases (see below).

For the remainder of this section we consider only safe and dangerous stability boundaries of codimension one. This allows us to use only one bifurcation parameter. We therefore assume that at $\varepsilon = 0$, the system

$$\dot{x} = X(x, \varepsilon) \tag{14.2.1}$$

lies on a boundary of the stability region; when $\varepsilon < 0$, it is inside the region of stability and outside when $\varepsilon > 0$.

14.2.1. Criteria for safe boundaries

(1) Let O_ε be an equilibrium state and let $O_{\varepsilon=0}$ have a single pair of purely imaginary eigenvalues. In this case, the system $X(\varepsilon)$ is written in the

form

$$\begin{aligned}
\dot{x} &= \rho(\varepsilon)x - \omega(\varepsilon)y + (L_1(\varepsilon)x - \Omega_1(\varepsilon)y)(x^2+y^2) + \cdots ,\\
\dot{y} &= \omega(\varepsilon)x + \rho(\varepsilon)y + (\Omega_1(\varepsilon)x + L_1(\varepsilon)y)(x^2+y^2) + \cdots ,\\
\dot{z} &= (A(\varepsilon) + h(x,y,z,\varepsilon))z\,,
\end{aligned} \tag{14.2.2}$$

where x, $y \in \mathbb{R}^1$, $z \in \mathbb{R}^{n-2}$, $\omega(0) \neq 0$, $\rho(0) = 0$, $\rho(\varepsilon)\varepsilon > 0$ at $\varepsilon \neq 0$; and the eigenvalues of the matrix $A(\varepsilon)$ have negative real parts. The corresponding boundary S_1 is safe if the Lyapunov value $L_1(0)$ is negative. When ε increases from zero, a unique stable periodic trajectory emerges from the weak focus $O_{\varepsilon=0}$ (Fig. 14.2.1).

(2) Let one multiplier of a periodic trajectory L_ε become equal to -1 on the stability boundary. The Poincaré map T on a cross-section transverse to the periodic trajectory may be represented in the form:

$$\begin{aligned}
\bar{x} &= \rho(\varepsilon)x + a_2(\varepsilon)x^2 + a_3(\varepsilon)x^3 + \cdots ,\\
\bar{y} &= (A(\varepsilon) + g(x,y,\varepsilon))y\,,
\end{aligned} \tag{14.2.3}$$

where $x \in \mathbb{R}^1$, $y \in \mathbb{R}^{n-2}$ $\rho(0) = -1$, $|\rho(\varepsilon)| < 1$ when $\varepsilon < 0, |\rho(\varepsilon)| > 1$ when $\varepsilon > 0$, and the eigenvalues of $A(\varepsilon)$ lie strictly inside a unit circle. The stability boundary S_2 is safe if the Lyapunov value $l_2 = -a_3(0) - a_2^2(0)$ is negative.

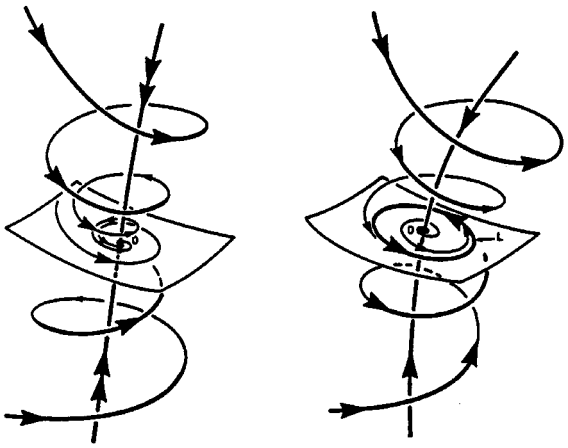

Fig. 14.2.1. Super-critical Andronov–Hopf bifurcation occurs on the safe boundary.

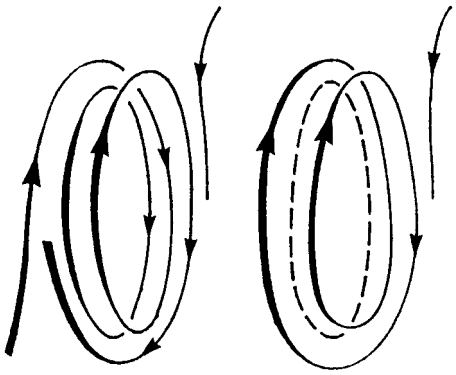

Fig. 14.2.2. A period-doubling bifurcation or a flip.

It follows from the form of the Poincaré map that the invariant center manifold, corresponding to $y = 0$, is a Möbius band in this case, with the periodic trajectory as its median line. At $\varepsilon > 0$, another, double-round periodic trajectory appears which inherits the stability and attracts all nearby trajectories, see Fig. 14.2.2.

(3) Let the system have a periodic trajectory with a pair of multipliers equal to $e^{\pm i\varphi(\varepsilon)}$, where $\varphi(0) \neq \{0, \pi/2, 2\pi/3, \pi\}$. The Poincaré map is then written in the form

$$\begin{aligned}
\bar{x} &= \rho(\varepsilon)(x\cos\varphi(\varepsilon) - y\sin\varphi(\varepsilon)) + (L_1(\varepsilon)x - \Omega(\varepsilon)y)(x^2+y^2) + \cdots ,\\
\bar{y} &= \rho(\varepsilon)(x\sin\varphi(\varepsilon) + y\cos\varphi(\varepsilon)) + (\Omega(\varepsilon)x + L_1(\varepsilon)y)(x^2+y^2) + \cdots , \quad (14.2.4)\\
\bar{z} &= (A(\varepsilon) + h(x,y,z,\varepsilon))z ,
\end{aligned}$$

where $x,\ y \in \mathbb{R}^1,\ z \in \mathbb{R}^{n-3}, |\rho(\varepsilon)| < 1$ when $\varepsilon < 0$, $|\rho(\varepsilon)| > 1$ when $\varepsilon > 0$, and the eigenvalues of $A(\varepsilon)$ lie strictly inside the unit circle. In this case, the boundary S_3 is safe provided that the Lyapunov value $L_1(0)$ is negative. Upon crossing S_3, a stable two-dimensional invariant torus emerges from the periodic trajectory, "the cycle loses its skin" as Andronov described this bifurcation, see Fig. 14.2.3. This is a mechanism responsible for a soft transition from self-oscillation to a beat modulation.

(4) In this case the limit of a periodic trajectory $\mathcal{L}_\varepsilon$ as $\varepsilon \to 0$ is a homoclinic cycle Γ^* composed of a simple saddle-node equilibrium state and its

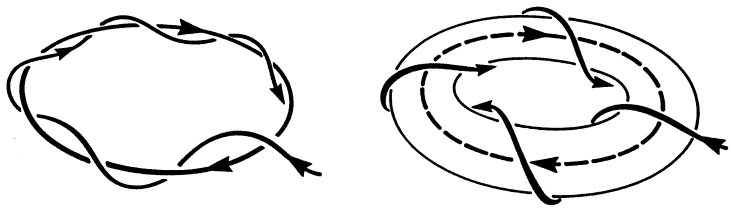

Fig. 14.2.3. Soft birth of an invariant torus. The cycle loses its skin.

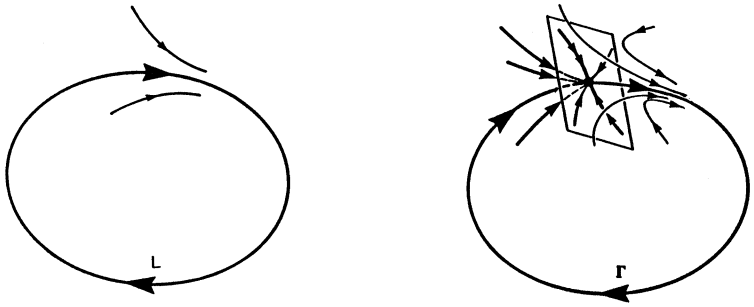

Fig. 14.2.4. The disappearance of the stable cycle may result in the appearance of a saddle-node with a bi-asymptotic trajectory.

separatrix, see Fig. 14.2.4. We also assume that the Γ^* is a smooth curve (i.e. the homoclinic trajectory does not lie in the non-leading manifold of the saddle-node). The given stability boundary S_4 is safe since the curve Γ^* is stable (it attracts every trajectory located inside a small neighborhood Γ^*). Beyond the bifurcation point, when $\varepsilon > 0$, a stationary regime emerges due to the appearance of the stable point.

(5) One more codimension-one boundary of stability of periodic trajectories which corresponds to the "blue sky catastrophe" [152]. It may occur in n-dimensional systems where $n \geq 3$.

In this case, the topological limit of the bifurcating periodic motion $\mathcal{L}_\varepsilon$ as $\varepsilon \to -0$ contains no equilibrium point, but a periodic trajectory $\mathcal{L}^*$ of the saddle-node type which disappears when $\varepsilon < 0$. The trajectory $\mathcal{L}^*$ is a simple saddle-node in the sense that it has only one multiplier, equal to 1, and the first Lyapunov value is not equal to zero.

The following conditions of general position are needed to define the stability boundary S_5: let us denote the unstable set of $\mathcal{L}^*$ by $W^u_{\mathcal{L}^*}$. It is locally

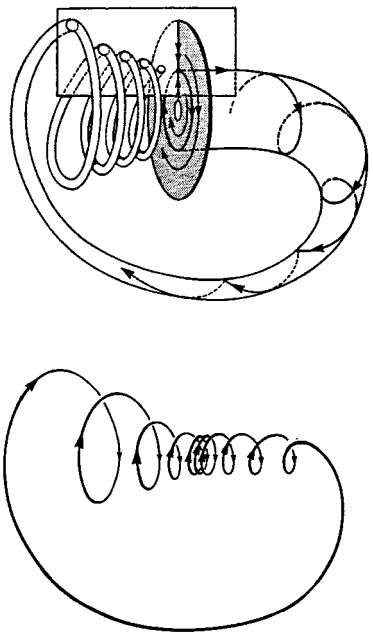

Fig. 14.2.5. A sketch of the blue sky catastrophe; the shape of the periodic orbit $L(\varepsilon)$ looks like a helix condensed near a saddle-node cycle.

homeomorphic to a semi-cylinder $\mathbb{R}^1 \times \mathbb{S}^1$. We suppose that all trajectories in $W^u_{\mathcal{L}^*}$ tend to $\mathcal{L}^*$ as $t \to +\infty$ and none lies in the strong stable subset $W^{ss}_{\mathcal{L}^*}$, i.e. $W^{ss}_{\mathcal{L}^*} \cap W^u_{\mathcal{L}^*} = \emptyset$. We require additionally that $W^u_{\mathcal{L}^*}$ adjoins to $\mathcal{L}^*$ from the side of the node region in such a way as it shown in Fig. 14.2.5; plus, some quantitative restrictions are imposed (see Sec. 12.4 for more detail).

The boundary S_5 is safe; when $\varepsilon > 0$, the periodic orbit $\mathcal{L}^*$ is split into two components: a stable cycle $\mathcal{L}^+_\varepsilon$ and a saddle $\mathcal{L}^-_\varepsilon$. The new stable limiting regime will therefore be given by $\mathcal{L}^+_\varepsilon$.

14.2.2. Criteria for dangerous boundaries

(6) In this case, the topological limit of a periodic trajectory $\mathcal{L}_\varepsilon$ is a separatrix loop $\overline{\Gamma}$ biasymptotic to a saddle equilibrium state. It is required that the roots $\rho_1,\ \rho_2, \ldots, \rho_n$ of the characteristic equation at the saddle are such that $\operatorname{Re}\rho_n \le \cdots \le \operatorname{Re}\rho_2 < 0 < \rho_1$ and the saddle value $\sigma = \operatorname{Re}\rho_2 + \rho_1$ is negative.

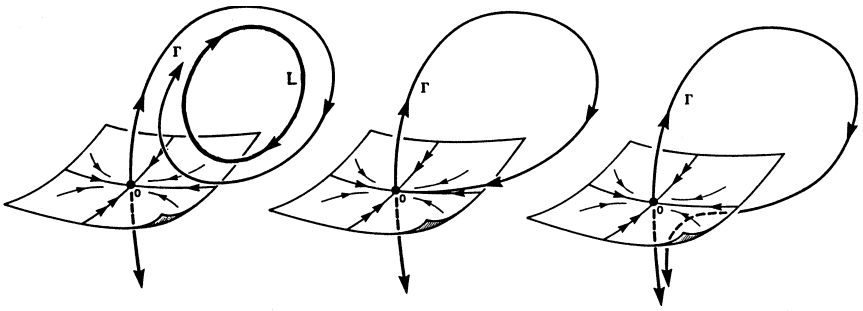

Fig. 14.2.6. A periodic orbit bifurcates into a homoclinic loop to a saddle.

The boundary S_6 is dangerous because the loop $\overline{\Gamma}$ is unstable: some trajectories will escape from its small neighborhood as $t \to \pm\infty$, see Fig. 14.2.6.

(7) Let one eigenvalue of an equilibrium state O_ε vanish at $\varepsilon = 0$. The system then can be represented in the form

$$\begin{aligned} \dot{x} &= R(x,\varepsilon) + f(x,y,\varepsilon)y\,, \\ \dot{y} &= (A(\varepsilon) + g(x,y,\varepsilon))y\,, \end{aligned} \tag{14.2.5}$$

where $x \in \mathbb{R}^1$, $y \in \mathbb{R}^{n-2}$, $R(0,\varepsilon) = \varepsilon$, $R_x(0,\varepsilon) = 0$. The generic case is selected by the condition $l_2 = R_{xx}(0,0) \neq 0$. Since we have supposed that the transition over the boundary starts from negative values of ε, let us assume $l_2 > 0$. The associated stability boundary S_7 is dangerous: when $\varepsilon \to -0$, another saddle equilibrium state is approaching O_ε and merging with it at $\varepsilon = 0$. When $\varepsilon > 0 (R(x,\varepsilon) > 0)$, the resulting saddle-node point O^* disappears and all trajectories diverge from it, see Fig. 14.2.7.

(8) This is similar to Case 1, but with $L_1(0) > 0$. As $\varepsilon \to -0$, a saddle periodic trajectory shrinks into a stable point O_ε. Upon moving through $\varepsilon = 0$, the equilibrium state becomes a saddle-focus: it spawns a two-dimensional unstable invariant manifold (i.e. the boundary S_8 is dangerous).

(9) This is the same as Case 2 but with $l_1 > 0$. The instability occurs because a period-two saddle periodic trajectory merges with a stable periodic orbit. When $\varepsilon \geq 0$, the latter becomes a saddle so that its unstable manifold is homeomorphic to a Möbius band.

(10) Same as Case 3 but $L_1(0) > 0$. The stable periodic orbit becomes unstable when an unstable two-dimensional invariant torus shrinks into it.

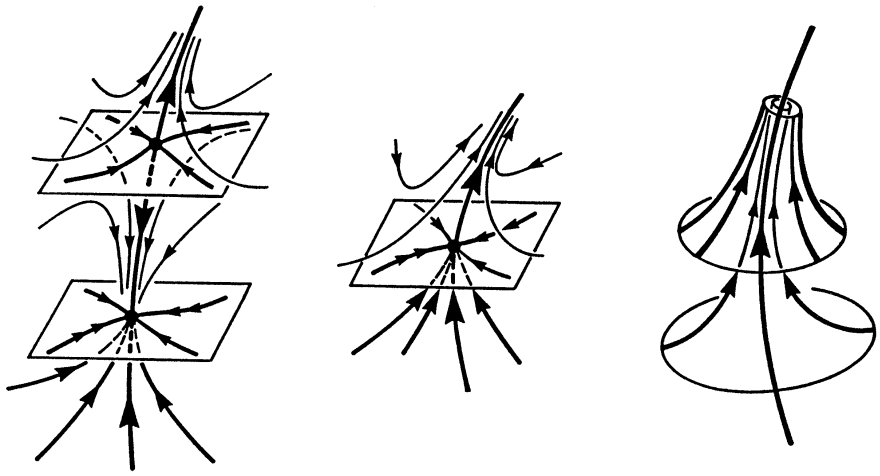

Fig. 14.2.7. A saddle-node bifurcation without homoclinics.

When $\varepsilon \geq 0$, the unstable invariant manifold W^u of the periodic trajectory has dimension three.

(11) Let one multiplier of a periodic trajectory $\mathcal{L}_\varepsilon$ become equal to $+1$ at $\varepsilon = 0$. The associated Poincaré map can be represented in the following form:

$$\begin{aligned} \bar{x} &= x + R(x, \varepsilon) \\ \bar{y} &= (A(\varepsilon) + g(x, y, \varepsilon))y\,, \end{aligned} \tag{14.2.6}$$

where $x \in \mathbb{R}^1$, $y \in \mathbb{R}^{n-2}$. Let $l_2 = R_{xx}(0,0) > 0$. Then, the boundary S_{11} exhibits a dangerous character because $\mathcal{L}_\varepsilon$ coalesces with a saddle periodic trajectory as $\varepsilon \to 0$. The bifurcating trajectory $\mathcal{L}^*$ is of saddle-node type and has an unstable invariant manifold W^u homeomorphic to a cylinder $\mathbb{S}^1 \times \mathbb{R}^+$, see Fig. 14.2.8.

Summary: The set of principal stability boundaries of equilibrium states consists of surfaces of three kinds: S_1, S_7 and S_8. Only the S_1-like boundaries are safe. As for periodic orbits, there are nine types of principal stability boundaries: among them S_6, S_9, S_{10}, S_{11} are dangerous, while S_2, S_3, S_4 S_5 and $\tilde{S}_1$, $\tilde{S}_2$ are safe (the latter two correspond to the subcritical Andronov–Hopf and flip bifurcations, respectively).

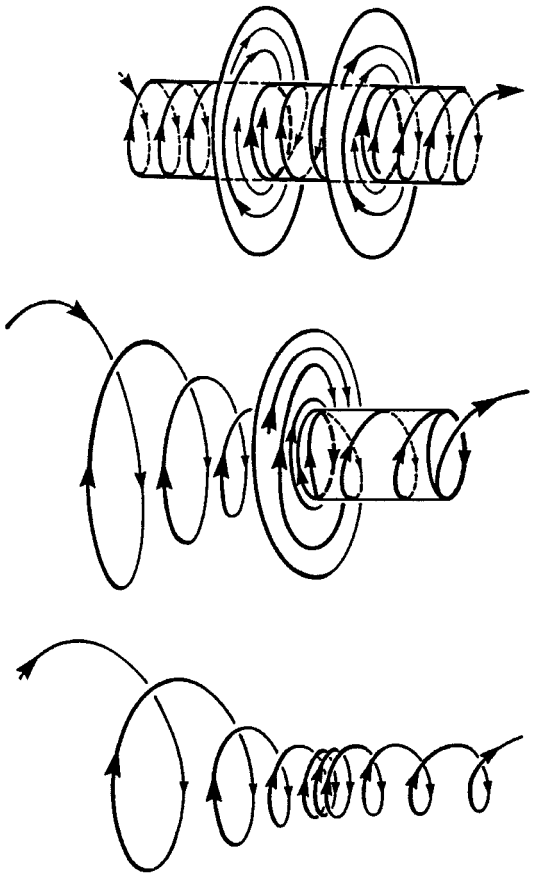

Fig. 14.2.8. A saddle-node (fold) bifurcation of periodic orbits in $\mathbb{R}^3$.

14.3. Dynamically definite and indefinite boundaries of stability regions

In this section we will attempt to answer the following question: where is the representative point heading for upon crossing over a stability boundary? Or, in other words, what is its Ω-limit set?

The answer is obvious when we deal with principal safe boundaries of stability regions: the representative point tends to a new stable regime which,

emerges from a soft bifurcation. The situation is dramatically different when a system passes through a dangerous boundary: the point escapes the old regime and runs away. In this situation the theory of local bifurcations does not provide a straightforward answer to the above question. Nevertheless, to figure out what may happen beyond the bifurcation it is useful to introduce two subtypes of the stability boundaries — *dynamically definite* and *dynamically indefinite boundaries* [137, 26]. Let us consider first a few examples.

The first example illustrates one of the most typical bifurcations which occur in dissipative systems; namely a stable periodic orbit L_1 adheres to the homoclinic loop of a saddle. Denote the unstable separatrices of the saddle by Γ_1 and Γ_2. Let Γ_1 form a homoclinic loop at the bifurcation point. Denote the limit set of the second separatrix by $\Omega(\Gamma_2)$. In the general case $\Omega(\Gamma_2)$ is an attractor; for instance, a stable equilibrium state, a stable periodic trajectory, or a stable torus, etc. Since immediately after bifurcation a representative point will follow closely along Γ_2, it seems likely that $\Omega(\Gamma_2)$ will become its new attractor.

The second example exhibits a stable equilibrium state which merges with a saddle to spawn a saddle-node. Denote by Γ, the only unstable trajectory leaving the saddle-node as $t \to +\infty$, and its limit set by $\Omega(\Gamma)$. If $\Omega(\Gamma)$ is an attractor, then the representative point will tend to it after the saddle-node has disappeared. However, another scenario is also possible; namely, when Γ tends to the same saddle-node as $t \to \pm\infty$. Then we have the situation described in the previous sections: a stable periodic trajectory that bifurcates from $\overline{\Gamma}$ becomes a new limit regime for the representative point.

Both cases have much in common in the sense that the unstable set of both bifurcating equilibrium states is one-dimensional. If the unstable set of the critical equilibrium state is of a higher-dimension, then the subsequent picture may be completely different. Figure 14.3.1 depicts such a situation. When the unstable cycle shrinks into the equilibrium state we have a dilemma: the representative point may jump either to the stable node O_1 or to the stable node O_2. Therefore this dangerous boundary must be classified as *dynamically indefinite*.

Consider the other hypothetical example. Let a two-dimensional diffeomorphism at $\varepsilon = 0$ have a phase portrait as shown in Fig. 14.3.2. Here, O_2 and O_3 are stable fixed points, and O_1 is a saddle. The unstable set W^u_O of the saddle-node O intersects transversely the stable manifold $W^s_{O_1}$

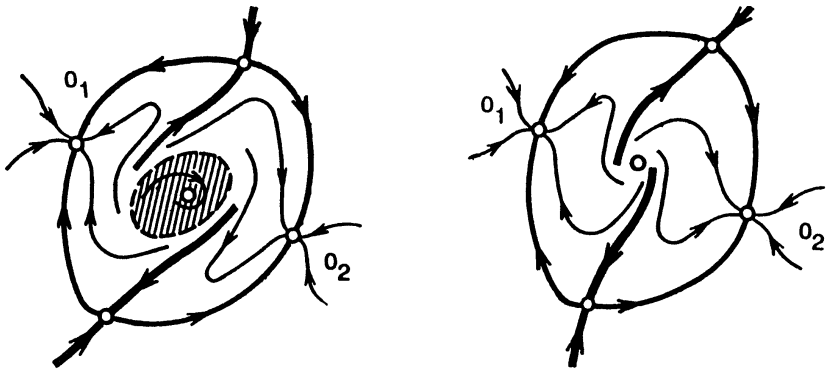

(a) (b)

Fig. 14.3.1. Uncertainty occurs when the unstable cycle vanishes at the origin.

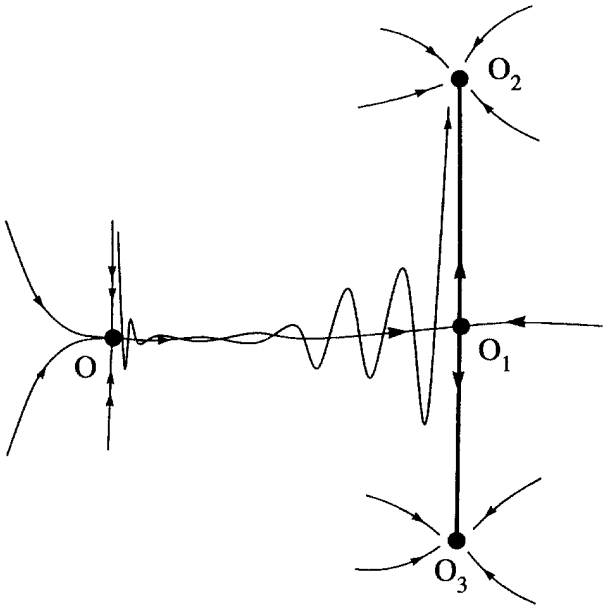

Fig. 14.3.2. Dynamical uncertainty due to heteroclinic wiggles.

of the saddle. When the saddle-node disappears there is an uncertainty on the choice of the new regime for a representative point because it may converge to either O_2 or O_3.

We can now assert that a stability boundary is *dynamically definite* if upon crossing over the boundary the behavior of the representative point is *uniquely defined*. This situation does occur in the case where the unstable set W^u of the equilibrium state (the periodic trajectory) contains at most one attractor at the critical parameter value.

In contrast, if the choice of the new regime for the representative point is ambiguously defined, then we can assert that such a boundary is *dynamically indefinite*. This occurs if at least two attractors belong to the boundary of the unstable set. It must also contain saddles whose unstable invariant manifolds separate the basins of the attractors.

Next, let us consider a particular case typical of symmetrical systems. For example, consider the family

$$\dot{x} = \varepsilon x - x^3 \,,$$

which is invariant with respect to $x \to -x$. The stability boundary $\varepsilon = 0$ is easily seen to be safe for the equilibrium state at the origin. When $\varepsilon > 0$, the origin looses its stability, which is inherited by two new equilibrium points $O_1(x = \sqrt{\varepsilon})$ and $O_2(x = -\sqrt{\varepsilon})$. So, $\varepsilon = 0$ is a dynamically indefinite safe boundary in view of the above arguments.

A more complicated example is the pendulum-like equation

$$\ddot{x} = f(x, \dot{x}, \varepsilon) \,,$$

where $f(x, \dot{x}, \varepsilon)$ is a periodic function in x, and $f(x, \dot{x}, \varepsilon) = -f(-x, -\dot{x}, \varepsilon)$. The transition through the boundary of the stability region of an "oscillating" limit cycle in this example results in the appearance of two stable periodic orbits which span the cylinder and correspond to two opposite directions of rotation of the pendulum. Here, an exit across the boundary occurs when the oscillating cycle merges with a heteroclinic connection between two saddles, as shown in Fig. 14.3.3. Observe from this picture that this boundary is dynamically indefinite.

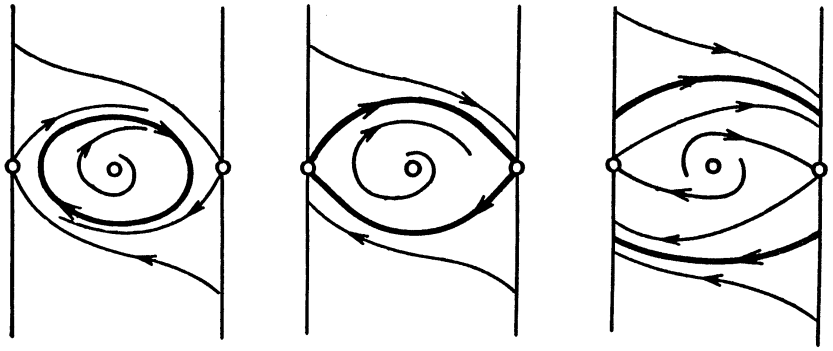

Fig. 14.3.3. Evolution of the phase cylinder. Anyone has experienced with the devil's wheel in fairs knows how it feels when situated up-side-down at the top point. For a fleeting moment which seems forever, you cannot tell which way the wheel will roll over down, clock-wise or counter-clock-wise. A.L.S. had, personally, made it once, and thereby had dramatically improved his qualitative understanding of the behavior near a saddle point.

Appendix C

EXAMPLES, PROBLEMS AND EXERCISES

We hope the examples presented in this appendix will provide some pedagogical illustrations and applications of the "qualitative" theory developed in this book. The range of instances varies from phenomenological problems to applications. Since very few nonlinear systems can be analyzed without computers, we will perform numerical computations where necessary. At some points, our *de facto* presentation will bear a descriptive character, avoiding technical details of computations. The two packages which have been used in the preparation of this appendix are Content [182] and Dstool [164].

C.1 Qualitative integration

C.1.#1. Classify the trajectories shown in Figs. 1.3.1, 1.3.2 and C.1.1 in the following terms: non-wandering, Poisson-stable, periodic, and homoclinic. What are the corresponding α- and ω-limit sets of these trajectories? □

C.1.#2. For different parameter values of a, construct the phase portraits for the following planar systems

(a) $$\dot r = r(a - r^2), \quad \dot\varphi = 1\,;$$

(b) $$\begin{cases} \dot y = x - (y^2-1)\left(\dfrac{x^2}{2} - y + \dfrac{y^3}{3} - \dfrac{2}{3}\right), \\ \dot x = 1 - y^2 - x\left(\dfrac{x^2}{2} - y + \dfrac{y^3}{3} - \dfrac{2}{3}\right); \end{cases}$$

(c) $$\dot x = y, \quad \dot y = 1 - ax^2 + y(x-2)\,;$$

(d) the van der Pol equation:

$$\ddot{x} + a(x^2 - 1)\dot{x} + x = 0\,;$$

(e) the Duffing equation:

$$\ddot{x} + a\dot{x} + x - x^3 = 0;$$

(f) the Bogdanov-Takens normal form:

$$\dot{x} = y, \quad \dot{y} = -x + ay + x^2\,;$$

(g) the Khorozov-Takens normal form:

$$\dot{x} = y, \quad \dot{y} = -x + ay + x^3\,. \qquad \square$$

C.1.#3. Discuss the phase portraits of the cells shown in Fig. C.1.1. What are the special trajectories here? $\square$

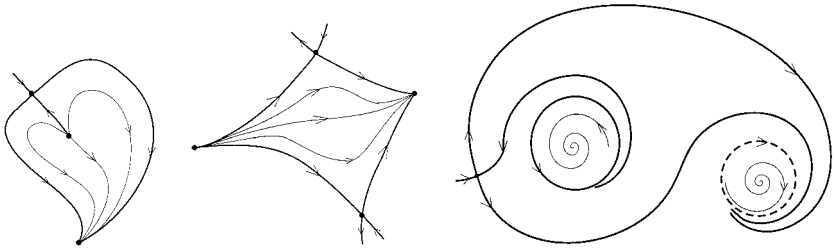

(a) (b) (c)

Fig. C.1.1. Examples of cells.

C.2 Rough equilibrium states and stability boundaries

C.2.1 *Routh-Hurwitz criterion*

Here we will formulate the rule that allows one to determine the structural stability of an equilibrium state and its topological type without solving explicitly the characteristic equation.

The problem in question is how many roots of the characteristic equation

$$\Xi(\lambda) = a_0\lambda^n + a_1\lambda^{n-1} + \cdots + a_n$$

lie to the left or to the right of the imaginary axis and how many roots lie on that axis. The number of zero roots is determined easily: there are s zero roots if and only if $a_n = \cdots = a_{n-s+1} = 0$ and $a_{n-s} \neq 0$. So, if we have a zero root of algebraic multiplicity s, we can just divide the characteristic equation by λ^s and proceed to the case where the last coefficient of the characteristic equation is non-zero, as we will assume to be the case. The next step is to compose the following Routh-Hurwitz matrix:

$$\begin{pmatrix} a_0; & a_2; & a_4; & \cdots \\ a_1; & a_3; & a_5; & \cdots \\ \dfrac{a_1a_2 - a_0a_3}{a_1}; & \dfrac{a_1a_4 - a_0a_5}{a_1}; & \cdots & \cdots \\ \dfrac{\dfrac{a_1a_2 - a_0a_3}{a_1}a_3 - \dfrac{a_1a_4 - a_0a_5}{a_1}a_1}{\dfrac{a_1a_2 - a_0a_3}{a_1}}; & \cdots & \cdots & \cdots \\ & \cdots & \cdots & \cdots \end{pmatrix} \tag{C.2.1}$$

Let us describe the algorithm for constructing the above matrix in detail. The entries of the first two rows are the coefficients of $\Xi(\lambda)$ with even and odd subscripts, respectively. The k-th row is built as follows: the entry r_{kj} at the j-th column is equal to the fraction

$$r_{kj} = \frac{r_{k-1,1}r_{k-2,j+1} - r_{k-2,1}r_{k-1,j+1}}{r_{k-1,1}}$$

whose numerator is taken with opposite sign of the determinant of the (2×2)-matrix at the intersection of the two previous rows with the first column and the $(j+1)$-th column, whereas the denominator is the entry located in the first column of the previous row. The algorithm is subsequently applied until the overall number of the rows in the matrix becomes equal to $(n + 1)$.

Such a construction for the matrix becomes possible only if all entries of the first column do not vanish. This is the *regular* case. Here, the number of the roots of $\Xi(\lambda)$ (including multiplicity) with positive real parts, is equal to the number q of sign changes of the entries in the first column. The polynomial $\Xi(\lambda)$ has no purely imaginary roots in the regular case. Therefore, the corresponding equilibrium state O is structurally stable in the regular case, and its topological type is given by $(n - q, q)$.

One can verify that the first column in (C.2.1) can be expressed through the main minors Δ_i of the Routh-Hurwitz matrix (2.1.10) as follows

$$a_0, \quad \Delta_1, \quad \frac{\Delta_2}{\Delta_1}, \quad \frac{\Delta_3}{\Delta_2}, \ldots, \frac{\Delta_n}{\Delta_{n-1}}\,.$$

In particular, if $a_0 > 0$ and $\Delta_i > 0$ $(i = 1, 2, \ldots, n)$, then the Routh-Hurwitz conditions hold (see Sec. 2.1).

While constructing the matrix (C.2.1) it may turn out that some entry $r_{m+1,1}$ $(1 \le m \le n)$ of the first column vanishes. In this *irregular* case one should find the first non-zero entry $r_{m+1,k+1}$ in the $(m+1)$-th row, as well as the last non-zero entries $r_{m,p}$ and $r_{m+1,s}$ in the m-th and $(m+1)$-th rows, respectively. Compute the deficiency number S_{m+1} by the following rule:

$$S_{m+1} = \begin{cases} k & \text{if } k \le s-p \\ s-p & \text{if } k > s-p \text{ and } (-1)^{s-p} r_{m,p} r_{m+1,s} < 0 \\ s-p+1 & \text{if } k > s-p \text{ and } (-1)^{s-p} r_{m,p} r_{m+1,s} > 0\,. \end{cases}$$

Then, shift the $(m+1)$-th row to the left over k positions, so that the element $r_{m+1,k+1}$ becomes the first one in the line, and multiply all other entries of this row through by $(-1)^k$. Since the first entry is now non-zero, one proceeds as in the regular case. Eventually, the number of roots of $\Xi(\lambda)$ with positive real parts will be equal to the number of sign changes in the first column added to the sum of deficiency numbers over all irregular rows.

There still remains a special case where for some m the entire $(m+1)$-th row of the matrix consists of zeros, i.e. $r_{m+1,j} = 0$ at all j. This is the only situation when pure imaginary roots are possible. If this case is encountered, we should replace the $(m+1)$-th row by a row consisting of the following numbers

$$(p-1)\, r_{m,1}; \quad (p-2)\, r_{m,2}; \quad (p-3)\, r_{m,3}; \quad \cdots\,,$$

where p is the number of the last non-zero entry in the m-th row, and proceed as before. Upon completing the construction (there may be other vanishing rows that should be replaced too) we count the number of sign changes in the first column plus the sum of deficiency numbers (if some irregular rows have appeared). The result equals the number of roots with positive real parts. The number of purely imaginary roots here is equal to $2(p-1-l)$, where p is the ordinal number of the last non-zero entry in the row which precedes the first

vanishing one, and l is the number of sign changes in the first column plus the sum of deficiency numbers computed after this row. The corresponding equilibrium state will be structurally stable only if $p = l + 1$.

C.2.#4. Determine the stability and the topological type of an equilibrium state whose characteristic equation is given below:

$$\Xi(\lambda) = \lambda^4 + 2\lambda^3 + \lambda^2 - 8\lambda - 20 = 0\,.$$

Solution. The corresponding Rough-Hurwitz matrix is given by

$$\begin{array}{rrl} 1 & 1 & -20 \\ 2 & -8 & \\ 5 & -20 & (p=2) \\ 5 & & (\text{zero entry replaced by } (p-1)r_{m,1}=5) \\ -20 & & \end{array}$$

Here there is one sign change in the first column, i.e. $\Xi(\xi)$ has one root in the right open half-plane. Let us count the number of purely imaginary roots: $2(p-1-l) = 2(2-1-1) = 0$. Thus, the equilibrium state O is structurally stable, and its topological type is saddle (3,1). □

C.2.2 *3D case*

Consider a three-dimensional system

$$\begin{aligned} \dot{y}_1 &= a_1^{(1)} y_1 + a_2^{(1)} y_2 + a_3^{(1)} y_3 + P_1(y_1, y_2, y_3), \\ \dot{y}_2 &= a_1^{(2)} y_1 + a_2^{(2)} y_2 + a_3^{(2)} y_3 + P_2(y_1, y_2, y_3), \\ \dot{y}_3 &= a_1^{(3)} y_1 + a_2^{(3)} y_2 + a_3^{(3)} y_3 + P_3(y_1, y_2, y_3)\,. \end{aligned} \tag{C.2.2}$$

Here, the functions P_i contain no linear terms. The characteristic equation of the system (C.2.2) is given by

$$\Xi(\lambda) = \begin{vmatrix} a_1^{(1)} - \lambda & a_2^{(1)} & a_3^{(1)} \\ a_1^{(2)} & a_2^{(2)} - \lambda & a_3^{(2)} \\ a_1^{(3)} & a_2^{(3)} & a_3^{(3)} - \lambda \end{vmatrix} = 0\,. \tag{C.2.3}$$

Equation (C.2.3) can be rewritten in the form of a cubic polynomial:

$$\lambda^3 + p\lambda^2 + q\lambda + r = 0\,, \tag{C.2.4}$$

where

$$
\begin{aligned}
p &= -(a_1^{(1)} + a_2^{(2)} + a_3^{(3)})\,, \\
q &= \begin{vmatrix} a_1^{(1)} & a_2^{(1)} \\ a_1^{(2)} & a_2^{(2)} \end{vmatrix} + \begin{vmatrix} a_1^{(1)} & a_3^{(1)} \\ a_1^{(3)} & a_3^{(3)} \end{vmatrix} + \begin{vmatrix} a_2^{(2)} & a_3^{(2)} \\ a_2^{(3)} & a_3^{(3)} \end{vmatrix}\,, \\
r &= -\begin{vmatrix} a_1^{(1)} & a_2^{(1)} & a_3^{(1)} \\ a_1^{(2)} & a_2^{(2)} & a_3^{(2)} \\ a_1^{(3)} & a_2^{(3)} & a_3^{(3)} \end{vmatrix}\,.
\end{aligned}
\tag{C.2.5}
$$

Here, the Routh-Hurwitz stability condition reduces to the following relation:

$$
p > 0, \quad q > 0, \quad r > 0, \quad \text{and} \quad R \equiv pq - r > 0\,. \tag{C.2.6}
$$

The boundaries of the stability region are two surfaces given by ($r = 0$, $p > 0, q > 0$) and ($R = 0, p > 0, q > 0$). The characteristic equation has at least one zero root on the surface $r = 0$, and a pair of purely imaginary roots on the surface ($R = 0, q > 0$).

C.2.#5. Show that the characteristic exponents of the equilibrium state on the bifurcation surface $R = 0$ are $(-p,\, i\sqrt{q}, -i\sqrt{q})$. □

The number of real roots of Eq. (C.2.4) depends on the sign of the discriminant of the cubic equation:

$$
\Delta = -p^2q^2 + 4p^3r + 4q^3 - 18pqr + 27r^2\,. \tag{C.2.7}
$$

(1) If $\Delta > O$, the cubic equation has one real root and two complex-conjugate ones;
(2) If $\Delta < O$, the cubic equation has three distinct real roots;
(3) When $\Delta = 0$, the equation has one real root of multiplicity 3 if $q = \frac{1}{3}p^2$ and $r = \frac{1}{27}p^3$, or two real roots (one of multiplicity 2).

The equation $\Delta = 0$ can be resolved as follows:

$$
r = \frac{1}{3}pq - \frac{2}{27}p^3 \pm \frac{2}{27}(p^2 - 3q)^{3/2}, \qquad q \le \frac{p^2}{3}\,.
$$

Hence, the characteristic equation has all the three roots real if and only if

$$
q \le \frac{p^2}{3} \quad \text{and} \quad r^-(p,q) \le r \le r^+(p,q)\,, \tag{C.2.8}
$$

where we denote

$$r^{\pm} = \frac{1}{3}pq - \frac{2}{27}p^3 \pm \frac{2}{27}(p^2 - 3q)^{3/2}\,.$$

When the equilibrium state is topologically saddle, condition (C.2.8) distinguishes between the cases of a simple saddle and a saddle-focus. However, when the equilibrium is stable or completely unstable, the presence of complex characteristic roots does not necessarily imply that it is a focus. Indeed, if the nearest to the imaginary axis (i.e. the leading) characteristic root is real, the stable (or completely unstable) equilibrium state is a node independently of what other characteristic roots are.

The boundary between real and complex leading characteristic roots is formed by a part of the surface $\Delta = 0$ which corresponds to the double roots and by the surface

$$r = \frac{p}{3}\left(q - \frac{2p^2}{9}\right), \qquad q \geq \frac{p^2}{3}\,, \tag{C.2.9}$$

which joins the surface $\Delta = 0$ along the line of triple roots. This surface corresponds to the existence of a pair of complex-conjugate roots whose real part is equal to the third root. When we cross this surface towards decreasing $|r|$ this pair is moved farther from the imaginary axis than the real root, so the equilibrium state becomes a node. To the other side of this surface the complex-conjugate pair becomes closer to the imaginary axis than the real root, so that the equilibrium state becomes a focus.

When studying homoclinic bifurcations, an important characteristic of saddle equilibria is the sign of the *saddle value* σ defined as the sum of the real parts of the two leading characteristic exponents nearest to the imaginary axis from the left and from the right.

In the case of a saddle, when both leading exponents $\lambda_{1,2}$ are real, the condition $\sigma = 0$ is a resonance relation $\lambda_1 + \lambda_2 = 0$. In terms of the coefficients of the cubic characteristic equation, this condition recasts as

$$R \equiv pq - r = 0, \qquad -p^2 < q < 0\,. \tag{C.2.10}$$

Observe that when $q > 0$, the surface $R = 0$, corresponds to the Andronov-Hopf bifurcation, whereas the part of the surface where $q < -p^2$, corresponds to the vanishing of the sum of one leading exponent and a non-leading one of opposite sign.

In the case of a saddle-focus of a three-dimensional system the condition $\sigma = 0$ reads as $\lambda_1 + \mathrm{Re}\lambda_2 = 0$ where λ_1 is a real root and $\lambda_{2,3}$ are the pair of complex-conjugate roots. This can be written as

$$r = -p(q + 2p^2), \qquad -p^2 < q\,. \tag{C.2.11}$$

When crossing this surface towards increasing r, the saddle value becomes positive.

Another important characteristic of saddle equilibria of three-dimensional systems is the *divergence* of the vector field at the equilibrium state. It is equal to the sum of the characteristic roots, i.e. to $-p$.

Summarizing, we can classify the rough equilibrium states in $\mathbb{R}^3$ as follows:

(1) The case $p > 0$ (div < 0) (See Table C.1).
(2) The case $p < 0$ (div > 0) (See Table C.2).
(3) The case $p = 0$ (div $= 0$) (See Table C.3).

C.2.#6. Draw the corresponding bifurcation diagrams on the (q, r)-plane with fixed p. □

Let us consider next a few examples. We will focus our consideration on the Lorenz equation, the Chua's circuit, the Shimizu-Morioka model and some others.

The Chua's circuit [179] is given by

$$\begin{aligned} \dot{x} &= a(y - f(x))\,, \\ \dot{y} &= x - y + z\,, \\ \dot{z} &= -by\,, \end{aligned} \tag{C.2.12}$$

with cubic nonlinearity $f(x) = -x/6 + x^3/6$. Here, a and b are some positive parameters. System (C.2.12) is invariant under the transformation $(x, y, z) \leftrightarrow (-x, -y, -z)$.

Let us find the equilibrium states in (C.2.12) by solving the following system:

$$\begin{aligned} 0 &= a(y + x/6 - x^3/6), \\ 0 &= x - y + z, \\ 0 &= -by\,. \end{aligned}$$

Table C.1

Parameter regions	Types of equilibria	σ	Eigenvalues $\lambda_i,\ i=1,2,3$
$0 < r < \begin{cases} r^+(p,q) & \text{for } 0 < q \le \dfrac{p^2}{3} \\ \dfrac{p}{3}\left(q - \dfrac{2p^2}{9}\right) & \text{for } q \ge \dfrac{p^2}{3} \end{cases}$	Stable node $\dim W^s = 3$ $\dim W^u = 0$	—	$0 > \lambda_1 > \mathrm{Re}\lambda_i$ $(i = 2, 3)$
$pq > r > \begin{cases} r^+(p,q) & \text{for } 0 < q \le \dfrac{p^2}{3} \\ \dfrac{p}{3}\left(q - \dfrac{2p^2}{9}\right) & \text{for } q \ge \dfrac{p^2}{3} \end{cases}$	Stable focus $\dim W^s = 3$ $\dim W^u = 0$	—	$0 > \mathrm{Re}\lambda_{1,2} > \lambda_3$
$r > \begin{cases} r^+(p,q) & \text{for } q \le 0 \\ pq & \text{for } q \ge 0 \end{cases}$	Saddle-focus (1,2)	$\sigma < 0$	$\mathrm{Re}\lambda_{2,3} > 0 > \lambda_1$
$0 < r < r^+(p,q),\ q < 0$	Saddle $\dim W^s = 1$ $\dim W^u = 2$	$\sigma < 0$	$\lambda_1 < 0 < \lambda_2 < \lambda_3$
$0 > r > \begin{cases} r^-(p,q) & \text{for } q \le -p^2 \\ pq & \text{for } -p^2 \le q < 0 \end{cases}$	Saddle $\dim W^s = 2$ $\dim W^u = 1$	$\sigma > 0$	$\lambda_1 > 0 > \lambda_2 > \lambda_3$
$r^-(p,q) < r < \begin{cases} pq & \text{for } -p^2 < q \le 0 \\ 0 & \text{for } 0 \le q < \dfrac{p^2}{4} \end{cases}$	Saddle $\dim W^s = 2$ $\dim W^u = 1$	$\sigma < 0$	$\lambda_1 > 0 > \lambda_2 > \lambda_3$
$-p(q+2p^2) < r < \begin{cases} r^-(p,q) & \text{for } -p^2 < q \le \dfrac{p^2}{4} \\ 0 & \text{for } q \ge \dfrac{p^2}{4} \end{cases}$	Saddle-focus (2,1)	$\sigma < 0$	$\lambda_1 > 0 > \mathrm{Re}\lambda_{2,3}$
$r < \begin{cases} r^-(p,q) & \text{for } q \le -p^2 \\ -p(q+2p^2) & \text{for } q \ge -p^2 \end{cases}$	Saddle-focus (2,1)	$\sigma > 0$	$\lambda_1 > 0 > \mathrm{Re}\lambda_{2,3}$

Table C.2

Parameter regions	Types of equilibria	σ	Eigenvalues $\lambda_i,\ i=1,2,3$
$0 > r > \begin{cases} r^-(p,q) & \text{for } 0 < q \le \dfrac{p^2}{3} \\ \dfrac{p}{3}\left(q - \dfrac{2p^2}{9}\right) & \text{for } q \ge \dfrac{p^2}{3} \end{cases}$	Repelling node $\dim W^s = 0$ $\dim W^u = 3$	—	$0 < \lambda_1 < \mathrm{Re}\lambda_i$ $(i = 2, 3)$
$pq < r < \begin{cases} r^-(p,q) & \text{for } 0 < q \le \dfrac{p^2}{3} \\ \dfrac{p}{3}\left(q - \dfrac{2p^2}{9}\right) & \text{for } q \ge \dfrac{p^2}{3} \end{cases}$	Repelling focus $\dim W^s = 0$ $\dim W^u = 3$	—	$0 < \mathrm{Re}\lambda_{1,2} < \lambda_3$
$r < \begin{cases} r^-(p,q) & \text{for } q \le 0 \\ pq & \text{for } q \ge 0 \end{cases}$	Saddle-focus (2,1)	$\sigma > 0$	$\mathrm{Re}\lambda_{2,3} < 0 < \lambda_1$
$0 > r > r^-(p,q),\ q < 0$	Saddle $\dim W^s = 2$ $\dim W^u = 1$	$\sigma > 0$	$\lambda_1 > 0 > \lambda_2 > \lambda_3$
$0 < r < \begin{cases} r^+(p,q) & \text{for } q \le -p^2 \\ pq & \text{for } -p^2 \le q < 0 \end{cases}$	Saddle $\dim W^s = 1$ $\dim W^u = 2$	$\sigma < 0$	$\lambda_1 < 0 < \lambda_2 < \lambda_3$
$r^+(p,q) > r > \begin{cases} pq & \text{for } -p^2 < q \le 0 \\ 0 & \text{for } 0 \le q < \dfrac{p^2}{4} \end{cases}$	Saddle $\dim W^s = 1$ $\dim W^u = 2$	$\sigma > 0$	$\lambda_1 < 0 < \lambda_2 < \lambda_3$
$-p(q+2p^2) > r > \begin{cases} r^+(p,q) & \text{at } q \in \left(-p^2, \dfrac{p^2}{4}\right) \\ 0 & \text{at } q \ge \dfrac{p^2}{4} \end{cases}$	Saddle-focus (1,2)	$\sigma > 0$	$\lambda_1 < 0 < \mathrm{Re}\lambda_{2,3}$
$r > \begin{cases} r^+(p,q) & \text{for } q \le -p^2 \\ -p(q+2p^2) & \text{for } q \ge -p^2 \end{cases}$	Saddle-focus (1,2)	$\sigma < 0$	$\lambda_1 < 0 < \mathrm{Re}\lambda_{2,3}$

Table C.3

Parameter regions	Types of equilibria	Eigenvalues $\lambda_i,\ i=1,2,3$	Dimensions of W^s and W^u
$0 < r < \frac{2}{9}\sqrt{3}\|q\|^{3/2},\ q<0$	Saddle	$\lambda_1 < 0 < \lambda_2 < \lambda_3$	$\dim W^s = 1$ $\dim W^u = 2$
$r > \begin{cases} \frac{2}{9}\sqrt{3}\|q\|^{3/2} & \text{for } q \le 0 \\ 0 & \text{for } q \ge 0 \end{cases}$	Saddle-focus (1,2)	$\lambda_1 < 0 < \mathrm{Re}\lambda_{2,3}$	$\dim W^s = 1$ $\dim W^u = 2$
$r < \begin{cases} -\frac{2}{9}\sqrt{3}\|q\|^{3/2} & \text{for } q \le 0 \\ 0 & \text{for } q \ge 0 \end{cases}$	Saddle-focus (2,1)	$\mathrm{Re}\lambda_{2,3} < 0 < \lambda_1$	$\dim W^s = 2$ $\dim W^u = 1$
$0 > r > -\frac{2}{9}\sqrt{3}\|q\|^{3/2},\ q<0$	Saddle	$\lambda_1 > 0 > \lambda_2 > \lambda_3$	$\dim W^s = 2$ $\dim W^u = 1$

□

From these equilibrium equations, we find that $y=0$, $x=-z$ and $x(1-x^2)=0$. Thus, there are always three equilibria: $O(0,0,0)$ and $O_{1,2}(\pm 1,0,\mp 1)$. The Jacobian matrix at the origin is given by

$$\begin{bmatrix} a/6 & a & 0 \\ 1 & -1 & 1 \\ 0 & -b & 0 \end{bmatrix}.$$

The characteristic equation at $O(0,0,0)$ is

$$\det \begin{bmatrix} a/6-\lambda & a & 0 \\ 1 & -1-\lambda & 1 \\ 0 & -b & -\lambda \end{bmatrix} = 0,$$

or

$$\lambda^3 + (1-a/6)\lambda^2 + (b-7a/6)\lambda - ab/6 = 0. \tag{C.2.13}$$

One can see that since the constant term is negative, it follows immediately from the Routh-Hurwitz criterion that the origin is an unstable equilibrium state. Furthermore, it may have no zero characteristic roots when a and b are positive. The codimension-2 point ($a=b=0$) requires special considerations. We postpone its analysis to the last section, where we discuss the bifurcation of double zeros in systems with symmetry.

The condition $R \equiv pq - r = 0$ reads here as

$$b = 7a/6 - 7a^2/36\,.$$

We have $q = -7a^2/36 < 0$ at $R = 0$. This means that the point at the origin cannot have a pair of purely imaginary eigenvalues. Thus, it is always structurally stable when $(a, b) \neq 0$. In accordance to the above classification table, its topological type is a saddle with a two-dimensional stable manifold, and a one-dimensional unstable manifold.

C.2.#7. In the (a, b)-parameter plane, find the transition boundary: saddle $\to$ saddle-focus for the origin, and equations for its linear stable and unstable subspaces. Detect the curves in the parameter plane that correspond to the vanishing of the saddle value σ of the equilibrium state at the origin. Find where the divergence of the vector field at the saddle-focus vanishes. Plot the curves found in the $(a\,b)$-plane. □

Let us examine next the stability of the non-trivial equilibria $O_{1,2}(\pm 1, 0, \mp 1)$. First, we linearize the system at either O_1 or O_2. The associated Jacobian matrix is given by

$$\begin{bmatrix} -a/3 & a & 0 \\ 1 & -1 & 1 \\ 0 & -b & 0 \end{bmatrix}.$$

The characteristic polynomial is given by

$$\lambda^3 + (1 + a/3)\lambda^2 + (b - 2a/3)\lambda + ab/3 = 0\,. \qquad \text{(C.2.14)}$$

Like O, the equilibria $O_{1,2}$ cannot have a zero characteristic exponent for $ab \neq 0$. The condition $R = 0$ reads here as

$$b = \frac{2}{9}a(3 + a)\,.$$

This bifurcation boundary is plotted in Fig. C.2.1. The corresponding expression for q is $q = 2a^2/9 > 0$. Therefore, at $R = 0$, the equilibria $O_{1,2}$ have a pair of pure imaginary characteristic exponents, namely,

$$\lambda_{1,2} = \pm i\frac{a\sqrt{2}}{3} \quad \text{and} \quad \lambda_3 = -(1 + a/3)\,.$$

This corresponds to the Andronov-Hopf bifurcation. When $R > 0$ the equilibria $O_{1,2}$ are stable foci, and when $R < 0$, they are saddle-foci (1,2). The

stability of $O_{1,2}$ in the critical case depends on whether the corresponding Andronov-Hopf bifurcation is sub- or super-critical (see Secs. 9.3 and 11.5), i.e. whether the point $O_{1,2}$ is a stable or unstable weak focus. To find out what occurs here we will need to determine the sign of the first Lyapunov value L_1. When $L_1 < 0$, $O_{1,2}$ are stable, and they are unstable if $L_1 > 0$. If the Lyapunov value vanishes on the Andronov-Hopf bifurcation curve, the sign of the next Lyapunov value L_2 must be computed, etc.

Consider the Lorenz equation [87]

$$\begin{aligned} \dot{x} &= -\sigma(x-y)\,, \\ \dot{y} &= rx - y - xz\,, \\ \dot{z} &= -bz + xy\,, \end{aligned} \tag{C.2.15}$$

where σ, r and b are positive parameters; we will assume, moreover, that $\sigma > b+1$. Notice that this equation is invariant under the involution $(x,y,z) \leftrightarrow (-x,-y,z)$.

Let us find the equilibrium states of this equation by solving the following system:

$$\begin{aligned} 0 &= -\sigma(x-y)\,, \\ 0 &= rx - y - xz\,, \\ 0 &= -bz + xy\,, \end{aligned}$$

We find that $x = y$, $x(r-1-z) = 0$ and $bz = x^2$. Plugging the last relation into the middle one, we arrive at the equation for the coordinates of equilibria:

$$x(b(r-1) - x^2) = 0\,. \tag{C.2.16}$$

One can see that the Lorenz equation always has one equilibrium state O at the origin. When $r > 1$, along with O there are two more equilibrium states $O_{1,2}(x_{1,2} = y_{1,2} = \pm b^{1/2}(r-1)^{1/2}, z_{1,2} = r-1)$.

The Jacobian matrix at the origin is given by

$$\begin{pmatrix} -\sigma & \sigma & 0 \\ r & -1 & 0 \\ 0 & 0 & -b \end{pmatrix}.$$

The characteristic equation

$$\det \begin{bmatrix} -\sigma-\lambda & \sigma & 0 \\ r & -1-\lambda & 0 \\ 0 & 0 & -b-\lambda \end{bmatrix} = 0$$

has three real roots:

$$\lambda_1 = -b \quad \text{and} \quad \lambda_{2,3} = \frac{-(\sigma+1) \pm \sqrt{(\sigma+1)^2 + 4\sigma(r-1)}}{2}\,.$$

Thus, when $r < 1$, the origin is a stable equilibrium state. When $r = 1$, the equilibrium state has one zero root. When $r > 1$, the origin becomes a saddle with a one-dimensional unstable manifold, and its stability is inherited by the stable equilibria $O_{1,2}$.

The unstable manifold W^u_O is composed of the saddle point itself and two trajectories $\Gamma_{1,2}$ that come from O as $t \to +\infty$. The stable manifold W^s_0 is two-dimensional. The leading stable direction in W^s_0 is given by the eigenvector corresponding to the smallest negative characteristic root. In our case, this is $\lambda_1 = -b$, and the corresponding eigenvector is $(0, 0, 1)$. Note that there is an invariant line $x = y = 0$ in W^s_O.

C.2.#8. Find the equations of $\mathcal{E}^u_O$ and $\mathcal{E}^{ss}_O$ at the origin. □

Let us carry out the stability analysis for $O_{1,2}$. We can choose either one; let it be O_1. The Jacobian matrix at O_1 is given by

$$\begin{bmatrix} -\sigma & \sigma & 0 \\ r - z_1 & -1 & -x_1 \\ x_1 & y_1 & -b \end{bmatrix}.$$

The corresponding characteristic equation is given by

$$\lambda^3 + (\sigma + b + 1)\lambda^2 + b(\sigma + r)\lambda + 2b\sigma(r-1) = 0\,.$$

The stability boundary of the equilibria $O_{1,2}$ is determined by the condition:

$$R \equiv b(\sigma + r)(\sigma + b + 1) - 2b\sigma(r-1) = 0\,. \qquad \text{(C.2.17)}$$

Thus, provided $\sigma > b + 1$, the equilibrium states $O_{1,2}$ are stable when

$$1 < r < \frac{\sigma(\sigma + b + 3)}{\sigma + b - 1}\,.$$

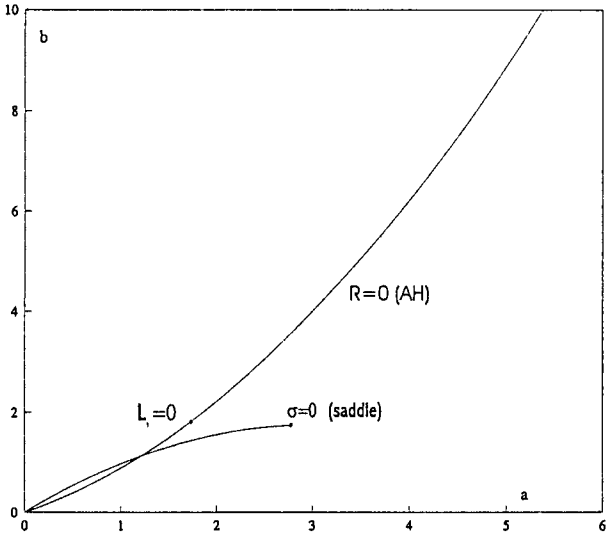

Fig. C.2.1. A part of the (a, b)-bifurcation diagram of the Chua's circuit; AH denotes the Andronov-Hopf bifurcation curve; $\sigma = 0$ corresponds to the vanishing of the saddle value when the origin is a saddle.

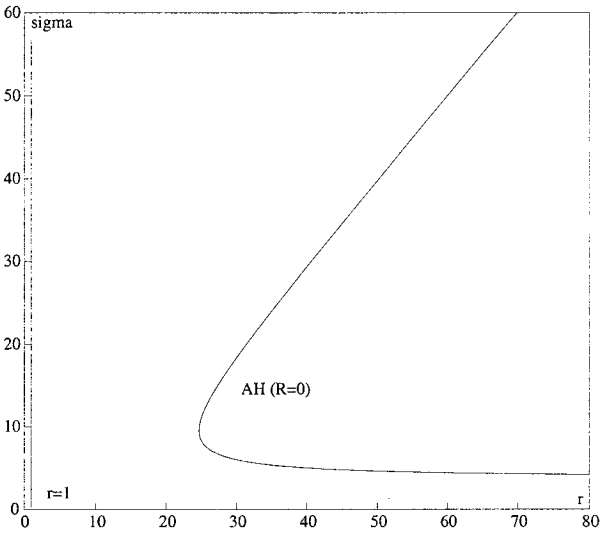

Fig. C.2.2. The Andronov-Hopf bifurcation curve AH and a pitch-fork curve $r = 1$ in the (r, σ)-plane of the Lorenz model at $b = 8/3$.

They become saddle-foci (1,2) when $R \leq 0$. This happens on, and to the right of the Andronov-Hopf bifurcation curve AH in the (r, σ)-parameter plane in Fig. C.2.2.

The stability of the bifurcating equilibria $O_{1,2}$ at the critical moment $R = 0$ is determined by the first Lyapunov value L_1. We will derive its analytical expression in Sec. C.5.

C.2.#9. Find a point in the (r, a)-parameter plane in Fig. C.2.3 where an equilibrium state of the asymmetric Lorenz model [189]

$$\begin{aligned} \dot{x} &= -10(x - y)\,, \\ \dot{y} &= rx - y - xz + a\,, \\ \dot{z} &= -\frac{8}{3}z + xy \end{aligned} \tag{C.2.18}$$

has a pair of zero eigenvalues. □

Consider next the following third-order system from atmospheric physics [128] and [183]

$$\begin{aligned} \dot{x} &= -y^2 - z^2 - ax + aF\,, \\ \dot{y} &= xy - bxz - y + G\,, \\ \dot{z} &= bxy + xz - z\,, \end{aligned} \tag{C.2.19}$$

where (a, b, F, G) are positive parameters. To find its equilibrium states (x_0, y_0, z_0), we equate the right-hand side of (C.2.19) to zero:

$$\begin{aligned} 0 &= -y_0^2 - z_0^2 - ax_0 + aF\,, \\ 0 &= x_0 y_0 - bx_0 z_0 - y_0 + G\,, \\ 0 &= bx_0 y_0 + x_0 z_0 - z_0\,. \end{aligned} \tag{C.2.20}$$

From the second and the third equations, we obtain

$$\begin{aligned} y_0 &= \frac{G(1 - x_0)}{1 - 2x_0 + (1 + b^2)x_0^2}\,, \\ z_0 &= \frac{bGx_0}{1 - 2x_0 + (1 + b^2)x_0^2}\,. \end{aligned} \tag{C.2.21}$$

Substituting (C.2.21) into the first equation in (C.2.20), we obtain

$$(1 + b^2)x_0^3 - [2 + (1 + b^2)F]x_0^2 + (1 + 2F)x_0 + \left(\frac{G^2}{a} - F\right) = 0\,. \tag{C.2.22}$$

Next, we introduce the new parameters

$$B = \frac{1}{1+b^2}, \quad G' = \frac{G^2}{a} - \frac{F}{1+b^2}\,,$$

and make a translation

$$x_0 = \bar{x} + \frac{2B+F}{3}\,.$$

Then (C.2.22) transforms into the cubic canonical equation

$$\bar{x}^3 + s\bar{x} + t = 0\,, \tag{C.2.23}$$

where

$$t = B(1+2F) - \frac{(2B+F)^2}{3}\,,$$
$$s = \frac{B(1+2F)(2B+F)}{3} + G' - \frac{2(2B+F)^3}{27}\,.$$

The discriminant of Eq. (C.2.23) is given by

$$\Delta = \frac{t^2}{4} + \frac{s^3}{27}\,.$$

The corresponding bifurcation curve determined by the condition $\Delta = 0$ is plotted in Fig. C.2.4. It breaks the parameter plane (F, G) into regions where system (C.2.19) possesses either one or three equilibrium states (inside the wedge in Fig. C.2.4). The precise location of the cusp, where all three equilibrium states coalesce, is determined by the simultaneous vanishing of s and t (the point labeled CP). This occurs when

$$G = \frac{2\sqrt{12}b\sqrt{ab}}{3(1+b^2)}, \quad F = \frac{1+\sqrt{3}b}{1+b^2}\,.$$

C.2.#10. Show that the system possesses an equilibrium state with characteristic exponents $(0, \pm i\omega)$ (Gavrilov-Guckenheimer bifurcation) at

$$F^* = \frac{3a^2 + 3a^2b^2 + 12ab^2 + 12b^2 + 4a}{4(a + ab^2 + 2b^2)}$$
$$G^* = \frac{\sqrt{a}(a^2 + a^2b^2 + 4ab^2 + 4b^2)}{4\sqrt{a + ab^2 + 2b^2}}\,.$$

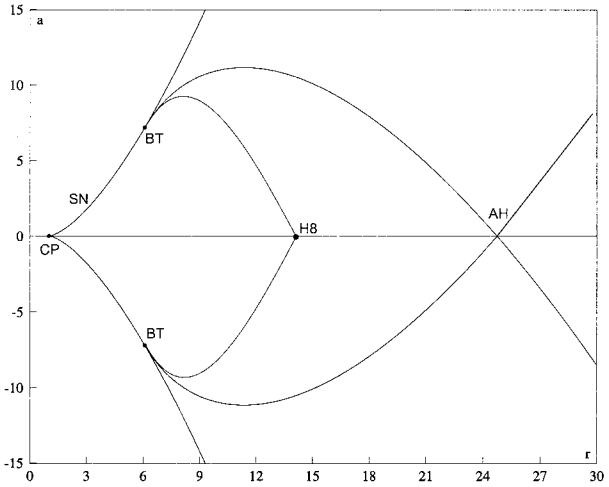

Fig. C.2.3. A partial bifurcation diagram for the asymmetric Lorenz model. The point CP is a cusp, at BT the system has a double-degenerate equilibrium state with two zero characteristic exponents (see Sec. 13.2).

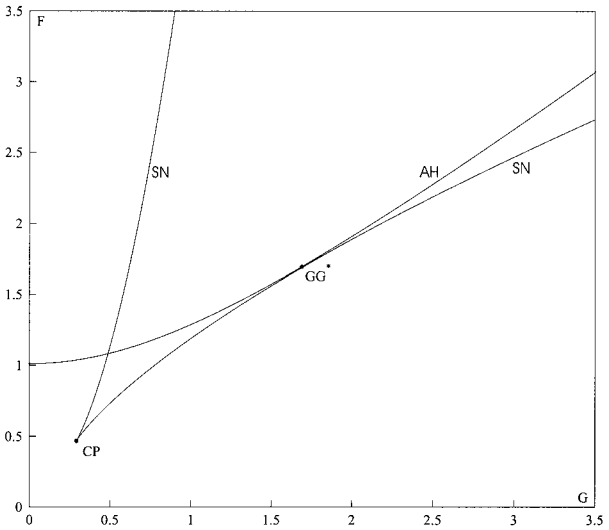

Fig. C.2.4. A fragment of the (F, G)-bifurcation portrait derived from a linear stability analysis for $a = 1/4$ and $b = 4$.

Hint: use the fact that at this bifurcation point the trace and the determinant of the Jacobian matrix must vanish simultaneously. □

C.2.#11. Carry out a linear stability analysis of the following system

$$\begin{aligned}\dot{r} &= r(\mu_1 + az + z^2)\,,\\ \dot{z} &= \mu_2 + z^2 + br^2\,,\\ \dot{\varphi} &= \omega + cz\,,\end{aligned}$$

where r, φ and z are cylindrical coordinates, $\mu_{1,2}$ are control parameters, and a, b, c assume the values ± 1. This is a truncated normal form for the Gavrilov-Guckenheimer bifurcation. □

C.2.#12. Find the transformation of coordinates and time which brings the Lorenz system (C.2.15) to the following form

$$\begin{aligned}\dot{x} &= y\,,\\ \dot{y} &= x - xz - ay + Bx^3\,,\\ \dot{z} &= -b'(z - x^2)\,.\end{aligned} \tag{C.2.24}$$

Hint: the corresponding relation between the parameters of both systems is

$$b' = \frac{b}{\sqrt{\sigma(r-1)}}, \quad a = \frac{1+\sigma}{\sqrt{\sigma(r-1)}}, \quad B = \frac{b}{2b-\sigma}\,. \qquad \square$$

The system (C.2.24) is the asymptotic normal form appearing in the study [129] of local codimension-three bifurcations of equilibria and periodic orbits of systems with a symmetry (see Sec. C.4). When $B = 0$, system (C.2.24) is the Shimizu-Morioka model [127], [191]

$$\begin{aligned}\dot{x} &= y\,,\\ \dot{y} &= x - xz - ay\,,\\ \dot{z} &= -bz + x^2\,,\end{aligned} \tag{C.2.25}$$

which can be viewed as the approximation of the Lorenz equation for large Raleigh numbers r. In a slightly different form, it can also be derived from PDEs describing a weekly nonlinear magneto-convection in the limit of tall, thin rolls [187].

The Shimizu-Morioka model has three equilibria when $b > 0$. The origin $O(0,0,0)$ is a saddle of type (2,1) with the characteristic exponents

$$\lambda_{1,2} = -a/2 \pm (a^2/4 + 1)^{1/2}, \quad \lambda_3 = -b\,.$$

The change of the leading direction in $\mathcal{E}^s$ occurs on the curve $a = (b^2 - 1)/b$ when $\lambda_2 = \lambda_3$. The saddle value $\sigma = \lambda_1 + \lambda_3$ vanishes on the curve $a = (1 - b^2)/b$.

C.2.#13. Write down the equations of the eigenspaces $\mathcal{E}^s$, $\mathcal{E}^u$, $\mathcal{E}^{sL}$ for the saddle at the origin. □

The characteristic equation at the non-trivial equilibria $O_{1,2}(\pm\sqrt{b},\, 0,\, 1)$ of the Shimizu-Morioka model is given by

$$\lambda^3 + (a+b)\lambda^2 + ab\lambda + 2b = 0\,.$$

The Andronov-Hopf bifurcation curve AH in Fig. C.2.5 is given by $(a + b)a - 2 = 0$. The characteristic exponents at $O_{1,2}$ on it are

$$\lambda_3 = -2/a, \qquad \lambda_{1,2} = \pm i\sqrt{2 - a^2}\,.$$

Above the curve AH the equilibria $O_{1,2}$ are stable foci; they are saddle-foci of type $(1, 2)$ below the curve.

The equilibrium states in the Rössler system [172, 188]

$$\begin{aligned} \dot{x} &= -y - z\,, \\ \dot{y} &= x + ay\,, \\ \dot{z} &= bx - cz + xz\,, \end{aligned}$$

are $O(0,0,0)$ and $O_1(c - ab,\, b - c/a,\, c/a - b)$. The characteristic equation at O is given by

$$\lambda^3 + (c-a)\lambda^2 + (1 + b - ac)\lambda + (c - ab) = 0\,.$$

It has the roots $(i\omega, -i\omega, \lambda)$ when

$$a = \frac{(1+c^2) + \sqrt{(1+c^2)^2 - 4bc^2}}{2c}, \quad \sqrt{c^2 + \frac{1}{4}} - \frac{1}{2} < b < \frac{(1+c^2)^2}{4c^2}$$

or

$$a = \frac{(1+c^2) - \sqrt{(1+c^2)^2 - 4bc^2}}{2c}, \quad b < \begin{cases} \sqrt{c^2 + \dfrac{1}{4}} - \dfrac{1}{2} & \text{for } c \geq \sqrt{2+\sqrt{5}}\,, \\ \dfrac{(1+c^2)^2}{4c^2} & \text{for } c \leq \sqrt{2+\sqrt{5}}\,. \end{cases}$$

This equilibrium state has one zero root when $a = c/b$.

The characteristic equation at O_1 assumes the form

$$\lambda^3 + a(b-1)\lambda^2 + \left(1 + \frac{c}{a} - a^2 b\right)\lambda + (ab - c) = 0\,.$$

It has a pair of purely imaginary roots on the curve

$$c = \frac{a}{b} + (b-1)a^3, \quad a^2 < 1 + \frac{1}{b}\,.$$

In addition, this equilibrium state may have a single zero root when $a = c/b$. Thus, the equilibrium states O_1 and O_2 coalesce when $ab = c$. The two other characteristic exponents of this degenerate point are given by

$$\lambda_{1,2} = \frac{a(1-b) \pm \sqrt{a^2(b+1)^2 - 4(b+1)}}{2}\,.$$

Hence, the exponents $\lambda_{1,2}$ become pure imaginary when

$$b = 1, \qquad 0 < a < \sqrt{2}\,.$$

The Rössler system and the new Lorenz system (C.2.19) are remarkable in that both have a doubly degenerate equilibrium state with characteristic exponents equal to $(0, \pm i\omega)$. The feature of this bifurcation is that the unfolding may contain a torus bifurcation curve along with curves corresponding to homoclinic loops to saddle-foci, and therefore non-trivial dynamics may emerge instantly in a neighborhood of the bifurcating equilibria. □

C.2.#14. Study the equilibria of the Hindmarsh-Rose model of neuronal activity [177]

$$\begin{aligned} \dot{x} &= y - z - x^3 + 3x^2 + I\,, \\ \dot{y} &= -y - 2 - 5x^2\,, \\ \dot{z} &= \varepsilon(2(x + 1.6) - z)\,, \end{aligned} \tag{C.2.26}$$

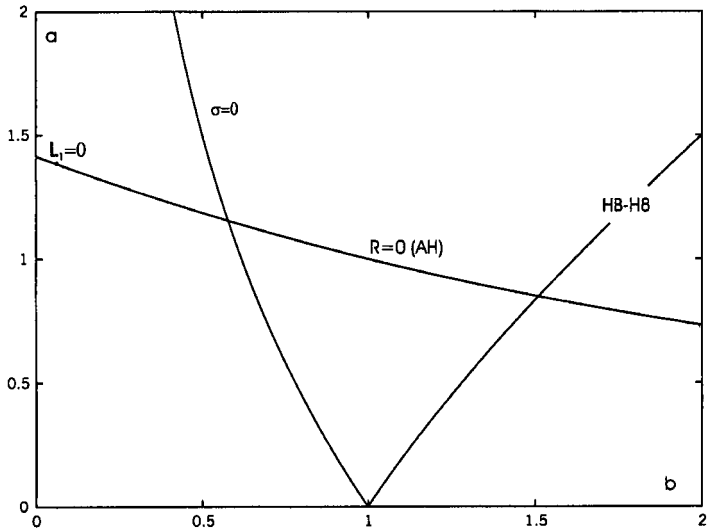

Fig. C.2.5. The (a, b)-bifurcation diagram in the Shimizu-Morioka system derived from a linear stability analysis. AH labels the Andronov-Hopf bifurcation curve; $\sigma = 0$ corresponds to zero saddle-value; $HB - H8$ corresponds to the change of the leading direction at the origin.

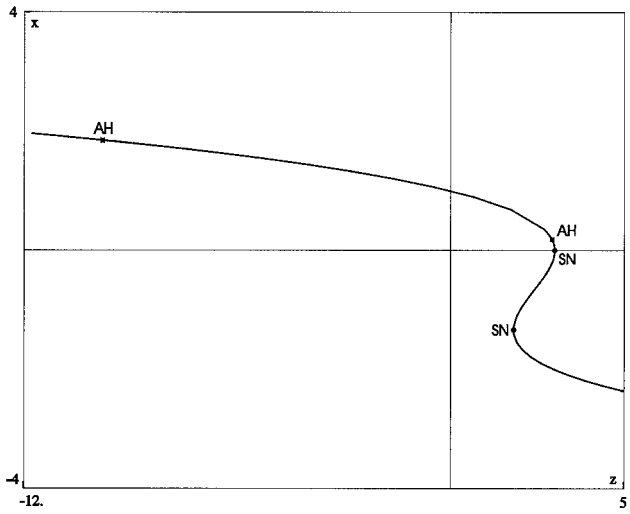

Fig. C.2.6. The x-coordinate of the equilibrium state versus z in the fast planar system at $I = 5$ and $\varepsilon = 0$. AH and SN denote, respectively, the Andronov-Hopf and the saddle-node bifurcations of the equilibria.

where I and ε are two control parameters. Start with the case $\varepsilon = 0$ (see Fig. C.2.6).

C.2.#15. Perform the linear stability analysis of the following systems describing bifurcations of an equilibrium state with three zero characteristic exponents in the case where the Jacobian matrix has a complete Jordan block [162, 163]:

$$\begin{aligned} &\dot{x} = y\,, && \dot{x} = y\,, \\ &\dot{y} = z\,, && \dot{y} = z\,, \\ &\dot{z} = ax - x^2 - by - z; && \dot{z} = ax - x^3 - by - z\,. \end{aligned} \tag{C.2.27}$$

How does the cubic term change the symmetry properties of the system? □

C.2.#16. The following "dimensional" perturbations of the Lorenz equation and the Shimizu-Morioka model are given by the following augmented systems

$$\begin{aligned} &\dot{x} = -\sigma(x - y)\,, && \dot{x} = y\,, && \dot{x} = y\,, \\ &\dot{y} = rx - y - xz\,, && \dot{y} = -ay + x - xz\,, && \dot{y} = -ay + x - xz\,, \\ &\dot{w} = z\,, && \dot{z} = -bz + \mu w + x^2\,, && \dot{z} = w\,, \\ &\dot{z} = -bw - az + xy\,, && \dot{w} = -bw - \mu z\,, && \dot{w} = -bw - \mu z + x^2 + cz^2\,. \end{aligned}$$

Find equilibrium states of these system and determine their types. □

C.2.#17. What are the minimum dimensions of W^s and W^u of the equilibrium state shown in Fig. C.2.7? □

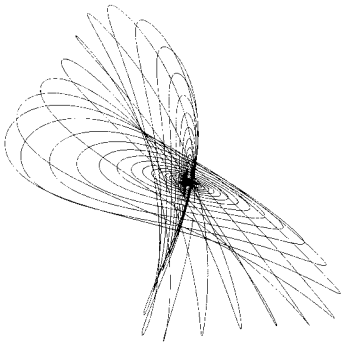

Fig. C.2.7. Trajectory homoclinic to a saddle-focus (2,2).

C.3 Periodically forced systems

Consider an n-dimensional system

$$\dot{x} = Ax + f(t)\,, \tag{C.3.1}$$

where $f(t)$ is a continuous periodic function of period 2π.

C.3.#18. Construct a Poincaré map of the plane $(x, y, t = 0)$ onto the plane $(x, y, t = \tau = 2\pi)$.

Solution. According to the Lagrange method of variations of parameters, the solution of (C.3.1) is given by

$$x(t) = e^{At}x_0 + \int_0^t e^{A(t-\tau)}f(\tau)d\tau\,.$$

Assuming $t = 2\pi$, we obtain the mapping

$$x_1 = e^{2\pi A}x_0 + \int_0^{2\pi} e^{A(2\pi-\tau)}f(\tau)d\tau\,. \tag{C.3.2}$$

□

C.3.#19. Determine the condition under which the above map has: (1) a unique fixed point and, (2) no fixed points.

Solution. The equation for the fixed points is given by

$$[I - e^{2\pi A}]x = C\,,$$

where C denotes the integral in (C.3.2). The two cases possible here are:

(1) $\det(I - e^{2\pi A}) \neq 0$. In this case there exists only one fixed point.
(2) $\det(I - e^{2\pi A}) = 0$. Then, it follows from the Kroneker-Capelli (consistency) theorem that if the rank of $(I - e^{2\pi A})$ is equal to that of the augmented matrix $(I - e^{2\pi A}|C)$, then there are infinitely many fixed points. Otherwise, there are no fixed points. □

C.3.#20. Show that the roots $z_1, \ldots, z_n$ of the characteristic equation $\det(zI - e^{2\pi A}) = 0$ are given by $e^{2\pi\lambda_1}, \ldots, e^{2\pi\lambda_n}$, where $\lambda_1, \ldots, \lambda_n$ are the eigenvalues of the linear system

$$\dot{x} = Ax\,. \tag{C.3.3}$$

□

C.3.#21. Prove that if the origin is a structurally stable equilibrium state of the system (C.3.3), then the corresponding fixed point of the map (C.3.2) is structurally stable as well. Furthermore, show that the topological types of the equilibrium state of (C.3.3) and the fixed point of (C.3.2) are the same. □

C.3.#22. Show that $\det(I - e^{2\pi A}) = 0$ if only one of the eigenvalues $\lambda_1, \ldots, \lambda_n$ is zero or is equal to $i\omega$ with integer ω. □

C.3.#23. Determine the condition under which the two-dimensional system

$$\begin{aligned} \dot{x} &= -\omega y + f(t)\,, \\ \dot{y} &= \omega x + g(t)\,, \end{aligned} \tag{C.3.4}$$

where f and g are continuous functions of period 2π, has an infinite number of periodic orbits of period $2\pi q$, where $q \geq 1$ is some integer.

Solution. The mapping T: $t = 0 \to t = 2\pi$ can be written in the form

$$\begin{aligned} x_1 &= x_0 \cos 2\pi\omega - y_0 \sin 2\pi\omega + C_1\,, \\ y_1 &= x_0 \sin 2\pi\omega + y_0 \cos 2\pi\omega + C_2\,, \end{aligned}$$

where

$$\begin{aligned} C_1 &= \int_0^{2\pi} (f(\tau)\cos\omega(2\pi - \tau) - g(\tau)\sin\omega(2\pi - \tau))d\tau\,, \\ C_2 &= \int_0^{2\pi} (f(\tau)\sin\omega(2\pi - \tau) + g(\tau)\cos\omega(2\pi - \tau))d\tau\,. \end{aligned}$$

When

$$\det \begin{pmatrix} \cos 2\pi\omega - 1 & -\sin(2\pi\omega) \\ \sin(2\pi\omega) & \cos(2\pi\omega) - 1 \end{pmatrix} = (\cos 2\pi\omega - 1)^2 + \sin^2 2\pi\omega \neq 0$$

this map has a unique fixed point. This condition is violated when ω is an integer. In the latter case, the map is recast as

$$x_1 = x_0 + C_1, \qquad y_1 = y_0 + C_2\,.$$

Therefore, if $C_1^2 + C_2^2 \neq 0$, it is clear that the map can have neither fixed nor periodic points; and if $C_1 = C_2 = 0$, all points are fixed ones.

Consider now the case where ω is not an integer. Let (x^*, y^*) be the coordinates of the fixed point. Applying the transformation $x = x^* + \xi$ and $y = y^* + \nu$ we translate the fixed point to the origin. Introducing polar coordinates, the map T assumes the form

$$\rho_1 = \rho_0\,,$$
$$\theta_1 = \theta_0 + 2\pi\omega \qquad \mod 2\pi\,.$$

One can see that every circle $r =$ constant is invariant here and that the map on every circle is the same:

$$\theta_1 = \theta_0 + 2\pi\omega \qquad \mod 2\pi\,.$$

The last one has no periodic points when ω is irrational. When $\omega = p/q$ with integer p and q, all the points are periodic with period q. □

Let us consider next a quasi-linear system

$$\begin{aligned} \dot{x} &= Ax + \mu f(x, y)\,, \\ \dot{y} &= By + \mu g(x, y)\,, \end{aligned} \tag{C.3.5}$$

where $x \in \mathbb{R}^n$ and $y \in \mathbb{R}^m$. The spectrum of A is supposed to lie on the imaginary axis, that of B lies in the left half-plane, and $f, g \in \mathbb{C}^k$.

C.3.#24. Prove the following theorem, which is analogous to the center manifold theorem:

Theorem C.1. *For any $R > 0$ there is a μ_0, such that for $|\mu| < \mu_0$ the sphere $\|(x, y)\| \le R$ contains an attracting invariant $\mathbb{C}^k$-smooth manifold $y = \mu\varphi(x, \mu)$.* □

It follows from the above theorem that the study of (C.3.5) is reduced to the study of the n-dimensional system

$$\dot{x} = Ax + \mu f(x, \mu\varphi(x, \mu)) = Ax + \mu\tilde{f}(x) + o(\mu)$$

where $\tilde{f}(x) = f(x, 0)$.

C.3.#25. Consider the analogous case of quasi-linear maps. □

C.3.#26. Prove the analog of Theorem C.1 for the following $(n + m)$-dimensional system

$$\begin{aligned} \dot{x} &= Ax + h_1(t) + \mu f(x, y, t)\,, \\ \dot{y} &= By + h_2(t) + \mu g(x, y, t)\,, \end{aligned} \tag{C.3.6}$$

where all functions are smooth and 2π-periodic. The spectra of A and B are supposed to lie on the imaginary axes and to the left of it, respectively.

Note that the truncated equation

$$\dot{y} = By + h_2(t)$$

has a unique 2π-periodic solution $y = \alpha(t)$. Thus, we can always make $h_2(t) \equiv 0$ (using the change $\tilde{y} \to y + \alpha(t)$). □

Let us consider the system

$$\dot{x} = \mu f(x,t)\,, \tag{C.3.7}$$

where $f(x,t) = f(x,t+2\pi)$ is a continuous function with respect to t and smooth with respect to x, $x \in \mathbb{R}^n$.

C.3.#27. Find the Poincaré map up to the terms of order μ^2.

Hint: the solution is found from the integral equation

$$x(t) = x_0 + \mu \int_0^t f(x(\tau),\tau)d\tau$$

using the method of successive approximations:

1st approximation is given by $\quad x(t) = x_0\,,$

2nd approximation is given by $\quad x(t) = x_0 + \mu \int_0^t f(x_0,\tau)d\tau\,,$

n-th approximation has the form $\quad x_{n+1}(t) = x_0 + \mu \int_0^t f(x_0,\tau)d\tau + O(\mu^2)\,.$

Solution:

$$x_1 = x_0 + \mu \int_0^{2\pi} f(x_0,\tau)d\tau + O(\mu^2)\,. \tag{C.3.8}$$

□

Denote $f_0(x) = \int_0^{2\pi} f(x_0,\tau)d\tau$.

C.3.#28. Show that the time 2π shift along the trajectories of the system

$$\dot{x} = \frac{\mu}{2\pi} f_0(x) \tag{C.3.9}$$

coincides with (C.3.8) up to the terms of order μ^2. The system (C.3.9) is called *an averaged system.* □

C.3.#29. Prove the following theorem

Theorem C.2. *Structurally stable equilibrium states of the averaged system correspond to structurally stable periodic orbits of the original system: if x^* is a structurally stable equilibrium state in* (C.3.9)*, then the Poincaré map* (C.3.8) *for the system* (C.3.7) *has a structurally stable fixed point close to x^* for all sufficiently small μ.* □

Proof. Let x^* be a structurally stable equilibrium state of the system (C.3.9); i.e.

$$f_0(x^*) = 0$$

and the roots $\lambda_1, \ldots, \lambda_n$ of the characteristic equation do not lie on the imaginary axis. Hence, we can seek them as $\lambda = \frac{\mu}{2\pi}\sigma$:

$$\det\left(\frac{\partial f_0}{\partial x}(x^*) - \sigma I\right) = 0\,. \tag{C.3.10}$$

The fixed points of (C.3.8) can be found from the equation

$$f_0(x) + O(\mu) = 0\,.$$

Since $f_0(x^*) = 0$ and $|\frac{\partial f_0}{\partial x}(x^*)| \neq 0$ because (C.3.10) has no zero roots, it follows that there exists a fixed point $x = x^* + O(\mu)$. The corresponding characteristic equation at this point is written in the form:

$$\det\left(I + \mu\frac{\partial f_0}{\partial x}(x^*) + O(\mu^2) - zI\right) = 0\,.$$

We seek the roots of this equation in the form $z = 1 + \mu\sigma$. Then we find that it recasts as

$$\det\left(\frac{\partial f_0}{\partial x}(x^*) + O(\mu) - \sigma I\right) = 0\,.$$

Therefore, for all small μ the roots σ will be close to those of (C.3.10). Thus, the fixed point will be structurally stable. Moreover, it has the same topological type as the equilibrium state of the averaged system. □

C.3.#30. Prove that in the general case

$$\dot{x} = Ax + \mu f(x,t)\,,$$

where $f(x,t)$ is a continuous function of time, smooth with respect to x, the associated Poincaré map is given by

$$x_1 = e^{2\pi A}x_0 + \mu\int_0^{2\pi} e^{A(2\pi-\tau)}f(e^{A\tau}x_0,\tau)d\tau + O(\mu^2)\,. \qquad \square$$

C.3.#31. Verify that if $\det(e^{2\pi A} - I) \neq 0$, it follows that for any given R, if μ is small enough, in the sphere of radius R there is a single fixed point $x^*(\mu)$ such that $x^*(\mu) \to 0$ as $\mu \to 0$. $\square$

Let us examine the system of two equations

$$\begin{aligned} \dot{x} &= -\omega y + \mu f(x,y,t), \\ \dot{y} &= \omega x + \mu g(x,y,t)\,. \end{aligned} \tag{C.3.11}$$

C.3.#32. Compute the map up to the terms of order μ^2.
Solution:

$$\begin{aligned} x_1 &= x_0\cos 2\pi\omega - y_0\sin 2\pi\omega + \mu\Phi_1(x_0,y_0) + \mu^2(\cdots)\,, \\ y_1 &= x_0\sin 2\pi\omega + y_0\cos 2\pi\omega + \mu\Phi_2(x_0,y_0) + \mu^2(\cdots)\,, \end{aligned} \tag{C.3.12}$$

where

$$\begin{aligned} \Phi_1 = \int_0^{2\pi} &[f(x_0\cos\omega\tau - y_0\sin\omega\tau, x_0\sin\omega\tau + y_0\cos\omega\tau,\tau)\cos\omega\tau \\ &+ g(x_0\cos\omega\tau - y_0\sin\omega\tau, x_0\sin\omega\tau + y_0\cos\omega\tau,\tau)\sin\omega\tau]d\tau \\ \Phi_2 = \int_0^{2\pi} &[-f(x_0\cos\omega\tau - y_0\sin\omega\tau, x_0\sin\omega\tau + y_0\cos\omega\tau,\tau)\sin\omega\tau \\ &+ g(x_0\cos\omega\tau - y_0\sin\omega\tau, x_0\sin\omega\tau + y_0\cos\omega\tau,\tau)\cos\omega\tau]d\tau\,. \end{aligned} \qquad \square$$

C.3.#33. Write the system (C.3.11) in polar coordinates $x = r\cos\theta$, $y = r\sin\theta$.
Solution:

$$\begin{aligned} \dot{r} &= \mu R(r,\theta,t), \\ \dot{\theta} &= \omega + \mu\Psi(r,\theta,t)\,, \end{aligned}$$

where

$$R = f(r\cos\theta, r\sin\theta, t)\cos\theta + g(r\cos\theta, r\sin\theta, t)\sin\theta$$

$$\Psi = \frac{1}{r}[-f(r\cos\theta, r\sin\theta, t)\sin\theta + g(r\cos\theta, r\sin\theta, t)\cos\theta]\,. \qquad \square$$

C.3.#34. Let

$$R(r,\theta,t) = \sum_{n=0}^{\infty}\sum_{m=0}^{\infty} a_{nm}(r)e^{i(m\theta+nt)}$$

$$\Psi(r,\theta,t) = \sum_{n=0}^{\infty}\sum_{m=0}^{\infty} b_{nm}(r)e^{i(m\theta+nt)}\,.$$

Construct the Poincaré map up to $O(\mu^2)$ for the case where ω is an integer.

Solution:

$$r_1 = r_0 + 2\pi\mu \sum_{m\omega+n=0} a_{nm}(r_0)e^{im\theta_0} + \mu^2(\cdots)$$

$$\theta_1 = \theta_0 + 2\pi\mu \sum_{m\omega+n=0} b_{nm}(r_0)e^{im\theta_0} + \mu^2(\cdots)\,. \qquad \square$$

If ω is an integer, the map (C.3.12) can be represented as follows

$$x_1 = x_0 + \mu\Phi_1(x_0, y_0) + \mu^2(\cdots)\,,$$

$$y_1 = y_0 + \mu\Phi_2(x_0, y_0) + \mu^2(\cdots)\,,$$

C.3.#35. Prove the following theorem:

Theorem C.3. (Averaging Theorem) *If ω is an integer, then for sufficiently small $\mu > 0$ structurally stable equilibrium states of the system*

$$\dot{x} = \frac{\mu}{2\pi}\Phi_1(x,y)\,,$$

$$\dot{y} = \frac{\mu}{2\pi}\Phi_2(x,y)$$

will correspond to structurally stable fixed points of the Poincaré map. Moreover, stable equilibria correspond to stable fixed points. $\square$

In polar coordinates the averaged system is given by

$$\dot{r} = \mu \sum_{mw+n=0} a_{nm}(r)e^{im\theta} = \mu R_0(r,\theta),$$

$$\dot{\theta} = \mu \sum_{mw+n=0} b_{nm}(r)e^{im\theta} = \mu \Psi_0(r,\theta)\,.$$

One should take into account that $r = 0$ is a singularity here.

C.3.#36. Find the associated averaged system for the van der Pol equation

$$\ddot{x} + \mu(1-x^2)\dot{x} + \omega^2 x = \mu A \sin t$$

provided that $\omega^2 = 1 + \mu\Delta$ (where Δ is called a detuning). Examine the types of equilibrium states as A and Δ vary. □

Consider now the case where ω is not an integer. According to C.3.#31, the map (C.3.12) has a unique fixed point close to zero in this case.

C.3.#37. Find the periodic motion $(x^*(t), y^*(t))$ corresponding to this fixed point and find the equations of the system after straightening this periodic solution (translate the origin into $(x^*(t), y^*(t))$).

Solution:

$$\dot{x} = -\omega y + \mu F(x,y,t) + \mu^2(\cdots)\,,$$

$$\dot{y} = \omega x + \mu G(x,y,t) + \mu^2(\cdots)\,,$$

where

$$F(x,y,t) = f(x,y,t) - f(0,0,t)\,,$$

$$G(x,y,t) = g(x,y,t) - g(0,0,t)\,.$$ □

Assume now $\omega = p/q$ where p and q are integers, $q > 1$. In this case, one is to find periodic motions of period $2\pi q$ that correspond to the fixed points of the map T^q. This map is written in the form

$$x_q = x_0 + \mu\Phi_1(x_0,y_0) + \mu^2(\cdots)\,,$$

$$y_q = y_0 + \mu\Phi_2(x_0,y_0) + \mu^2(\cdots)\,,$$

where

$$\Phi_1 = \int_0^{2\pi q} [f(\cdot)\cos\omega\tau + g(\cdot)\sin\omega\tau]d\tau\,,$$

$$\Phi_2 = \int_0^{2\pi q} [-f(\cdot)\sin\omega\tau + g(\cdot)\cos\omega\tau]d\tau\,,$$

where $(\cdot)$ stands for $(x_0\cos\omega\tau - y_0\sin\omega\tau, x_0\sin\omega\tau + y_0\cos\omega\tau)$ as above in (C.3.12), and $\omega = \frac{p}{q}$.

In the same manner as in the previous case, we can treat the averaged system

$$\dot{x} = \frac{\mu}{2\pi q}\Phi_1(x,y)\,,$$

$$\dot{y} = \frac{\mu}{2\pi q}\Phi_2(x,y)\,.$$

In polar coordinates, the map T^q can be recast as

$$r_q = r_0 + 2\pi q\mu \sum_{mp+nq=0} a_{nm}(r_0)e^{im\theta_0} + \mu^2(\cdots)\,,$$

$$\theta_q = \theta_0 + 2\pi q\mu \sum_{mp+nq=0} b_{nm}(r_0)e^{im\theta_0} + \mu^2(\cdots)\,.$$

Here, the averaged system is given by

$$\dot{r} = \mu R_0(r,\theta)\,,$$

$$\dot{\theta} = \mu\Psi_0(r,\theta)\,,$$

where $R_0 = \sum_{mp+nq=0} a_{nm}(r)e^{im\theta}$ and $\Psi_0 = \sum_{mp+nq=0} b_{nm}(r)e^{im\theta}$. It should be noted that $f(0,0,t) \equiv 0$ and $g(0,0,t) \equiv 0$ in this case, i.e. the averaged system in polar coordinates no longer has a singularity at $r = 0$. □

C.3.#38. Consider the case of irrational ω. As above, one may assume $f(0,0,t) \equiv 0$, $g(0,0,t) \equiv 0$ in (C.3.11). The system in polar coordinates takes the form

$$\dot{r} = \mu \sum_{n=0}^{\infty}\sum_{m=0}^{\infty} a_{nm}(r)e^{i(m\theta+nt)}, \qquad \dot{\theta} = \omega + \mu \sum_{n=0}^{\infty}\sum_{m=0}^{\infty} b_{nm}(r)e^{i(m\theta+nt)}$$

with non-singular (smooth) coefficients a_{nm}, b_{nm}. Prove that for any given N, M there exists a smooth coordinate transformation which brings the system to the form

$$\dot{r} = \mu a_{00}(r) + O(\mu^2) + \mu \sum_{n=N}^{\infty} \sum_{m=M}^{\infty} a_{nm}(r) e^{i(m\theta+nt)},$$

$$\dot{\theta} = \omega + \mu b_{00}(r) + O(\mu^2) + \mu \sum_{n=N}^{\infty} \sum_{m=M}^{\infty} b_{nm}(r) e^{i(m\theta+nt)}\,.$$

Note that since the series here tend to zero as $N, M \to +\infty$, it follows that for an arbitrarily small δ the map T in appropriate coordinates can be written as follows

$$r_1 = r_0 + 2\pi\mu a_{00}(r_0) + \delta O(\mu)\,,$$

$$\theta_1 = \theta_0 + 2\pi\omega + 2\pi\mu b_{00}(r_0) + \delta O(\mu)\,. \qquad \square$$

C.3.#39. Examine the shortened map

$$r_1 = r_0 + 2\pi\mu a_{00}(r_0)\,,$$

$$\theta_1 = \theta_0 + 2\pi\omega + 2\pi\mu b_{00}(r_0)\,.$$

Show that in addition to the trivial fixed point $(0, 0)$, the above map may have invariant closed curves determined by the zeros of the equation

$$a_{00}(r_0) = 0\,. \qquad \square$$

C.3.#40. Prove that for small $\mu > 0$, each root r^* of the equation

$$a_{00}(r_0) = 0\,,$$

for which

$$a'_{00}(r^*) < 0$$

corresponds to the stable invariant closed curve $r = r^*(\mu) = r^* + O(\mu)$.

Direction: take δ sufficiently small and apply the annulus principle. $\square$

In the case of irrational ω, the averaged system is given by

$$\dot{r} = \mu a_{00}(r)\,,$$

$$\dot{\theta} = \omega + \mu b_{00}(r)\,.$$

Here $r = 0$ is an equilibrium state, while the non-zero roots of $a_{00}(r) = 0$ correspond to the limit cycles.

C.3.#41. The next problem is almost equivalent to the previous one: show that for small $\mu > 0$ stable (unstable) limit cycles of the averaged system correspond to stable (unstable) invariant tori of the original system. □

Let us return to the resonant case ($\omega = p/q, q \geq 1$). The corresponding averaged system can then be recast as

$$\dot{r} = \mu R_0(r, \theta)\,,$$
$$\dot{\theta} = \mu \Psi_0(r, \theta)\,.$$

Assume that the system

$$\begin{aligned} \dot{r} &= R_0(r, \theta)\,, \\ \dot{\theta} &= \Psi_0(r, \theta) \end{aligned} \tag{C.3.13}$$

has a structurally stable periodic orbit $L : \{r = \alpha(t),\, \theta = \beta(t)\}$ of period τ, and let

$$\lambda = \int_0^\tau \left[\frac{\partial R_0}{\partial \tau}(\alpha(t), \beta(t)) + \frac{\partial \Psi_0}{\partial \tau}(\alpha(t), \beta(t)) \right] d\tau < 0.$$

This implies that the averaged system has a periodic solution $\{r = \alpha(\mu t),\, \theta = \beta(\mu t)\}$ of period τ/μ.

C.3.#42. Prove that the original system has a stable invariant torus for small $\mu > 0$.

Hint: modify (C.3.13) first. Introduce the normal coordinates (u, φ) near L (see Sec. 3.10). Then the system is written in the form

$$\dot{u} = A(\varphi)u + O(u^2)\,,$$
$$\dot{\varphi} = 1 + O(u)\,,$$

where the right-hand side is a periodic function of period τ_0. Note that

$$\lambda = \int_0^\tau A(\varphi) d\varphi\,,$$

and therefore

$$A(\varphi) = \lambda + A_0(\varphi)\,,$$

where $\int_0^\tau A_0(\varphi)d\varphi = 0$. Having introduced $v = ue^{-\int A_0(\varphi)d\varphi}$, the system assumes the form

$$\dot{v} = \lambda v + O(v^2)\,,$$
$$\dot{\varphi} = 1 + O(v)\,.$$

It follows from here that the averaged system in the new coordinates (v, φ) can be recast as

$$\dot{v} = \mu[\lambda v + O(v^2)]\,,$$
$$\dot{\varphi} = \mu[1 + O(v)]\,.$$

The corresponding *shift map* over $2\pi q$ is given by

$$v_1 = v_0 + \mu[2\pi q\lambda v_0 + O(v_0^2)] + O(\mu^2)\,,$$
$$\varphi_1 = \varphi_0 + 2\pi q\mu + O(\mu v_0) + O(\mu^2)\,.$$

The same form has the $2\pi q$-shift map of the original system (C.3.11). Introduce $v = \mu w$, after which the Poincaré map becomes

$$w_1 = w_0 + 2\pi q\mu\lambda w_0 + O(\mu^2)\,,$$
$$\varphi_1 = \varphi_0 + 2\pi q\mu + O(\mu^2)\,.$$

To complete the solution, apply the annulus principle. □

C.3.#43. Examine the Mathieu equation written in the following form

$$\dot{x} = y, \qquad \dot{y} = -\omega^2(1 + \varepsilon\cos\omega_0 t)x\,. \tag{C.3.14}$$

Show that the instability zones, which correspond to the parametric oscillations, are adjoined to the points $\omega/\omega_0 = k/2$ $(k = 1, 2, \ldots)$ in the plane $(\omega/\omega_0, \varepsilon)$ on the surface $\varepsilon = 0$ [20].

The solution of (C.3.14) starting from an initial point (x_0, y_0) has the following form at $\varepsilon = 0$:

$$\begin{aligned} x(t) &= \frac{y_0}{\omega_0}\sin\omega t + x_0\cos\omega t\,,\\ y(t) &= y_0\cos\omega t - \omega x_0\sin\omega t\,. \end{aligned} \tag{C.3.15}$$

Next we construct the map of the plane $(x, y, t = 0)$ onto the plane $(x, y, t = \tau = 2\pi/\omega_0)$. To do this, we substitute $t = 2\pi/\omega_0$ into (C.3.15) and replace $(x(t), y(t))$ by $(\bar{x}, \bar{y})$, and (x_0, y_0) by (x, y). The resulting operator $(x, y) \mapsto (\bar{x}, \bar{y})$ is given by

$$\begin{pmatrix} \bar{x} \\ \bar{y} \end{pmatrix} = \begin{pmatrix} \cos 2\pi \dfrac{\omega}{\omega_0} & \dfrac{1}{\omega} \sin 2\pi \dfrac{\omega}{\omega_0} \\ -\omega \sin 2\pi \dfrac{\omega}{\omega_0} & \cos 2\pi \dfrac{\omega}{\omega_0} \end{pmatrix} \begin{pmatrix} x \\ y \end{pmatrix}. \tag{C.3.16}$$

The characteristic equation of (C.3.16) is

$$\rho^2 + p\,\rho + q = 0\,,$$

where

$$p \equiv \text{tr T} = -2\cos 2\pi \frac{\omega}{\omega_0} \quad \text{and} \quad q \equiv \det T = 1\,.$$

This is an *area-preserving map*. The multipliers of the fixed point $O(x = y = 0)$ satisfy the relations

$$\rho_1 + \rho_2 = -p \quad \text{and} \quad \rho_1 \rho_2 = q = 1\,.$$

Therefore, when $|p| < 2$, the above map is a rotation through the angle $2\pi\omega/\omega_0$ such that all of its trajectories are stable.

Find a correction of the first order in ε to formula (C.3.15) (use C.3.#30). Note that the origin of the perturbed map becomes a saddle when $|p| > 2$. Furthermore, it is a saddle $(+,+)$ or a saddle $(-,-)$ if $p > 2$ and $p < -2$, respectively. □

C.3.#44. [166] Consider the system

$$\dot{\psi}_1 = \omega_1\,,$$
$$\dot{\psi}_2 = \omega_2\,,$$

where $\omega_{1,2} > 0$, which can be interpreted as a pair of two non-interacting harmonic oscillators.

The above system can be reduced to one equation

$$\frac{d\psi_1}{d\psi_2} = \frac{\omega_1}{\omega_2} \triangleq r\,.$$

We can always assume $r < 1$. The above system has the solution $\psi_1 = r\psi_2 + \psi_2^0$. Introducing the normalized coordinates $\theta = \psi_2^0/2\pi$ and $\bar{\theta} = (r2\pi + \psi_2^0)/2\pi$, one obtains the circle map

$$\bar{\theta} = \theta + r, \qquad \mod 1\,, \tag{C.3.17}$$

which can also be represented by the following map on the interval $[0, 1]$:

$$\bar{\theta} = \begin{cases} \theta + r & \text{for } 0 \le \theta \le 1 - r\,, \\ \theta - (1 - r) & \text{for } 1 - r \le \theta \le 1\,, \end{cases} \tag{C.3.18}$$

where the end points $\theta = 0$ and $\theta = 1$ are identified.

Let r be a rational number, i.e. $r = p/q$ where p and q are some mutually prime integers. Let us partition the segment $[0, 1]$ into p intervals of length $1/p$: $[0, 1/p]$, $[1/p, 2/p], \ldots, [(p-1)/p, 1]$. Choose an initial point $\theta_0 \in [0, 1/p]$. The positive semi-trajectory of (C.3.17) starting from θ_0 is the sequence of iterates

$$\left(\theta_0, \theta_1 = \theta_0 + \frac{p}{q} (\mod 1), \theta_2 = \theta_0 + \frac{2p}{q} (\mod 1), \ldots, \theta_i = \theta_0 + \frac{ip}{q} (\mod 1), \ldots\right).$$

The cycle of period n is given by

$$\left\{\theta_0 = \theta_0 + \frac{np}{q} \quad \mod 1, \quad \theta_i \neq \theta_0, \quad i = 1, 2, \ldots, n-1\right\}.$$

Under the above condition imposed on p and q it follows that the minimal period $n = p$. Therefore, there is only one point on the cycle on each interval $[(k-1)/p, k/p]$, $k = 1, \ldots, p$ because the number of points on the cycle and that of the intervals both equal p. Otherwise $n < p$, but this is impossible because two iterates of the cycle cannot belong to the same interval. Since θ_0 is an arbitrary point of $[0, 1/p]$, it follows that the segment $[0, 1]$ is filled in by p-period cycles entirely. Thus, when the rotation number is rational there is a continuum of coexisting cycles of period p in the system under consideration.

If the number r is irrational, it can be represented as

$$r = \lim_{l \to \infty} \frac{q_l}{p_l}$$

such that $p_l \to \infty$ as $l \to \infty$. In addition, the number of intervals $[(k-1)/p_l, k/p_l]$ on $[0, 1]$ also increases without bound. Therefore, the length of each interval decreases, and as $l \to \infty$ the whole segment [0, 1] is filled out by a quasi-periodic covering. □

C.3.#45. Examine the circle map:

$$\bar{\theta} = \theta + \omega + k \sin\theta \qquad \mod (2\pi)\,, \tag{C.3.19}$$

where ω is a frequency and k is some parameter.

Compute numerically the rotation number $R(\omega)$:

$$R = \frac{1}{2\pi} \lim_{N\to+\infty} \frac{1}{N} \sum_{n=0}^{N-1} (\theta_{n+1} - \theta_n)$$

for $\omega \in [0,\, 2\pi]$.

Hint: compute the iterates of the following two-dimensional mapping

$$\begin{aligned} \theta_{n+1} &= (\theta_n + \omega + k \sin x_n) \qquad \mod 2\pi\,, \\ R_{n+1} &= \frac{1}{n+1} \left(n R_n + \omega + \frac{\theta_{n+1} - \theta_n}{2\pi} \right), \end{aligned} \tag{C.3.20}$$

as ω varies from 0 to 2π.

As $n \to +\infty$, the iterates of R_n converge to the rotation number R at the given ω. Next plot the bifurcation diagram of R versus ω as in Fig. C.3.1. □

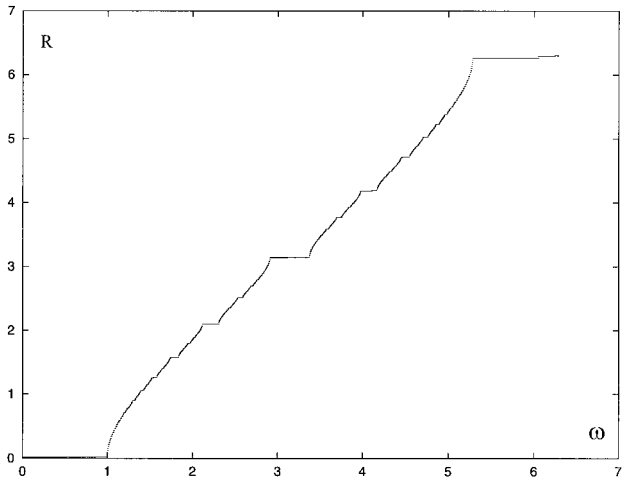

Fig. C.3.1. "Devil staircase" in (C.3.20).

C.4 Derivation of normal forms

In this section, we will discuss some algorithms for constructing normal forms. Due to the reduction principle, it is sufficient to construct the normal forms for the system on the center manifold only. Therefore, in order to consider bifurcations of an equilibrium state with a *single zero* characteristic root, we need a one-dimensional normal form. If it has a pair of zero characteristic exponents, one should examine the corresponding family of two-dimensional normal forms, and so on.

In certain situations the global properties of the original system must be taken into account. So, for instance, if the original system restricted to the center manifold is symmetric, the associated normal form will inherit this property as well. In essence, a normal form for a given bifurcation is a parameterized system of differential or difference equations, depending on what the problem under consideration is, whose right-hand sides are in the simplest form but sufficient to describe the main bifurcations in the given family.

In order to study bifurcations near a stability boundary one must introduce small governing parameters the number of which is at least equal to the order of degeneracy of the linear problem, or this number may even be greater provided that there are extra degeneracies due to the nonlinear terms. Since the unfolding parameters are small, the orbits on the center manifold may stay in a small neighborhood of the equilibrium state for a rather long time (there is no fast instability in the center manifold because all characteristic exponents of the reduced linearized system are nearly zero). Thus, it is reasonable to rescale the parameters and phase variables so that they assume finite values instead of asymptotically vanishing ones; the time variable must then be rescaled too.

This approach is a rather general one. Its advantage is that when the rescaling procedure has been carried out, many resonant monomials disappear. The most trivial example is a saddle-node bifurcation with a single zero eigenvalue. In this case the center manifold is one-dimensional. The Taylor expansion of the system near the equilibrium state may be written in the following form

$$\dot{x} = \mu + x^2 + l_3 x^3 + \cdots ,$$

where μ is a small governing parameter. The rescaling $x \to \sqrt{|\mu|}x$, $t \to t/\sqrt{|\mu|}$ brings the system to the form

$$\dot{x} = \pm 1 + x^2 + O(\sqrt{|\mu|}) ,$$

so that the second degree monomial only survives in the limit $\mu \to 0$.

An analogous algorithm can be applied to the multi-dimensional case. The limit of the rescaled system as governing parameters tend to zero gives a description "in the main order" of the behavior of the system near a bifurcation point. Such a limit system is called *an asymptotic normal form*.

The asymptotic normal forms that arise in the study of equilibria with single or double zero eigenvalues are one- or two-dimensional, respectively. The analysis of such forms is often very comprehensive so most effort is applied to establishing the rigorous correspondence between the dynamics in the asymptotic normal form and that in the original system [20, 64]. However, the analysis of bifurcations in two-dimensional normal forms may already require consideration of some other global bifurcations, sometimes of codimension two. Moreover, accounting for the dropped terms of higher order may also destroy the idealized picture occurring in truncated normal forms. The most vivid example is the bifurcations of an equilibrium state with exponents $(0, \pm i\omega)$ where the normal form possesses a rotational symmetry. If the original system does not support this symmetry, the simple dynamics in the shortened normal form may transform into chaos in the enlarged system.

The situation becomes different when one considers normal forms of higher dimensions. Three- (and higher) dimensional asymptotic normal forms may exhibit non-trivial dynamics by themselves. For example, a homoclinic loop to the saddle-focus was found in the asymptotic normal form

$$\begin{aligned} \dot{x} &= y\,, \\ \dot{y} &= z\,, \\ \dot{z} &= -z - by + ax - x^2\,, \end{aligned}$$

corresponding to the bifurcation of triple zero eigenvalues with a complete Jordan box [163]. Notably, the equations in some asymptotic normal forms coincide with some well-known models coming from different applications: the third-order Duffing equation, the Chua's circuit, the Shimizu-Morioka system and the Lorenz equation.

C.4.#46. Derive the normal form for the Shimizu-Morioka equation in the form [187]

$$\begin{aligned} \dot{x} &= y\,, \\ \dot{y} &= ax - ky - xz\,, \\ \dot{z} &= -z + x^2\,, \end{aligned} \tag{C.4.1}$$

near the codimension-two point $(k = a = 0)$.

First we should determine the characteristic exponents at the origin. It is easy to see that there is a pair of zero exponents and one equal to -1. The eigenspace corresponding to the zero pair is given by $\{z = 0\}$. The center invariant manifold, tangent to this plane at the origin, is written as

$$z = x^2 - 2xy + 2y^2 + \cdots$$

where the dots stand for the cubic and higher order terms in (x, y, z, a, k). The system on the center manifold thus takes the form

$$\begin{aligned} \dot{x} &= y\,, \\ \dot{y} &= ax - ky - x^3 + 2x^2y - 2xy^2 + \cdots\,, \end{aligned} \tag{C.4.2}$$

where the dots stand for the terms of the fourth order, at least.

Let us next rescale

$$(x, y, t, k, a) \to (\varepsilon x_{\rm new}, \varepsilon^2 y_{\rm new}, t_{\rm new}/\varepsilon, \varepsilon k_{\rm new}, \varepsilon^2 a_{\rm new})\,.$$

The system recasts as

$$\begin{aligned} \dot{x} &= y\,, \\ \dot{y} &= ax + ky - x^3 + 2\varepsilon x^2 y + O(\varepsilon^2)\,, \end{aligned} \tag{C.4.3}$$

where the new parameters $k_{\rm new}$ and $a_{\rm new}$ can now be arbitrary. Observe that the reflection symmetry $(x, y) \to (-x, -y)$ in (C.4.3) is inherited from the original system (C.4.1). Due to this fact the Taylor expansion of the functions in the right-hand side does not contain quadratic terms (and other terms of even order) in (x, y). In contrast to the generic Bogdanov-Takens bifurcation, which we analyze in Sec. 13.2, the bifurcations in the symmetric system are somewhat different: the equilibrium state at the origin always exists, and it undergoes a pitch-fork bifurcation instead of a saddle-node one. The bifurcation unfolding of the symmetric system also contains an additional curve which corresponds to the double semi-stable periodic orbit with multiplier equal to $+1$. The signs of the Lyapunov values on the Andronov-Hopf stability boundary for the origin and for the non-trivial equilibria are determined by the sign of ε. Note that when $\varepsilon = 0$ and $k = 0$, the system (C.4.3) becomes integrable with Hamiltonian

$$H(x, y) = \frac{y^2}{2} - \frac{x^2}{2} + \frac{x^4}{4}\,. \qquad \square$$

C.4.#47. Let us consider next the following version of Chua's circuit [168]

$$\dot{x} = \beta(g(y-x) - f(x))\,,$$
$$\dot{y} = g(x-y) + z\,,$$
$$\dot{z} = -y\,,$$

where α, β and g are some positive parameters. Here $f(x) = \alpha x(x^2-1)$ is the cubic approximation for the nonlinear element, and therefore this system possesses odd symmetry $(x, y, z) \to (-x, -y, -z)$. When $g > \alpha$, there is a single equilibrium state O at the origin. When $g < \alpha$, there also exists a pair of symmetric equilibrium states $O_{1,2}(\pm\sqrt{1-g/a}, 0, \mp g\sqrt{1-g/a})$. On the line $g = \alpha$, the characteristic equation at O has a single zero root when $\beta \neq 1/g^2$, and two zero roots at $\beta = 1/g^2$ (the third root is equal to $-g$ in this case). Like the case of the Shimizu-Morioka system, the structure of the bifurcation set in a plane transverse to this curve in the parameter space is determined by the Khorozov-Takens normal form with reflection symmetry. The outline of the reduction to this normal form on a two-dimensional center manifold is discussed below.

The Jacobian matrix corresponding to two null roots is given by

$$D = \begin{pmatrix} 0 & 1 & 0 \\ 0 & 0 & 0 \\ 0 & 0 & -\alpha \end{pmatrix}.$$

The linear part of the system reduces to the form

$$\begin{pmatrix} \dot{\xi} \\ \dot{\eta} \\ \dot{\zeta} \end{pmatrix} = D \begin{pmatrix} \xi \\ \eta \\ \zeta \end{pmatrix}$$

at $\alpha = g = 1/\sqrt{\beta}$ by means of the transformation

$$\begin{pmatrix} x \\ y \\ z \end{pmatrix} = \xi \begin{pmatrix} 1 \\ 0 \\ -g \end{pmatrix} + \eta \begin{pmatrix} 0 \\ g \\ g^2 \end{pmatrix} + \zeta \begin{pmatrix} 1 \\ -g^2 \\ -g \end{pmatrix}.$$

It is easy to compute and verify that in these coordinates the system assumes the form

$$\dot{\xi} = \eta + \left(1 - \frac{1}{g^2}\right) F\,,$$

$$\dot{\eta} = \frac{1}{g} F\,,$$

$$\dot{\zeta} = \frac{1}{g^2} F\,,$$

where

$$F = \gamma_1 \xi + \gamma_2 \eta + (\gamma_1 - g\gamma_2)\zeta - \beta\alpha(\xi + \zeta)^3\,,$$

and $\gamma_{1,2}$ are small parameters:

$$\gamma_1 = \beta(\alpha - g), \qquad \gamma_2 = \beta g^2 - 1\,.$$

The center manifold has the form

$$\zeta = \frac{\gamma_1}{g^3}\xi + \left(\frac{\gamma_2}{g^3} - \frac{\gamma_1}{g^4}\right)\eta + \cdots\,,$$

where the dots stand for the cubic and higher order terms with respect to $(\xi, \eta, \gamma_1, \gamma_2)$. The system on the center manifold is written as

$$\begin{aligned}
\dot{\xi} &= \eta\left(1 + \left(1 - \frac{1}{g^2}\right)\left(\gamma_2 + (\gamma_1 - g\gamma_2)\left(\frac{\gamma_2}{g^3} - \frac{\gamma_1}{g^4}\right)\right)\right) \\
&\quad + \xi\left(1 - \frac{1}{g^2}\right)\left(\gamma_1 + (\gamma_1 - g\gamma_2)\frac{\gamma_1}{g^3}\right) - \frac{1}{g}\left(1 - \frac{1}{g^2}\right)\xi^3 + \cdots\,, \\
\dot{\eta} &= \eta\frac{1}{g}\left(\gamma_2 + (\gamma_1 - g\gamma_2)\left(\frac{\gamma_2}{g^3} - \frac{\gamma_1}{g^4}\right)\right) + \xi\frac{1}{g}\left(\gamma_1 + (\gamma_1 - g\gamma_2)\frac{\gamma_1}{g^3}\right) \\
&\quad - \frac{1}{g^2}\xi^3 + \cdots\,,
\end{aligned}$$

where the dots denote terms of order higher than *three* with respect to $(\xi, \eta, \gamma_1, \gamma_2)$. Now the last step is to change the variable η so that the first equation would become $\dot{\xi} = \eta$. The final form of the system is given by

$$\dot{\xi} = \eta\,,$$

$$\dot{\eta} = \varepsilon_1\xi + \varepsilon_2\eta - \frac{1}{g^2}\xi^3 + 3\frac{1 - g^2}{g^3}\xi^2\eta + \cdots\,,$$

where

$$\varepsilon_1 = \frac{\gamma_1}{g}\left(1+\gamma_1\frac{1}{g^3}+\gamma_2\left(1-\frac{2}{g^2}\right)\right)$$

and

$$\varepsilon_2 = \gamma_1 - (\gamma_1 - g\gamma_2)\frac{g^3+1}{g^5} - (\gamma_1 - g\gamma_2)^2\frac{1}{g^5}\,. \qquad \square$$

C.4.#48. The equation of Chua's circuit can be re-parametrized in a way so that the system is written as

$$\begin{aligned}\dot{x} &= a(y + c_0 x - c_1 x^3)\,,\\ \dot{y} &= x - y + z\,,\\ \dot{z} &= -by\,.\end{aligned} \tag{C.4.4}$$

Then, y becomes a fast variable in the limit $(a,b)\to 0$, and all the dynamics of the original system (C.4.4) concentrates on the slow manifold $y = x + z$. The corresponding slow system is given by the following set of equations

$$\begin{aligned}\dot{x} &= \gamma(x + z + c_0 x - c_1 x^3)\,,\\ \dot{z} &= -x - z\,,\end{aligned} \tag{C.4.5}$$

where $\gamma = a/b$ is a parameter. Let us solve the first equation for z:

$$z = \dot{x}/\gamma - x - c_0 x + c_1 x^3\,,$$

and substitute this expression into the second equation in (C.4.5)

$$\dot{z} = -\dot{x}/\gamma + c_0 x - c_1 x^3\,.$$

Since

$$\dot{z} = \ddot{x}/\gamma - (1 + c_0 - 3c_1 x^2))\dot{x}\,,$$

we obtain

$$\ddot{x} - (\gamma(1 + c_0 - 3c_1 x^2) - 1)\dot{x} + \gamma(c_0 x - c_1 x^3) = 0\,.$$

Letting $\dot{x} = u$, we can rewrite this equation in the form

$$\begin{aligned}\dot{x} &= u\,,\\ \dot{u} &= c_0 x + (\gamma - 1 + \gamma c_0)y - 3\gamma c_1 x^2 y - \gamma c_1 x^3\,,\end{aligned}$$

which can be identified as the Khorozov-Takens normal form. $\square$

C.4.#49. Derivation of the normal form for an equilibrium state with three zero characteristic exponents in the model of a laser with saturable absorber [191]:

$$\begin{aligned}
\dot{E} &= -E + P_1 + P_2\,, \\
\dot{P}_1 &= -\delta_1 P_1 - E(m_1 + M_1)\,, \\
\dot{P}_2 &= -\delta_2 P_2 - E(m_2 + M_2)\,, \\
\dot{M}_1 &= -\rho_1 M_1 + E P_1\,, \\
\dot{M}_2 &= -\rho_2 M_2 + \beta E P_2\,.
\end{aligned} \tag{C.4.6}$$

Here E, P_1, and P_2 are the slow envelopes of electric field and atomic polarizations in the active and passive media. M_1 and M_2 are the deviations of the population differences in the active and passive medium from their values $m_1 < 0$ and $m_2 > 0$ in the absence of a laser field. δ_1 and δ_2 (ρ_1 and ρ_2) are transverse (longitudinal) relaxation rates in the active and passive media normalized by the cavity relaxation rate, β is the ratio of the saturation intensities of the intracavity media.

Linear stability of the trivial steady state

$$E = P_1 = P_2 = M_1 = M_2 = 0$$

is determined by the eigenvalues of the Jacobian matrix

$$\mathrm{J} = \begin{pmatrix}
-1 & 1 & 1 & 0 & 0 \\
-m_1 & -\delta_1 & 0 & 0 & 0 \\
-m_2 & 0 & -\delta_2 & 0 & 0 \\
0 & 0 & 0 & -\rho_1 & 0 \\
0 & 0 & 0 & 0 & -\rho_2
\end{pmatrix},$$

which are the roots of the characteristic equation

$$(\lambda^3 + a_2\lambda^2 + a_1\lambda + a_0)(\lambda + \rho_1)(\lambda + \rho_2)\,,$$

where

$$\begin{aligned}
a_2 &= 1 + \delta_1 + \delta_2\,, \\
a_1 &= m_1 + m_2 + \delta_1 + \delta_2 + \delta_1\,\delta_2\,, \\
a_0 &= m_2\delta_1 + m_1\delta_2 + \delta_1\delta_2\,.
\end{aligned}$$

Let $\delta_1 - \delta_2 > 0$, then at the codimension-three point given by

$$\begin{aligned} m_1 = m_{01} &= -\frac{\delta_1^2(1+\delta_2)}{\delta_1-\delta_2} < 0\,, \\ m_2 = m_{02} &= \frac{\delta_2^2(1+\delta_1)}{\delta_1-\delta_2} > 0, \qquad \rho_1 = 0\,, \end{aligned} \tag{C.4.7}$$

the Jacobian matrix J has a triply degenerate zero eigenvalue with geometric multiplicity two:

$$\lambda_{1,2,3} = 0, \quad \lambda_4 = \rho_2, \quad \lambda_5 = -\Lambda = -(1+\delta_1+\delta_2)\,.$$

By introducing the linear transformation of the coordinates

$$\begin{pmatrix} x_1 \\ x_2 \\ x_3 \\ x_4 \\ x_5 \end{pmatrix} = U \begin{pmatrix} E \\ P_1 \\ P_2 \\ M_1 \\ M_2 \end{pmatrix},$$

where

$$U = \begin{pmatrix} 1+\delta_2 & \dfrac{\delta_1(1+\delta_2)-\delta_2}{\delta_1^2} & 1 & 0 & 0 \\ \delta_2 & \dfrac{\delta_2}{\delta_1} & 1 & 0 & 0 \\ 0 & 0 & 0 & 1 & 0 \\ -(1+\delta_1) & \dfrac{1+\delta_1}{1+\delta_2} & 1 & 0 & 0 \\ 0 & 0 & 0 & 0 & 1 \end{pmatrix}$$

is such that

$$\mathrm{UJU}^{-1} = \begin{pmatrix} 0 & 1 & 0 & 0 & 0 \\ 0 & 0 & 0 & 0 & 0 \\ 0 & 0 & 0 & 0 & 0 \\ 0 & 0 & 0 & -\Lambda & 0 \\ 0 & 0 & 0 & 0 & -\rho_2 \end{pmatrix},$$

the system (C.4.6) assumes the form

$$\dot{x}_1 = x_2 - \frac{1}{\Lambda^2}\left[\frac{\delta_1 - \delta_2(1-\delta_1)}{{\delta_1}^2}(x_3+\xi_1) + (x_5+\xi_2)\right] S(x_1,x_2,x_4)\,,$$

$$\dot{x}_2 = -\frac{1}{\Lambda^2}\left(\frac{\delta_2}{\delta_1}(x_3+\xi_1) + (x_5+\xi_2)\right) S(x_1,x_2,x_4)\,,$$

$$\dot{x}_3 = -\rho_1 x_3 - \frac{m_{01}}{\Lambda^4}[\Lambda x_1 - (1+\Lambda)x_2 + x_4] S(x_1,x_2,x_4)\,,$$

$$\dot{x}_4 = -\Lambda x_4 - \frac{1}{\Lambda^2}\left(\frac{1+\delta_1}{1+\delta_2}(x_3+\xi_1) + (x_5+\xi_2)\right) S(x_1,x_2,x_4)\,,$$

$$\dot{x}_5 = -\rho_2 x_5 - \frac{\beta}{\Lambda^4}\left[\frac{m_{02}}{\delta_2^2}(\Lambda\delta_1\delta_2 x_1 - (\Lambda\delta_1 - \delta_2)(1+\delta_2)x_2) - \frac{\delta_2^2 m_{01}}{\delta_1^2}x_4\right]$$
$$\times\, S(x_1,x_2,x_4)\,.$$

Here m_{01} and m_{02} are defined in (C.4.7), $\xi_1 = m_1 - m_{01}$, $\xi_2 = m_2 - m_{20}$ and ρ_1 are small parameters, and

$$S(x_1,x_2,x_4) = \delta_1\Lambda(x_1 - x_2) + (1+\delta_2)(x_2 - x_4)\,.$$

After reduction to center manifold (we simply substitute $x_4 = x_5 = 0$ into the first three equations) we obtain (the dots stand for the terms of order 3 and higher):

$$\dot{x}_1 = x_2 + ax_1(x_3+\xi_1) + bx_2(x_3+\xi_1) + \xi_2 s(x_1,x_2) + \cdots\,,$$

$$\dot{x}_2 = -cx_1(x_3+\xi_1) + dx_2(x_3+\xi_1) + \xi_2 s(x_1,x_2) + \cdots\,,$$

$$\dot{x}_3 = -\rho_1 x_3 + ex_1^2 + fx_1x_2 + gx_2^2 + \cdots\,,$$

where

$$s(x_1,x_2) = -\frac{\delta_1}{\Lambda}x_1 - \frac{1+\delta_2-\delta_1\Lambda}{\Lambda^2}x_2, \qquad a = -\frac{\delta_1 - (1-\delta_1)\delta_2}{\Lambda\delta_1}\,,$$

$$b = \frac{(\delta_1 - (1-\delta_1)\delta_2)(\Lambda\delta_1 - (1+\delta_2))}{\Lambda^2\delta_1^2}, \qquad c = \frac{\delta_2}{\Lambda}\,,$$

$$d = \frac{\delta_2(\Lambda\delta_1 - 1 - \delta_2)}{\Lambda^2\delta_1}, \qquad e = -\frac{\delta_1 m_{01}}{\Lambda^2}$$

and

$$f = \frac{m_{01}(\delta_1(1+2\Lambda)-1-\delta_2)}{\Lambda^3}, \qquad g = -\frac{m_{01}(1+\Lambda)(\Lambda\delta_1-1-\delta_2)}{\Lambda^4}\,.$$

Finally, applying the coordinate transformation

$$\begin{aligned} x_1 &= z_1\,,\\ x_2 &= z_2 - az_1(z_3+\xi_1) - bz_2(z_3+\xi_1) - \xi_2 s(z_1,z_2)\,,\\ x_3 &= z_3 + \frac{f}{2}z_1^2 + gz_2z_1\,, \end{aligned}$$

we obtain

$$\begin{aligned} \dot z_1 &= z_2 + \cdots\,,\\ \dot z_2 &= \epsilon_1 z_1 + \epsilon_2 z_2 - cz_1z_3 + d'z_2z_3 + \cdots\,,\\ \dot z_3 &= -\rho_1 z_3 + ez_1^2 + \cdots\,, \end{aligned} \tag{C.4.8}$$

where

$$c = \frac{\delta_2}{\Lambda}, \qquad e = -\frac{\delta_1 m_{01}}{\Lambda^2}, \qquad d' = -\frac{1+\delta_1}{\Lambda^2}\,,$$

and the small parameters $\varepsilon_{1,2}$ are given by

$$\varepsilon_1 = -\frac{\xi_1\delta_2+\delta_1\xi_2}{\Lambda}, \qquad \varepsilon_2 = -\frac{(1+\delta_1)\xi_1+(1+\delta_2)\xi_2}{\Lambda^2}\,.$$

We can rescale the small parameters as follows:

$$\epsilon_1 = \varepsilon^2 \qquad \epsilon_2 = \mu\varepsilon, \qquad \rho_1 = \rho\varepsilon\,.$$

By neglecting the third order terms and rescaling the variables $z_1 = x\varepsilon^{3/2}/\sqrt{ce}$, $z_2 = y\varepsilon^{5/2}/\sqrt{ce}$, $z_3 = z\varepsilon^2/c$, we arrive at the following asymptotic normal form

$$\frac{dx}{d\tau} = y, \qquad \frac{dy}{d\tau} = x + \mu y - xz, \qquad \frac{dz}{d\tau} = -\rho z + x^2 \tag{C.4.9}$$

which coincides with the Shimizu-Morioka model. □

C.4.#50. Let a Jacobian of the system linearized at the equilibrium state have three zero eigenvalues. In addition, let the system on the center manifold

possess the symmetry $(x, y, z) \to (-x, -y, z)$, where y, z are the coordinate projections on the eigenvectors and x is the projection onto the adjoined vector. Then, generically, the system may be reduced to the following form

$$\begin{aligned}
&\dot{x} = y\,,\\
&\dot{y} = x[\bar{\mu} - az(1 + g(x, y, z)) - a_1(x^2 + y^2)(1 + \cdots)]\\
&\qquad - y[\bar{\alpha} + a_2 z(1 + \cdots) + a_3(x^2 + y^2)(1 + \cdots)]\,,\\
&\dot{z} = -\bar{\beta} + z^2(1 + \cdots) + b(x^2 + y^2)(a + \cdots)\,,
\end{aligned} \tag{C.4.10}$$

where $a_i \neq 0$, $i = 1, 2, 3$ and $b \neq 0$. Here, $\bar{\mu}$, $\bar{\alpha}$ and $\bar{\beta}$ are small parameters, and g and the dots denote the terms which vanish at the origin. Suppose $ab > 0$. Let $\tau^2 = \mu + a\sqrt{\bar{\beta}}(1 + g(0, 0, -\sqrt{\bar{\beta}})) > 0$, $\bar{\beta} > 0$. By scaling the time $t \to s/\tau$, changing the variables

$$x \to x\sqrt{\frac{\tau^3}{ab}}, \qquad y \to \tau y\sqrt{\frac{\tau^3}{ab}}, \qquad z \to -\sqrt{\bar{\beta}} + \frac{\tau^2}{a} z$$

and defining the new parameters as $\bar{\alpha} = \alpha\tau$ and $\bar{\beta} = (\beta\tau/2)^2$, we obtain the following system

$$\begin{aligned}
&\dot{x} = y\\
&\dot{y} = x(1 - z) - \alpha y + O(\tau)\,,\\
&\dot{z} = -\beta z + x^2 + O(\tau)\,,
\end{aligned} \tag{C.4.11}$$

where α and β are parameters which are no longer small. Dropping the terms of order τ, we obtain the Shimizu-Morioka model. □

C.4.#51. In addition to the conditions of the above case, let the system be invariant with respect to the involution $(x, y, z) \to (x, y, -z)$, i.e. it possesses two symmetries. The normalized system can then be recast as

$$\begin{aligned}
&\dot{x} = y\,,\\
&\dot{y} = x[\bar{\mu} - az^2(1 + g(x, y, z^2)) - b(x^2 + y^2)(1 + \cdots)]\\
&\qquad - y[\bar{\alpha} + a_1 z^2(1 + \cdots) + b_1(x^2 + y^2)(1 + \cdots)]\,,\\
&\dot{z} = z(\bar{\beta} - cz^2(1 + \cdots) + d(x^2 + y^2)(a + \cdots)\,.
\end{aligned} \tag{C.4.12}$$

Suppose $c > 0$ and $ad > 0$. In the parameter region $\tau^2 = \bar{\mu} - a\bar{\beta}c(1 + g(0, 0, \bar{\beta}/c)) > 0$ and $\beta > 0$, let us introduce the renormalization:

$$t \to s/\tau, \quad x \to x\tau\sqrt{\frac{c}{ad}}, \quad y \to \tau^2 y\sqrt{\frac{c}{ad}}, \quad z \to \sqrt{\frac{\bar{\beta}}{c} + \frac{\tau^2}{a}}z$$

and $\bar{\alpha} = \tau\alpha$, $\bar{\beta} = \tau\beta/2$. Denoting $B = \frac{bc}{ad}$ and omitting the terms of order τ we arrive at the following system

$$\begin{aligned} \dot{x} &= y\,, \\ \dot{y} &= x(1 - z) - \alpha y + Bx^3\,, \\ \dot{z} &= -\beta(z - x^2)\,. \end{aligned} \tag{C.4.13}$$

The above system is remarkable because the Lorenz equation can be reduced to it when $r > 1$. The relations between the parameters of two systems are given by

$$\beta = \frac{b}{\sigma(r-1)}, \quad \alpha = \frac{1+\sigma}{\sigma(r-1)}, \quad B = \frac{b}{2\sigma - b}\,.$$

It follows from the above relations that the region of the positive parameters (r, b, σ) in the Lorenz equation is bounded by the plane $\beta = 0$ and the surface $\frac{\alpha}{\beta} = \frac{1}{2}(\frac{1}{B} + 1)$, which tends to $\beta = 0$ as $B \to 0$.

We should also note that the Shimizu-Morioka system is a particular case (i.e. $B = 0$) of the Lorenz system in the form (C.4.13). □

C.4.#52. *The bifurcation of a periodic orbit with three multipliers* $+1$. On the center manifold we introduce the coordinates (x, y, z, ψ), where ψ is the angular coordinate and (x, y, z) are the normal coordinates (see Sec. 3.10). Assuming that the system is invariant under the transformation $(x, y) \to (-x, -y)$, the normal form truncated up to second order terms is given by

$$\begin{aligned} \dot{x} &= y\,, \\ \dot{y} &= x(\bar{\mu} - az) - y(\bar{\alpha} + a_2 z)\,, \\ \dot{z} &= -\bar{\beta} + z^2 + b(x^2 + y^2)\,, \\ \dot{\psi} &= 1\,, \end{aligned} \tag{C.4.14}$$

where the periodic orbit is supposed to be of period 1. Because the first three equations in the above system are independent of the fourth one, the resulting normal form is analogous to the Shimizu-Morioka system. □

C.4.#53. Below we present (following [185]) a *list* of asymptotic normal forms which describe the trajectory behavior of a triply-degenerate equilibrium state near a stability boundary in systems with discrete symmetry. We say there is a *triple instability* when a dynamical system has an equilibrium state such that the associated linearized problem has a triplet of zero eigenvalues. In such a case, the analysis is reduced to a three-dimensional system on the center manifold. Assuming that (x, y, z) are the coordinates in the three-dimensional center manifold and a bifurcating equilibrium state resides at the origin, we suppose also that our system is equivariant with respect to the transformation $(x, y, z) \leftrightarrow (-x, -y, z)$.

We note that the listed systems have a natural "physical" meaning and do appear in some realistic applications, see for example the above laser equations. Thus, this method may be viewed as a recipe for exclusion of irrelevant terms in the nonlinearity as well as for selection of those nonlinear terms which are responsible for specific details of such behavior.

In addition to the symmetry assumption, we will also suppose that the linear part of the system near the origin O restricted to the invariant plane $z = 0$ has a complete Jordan block. Then, the system in the restriction to the center manifold may locally be written in the form

$$\begin{cases} \dot{x} = y\,, \\ \dot{y} = x(az + F(x^2, xy, y^2, z)) + yG(y^2, z)\,, \\ \dot{z} = H(x^2, xy, y^2, z)\,, \end{cases} \tag{C.4.15}$$

where neither $H(0, 0, 0, z)$ nor $F(0, 0, 0, z)$ contain linear terms.

Let us consider a three-parameter perturbation of the system in the form

$$\begin{cases} \dot{x} = y\,, \\ \dot{y} = x(\mu_1 + az + F(x^2, xy, y^2, z)) + y(-\mu_2 + G(y^2, z))\,, \\ \dot{z} = -\mu_3 z + H(x^2, xy, y^2, z)\,, \end{cases} \tag{C.4.16}$$

where $\mu = (\mu_1, \mu_2, \mu_3)$ are small parameters, and the functions F, G and H may also depend on μ.

Let us also suppose that

$$a \neq 0\,. \tag{C.4.17}$$

It is then obvious that a change of the z-coordinate reduces (C.4.16) to the following form (with some new functions G and H)

$$\begin{cases} \dot{x} = y\,, \\ \dot{y} = x(\mu_1 - z) + y(-\mu_2 + G(y^2, z))\,, \\ \dot{z} = -\mu_3 z + H(x^2, xy, y^2, z)\,. \end{cases} \tag{C.4.18}$$

Let us rescale the variables and time:

$$x \to \delta_x x, \quad y \to \delta_y y, \quad z \to \delta_z z, \quad t \to t/\tau\,,$$

where δ_x, δ_y, δ_z and τ are some small quantities. We assume $\mu_1 \neq 0$ and let

$$\delta_y = \tau\delta_x, \quad \delta_z = \tau^2 = |\mu_1|\,.$$

Then (C.4.18) assumes the form

$$\begin{cases} \dot{x} = y\,, \\ \dot{y} = x(\pm 1 - z) - \lambda y + O(\tau)\,, \\ \dot{z} = -\alpha z + H(\delta_x^2\, x^2, \tau\delta_x^2\, xy, \tau^2\delta_x^2\, y^2, \tau^2 z)/\tau^3\,, \end{cases} \tag{C.4.19}$$

where α and λ are new rescaled parameters, which are no longer small:

$$\alpha = \mu_3/\sqrt{|\mu_1|}, \quad \lambda = \mu_2/\sqrt{|\mu_1|}\,.$$

The asymptotic normal form is a finite limit of the system (C.4.19) as $\mu \to 0$. Note that different choices of proportion between the scaling factors δ_x and τ yield different normal forms.

In the last equation of (C.4.19), the terms which contain z^2, y^3 and yz, tend to zero as $\tau \to 0$. Thus, by cutting out small terms, we transform (C.4.19) to

$$\begin{cases} \dot{x} = y\,, \\ \dot{y} = x(\pm 1 - z) - \lambda y\,, \\ \dot{z} = -\alpha z + \delta_x^2 x^2 H_1(\delta_x^2 x^2)/\tau^3 + \delta_x^2 xy H_2(\delta_x^2 x^2)/\tau^2 \\ \qquad + \delta_x^2 y^2 H_3(\delta_x^2 x^2)/\tau + \delta_x^2 z x^2 H_4(\delta_x^2 x^2)/\tau\,. \end{cases} \tag{C.4.20}$$

The right-hand side in (C.4.20) is to be finite, i.e. if the Taylor expansions of the functions H_i begin with x^{2m_i} for zero values of the perturbation parameters

μ_1, μ_2, and μ_3, then the following inequalities must hold

$$\delta_x^{2(m_1+1)}/\tau^3 < \infty\,,$$
$$\delta_x^{2(m_2+1)}/\tau^2 < \infty\,,$$
$$\delta_x^{2(m_3+1)}/\tau < \infty\,,$$
$$\delta_x^{2(m_4+1)}/\tau < \infty\,.$$

Therefore, we can choose τ so that

$$\tau \sim \delta_x^{\beta}\,, \tag{C.4.21}$$

where

$$\beta = \min\left\{\frac{2}{3}(m_1+1),\ m_2+1,\ 2(m_3+1),\ 2(m_4+1)\right\}. \tag{C.4.22}$$

For example, in the most generic case where $H_i(0) \neq 0$ $(i = 1, \ldots, 4)$, the exponent $\beta = 2/3$ in (C.4.21) and (C.4.22). Then, system (C.4.20) reduces to the form

$$\begin{cases} \dot{x} = y\,, \\ \dot{y} = x(\pm 1 - z) - \lambda y\,, \\ \dot{z} = -\alpha z + x^2 H_1(0) + O(\tau)\,. \end{cases} \tag{C.4.23}$$

In the limit $\tau \to 0$, this system becomes the Shimizu-Marioka model, where the parameters α and λ may take arbitrary finite values.

Let us now consider an extra degeneracy: $H_1(0) = 0$ and $H_1'(0) \neq 0$. In order to study bifurcations in this case one should introduce a new independent governing parameter which is the constant term of the Taylor expansion of H_1. If we set $\beta = 1$ according to relation (C.4.22), then system (C.4.20) reduces to the following asymptotic form:

$$\begin{cases} \dot{x} = y\,, \\ \dot{y} = x(\pm 1 - z) - \lambda y\,, \\ \dot{z} = -\alpha z + x^2 \tilde{h}_{10} + H_2(0) xy\,. \end{cases} \tag{C.4.24}$$

This is equivalent to the Lorenz equations. Here, $\tilde{h}_{10} = H_1(0)/\tau$ is the third rescaled governing parameter which may take arbitrary finite values.

The next degeneracy $H_2(0) = 0$, $H_2'(0) \neq 0$ modifies the third equation in (C.4.24) in the following way:

$$\dot{z} = -\alpha z + x^2\tilde{h}_{10} + \tilde{h}_{20}xy + H_1'(0)x^4\,, \tag{C.4.25}$$

where $\tilde{h}_{10} = H_1(0)/\tau^{3/2}$ and $\tilde{h}_{20} = H_2(0)/\tau^{1/2}$. Here, $\beta = 4/3$.

By repeating this procedure we can get a hierarchy of the asymptotic normal forms. Let us denote

$$H_i(x^2) = \sum_j^{\infty} H_{ij}x^{2j}\,.$$

We assume that at the moment of bifurcation the values of H_{ij} for $j = 0, \ldots, m_i - 1$ vanish. As before, we can treat these non-zero H_{ij} as additional independent small parameters.

It is obvious that in the rescaled system (C.4.20) there are non-zero coefficients in front of those terms which correspond to such m_i for which the minimum in (C.4.22) is achieved; all terms of higher order vanish in the limit $\tau \to 0$. The terms of degree less then $2m_i$, which appear in H_i for non-zero parameter values, also survive after the rescaling; their normalized coefficients appear as the independent parameters that may assume arbitrary finite values.

Thus, if we get rid of all asymptotically vanishing terms, system (C.4.20) takes the form

$$\begin{cases} \dot{x} = y\,, \\ \dot{y} = x(\pm 1 - z) - \lambda y\,, \\ \dot{z} = -\alpha z + x^2\tilde{H}_1(x^2) + xy\tilde{H}_2(x^2) + y^2\tilde{H}_3(x^2) + zx^2\tilde{H}_4(x^2)\,, \end{cases} \tag{C.4.26}$$

where $\tilde{H}_i$'s are polynomials of degree n_i such that

$$\begin{aligned} &\max\left\{\frac{2}{3}(n_1+1),\ n_2+1,\ 2(n_3+1),\ 2(n_4+1)\right\} \\ &\qquad = \frac{1}{\beta} < \min\left\{\frac{2}{3}(n_1+2),\ n_2+2,\ 2(n_3+2),\ 2(n_4+2)\right\} \end{aligned} \tag{C.4.27}$$

(if some $\tilde{H}_i$ vanish identically, then we let $n_i = -1$). The coefficients of $\tilde{H}_{ij}$ are defined as follows:

$$\tilde{h}_{ij} = H_{ij}/\tau^{s_i - \frac{2(j+1)}{\beta}}\,,$$

where $s_1 = 3, s_2 = 2, s_3 = s_4 = 1$.

It follows immediately from (C.4.27) that $n_3 = n_4$, i.e. the degrees of $\tilde{H}_3$ and $\tilde{H}_4$ are always equal. Hence, the list of asymptotic normal forms which are given by (C.4.26) and (C.4.27) can be ordered as the common degree $n(= n_3 = n_4)$ increases.

The first in the list are the systems given by (C.4.23), (C.4.24) and (C.4.25), which correspond to $n = -1$. For each of the greater values of n there are four sub-cases below. Each consecutive case corresponds to additional degeneracies. This is a cyclic list: after the fourth case, we return to the beginning with $n = n + 1$ and so forth.

(1) $n_1 = 3n + 2$, $n_2 = 2n + 1$; at the moment of bifurcation the first $(n-1)$ coefficients vanish in both H_3 and H_4, the first $2n$ and $(3n+1)$ coefficients vanish in H_2 and H_1, respectively.
(2) $n_1 = 3n + 3$, $n_2 = 2n + 1$; at the moment of bifurcation the first n coefficients vanish in both H_3 and H_4, the first $(2n + 1)$ and $(3n + 2)$ coefficients vanish in H_2 and H_1, respectively.
(3) $n_1 = 3n + 3$, $n_2 = 2n + 2$; at the moment of bifurcation the first n coefficients vanish in both H_3 and H_4, the first $(2n + 1)$ and $(3n + 3)$ coefficients vanish in H_2 and H_1, respectively.
(4) $n_1 = 3n + 4$, $n_2 = 2n + 2$; at the moment of bifurcation the first n coefficients vanish in both H_3 and H_4, the first $(2n + 2)$ and $(3n + 3)$ coefficients vanish in H_2 and H_1, respectively. □

C.5 Behavior on stability boundaries

C.5.#54. A stable limit cycle bifurcates from infinity in the system

$$\begin{aligned} \dot{x} &= x - y - a(x^2 + y^2)x\,, \\ \dot{y} &= x + y - a(x^2 + y^2)y\,, \end{aligned} \tag{C.5.1}$$

at $a = 0$. At this value, the system becomes linear

$$\begin{aligned} \dot{x} &= x - y\,, \\ \dot{y} &= x + y\,, \end{aligned} \tag{C.5.2}$$

and it has an unstable focus at the origin. One can compose the Lyapunov function $V(x, y) = x^2 + y^2$ and verify that all the orbits diverge to infinity (i.e. the infinity is stable) since the time derivative of the Lyapunov function

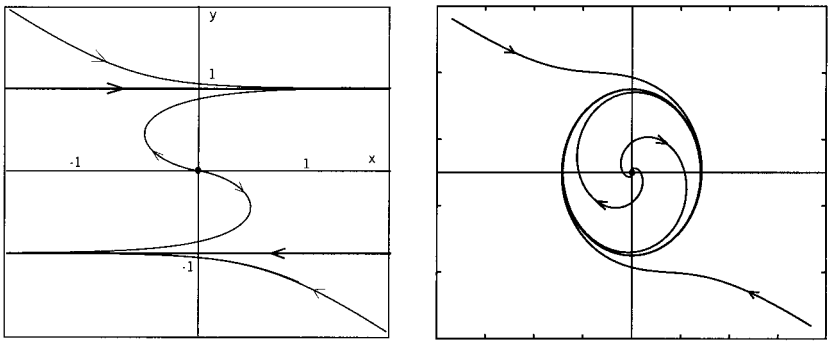

(a) (b)

Fig. C.5.1. Limit cycle in (C.5.3) for $a > 0$ (b) and at $a = 0$ (a).

$\dot{V}(x, y) = 2(x^2 + y^2)$ is positive, and hence each level $(x^2 + y^2) = C$ is a curve without contact and every trajectory must flow outside of every such curve C as time increases.

When $a \neq 0$, we have

$$\frac{d\,(x^2 + y^2)}{dt} = 2(x^2 + y^2)(1 - a(x^2 + y^2))\,.$$

It is apparent that $\dot{V}(x, y) < 0$ if $x^2 + y^2 > 1/a$, and $\dot{V}(x, y) > 0$ when $V < 1/a$. Thus, $x^2 + y^2 = 1/a$ is a stable invariant curve (a limit cycle), and all trajectories (except for the equilibrium state at the origin) tend to it as $t \to +\infty$.

C.5.#55. [25] Explain how the stable limit cycle in Fig. C.5.1 of the system

$$\begin{aligned} \dot{x} &= y - x(ax^2 + y^2 - 1)\,, \\ \dot{y} &= -ay - y(ax^2 + y^2 - 1) \end{aligned} \tag{C.5.3}$$

evolves as $a \to +0$. □

C.5.#56. Find a Lyapunov function for Khorozov-Takens normal form

$$\begin{aligned} \dot{x} &= y\,, \\ \dot{y} &= -x^3 - x^2 y\,. \end{aligned}$$

□

C.5.#57. Reveal the role of the cubed y in making the following system asymptotically stable: find a proper Lyapunov function.

$$\dot{x} = y\,,$$
$$\dot{y} = ay + x - x^3 - by^3\,.$$

Here a and b are some control parameters. □

C.5.#58. Prove the global asymptotic stability of solutions of the Lorenz equation

$$\begin{aligned} \dot{x} &= -\sigma(x-y)\,, \\ \dot{y} &= rx - y - xz\,, \\ \dot{z} &= -bz + xy\,, \end{aligned} \tag{C.5.4}$$

when $r < 1$, $\sigma > 0$ and $b > 0$.

The following function

$$V_0(x,y,z) = \frac{1}{2}(x^2 + \sigma y^2 + \sigma z^2)$$

is a Lyapunov function, since its time derivative

$$\dot{V}_0 = -\sigma(x^2 - (1-r)xy + y^2 + bz^2)$$

is a negatively defined quadratic form. □

C.5.#59. Prove that the infinity is unstable in the Lorenz system.

Solution. The time derivative of the function

$$V(x,y,z) = \frac{x^2}{2} + \frac{y^2}{2} + (z - r - \sigma)^2$$

is given by

$$\dot{V}(x,y,z) = x\dot{x} + y\dot{y} + (z-\sigma-r)\dot{z} = -\sigma x^2 - y^2 - b\left(z - \frac{r+\sigma}{2}\right)^2 + \frac{b}{4}(r+\sigma)^2\,.$$

The condition $\dot{V} = 0$ determines an ellipsoid outside of which the derivative is negative. Therefore, all "outer" positive semi-trajectories of the Lorenz system flow inside the surface

$$\sigma x^2 + y^2 + b\left(z - \frac{r+\sigma}{2}\right)^2 = \frac{b}{4}(r+\sigma)^2\,.$$ □

C.5.#60. Prove that infinity is unstable in a Chua's circuit modeled by

$$\begin{aligned} \dot{x} &= a(y + x/6 - x^3/6)\,, \\ \dot{y} &= x - y + z\,, \\ \dot{z} &= -by\,. \end{aligned} \tag{C.5.5}$$

Use the Lyapunov function

$$V_0(x, y, z) = \frac{x^2}{2a} + \frac{y^2}{2} + \frac{z^2}{2b}\,,$$

and analyze its time-derivative

$$\dot{V}_0 = \frac{x\dot{x}}{a} + y\dot{y} + \frac{z\dot{z}}{b} = \frac{1}{6}(x^2 - x^4) + 2xy - y^2$$

for large x and y. □

C.5.#61. Consider the following perturbation of the Bogdanov-Takens normal form:

$$\begin{aligned} \dot{x} &= y\,, \\ \dot{y} &= \mu y - \varepsilon^2 x + a_{20}x^2 + a_{11}xy + a_{02}y^2 + Q(x, y)\,, \end{aligned} \tag{C.5.6}$$

where μ and ε are small, and $Q(x, y)$ starts with cubic terms. One can see that the origin $O(0, 0)$ is a weak focus for the above system at $\mu = 0$ and small $\varepsilon \neq 0$: the characteristic roots are $\pm i\varepsilon$. To determine the stability of the weak focus, let us rescale first the variables $x \mapsto \varepsilon^2 x$, $y \mapsto \varepsilon^3 y$, and the time $t \mapsto \varepsilon^{-1}t$. The system will take the form

$$\begin{aligned} \dot{x} &= y\,, \\ \dot{y} &= -x + a_{20}x^2 + \varepsilon a_{11}xy + O(\varepsilon^2)\,. \end{aligned} \tag{C.5.7}$$

The following normalizing coordinate transformation

$$x_{\text{new}} = x - \frac{a_{20}}{3}(x^2 + 2y^2) + \frac{\varepsilon}{3}a_{11}xy, \qquad y_{\text{new}} = \dot{x}_{\text{new}}$$

brings the system to the form

$$\begin{aligned} &\dot{x} = y\,, \\ &\dot{y} = -x + 2a_{20}^2\left(x^3 - \frac{4}{3}xy^2\right) + \varepsilon a_{20}a_{11}\left(5x^2y - \frac{4}{3}y^3\right) + O(\varepsilon^2) + \cdots\,, \end{aligned}$$

where the dots stand for the terms of order higher than three. So, we eliminate all quadratic terms (up to $O(\varepsilon^2)$-terms) and now the first Lyapunov value can be immediately computed. Thus, let us introduce the complex variable $z = x + iy$ so that the system will recast as

$$\dot{z} = -iz + \left(\frac{\varepsilon}{8}a_{20}a_{11} + i\frac{5}{12}a_{20}^2 + O(\varepsilon^2)\right) z^2 z^* + \cdots ,$$

where the dots stand for negligible cubic and higher order terms. The first Lyapunov value is the real part of the coefficient of $z^2 z^*$, i.e. it is equal to

$$L_1 = \frac{\varepsilon}{8}[a_{20}a_{11} + O(\varepsilon)] .$$

It follows that the weak focus is stable when $a_{20}a_{11} < 0$, and unstable for $a_{20}a_{11} > 0$ for small ε. At $\varepsilon \neq 0$, only one limit cycle is born from the weak focus, provided $a_{20}a_{11} \neq 0$. □

C.5.#62. Let us give a general formula for the first Lyapunov value at a weak focus of the three-dimensional system

$$\dddot{\xi} + P\ddot{\xi} + Q\dot{\xi} + R\xi = f(\xi, \dot{\xi}, \ddot{\xi})$$

where f is a nonlinearity, i.e. its Taylor expansion at the origin begins with quadratic terms, and the coefficients P, Q, R satisfy the relation

$$PQ = R, \qquad Q > 0 .$$

Denoting $y \equiv (y_1, y_2, y_3) = (\xi, \dot{\xi}, \ddot{\xi})$ we can rewrite the above equation as

$$\dot{y} = Ay + f(y) \cdot \begin{pmatrix} 0 \\ 0 \\ 1 \end{pmatrix} ,$$

where

$$A = \begin{pmatrix} 0 & 1 & 0 \\ 0 & 0 & 1 \\ -R & -Q & -P \end{pmatrix} .$$

The eigenvalues of the matrix A are $-P$ and $\pm i\omega$, with $\omega^2 = Q$. The corresponding eigenvectors are

$$\begin{pmatrix} 1 \\ -P \\ P^2 \end{pmatrix} , \quad \begin{pmatrix} 1 \\ i\omega \\ -Q \end{pmatrix} , \quad \text{and} \quad \begin{pmatrix} 1 \\ -i\omega \\ -Q \end{pmatrix} ,$$

and the eigenvectors of the adjoint matrix are respectively given by

$$\begin{pmatrix} Q \\ 0 \\ 1 \end{pmatrix}, \quad \begin{pmatrix} P\omega \\ \omega - iP \\ -i \end{pmatrix}, \quad \text{and} \quad \begin{pmatrix} P\omega \\ \omega + iP \\ i \end{pmatrix}.$$

Thus, we can introduce the new variables $u \in R^1$ and $z \in C^1$ as follows:

$$y = u \begin{pmatrix} 1 \\ -P \\ P^2 \end{pmatrix} + z \begin{pmatrix} 1 \\ i\omega \\ -Q \end{pmatrix} + z^* \begin{pmatrix} 1 \\ -i\omega \\ -Q \end{pmatrix}.$$

The derivatives $\dot{u}$ and $\dot{z}$ are computed by the following rule

$$\dot{u} = \frac{1}{Q + P^2}(Q\dot{y}_1 + \dot{y}_3), \qquad \dot{z} = \frac{1}{2P\omega}(P\omega\dot{y}_1 + (\omega - iP)\dot{y}_2 - i\dot{y}_3)\,,$$

so that we arrive at the system whose linear part is already diagonal

$$\begin{aligned} \dot{u} &= -Pu + \alpha_1 z^2 + \alpha_2 z z^* + \cdots\,, \\ \dot{z} &= i\omega z + \beta_1 z^2 + \beta_2 z z^* - \beta_1^* z^{*2} + \gamma u z - \gamma^* u z^* + \delta z^2 z^* + \cdots\,, \end{aligned} \tag{C.5.8}$$

where the dots stand for the nonlinear terms which are negligible for the computation of the first Lyapunov value. If we expand the nonlinearity up to the third order in y:

$$f(y) = \sum c_{kj} y_j y_k + \sum d_{kjl} y_k y_j y_l + \cdots\,, \tag{C.5.9}$$

then the coefficients $\alpha, \beta, \gamma, \delta$ in (C.5.8) are found as follows:

$$\begin{aligned} &(Q + P^2)\alpha_1 = 2iP\omega\beta_1 = \textstyle\sum c_{kj}(i\omega)^{k+j-2}\,, \\ &(Q + P^2)\alpha_2 = 2iP\omega\beta_2 = -\textstyle\sum((-1)^k + (-1)^j)c_{kj}(i\omega)^{k+j-2}\,, \\ &\gamma = \frac{1}{2}\textstyle\sum c_{kj}((-P)^{k-2}(i\omega)^{j-2} + (-P)^{j-2}(i\omega)^{k-2})\,, \\ &\delta = -\frac{1}{2PQ^2}\textstyle\sum d_{kjl}(i\omega)^{k+j+l}((-1)^k + (-1)^j + (-1)^l)\,. \end{aligned} \tag{C.5.10}$$

System (C.5.8) has a center manifold given by

$$u = \frac{\alpha_1}{P + i\omega} z^2 + \frac{\alpha_2}{P} z z^* + \cdots\,.$$

On the center manifold the system assumes the form

$$\dot{z} = i\omega z + \beta_1 z^2 + \beta_2 z z^* - \beta_1^* z^{*2} + \left(\gamma \frac{\alpha_2}{P} - \gamma^* \frac{\alpha_1}{P + i\omega} + \delta\right) z^2 z^* + \cdots . \quad \text{(C.5.11)}$$

The normalizing transformation

$$z_{\rm new} = z + i\frac{\beta_1}{\omega} z^2 - i\frac{\beta_2}{\omega} z z^* + i\frac{\beta_1^*}{3\omega} z^{*2}$$

kills all quadratic terms, so that the system on the center manifold takes the form

$$\dot{z} = i\omega z + (L_1 + i\Omega_1) z^2 z^* + \cdots ,$$

where

$$L_1 + i\Omega_1 = \frac{i}{\omega}\left(\beta_1\beta_2 - |\beta_1|^2 - \frac{2}{3}|\beta_2|^2\right) + \gamma\frac{\alpha_2}{P} - \gamma^*\frac{\alpha_1}{P + i\omega} + \delta\,. \quad \text{(C.5.12)}$$

By definition, L_1 is the *first* Lyapunov value. □

C.5.#63. Let us apply the above algorithm to determine the stability of the structurally unstable equilibria $O_{1,2}$ in the Lorenz model, see Sec. C.2. To find whether the corresponding Andronov-Hopf bifurcation is sub- or supercritical on the stability boundary of these equilibria we will compute the analytical expression for the first Lyapunov value L_1.

Following [165, 186], let us first bring the original system

$$\dot{x} = -\sigma(x - y)\,,$$
$$\dot{y} = rx - y - xz\,,$$
$$\dot{z} = -bz + xy$$

to a single third-order differential equation

$$\dddot{x} + (\sigma + b + 1)\ddot{x} + b(1 + \sigma)\dot{x} + b\sigma(1 - r)x = \frac{(1 + \sigma)\dot{x}^2}{x} + \frac{\dot{x}\ddot{x}}{x} - x^2\dot{x} - \sigma x^3\,. \quad \text{(C.5.13)}$$

Then, we introduce the new variable $\xi = x - x_0$, where $x_0 = \pm\sqrt{b(r-1)}$ for $O_{1,2}$, respectively. We stress that only quadratic and cubic terms in the nonlinearity are needed and hence the first order terms of the expansion of

$(x_0+\xi)^{-1}$ are sufficient in order to find the first Lyapunov value. Taking into account the needed terms, the equation (C.5.13) can be rewritten as follows

$$\dddot{\xi} + (\sigma+b+1)\ddot{\xi} + [b(1+\sigma)+x_0^2]\dot{\xi} + [b\sigma(1-r)+3\sigma x_0^2]\xi$$
$$= -3\sigma x_0\xi^2 - 2x_0\xi\dot{\xi} + \frac{1+\sigma}{x_0}\dot{\xi}^2 + \frac{1}{x_0}\dot{\xi}\ddot{\xi} - \sigma\xi^3 - \xi^2\dot{\xi}$$
$$- \frac{1+\sigma}{x_0^2}\xi\dot{\xi}^2 - \frac{1}{x_0^2}\xi\dot{\xi}\ddot{\xi} + \cdots . \qquad \text{(C.5.14)}$$

The stability boundary for both O_1 and O_2 is given by

$$r = \sigma(\sigma+b+3)(\sigma-b-1)^{-1} .$$

The first Lyapunov value computed by the above algorithm is

$$L_1 = b[p^3q(p^2+q)(p^2+4q)(\sigma-b-1)]^{-1}B , \qquad \text{(C.5.15)}$$

where

$$B = [9\sigma^4 + (20-18b)\sigma^3 + (20b^2+2b+10)\sigma^2$$
$$- (2b^3-12b^2-10b+4)\sigma - b^4 - 6b^3 - 12b^2 - 10b - 3] .$$

On the stability boundary, the inequality $\sigma > b+1$ is fulfilled. Upon substituting $\sigma = \sigma_* + b + 1$, the expression for B becomes a polynomial of σ_* and b with positive coefficients. Hence, if $\sigma_* > 0$ and $b > 0$, then $L_1 > 0$. Thus, both equilibria $O_{1,2}$ are unstable (saddle-foci) on the stability boundary. The boundary itself is dangerous in the sense of the definition suggested in Chap. 14. Therefore, the corresponding Andronov-Hopf bifurcation of $O_{1,2}$ is sub-critical. □

C.5.#64. Compute the first Lyapunov value in the Chua's circuit (C.5.5). Verify that for $c_1 = c_3 = 1/6$ it vanishes at the point ($a \simeq 1.72886$, $b \simeq 1.816786$), labeled by $L_1 = 0$ on the Andronov-Hopf curve in Fig. C.2.1. This is the point of codimension two from which a curve of saddle-node periodic orbit originates. □

C.5.#65. Find the expression for the first Lyapunov value in the Shimizu-Marioka system (C.2.25) reduced to the following third order differential equation

$$\dddot{x} + (a+b)\ddot{x} + ab\dot{x} - bx + x^3 - \frac{a}{x}\dot{x}^2 - \frac{\dot{x}\ddot{x}}{x} = 0 . \qquad \text{(C.5.16)}$$

Show that it is negative (positive) to the right (left) of the point ($a \simeq 1.359, b \simeq 0.1123$) on the Andronov-Hopf bifurcation curve given by $(a+b)a - 2 = 0$. □

C.6 Bifurcations of fixed points and periodic orbits

C.6.#66. Consider the *logistic* map

$$\bar{x} = ax(1-x) \equiv f(x)\,,$$

with $0 < a < 4$ and $x \in I = [0,1]$. When $0 < a < 1$, the origin is a unique stable fixed point. It is semi-stable at $a = 1$ since $f'(0) = 1$. It becomes unstable as a increases, and another fixed point $O_1(x_1 = (a-1)/a)$ bifurcates from the origin (hence we have a transcritical bifurcation here). The point O_1 is stable when $1 < a \le a_1 = 3$ [see Fig. C.6.1(a)]. It flip-bifurcates when $f'(O_1) = a - 2ax_1 = -1$ at $a = 3$. The first Lyapunov value at this point is equal to $-\frac{1}{6}(f'''(O_1) + \frac{3}{2}f''(O_1)^2) = -\frac{2}{3}a_1 = -2$. Since it is negative, the point is asymptotically stable at $a = 3$. Thus, a stable cycle C_2 of period 2 bifurcates from O_1 as a exceeds 3, as shown in Fig. C.6.1(b).

The cycle of period two consists of a pair of period-two points

$$x_2^{(1,2)} = \frac{a+1 \pm \sqrt{a^2-2a-3}}{2a}\,,$$

which are the roots of the equation $x = f^2(x)$ other than those corresponding to O and O_1. The direct computation of the multiplier of the cycle, which is given by $f'(x_2^{(1)}) \cdot f'(x_2^{(2)})$, reveals that it is stable when $3 < a < 1 + \sqrt{6}$. Moreover, the multiplier is positive when $3 < a < 1 + \sqrt{5}$, and negative when $1 + \sqrt{5} < a$, but still less than 1 in absolute value. This cycle becomes repelling when $a > 1 + \sqrt{6}$, and its stability switches to the cycle C_4 of period 4, shown in Fig. C.6.1(c). When this cycle goes through the flip bifurcation at $a = a_3 \simeq 3.54$, then a stable period-8 cycle is born, and so forth [see Fig. C.6.2(d)–(f)].

Note that the first Lyapunov value is always negative for a flip-bifurcation of any periodic orbit in the logistic map. Indeed, the Schwarzian derivative:

$$S(f)(x) = \frac{f'''}{f'} - \frac{3}{2}\left(\frac{f''}{f'}\right)^2$$

is negative everywhere within the interval $[0,1]$ where the map is defined. It is easy to check that if for some map $S(f) < 0$ everywhere, then $S(f \circ f \circ \cdots \circ f) < 0$ everywhere too, i.e. it is negative for every power of the map. It remains to note that $\frac{1}{6}S(f)$ coincides with the first Lyapunov value at the fixed point at the moment of flip-bifurcation (when $f'(x) = -1$).

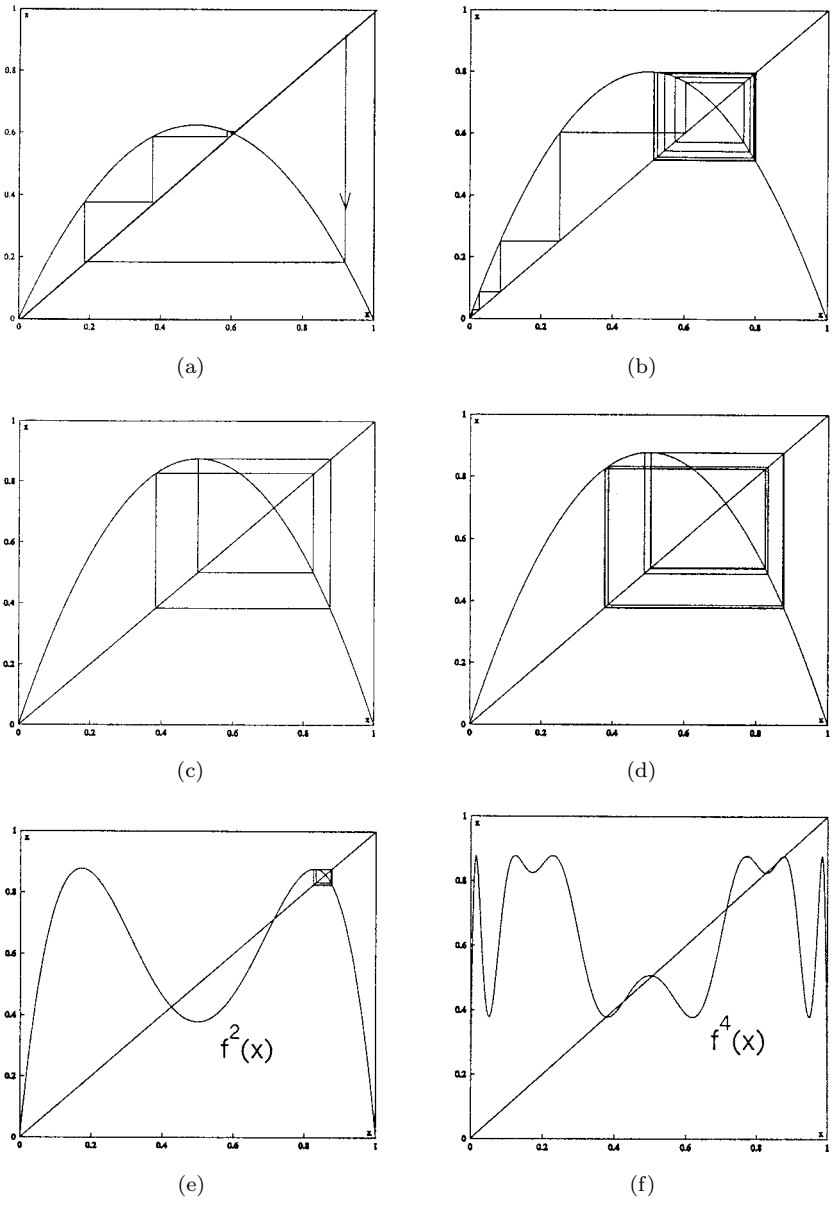

Fig. C.6.1. Period doubling in the logistic map.

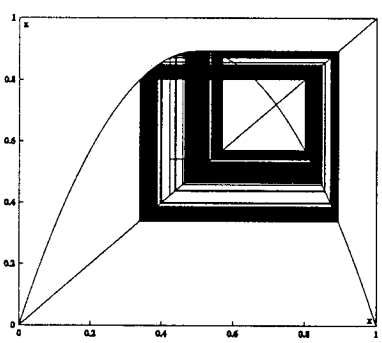

(g)

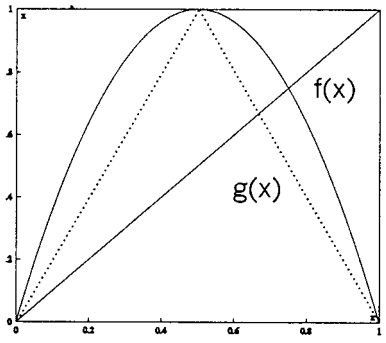

(h)

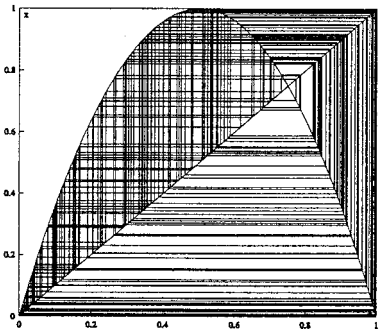

(i)

Fig. C.6.1. (*Continued*)

This sequence of period-doubling bifurcations ends up at approximately $a \simeq 3.569$, after which the logistic map exhibits chaotic behavior, see Fig. C.6.1(g) and (i).

Feigenbaum [170] noticed that the bifurcation values of a_n, $n = 1, 2, \ldots$ increase asymptotically in geometrical progression with the multiplier

$$\delta = \lim_{n\to\infty} \frac{a_n - a_{n-1}}{a_{n+1} - a_n} \simeq 4.66920\,. \qquad \square$$

C.6.#67. Find the critical value of a that corresponds to the situation depicted in Fig. C.6.1(h). Can this map have stable orbits at this moment? To answer this question reduce it first to a piece-wise linear map.

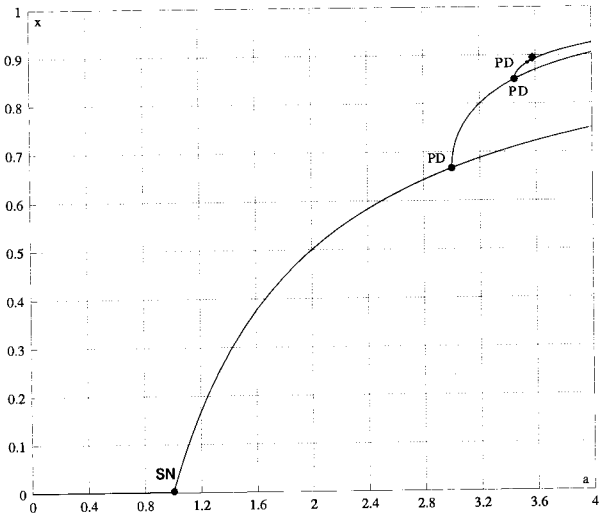

Fig. C.6.2. (x versus a) bifurcation diagram of the logistic map in the period-doubling process.

Evaluate the values of a_n that correspond to the flip bifurcations of the orbits of period 16, 32, respectively. Find the corresponding maximal x-coordinates of these cycles and plot them on Fig. C.6.2. □

C.6.#68. Examine the map

$$\bar{x} = x + x(a(1-x) - b(1-x)^2) = f(x)\,,$$

where a and b are some positive parameters. Find its fixed points, and detect the corresponding stability boundaries. Determine the asymptotic stability of the fixed points and period-2 cycle at critical cases. □

C.6.#69. Examine the maps $\bar{x} = \mu_1 + Ax^{1+\mu_2}$ and $\bar{x} = \mu_1 - \mu_2 x^\nu + x^{2\nu}$, where $0 < \nu < 1$, and $|\mu_1| \ll 1$. Consider the subcases $0 < \nu < 1/2$ and $1/2 < \nu$ separately. What happens at $\nu = 1/2$? Analyze bifurcations of symmetric periodic points in the two maps $\bar{x} = (\mu_1 + A|x|^{1+\mu_2})\,\mathrm{sign}(x)$ and $\bar{x} = (\mu_1 - \mu_2|x|^\nu + |x|^{2\nu})\,\mathrm{sign}(x)$, $|\mu_{1,2}| \ll 1$. Such maps appear in the study of homoclinic bifurcations of codimension two (see Sec. 13). □

C.6.#70. Consider the Hénon map:

$$\bar{x} = y\,, \qquad \bar{y} = a - bx - y^2\,.$$

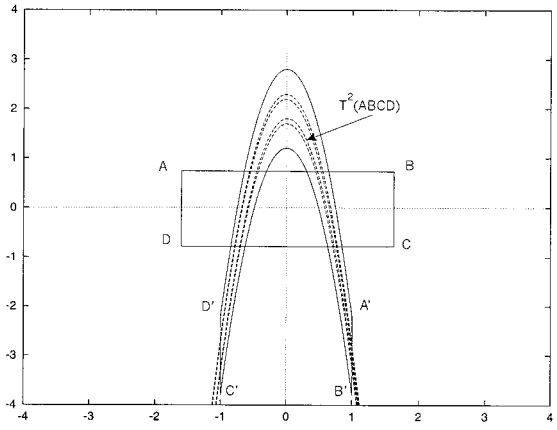

(a)

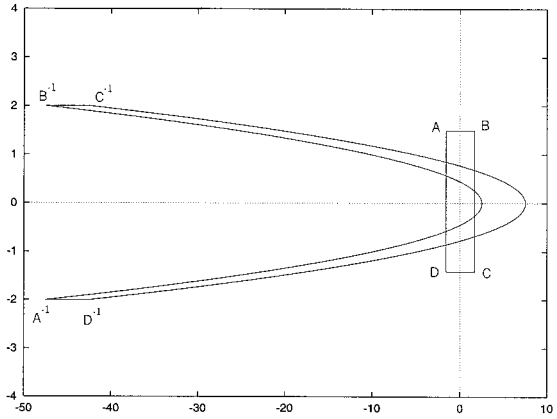

(b)

Fig. C.6.3. Horseshoe in the Hénon map for $a = 2$ and $b = 0.4$ and in its inverse.

This map is a canonical example illustrating the chaotic behavior. For certain parameter values the Hénon map models the mechanism of the creation of the Smale horseshoe as illustrated in Fig. C.6.3, for the map and for its inverse:

$$y = \bar{x}\,,$$
$$x = (a - \bar{y} - \bar{x}^2)/b\,,$$

defined for $b \neq 0$.

The Jacobian of the Hénon map is constant and equal to b. Therefore, when $b > 0$, the Hénon map preserves orientation in the plane, whereas orientation is reversed when $b < 0$. Note also that if $|b| < 1$, the map contracts areas, so the product of the multipliers of any of its fixed or periodic points is less than 1 in absolute value. Hence, in this case the map cannot have completely unstable periodic orbit (only stable and saddle ones). On the contrary, when $|b| > 1$, no stable orbits can exist. When $|b| = 1$, the map becomes conservative. At $b = 0$, the Hénon map degenerates into the above logistic map, and therefore one should expect some similar bifurcations of the fixed points when b is sufficiently small.

Next, let us find the fixed points in the Hénon map and analyze how they bifurcate as the parameters a and b vary. The bifurcation portrait is shown in Fig. C.6.4. It contains three bifurcation curves: SN: $a = -\frac{1}{4}(1+b)^2$, PD: $a = \frac{3}{4}(1+b)^2$, and AH: $b = 1, -1 < a < 3$. For $(a,b) \in SN$ the map has a fixed point with one multiplier $+1$; when $|b| < 1$, this point is a saddle-node with an attracting sector, while when $|b| > 1$, this is a saddle-node with a repelling zone. For $(a,b) \in PD$ the map has a fixed point with multiplier -1; when $|b| < 1$, the other multiplier is less than 1 in absolute value and the first Lyapunov value is negative, so the bifurcating point is stable. For $|b| > 1$,

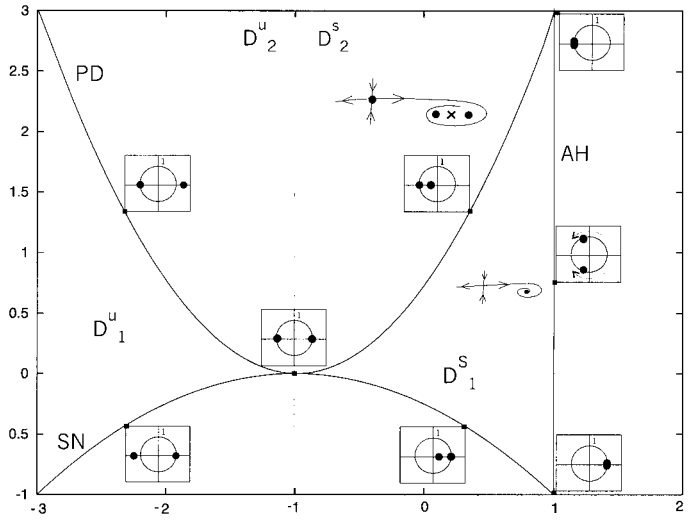

Fig. C.6.4. Bifurcation portrait of the fixed points in the Hénon map.

the other multiplier is greater than 1 in absolute value and the first Lyapunov value is positive, so the bifurcating point is completely unstable. (Check the equations for the bifurcation curves and compute the Lyapunov values.)

In the region D_1 there are two fixed points, one of which is a saddle, and the other one is stable for $(a,b) \in D_1^s$, and repelling when $(a,b) \in D_1^u$. Transition from D_1 to D_2 is accompanied with the period-doubling bifurcations of the fixed point, correspondingly, stable on the route $D_1^s \to D_2^s$, and repelling on the route $D_1^u \to D_2^u$. Meanwhile the point becomes a saddle $(-)$, and in its neighborhood a stable cycle of period two bifurcates from it when $(a,b) \in D_2^s$; in the region D_2^u, this period-two cycle is repelling.

When $b = 1$, the Hénon map becomes conservative, as its Jacobian equals $+1$. At $b = 1$ and $a = -1$, it has an unstable parabolic fixed point with two multipliers $+1$; at $b = 1$ and $a = 3$, it is a stable parabolic fixed point with two multipliers -1. In between these points, for $-1 < a < 3$ (i.e. $(a,b) \in T$), the map has a fixed point with multipliers $e^{\pm i\psi}$ where $\cos\psi = 1 - \sqrt{a+1}$. This is a generic elliptic point for $\psi \notin \{\pi/2, 2\pi/3, \arccos(-1/4)\}$ [167]. Since the Hénon map is conservative when $b = 1$, the Lyapunov values are all zero. When we cross the curve AH, the Jacobian becomes different from 1, hence the map either attracts or expands areas which, obviously, prohibits the existence of invariant closed curves. Thus, no invariant curve is born upon crossing the curve AH. □

C.6.#71. Let us consider the following map

$$\begin{aligned} \bar{x} &= y + \alpha y^2\,, \\ \bar{y} &= a - bx - y^2 + \beta xy \end{aligned} \tag{C.6.1}$$

with small α and β. This map can therefore be treated as a slight perturbation of the Hénon map. We may wonder what bifurcations occur in some bounded subregion in the (x,y)-plane which remains of finite size as both α and β tend to zero. This question is typical in the study of bifurcations of a quadratic homoclinic tangency between the stable and unstable manifolds of a neutral saddle fixed point (with the multipliers $|\nu| < 1 < |\gamma|$ such that $|\nu\gamma| = 1$) [175].

Let us derive the equations of the bifurcation curves $\widetilde{SN}$, $\widetilde{PD}$ and $\widetilde{AH}$ for (C.6.1) for small α and β; these curves correspond to the saddle-node, period-doubling and torus creation, respectively.

Consider the characteristic equation for (C.6.1)

$$\det \begin{pmatrix} -\lambda & 1+2\alpha y \\ -b+\beta y & -2y+\beta x-\lambda \end{pmatrix} = 0\,.$$

Since $x = y + \alpha y^2$ at a fixed point, this equation recasts as

$$\lambda^2 + \lambda(2y - \beta y - \alpha\beta y^2) + b + y(2b\alpha - \beta) - 2\alpha\beta y^2 = 0\,. \tag{C.6.2}$$

The equation for the coordinate y of a fixed point of (C.6.1) is given by

$$a - y(1+b) - y^2(1 + b\alpha - \beta) + \alpha\beta y^3 = 0\,. \tag{C.6.3}$$

Let us derive the equation of the curve $\widetilde{SN}$ of saddle-node fixed points. Since one of the eigenvalues of such points equals 1, plugging $\lambda = 1$ into (C.6.2) yields

$$1 + b + 2y(1 + b\alpha - \beta) - 3\alpha\beta y^2 = 0\,. \tag{C.6.4}$$

This equation has only one solution in any fixed finite region, provided that α and β are sufficiently small:

$$y = -\frac{1+b}{2(1+b\alpha-\beta)} + O(\alpha\beta)\,.$$

Substituting this in (C.6.3) gives the following equation for $\widetilde{SN}$

$$a = -\frac{(1+b)^2}{4}(1 - b\alpha + \beta) + O(\alpha^2 + \beta^2)\,. \tag{C.6.5}$$

Analogously, the equation of the curve $\widetilde{PD}$ corresponding to a period-doubling bifurcation is given by

$$a = \frac{3}{4}(1+b)^2\left(1 + \frac{4}{3}b\alpha - \frac{\beta}{3}\right) + O(\alpha^2 + \beta^2)\,. \tag{C.6.6}$$

Note that the curves $\widetilde{SN}$ and $\widetilde{PD}$ are close to the curves SN and PD of the original Hénon map.

Let us derive next the equation for the curve $\widetilde{AH}$ which corresponds to the creation of an invariant curve (the Andronov-Hopf bifurcation for maps). Since eigenvalues of such a point are $\lambda_{1,2} = e^{\pm i\varphi}$, it follows that the Jacobian

of the map at the fixed point equals 1 and the trace of the Jacobian matrix equals $2\cos\varphi$. This yields the following system for solving y and b:

$$\begin{aligned} &2y - \beta y - \alpha\beta y^2 = -2\cos\varphi \\ &b + y(2b\alpha - \beta) - 2\alpha\beta y^2 = 1\,. \end{aligned} \tag{C.6.7}$$

We obtain from the first equation that

$$y = -\frac{\cos\varphi}{1-\beta/2} + O(\alpha\beta)\,, \tag{C.6.8}$$

and from the second one that

$$b = 1 - (\beta - 2\alpha)\cos\varphi + O(\alpha^2 + \beta^2)\,. \tag{C.6.9}$$

Finally, we find from (C.6.3) that

$$a = \cos^2\varphi[1 + \beta - \alpha] - 2\cos\varphi[1 + \beta/2] + O(\alpha^2 + \beta^2)\,. \tag{C.6.10}$$

The curve $\widetilde{AH}$ is given by (C.6.9)–(C.6.10). Since the Jacobian of the map (C.6.1) is no longer constant, one should expect that the corresponding bifurcation of the birth of the invariant curve will be non-degenerate at the fixed point. To make sure, let us compute the first Lyapunov value L_1.

Let $(a, b) \in \widetilde{AH}$. Then $b = -1+O(\alpha,\beta)$ and $-1+O(\alpha,\beta) < a < 3+O(\alpha,\beta)$. The bifurcating fixed point with multipliers $e^{\pm i\varphi}$ has coordinates

$$\begin{aligned} x &= -\cos\varphi(1 + \beta/2) + \alpha\cos^2\varphi + O(\alpha^2 + \beta^2)\,, \\ y &= -\cos\varphi(1 + \beta/2) + O(\alpha^2 + \beta^2)\,. \end{aligned} \tag{C.6.11}$$

Let us translate the origin to the fixed point. The map (C.6.1) then assumes the form

$$\begin{aligned} \bar{x} &= y(1 + \rho) + \alpha y^2 + \cdots\,, \\ \bar{y} &= -x/(1 + \rho) + 2y\cos\varphi - y^2 + \beta xy + \cdots\,. \end{aligned}$$

where $\rho = 2\alpha\cos\varphi + O(\alpha^2 + \beta^2)$ and the dots stand for nonlinear terms of order $O(\alpha^2 + \beta^2)$. By rescaling the x-variable to $(1 + \rho)$, the map is brought to the form

$$\begin{aligned} \bar{x} &= y + \alpha y^2 + \cdots\,, \\ \bar{y} &= -x + 2y\cos\varphi - y^2 + \beta xy + \cdots\,. \end{aligned} \tag{C.6.12}$$

Now, make a linear transformation $x = \xi$ and $y = (\cos\varphi)\xi - (\sin\varphi)\eta$ after which the linear part of the map becomes a rotation through an angle φ:

$$\begin{aligned}
\bar{\xi} &= \xi\cos\varphi - \eta\sin\varphi + \alpha(\xi\cos\varphi - \eta\sin\varphi)^2 + \cdots\,,\\
\bar{\eta} &= \xi\sin\varphi + \eta\cos\varphi + \frac{1}{\sin\varphi}(\xi\cos\varphi - \eta\sin\varphi)^2(1+\alpha\cos\varphi)\\
&\quad - \frac{\beta}{\sin\varphi}\xi(\xi\cos\varphi - \eta\sin\varphi) + \cdots\,.
\end{aligned} \tag{C.6.13}$$

Denoting $z = \xi + i\eta$, we obtain

$$\bar{z} = ze^{i\varphi} + c_{20}z^2 + c_{11}zz^* + c_{02}(z^*)^2 + \cdots\,, \tag{C.6.14}$$

where z^* is complex-conjugate to z and the coefficients c_{ij} are given by

$$\begin{aligned}
c_{20} &= \frac{1}{4}[-2\cos\varphi - \alpha + \beta] + \frac{i}{4}\left[\frac{\cos 2\varphi}{\sin\varphi} + \frac{\cos\varphi}{\sin\varphi}(\alpha-\beta)\right],\\
c_{11} &= \frac{\alpha}{2} + \frac{i}{2}\left[\frac{1}{\sin\varphi} + \frac{\cos\varphi}{\sin\varphi}(\alpha-\beta)\right],\\
c_{02} &= \frac{1}{4}[2\cos\varphi + \alpha(3\cos^2\varphi - \sin^2\varphi) - \beta]\\
&\quad + \frac{i}{4}\left[\frac{\cos 2\varphi}{\sin\varphi} + \alpha\frac{\cos\varphi}{\sin\varphi}(\cos^2\varphi - 3\sin^2\varphi) - \beta\frac{\cos\varphi}{\sin\varphi}\right].
\end{aligned} \tag{C.6.15}$$

According to Sec. 3.13, the quadratic terms are eliminated by the following normalizing transformation (when $\varphi \neq 2\pi/3$):

$$z_{\text{new}} = z - \frac{c_{20}}{e^{2i\varphi} - e^{i\varphi}}z^2 - \frac{c_{11}}{1 - e^{i\varphi}}zz^* - \frac{c_{02}}{e^{-2i\varphi} - e^{i\varphi}}(z^*)^2 + \cdots\,. \tag{C.6.16}$$

This transformation does not change the linear part and it is known to eliminate all quadratic terms. Thus, we need only to collect the coefficients in front of the cubic term z^2z^*. This gives

$$\bar{z}_{\text{new}} = e^{i\varphi}z_{\text{new}} + e^{i\varphi}z_{\text{new}}^2 z_{\text{new}}^*(L + i\Omega) + O_3(z)\,, \tag{C.6.17}$$

where $O_3(z)$ stands for the remaining cubic and higher order terms, and

$$L + i\Omega = -c_{20}c_{11}e^{-2i\varphi}\frac{1 - 2e^{i\varphi}}{1 - e^{i\varphi}} - |c_{11}|^2\frac{1}{1 - e^{i\varphi}} - |c_{02}|^2\frac{2}{1 - e^{3i\varphi}}\,. \tag{C.6.18}$$

Taking the real part of the right-hand side we arrive at the following formula for the first *Lyapunov value* L_1 [184]

$$L_1 = \mathrm{Re}(c_{20}c_{11})\frac{\cos 3\varphi - 3\cos 2\varphi + 2\cos\varphi}{2(1-\cos\varphi)} + \mathrm{Im}(c_{20}c_{11})\frac{\sin 3\varphi - 3\sin 2\varphi + 2\sin\varphi}{2(1-\cos\varphi)} - |c_{02}|^2 - \frac{1}{2}|c_{11}|^2 . \quad \text{(C.6.19)}$$

When we plug (C.6.15) into the above formula, we finally obtain the following expression:

$$L_1 = \frac{1}{16(1-\cos\varphi)}[\beta - 2\alpha] + O(\alpha^2 + \beta^2) . \quad \text{(C.6.20)}$$

Observe that L_1 vanishes at $\alpha = \beta = 0$ as it is to be identically zero in the Hénon map.

Thus, when α and β are small, the sign of the first Lyapunov value equals the sign of the difference $(\beta - 2\alpha)$. If it is negative, the stable invariant curve is born through the super-critical Andronov-Hopf bifurcation when crossing the curve $\widetilde{AH}$ towards larger β. □

C.6.#72. Using a computer, trace the evolution of the invariant curve as b grows (choose $\alpha = \beta = 0.001$).

Let us first discuss the case $L_1 < 0$. In the region to the left of $\widetilde{AH}$ the point O is stable, see Fig. C.6.5. The point O becomes unstable to the right of the Andronov-Hopf bifurcation curve $\widetilde{AH}$, and a stable invariant curve bifurcates from it. The stable curve evolves in the following way: as the parameter increases further, it "glues" to a homoclinic loop to the saddle fixed point O_1. By the term "gluing" we mean that the stable invariant curve becomes a part of the non-wandering set of the complex homoclinic structure existing due to intersections of the stable and unstable manifolds of the saddle fixed point O_1. As the parameters vary further, this non-wandering set vanishes as the result of the homoclinic tangency.

Such a scenario of stability loss is often referred to in the literature as "soft" (see Chap. 14). In the case $L_1 > 0$, the loss of stability develops in a *dangerous* way: the point O is stable initially; meanwhile an unstable invariant curve "materializes" from the homoclinic tangles of O_1, and shrinks to the origin as the curve $\widetilde{AH}$ is reached. The fixed point at the origin becomes unstable upon crossing $\widetilde{AH}$, and all nearby trajectories escape from its neighborhood. □

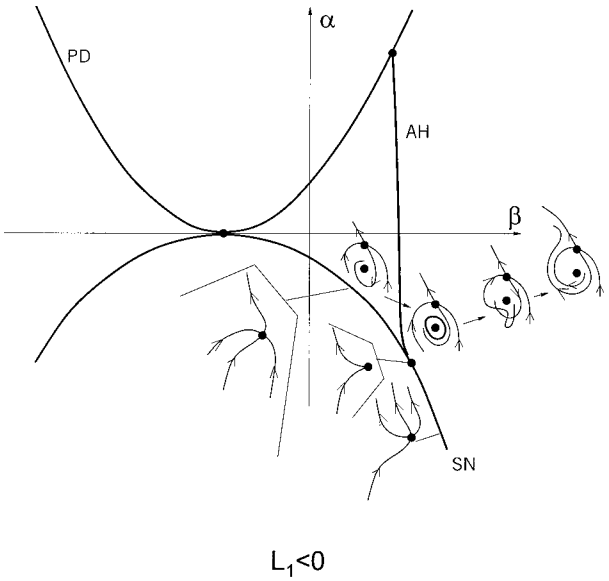

Fig. C.6.5. Bifurcation portrait of the perturbed Hénon map.

C.6.#73. Examine the following map

$$\bar{x} = y\,,$$
$$\bar{y} = \mu_1 + \mu_2 y + dy^3 - bx\,,$$

where μ_1, μ_2, b are control parameters, and $d = \pm 1$. Such maps appear in the study of the Lorenz attractor, as well as in modeling the behavior of the periodic forced equations with cubic nonlinearity, like the Duffing system [176, 184].

The Jacobian of the map is equal to b, and therefore, when $b \neq 0$, it is a diffeomorphism. The inverse is given by

$$\bar{y} = x\,,$$
$$\bar{x} = \frac{1}{b}(\mu_1 + \mu_2 x + dx^3 - y)\,.$$

One can easily see from the above formula that the cases $|b| > 1$ and $|b| < 1$ are symmetric. When $b = 0$, the original map becomes "one-dimensional" in the

sense that it has an invariant curve $y = dx^3+\mu_2 x+\mu_1$ to which any point of the plane is mapped onto after one iteration. It should be noticed that the map is invariant with respect to the transformation $(x, y, \mu_1, \mu_2) \to (-x, -y, -\mu_1, \mu_2)$, and hence bifurcations curves in the (μ_1, μ_2)-parameter plane are symmetric with respect to the μ_2-axis. □

C.6.#74. Find analytically the equations of the basic bifurcation curves of the fixed points and period-2 cycles of these maps.

Partial solution: the curve SN corresponding to a fixed point with multiplier $+1$ is given by

$$\mu_1 = \pm\frac{2}{3}\left(\frac{-1+b-\mu_2}{3d}\right)^{\frac{1}{2}} ;$$

that with multiplier -1 is given by

$$\mu_1 = \pm\frac{2}{3}\left(\frac{-1+b-\mu_2}{3d}\right)^{\frac{1}{2}} (2+2b-\mu_2)\,.$$

The bifurcation curves of the period-2 cycle with multiplier $+1$ are given by

$$\mu_1 = \pm\frac{2}{3\sqrt{3}}(-\mu_2-2(b+1))^{\frac{3}{2}}, \qquad \text{at } d=+1\,,$$

$$\mu_1 = \pm\frac{2}{3\sqrt{3}}(\mu_2+2b-1)^{\frac{3}{2}}, \quad \mu_2 > -\frac{2}{3}(b+1), \qquad \text{at } d=-1\,,$$

Those corresponding to period-4 doubling are given by

$$\mu_1^2 = \frac{1}{216d}(b(b+1)+\mu_2 \pm q)^2(-5\mu_2-6(b+1)\pm q)\,,$$

where $q = \sqrt{(3\mu_2+2b+2)^2-8(b^2+1)}$. □

C.6.#75. The following system is an asymptotic normal form for the bifurcation of an equilibrium state with triple zero characteristic exponent [162, 163]

$$\dot{x} = y\,,$$

$$\dot{y} = z\,,$$

$$\dot{z} = ax - x^2 - by - z\,,$$

in the case of complete Jordan block (continued from Sec. C.2). Here a and b are control parameters. A fragment of the bifurcation diagram of this system

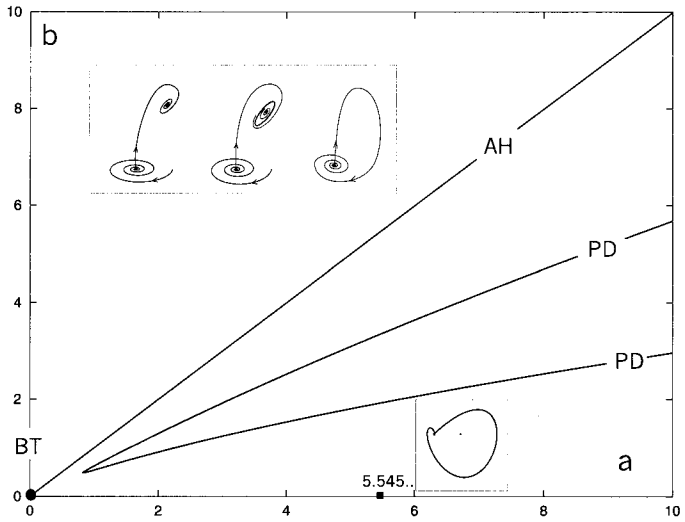

Fig. C.6.6. A part of the bifurcation diagram. AH labels the Andronov-Hopf bifurcation of the non-trivial equilibrium state O_1; PD labels a flip-bifurcation of the stable periodic orbits that generates from O_1.

is shown in Fig. C.6.6. For $a, b \geq 0$, this system has two equilibrium states: $O(0,0,0)$ and $O_1(a,0,0)$. The origin $a = b = 0$ corresponds to the Bogdanov-Takens bifurcation of codimension two (see Sec. 13.4).

Let us describe the essential bifurcations in this system on the path $b = 2$ as μ increases. On the left of the curve AH, the equilibrium state O_1 is stable. It undergoes the super-critical Andronov-Hopf bifurcation on the curve AH. The stable periodic orbit becomes a saddle through the period-doubling bifurcation that occurs on the curve PD. Figure C.6.7 shows the unstable manifold of the saddle periodic orbit homeomorphic to a Möbius band. As a increases further, the saddle periodic orbit becomes the homoclinic loop to the saddle point $O(0,0,0,)$ at $a \simeq 5.545$. What can one say about the multipliers of the periodic orbit as it gets closer do the loop? Can the saddle periodic orbit shown in this figure get "pulled apart" from the double stable orbit after the flip bifurcation? In other words, in what ways are such paired orbits linked in $\mathbb{R}^3$, in $\mathbb{R}^4$? □

C.6.#76. Using a computer detect the bifurcation curve in the (a, b)-parameter plane that corresponds to the pitch-fork bifurcation of a symmetric

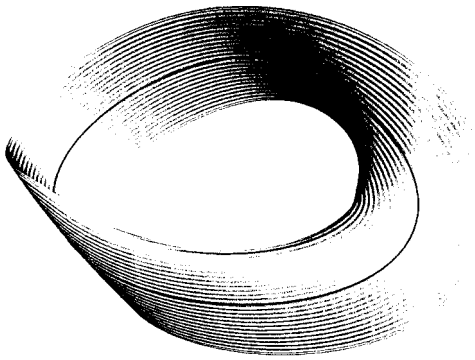

Fig. C.6.7. Shown is a piece of the stable manifold of the saddle periodic orbit (dark circle) at $a = 3.2$; courtesy of H. Osinga and B. Krauskopf [181].

periodic orbit in the Shimizu-Morioka model [191]:

$$\begin{aligned} \dot{x} &= y\,, \\ \dot{y} &= x - xz - ay\,, \\ \dot{z} &= -bz + x^2\,, \end{aligned} \tag{C.6.21}$$

at $a \simeq 0.4$ and $b \simeq 0.45$. Can a symmetric limit cycle go through a period-doubling bifurcation in this system? In the Lorenz equation? In a Chua circuit? What makes the difference? □

C.6.#77. Let us consider an example of a system with torus bifurcation. Our example here is the following model coming from meteorology [128, 183]

$$\begin{aligned} \dot{x} &= -y^2 - z^2 - ax + aF\,, \\ \dot{y} &= xy - bxz - y + G\,, \\ \dot{z} &= bxy + xz - z\,. \end{aligned} \tag{C.6.22}$$

It follows from the linear stability analysis (see Sec. C.2) that the (a, b)-parameter plane has a codimension-two point corresponding to an equilibrium state with characteristic exponents $(0, \pm i\omega)$. Therefore, the dimension of the center manifold in such a case must be equal to 3 at least. For the complete account on this bifurcation the reader is referred to [51, 64]. Below, we will give its brief outline.

Observe that at such a codimension-two point the Andronov-Hopf and saddle-node bifurcations occur simultaneously. Let μ_1 and μ_2 be the same

parameters that govern these bifurcations in each versal family, respectively:

$$\begin{cases} \dot{r} = r(\mu_1 + L_1 r^2) + \cdots , \\ \dot{\varphi} = \omega(\mu_1) + \Omega(\mu_1) r^2 + \cdots , \\ \dot{z} = \mu_2 - z^2 + \cdots , \end{cases}$$

where $\omega(0) \neq 0$, $\Omega(0) \neq 0$, and L_1 denotes a Lyapunov value. Taking the interaction into account, the resulting normal form can be written as

$$\begin{aligned} \dot{r} &= r(\tilde{\mu}_1 + L_1 r^2 + az + z^2) + O(|(r,z)|^4) , \\ \dot{z} &= \tilde{\mu}_2 + z^2 + br^2 + O(|(r,z)|^4) , \\ \dot{\varphi} &= \omega + cz + O(|(r,z)|^2)) , \end{aligned}$$

where a, b may be set ± 1. Note that if we drop the $O(|(r,z)|^4)$-terms, the system becomes invariant with respect to rotation around the z-axis, so its trajectories lie on integral surfaces determined by trajectories of the planar system consisting of the first two equations, which are decoupled from the third one. In this planar system, equilibrium states with $r = 0$ correspond to equilibrium states of the three-dimensional normal form, those with $r \neq 0$ correspond to periodic orbits, and a structurally stable limit cycle will correspond to an invariant torus. Depending on the signs of a and b, there may be four essentially different cases. We will focus on the case $a = -1$ and $b = 1$ only where the torus-bifurcation takes place, and leave the other ones for exercises on linear stability analysis. The corresponding bifurcation diagram is shown in Fig. C.6.8. Let us describe next the corresponding bifurcations in terms relevant to the original three-dimensional system (C.6.22).

The point O_1 is repelling in the region to the right of AH. On the left of AH it becomes a saddle-focus (2,1) and a repelling periodic orbits generates from it. This periodic orbit is the edge of the stable manifold of O_1 (Fig. C.6.9(a)). This periodic orbit becomes stable upon crossing TB, and a repelling two-dimensional invariant torus bifurcates from it (see Fig. C.6.9(b)). This torus becomes the heteroclinic connection between both saddle-foci (Fig. C.6.9(c)) on the curve H in Fig. C.6.8.

The bifurcations described above are subject to the condition of invariance with respect to rotation around the z-axis. The straight-line $r = 0$ is then an integral curve, and in the case where O_1 and O_2 are both saddles, this is

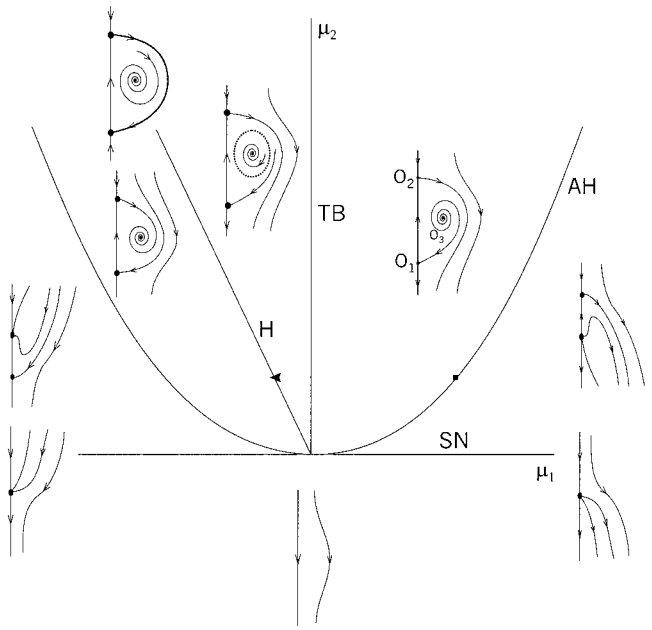

Fig. C.6.8. Unfolding of the planar system with $a = -1$ and $b = 1$.

their common one-dimensional separatrix. Moreover, in such symmetrical systems, both two-dimensional stable and unstable invariant manifolds of these saddles may either coalesce or have no common points. In generic systems which are not rotationally invariant, one-dimensional separatrices of the saddles may coincide at particular (codimension-two) parameter values, whereas two-dimensional manifolds of the saddles may cross transversely each other along some trajectories for an open set of parameters. Taking into account the terms destroying the rotational symmetry may significantly change the structure of the heteroclinic connection, namely it may split. If this is the case, the situation is likely where a one-dimensional separatrix becomes bi-asymptotic to either saddle-focus shown in Fig. C.6.9(d). Moreover, if the saddle value is positive at either saddle-focus, the separatrix loop will give rise to a homoclinic explosion when the neighborhood is filled by infinitely many saddle periodic orbits (see Sec. 13). □

C.6.#78. The Medvedev's construction of the blue-sky catastrophe on the torus [95] is illustrated by Fig. C.6.11. It is supposed that there exists a pair

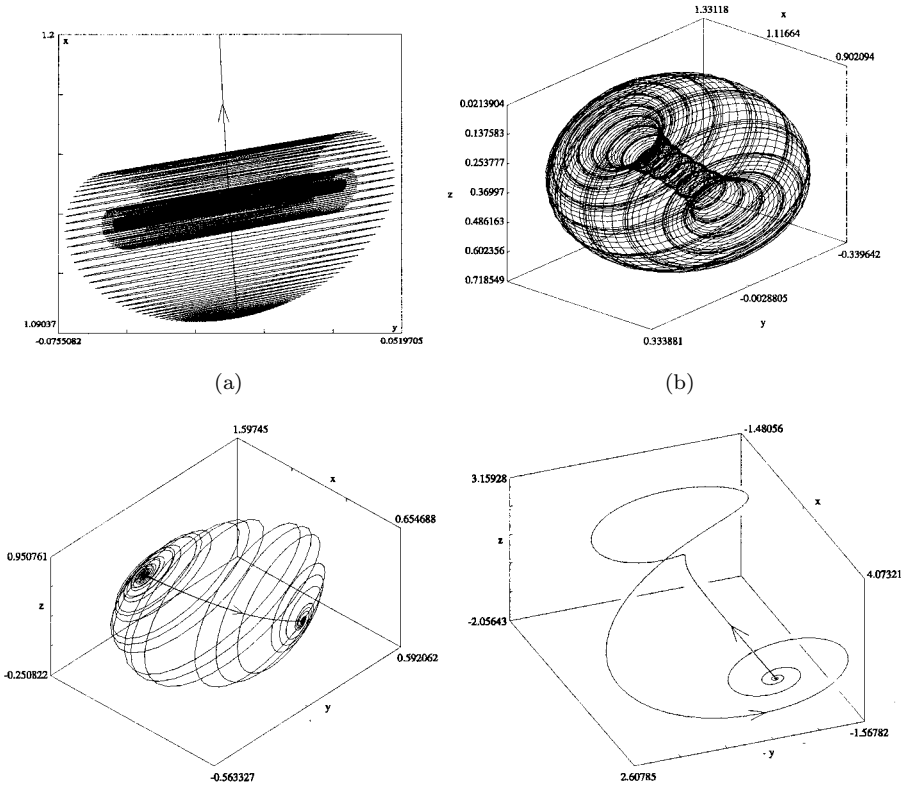

(a) (b)

(c) (d)

Fig. C.6.9. Phase portraits of system (C.6.22): (a) $(F = 1.77, G = 1.8)$; (b) $(F = 1.8, G = 1.65)$; (c) $(F = 1.8, G = 1.5)$; (d) $(F \simeq 1.416, G \simeq 2.195)$.

of saddle-node cycles C_1 and C_2 on the torus at some $\mu = 0$. By introducing the direction of the motion of the torus, one can assign that one cycle rotates in the clockwise direction whereas the other one spins in the opposite direction. Discuss the way on how the blue-sky catastrophe may flow in. How many cycles of what stability can appear through this bifurcation? Let $n_1(\mu)$ and $n_2(\mu)$, $\mu > 0$ be the number of gyrations which a closed trajectory on the torus makes near the ghosts of $C_{1,2}$. What is $\lim_{\mu \to +0} n_{1,2}(\mu)$? □

C.6.#79. Challenge: following the underlying idea on the development of the blue-sky catastrophe in a two time scales system which is discussed in

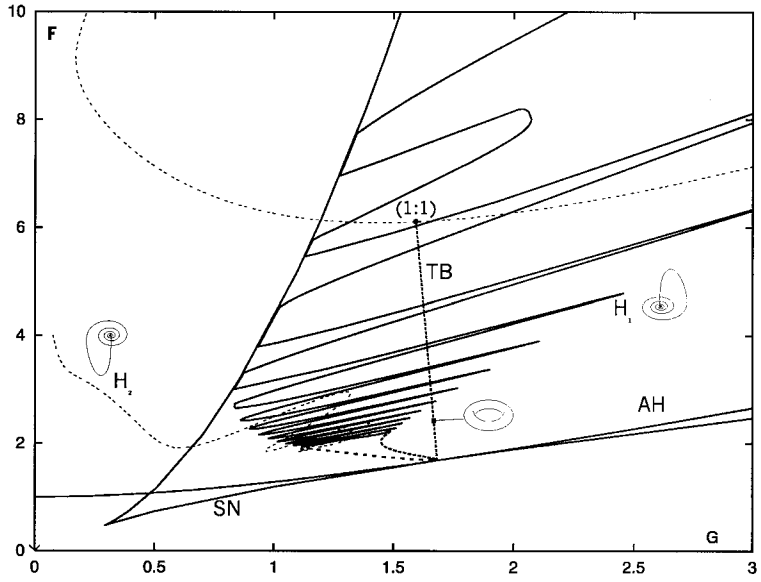

Fig. C.6.10. Part of the bifurcation diagram of the system (C.6.22).

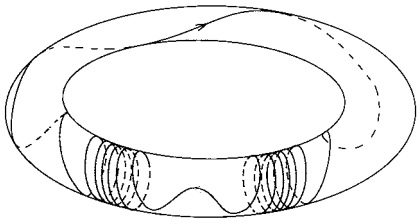

Fig. C.6.11. Blue-sky catastrophe on a torus.

Sec. 12.4, find the blue-sky catastrophe in the modified Hindmarsh-Rose model of neuronal activity

$$\begin{aligned} \dot{x} &= y - z - x^3 + 3x^2 + 5\,, \\ \dot{y} &= -y - 2 - 5x^2\,, \\ \dot{z} &= \varepsilon(2(x + 2.1) - z) - \frac{A}{(z - 1.93)^2 + 0.003}\,, \end{aligned} \tag{C.6.23}$$

where A and ε are two control parameters. Figure C.6.12 represents the bifurcation diagram of the slow system. Prove the stability of the resulting periodic

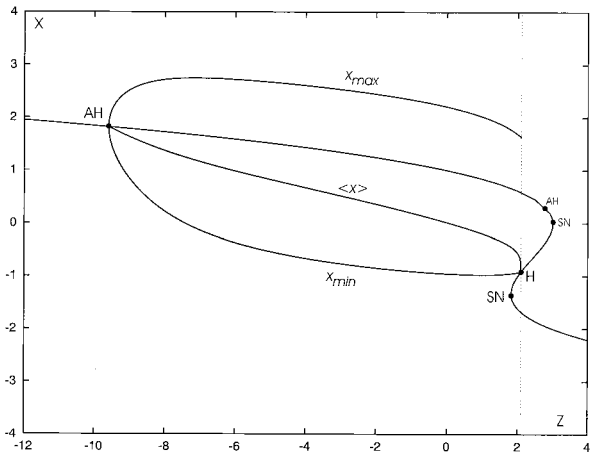

Fig. C.6.12. Plot of the x-coordinate of the equilibrium state versus z at $\varepsilon = 0$. The symbols $x_{\min}$, $x_{\max}$ and $\langle x \rangle$ denote, respectively, the maximal, minimal and averaged values of the x-coordinates of the stable limit cycle which bifurcates from a stable focus at AH and terminates in the separatrix loop to the saddle O (see the next figure) at the point H: $z \simeq 2.086$.

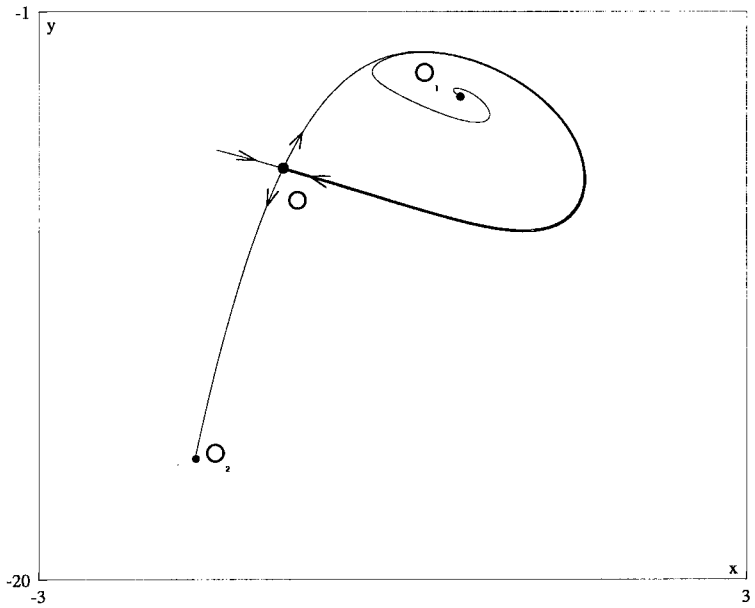

Fig. C.6.13. A separatrix loop to the saddle O at $z \simeq 2.086$ and $\varepsilon = 0$.

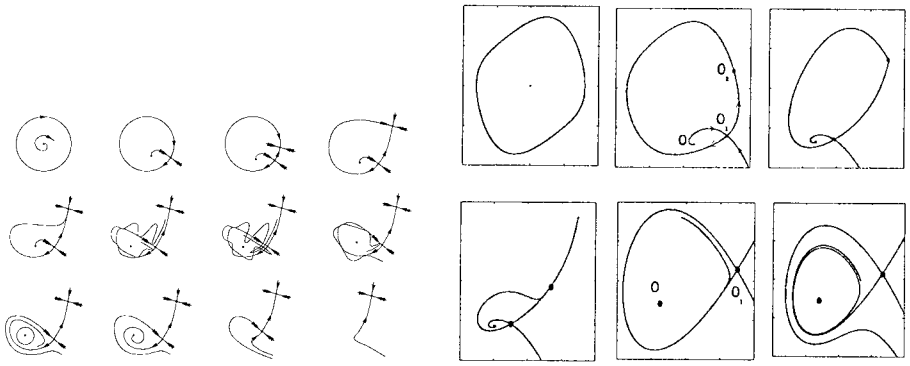

(a) (b)

Fig. C.6.14. Shift map over $2\pi/\omega$: ideal bifurcation puzzle (a) and numeric result (b) for $a = 0.4$, $\omega = 0.893$, and at $\beta = 0.0, 0.37, 0.37409, 0.375, 0.376, 0.3761$. Both figures are courtesy of B. Krauskopf and H. Osinga [180].

orbit. How can you explain the delayed loss of stability of the equilibrium state O_1: contrast the corresponding diagram at zero and small nonzero ε. The curious reader is advised to consult [21] for more details concerning this phenomenon. □

C.6.#80. Study a mechanism of the appearance and breakdown of an invariant torus in the periodically forced Van der Pol equation

$$\begin{aligned} \dot{x} &= y\,, \\ \dot{y} &= -x - a(x^2-1)y + \beta\cos\omega t\,, \\ \dot{t} &= \omega\,, \end{aligned} \tag{C.6.24}$$

as β increases from zero; Start with the Andronov-Hopf bifurcation of the origin in the unperturbed equation. What occurs with the limit cycle at $a = 2$? The phenomenological scenario of the evolution of the torus is shown in Fig. C.6.14. What bifurcations precede its breakdown, and when does it lose its smoothness? Attention should be drawn to the behavior of the separatrices of the saddle near the stable resonant cycle. □

C.7 Homoclinic bifurcations

Homoclinic bifurcations are *a priori* not a local problem. The detection of a homoclinic bifurcation in a specific set of ODE's is an art in itself. Besides,

it often requires performing rather sophisticated numerical computations. However, as we have seen in our study of the Bogdanov-Takens normal form, in some specific cases one can prove analytically the existence of a homoclinic loop. This concerns systems close to integrable ones. Another instance is that of systems with piece-wise linear right hand sides, as well as by two time scales systems with slow and fast variables. Nevertheless, these examples are exceptions. As for generic nonlinear dissipative systems are concerned, the situation is quite non-trivial, especially if the saddle in question has unstable and stable manifolds of dimensions equal or exceeding two (so far, the known regular numerical methods are applied well to saddles with one-dimensional stable or unstable separatrices). What really simplifies the problem is that there are not so many bifurcation scenarios that usually precede the appearance of the homoclinic loop. We will illustrate some of them below. However, this list is undoubtedly incomplete, and we hope that the lucky reader will run into novel bifurcations in further research.

A homoclinic bifurcation is a composite construction. Its first stage is based on the local stability analysis for determining whether the equilibrium state is a saddle or a saddle-focus, as well as what the first and second saddle values are, and so on. On top of that, one deals with the evolution of ω-limit sets of separatrices as parameters of the system change. A special consideration should also be given to the dimension of the invariant manifolds of saddle periodic trajectories bifurcating from a homoclinic loop. It directly correlates with the ratio of the local expansion versus contraction near the saddle point, i.e. it depends on the signs of the saddle values.

C.7.#81. Following the same steps as in the study of the generic Bogdanov-Takens normal form, analyze the structure of the bifurcation set near the origin $\mu_1 = \mu_2 = 0$ in the Khorozov-Takens normal form with reflection symmetry:

$$\dot{x} = y\,,$$

$$\dot{y} = \mu_1 x + \mu_2 y \pm x^3 - x^2 y\,.$$

The rescaling

$$x \to \varepsilon u, \quad y \to \varepsilon^2 v, \quad |\mu_1| \to \varepsilon^2, \quad \mu_2 \to \varepsilon^2 \nu, \quad t \to t/\varepsilon$$

gives

$$\dot{u} = v\,,$$
$$\dot{v} = \gamma u + \nu v \pm u^3 - \varepsilon u^2 v\,,$$

where $\gamma = \text{sign}\ \mu_1 = \pm 1$. Then, at $\varepsilon = 0$, the system becomes a Hamiltonian one

$$\dot{u} = -\frac{\partial H}{\partial v}\,,$$
$$\dot{v} = \frac{\partial H}{\partial u}\,,$$

with the first integral

$$H = \frac{v^2}{2} + \gamma\frac{u^2}{2} \pm \frac{u^4}{4}\,.$$

The most interesting case is when the sign of γ is opposite to the sign of the coefficient of the fourth-order term in H, so let us assume further

$$H = \frac{v^2}{2} + \gamma\frac{u^2}{2} - \gamma\frac{u^4}{4}\,.$$

This integrable system has three equilibrium states $O(0,0)$ and $O_{1,2}(\pm 1, 0)$. When $\gamma = 1$, the origin is a center while $O_{1,2}$ are the saddles [see Fig. C.7.1(a)].

The saddles have a closed symmetric heteroclinic connection at the level $H = 1/4$. The equations of the trajectories connecting the saddles can be found explicitly, and for the upper one it is given (verify this) by

$$u = \frac{e^{\sqrt{2}t} - 1}{e^{\sqrt{2}t} + 1}, \qquad v = \frac{2\sqrt{2}e^{\sqrt{2}t}}{(e^{\sqrt{2}t} + 1)^2}\,.$$

In the case $\gamma = -1$, the origin becomes a saddle and $O_{1,2}$ are centers [see Fig. C.7.1(b)]. The distinguishable figure-of-eight lies at the zero level of the associated Hamiltonian. The equation of its right lobe is given by

$$u(t) = \frac{2\sqrt{2}e^{t}}{1 + e^{2t}}, \qquad v(t) = \frac{2\sqrt{2}e^{t}(1 - e^{2t})}{(1 + e^{2t})^2}\,.$$

The heteroclinic connection or the homoclinic-8 in a perturbed system persists on the curve $\mu_2 = \nu\mu_1 + O(\mu_1^2)$, where ν is found from the condition

$$\int_{-\infty}^{+\infty} \frac{\partial}{\partial\varepsilon}\,\frac{d}{dt} H(u(t), v(t))dt\Big|_{\varepsilon=0} = 0\,.$$

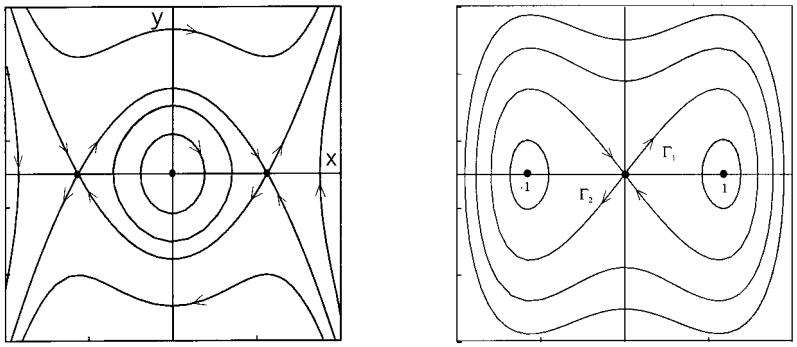

(a) (b)

Fig. C.7.1. Integral curves of the Hamiltonian systems: cases $\gamma = 1$(a) and $\gamma = -1$(b).

The latter can be rewritten as

$$\nu = \frac{\int_{-\infty}^{+\infty} u^2(t)v(t)dt}{\int_{-\infty}^{+\infty} v(t)dt}\,,$$

which gives

$$\nu = \frac{1}{5}, \quad \text{and} \quad \frac{4}{5}\,,$$

respectively, for each case. Compute the saddle value on the curve $H8$ in the case $\gamma = -1$. Show that the stable symmetric limit cycle cannot terminate in the homoclinic-8 on this curve. See the complete bifurcation diagrams in Fig. C.7.2.

C.7.#82. Apply the Shilnikov theorem and explain what kind of behavior one should anticipate in the Rössler system [172, 188]

$$\dot{x} = -y - z\,,$$

$$\dot{y} = x + ay\,,$$

$$\dot{z} = 0.3x - cz + xz\,,$$

near the homoclinic loops of the saddle-foci O shown in Fig. C.7.3. Determine the corresponding characteristic exponents, and evaluate the saddle values.

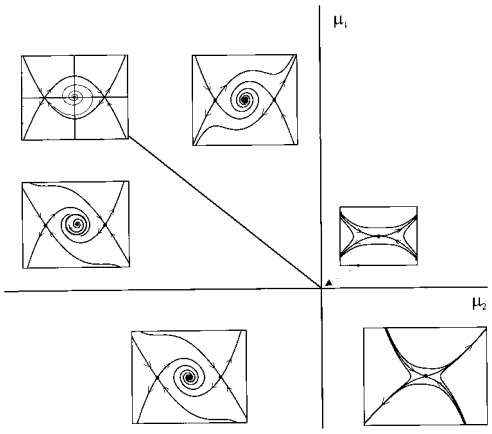

(a)

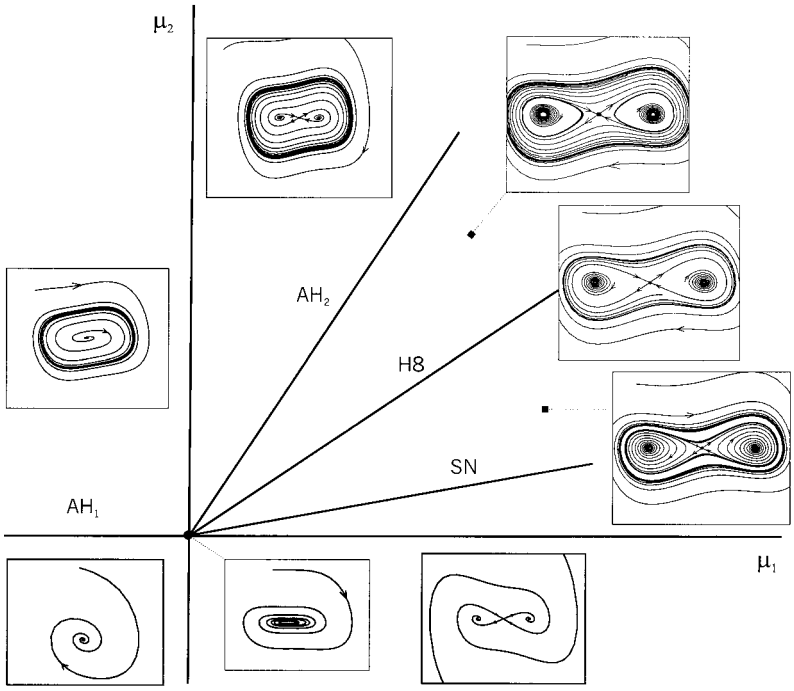

(b)

Fig. C.7.2. Bifurcation diagrams of the Khorozov-Takens normal form.

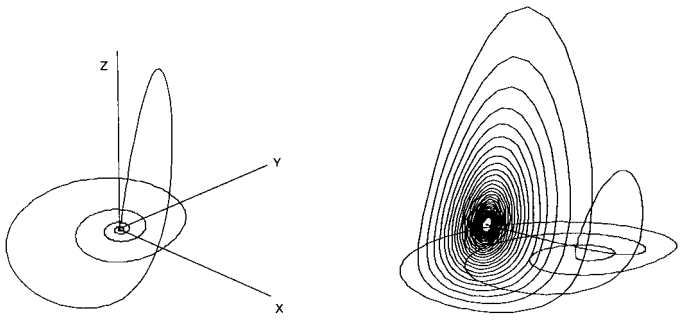

(a) (b)

Fig. C.7.3. Homoclinic loops to the saddle-foci O and O_1 in the Rössler model for $(a = 0.380, c = 4.820)$ and $(a = 0.4853, c = 4.50)$, respectively. Initial conditions are chosen on the unstable manifolds at a distance of about 0.47 from O on the plane $y = 0$, and about 0.14 from O_1, respectively.

Direct computation reveals that for the given parameters the saddle-focus O has the exponents $\lambda_{1,2} \simeq 0.1597 \pm i0.9815$ and $\lambda_3 \simeq -4.7594$. Since the complex exponents $\lambda_{1,2}$ are nearest to the imaginany axis, the homoclinic loop implies the emergence of infinitely many saddle periodic orbits. Moreover, since the second saddle value $\sigma_2 = \lambda_3 + 2\mathrm{Re}\lambda_{1,2}$ is negative (here it is equal to the divergence of the vector field at O), it follows that near the homoclinic loop there may also exist stable periodic orbits along with saddle ones. These stable orbits have long periods and weak attraction basins, and therefore they are practically invisible in numerical experiments.

In the second case, the equilibrium state O_2 has the characteristic exponents $(-0.0428 \pm 3.1994, 0.4253)$. In contrast to the first case, there are no stable periodic ordits in a small neighborhood of the loop, because the divergence of the vector field at O_2 is positive. □

C.7.#83. Consider the following $\mathbb{Z}_2$-symmetric Chua's circuit with cubic nonlinearity [179]:

$$\begin{aligned} \dot{x} &= a\left(y - \frac{x}{6} + \frac{x^3}{6}\right), \\ \dot{y} &= x - y + z, \\ \dot{z} &= -by, \end{aligned} \tag{C.7.1}$$

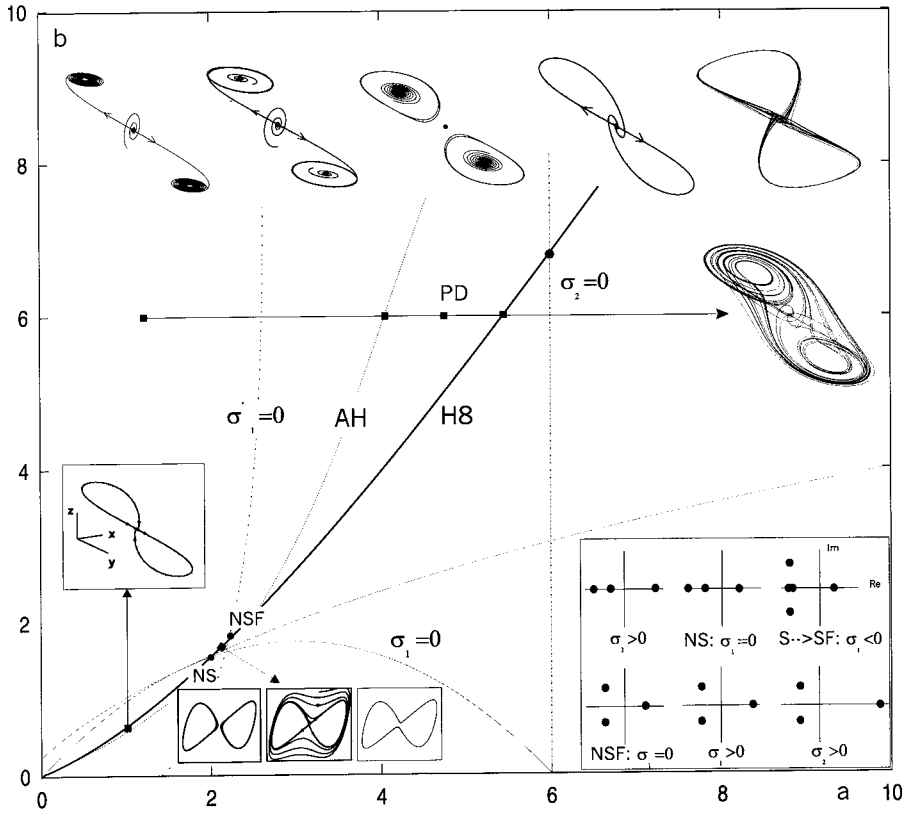

Fig. C.7.4. Bifurcation diagram for the Chua's circuit.

where $a \geq 0$ and $b \geq 0$ are control parameters. When $a = b = 0$, the bifurcation unfolding of (C.7.1) is the same as that of the Khorozov-Takens normal form. In particular, it includes the bifurcation of a homoclinic-8. Thus, the corresponding bifurcation curve, labeled $H8$, starts from the origin in the (a, b)-parameter plane in Fig. C.7.4. Of special consideration here are the four codimension-two points on this curve at which the following resonant conditions hold (after Sec. C.2):

(1) NS ($a \simeq 1.13515, b \simeq 1.07379$) corresponds to the saddle (at the origin) with zero saddle value σ. Below this point, σ is positive.

(2) The point $S \to SF$ ($a \simeq 1.20245, b \simeq 1.14678$) corresponds to the transition from a saddle to a saddle-focus (2,1). It is important that $\sigma < 0$ at this point.
(3) The abbreviation NSF stands for the neutral saddle-focus at which the saddle value σ vanishes.
(4) Introduce the second saddle value σ_2 as the sum of the three leading characteristic exponents at the saddle-focus. In the three-dimensional case, it is the divergence of the vector field at the origin. Here, the curve $\sigma_2 = 0$, given by the equation $a = 6$, intersects $H8$ at ($a = 6, b = 7.19137$). Above this point, $\sigma_2 > 0$.

These points break the bifurcation curve $H8$ into the four segments the trajectory behaviour on which is described next.

Segment $(0, NS)$:

On this interval, the homoclinic-8 bifurcates in the same way as in the Khorozov-Takens normal form. Both loops, which form the homoclinic-8 are orientable. The dimension of the center homoclinic manifold is equal to 2. The third dimension does not yet play a significant role. Therefore, it follows from the results in Sec. 13.7 that on the right of $H8$, there are two unstable cycles (*cycles* 1 *and* 2 in Fig. 13.7.9). To the left of $H8$, a symmetric saddle periodic orbit (cycle 12) bifurcates from the homoclinic-8 (see also Fig. C.7.5).

The point NS. This point is of codimension two as $\sigma = 0$ here. The behavior of trajectories near the homoclinic-8, as well as the structure of the bifurcation set near such a point depends on the separatrix value A (see formula (13.3.8)). Moreover, they do not depend only on whether A is positive (the loops are orientable) or negative (the loops are twisted), but it counts also whether $|A|$ is smaller or larger than 1. If $|A| < 1$, the homoclinic-8 is "stable", and unstable otherwise. To find out which case is ours, one can choose an initial point close sufficiently to the homoclinic-8 and follow numerically the trajectory that originates from it. If the figure-eight repels it (and this is the case in Chua's circuit), then $|A| > 1$. Observe that a curve of double cycles with multiplier $+1$ must originate from the point NS by virtue of Theorem 13.5.

On the segment between NS and NSF, the saddle value is negative, i.e., $\sigma < 0$. Moving up along $H8$, we go through the point above which the origin becomes a saddle-focus. By virtue of Theorem 13.11, in either case (i.e., when the origin is a saddle, or a saddle focus with $\sigma < 0$), only two stable cycles, or a single symmetric stable cycle bifurcate from the homoclinic-8 on

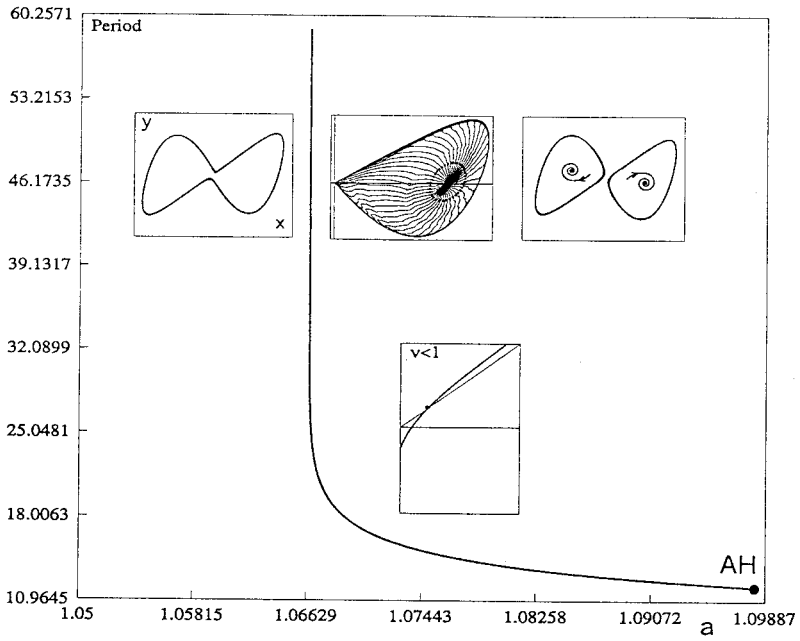

Fig. C.7.5. Period T of the periodic orbit born through a sub-critical Andronov-Hopf bifurcation versus the parameter a ($b = 1$), as the cycle approaches the homoclinic loop. The origin is a saddle with $\sigma > 0$.

the opposite sides from $H8$. Therefore, the point $S \to SF$ is not a bifurcation point. However, by introducing a small perturbation, that breaks down the symmetry of Chua's circuit, one can make the resulting bifurcation unfolding essentially different (see the contrast in Figs. 13.7.5 and 13.7.9). It should be merely noted that the transition from saddle to saddle-focus would cause dramatical changes in the dynamics of the system if σ were positive at such a point. Taking into consideration one homoclinic loop only, this would cause a homoclinic explosion from a single saddle periodic orbit in the case of a saddle to infinitely many ones in the case of a saddle-focus (see Theorems 13.7–10 and [29]).

The point NSF: $\sigma = 0$ corresponds to a neutral saddle-focus. At this codimension-two point the dynamics of the trajectories near the homoclinic loops to the saddle-focus becomes chaotic. This bifurcation indeed preceeds the origin of the chaotic double scroll attractor in Chua's circuit. In the general case, this bifurcation was first considered in [29]. The complete unfolding of

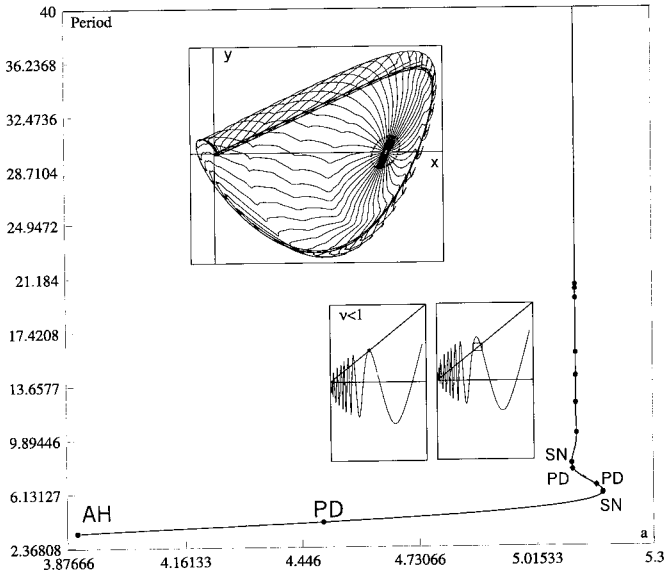

Fig. C.7.6. Dependence of period T of the periodic orbit generating via a super-critical Andronov-Hopf bifurcation on the parameter a ($b = 6$) as the cycle approaches the homoclinic loop to a saddle-focus with $\sigma > 0$.

such bifurcation is unknown. The brief outline of [29] is as follows: there is an infinite series of codimension-1 bifurcation curves that accumulate to the curve $H8$ above the point NSF. These curves correspond to subsequent homoclinic bifurcations, saddle-node and period doubling bifurcations of periodic orbits close to the primary homoclinic one. To understand this phenomena (homoclinic explosion) one may examine a simplified picture of the evolution of the one-dimensional map with the saddle index $\nu > 1$ (corresponding to $\sigma < 0$), and $\nu < 1$ ($\sigma > 0$) shown in Fig. C.7.6. Recall that in the case under consideration, $\nu = |\mathrm{Re}\lambda^*|/\lambda_1$, where $\lambda_1 > 0$ and λ^* is the real part of the complex-conjugate pair of the exponents at the saddle-focus. One can see from this figure that the period of the periodic orbit tends to infinity as the parameter converges to the critical value. In the saddle-focus case with $\nu < 1$, it has a distinctive oscillatory component. Every turning point, corresponds to the saddle-node bifurcation which is followed by a period-doubling bifurcation. Therefore, there takes place an infinite sequence of such bifurcations accumulating to the homoclinic one [173].

Thus, in a neighborhood of the homoclinic loop to the saddle-focus with $\nu < 1$, there may exist structurally unstable periodic orbits, in particular saddle-nodes. This gives rise to the question: does the saddle-node bifurcations of periodic orbits result in the appearance of stable ones?

To answer it, one must examine the two-dimensional Poincaré map instead of the one-dimensional one, and evaluate the Jacobian of the former map. If its absolute value is larger than one, the map has no stable periodic points, and hence there are no stable orbits in a neighborhood of the homoclinic trajectory because the product of the multipliers of the fixed point is equal to the determinant of the Jacobian matrix of the map. One can see from formula (13.4.2) that the value of the Jacobian is directly related to whether $2\nu - 1 > 0$ or $2\nu - 1 < 0$, or, equivalently, $\nu > 1/2$ or $\nu < 1/2$. Rephrasing in terms of the characteristic exponents of the saddle-focus, the above condition translates into whether the second saddle value $\sigma_2 = \lambda_1 + 2\mathrm{Re}\lambda^*$ is positive or negative. It can be shown [100] that if $\sigma > 0$ but $\sigma_2 < 0$ ($a < 6$ in Fig. C.7.4), there may be stable periodic orbits near the loop, along with saddle ones. However, when $\sigma_2 > 0$ ($\sigma > 0$, automatically), totally unstable periodic orbits emerge from the saddle-node bifurcations.

The last comment on the Chua circuit concerns the bifurcations along the path $b = 6$ (see Fig. C.7.4). Notice that this sequence is very typical for many symmetric systems with saddle equilibrium states. We follow the stable periodic orbit starting from the super-critical Andronov-Hopf bifurcation of the non-trivial equilibrium states at $a \simeq 3.908$. As a increases, both separatrices tend to the stable periodic orbits. The last ones go through the pitch-fork bifurcations at $a \simeq 4.496$ and change into saddle type. Their size increases and at $a \simeq 5.111$, they merge with the homoclinic-8. This, as well as subsequent bifurcations, lead to the appearance of the strange attractor known as the double-scroll Chua's attractor in the Chua circuit. □

C.7.#84. Homoclinic bifurcations in the Shimizu-Morioka model [127]:

$$\begin{aligned} \dot{x} &= y\,, \\ \dot{y} &= x - ay - xz\,, \\ \dot{z} &= -bz + x^2\,. \end{aligned} \tag{C.7.2}$$

We will be seeking homoclinic bifurcations by starting from the Andronov-Hopf bifurcation at the non-trivial equilibria $O_{1,2}$ that takes place on the curve AH: $b = \frac{(2-a^2)}{a}$ (see Sec. C.2). This bifurcation can be super-critical — the first

Lyapunov value is negative to the right of the point GH, and it is subcritical to the right of the point GH. Let us consider next the evolution of the behavior of the separatrices of the saddle O at the origin as the parameter a decreases while keeping $b = 0.9$ fixed. Above AH the separatrices tend to the stable equilibria $O_{1,2}$ which looses stability via an Andronov-Hopf bifurcation at $a \simeq 1.0341$. In the region between AH and HB the separatrices are attracted to the newborn stable periodic orbits. As a decreases further, the amplitude of the stable orbits increases, and they both merge with the origin at $a \simeq 0.8865$, thereby forming a homoclinic butterfly. Such a symmetric homoclinic bifurcation with $\sigma < 0$ is often called a *gluing* bifurcation regardless of the geometry the homoclinic configuration which can be a butterfly or a figure-eight. One can see that the leading direction at the saddle in the given parameter values is the z-axis corresponding to the eigenvalue $\lambda_2 = -b$. Therefore, in our classification we are dealing with a homoclinic butterfly: both separatrices enter the saddle touching each other. The homoclinic butterfly transforms into a figure-8 when the separatrices enter the saddle from the opposite direction given by the eigenvector of the other negative eigenvalue which becomes leading when $\lambda_2 < \lambda_3 = -a/2 - \sqrt{a^2/4 + 1}$ on HB. In both cases, upon exiting from the homoclinic bifurcation a stable symmetric periodic orbit appears. Thus, the results of the homoclinic metamorphosis is always the same if $\sigma < 0$. This is not the case when $\sigma > 0$ where the geometry of the homoclinics is a key factor.

The more important resonant condition on HB takes place at ($a \simeq 1.044$, $b \simeq 0.608$) where the saddle value σ vanishes (see Sec. 13.6). Near such a point the local consideration reduces to the corresponding truncated"normal form" — a one-dimensional Poincaré map

$$\bar{x} = (-\mu + A|x|^{1+\sigma})\,\mathrm{sign}(x)\,, \tag{C.7.3}$$

where $\|\mu, \sigma\| \ll 1$, A is a separatrix value. In our interpretation, the fixed point at the origin at $\mu = 0$ corresponds to the homoclinic butterfly. It follows from Sec. 13.6 that the structure of the bifurcation unfolding near such a codimension-two point counts strongly on the magnitude and the sign of A. We have earlier emphasized the role of A, but it is worth repeating that the sign of A determines the orientation of homoclinic loops. Moreover, in the "linear case" (i.e. at $\sigma = 0$), the value of A also determines the stability of the homoclinic butterfly. There is almost no way to find the value of A in the specific set of ODE's without computer simulations. The simplest way to do that is to carry out a numerical experiment analogous to that we have already used in the

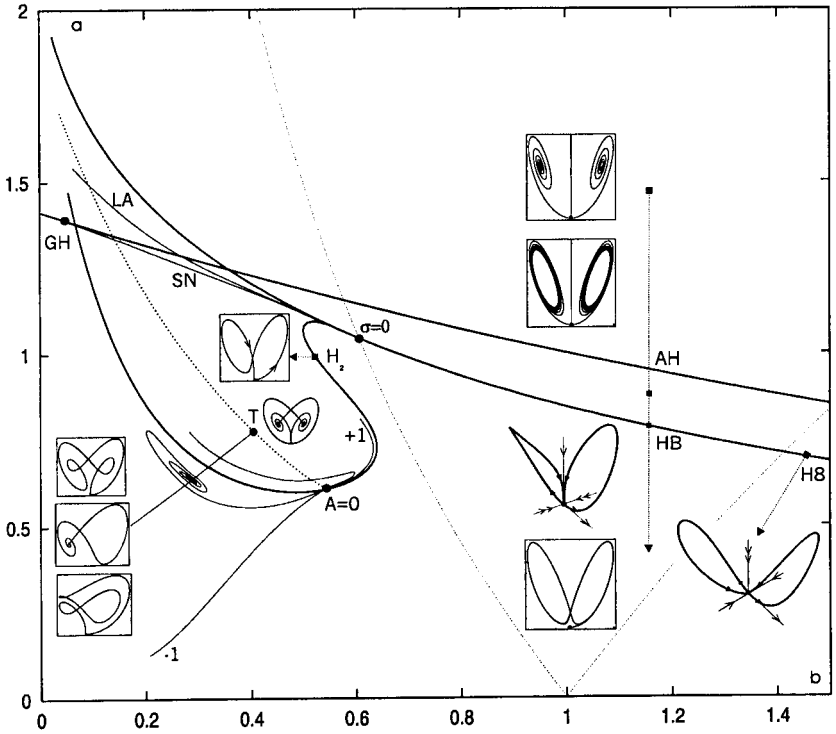

Fig. C.7.7. Fragment of bifurcation diagram of the Shimizu-Morioka model.

analysis of the Chua's circuit. The separatrix value will satisfy $|A| < 1$ if the separatrices of the saddle remain in a small neighborhood of the homoclinic butterfly after it splits. The other issue is how to determine the "orientation" condition, i.e., to find whether A is positive or negative; and we will return to this question later.

It is not hard to conclude from numerical experiments, which reveal the manner in which the separatrices converge to the homoclinic butterfly that A must be within the range (0,1). In this case, when $\sigma < 0$, everything is simple: the homoclinic butterfly splits into either two stable periodic orbits (Fig. C.7.8(g)), or just one stable symmetric periodic orbit (Fig. C.7.8(i)). It follows from Sec. 13.6 that when $\sigma > 0$, two bifurcation curves originate from this codimension-two point. They correspond to the saddle-node bifurcation (Fig. C.7.8(d)) and to the double homoclinic loop (Fig. C.7.8(f)). The

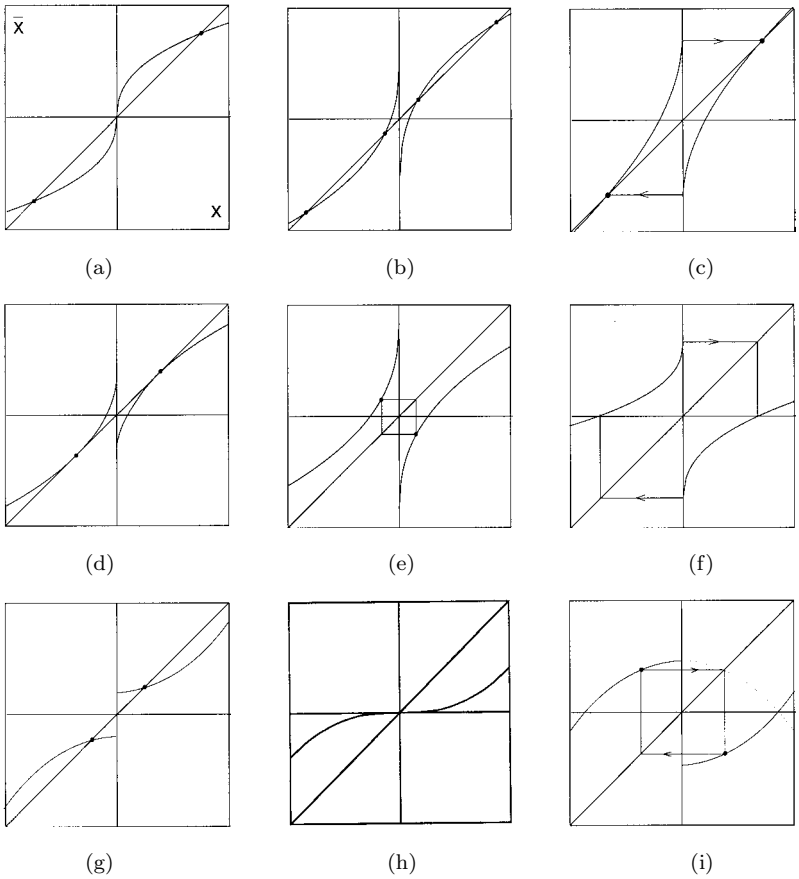

Fig. C.7.8. Bifurcations in one-dimensional map near the codimension-two point $\sigma = 0$; (a)–(f) corresponds to the case $\sigma > 0$, whereas (g)–(i) correspond to $\sigma < 0$.

symmetry adds to the problem a plethora of other bifurcation phenomena. Of very special interest is the bifurcation shown in Fig. C.7.8(c). It leads to the formation of the closed interval which is mapped onto itself. Furthermore, since the derivative of the map is larger than 1 on this integral, it contains no stable periodic points but infinitely many unstable ones. This is the moment of the appearance of the invariant attractive set without stable trajectories — a Lorenz-like attractor. In terms of the flow, this bifurcation occurs when the one-dimensional separatrices of the saddle at the origin lie on two-dimensional

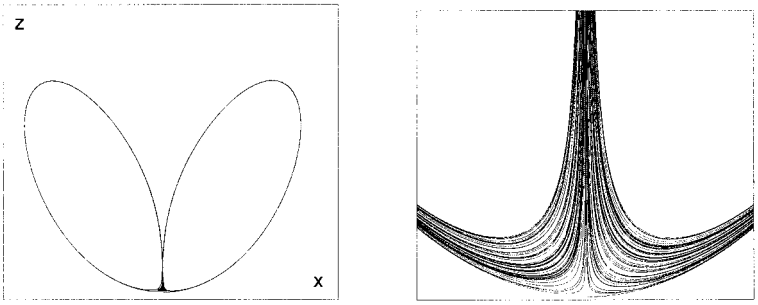

Fig. C.7.9. The Lorenz-like attractor in the Shimizu-Morioka model near the point $\sigma = 0$.

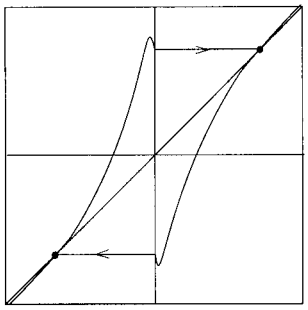

Fig. C.7.10. The Lorenz attractor does not appear if $A < 0$ on the curve LA.

stable manifolds of the saddle periodic orbits that have earlier bifurcated from each loop (see an analogous bifurcation for the Lorenz equation shown in Fig. C.7.14). Since $A > 0$, these manifolds are homeomorphic to a cylinder. This bifurcation occurs on the curve LA in Fig. C.7.7. Near the codimension-two point $\sigma = 0$, the Lorenz attractor is very thin, and looks like a stable periodic orbit (see Fig. C.7.9). Note that one should verify that the separatrix value A does not vanish anywhere on the curve LA. If so, there may arise the situation sketched in Fig. C.7.10 which shows schematically how the primary bifurcation of the Lorenz attractor can be ruined when the separatrix value A becomes negative. We will discuss this possibility below.

So far an important conclusion: since there is a homoclinic butterfly with $|A| < 1$, the region of the existence of the Lorenz attractor adjoins to the codimension-two point in the parameter space. The interested reader is advised to consult [127, 129, 187] on the bifurcations of Lorenz attractor in the

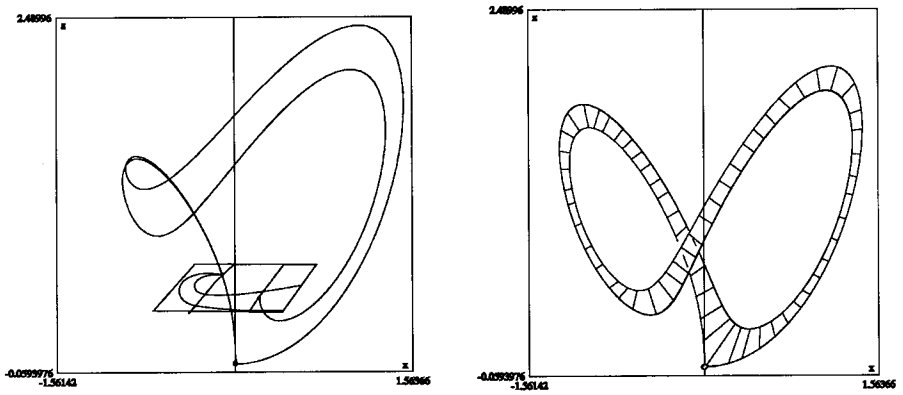

Fig. C.7.11. Twisted ($A < 0$) and orientable ($A > 0$) double homoclinic loops. The two-dimensional Poincaré map has a distinctive hook-like shape after the separatrix value A becomes negative.

Shimizu-Morioka model, and [114, 115, 117, 161] for the original Lorenz and some other Lorenz-like equations. □

C.7.#85. Consider the bifurcations of the symmetric cycle as σ evolves from positive to negative values. Can it undergo a period-doubling bifurcation? saddle-node one? Exploit the symmetry of the problem. For the map (C.7.3), find the analytical expression for the principal bifurcation curves. Does the saddle-node bifurcation here precede the appearance of the Lorenz attractor (i.e. can chaos "emerge through the intermittence")? Vary A from positive to negative values. Examine the piece-wise linear map with $A > 1$, and determine the critical value of A, after which the Lorenz attractor emerges. □

Another codimension-two homoclinic bifurcation in the Shimizu-Morioka model occurs at ($a \simeq 0.605, b \simeq 0.549$) on the curve H_2 corresponding to the double homoclinic loops. At this point, the separatrix value A vanishes and the loops become twisted, i.e. we run into inclination-flip bifurcation [see Figs. 13.4.8 and C.7.11]. The geometry of the local two-dimensional Poincaré map is shown in Fig. 13.4.5 and 13.4.6. To find out what our case corresponds to in terms of the classification in Sec. 13.6, we need also to determine the saddle index ν at this point. Again, as in the case of a homoclinic loop to the saddle-focus, it is very crucial to determine whether $\nu < 1/2$ or $\nu > 1/2$. Simple calculation shows that $\nu > 1/2$ for the given parameter values. Therefore,

the bifurcation unfolding for each of the homoclinic loops in the butterfly is the same as in Sec. 13.6. The following four bifurcation curves originate from such a point. They correspond to a saddle-node bifurcation (labeled "+1" in Fig. C.7.7), the period doubling ("−1"), and to two curves of the doubled separatrix loops (these curves end up spiraling to T-points in the (a, b)-plane). The dashed curve in the (a, b)-plane corresponds to the $A = 0$-axis in the bifurcation diagram in Fig. 13.6.4. Above this curve all homoclinic loops of the origin are orientable, and they are twisted below it. At each point of intersection of the curve $A = 0$ and a homoclinic bifurcation curve the structures of the bifurcation sets are similar, unless $\nu < 1/2$. The importance of this ratio becomes evident upon studying the one-dimensional Poincaré map

$$\bar{x} = (\mu + A|x|^{\nu} + |x|^{\gamma}) \operatorname{sign}(x)\,, \tag{C.7.4}$$

where $|\mu, A| \ll 1$, $\nu = |\lambda_2|/\lambda_1$, and $\gamma = |\max\{2\lambda_2, \lambda_3\}|/\lambda_1$; here $\lambda_{1,2}$ are, respectively, the leading unstable and stable characteristic exponents at the saddle, and λ_3 is a non-leading stable characteristic exponent.

When $A = 0$, the stability of the trajectories of the above map is determined by the third term. It is clear that depending on γ, the map for the parameter values on the curve $A = 0$ may be either a contraction if $\gamma > 1$, or an expansion if $\gamma < 1$. Assuming $2\lambda_2 > \lambda_3$, the condition on γ reduces to either $\nu < 1/2$ or $\nu > 1/2$. Thus, it is not hard to see that the map may have the form shown in Fig. C.7.8(a) at $\nu < 1/2$ and in Fig. C.7.8(h) at $\nu > 1/2$. If $\nu < 1/2$, there can be no stable points for zero values of A.

The structure of the bifurcation set of the truncated map (without the term $|x|^{\gamma}$) with $1/2 < \nu < 1$ and $A > 0$ is the same as in the above resonant case $\nu = 1$. The case $A < 0$ is presented in Fig. C.7.12(a)–(c). The reader is challenged to examine the bifurcations in this map. The feature of the case $A < 0$ is that the map may have an invariant attracting interval, which is mapped onto itself (Fig. C.7.12(c)). We can identify the chaotic behavior on this interval with a "non-orientable Lorenz attractor" [127, 129].

In terms of the flow, this means that for the parameter values from an exponentially narrow region in the parameter space, which adjoins to the point $A = 0$ on $H8$ from the side of $A < 0$, there exists a Lorenz-like attractor containing infinitely many saddle periodic orbits whose stable and unstable manifolds are homeomorphic to a Möbius band.

The one-dimensional map (C.7.4) has, when $A < 0$, a parabola-like graph shown in Fig. C.7.12(d)–(f). Obviously, one should foresee the period-doubling

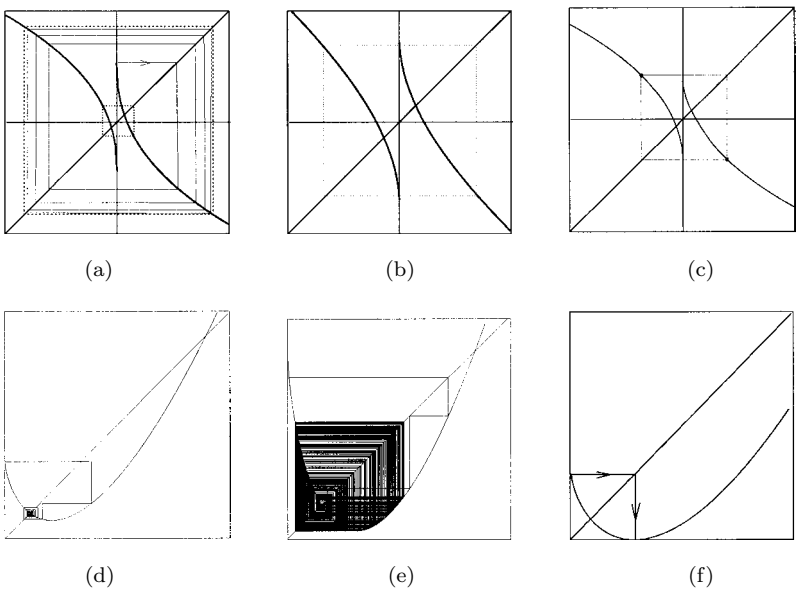

Fig. C.7.12. Transformations of the map (C.7.4) near $A \leq 0$.

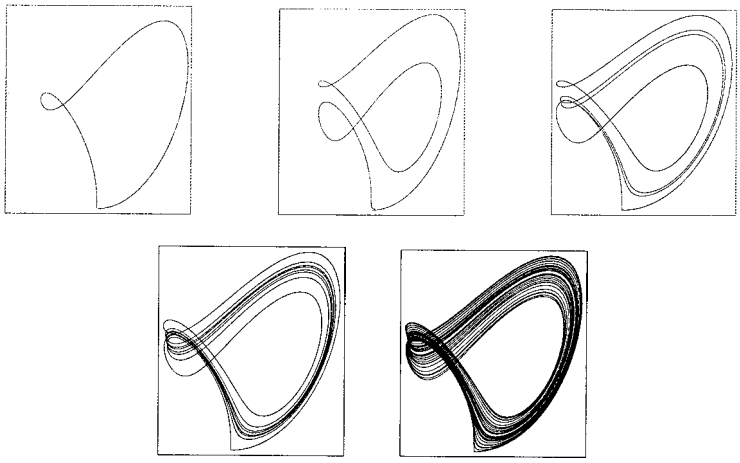

Fig. C.7.13. Homoclinic doubling cascade in the Shimizu-Morioka model, as the parameter a varies ($b = 0.40$). Using the *shooting* approach, find the corresponding values of parameter a.

cascades (Figs. C.7.12(c) and C.7.11(e)) similar to those that appear in the study of the purely quadratic map in Sec. C.11. The contrast is the infinite derivative at the discontinuity point that guarantees strong expansion near the origin.

The period-doubling cascade is closely related here to the homoclinic doubling cascade [71, 120, 126], see Fig. C.7.13.

The two-dimensional map has the shape of a distinguishable "hook" for the parameter values along the curve $H8$ in the region $A < 0$, as shown in Fig. C.7.10. In fact, this observation suggests the simplest recipe for computing the orientation of the homoclinic loop; namely, having chosen a point on the cross-section close to the stable manifold and computing the corresponding trajectory, one verifies if the initial and the final points of the trajectory lie on the same side from W^s on the cross-section. If this is the case, then $A > 0$, and $A < 0$ otherwise. The initial point should be reasonably close to W^s because when A changes its sign one more time and becomes positive again, the loop becomes twice twisted and so forth. Figure C.7.7 shows two such secondary bifurcation curves which originate from the point $A = 0$ and end up spiraling to two T-points in the (a, b)-parameter plane (examine the fine structure of T-point in [35, 174]). Such codimension-two point (approximately $a \simeq 0.781, b \simeq 0.39$ in Fig. C.7.7) corresponds to a heteroclinic cycle involving the saddle at the origin and the non-trivial saddle-foci. It follows from [35] that near the primary T-point there is an accumulating series of similar ones that lie within a sector bounded by the bifurcation curves corresponding to homoclinics and heteroclinics to these saddle-foci. This, in part, explains why the separatrix value A alters its sign here, and as a result, the loops change orientation (remember the 2D Poincaré map near a saddle-focus).

C.7.#86. Assume there is a homoclinic loop to a saddle-focus in the Shimizu-Morioka model (like a T-point). Without computing the characteristic exponent of the saddle-focus, what can we say about the local structure: is it trivial (one periodic orbit), or complex (infinitely many periodic orbits)? □

The classical Lorenz equation

$$\begin{aligned} \dot{x} &= -\sigma(x - y)\,, \\ \dot{y} &= rx - y - xz\,, \\ \dot{z} &= -\frac{8}{3}z + xy\,. \end{aligned} \tag{C.7.5}$$

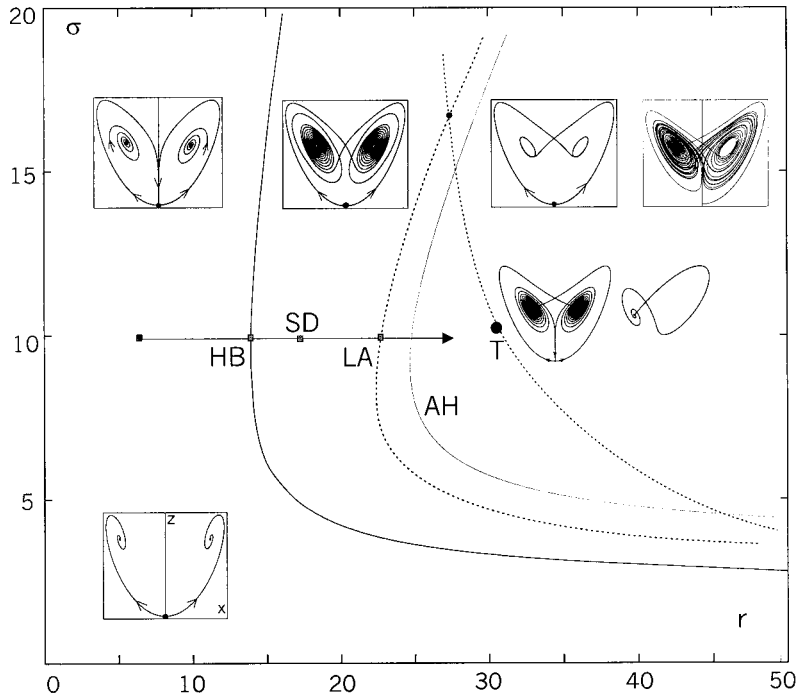

Fig. C.7.14. Famous path to the Lorenz attractor. The T-point is located at ($r \simeq 30.4$, $\sigma \simeq 10.2, b = 8/3$).

A fragment of its (r, σ) bifurcation diagram is shown in Fig. C.7.14. Detect the points where the path $\sigma = 10$ intersect the curve HB of the homoclinic butterfly and the curve LA on which the one-dimensional separatrices of the saddle tend to the saddle periodic orbits. Find the point on the curve LA above which the Lorenz attractor does not arise upon crossing LA towards larger values of r. The dashed line passing through the T-point in Fig. C.7.14 corresponds to the moment of the creation of the hooks in the two-dimensional Poincaré map when the separatrix value varishes: $A = 0$ (see discussion on the Shimizu-Morioka model). □

We have seen that homoclinic bifurcations in symmetric systems have much in common. Let us describe next the universal scenario of the formation of a homoclinic loop to a saddle-focus in a "typical" system. In particular, this mechanism works adequately in the Rössler model, in the new Lorenz models, in the normal form (C.2.27), and many others.

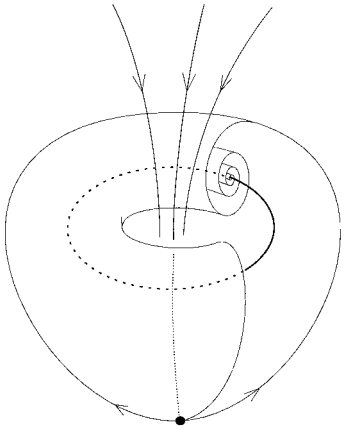

Fig. C.7.15. An attracting whirlpool.

The first step on the route to such a homoclinic bifurcation is a super-critical Andronov-Hopf bifurcation: the stable equilibrium states losses its stability and becomes a saddle-focus. The edge of its two-dimensional unstable manifold is the new-born stable periodic orbit. Next, let a real leading multiplier of the stable periodic orbit coalesce with the other one after which they become a complex conjugate pair remaining inside the unit circle. Then, the unstable manifold of the saddle-focus starts winding to the stable periodic orbit thereby forming an attractive "cup" or "a whirl-pool", as shown in Fig. C.7.15. As a parameter of the system varies further, the sizes of the scrolls increase, and eventually the unstable manifold of the saddle-focus touches its stable manifold. Usually, this homoclinic bifurcation follows the preceding stability-loss bifurcations of the periodic orbit via either a flip- or a torus-bifurcation. Moreover, if the saddle value is positive at the saddle-focus, then the whirlpool will contain an attracting set of non-trivial structure.

Let us visualize these steps using the example of the new Lorenz model [128]

$$\begin{aligned} \dot{x} &= -y^2 - z^2 - ax + aF\,, \\ \dot{y} &= xy - bxz - y + G\,, \\ \dot{z} &= bxy + xz - z\,, \end{aligned} \tag{C.7.6}$$

where (F, G) are control parameters and $(a = 1/4, b = 4.0)$ (see Fig. C.7.16).

The new Lorenz model is very rich in the sense of bifurcations. One of them is a non-transverse homoclinic saddle-node bifurcation. In Sec. C.2, we have

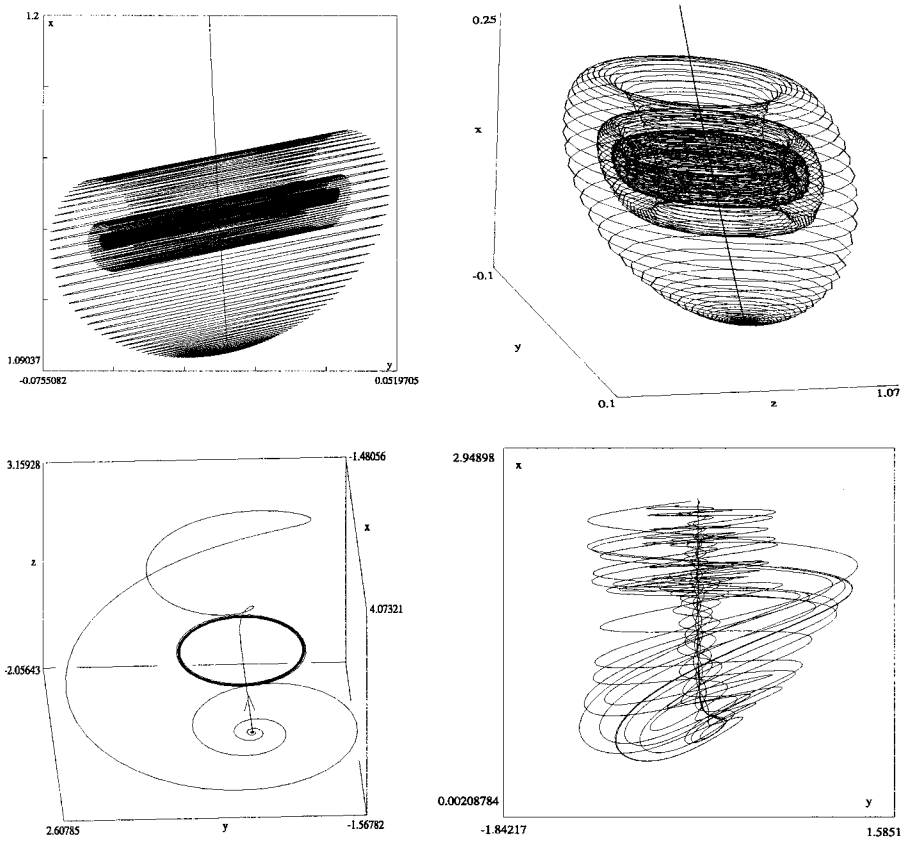

Fig. C.7.16. Creation of a whirlpool in the new Lorenz system.

already found the regular saddle-node bifurcation curve SN. Figure C.7.17 is the enlargement of the bifurcation diagram of the system near the upper branch of SN, compare with Figs. C.6.10 and C.2.4. This branch corresponds to a structurally unstable equilibrium state with one zero characteristic exponent, the other two have a negative real part. To the left of SN, this critical equilibrium disappears, whereas to the right of SN it splits into two: a stable one and and a saddle-focus (2,1). The curve H_1 corresponds to the homoclinic loop of the saddle-focus. The points where H_1 merges with SN correspond to the non-transverse homoclinic saddle-node bifurcations of codimension two.

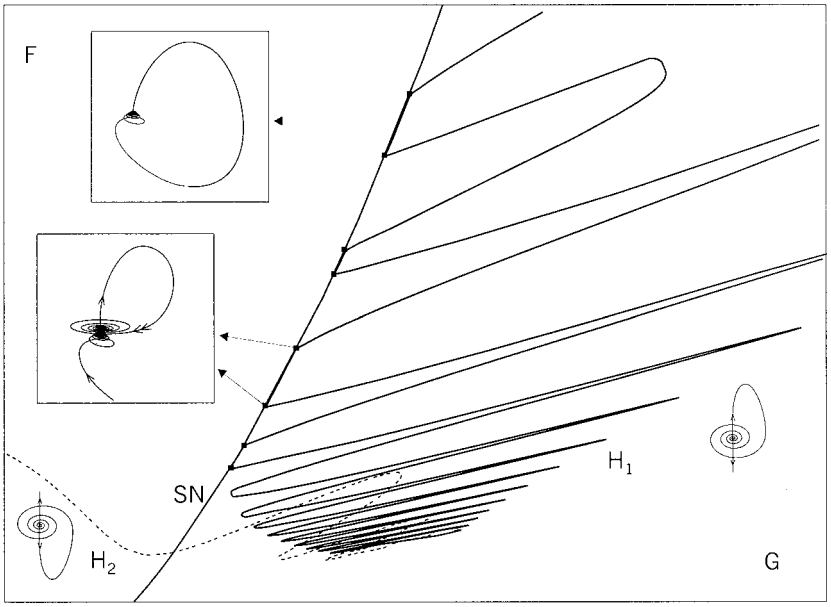

Fig. C.7.17. Enlargement of the bifurcation diagram in Fig. C.6.10. The marked points correspond to the non-transverse homoclinic saddle-node bifurcation.

At such a point the unstable manifold of the saddle-node returns to the equilibrium state along the strongly stable manifold. The rest of the curve SN is a bifurcation surface of codimension-one broken by these points into alternating intervals of two types. Bifurcation sequences on the route from the right to the left over these intervals differ significantly. In the first case, this is a plain saddle-node bifurcation: two equilibrium states coalesce and vanish. A point on the second type segments corresponds to the saddle-node equilibrium state with a homoclinic orbit which becomes an attractive limit cycle after the saddle-node point disappears on the left of SN. It is curious to note that this bifurcation sequence is reversible: having crossed over SN from the left to the right, the stability of the periodic orbit returns to the attractive equilibrium state. In this connection, see the discussion on "safe" and "dangerous" bifurcations in Chap. 14. □

Let us complete this section by an illustration corresponding to the homoclinic butterfly of the saddle-focus in the four-dimensional case. Let us consider

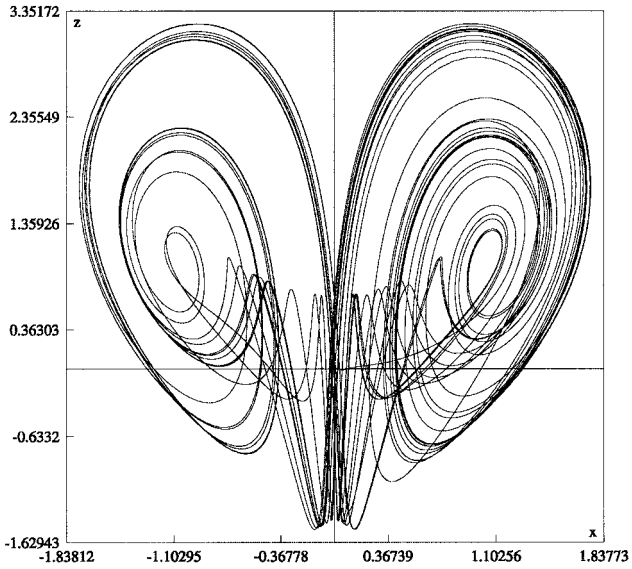

Fig. C.7.18. Homoclinic explosion caused by a homoclinic butterfly to a saddle-focus in system (C.7.7) at $a = 2, b = 0.5, \mu = 1.2$.

a four-dimensional perturbation of the Lorenz equation

$$\begin{aligned} \dot{x} &= -10(x - y)\,, \\ \dot{y} &= rx - y - xz\,, \\ \dot{z} &= -\frac{8}{3}z + \mu w + xy\,, \\ \dot{w} &= -\frac{8}{3}w - \mu z\,, \end{aligned}$$

and that of the Shimizu-Morioka model

$$\begin{aligned} \dot{x} &= y\,, \\ \dot{y} &= -ay + x - xz\,, \\ \dot{z} &= w\,, \\ \dot{w} &= -bw - \mu z + x^2\,, \end{aligned} \tag{C.7.7}$$

where a new parameter $\mu \geq 0$ is introduced so that the saddle equilibrium state at the origin restricted to the (z, w)-subspace becomes a stable focus.

C.7.#87. Find the stable, strongly stable and unstable linear subspaces of the equilibria at the origin. Detect numerically the primary homoclinic loops to the origin ($\mu = 0$ is a good initial guess). Classify them in terms of a homoclinic butterfly or a figure-eight. What are the first and the second saddle values at homoclinic bifurcations? What can you say about the dimensions of the stable and unstable manifolds of the periodic orbits that appear through a homoclinic explosion in both models? Construct the Poincaré maps. □

Index — Parts I & II

Bibliography

[*] This bibliography does not pretend to be complete and includes only references directly related to the content of this book. Besides, the references to some books that are particularly pertinent to the subject of this book are marked with an asterisk $*$.

[1] Afraimovich, V. S., Bykov, V. V. and Shilnikov, L. P. [1977] "The Origin and structure of Lorenz attractor," *Sov. Phys. Dokl.* **22**(5), 253–255.

[2] Afraimovich, V. S. and Shilnikov, L. P. [1973] "On critical sets of Morse–Smale systems," *Trans. Moscow Math. Soc.* **28**, 1761–1765.

[3] Afraimovich, V. S. and Shilnikov, L. P. [1974] "On some global bifurcations connected with the disappearance of fixed point of a saddle-node type," *Soviet Math. Dokl.* **15**, 1761–1765.

[4] Afraimovich, V. S. and Shilnikov, L. P. [1974] "On small periodic perturbations of autonomous systems," *Doclady AN SSSR* **5**, 734–742.

[5] Afraimovich, V. S. and Shilnikov, L. P. [1977] "The annulus principle and problems on interaction of two self-oscillation systems," *Prikladnaja Matematika i Mehanika* **41**, 618–627.

[6] Afraimovich, V. S. and Shilnikov, L. P. [1982] "On a bifurcation of codimension-one leading to the appearance of a countable set of tori," *Soviet Math. Dokl.* **25**, 101–105.

[7] Afraimovich, V. S. and Shilnikov, L. P. [1991] "Invariant tori, their breakdown and stochasticity," *Amer. Math. Soc. Transl.* **149**, 201–211.

[8] Andronov, A. A. [1933] "Mathematical problems of the theory of self-oscillations," in *All-Union Conference on Auto-oscillations*, November 1933 (GTTI: Moscow-Leningrad), 32–71.

[9] Andronov, A. A. and Leontovich, E. A. [1937] "Some cases of the dependence of the limit cycles upon parameters," *Uchenye zapiski Gorkovskogo Universiteta* **6**, 3–24.

[10] Andronov, A. A. and Leontovich, E. A. [1968] "Dynamical systems of first degree of roughness on the plane," *Am Math. Soc., Transl., II, Ser.* **75**, 149–199.

[11] * Andronov, A. A., Leontovich, E. A., Gordon, I. E. and Maier, A. G. [1971] *The Theory of Bifurcations of Dynamical Systems on a Plane* (Israel program of scientific translations, Jerusalem).

[12] * Andronov, A. A., Leontovich, E. A., Gordon, I. E. and Maier, A. G. [1973] *The Theory of Dynamical Systems on a Plane* (Israel program of scientific translations, Jerusalem).

[13] Andronov, A. A. and Pontryagin, L. S. [1937] "Systèmes grossières," *Dokl. Acad. Nauk SSSR* **14**(5), 247–251.

[14] Andronov, A. A. and Vitt, A. A. [1930] "Zur Theorie des Mitmehmens von van der Pol," *Archiv für Elektrotechnik*, Bd. XXIV, 99.

[15] Andronov, A. A. and Vitt, A. A. [1933] "On Lyapunov stability," *Zhurnal Eksperimental'noi i Teoreticheskoi Fisiki* **5**.

[16] Anosov, D. V., Bronshtejn, I. U., Aranson, S. Kh. and Grines, V. Z. [1988] *Smooth Dynamical Systems*, *Dynamical Systems I*, Encyclopedia of Mathematics Science I (Springer-Verlag: New York), 149–233.

[17] * Andronov, A. A., Vitt, A. A. and Khaikin, S. E. [1966] *Theory of Oscillations* (Pergamon Press: Oxford).

[18] Arneodo, A., Coullet, P., Spiegel, E. and Tresser, C. [1981] "Asymptotic chaos," *Physica* **D14**, 327–347.

[19] Arnold, V. I. [1973] "Lectures on bifurcations and versal families," *Recrs. Math. Surv.* **27**(5), 54–123.

[20] * Arnold, V. I. [1982] *Geometrical Methods in the Theory of Ordinary Differential Equations* (Springer-Verlag: New York).

[21] * Arnold, V. I., Afraimovich, V. S., Ilyashenko, Y. S. and Shilnikov, L. P. [1994] *Bifurcation Theory*, Dynamical Systems V. Encyclopaedia of Mathematical Sciences (Springer-Verlag: New York).

[22] Arnold, V. I. and Ilyashenko, Y. S. [1985] *Ordinary Differential Equations*, Dynamical Systems I. Encyclopaedia of Mathematical Sciences (Springer-Verlag: New York).

[23] Auslander, L., Green, L. and Hahn, F. [1963] "Flows on homogeneous spaces," *Annals of Mathematics Studies* **53** (Princeton University Press: Princeton, N.J.).

[24] * Bautin, N. N. [1949] *Behavior of Dynamical Systems near the Boundaries of Stability Regions* (OGIZ GOSTEHIZDAT: Leningrad).

[25] * Bautin, N. N. and Leontovich, E. A. [1976] *Methods and Rules for the Qualitative Study of Dynamical Systems of the Plane* (Nauka: Moscow).

[26] Bautin, N. N. and Shilnikov, L. P. [1980] "Suplement I: Safe and dangerous boundaries of stability regions," *The Hopf Bifurcation and Its Applications*, Russian translation of the book by Marsden, J. E. and McCracken, M. (Mir: Moscow).

[27] Belitskii, G. R. [1979] *Normal Forms, Invariants, and Local Mappings* (Naukova Dumka: Kiev).

[28] Belogui, J. A. [1981] *Module de estabilidade para campos vetoriais em variedades tridimensionais* (Ph.D. Thesis, I.M.P.A., Brazil).

[29] Belyakov, L. A. [1974] "A case of the degeneration of a periodic motion with homoclinic curves," *Math. Zametki* **15**, 336–341; [1980] "The bifurcation set in a system with a homoclinic saddle curve," *ibid.* **28**, 910–916; [1984] "Bifurcation of systems with homoclinic curve of a saddle-focus with saddle quantity zero," *ibid.* **36**, 838-843.

[30] Bendixson, J. [1901] "Sur les courbes definies par les equations differentielles," *Acta Math.* **24**.

[31] Birkhoff, G. D. [1927] "Dynamical systems," *Amer. Math. Soc., Colloquium Publications* **9**.

[32] Birkhoff, G. D. [1935] "Nouvelles recherche sur les systèmes dynamiques," *Memorie Pont Acad. Sci. Novi Lyncaei* **53**(1), 85–216.

[33] Bogdanov, R. I. [1975] "Versal deformations of a singular point on the plane in the case of zero eigenvalues," *Functional Analysis and Its Applications* **9**(2), 144–145.

[34] Bykov, V. V. [1978] "On the structure of a neighborhood of a separatrix contour with a saddle-focus," in *Methods of Qualitative Theory of Differential Equation* (Gorky: Gorky State University), 3–32; [1980] "On bifurcations of dynamical systems with a separatrix contour containing a saddle-focus," *ibid.* 44–72; [1988] "On the birth of a non-trivial hyperbolic set from a contour formed by separatrices of a saddle," *ibid.* 22–32.

[35] Bykov, V. V. [1993] "The bifurcations of separatrix contours and chaos," *Physica* **D62**, 290–299.

[36] Cartwright, M. L. and Littlewood, J. E. [1945] "On nonlinear differential equations of the second order, I: The equation $\ddot{y} + k(1 - y^2)\dot{y} + y = b\,\lambda\,k\cos(\lambda t + a)$, k large," *J. Lond. Math. Soc.* **20**, 180–189.

[37] Chenciner, A. [1981] "Courbes fermées invariantes non-normalement hyperboliques au voisinage d'une bifurcation de Hopf dégénerée de diffeomorphismes $\mathbb{R}^2$," *Comptes Rendus Acad. Sci. 292, Ser.* **1**, 507–510.

[38] Chow, S.-N., Deng, B. and Fiedler, B. [1990] "Homoclinic bifurcations of resonant eigenvalues," *J. Dyn. Diff. Eq.* **2**(2), 177–245.

[39] * Chow, S.-N. and Hale, J. [1982] *Methods of Bifurcation Theory* (Springer-Verlag: New York).

[40] * Chow, S.-N., Li, C. and Wang, D. [1994] *Normal Forms and Bifurcations of Planar Vector Fields* (Cambridge University Press: Cambridge).

[41] Chua, L. O. [1998] *CNN: A Paradigm for Complexity* (World Scientific: Singapore).

[42] de Melo, W. [1980] "Moduli of stability of two-dimensional diffeomorphisms," *Topology* **19**, 9–21.

[43] de Melo, W. and van Streen, S. J. [1987] "Diffeomorphisms on surfaces with finite number of moduli," *Erg. Theory Dynam. Systems* **7**, 415–462.

[44] Deng, B. [1993] "Homoclinic twisting bifurcations and cusp horseshoe maps," *J. Dyn. Diff. Eq.* **5**, 417–467.

[45] Diaz, L., Rocha, J. and Viana, M. [1996] "Strange attractors in saddle-node cycles: prevalence and globality," *Invent. Math.* **125**, 37–74.

[46] Doedel, E. [1997] "Nonlinear numerics," *Int. J. Bif. Chaos* **7**(9–10), 2127–2143.

[47] Dulac, H. [1923] "Sur les cycles limites," *Bull. Soc. Math. France* **51**, 45–188.

[48] Fenichel, N. [1971] "Persistence and smoothness of invariant manifolds for flows," *Indiana Univ. Math. J.* **21**, 193–226.

[49] Fink, A. M. [1974] *Almost Periodic Differential Equations*, Lecture Notes in Mathematics **377** (Springer-Verlag: Berlin, New York).

[50] Gambaudo, J. M., Glendinning, P. and Tresser, C. [1988] "The gluing bifurcation. I: Symbolic dynamics of the closed curves," *Nonlinearity* **1**(1), 203–214.

[51] Gavrilov, N. K. [1978] "On some bifurcations of an equilibrium state with one zero and a pair of purely imaginary roots," in *Methods of Qualitative Theory of Differential Equations* (Gorky State University: Gorky); [1987] "On bifurcations of equilibrium with one zero and pair of pure imaginary eigenvalues and additional degeneracy," *ibid.* 43–51.

[52] Gavrilov, N. K. and Roshchin, N. V. [1983] "On the stability of an equilibrium with one zero and a pair of pure imaginary eigenvalues," in *Methods of Qualitative Theory of Differential Equations* Leontovich–Andronova, ed., (Gorky State University: Gorky), 41–49.

[53] Gavrilov, N. K. and Shilnikov, A. L. [1996] "On a blue sky catastrophe model," Proc. Int. Conf. *Comtemp. Problems of Dynamical Systems Theory*, ed. Lerman, L. (Nizhny Novgorod State University: Nizhny Novgorod). [1999] "An Example of blue sky catastrophe," in *Ams Transl. Series II.* "Methods of qualitative theory of differential equations and related topics." (AMS, Providence, Rhode Island).

[54] Gavrilov, N. K. and Shilnikov, L. P. [1972] "On three-dimensional dynamical systems close to systems with a structurally unstable homoclinic curve I," *Math. USSR Sbornik* **88**(44), 467–485.

[55] Gavrilov, N. K. and Shilnikov, L. P. [1973] "On three-dimensional dynamical systems close to systems with a structurally unstable homoclinic curve II," *ibid.* **90**(1), 139–156.

[56] * Golubitsky, M. and Schaeffer, D. [1985] *Singularities and Groups in Bifurcation Theory I* (Springer-Verlag: New York).

[57] * Golubitsky, M., Stewart, I. and Schaeffer, D. [1988] *Singularities and Groups in Bifurcation Theory II* (Springer-Verlag: New York).

[58] Gonchenko, S. V. and Shilnikov, L. P. [1990] "Invariants of Ω-conjugacy of diffeomorphisms with a structurally unstable homoclinic trajectory," *Ukrainian Math. J.* **42**(2), 134–140.

[59] Gonchenko, S. V. and Shilnikov, L. P. [1993] "On moduli of systems with a structurally unstable homoclinic Poincaré curve," *Russian Acad. Sci. Izv. Math.* **41**(3), 417–445.

[60] Gonchenko, S. V., Turaev, D. V. and Shilnikov, L. P. [1993a] "On models with non-rough Poincaré homoclinic curves," *Physica* **D62**, 1–14.

[61] Gonchenko, S. V., Turaev, D. V. and Shilnikov, L. P. [1993b] "Dynamical phenomena in multi-dimensional systems with a structurally unstable homoclinic Poincaré curve," *Russian Acad. Sci. Dokl. Math.* **47**(3), 410–415.

[62] Gonchenko, S. V., Shilnikov, L. P. and Turaev, D. V. [1996] "Dynamical phenomena in systems with structurally unstable Poincaré homoclinic orbits," *Interdisc. J. Chaos* **6**(1), 1–17.

[63] Gonchenko, S. V., Sten'kin. O. V. and Turaev, D. V. [1996] "Complexity of homoclinic bifurcations and Ω-moduli," *Int. J. Bifurcation & Chaos* **6**(6), 969–989.

[64] * Guckenheimer, J. and Holmes, P. [1983] *Nonlinear Oscillations, Dynamical Systems, and Bifurcations of Vector Fields* (Springer-Verlag: New York), Series title: Applied Mathematical Sciences **42**.

[65] Guimond, L. S. [1999] "Homoclinic loop bifurcations on a Möbius band," *Nonlinearity* **12**(1), 59–78.

[66] Halanay, A. [1966] *Differential Equations; Stability, Oscillations* (Academic Press: New York) Series title: Mathematics in Science and Engineering **23**.

[67] Hale, J. and Kocak, H. [1991] *Dynamics and Bifurcations* (Springer-Verlag: New York).

[68] Hermann, M. [1971] "Mesure de Lebesgue et nombre de rotation," *Proc. Symp. Geometry Topology*, Lecture Notes in Mathematics, Vol. 597 (Springer-Verlag: New York), 371–295.

[69] Homburg, A. J. [1996] "Global aspects of homoclinic bifurcations of vector fields," *Memoirs of the A.M.S.* **578**.

[70] Homburg, A. J., Kokubu, H. and Krupa, M. [1994] "The cusp horseshoe and its bifurcations in the unfolding of an inclination flip homoclinic orbit," *Ergod. Th. Dynam. Syst.* **14**, 667–693.

[71] Homburg, A. J., Kokubu, H. and Naudot, V. [1997] "Homoclinic-doubling cascades," preprint.

[72] Homburg, A. J. and Krauskopf, B. [1998] "Resonant homoclinic flip bifurcations," preprint, Free University-Berlin.

[73] Ilyashenko, Yu. S. and Yakovenko, S. Yu. [1991] "Finite-smooth normal forms of local families of diffeomorphisms and vector fields," *Uspechi Mat. Nauk*, Vol. 46, **1**(277), 1–39.

[74] Ilyashenko, Yu. S. and Yakovenko, S. Yu. [1993] "Nonlinear Stokes phenomena in smooth classification problems," *Adv. Soviet Math.*, Vol. 14, 235–287.

[75] Khazin, L. G. and Shnol, E. E. [1991] *Stability of Critical Equilibrium States* (Manchester University Press).

[76] Khibnik, A. I, Kuznetsov, Y. A., Levitin, V. V. and Nikolaev, E. V. [1993] "Continuation techniques and interactive software for bifurcation analysis of ODE's and iterated maps," *Physica* **D62**(1–4), 360–371.

[77] Kisaka, M., Kokubu, H. and Oka H. [1993] "Bifurcations to N-homoclinic orbits and N-periodic orbits in vector fields," *J. Dyn. Diff. Eq.* **5**, 305–357.

[78] Kokubu, H., Komuro, M. and Oka, H. [1996] "Multiple homoclinic bifurcations from orbit flip. I. Successive homoclinic-doublings," *Int. J. Bif. Chaos* **6**, 833–850.

[79] Kokubu, H. and Naudot, V. [1997] "Existence of infinitely many homoclinic-doubling bifurcations from some codimension-three homoclinic orbits," *J. Dyn. Diff. Eq.* **9**, 445–462.

[80] Krauskopf, B. [1994] "Bifurcation sequences at 1:4 resonance: An inventory," *Nonlinearity* **7**(3), 1073–1091.

[81] Krylov, N. M. and Bogolyubov, N. N. [1947] *Introduction to Nonlinear Mechanics* (Princeton University Press: Princeton).

[82] * Kuznetsov, Yu. A. [1998] *Elements of Applied Bifurcation Theory* (Springer-Verlag: New York).

[83] Kuznetsov, Yu. A. and Levitin, V. V. [1996] "CONTENT: A multiplatform environment for analyzing dynamical systems" (Centrum voor Wiskunde en Informatica, Amsterdam), ftp.cwi.nl/pub/CONTENT.

[84] Levitan, B. M. and Zhikov, V. V. [1982] *Almost Periodic Functions and Differential Equations* (Cambridge University Press: Cambridge [Cambridgeshire]; New York).

[85] Leontovich, E. A. [1951] "On birth of limit cycles from separatrices," *DAN SSSR* **74**4, 641–644.

[86] Li, W. and Zhang, Z. F. [1991] "The "blue sky catastrophe" on closed surfaces," *Adv. Series Dynam. Syst.* **9** (World Scientific, River Edge, N.J.), 316–332.

[87] Lorenz, E. N. [1963] "Deterministic non-periodic flow," *J. Atmos. Sci.* **20**, 130–141.

[88] Lukyanov, V. [1982] "On bifurcations of dynamical systems with a separatrix loop to a saddle-node," *Diff. Eq.* (*Russian*) **58**, 1493–1506.

[89] Lyapunov, A. M. [1950] "Problème général de la stabilité du mouvement," *Ann. de la Faculté des Sciences de Toulouse* **9**, 203–474.

[90] Lyapunov, A. M. [1966] *Stability of Motion* (Academic Press: New York).

[91] Malkin, I. G. [1952] *Theory of Stability of Motion* (Washington, D. C., United States Atomic Energy Commission, Series title: Translation series: AEC-tr-3352).

[92] Markov, A. A. [1933] "Stabilitat im Liapunoffschen Sinne und Fastperiodizitat," *Math. Zeitschr.* **36**.

[93] Mayer, A. G. [1943] "On center trajectories and a Birkhoff problem," *Mat. Sbornik* **12**(1).

[94] Meyer, K. R. [1968] "Energy functions for Morse–Smale systems," *Anter. J. Math.* **90**(4), 1031–1040.

[95] Medvedev, V. S. [1980] "On a new type of bifurcations on manifolds," *Mat. Sbornik* **113**, 487–492.

[96] Naudot, V. [1996] "Bifurcations homoclines des champs de vecteurs en dimension trois," thesis, l'Université de Bourgogne, Dijon.

[97] Newhouse, S., Palis, J. and Takens, F. [1983] "Bifurcations and stability of families of diffeomorphisms," *Publ. Math. IHES* **57**, 5–71.

[98] * Nemytskii, V. V. and Stepanov, V. V. [1960] *Qualitative Theory of Differential Equations* (Princeton, N.J., Princeton University Press. Series title: Princeton Mathematical Series **22**).

[99] Nozdracheva, V. P. [1982] "Bifurcation of a noncoarse separatrix loop," *Differ. Equations* **18**, 1098–1104.

[100] Ovsyannikov, I. M. and Shilnikov, L. P. [1987] "On systems with a saddle-focus homoclinic curve," *Math. USSR Sb.* **58**, 557–574.

[101] Ovsyannikov, I. M. and Shilnikov, L. P. [1992] "Systems with a homoclinic curve of multi-dimensional saddle-focus type, and spiral chaos," *Math. USSR Sb.* **73**, 415–443.

[102] Palis, J. [1969] "On Morse–Smale dynamical systems," *Topology* **4**, 385–404.

[103] Palis, J. [1978] "A differentiable invariant of topological conjugacies and moduli of stability," *Asterisque* **51**, 335–346.

[104] Palis, J. and de Melo, W. [1982] *Geometric Theory of Dynamical Systems. An Introduction* (Springer-Verlag: New York).

[105] Palis, J. and Pugh, C. [1975] "Fifty problems in dynamical systems," *Lecture Notes in Mathematics* Vol. 486, 34–353.

[106] Palis, J. and Smale, S. [1969] "Structural stability theorem," preprint.

[107] Peixoto, M. M. [1962] "Structural stability on two-dimensional manifolds," *Topology* **1**, 101–120.

[108] Poincaré, H. [1903] "Sur l'equilibre d'une masses fluide animés d'un mouvement de rotation," *Acta Mathematica* **7**.

[109] Poincaré, H. [1885] "Sur les courbes définies par des équations différentielles," *J. de Math. Pures et Appl.* **1**, 167–244.

[110] Poincaré, H. [1903] *Figures d'equilibre d'une masse fluide* (Paris).

[111] Poincaré, H. [1921] "Analyse des travans de Henri Poincaré faite par luimeme," *Acta Mathematica* **38**, 36–135.

[112] Pontryagin, L. S. [1933] "Les fonctions presque périodiques et l'analysis situs," *C.R. Acad. Sci.* **196**(17), 1201–1203.

[113] Pugh, C. C. [1967] "The closing lemma," *Amer. J. Math.* **89**, 956–1009.

[114] Robinson, C. [1989] "Homoclinic bifurcation to a transitive attractor of Lorenz type," *Nonlinearity* **2**, 495–518.

[115] Robinson, C. [1992] "Homoclinic bifurcation to a transitive attractor of Lorenz type II," *SIAM J. Math. Anal.* **23**, 1255–1268.

[116] Roussarie, R. [1986] "On the number of limit cycles which appear by perturbation of separatrix loop of planar vector fields," *Bol. Soc. Math. Brasil* **17**(2), 67–101.

[117] Rychlik, M. R. [1990] "Lorenz attractors through Sil'nikov-type bifurcation. Part I," *Ergod. Th. Dynam. Syst.* **10**, 793–821.

[118] Sacker, R. [1964] "On invariant surfaces and bifurcations of periodic solutions of ordinary differential equations," *IMM-NUY* **333**, New York State University.

[119] Sanstede, B. [1993] "Verzweigungstheorie homokliner Verdopplungen," Ph.D. Thesis, Free University of Berlin, Institut für Angewandte Analysis und Stochastic, Report No. 7, Berlin.

[120] Sanstede, B. [1995] "Center manifold for homoclinic solutions," *Weierstrass Inst. Appl. Analysis Stochastic*, preprint N 186.

[121] Shashkov, M. V. [1994] "Bifurcations of separatrix contours," Ph.D. Thesis, Nizhny Novgorod State University.

[122] Shashkov, M. V. [1992] "On bifurcations of separatrix contours with two saddles," *Int. J. Bif. Chaos* **2**(4), 911–914.

[123] Shashkov, M. V. [1992] "On the bifurcations of separatrix contours on two-dimensional surfaces. I," *Selecta Math. Sovietica* **11**(4), 341–353.

[124] Shashkov, M. V. [1994] "On the bifurcations of separatrix contours on two-dimensional surfaces. II," *ibid.* **13**(2), 175–182.

[125] Shashkov, M. V. and Turaev, D. V. [1996] "On the complex bifurcation set for a system with simple dynamics," *Int. J. Bif. Chaos* **6**(5), 949–968.

[126] Shilnikov, A. L. [1990] "Qualitative and numerical analysis of Lorenz-like systems," Ph.D Thesis, Gorky State University.

[127] Shilnikov, A. L. [1993] "Bifurcations of the Lorenz attractors in the Morioka–Shimizu model," *Physica* **D62**, 338–346.

[128] Shilnikov, A. L., Nicolis, G. and Nicolis, C. [1995] "Bifurcation and predictability analysis of a low-order atmospheric circulation model," *Int. J. Bif. Chaos* **5**(6), 1701–1711.

[129] Shilnikov, A. L., Shilnikov, L. P. and Turaev, D. V. [1993] "Normal forms and Lorenz attractors," *Int. J. Bif. Chaos* **1**(4), 1123–1139.

[130] Shilnikov, L. P. [1963] "Some cases of generation of periodic motion from singular trajectories," *Math. USSR Sbornik* **61**(103), 443–466.

[131] Shilnikov, L. P. [1965] "A case of the existence of a denumerable set of periodic motions," *Sov. Math. Dokl.* **6**, 163–166.

[132] Shilnikov, L. P. [1967] "The existence of a denumerable set of periodic motions in four-dimensional space in an extended neighborhood of a saddle-focus," *Soviet Math. Dokl.* **8**(1), 54–58.

[133] Shilnikov, L. P. [1967] "On a Poincaré-Birkhoff problem," *Math. USSR Sbornik* **3**, 415–443.

[134] Shilnikov, L. P. [1968] "On the generation of periodic motions from trajectories doubly asymptotic to an equilibrium state of saddle type," *Math. USSR Sbornik* **6**, 427–437.

[135] Shilnikov, L. P. [1969] "On a new type of bifurcation of multi-dimensional dynamical systems," *Soviet Math. Dokl.* **10**, 1368–1371.

[136] Shilnikov, L. P. [1970] "A contribution to the problem of the structure of an extended neighborhood of a rough equilibrium state of saddle-focus type," *Math. USSR Sbornik* **10**, 91–102.

[137] Shilnikov, L. P. [1975] "Theory of the bifurcations of dynamical systems," *Math. Physics* **20**, 674–676.

[138] Shilnikov, L. P. [1981] "The bifurcation theory and quasihyperbolic attractors," *Uspehi Mat. Nauk* **36**, 240–241.

[139] Shilnikov, L. P. and Turaev, D. V. [1997] "Simple bifurcations leading to hyperbolic attractors," *Computers Math. Applic.* **34**(2–4), 173–193.

[140] Shilnikov, L. P. and Turaev, D. V. [2000] "A new simple bifurcation of a periodic orbit of blue sky catastrophe type," in AMS Transl. Series II. "Methods of qualitative theory of differential equations and related topics" (AMS, Rhode Island, Providence).

[141] Simonov, A. A. [1978] "An investigation of bifurcations in some dynamical systems by the methods of symbolics dynamics," *Sov. Math. Dokl.*, **19**, 759–763.

[142] Smale, S. [1960] "Morse inequalities for a dynamical system," *Bull. Amer. Math. Soc.* **66**, 43–49.

[143] Smale, S. [1963] "Diffeomorphisms with many periodic points," in *Diff. Combin. Topology*, ed. S. Cairus (Princeton University Press: Princeton), 63–86.

[144] Sotomayor, J. [1971] "Generic bifurcations of dynamical systems," in *Dynamical Systems Proc. Symp. Univ. Bahia*, Salvador, 561-582, Zbl.296.58007.

[145] Sotomayor, J. [1971] "Structural stability and bifurcation theory," in *Dynamical Systems Proc. Symp. Univ. Bahia*, Salvador, 549-560, Zbl.293.34081.

[146] Takens, F. [1974] "Singularities of vector fields," *Publ. Math. IHES* **43**, 47–100.

[147] Tresser, C. [1984] "About some theorems by L. P. Sil'nikov," *Ann. Inst. Henri Poincaré, Phys. Theor.* **40**, 441–461.

[148] Turaev, D. V. [1984] "On a case of bifurcations of a contour composed by two homoclinic curves of a saddle," in *Methods of Qualitative Theory of Differential Equations* (Gorky State University), 162–175.

[149] Turaev, D. V. [1991] "On bifurcations of dynamical systems with two homoclinic curves of the saddle," Ph.D. Thesis, Nizhny Novgorod State University.

[150] Turaev, D. V. [1996] "On dimension of nonlocal bifurcational problems," *Int. J. Bif. Chaos* **2**(4), 911–914.

[151] Turaev, D. V. and Shilnikov, L. P. [1987] "On bifurcations of a homoclinic "figure-eight" for a saddle with a negative saddle value," *Soviet Math. Dokl.* **44**(2), 422–426.

[152] Turaev, D. V. and Shilnikov, L. P. [1995] "On a blue sky catastrophe," *Soviet Math. Dokl.* **342**(5), 596–599.

[153] Turaev, D. V. and Shilnikov, L. P. [1998] "An example of a wild strange attractor," *Sbornik. Math.* **189**(2), 291–314.

[154] van der Pol, B. [1927] "Forced oscillations in a circuit with nonlinear resistance (receptance with reactive triode)," *London, Edinburgh and Dublin Phil. Mag.* **3**, 65–80 (Reprinted in Bellman and Kakaba [1964]).

[155] Van Strien, S. J. [1982] *On Parameter Families of Vector Fields. Bifurcations Near Saddle-connections*, Ph.D. Thesis, Utrecht University.

[156] * Wiggins, S. [1988] *Global Bifurcations and Chaos* (Springer-Verlag: New York).

[157] Eleonsky, V. M., Kulagin, N. E., Turaev, D. V. and Shilnikov, L. P. [1988] "On the classification of self-localized states of the electromagnetic field within nonlinear medium," DAN SSSR **309**(9) 898–852.

[158] Shashkov, M. [1999] "Impossibility of complete bifurcation description for some classes of systems with simple dynamics", Abstracts of Int. Conference, *Equadiff 99* (Berlin), 22.

[159] Shilnikov, L. P., Turaev, D. V. [1997] "Superhomoclinic orbits and multipulse homoclinic loops in Hamiltonion systems with discrete symmetries", Regular and Chaotic Dynamics **2**(3/4) 126–138.

[160] ∗ Ilyashenno, Y. Li, Weigu [1999] Nonlocal bifurcations. *Math. Surveys and Monographs* **66** (AMS, Rhode Island, Providence).

[161] Afraimovich, V., Bykov, V. V. and Shilnikov L. P. [1983] "On attracting structurally unstable sets of Lorenz attrcator type", *Trans. Moscow. Math. Soc.* **44**, 150–213.

[162] Arneodo, A. Couller, P. H. and Spiegel, E. A. [1985] "The dynamics of triple convection", *Geophys. Astrophys. Fluid Dynamics* **31**, 1–48.

[163] Arneodo, A. Coulle r, P. H., Spiegel, E. A. and Tresser, C. [1985] "Asymptotic chaos", *Physica* **14D**, 327–347.

[164] Back, A., Guckenheimer, J., Myers, M. R., Wicklin, F. J. and P. A. Worfolk [1992] "DsTool: Computer assisted exploration of dynamical systems", *Notices Amer. Math. Soc.* **39**(4), 303–309; ftp://cam.cornell.edu/pub/dstool/.

[165] Bautin, N. N. [1984] *Behavior of Dynamical Systems near the Boundaries of Stability Regions* (Nauka: Moscow).

[166] Belykh, V. N. [1980] Qualitative methods of the theory of nonlinear oscillations of concentrated systems, Gorky State Univerosity press: Gorky.

[167] Byragov, V. S. [1987] "Bifurcations in a two-parameter family of conservative mappings that are close to the Henon mapping", in *Methods of the Qualitative Theory of Differential Equations* (Gorky: Gorky State Univ. Press), 10–24.

[168] Bykov, V. V. [1998] "On bifurcations leading to chaos in Chua's circuit", *Int. J. Bifurcation & Chaos* **8**(4), 685–699.

[169] Bykov, V. V. and Shilnikov, A. L. [1992] "On boundaries of the region of existence of the Lorenz attractor", *Selecta Math. Sovietica* **11**(4), 375–382.

[170] Feigenbaum, M. [1978] "Quantative universality for a class of nonlinear transformations", *J. Statist. Phys.* **19**, 25–52.

[171] Gaspard, P. [1993] "Local birth of homoclinic chaos", *Physica* **D62**, 94–122.

[172] Gaspard, P. and Nicolis, G. [1983] "What can we learn from homoclinic orbits in chaotic dynamics?" *J. Stat. Phys.* **27**(1), 499–518.

[173] Glendenning, P. and Sparrow, C. [1984] "Local and global behavior near homoclinic orbits", *J. Stat. Phys.* **35**, 645–696.

[174] Glendenning, P. and Sparrow, C. [1985] "T-point: a codimension-two heteroclinic bifurcation", *J. Stat. Phys.* **43**, 479–488.

[175] Gonchenko, S. V. and Gonchenko, V. S. [2000] "On Andronov-Hopf bifurcations of two-dimensional diffeomorphisms with homoclinic tangencies", Preprint No. 556, WIAS, Berlin.

[176] Gonchenko, S. V. and Komlev, Yu. A [1988] "Bifurcations and chaos in a cubic map of the plane", in *Methods of Qualitative Theory of Diff. Equations* (Gorky University Press: Gorky), 33–39.

[177] Hindmarsh, J. L. and Rose, R. M. [1984] "A model of neuronal bursting using three cioupled first order differential equations", *Proc. R. Soc. Lond.* **B221**, 87–102.

[178] Khibnik, A. I., Kuznetsov, Yu. A., Levitin, V. V. and Nikolaev, E. V. [1993] "Continuation techniques and interactive software for bifurcation analysis of ODEs and iterated maps", *Physica* **62D**, 360–371.

[179] Khibnik, A. I., Roose, D. and Chua, L. O. [1993] "On periodic orbits and homoclinic bifurcations in Chua's circuit with smooth nonlinearity", *Int. J. Bifurcation & Chaos* **3**(2), 363–384.

[180] Krauskopf, B. and Osinga H. M. [1999] "Investigating torus bifurcations in the forced Van der Pol oscillator", in *Numerical Methods for Bifurcation Problems and Large-Scale Dynamical Systems* eds. E. J. Doedel, L. S. Tuckerman, IMA Volumes in Mathematics and its Applications **119**, Springer-Verlag, to appear.

[181] Osinga H. M. [1999] "Non-orientable manifolds of periodic orbits", *Proceedings of Equadiff 99*, Berlin, to appear.

[182] Kuznetsov, Yu. A. [1998] "CONTENT — integrated environment for analysis of dynamical systems Tutorial", Ecole Normale Superieure de Lyon, Rapport de Recherche UPMA-98-224; ftp://ftp.cwi.nl/pub/CONTENT.

[183] Lorenz, E. N. [1984] "Irregularity: A fundumental property of the athmosphere", *Tellus* **A36**, 98–110.

[184] Mira, C. [1987] *Chaotic Dynamics: From the One-dimensional Endomorphism to the Two-Dimensional Diffeomorphism.* (World Scientific: Singapore-New Jersey-Hong Kong).

[185] Pisarevskii, V., Shilnikov, A. L. and Turaev, D. V. [1998] "Asymptotic normal forms for equilibria with a triplet of zero charactersitic exponents in systems with symmetry", *Regular and Chaotic Dynamics* **3**(1), 19–27.

[186] Roschin, N. V. [1978] "Unsafe stability boundaries of the Lorenz model", *J. Appl. Math. Mech.* **42**(5), 1038–1041.

[187] Rucklidge, A. M. [1994] "Chaos in magnetoconvection", *Nonlinearity* **7**, 1565–1591.

[188] Rössler, O. [1976] "An equation for continuous chaos", *Phys. Lett.* **57A**, 397–398.

[189] Shilnikov, A. L. and Shilnikov, L. P. [1991] "On the nonsymmetric Lorenz model", *Int. J. Bifurcation & Chaos* **1**(4), 773–776.

[190] Shimizu, T. and Morioka, N. [1980] "On the bifurcation of a symmetric limit cycle to an asymmetric one in a simple model", *Phys. Lett.* **76A**, 201–204.

[191] Vladimirov A. G. and Volkov, D. Yu. [1993] *Optics Commun.* **100**, 351–360.